AGARD-AR-332

AGARD

ADVISORY GROUP FOR AEROSPACE RESEARCH & DEVELOPMENT
7 RUE ANCELLE, 92200 NEUILLY-SUR-SEINE, FRANCE

AGARD ADVISORY REPORT NO. 332

Recommended Practices for the Assessment of the Effects of Atmospheric Water Ingestion on the Performance and Operability of Gas Turbine Engines

(Recommandations concernant les méthodes à utiliser pour le traitement de l'humidité dans les turbines à gaz)

Report of the Propulsion and Energetics Panel Working Group 24.

This Advisory Report was prepared at the request of the Propulsion and Energetics Panel of AGARD.

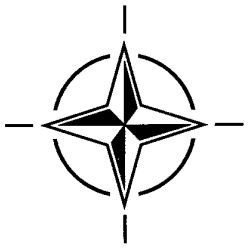

NORTH ATLANTIC TREATY ORGANIZATION

Published September 1995

Distribution and Availability on Back Cover

AGARD

ADVISORY GROUP FOR AEROSPACE RESEARCH & DEVELOPMENT
7 RUE ANCELLE, 92200 NEUILLY-SUR-SEINE, FRANCE

AGARD ADVISORY REPORT NO. 332

Recommended Practices for the Assessment of the Effects of Atmospheric Water Ingestion on the Performance and Operability of Gas Turbine Engines

(Recommandations concernant les méthodes à utiliser pour le traitement de l'humidité dans les turbines à gaz)

Report of the Propulsion and Energetics Panel Working Group 24.

This Advisory Report was prepared at the request of the Propulsion and Energetics Panel of AGARD.

North Atlantic Treaty Organization
Organisation du Traité de l'Atlantique Nord

The Mission of AGARD

According to its Charter, the mission of AGARD is to bring together the leading personalities of the NATO nations in the fields of science and technology relating to aerospace for the following purposes:

- Recommending effective ways for the member nations to use their research and development capabilities for the common benefit of the NATO community;
- Providing scientific and technical advice and assistance to the Military Committee in the field of aerospace research and development (with particular regard to its military application);
- Continuously stimulating advances in the aerospace sciences relevant to strengthening the common defence posture;
- Improving the co-operation among member nations in aerospace research and development;
- Exchange of scientific and technical information;
- Providing assistance to member nations for the purpose of increasing their scientific and technical potential;
- Rendering scientific and technical assistance, as requested, to other NATO bodies and to member nations in connection with research and development problems in the aerospace field.

The highest authority within AGARD is the National Delegates Board consisting of officially appointed senior representatives from each member nation. The mission of AGARD is carried out through the Panels which are composed of experts appointed by the National Delegates, the Consultant and Exchange Programme and the Aerospace Applications Studies Programme. The results of AGARD work are reported to the member nations and the NATO Authorities through the AGARD series of publications of which this is one.

Participation in AGARD activities is by invitation only and is normally limited to citizens of the NATO nations.

Published September 1995

ISBN 92-836-1022-9

Printed by Canada Communication Group
45 Sacré-Cœur Blvd., Hull (Québec), Canada K1A 0S7

Contents

Recent Publications of the Propulsion and Energetics Panel

CONFERENCE PROCEEDINGS (CP)

Interior Ballistics of Guns
AGARD CP 392, January 1986

Advanced Instrumentation for Aero Engine Components
AGARD CP 399, November 1986

Engine Response to Distorted Inflow Conditions
AGARD CP 400, March 1987

Transonic and Supersonic Phenomena in Turbomachines
AGARD CP 401, March 1987

Advanced Technology for Aero Engine Components
AGARD CP 421, September 1987

Combustion and Fuels in Gas Turbine Engines
AGARD CP 422, June 1988

Engine Condition Monitoring — Technology and Experience
AGARD CP 448, October 1988

Application of Advanced Material for Turbomachinery and Rocket Propulsion
AGARD CP 449, March 1989

Combustion Instabilities in Liquid-Fuelled Propulsion Systems
AGARD CP 450, April 1989

Aircraft Fire Safety
AGARD CP 467, October 1989

Unsteady Aerodynamic Phenomena in Turbomachines
AGARD CP 468, February 1990

Secondary Flows in Turbomachines
AGARD CP 469, February 1990

Hypersonic Combined Cycle Propulsion
AGARD CP 479, December 1990

Low Temperature Environment Operations of Turboengines (Design and User's Problems)
AGARD CP 480, May 1991

CFD Techniques for Propulsion Applications
AGARD CP 510, February 1992

Insensitive Munitions
AGARD CP 511, July 1992

Combat Aircraft Noise
AGARD CP 512, April 1992

Airbreathing Propulsion for Missiles and Projectiles
AGARD CP 526, September 1992

Heat Transfer and Cooling in Gas Turbines
AGARD CP 527, February 1993

Fuels and Combustion Technology for Advanced Aircraft Engines
AGARD CP 536, September 1993

Technology Requirements for Small Gas Turbines
AGARD CP 537, March 1994

Erosion, Corrosion and Foreign Object Damage Effects in Gas Turines
AGARD CP 558, February 1995

Environmental Aspects of Rocket and Gun Propulsion
AGARD CP 559, February 1995

ADVISORY REPORTS (AR)

Producibility and Cost Studies of Aviation Kerosines *(Results of Working Group 16)*
AGARD AR 227, June 1985

Performance of Rocket Motors with Metallized Propellants *(Results of Working Group 17)*
AGARD AR 230, September 1986

Recommended Practices for Measurement of Gas Path Pressures and Temperatures for Performance Assessment of Aircraft Turbine Engines and Components *(Results of Working Group 19)*
AGARD AR 245, June 1990

The Uniform Engine Test Programme *(Results of Working Group 15)*
AGARD AR 248, February 1990

Test Cases for Computation of Internal Flows in Aero Engine Components *(Results of Working Group 18)*
AGARD AR 275, July 1990

Test Cases for Engine Life Assessment Technology *(Results of Working Group 20)*
AGARD AR 308, September 1992

Terminology and Assessment Methods of Solid Propellant Rocket Exhaust Signatures *(Results of Working Group 21)*
AGARD AR 287, February 1993

Guide to the Measurement of the Transient Performance of Aircraft Turbine Engines and Components *(Results of Working Group 23)*
AGARD AR 320, March 1994

Experimental and Analytical Methods for the Determination of Connected — Pipe Ramjet and Ducted Rocket Internal Performance *(Results of Working Group 22)*
AGARD AR 323, July 1994

LECTURE SERIES (LS)

Engine Airframe Integration for Rotocraft
AGARD LS 148, June 1986

Design Methods Used in Solid Rocket Motors
AGARD LS 150, April 1987
AGARD LS 150 (Revised), April 1988

Blading Design for Axial Turbomachines
AGARD LS 167, June 1989

Comparative Engine Performance Measurements
AGARD LS 169, May 1990

Combustion of Solid Propellants
AGARD LS 180, July 1991

Steady and Transient Performance Prediction of Gas Turbine Engines
AGARD LS 183, May 1992

Rocket Motor Plume Technology
AGARD LS 188, June 1993

Research and Development of Ram/Scramjets and Turboramjets in Russia
AGARD LS 194, December 1993

Turbomachinery Design Using CFD
AGARD LS 195, May 1994

Mathematical Models of Gas Turbine Engines and their Components
AGARD LS 198, December 1994

AGARDOGRAPHS (AG)

Measurement Uncertainty within the Uniform Engine Test Programme
AGARD AG 307, May 1989

Hazard Studies for Solid Propellant Rocket Motors
AGARD AG 316, September 1990

Advanced Methods for Cascade Testing
AGARD AG 328, August 1993

REPORTS (R)

Application of Modified Loss and Deviation Correlations to Transonic Axial Compressors
AGARD R 745, November 1987

Rotocraft Drivetrain Life Safety and Reliability
AGARD R 775, June 1990

Preface

Over the past three years the AGARD(PEP) Working Group 24 has met twice a year to produce this "Recommended Practices for the Assessment of the Effects of Atmospheric Water Ingestion on the Performance and Operability of Gas Turbine Engines". Each member of the group, whether from the PEP panel or by invitation, has brought their wide range of experience and knowledge for the advancement of understanding in the area of gas turbine operation. The resulting report is intended for use by all concerned with the gas turbine — from student through to Certification Authority. Although the report is made up from the individuals' contributions, which in these current difficulties has called for excessive workload for many, the work of our Technical Editor Earl Dudgeon (Canada) has been invaluable to all the contributors. On behalf of WG24 I trust that the effort and knowledge contained herein will help you continue to advance the safety, reliability and capability of the gas turbine engine.

K.R. Garwood
Chairman of Working Group 24
August, 1994.

Préface

Au cours des trois dernières années, le groupe de travail No. 24 du panel AGARD de propulsion et d'énergétique s'est réuni deux fois par an pour préparer la rédaction du présent document «Recommandations concernant les méthodes à utiliser pour le traitement de l'humidité dans les turbines à gaz». Chaque membre du groupe, qu'il s'agisse d'un membre du Panel PEP ou d'un invité, a apporté au projet l'ensemble de son expérience et de ses connaissances afin de permettre l'avancement des idées dans le domaine de l'exploitation des turbines à gaz. Le rapport qui en résulte est destiné à tous ceux qui s'intéressent aux turbines à gaz — des étudiants aux membres des services officiels. Bien que le rapport soit composé par les contributions de chacun des membres du groupe, et que l'établissement des ces rapports, par ces temps difficiles, ait dû représenter une charge de travail onéreuse pour beaucoup des membres, les efforts fournis par notre éditeur technique, Earl Dudgeon (Canada) ont été d'une valeur inestimable pour chacun des auteurs. Au nom du WG24, j'ose espérer que les connaissances et les efforts consentis par les auteurs de ce volume vous seront profitables et vous permettront de poursuivre les travaux destinés à faire avancer la sécurité, la fiabilité et la capacité des turbomoteurs.

Propulsion and Energetics Panel Working Group 24 Members

Chairman: Mr. Keith R. Garwood
Rolls Royce plc.
Whittle House 62
P.O. Box 3
Filton, Bristol BS12 7QE
United Kingdom

MEMBERS

Belgium:
Prof. René Jacques
Ecole Royale Militaire
30 Avenue de la Renaissance
1040 Bruxelles

Canada:
Mr. J. Bird
Institute for Aerospace Research
National Research Council
Bldg. M-7, Montreal Rd.
Ottawa, ON K1A 0R6

Dr. Earl H. Dudgeon
c/o Propulsion Laboratory, Bldg. M-7
National Research Council
Ottawa, ON K1A 0R6
(Technical Editor)

Mr. Don M. Rudnitski
Institute for Aerospace Research
National Research Council
Ottawa, ON K1A 0R6

France:
M. le Prof. Jacques Chauvin
LEMFI
Batiment 502
Campus Universitaire
91405 Orsay Cedex

M. Jean-Pierre Duponchel
SNECMA
Engineering Division
Villaroche Centre
77550 Moissy-Cramayel

M. Alain Kleitz
Electricité de France
Direction des Etudes et Recherches
Departement Machines
6 Quai Watier BP 49
78400 Chatou CEDEX

Germany:
Prof. Dr.-Ing. Wolfgang Braig
Institut für Luftfahrtantriebe
Universität Stuttgart
Pfaffenwaldring 6
70569 Stuttgart

Prof. Dr.-Ing. Klaus Broichhausen
MTU München GmbH
Dachauer Str. 665
80995 München

Dr. Joachim Kurzke
MTU München GmbH
Dachauer Str. 665
80995 München

Greece:
Prof. Dr. Peter Kotsiopoulos
Hellenic Air Force Academy
Chair of Propulsion Systems
Dekelia, Attiki

Italy:
Ing. Claudio Vinci
FiatAvio S.p.A.
Corso Ferrucci, 12
10138 Torino

Norway:
Mr. Ivar Skoe
IA-T
Kristian Sonjusvei 20
N-3600 Kongsberg

Turkey:
Capt. Erdogan Günes
1 NCI Hava Ikmal Baim Merkezi
26030 Eskisehir

United Kingdom:
Mr. Christopher Begley
Rolls-Royce plc.
Whittle House 37
P.O. Box 3
Filton, Bristol BS12 7QE

Prof. Robin Elder
School of Mech. Engineering
Cranfield University
Cranfield, Bedford MK43 OAL

United States:
Mr. Ralph Campbell
(General Electric Co.
Cincinnati, OH)*
10410 Storybook Drive
Cincinnati, OH 45242

Mr. Glen Lazalier
Sverdrup Technology Inc. AEDC Div.
MS-5051
877 Avenue E
Arnold AFB, TN 37389-5051

Mr. John Rampy
AEDC
Arnold AFB, TN 37389

Mr. John Roberts
Pratt & Whitney
Performance Group MS 163-17
400 Main St.
East Hartford, CT 06108

Mr. Robert E. Smith, Jr.
(Sverdrup Technology Inc., AEDC Div.)*
1207 Sycamore Circle
Manchester, TN 37355

* Retired — current address given.

PANEL EXECUTIVE

Dr. Peter Tonn

Mail from Europe
AGARD-OTAN
7, rue Ancelle
92200 Neuilly-sur-Seine
France

Tel: (1) 47 38 57 85
Telex: 610176F
Telefax: (1) 47 38 57 99

Mail from US and Canada
AGARD-NATO
Attn: PEP Executive
Unit 21551
APO New York 09777

NOMENCLATURE

Parameters	Definitions	Text Reference[1]
a	Thickness of hail debris	Eq. 5-13
A	Area	Eq. 3-19
b	Normal displacement of hailstone at time t after impact	Eq. 5-17
B	Probe separation	Fig. 7-4
c_p	Specific heat at constant pressure	Eq. 3-1
C	Correction factor	Sect. 3.4.3
C_D	Drag coefficient	p. 4-7
COR	Coefficient of restitution	Eq. 5-19
dp	Dew point	p. 7-3
D	Diameter	Eq. 2-6
Do	Particle diameter before impact	Eq. 5-10
f	Function	Eq. 2-1
f_D	Frequency distribution	Eq. 2-22
far	Fuel-air ratio	Fig. 3-1
F	Thrust	Eq. 3-59
F_D	Drag force	Eq. 5-1
g	Function	Eq. 2-4
ΔG_c	Cluster potential barrier	Eq. 4-13(c)
h	Enthalpy	Eq. 3-15
h_{fg}	Specific enthalpy of evaporation	Eq. 4-7
H	Height	Fig. 2-15
Ho	Height for freezing	Fig. 2-15
I	Intensity	Eq. 7-8
J	Rate of nucleation	Eq. 4-13(a)
k	Unit conversion factor	Eq. 3-38
k	Proportionality factor	Eq. 7-8
k(HWC)	Probability correction factor	Eq. 2-11
K	Boltzmann constant	Eq. 4-13(b)
K_c	Parameter to describe the formation of a water droplet	Eq. 4-13(a)
Kn	Knudsen number	Eq. 4-15
lcc	Linear correlation coefficient	Eq. 4-10
L	Distance across hailshaft	Eq. 2-17
m	Mass	Eq. 3-8
M	Molecular weight	Eq. 3-2
Ma	Mach number	Eq. 3-19
Mw	Water content	Eq. 2-3
n	Number of hail storms	Eq. 2-11
N	Rotation speed	Eq. 3-38
N	Rosin-Rammler width parameter	Eq. 5-9
N	Number of particles	Fig. 4-46
N_c	Number of clusters of critical radius	Eq. 4-13(b)
N(D)	Number of drops of diameter D	Eq. 2-6
N_o	Intercept	Eq. 2-6
P	Pressure	Eq. 3-4
P_s	Static pressure	Eq. 3-4
P_T	Total pressure	Eq. 3-19
P_v	Vapour pressure	Eq. 4-5
PW	Power	Eq. 3-27
P	Probability	Eq. 2-1
Pc	Conditional Probability	Eq. 2-9
Pj	Probability (Hail)	Fig. 2-10
Pp	Prior Probability	Eq. 2-9
Pt	Duration Probability	Eq. 2-23

[1] Equation, Page, Table or Figure of first use

Q_L	Heating value of fuel	Eq. 3-61
r	Radius	Eq. 4-12
r_r	Recovery factor	Eq. 7-10
ri	Refractive index	Fig. 7-10
R	Gas constant	Eq. 3-1
Re	Reynolds number	Eq. 5-3
RH	Relative humidity	Table 3-2
Rr	Rain rate	p. 2-6
$\Re$	Universal gas constant	Eq. 3-2
S	Supersaturation ratio	Eq. 4-5(b)
t	Time	Eq. 2-11
tw	Thickness of liquid water coating on hailstone	p. 2-9
T	Temperature	Eq. 3-4
Tf	Frost point temperature	Eq. 7-5
Td	Dew point temperature	Eq. 7-5
ΔTe	Subcooling temperature due to expansion in nozzle	Eq. 4-6
ΔTr	Reheating due to latent heat released by condensation	Eq. 4-6
U	Tangential velocity	Eq. 3-25
V	Velocity	Eq. 3-23
V	Volume	Eq. 3-16
Vc	Hail particle shattering velocity	Eq. 5-18
war	Absolute humidity (water to dry air mass ratio)	Eq. 3-8
W	Mass flow rate	Eq. 3-19
We	Weber number	Eq. 5-6
Wr	Mass flow ratio	Eq. 4-7
x	Mass fraction	Eq. 3-9
x_v	Specific humidity	Eq. 3-9
$\overline{X}$	Rosin-Rammler mean diameter	Eq. 5-8
Y	Linear distance from hail particle to surface parallel to V_N	Eq. 5-13
z_1, z_2	Constants	p. 7-9
Z	Radar reflectivity factor	Eq. 2-10
α	Exponent of raindrop diameter	Eq. 2-7
α	Particle size parameter	p. 7-7
β	Hail particle impact angle	p. 5-6
γ	Isentropic exponent (ratio of specific heats)	Eq. 3-1
γ_R	Restitution ratio	Eq. 5-15
δ	Standardized pressure ratio	Eq. 3-62
δ	Droplet fractional deposition	Fig. 5-5
δ_{Film}	Film thickness	Eq. 5-21
Γ	Ratio of isentropic exponents	Eq. 3-63
ζ	Loss coefficient	Eq. 3-29
η	Efficiency	Eq. 3-30
θ	Flight path angle	Eq. 2-17
θ	Spread angle of shattered hail particles	Eq. 5-15
Θ	Standardized temperature ratio	Eq. 3-62
λ	Flight path length	Eq. 2-18
λ	Wavelength of light	p. 7-7
Λ	Slope parameter	Eq. 2-6
μ	Absolute viscosity	Eq. 4-15
V	Droplet mass fraction	Eq. 5-9
ξ	Hailshaft diameter	Eq. 2-18
ρ	Density	Eq. 2-8
σ	Liquid surface tension	Eq. 4-12
Φ	Entropy function	Eq. 3-6
φ	Degree of saturation	Eq. 3-17
ψ	Angle of hail fragments	Eq. 5-14
	Stream function	p. 4-16

Engine Stations are indicated as numerals attached to the referenced pressure or temperature, e.g. P2, T54. See AGARD Advisory Report 320, March 1994.

Subscripts

a	air
ar	aircraft
amb	ambient
ax	axial
A	airflow
b	combustor
c	component, cluster
C	carbon
comp	compressor
crit	critical
d	dry
db	dry bulb
ef	effective
equiv	equivalent
exp	expansion
f	condensate
F	fuel
Film	film
h	hailshaft
h	hailstone
H	Hydrogen
i	inlet
is	ideal specific
j	vane stage number
k	blade stage number
local	local
Loss	loss
max	maximum
med	median
min	minimum
mix	mixture
N	normal component
N	rotation
o	outlet
O_2	Oxygen
p	particle
P	parallel component
r	recovery
stoich	stoichiometric
sat	saturated
S	static
t	turbine
T	temperature
T	total
v	vapour
w	water
wb	wet bulb
wm	mass mean
x	thrust
1,2	first, second

Descriptive Symbols

AOA	Angle of attack
ATF	Altitude test facility
BPR	Bypass ratio
CCD	Charge coupled device
CFD	Computational fluid dynamics
CNC	Condensation nucleus counter
DGV	Doppler global velocimetry
DMA	Differential mobility analyser
DMPSA	Differential mobility particle size analyser
EGT	Exhaust gas temperature
EPR	Engine pressure ratio
FAR	Federal aviation regulation
HPC	High pressure compressor
HWC	Hail water concentration
IPS	Inertial particle separator
ISA	International standard atmosphere
JAR	Joint airworthiness requirement
K FACTOR	Condensation correction factor
KIAS	Knots indicated air speed
LDA	Laser doppler anemometry
LWC	Liquid water concentration
MCS	Mesoscale convective system
MIL-STD	Military-standard
MSL	Mean sea level
NG	Gas generator speed
NH	High pressure compressor speed
NL	Low pressure compressor speed
NPRM	Notice of proposed rulemaking
NPT	Power turbine speed
PIV	Particle image velocimetry
PRT	Platinum resistance thermometer
RSS	Root sum square
SFC	Specific fuel consumption
SHP	Shaft horsepower
TAT	Total air temperature
T/E	Trailing edge
TGT	Turbine gas temperature
TRISE	Temperature rise due to condensation
TWC	Total water content
VWC	Vapour water concentration

ACRONYMS

AEDC	Arnold Engineering Development Center (USA)
AGARD	Advisory Group for Aerospace Research & Development (NATO)
AIA	Aerospace Industries Association (USA)
AIAA	American Institute of Aeronautics and Astronautics
ANSI	American National Standards Institute
ARC	Alberta Research Council (Canada)
ASME	American Society of Mechanical Engineers
ASTM	American Society of Testing Materials
BCAR	British Civil Aviation Regulations
CAA	Civil Aviation Authority (UK)
CEPr	Centre d'Essais des Propulseurs (France)
CFMI	A joint company GE/SNECMA
FAA	Federal Aviation Authority (USA)
GNEFA	Groupement National d'Etudes des Fléaux Atmosphériques (France)
IPTS	International Practical Temperature Scale
ISO	International Standards Organization
JAA	Joint Aviation Authority (Europe)
MCAS	Marine Corps Air Station (USA)
NAS	Naval Air Station (USA)
NASA	National Aeronautics and Space Administration (USA)
NATO	North Atlantic Treaty Organization
NIST	National Institute for Standards and Technology (USA)
NRCC	National Research Council (Canada)
PEP	Propulsion and Energetics Panel (AGARD)
RAE	Royal Aerospace Establishment (UK)
SI	Système International (System of units of measurement)
SNECMA	Société Nationale d'Etude et de Construction de Moteurs d'Aviation
USAF	United States Airforce
UTRC	United Technologies Research Centre

GLOSSARY

Absolute Humidity	The ratio of the mass of water vapour to the mass of dry air with which the water vapour is associated in a given volume (often referred to as the mixing ratio).
Air-mass Thunderstorm	A convective-scale, isolated thunderstorm cell.
Atmospheric Water	Water in any of its physical states: solid, liquid or vapour.
Certification	Process by which compliance with applicable regulations or specifications is achieved.
Degree of Saturation	The ratio of the mass of water vapour in a volume of air to the maximum amount of water which the air can hold as vapour at the same temperature.
Dew Point Temperature	The temperature to which humid air has to be brought (at constant pressure and mixing ratio) in order that its water vapour pressure is equal to the saturated water vapour pressure (liquid) at this temperature.
Drizzle	Rain with droplet sizes below 0.5 millimetres.
Frontal Systems	Synoptic-scale weather systems that are tracked daily on weather maps. They are responsible for much of the day-to-day weather in the mid-latitudes.
Frost Point Temperature	The temperature to which humid air has to be brought (at constant pressure and mixing ratio) in order that its water vapour pressure is equal to the saturated water vapour pressure (ice) at this temperature.
Graupel	Graupel is a form of hail, consisting of small (under 0.5 centimetres in diameter) pellets of a soft mixture of ice and liquid water.
Hail	Frozen water, in the form of hail stones, is formed in convective updrafts. Hail stones vary in size from 0.5 centimetres up to 3 centimetres.
Hail Water Content	The quantity of water in the form of hail in air, expressed in grams per cubic metre of air.
Hoarfrost	The sublimation of water vapour on a solid surface when the temperature of the ambient still air drops below the frost point.
Liquid Suspension	Atmospheric liquid suspensions in the form of clouds or fog are the product of natural condensation with water droplets ranging from hundredths of a micron up to 20 to 25 microns in diameter.
Liquid Water Concentration	The quantity of liquid water in air, expressed in grams of water per cubic metre of air.
Mesoscale Convective System	An organized system of convective thunderstorm cells.
Precipitation	The general atmospheric form of liquid water precipitation is rain.
Rainfall Rate	The linear accumulation depth of rainfall at ground level per unit time.
Relative Humidity	The ratio of the actual partial pressure of water vapour to the saturated partial pressure of the vapour at the same temperature. For the temperatures and pressures typical of gas turbine conditions, the relative humidity approximates closely the degree of saturation. Relative humidity is usually expressed as a percent.
Saturated Water Vapour Pressure	The pressure of water vapour (at a given temperature, liquid or ice) in equilibrium with a plane surface of liquid water or pure ice.
Scoop Factor	A ratio quantifying the relative increase in rain/hail concentration (weight of water/weight of air in a given volume) between the atmosphere and the airstream at the engine inlet plane. The change in concentration between the ambient atmosphere and the inlet is a result of the inlet airstream expanding to fill the inlet while the rain and hail do not. The ratio is equal to *Ainlet/Ao* where *Ainlet* is the frontal area of the inlet at the reference plane and *Ao* is the area of the inlet flow stream tube far upstream of the engine.
Specific Humidity	The ratio of the mass of water vapour in a volume of air to the total mass of the humid air.

International Standard Atmosphere

Dry Air:

Pressure P		101.325 kPa (14.696 lb/in^2)
Temperature T		288.15 K (518.7° R)
Molecular weight M		28.966 gm/mole
Density ρ		1.2255 kg/m^3 (.07651 lb/ft^3)
Gas constant R		287.05 J/kg-K (53.34 ft lb/lb-°R)
Acoustic velocity a		340.4 m/sec (1117 ft/sec)
Absolute viscosity μ		1.790 x 10^{-5} kg/m-sec (1.203 x 10^{-5} lb/ft-sec)
Specific heat c_p		1005 J/kg-K (.240 BTU/lb-°R)
Ratio of specific heats γ		1.400
Composition	N_2	0.78084 moles/mole
	O_2	0.20948
	Ar	0.00937
	CO_2	0.00032

1. INTRODUCTION

1.1 PURPOSE

The understanding of fundamental gas and thermodynamics in the gas turbine engine has advanced significantly in the last decade as the availability of high speed digital computational methods have become widespread. Engine design and off design performance simulations with optimising algorithms are available to industry and students with little of the prior correlative arts now incorporated into exact solutions. Similarly the test stand operators now have near real-time analysis of the engine operation as the testing proceeds, with comparison to required or desired performance and mechanical targets and limits easily made. With such exactness of assessment it is vital that all known and measurable disturbances from the ideal dry air performance are correctly incorporated into the prediction and analysis of the components and the engine.

This AGARD report is intended to establish a modern 'Recommended Practices' for the treatment of water ingestion in the gas turbine system. All forms of water ingestion are covered, from the analytically handleable gaseous, through the difficult but semi analytical condensing, to the empirical with modelling support of the liquid droplets. Excluded from the analysis is the effect of mechanical damage such as blade deformation and tip rubbing. However the important operability factor of ice blocking of handling bleed slots is addressed. This is the first collation of such a wide knowledge base within one document, and represents the state of the art in the mathematical modelling and of the instrumentation necessary for assessing the state of the water content in the air. It is hoped that the general awareness of the ever present but often overlooked effects of humidity effects in gas turbines will be enhanced in all the areas that have responsibilities for the performance, handling, testing and contracting of gas turbine engines.

Advantage has been taken of the work initiated by the A.I.A. on determining the weather threats. This work, and the methodology of encounter probability are outlined here. Such weather threats and encounter probabilities are functions of the operational requirement, aircraft speed and throttle setting. As such each airframe and engine configuration need to be assessed against the operational requirements. Sufficient information and sources of information are given to enable the reader to initiate such an assessment.

Also given within this document are some of the current test requirements concerning certification. The reader is cautioned that these are included for indication only and should not be used as authoritative, but should contact the relevant regulatory body for further information.

1.2 BACKGROUND

This publication is the result of a wide range of experienced gas turbine designers, testers, component and instrumentation specialists meeting twice a year over a three year period as AGARD (PEP) Working Group 24. Their background and skills have been focused in the common aim of producing a document that will be a significant contribution to the gas turbine fraternity. In the fullness of time it is anticipated that this publication will benefit from a re-examination of content, when further information is available. At this time the contents are to the most current state of the art. Wherever possible indications are made of the areas of uncertainty and lack of knowledge.

The Working Group was established following early work at NRC of Canada where inconsistencies between engine gaseous humidity test stand corrections were discovered. It was apparent that different manufacturers used different corrections, some being more theoretically based than others. Discussions within the Ad-hoc committee which preceded the Working Group confirmed the inconsistency of approach, not only engine manufacturer to manufacturer (mostly on older generation engines) but also in component rig to whole engine accounting. Whilst in general these effects are small compared to say tip clearance and heat transfer effects, they are nonetheless measurable and accountable with both seasonal and daily variations. This becomes more important as the engine comes towards the overhaul period when marginal testing ignoring these effects can lead to unnecessary premature overhaul or rejection from post overhaul test.

A survey of the NATO nations indicated that the treatment of gaseous humidity in the more recent engines was more correctly handled, but that concerns persisted in the treatment of condensing flows and even greater concern in the low understanding in the small

droplet, rain, hail, and snow effects. Much of this concern followed from civil engine operation where incidents of total loss of power, particularly from low power settings in inclement weather had led to loss of aircraft and associated fatalities. Such throttle settings would not be dissimilar to those of high performance military aircraft in 1g flight with weapons gone. It was with this widened scope that approval from the Military Committee was gained for the formation of Working Group 24.

During the course of preparation of this report the participants of WG24 have had particular responsibilities for the areas of the report relating closely to their particular skills. The major outline was quickly established and the last three meetings of the WG24 took the form of critical reviews of each section by the whole of WG24. By this approach the final report has benefited from the experience and critique of all of the authors.

1.3 AUDIENCE , AND HOW TO USE

In writing this report consideration has been given to the anticipated wide experience and expertise range of the readers. Each chapter (with the exclusion of Chapter 6) can be read either as authoritative or as a source of background information, theory and logic, from which to explore more deeply into the references. Chapter 2 gives the most up to date assessment of the hazardous weather threat using data collected from national organisations. The main body of the report is contained in Chapters 3,4 and 5. For both new and old student there is sufficient theory, particularly in Chapter 3 to allow them to follow on from the ideal world of dry air to the real world of ever present gaseous humidity. With the foundation from Chapter 3, the increasing difficulties and uncertainties of phase change in condensing flows in Chapter 4 followed by the multiple phase changes and particle trajectory and break-up of Chapter 5 can be followed.

The engine designer and developer should be able to use this publication as a reference to their everyday work. Chapters 7 and 8 deal with the more practical aspects of the topic, giving consideration to the ability to measure in the presence of humidity and the droplets and particulate in the humidity, then to discuss the implications and considerations to be given whilst testing components and engines.

The certificator, whether from the contractual and requirements point of view, or from the validators point of view should be able to use Chapters 2, 3, 4, 5, 6, and 8 . Work of assessing the real threat probability of particular aircraft/engine combinations under required flight profiles should lead to better definitions for the certification bodies. Such work would also lead to an improved understanding of real operational limitations.

If all of the above were available for the engines in current service, then the task of the flight line manager and the pass-off tester would be one of greater simplicity. It must be acknowledged that currently the majority of in-service engines have not been as rigorously treated as can be achieved today. With suitable application of the principles in Chapters 3 and 4 then some of the apparent random scatter can be reduced and better assessments made on the state of the propulsion unit.

Chapter 9 should be carefully read by anyone that uses this report. Although each individual chapter attempts to highlight the state of knowledge and its influence on the engine, these are collated in this final chapter and a balanced view can then be formed. Areas of lack of information and knowledge are identified which gives rise to indications of where further research or application should be made. Above all it is hoped that any reader of this report will have had their awareness raised and that throughout their dealings with the gas turbine will note the efforts made to make flying a safe situation whatever the weather!

2. ASSESSMENT OF ENVIRONMENTAL WATER[1]

Water appears in nature in many forms (phases, shapes, sizes and concentrations) which affect the operation of gas turbine engines in testing environments and installed in aircraft. The specific effects will depend on the elemental forms of water. In order to determine the possible effects on engine performance and operability it is necessary to have a clear understanding of these various forms of water.

2.1 DEFINITION AND SOURCES OF ENVIRONMENTAL WATER

2.1.1 Ambient Water

Ambient water may be present in any of its physical states: vapour, liquid, or solid.

2.1.2 Water Vapour

Water vapour is virtually always present to some extent in the atmosphere. The environmental vapour water content (VWC) is the concentration of water vapour in air expressed in grams of water per cubic metre of air, (g m^{-3}). The meteorological term for water in the vapour phase is humidity, for which the two most useful definitions are absolute and relative humidity.

Absolute Humidity, often referred to as mixing ratio or water-air ratio (**war**), is the ratio of the mass of water vapour to the mass of dry air with which the water vapour is associated in a given volume. A related term, **Specific Humidity**[2], is used here to express the ratio of the mass of water vapour to the total mass of humid air (see Table 3-2, Chapter 3).

Dew or **Frost Point Temperature** (Td or Tf) is the temperature to which the humid air must be brought (at constant pressure and mixing ratio) in order that its water vapour pressure is equal to the saturated water vapour pressure ($P_{S\ sat}$) at this temperature. The **Saturated Water Vapour Pressure** is the pressure of the water vapour (at a given ambient temperature and pressure) in equilibrium with a plane surface of liquid water or pure ice.

Relative Humidity is the ratio of the actual partial pressure of the water vapour to the saturated water vapour pressure at the same temperature. For typical gas turbine conditions, it is closely equivalent to the degree of saturation (see Table 3-2), and is usually expressed as a percent.

Under certain situations, usually when condensing nuclei are not present, water can remain in the vapour phase far beyond the saturation limit. This condition is defined as **supersaturation**, and is expressed as a ratio relative to the saturation limit.

Hoarfrost is the sublimation of water vapour on solid surfaces when the temperature of the ambient still air drops below the frost point. Water concentrations can be quite high, and hoarfrost formations can be a considerable problem in blocking air passages through debris screens and air filters in stationary gas turbine installations (Chappell and Grabe, 1974 (Reference 2.1)).

2.1.3 Liquid Water

Liquid water concentration (LWC) is the quantity of liquid water in air, expressed in grams of water per cubic metre of air. As the water and air mixture comes under the influence of the propulsion system it becomes useful to specify the liquid water concentration in terms of the mass of liquid water per unit mass of dry air. This definition specifies the water-air mass ratio which is more conveniently handled in the thermodynamic cycle modeling of the propulsion system.

The liquid water entering the engine may be a result of precipitation, inlet condensation, droplet suspension or liquid spray.

Precipitation - Rain is the most commonly encountered form of liquid water. It is present in a wide variety of weather systems, reaching its highest level of concentration during heavy convective precipitation associated with supercell thunderstorms.

---

[1] Tables and Figures for Chapter 2 begin on page 2-18.

[2] Many references use "Specific Humidity" to mean absolute humidity. Care should be taken in interpreting different technical articles. The distinction between absolute and specific humidities, as defined above, is maintained throughout this report.

Rain droplet sizes commonly range from one to two millimeters, with extremes of five to eight millimeters observed in tropical rain storms. Drizzle is a special form of rain with droplet sizes below 0.5 millimeters.

Inlet Condensation - Condensation can occur under conditions of high inlet velocity and humidity. The reduced static temperature causes the water vapour to condense out into fine droplets in a process not unlike that which creates clouds and fog. During the condensation process the latent heat of vaporization is released thereby raising the temperature of the water and air mixture entering the engine, Section 4.2.2.

Liquid Suspension - Suspensions in the form of clouds and fog are the product of natural condensation which creates very fine water droplets ranging from hundredths of a micron up to 20 to 25 microns in diameter. The cloud water concentration varies between 0.1 and 2 grams per cubic meters. Sometimes the water droplets are supercooled and form ice on contact with a solid surface. This can create severe icing problems for passing aircraft and their engines.

Water Spray - Water is sometimes sprayed into the engine inlet by the aircraft under-carriage and from puddles on the runway, or from the pontoons of a seaplane. This water is concentrated and highly localized when it enters the engine.

2.1.4 Solid Water

Frozen water, in the form of hail, graupel, ice crystals, and snow, is sometimes ingested by the engine. Since hail is by far the most serious threat, the concentration of frozen water will be referred to as the hail water concentration (HWC), which is the quantity of solid water in air, expressed in grams of water per cubic meter of air.

Hail/Graupel - Hail stones are formed in convective updrafts and vary in size from 0.5 centimeters up to 3 centimeters. The record hail stone, found in Coffeyville, Kansas, in 1970, was 44 centimeters in circumference and weighed 776 grams. Hail is a well-known hazard to airframes and engines, and specific hail ingestion tests have to be passed by aviation gas turbines before certification. Graupel is a form of hail, consisting of small (under 0.5 centimeters in diameter) pellets of a soft mixture of ice and liquid water.

Snow/Ice Crystals - Snowflakes, delicate combinations of tiny ice crystals, do not represent a danger to gas turbine engines, however they may affect the engine cycle performance. The flake configurations are numerous; the concentrations in a snow cloud have been determined to be between 0.1 and 1.2 grams per cubic meter. In reverse-flow engines, icing and air passage blockage problems may arise. Snow ingestion during thrust reverser operation may result in operability problems during aircraft landing. Ice crystals, which are found in the upper regions of decaying cumulo-nimbus clouds, may also cause icing problems.

Blowing snow is a special problem, created by strong winds which pick up surface snow and blow it into openings, for example, the air intakes of stationary gas turbines (Reference 2.1). Concentrations are highest close to the surface, where they may reach 390 grams per cubic metre. Modern stationary gas turbines, installed in regions with appreciable snowfalls, have their air intakes placed high above the ground, out of the danger zone of blowing snow.

2.2 WEATHER SYSTEMS PRODUCING HIGH WATER CONCENTRATIONS

Weather systems occur in nature over a wide variety of spatial and temporal scales. As a general rule the larger the horizontal extent of the system, the longer lifetime it is likely to have. Table 2.1 identifies the scales of interest for this discussion.

Air-mass Thunderstorms - These are convective-scale, isolated thunderstorm "Cells" that often develop in the late afternoon, especially over land in the spring and summer months. They also often accompany a frontal system. These cells generally do not pose as significant a threat as those found in larger mesoscale convective systems, however they are capable of producing heavy rain and/or hail.

Mesoscale Convective Systems (MCS) - An MCS is an organized system of convective thunderstorm cells. A familiar example of an MCS is a squall line: a line of convective cells. While the individual cells may have lifetimes as short as 15 to 20 minutes, the squall-line system may persist for several hours as new cells continually form out ahead of the leading edge of the storm. Other MCSs may appear less organized than a squall-line system. In

general the entire MCS should be avoided since new cells can develop as quickly as 10 minutes. Because of the more organized nature of MCSs, the individual cells are stronger, and can be more of a threat, than airmass thunderstorm cells. Heavy rain and/or hail, high wind shear and turbulence, strong vertical motions, and lightning can be produced by MCSs.

Supercell Thunderstorms - When certain atmospheric conditions are present, supercell thunderstorms can develop, as shown in Figure 2-1. A supercell storm is really an MCS that, rather than having a multi-cellular structure, effectively acts as a single strong cell with a continuous updraft and downdraft. In multicellular MCSs, the individual cells are self-destructive in that the downdraft that eventually develops tends to cut off the inflow into the updraft, thereby killing off the supply of moisture and energy to the cell. Supercell storms on the other hand are characterized by an updraft-downdraft couplet that is non-interfering. As a consequence, the supercell thunderstorm can be very long-lived, with lifetimes often exceeding six hours. Supercells are the most severe storms that can be encountered. The largest hailstones and most tornadoes are spawned by supercell storms. Extreme hail and/or rain, strong wind shear and turbulence including tornadoes, strong vertical air motions (updraft can exceed 75 knots), and lightning are hazards that can be encountered in and around supercell storms. They frequently occur as isolated single-cell systems, but they can occur with ordinary cells in multi-cellular MCSs or even in a squall line.

Hurricanes and Tropical Storms - It is unlikely that engine or airplane operation would be concerned with a hurricane or tropical storm since these storm systems are very long-lived and are well monitored by various meteorological agencies. Therefore, these types of storms will not be discussed here. Numerous publications on tropical storms exist and can easily be found in the meteorological literature.

Extratropical Cyclones (Frontal Systems) - These are the synoptic-scale weather systems that are tracked daily on weather maps. They are responsible for much of the day-to-day weather in the mid-latitudes. Most of the precipitation from extratropical cyclones occurs in the vicinity of "fronts", so named because they mark the boundary of two different air masses. There is a discontinuity of sorts in relative humidity, temperature, wind, and atmospheric pressure across a front. There are three basic types of fronts that occur in extratropical cyclones; cold, warm and occluded[3] . The vertical air motions, liquid water contents, and precipitation rates associated with frontal systems are commonly much smaller than those associated with convective and mesoscale weather systems. There are, however, important exceptions to this rule. Squall lines can occur several miles ahead of or behind cold fronts. Significant convection also commonly occurs in conjunction with the cold front, and less commonly with the warm or occluded front. If a strong cold front moves through a region of warm moist air, as indicated by surface observations, then convection is likely to occur ahead of or along the cold frontal boundary. When extratropical cyclones are over the ocean, convection commonly occurs behind the cold front. Figures 2-2(a) to (e) illustrate an extratropical cyclone in various stages of its development and indicate the locations of different fronts. In its initial stage (Figure 2-2(a)), a cloud band will probably be present in conjunction with the front, but precipitation, if any, will most likely be light. As the system develops (Figures 2-2(b) to 2-2(d)), the precipitation intensity increases and a kink, marking the junction of the warm and cold air masses, forms along what had been the stationary front. Convective precipitation starts developing. Figure 2-2(e) shows wind direction, cloud formations, and typical cross sectional profiles for a mature extratropical cyclone. The regions where convective precipitation is likely to occur are also indicated in this figure. If convection does develop, it presents the same hazards to aircraft as those associated with convection in MCSs. This is especially true of the convection that can occur ahead of and along the cold front.

Seasonal Variation in the Occurrence of Weather Systems - All of the weather systems listed above, except extratropical cyclones, are convective or are systems of convective cells. Convective precipitation is more common in the spring and summer months. Convection results when the vertical temperature profile of the atmosphere is unstable. In simple terms, this occurs when temperatures near the surface of the earth are warm and temperatures aloft are cold. During the spring and summer, solar heating at the ground is strong and contributes towards creating an unstable atmosphere. In addition, there is a certain lag time in the heating of the atmosphere. As the spring season progresses, atmospheric instability increases since the earth's surface warms quickly while the atmosphere is slower to warm. Consequently, in most areas of the

---

[3] Actually, there is a fourth front, the stationary front, but it is simply a warm or cold front that isn't moving.

world, spring is the season in which convective weather is most likely to occur.

Extratropical cyclones develop in regions of enhanced synoptic-scale horizontal temperature gradients. The gradients necessary for the development of frontal systems are most likely to develop in the winter season when the gradient of solar heating between the pole and equator is at its largest. Hence, frontal systems occur most commonly in the winter months. Convection in frontal systems, however, is more frequent in the spring for the same reasons discussed above. It should be pointed out, though, that frontal systems can occur virtually any time of the year and, likewise, any of the convective and mesoscale systems can occur in the fall and winter as well as in the spring and summer.

Daily Variations of Weather - The above discussions have dealt mainly with precipitation resulting from the weather systems given in Table 2-1. Accurate forecasting of these events is essential to productive engine testing. Another important consideration in test planning is the expected daily variations of temperature and humidity for the test locality. This information, obtained from the sources given in Section 2.6, enables the test planner to select the time when ambient conditions are best suited to the test objectives. For example, testing at high power settings would be planned during the coolest period, early mornings, to minimize the temperatures of hot parts, thereby preserving engine life, and performance testing would take place when the relative humidity was lowest, mid-afternoon, to minimize the possibility of inlet condensation.

2.3 OTHER SOURCES OF AMBIENT WATER

2.3.1 Humidity

The most severe humidity conditions are defined in Reference 2.2: "Climatic Information to Determine Design and Test Requirements for Military Systems and Equipment". In this document the land areas of the world are divided into regional types of climate based mainly on temperature differences. Humidity values representative of extreme conditions during the most severe month in each of these regions are presented. Since the amount of water vapour that air can hold increases with temperature, areas with the highest absolute humidities are hot locations (usually at the edge of a desert) adjacent to very warm bodies of water, i.e. the narrow coastal deserts of the Red Sea or Gulf of Aden. Table 2-2 lists the percentage extremes of humidity and associated dew points for the most severe conditions. Also shown in this table is the humidity lapse rate with altitude. This table represents the highest level of absolute humidity obtained during the daily cycle. A synthetic daily cycle of humidity, temperature and other elements associated with the 1-percent high absolute humidity value is given in Table 2-3.

Typical humidity conditions for specific locations can usually be obtained from summaries of local climatological data issued by many of the national climatic data organizations listed in Section 2.6. For example, monthly averages of the daily cycle of relative humidity for seven regions in France are shown in Figure 2-3. Likewise a composite of climatological data issued for Cincinnati, Ohio is shown in Figure 2-4. These data also show monthly averages of relative humidity four times each day in six hour intervals.

2.4 ENCOUNTER THREAT FOR RAIN AND HAIL DEFINED BY THE AIA[4]

2.4.1 Introduction

The focus of the Aerospace Industries Association (AIA) PC 338-1 project (1990) "Investigation of Engine Powerloss and Instability in Inclement Weather" was directed at defining the rain and hail weather threat and at establishing also an appropriate means for demonstrating suitable engine performance and operability while ingesting the appropriate amounts of rain or hail. To accomplish this it was necessary to quantify the rain and hail threat in terms of a probability of occurrence. This was accomplished by developing the probability of various rain and hail intensity levels

---

[4] This section is a condensation of Reference 2.3. This document is an internal report of the Boeing Company, not generally available to the public, and most of the material has been transcribed verbatim.

occurring in the atmosphere and then comparing these intensity values against current certification requirements. In the context of this study, "intensity" refers to the concentration of rain or hail given in units of grams of water per cubic meter (g/m^{-3}).

Considerably more data have been published on rain than on hail. A couple of likely explanations for this are: 1) rain occurs much more frequently than hail, and 2) there are more research aircraft equipped to fly into rain storms than into hail storms. Because of the scarcity of published hail data, the Boeing Company initiated a contract with the atmospheric research group of the Alberta Research Council (ARC) in Edmonton, Alberta, Canada. This agency was contracted to supply hail data in terms of radar reflectivity measurements, storm size, etc. The analysis of these data was done by Boeing to provide a definition of the hail threat. Likewise CFM International (CFMI) contracted with the Groupement National d'Etudes des Fléaux Atmosphériques (GNEFA) in Aubiere, France to supply hail data which was analyzed by CFMI. These analyzed data were provided to the AIA Propulsion Committee (PC) Project PC 338-1, for their use in the study. All decisions on the use of these data were made by the project study group.

The results of the weather threat analysis are considered to apply at a single point in space in the "worst case" location. In other words, the rain and hail probability curves describe the likelihood of rain or hail, of a given intensity, occurring at the location in the world most likely to have that given intensity.

2.4.2 Threat Definition

Water concentration was used to describe the level of intensity of rain and hail. When discussing water concentration, the term liquid water content (LWC) will be used in association with rain. Hail water content (HWC) will be used when discussing hail. Unless stated otherwise, LWC and HWC will not include the contribution of water from cloud droplets. The basis for ignoring cloud water is the assumption that, at high concentrations of precipitation, cloud water is swept out by the precipitation particles faster than it is generated in the cloud updraft. As previously mentioned, LWC and HWC are given in units of grams of water per cubic meter ($g\ m^{-3}$).

This study assigns probability levels to given LWC and HWC values. In other words, it describes LWC and HWC as functions of probability:

$$LWC = f_1(P) \qquad 2\text{-}1$$

$$HWC = f_2(P) \qquad 2\text{-}2$$

In Equations 2-1 and 2-2, P is the joint probability of a rain or hail storm occurring at a given point and of the given LWC or HWC being equalled or exceeded at that point. Expressed symbolically:

$$P = P(\text{joint}) = P(\text{storm} \cap \text{Mw}) = P(\text{storm}) \times P(\text{Mw} \mid \text{storm}) \qquad 2\text{-}3$$

where Mw is water content excluding water from cloud droplets (either LWC or HWC), P(storm) is the probability of a storm occurring at a given point and at a given instant, and P(Mw | storm) is the conditional probability of a given water concentration (Mw) value occurring at that point and time given the occurrence of the storm. It was assumed that LWC (or HWC) and P have a one-to-one relationship; therefore the probability of a given LWC value, P(LWC), or of a given HWC value, P(HWC), can also be expressed as functions of LWC and HWC:

$$P(\text{LWC}) = g_1\ (\text{LWC}) \qquad 2\text{-}4$$

$$P(\text{HWC}) = g_2\ (\text{HWC}) \qquad 2\text{-}5$$

where g_1 and g_2 are the inverse functions of f_1 and f_2 respectively.

Because the probability of a given water concentration (Mw) varies significantly as a function of location, the approach used was to consider the known "worst case" locations for rain and hail intensity, that is, those locations in the world where high LWC and HWC values have been reported to occur most frequently. This ensures that any point in the world could be randomly chosen, at any random instant, and the probability of a given LWC or HWC occurring at that instant would be no higher than that given by Equations 2-4 or 2-5, respectively.

2.4.3 Rain Threat

In this section the weather analysis pertaining to rain is divided into three parts. In the first part, data sources are given and discussed. In the second part, the methodology used to develop the LWC probability curve is explained, and in the third, the results and a discussion are presented.

Data Sources - As discussed previously, P(LWC) and P(HWC) were defined as "instantaneous" probabilities (i.e., as the probability of a given LWC or HWC occurring at a given instant). In practice, though, there is a finite time interval over which a datum point is collected. Traditionally, rain data with a temporal resolution of one minute are considered indicative of the

instantaneous rain rate. Most of the rain data used in this analysis were taken over one-minute intervals.

An important source of data came from Tattelman and Larson (1989) (Reference 2.4). They analyzed one-minute rain rate data collected by weighing rain gauges. Their data spans 10 years (1970-79) and includes 41 stations in the continental United States and one station in Puerto Rico (6 1/2 year data base).

Bodtmann and Ruthroff (1976) (Reference 2.5) analyzed five years (1966-70) of weighing rain gauge data at 20 U.S. stations. They found the highest rain rates in their data occurred at Miami, Florida. Jones and Wendland (1984) (Reference 2.6) gave the percent frequency above threshold rain rates for Urbana, Illinois. These data, taken over a ten-year period from 1970-79, were particularly useful because the upper end was higher than any data given by References 2.4 or 2.5.

Roys and Kessler (1966) (Reference 2.7) discussed water contents of thunderstorms in Oklahoma. Data were collected at altitudes above 7600 m (25,000 feet) by an F-100 airplane during the 1962 National Severe Storms Project. Water entering the F-100's jet engine was evaporated as the air was warmed through compression. The compressed air was analyzed by a water vapour analyzer and compared to air collected in a reference cavity. This comparison yielded the amount of water ingested in the engine.

Finally, Briggs (1972) (Reference 2.8) presented data from Freetown, Sierra Leone, Singapore, and London (Heathrow) in a paper in which he derived curves of the intensity of rain, as a function of altitude, predicted to be met once in 10^5 flight hours by a Concorde airplane. Of the three locations, Freetown has the highest probability of instantaneous rainfall occurrence at or exceeding 25, 50, and 100 mm/ hr.

Method of Analysis - Data from the disparate sources were evaluated so that individual data points could be plotted on a common graph with probability on the abscissa and LWC on the ordinate. An "envelope" fit gave LWC as a function of probability.

A straightforward technique was used to convert the data of References 2.4, 2.5 and 2.6 to a common format. All three of these studies used rain rate on one of the axes of their plotted data. The other axis was either annual average occurrences (Reference 2.4), number of minutes per year rain rate is exceeded (Reference 2.5), or percent frequency above threshold rate (Reference 2.6). Likewise, the methods to convert the data of Reference 2.8 to the common format for this study were straightforward. The first step was to convert rain rates to LWC, the second step was to convert the other axis to exceedance probability.

There are a number of studies in which correlations between LWC (frequently designated "Mw") and rain rate (Rr) are reported. Rain rate and LWC are measured independently, but at the same time and location. A plot like that shown in Figure 2-5 is the result. The points, when plotted on log-log paper, can usually be fitted with a straight line, thus defining a power law relationship between Mw and Rr. Table 2-4 shows the Mw-Rr relations used in the rain analysis described here.

From the Tattelman and Larson (1989) data: Miami and Tallahassee, Florida, and Oklahoma City, Oklahoma, were the stations chosen to provide data points for the LWC versus probability graph. Miami and Tallahassee were chosen because high intensity one-minute rain rates were most frequent at these two locations. Oklahoma City is a significant location, because the Roys and Kessler data (Reference 2.7) were also collected in Oklahoma. The rain rates at Miami and Tallahassee were converted to LWC using the Mueller and Sims (1966) (Reference 2.9) equation from Table 2-4. The Oklahoma City data were converted using the Jones (1956) equation (Reference 2.10). The other axis of the plots from Reference 2.4 is the annual average occurrences. For this study the one-minute duration curves were used and the assumption was made that the probability of a given LWC value being exceeded is equal to the annual average number of minutes per year it is exceeded divided by the number of minutes in a year. The larger the sample population, the better is this assumption.

To clarify how a data point is generated, it is useful to go through the process step by step. For example, in Figure 2-6 the one-minute duration curve (uppermost curve) shows that the 2.5 mm/min rain rate occurs ~11 times annually. So the LWC value, using the Mueller and Sims (1966) (Reference 2.9) equation is:

$$LWC = Mw = 0.0528 \times Rr\ (= 150\ mm/hr)^{0.95}$$

$$= 6.2\ g\ m^{-3}$$

The probability level is calculated by taking the number of one-minute occurrences divided by the number of minutes in a year:

$$P(LWC) = \sim 11/(365.25 \times 24 \times 60) = 2.1 \times 10^{-5}$$

Therefore, the data point (P, LWC), is (2.1×10^{-5}, 6.2). This particular point can be seen plotted on Figure 2-7.

Three data points were calculated from the Miami data of Reference 2.5. Miami had the highest rain rates of the 20 stations in their database. The methods used to calculate the data points were the same as those used to re-analyze the data of Reference 2.4.

Two data points were calculated from the Urbana, Illinois, data of Reference 2.6. LWC was calculated from rain rates using the Jones (1956) equation in Table 2-4. Probability was calculated by dividing the axis labelled "percent frequency above threshold rate" by 100.

Two data points were calculated from the Freetown data of Reference 2.8. The 100 mm/hr data point, and an interpolated data point at 75 mm/hr, were inverted to LWC using the Willis (1984) (Reference 2.11) M-R equation from Table 2-4. Exceedance probability was already given, so no conversion was necessary.

As mentioned earlier, the methods to convert the data of References 2.4, 2.5, 2.6 and 2.8 to a common format for this study were straightforward. Converting the Roys and Dessler (1966) data of Reference 2.7, however, was considerably more complicated and the details are given in Reference 2.3.

Results - Figure 2-7 shows the rain curve with the various data points. At probability levels of 10^{-7}, 10^{-8}, and 10^{-9}, the corresponding LWC values are 15.3, 18.9, and 22.4 g m^{-3}. The curve was determined by selecting only the highest LWC values in a cluster of data points and curve fitting the selected points. The values were chosen in this manner in order to define a curve that would apply in the worst case location. For example, data points from a location in the Sahara desert could easily have been plotted on Figure 2-7, but it is clear that it would be unrepresentative for these points to influence the curve fit, since they obviously do not represent a worst case location. Points chosen for the curve fit were: the three Tallahassee points (Reference 2.4), the two Oklahoma points (Reference 2.7), the three Miami points (Reference 2.6), the two Freetown, Sierra Leone points (Reference 2.8), and the Urbana, Illinois points (Reference 2.6) at 14.2 g m^{-3}. The Miami points of Reference 2.4 were not used, because the Tallahassee points at the same probability level were higher. The Oklahoma data points of Reference 2.4 also were not used, nor was the Urbana, Illinois data point of Reference 2.6 at 6.7 g m^{-3} .

The data imply that subtropical locations like Florida have the highest probability of LWC values below 10 g m^{-3}, while mid-latitude continental interior locations like Urbana and/or Oklahoma have the highest probability of LWC values above 10 g m^{-3}. Physical arguments can be constructed to support this implication. Florida is located at latitudes below 31°N where it gets relatively strong surface heating throughout the year. In addition, the state is surrounded by warm ocean water thus ensuring a nearly constant supply of moisture laden air. Strong surface heating and an abundant moisture supply are the ideal recipe for convective precipitation, so it is not surprising that Florida experiences convective rainfall year-round. In the midwestern United States, like Oklahoma, there is strong surface heating in the spring and summer. Often the low-level winds are from the south to southeast at this time of the year, bringing warm moisture-laden air from the Gulf of Mexico. Unlike Florida, however, a mid-level inversion often sets up under these conditions, particularly in the spring and early summer. The inversion inhibits convection until either the low-level temperatures are high enough to allow thermals (rising "bubbles" of warm air) to penetrate the inversion level or until low-level air is forced above the inversion level by a front. When the convection finally is released it can be more vigorous than Florida convection, thereby producing high LWC values. Oklahoma has the potential for very severe convection more often than Florida, but since convection is inhibited by the season and inversions, Florida has moderate convection more often than Oklahoma.

A reasonable check of the rain curve in Figure 2-7 is to compare it with the MIL-STD-210C (Reference 2.2) worst case 0.01%, 0.1% and 0.5% values (Table 2-5). Figure 2-8 shows the rain curve with the three MIL-STD-210C points plotted. These points lie above the curve, but it should be kept in mind that the MIL-STD-210C data, taken from Tattelman and Grantham (1983) (Reference 2.12), are the probabilities during the worst month, whereas the curve in Figure 2-7 is based on annual probabilities. Considering this difference, then, the portion of the probability curve near the MIL-STD-210C points seems reasonable, although it cannot be concluded that the MIL-STD-210C points validate the curve because of the differences in temporal scale.

Besides the data used to establish the rain probability curve in Figure 2-7, a number of extreme LWC data points have been reported. The largest *in situ* rain LWC value is 44 g m^{-3} from an Oklahoma thunderstorm as reported by Roys and Kessler (1966). The world's record 1-minute and 42-minute rainfall of 15 mm (1.23 inches) at Unionville, Maryland on 4 July 1956 and 305 mm (12 inches) at Holt, Missouri on 22 June 1947 (Riordan and Bourget, 1985) (Reference

2.13) translate to LWC values of 60.3 and 15.8 g m^{-3}, respectively (References 2.2 and 2.11). Table 2-6 shows some extreme rain LWC data and associated data sources.

An important aspect of the weather threat analysis is the vertical distribution of rain LWC in the atmosphere. Table 2-7 shows the assumed profile for LWC used in this study. It implies that LWC is constant from the surface to 6 km MSL and drops off to 0 g m^{-3} at 20 km MSL (References 2.2, 2.14). Figure 2-9 shows the vertical distribution of LWC as determined using the values given in Table 2-7. This distribution is described as all liquid below ~4570 m (15,000 ft) MSL, mostly liquid between ~ 4570 - 6100 m (15,000 - 20,000 ft) MSL and nearly all ice above ~7000 m (23,000 ft) MSL (Reference 2-2). However, recall that this distinction is not made here, i.e. the condensate is assumed to be liquid all the way to 6100 m (20,000 ft) MSL.

Another important aspect of the weather threat analysis is the raindrop size distribution. Marshall and Palmer (1948) (Reference 2.15) reported an exponential distribution of the form:

$$N(D) = N_0 e^{-\Lambda D} \qquad (\text{for } 0 < D < D_{max}) \qquad 2\text{-}6$$

where D is the raindrop diameter, N(D) is the number of drops having diameters between D and D +dD, Λ is the slope parameter, N_0 is the intercept, and D_{max} is the maximum drop diameter (usually taken to be ~0.6 - 0.65 mm since drops larger than that tend to break up when falling). A refinement of Equation 2-6 is a gamma distribution:

$$N(D) = N_0 D^{\alpha} e^{-\Lambda D} \qquad (0 < D < D_{max}) \qquad 2\text{-}7$$

which reduces to Equation 2-6 when $\alpha = 0$. Equation 2-8 below gives LWC:

$$LWC = \frac{1}{6}\rho_w \int_0^{D_{max}} N(D) D^3 dD \qquad 2\text{-}8$$

where ρ_w is the density of rain water. Reference 2.14 uses Equation 2-7 to describe the drop size distribution with values for N_0, α, and Λ dependent on rainrate. Figure 2-10a shows the drop size distribution for the 42-minute world record rainrate of 432 mm hr^{-1} (15.8 g m^{-3}) (Reference 2.14). Approximately 72% of the rain drops are between 0.5 and 2.0 mm. The size category with the most raindrops is $1.0 < D < 1.5$ mm, while the mean drop size is 1.4 mm in diameter. Figure 2-10b shows the percent contribution to the total water content from each 0.5 mm size interval. Approximately 75% of the total water content is from drops with diameters between 1.5 and 3.9 mm. The size category contributing the most to the total water content is $2.0 < D < 2.4$ mm, while the median volume diameter, D_0 (i.e., the drop size which separates the distribution such that all drops smaller than D_0 contribute the same liquid water content as all drops larger than D_0) is 2.6 mm.

2.4.4 Hail Threat

For the purpose of this study, hail is defined as frozen precipitation of a particle of size 0.5 cm diameter or greater. This definition excludes smaller sized frozen precipitation, viz. graupel, sleet, snow pellets, etc. This section documents the portion of the weather analysis based on the data supplied to the Boeing company by the Alberta Research Council (ARC). While ARC supplied the data, the actual analysis was carried out by the Boeing Company. In the first part of this section, the ARC data is discussed. In the second part, the methodology used by Boeing to develop a HWC curve, based on the ARC data, is explained. In the third part, the ARC curve is presented and discussed. Data supplied by the Groupement National d'Etudes des Fléaux Atmosphériques (GNEFA) are discussed in the last part of this section.

2.4.4.1 *ARC Data*

The Alberta Research Council (ARC), located in Edmonton, Alberta, Canada has been collecting weather data for many years. They are world leaders in hail research. As part of their extensive convective storm data base, they have S-band (10-cm wavelength, or 3 GHz) dual-polarization weather radar data from 1974-1985. Their S-band radar was operated any time significant weather was within the radar's range.

ARC signed a contract with the Boeing Company in early 1989 to provide Boeing with radar data processed to Boeing's specifications. Data from the month of July, the peak month of Alberta's hail season, from 1983, 1984, and 1985, the years with the best and most complete sets of S-band data, were processed. The polarization capabilities of the radar allowed ARC to differentiate between regions of rain, hail only, or mixed (rain and hail) using algorithms developed at the University of Essex in the United Kingdom. Within each region of a given category, the maximum reflectivity was recorded. The area of each hail and mixed cell was also recorded and the equivalent diameter was computed ("equivalent diameter" in this case refers to the diameter of a circular region of the same area).

Table 2-8 gives a summary of the total hail data points. There are 414 maximum hail reflectivity data

points (30-minute data) from the three July months of 1983-85. Additionally, there are 2868 hailshaft area (equivalent diameter) data points. There are more hailshaft area points than maximum hail reflectivity points because the hailshaft area data include the mixed (rain and hail) regions. The data points were used to construct cumulative distribution plots of both equivalent diameter and maximum reflectivity.

Methods of Analysis - The hail curve, given by *P*(HWC), is a product of the prior probability of a hail storm occurring at a given point and the conditional probability of a given HWC value occurring within that hailstorm:

$$P(\text{HWC}) = Pp(\text{HWC}) \times Pc(\text{HWC}) \qquad 2\text{-}9$$

Equation 2-9 applies specifically to hail, while Equation 2-3 is a more general expression of the joint probability of a given water content from a convective storm. Comparing Equations 2-3 and 2-9, *P*(HWC) corresponds to *P*(storm ∩ Mw), the prior probability of a hailstorm occurring at a given point is *Pp*(HWC) in Equation 2-9 corresponding to *P*(storm) in Equation 2-3, and the conditional probability of HWC, given a hailstorm, is *Pc*(HWC) in Equation 2-9 and *P*(Mw | storm) in Equation 2-3.

The first step in the analysis was to convert the 414 hail reflectivity data points into HWC data points. There are a number of Z-Mw conversions for hail. The Ulbrich and Atlas (1982) (Reference 2.16) conversion equation was used in this analysis.

Because hail reflectivity is strongly influenced by the liquid water coating thickness, tw, on the hailstones, the reflectivity values were corrected to account for this effect. The equation of Reference 2.16:

$$Z = 9.22 \times 10^{5} (\text{Mw})^{1.23} \qquad 2\text{-}10$$

assumes tw = 0.01 cm. Because water coating thickness cannot be measured directly, it was necessary to estimate tw for the Alberta constant-altitude plan-position indicator (CAPPI) altitudes. The reflectivity values were corrected and then converted to HWC using Equation 2-10.

Figure 2-11 shows the cumulative distribution of HWC values from the ARC data at 2.7, 4.7, and 6.7 km MSL. The 2.7 km MSL CAPPI level has the largest HWC values and therefore these data were used to estimate *Pc* (HWC) in Equation 2-9.

The other term on the right hand side of Equation 2-9, *Pp*(HWC), was calculated by estimating the mean annual minutes of hail at a worst case location for hail and then dividing this number by the number of minutes in a year. Equation 2-11 below shows how *Pp* (HWC) was estimated:

$$Pp(\text{HWC}) = \text{n} \times \text{t} \times \text{k(HWC)} / 525960 \qquad 2\text{-}11$$

where n is the number of hail storms at a point representing the worst case location, t is the mean point hailfall duration, 525960 is the number of minutes in a year, and the correction factor k(HWC), is necessary because it was recognized that the higher HWC values within a hailshaft occupy a smaller cross-sectional area and therefore the duration of larger HWC values at a point will be considerably smaller than the overall hail duration. Southeastern Wyoming has the highest number of haildays in the United States at 9. For this reason a value of 9 haildays per year was used as the peak value in the U.S. for the purposes of this study. There is a precedent for using the peak value of the U.S. as a worst case value globally (c.f., Gringorten, 1971) (Reference 2.17). Gokhale (1975) (Reference 2.18) shows maps similar to the U.S. hailday map for Africa, Argentina, and India that support a value of 9 as worst case. Similarly, Omoto (1974) (Reference 2.19) shows a hailday map for Japan where a value of 5 haildays annually is the maximum. Sulakvelidze (1967) (Reference 2.20) reports a point hailday maximum of 8-10 days for the Soviet Union. To reiterate, the value of 9 haildays per year in southeastern Wyoming was considered the worst case frequency for the purposes of this study. Furthermore, since hail occurs so infrequently (only 9 days out of 365), it was assumed that only one hailfall per hailday occurs at a given point. In other words, n, from Equation 2-11 was assigned a value of 9.

Results - With *Pp*(HWC) *and* *Pc*(HWC) known, then Equation 2-9 was used to solve for *P*(HWC). The three *Pc*(HWC) points, indicated in Figure 2-11, were multiplied by *Pp*(HWC), then curve fitted. The resulting curve, which is defined by *P*(HWC) = $Pj = 1.39 \times 10^{-5}$. exp(-HWC/1.73), is shown in Figure 2-12. At probability levels of 10^{-7},10^{-8}, and 10^{-9}, the HWC values are 8.5, 12.5, and 16.5 g m^{-3}, respectively. The highest measured value from the ARC 30-minute data was 9.3 g m^{-3}, which has a corresponding probability of occurrence of 6.4×10^{-8}. All values to the left of ($9.3, 6.4 \times 10^{-8}$) were extrapolated.

Figure 2-13 shows a comparison of the rain and the ARC-derived hail curves. As might be expected, *P*(LWC) exceeds *P*(HWC) at all probability levels along the abscissa. The two curves tend to converge to the left, which also might be expected since atmospheric

conditions favorable for producing extreme rainfall often are also conducive to hail storm formation.

It should be re-emphasized that the curve in Figure 2-13 represents the probability of hail occurring at a point at a worst case location for hail. *P*(HWC) does not give the probability of an airplane encountering hail of various intensity.

An important aspect of the weather threat analysis is the hailstone size distribution as discussed in Federer and Waldvogel (1975) (Reference 2.24). The size distribution is usually considered to be exponential as given by Equation 2-12.

$$N(D) = N_o e^{-\Lambda D} \qquad \text{for } (D_{min} < D < D_{max}) \quad 2\text{-}12$$

where N_o and Λ are defined in Section 2.4.3. The minimum hailstone diameter, D_{min}, is specified as 5 mm, while the maximum hailstone diameter D_{max} is often considered infinite for calculation purposes. Equation 2-13 below gives HWC:

$$HWC = \frac{1}{6}\rho_h \int_{D_{min}}^{D_{max}} N(D) D^3 dD \qquad 2\text{-}13$$

where ρ_h is the density of the hailstones. Equations 2-14 and 2-15 below, from Reference 2.16, can be rearranged and combined with the empirical relationship Equation 2-16, also from Reference 2.16, to give equations for No and Λ as a function of HWC.

$$No = 95.6\ D_{med}^{0.39} \qquad 2\text{-}14$$

$$HWC = \pi \rho_h\ No/\Lambda^4 \qquad 2\text{-}15$$

$$HWC = 1.49\ (D_{med})^{0.39} \qquad 2\text{-}16$$

So, for a given HWC, Equations 2-12 and 2-13 can be used to estimate the contribution of the total number of hailstones and HWC from selected hailstone size intervals (similar to Figure 2-10 but for hail). Figure 2-14(a) shows the hailstone size distribution as calculated from Equation 2-12 with No and Λ calculated by assuming an HWC of 13 g m^{-3} and assuming D_{min} = 5 mm and $D_{max} = \infty$. Approximately 89% of the hailstones are between 0.5 and 1.5 cm. The size category with the most hailstones is $0.5 < D < 1.0$ cm, while the mean stone size is 0.95 cm in diameter. Figure 2-14(b) shows the percent contribution to the total HWC from each 1 mm size interval as calculated from Equation 2-13 with HWC = 13 g m^{-3}, D_{min} = 5 mm, $D_{max} = \infty$, and $\rho_h = 9 \times 10^5$ g m^{-3}. Approximately 48% of the total HWC is from stones with diameters between 1.0 and 2.0 cm. The size category contributing the most to the total HWC is $1.0 < D < 1.5$ cm, while the median volume diameter, D_{med}, is 1.6 cm.

Vertical Distribution of Hail in the Atmosphere - A significant aspect of the weather threat study concerns the vertical distribution of hail in the atmosphere. In particular it is important to identify the level in the atmosphere at which the hail curve in Figure 2-12 applies. A majority of above-ground-level hail data in the available literature has been collected by weather radar, therefore altitude distributions have been derived from reflectivity profiles of hailstorms.

ARC data were used to determine the variation of HWC with altitude above the freezing level. As indicated in Figure 2-11 the probability of a given HWC value decreases with increasing altitude above the freezing level. Stated alternatively, the HWC value at a given probability level decreases with increasing altitude. The rate at which HWC decreases with altitude depends on the probability level of interest.

To calculate the change in HWC with altitude, ARC cumulative hail probability curves (Figure 2-11 were examined at the probability level corresponding to 9.5 g m^{-3} on the 2 km AGL curve, i.e., 99.8%. Data shown in Figure 2-11 were curve fitted and then the 6 km AGL data were extrapolated to 99.8% cumulative probability. Variation of HWC with increasing altitude above the freezing level was calculated from the HWC values at 99.8% cumulative hail probability at 3.5, 4.7 and 6.7 km MSL. This provided three points, which were subsequently curve-fitted, as indicated in Figure 2-15 by the portion of the curve to the right of H = Ho, where Ho is the freezing level.

To calculate the variation of HWC with altitude below the freezing level, the modeled hailstone was allowed to fall below the freezing level until the critical amount of liquid water, before the onset of water shedding, had been reached. Figure 2-15 shows the variation of normalized HWC as a function of altitude from the freezing level. The portion of the curve to the left of H = Ho was derived from the Rasmussen and Heymsfield (1987) (Reference 2.21) melting model as described above.

2.4.4.2 *GNEFA Data*

The Groupement National d'Etudes des Fléaux Atmosphériques (GNEFA), located in Aubiere, France enjoys the reputation of being among the world's leading experts on hail and hailstorms.

They were engaged by CFM International (CFMI) [through the Société National d'Etude et de Construction de Moteurs d'Aviation (SNECMA)], to provide data taken during hail storms in Europe.

Included in the data were S-band weather radar collected in the Napf region of Switzerland (near Zurich) as part of the Grossversuch IV program (Federer et al. 1978 (Reference 2.22), Waldvogel et al. 1978 (Reference 2.23) and Federer and Waldvogel 1975 (Reference 2.24)).

The radar data consists of a set of 253 Z_{max} values, where Z_{max} is defined as the maximum reflectivity value of a "potential hail-producing" cell. A cell is defined as a potential hail producer if a plan-position indicator (PPI) radar echo contour exceeds 45 dB Z and a hail hazard criterion, measured in range-height indicator (RHI) mode by another radar, is met. All cells which had produced hail at the ground were considered hail producers, but not all cells considered hail producers discharged hail measured at ground level. The 253 cells providing Z_{max} values make up the complete Grossversuch IV radar-identified cell data of the years 1977-1982.

While GNEFA supplied the data, the actual analysis was carried out by CFMI. Much of the same methodology used to develop the ARC hail curve, previously described, was also used to develop the GNEFA hail curve. The most important difference between the Boeing and CFMI methodologies is that a correction factor was applied to the GNEFA reflectivity data. The GNEFA data differs from the ARC data in that ARC values represent maximum reflectivity within a hail cell at the time it happened to be scanned. A GNEFA value, on the other hand, represents the single highest reflectivity value within a hail cell that occurred sometime during the life of the cell (or at least throughout the portion of the cell's life when it was within the range of the radar). Consequently the HWC values, converted from the GNEFA reflectivity values using Equation 2-9, were multiplied by a constant correction to get an "average" HWC. The resulting curve, defined by $P(\text{HWC}) = 6.75 \times 10^{-6} \exp(-\text{HWC}/2.05)$, is shown in Figure 2-16. At probability levels of 10^{-7}, 10^{-8}, and 10^{-9} the HWC values are 8.6, 13.4, and 18.1 g m^{-3}, respectively. The largest HWC value of the four fitted points is 10.2 g m^{-3}, which has a corresponding probability of occurrence of 4.7×10^{-8}. So all values to the left of (10.2, 4.7×10^{-8}) were extrapolated.

Figure 2-16 shows both the Boeing-derived and CFMI-derived hail curves. The two curves cross each other at about $P(9 \text{ g m}^{-3}) = 8.5 \times 10^{-8}$. The CFMI curve has larger HWC values than the Boeing curve at probabilities less than 8.5×10^{-8}, whereas the Boeing curve has higher HWC values for probabilities greater than 8.5×10^{-8}. In general, though, there is good agreement between the two curves. At a probability level of 10^{-9}, for example, the Boeing HWC is 16.5 g m^{-3} and the CFMI HWC is 18.1 g m^{-3}, a difference of only 1.6 g m^{-3}.

2.4.5 Airplane Threat Analysis

2.4.5.1 *Introduction*

Previous sections discussed rain and hail concentrations occurring at a point for an instant of time. The airplane threat analysis evaluates the conditional probability of an airplane spending a finite period of time in an extreme rain or hail encounter. This conditional probability will be called the duration probability P_t. The duration probability accounts for the transient nature of encounters by an aircraft with extreme concentrations of rain or hail. The duration probability is also necessary to establish a correlation between actual aircraft rain and hail threat levels and engine test requirements.

The horizontal extent of extreme rain concentrations is large relative to hail. Because of this size difference, the duration probability of rain is assumed to be 1.0. The following analysis evaluates the duration probability of hail encounters.

2.4.5.2 *Assumptions*

The duration probability analysis is based on the following assumptions:

1) Hailshafts are circular - that is, there is no preferred direction or orientation relative to the airplane path.
2) The airplane enters the hailshaft at its perimeter.
3) The airplane passes through the hailshaft in level flight.
4) Hailshafts are stationary relative to airplane motion.
5) The HWC distribution through the hailshaft is uniform.
6) The airplane passes through the hailshaft along a straight line.
7) The duration probability is independent of HWC.

The above assumptions simplify the analysis and provide a conservative estimate of the duration probability.

2.4.5.3 *Definitions*

Figure 2-17 shows the geometry imposed by the above assumptions. The diameter of the hailshaft is D_h. The angle of the airplane path relative to the hailshaft is θ. The distance across the hailshaft at angle θ is L. The flight path length, that is the distance travelled over the duration period, is λ.

Figure 2-18 shows the relative frequency distribution of equivalent hailshaft diameters derived from data provided by ARC. The relative frequency distribution is the number of hailshaft measurements in each diameter interval distribution and was derived from dual-polarization radar measurements. The following analysis uses the ARC hailshaft diameter frequency distribution.

2.4.5.4 ***Formulation***

The first step in calculating the duration probability is to determine the airplane flight path length, λ. The flight path length is the product of true airspeed and duration time. The airspeed and duration time used in the following example calculation are representative values for large commercial airplanes. A typical airspeed for a large commercial airplane penetrating inclement weather is 280 Knots Indicated Airspeed (KIAS). The true airspeed can be calculated from indicated airspeed, altitude and ambient temperature. The altitude and ambient temperature for this calculation were chosen as 4570 m (15,000 ft) above mean sea level (MSL) and 0°C. These conditions correspond to the altitude and ambient temperature of the maximum HWC in a North American hailshaft. Under these conditions, 280 KIAS corresponds to a true airspeed of 184 m/sec (603 ft/sec). Flight crews who have flown large commercial airplanes through extreme hail conditions have reported that the encounter lasted about 30 seconds. For this reason, 30 seconds was chosen as the duration time for the airplane threat analysis. The flight path length for a 30 second duration at 184 m/sec is 5514 metres (18090 feet).

The second step is to relate the flight path across the hailshaft to hailshaft diameter D_h and flight path angle θ (refer to Figure 2-17). The distance across the hailshaft at angle θ can be written:

$$L = D_h \cdot \sin\theta. \qquad 2\text{-}17$$

The third step is to evaluate the duration probability in terms of the above geometrical considerations. The probability that L is greater than λ at a given hailshaft diameter can be written $P\{L>\lambda, D_h = \xi\}$. This expression can be rewritten as the conditional probability $L>\lambda$, with the condition that $D_h = \xi$, multiplied by the probability that $D_h = \xi$.

$$P\{L>\lambda, D_h = \xi\} = P\{L>\lambda \mid D_h = \xi\} \cdot P\{D_h = \xi\} \qquad 2\text{-}18$$

Equation 2-18 can be further modified by substituting Equation 2-17 for L and rearranging the terms to give:

$$P\{L>\lambda, D_h = \xi\} = P\{\theta > \arcsin(\lambda/D_h) \mid D_h = \xi\} \cdot P\{D_h = \xi\} \qquad 2\text{-}19$$

The term $\theta > \arcsin(\lambda/D_h)$ in Equation 2-19 can be interpreted as the angle in which L is greater than the flight path length λ. In other words, if the flight path angle is θ or greater, a hailshaft will encompass the airplane flight path,. For a given flight path length and hailshaft diameter, the ratio of angles in which L exceeds λ is $(\pi/2 - \theta)/(\pi/2)$. Although the geometry was developed for angles from zero to $\pi/2$, this ratio also applies to angles from zero to π.

The probability that the line segment L exceeds the flight path length λ, for a given hailshaft diameter, can be written:

$$P\{\theta > \arcsin(\lambda/D_h) \mid D_h = \xi\} = (\pi/2 - \arcsin(\lambda/\xi))/(\pi/2) \qquad 2\text{-}20$$

Substituting Equation 2-20 into 2-19 gives:

$$P\{L>\lambda, D_h = \xi\} = [(\pi/2 - \arcsin(\lambda/\xi))/(\pi/2)] \cdot P\{D_h = \xi\} \qquad 2\text{-}21$$

The term $P\{D_h = \xi\}$ can be expressed as the frequency distribution of hailshaft diameters from Figure 2-16:

$$P\{D_h = \xi\} = f_D(\xi) \qquad 2\text{-}22$$

The final step is to consider the duration probability over the relevant range of hailshaft diameters and flight path lengths. The duration probability for all hailshaft diameters greater than the flight path length is determined by substituting Equation 2-22 into 2-21 and integrating from λ to infinity:

$$Pt = P\{L>\lambda\} = \int_{\lambda}^{\infty} \left[\left(\frac{\pi}{2} - \arcsin\left(\frac{\lambda}{\xi}\right)\right)/\left(\frac{\pi}{2}\right)\right] f_D(\xi)\, d\xi \qquad 2\text{-}23$$

2.4.5.5 ***Results***

Figure 2-19 shows the results of numerically integrating Equation 2-23 for flight path lengths up to 11,970 m (36,000 ft). Given a flight path length λ = 5514 m (18,090 ft), the duration probability is 0.16. In other words, given the condition that an airplane is travelling 184 m/sec (603 ft/sec) and has encountered a hailshaft,

there is a 0.16 probability that the airplane will spend 30 seconds or more in the hailshaft.

Under the assumption that the duration probability is independent of HWC, the threat to an airplane can be written as the product of *Pj* (from Figure 2-12) and *Pt* (from Figure 2-19).

$$P = Pj \cdot Pt \qquad 2\text{-}24$$

The curve shown in Figure 2-12 can be factored to account for a given *Pt*. The *Pt* for the example condition (4570m, 280 KIAS and 0°C Tamb) is 0.16. The airplane threat curve is obtained by multiplying the abscissa in Figure 2-12 by 0.16. An airplane threat curve for the example condition is shown in Figure 2-20. Equations given in Section 2.3.4 can be modified to calculate the HWC for other values of *Pt*:

$$HWC = -1.73 \cdot \ln[(P)/(Pt \cdot 1.39 \cdot 10^{-5})] \qquad 2\text{-}25$$

where *P* is the over-all threat probability, and *Pt* is the duration probability.

2.4.5.6 *Conclusions*

The airplane threat analysis discussed in this section provides a means of estimating the conditional probability that the airplane will remain in rain or hail for a given period of time. This conditional probability has been called duration probability *Pt*. For extreme rain, *Pt* was chosen as 1.0. For extreme hail, *Pt* can be determined from the curve shown in Figure 2-19.

2.5 THREAT DEFINITION AND TEST REQUIREMENTS

2.5.1 Threat Definition

This section defines the levels of LWC (rain) and HWC (hail) which are recommended for engine water ingestion certification testing. The probability curves for rain and hail were developed such that they are representative of an aircraft flying at the worst case world-wide location. These curves provide the starting point for determining the aircraft threat. The AIA committee recommended evaluating the engine tolerance to water ingestion at a threat level of 10^{-8} probability per flight. Figure 2-20 shows the probability of an aircraft encountering a specified HWC value for 30 seconds, assuming the aircraft enters the hail shaft at an indicated airspeed of 280 knots and an ambient temperature of 0°C. At this condition the HWC value corresponding to 10^{-8} probability is 9.5 gm^{-3}.

Radar data shows that the maximum HWC concentration occurs at the freezing level altitude and lapses as shown in Figure 2-15. Hail storms that occur in the Central United States are representative of the most frequent and most severe world wide. During June, the peak month of hailstorm frequency, a freezing level height of 4600 m (15,000 ft) appears to represent the upper limit within the region of the most severe hail activity. Therefore the maximum HWC in the USA is expected to occur at the 4600 m level. The most severe hail activity in Europe occurs in France and Switzerland, also during June. At this location the freezing level heights are around 3660 m (12,000 ft). For these conditions the maximum hail threat is closely similar to that of Figure 2-20 and an HWC value of 9.5 g m^{-3} at 10^{-8} probability is appropriate.

As specified in Section 2.4.5.1, the duration probability for an airplane encounter with the worst location rain storm is considered to be 1.0. With this assumption the rain curve in Figure 2-7 can be directly applied to represent an aircraft encounter probability. This curve gives a LWC value at 10^{-8} probability of 18.9 gm^{-3}. Figure 2-9 shows the LWC lapse characteristic with altitude based on the MIL-STD-210C rain lapse model.

2.5.2 Test Requirements

The rain and hail 10^{-8} probability threat levels described in Section 2.5.1 are shown in Table 2-9. The recommended certification water ingestion levels have been increased by approximately 5% to ensure margin during the certification test to accommodate minimum quality and/or deteriorated product engines. This table also defines the certification requirement in terms of ambient water-air ratio. The test duration for hail is 30 seconds, which is consistent with the hail shaft duration probability described in Section 2.4. A duration time of three minutes has been specified for rain. This amount of time should be more than adequate to allow the engine to achieve operability stabilization.

The requirements shown in Table 2-9 were derived for high bypass commercial engines. Since military aircraft vary widely in their missions, in terms of altitude, flight velocity and power setting, these requirements need to be established for the different military applications.

An overview of the AIA recommended rain and hail altitude certification requirements, and how they

relate to the ground proof test demonstration, is shown in Figure 2-21. The commercial engine certification requirements are described in Chapter 6.

The following is an example of the AIA proposed rain threat shown in Figure 2-21 and how it compares with the current United States Federal Aviation Regulations (FAR) Part 33 test requirement. This figure shows that the 20 g m^{-3} maximum rain concentration level occurs between sea level and 6100 m (20,000 ft) altitude. Also shown on Figure 2-21 is the 10 g m^{-3} maximum hail concentration level which occurs between 3600 m (12,000 ft) and 4600 m (15,000 ft).

It should be noted that for a given concentration level, the amounts of rain and/or hail that are ingested during a test at sea level conditions are much higher than at altitude conditions. This is a result of the difference in air density between altitude and sea level. For example, the 20 g m^{-3} rain threat equates to a maximum concentration level of approximately 3% water-air ratio at 6100 m (20,000 ft); this water-air ratio corresponds to 37.5 g m^{-3} at sea level conditions.

In order to validate the engine's capacity to adequately withstand a severe rain and hail encounter, the critical operating points throughout the flight envelope are identified through analysis. This analysis encompasses the full range of all pertinent variables discussed in Chapter 5. These variables include altitude, flight velocity, engine power setting, inlet aerodynamic flow field, rain droplet break-up, engine air-bleed systems, and typical operability margins, including surge/stall margin, fuel control rollback margin, combustor blowout margin and instrumentation sensing errors. The analysis, confirmed by operational experience, often indicates that the primary area of concern is high altitude, low power operating conditions, such as the top of idle descent. This is the flight condition where the maximum scoop factor and the maximum water-air ratio both occur. Figure 5-25 shows the scoop factor during idle descent can produce a 2.5 amplification of the ambient rain threat. The resulting certification test then requires 3% water-air ratio multiplied by the 2.5 amplification factor, or 7.5% engine face water-air ratio, which is almost twice as severe as the 4% current FAR requirement for rain. There is no current FAR 33 maximum hail level concentration test requirement for engine operation.

It appears that the current FAR 33 rain and hail ingestion requirements are valid tests for addressing permanent mechanical damage due to hail impact and case contraction from water ingestion. However, these standards do not adequately address engine power loss anomalies such as rollback and flameout.

2.6 SOURCES OF METEOROLOGICAL DATA

2.6.1 Canada

Atmospheric Environment Service,
Environment Canada,
LaSalle Academy, Block E,
373 Sussex Dr.,
Ottawa, ON
Canada. K1A 0H3

2.6.2 France

Météo-France,
Central d'Exploitation de la Météorologie-climatologie et Banque de Données,
42 Avenue Coriolis
31057 Toulouse
France
Tel. 33-61-07-83-49
Fax. 33-61-07-83-09

2.6.3 Germany

Deutscher Wetterdienst
Zentralamt
Postfach 10 04 65
63004 Offenbach

2.6.4 Turkey

Ministry of Environment,
Meteorological General Management
Bakanhkar 06700
Ankara
Turkey

2.6.5 United Kingdom

Air Ministry,
Meteorological Office,
Tables of Temperature, Relative Humidity and Precipitation for the World,
Her Majesty's Stationery Office, London.

2.6.6 United States

US Department of Commerce,
National Oceanic and Atmospheric Center
Federal Building
Asheville, NC 28801-2733 (704)259-0682

2.7 CONCLUSIONS AND RECOMMENDATIONS

The results of this section are summarized in Table 2-10.

FINDINGS:

- The most severe rain and hail threat conditions are produced by well developed convective clouds.
- The probability of encountering a given quantity of rain and hail at the world 's worst location is shown in Figure 2-13. Since the values for hail probabilities below 10^{-7} are extrapolated, more data are needed. Future weather satellites offer the greatest potential for obtaining these data and should be capable of making 10^8 measurements in a relatively short period of time.
- The AIA recommended rain and hail certification requirements for high bypass commercial engines are presented in Table 2-9. The values shown, 20 g/m^3 for rain and 10 g/m^3 for hail, represent an aircraft encounter probability of 10^{-8} at the most limiting flight conditions of altitude, Mach number, and power setting for a minimum quality engine.
- Specified levels of rain and hail ingestion for military engine qualification should be established in consideration of their mission requirements and an acceptable level of risk. Adapting the methodology used by the AIA for commercial engines would be a reasonable approach.
- There are still many unknowns that need to be resolved for the complete definition of the water ingestion threat. For example, - what are the effects of the temperature and hardness of hail on the engine's ability to process it; what is the threat of rain and hail in combination; does icing aggravate the operability problem; testing is generally conducted with warm air and water, would the results be different in a sub-freezing environment with chilled water?

2.8 REFERENCES

2.1 Grabe, W., Chappell M.S., *Stationary Gas Turbine Icing: Some Design Guidelines for Blowing Snow Environments,* National Research Council Canada, LTR-ENG-30, Sept. 1974.

2.2 U.S. Department of Defense, 1987: Military Standard, *Climatic Information to Determine Design and Test Requirements for Military Systems and Equipment*, MIL-STD-210C, 9 January 1987, Office of the Under Secretary of Defence, Research and Engineering, Washington, D.C.

2.3 Tank W.G., Pataoe, M.W., Moravec, B.A., Edalati, N.K., *Inclement Weather Study; Rain and Hail Threat Definition and Analysis*. D6-56394 (unpublished internal report of The Boeing Company), 1992.

2.4 Tattelman, P., and Larson K.P., *Effects of Rain Attenuation on Satellite EHF Communications in the United States*, AFGL-TR-89-0012, 1989.

2.5 Bodtmann, W.F. and Ruthroff, C.L., *The Measurement of 1 min Rain Rates from Weighing Raingage Recordings*, J. Appl. Meteor., **15**, pp 1160-1166, 1976.

2.6 Jones, D.M.A. and Wendland, W.A., *Some Statistics of Instantaneous Precipitation*, J. Climate Appl. Meteor., **24**, pp 1059-1067, 1984.

2.7 Roys, G.P. and Kessler, E., *Measurements by Aircraft of Condensed Water in Great Plains Thunderstorms.* National Severe Storms Project Rep. No. 19, Washington, D.C., 1966.

2.8 Briggs, J., *Probabilities of Aircraft Encounters with Heavy Rain*, Meteor. Mag., **101**, pp 8-13, 1972.

2.9 Mueller, E.A., and A. L. Sims, *Investigation of the Quantitative Determination of Point and Areal Precipitation by Radar Echo Measurements*, Tech Rep. ECOM-00032-F, Contract DA-28-043 AMC-00032 (E) Illinois State Water Survey, Urbana, 88 pp, 1966 [AD 645218.]

2.10 Jones, D.M.A., *Rainfall Drop-Size Distribution and Radar Reflectivity*, Res. Rept No. 6, Urbana: Meteor. Lab., Illinois State Water Survey, 1956.

2.11 Willis, P.T., *Functional Fits to Some Observed Drop Size Distributions and Parameterizations of Rain*, J. Atmos. Sci., 41, 1648-1661, 1984.

2.12 Tattelman, P., and Grantham D.D., *Northern Hemisphere Atlas of 1-Minute Rainfall Rates*, AFGL-TR-83-0267, 81 pp [ADA145411], 1983.

2.13 Riordan, P. and Bourget, P.G., *World Weather Extremes*, ETL-0416, 77 pp, 1985.

2.14 Tattleman, P., and Willis, P.T., *Model Vertical Profiles of Extreme Rainfall Rate, Liquid Water Content, and Drop-Size Distribution*, AFGL-TR-85-0200, 34 pp, 1985.

2.15 Marshall, J.S., and Palmer, W.M.K., *The Distribution of Raindrops with Size*, J. Meteor., **5**, pp 165-166, 1948.

2.16 Ulbrich, C. W., and Atlas D., *Hail Parameter Relations: A Comprehensive Digest*, J. Appl. Meteor., **21**, pp 22-43, 1982.

2.17 Gringorten, L.L., *Hailstone Extremes for Design.* AFCRL-72-0081, 23 pp, 1971.

2.18 Gokhale, N.R., *Hailstorms and Hailstone Growth*, State University of New York Press, Albany, New York, 465 pp, 1975.

2.19 Omoto, Y., *Hailstorms in Japan.*, World Meteorological Society, Geneva, WMO 339, 207-215, 1974.

2.20 Sulakvelidze, G. K., *Rainstorms and Hail*, Gidromet., Leningrad, 1967. [Translated Israel Program for Scientific Translations, Jerusalem, 1969.]

2.21 Rasmussen, R., and Heymsfield, A.J., *Melting and shedding of graupel and hail. Part II: Sensitivity study*, J. Atmos. Sci., **44**, pp 2764-2782, 1987.

2.22 Federer, B., Waldvogel, A., Schmid, W., Hampel F., Rosini, E., Vento, D., Admirat, P., and Mezeix, J.F., *Plan for the Swiss randomized hail-suppression experiment. Design of Grossversuch IV.* Pure and Appl, Geophys., **117**, 548-571, 1978.

2.23 Waldvogel, A., Federer, B., Schmid, W., and Mezeix, J.F., *The Kinetic Energy of Hailfalls. Part II: Radar and Hailpads*, J. Appl Meteor., **17**, pp 1680-1693, 1978.

2.24 Federer, B. and Waldvogel, A., *Hail and Raindrop Size Distributions from a Swiss Multicell Storm*, J. Appl. Meteor., **14**, pp 91-97, 1975.

2.25 Kyle, T.G. and Sand, W.R., *Water Content in Convective Storm Clouds*, Science, **180**, pp 1274-1276, 1973.

Table 2-1

WEATHER SYSTEMS PRODUCING HIGH WATER CONCENTRATIONS

Scale	Horizontal Extent	Temporal Extent
Convective	tens of kilometres	to ~ 1 hour
Mesoscale	tens to a few hundred kilometres	~ 1 to 10 hours
Synoptic	a few hundred to a few thousand kilometres	~ 10 hours to several days

Table 2-2

MODEL PROFILES OF ABSOLUTE HUMIDITY FOR WORLD WIDE ENVIRONMENT

(Reference 2.2)

Geometric Altitude	BELIZE CITY						ABADAN, IRAN		SHARJAH, ARABIA	
	20% Worst Month Tropics		10% Worst Month Tropics		5% Worst Month Tropics		1% Worst Month Tropics		Highest Recorded	
	Mixing Ratio	Dew Point	Mixing Ratio	Dew Point	Mixing Ratio	Dew Point	Mixing Ratio	Dew Point	Mixing Ratio	Dew Point
(ft)	*% war*	*°F*	*% war*	*°F*	*% war*	*°F*	*% war*	*°F*	*% war*	°F
km	PPM x 10^3	° K	PPM x 10^3	° K	PPM x 10^3	° K	PPM x 10^3	° K	PPM x 10^3	° K
(0)	*1.55*	*83*	*1.62*	*84*	*1.74*	*86*	*1.93*	*88*	*2.18*	*93*
0	25	301	26	302	28	303	30	304	35	307
(3,281)	*1.37*	*77*	*1.49*	*79*	*1.62*	*81*	*1.80*	*84*	*1.93*	*86*
1	22	298	24	299	26	300	29	302	31	303
(6562)	*1.18*	*68*	*1.24*	*70*	*1.31*	*72*	*1.49*	*75*	*1.74*	*79*
2	19	193	20	294	21	295	24	297	28	299
(13,123)	*0.75*	*48*	*0.87*	*52*	*1.00*	*55*	*1.18*	*61*	*1.37*	*64*
4	12	282	14	284	16	286	19	289	22	291
(19,685)	*0.44*	*28*	*0.48*	*30*	*0.52*	*32*	*0.62*	*37*	*0.62*	*37*
6	7.1	271	7.7	272	8.3	273	10	276	10	276
(26,246)	*0.25*	*9*	*0.27*	*10*	*0.29*	*12*	*0.37*	*18*	*0.39*	*19*
8	4.0	260	4.3	261	4.7	262	5.9	265	6.4	266
(32,808)							0.08	-20		
10							1.3	244		
(39,370)							*0.01*	*-49*		
12							0.23	228		
(45,931)							*0.003*	*-76*		
14							0.05	213		

Mixing Ratios are based upon a typical surface atmospheric pressure of 1000 millibars and dew points in adjacent column.

Table 2-3

DAILY CYCLE OF HUMIDITY, TEMPERATURE, AND OTHER ELEMENTS ASSOCIATED WITH THE WORLDWIDE HIGH ABSOLUTE HUMIDITY - 1-PERCENT VALUE

(This cycle also represents the Hot-Humid condition for the Hot Regional Type)

(Reference 2.2)

TIME	ABSOLUTE HUMIDITY			TEMPERATURE		RH	SOL. RAD.	
(LST)	Mix.Ratio (ppm)	Dew Point (° K)	(°F)	(° K)	(°F)	(%)	(W/m^2)	(Bph)
01	26 x 10^3	302	84	304	88	88	0	0
02	26 x 10^3	302	84	304	88	88	0	0
03	26 x 10^3	302	84	304	88	88	0	0
04	26 x 10^3	302	84	304	88	88	0	0
05	26 x 10^3	302	84	304	88	88	0	0
06	27 x 10^3	302	85	305	91	88	45	15
07	28 x 10^3	303	86	307	93	83	315	100
08	29 x 10^3	304	87	309	96	78	560	177
09	30 x 10^3	304	88	310	98	73	790	251
10	30 x 10^3	304	88	311	100	70	950	302
11	30 x 10^3	304	88	312	102	66	1035	328
12	30 x 10^3	304	88	313	104	63	1080	343
13	30 x 10^3	304	88	314	105	60	1000	317
14	30 x 10^3	304	88	314	105	60	885	280
15	30 x 10^3	304	88	314	105	60	710	225
16	30 x 10^3	304	88	314	105	60	465	147
17	29 x 10^3	304	88	312	102	64	210	66
18	29 x 10^3	304	87	310	99	69	15	4
19	28 x 10^3	304	87	309	97	74	0	0
20	28 x 10^3	303	86	307	94	79	0	0
21	28 x 10^3	303	86	306	91	85	0	0
22	27 x 10^3	302	85	305	90	86	0	0
23	26 x 10^3	302	85	305	89	87	0	0
24	26 x 10^3	302	84	304	88	88	0	0

Note: Mixing ratios are based upon a typical surface atmospheric pressure of 1000 mb and dew points in adjacent column.

Table 2-4

VARIOUS EQUATIONS USED TO CONVERT RAIN RATE, Rr, in mm hr^{-1} TO LIQUID WATER CONTENT, Mw, in gm m^{-3}

Source	Climate Region	Mw-Rr Equation	Locations Where Data Were Collected
Jones, 1956 (Reference 2.10)	mid-latitude continental	$Mw = 0.052\ Rr^{0.95}$	Illinois
Mueller & Sims, 1956 (Reference 2.9)	subtropical	$Mw = 0.0528\ Rr^{0.95}$	Miami
Willis, 1984 (Reference 2.11)	tropical	$Mw = 0.062\ Rr^{0.913}$	Hurricanes Anita & Frederic

Table 2-5

MODEL PROFILES OF PRECIPITATION RATE, TOTAL WATER CONCENTRATIONS AND DEDUCED TOTAL WATER-AIR RATIOS (percent by weight)

(Total water is summation of precipitation and cloud water)

(Reference 2.2)

Geometric Altitude (ft) km	Northeast Brazil and Cherrapunji, India									Holt, Missouri			Unionville, Maryland		
	0.5% Worst Month Tropics			0.1% Worst Month Tropics			0.01% Worst Month Tropics			42 Minute World Record			1 Minute World Record		
	Rate	*Total Water*		Rate	*Total Water*		Rate	*Total Water*		Rate	*Total Water*		Rate	*Total Water*	
		g m⁻³	% war		*g m⁻³*	% war		*g m⁻³*	% war		*g m⁻³*	% war		*g m⁻³*	% war
		Prec	CLD		Prec	CLD		Prec	CLD		Prec	CLD		Prec	CLD
	mm/min	g m⁻³	g m⁻³	mm/min	g m⁻³	g m⁻³	mm/min	g m⁻³	g m⁻³	mm/min	g m⁻³	g m⁻³	mm/min	g m⁻³	g m⁻³
(0) 0	0.60	*1.6*	*0.13*	1.40	*3.5*	*0.29*	2.80	*6.7*	*0.55*	7.2	*15.8*	*1.29*	31.2	*60.3*	*4.92*
		1.6	0		3.5	0		6.7	0		15.8	0		60.3	0
(6,562) 2	0.60	*3.7*	*0.37*	1.40	*6.5*	*0.64*	2.80	*10.1*	*1.00*	7.2	*19.2*	*1.91*	31.2	*63.7*	6.33
		1.6	2.1		3.5	3.0		6.7	3.4		15.8	3.4		60.3	3.4
(13,123) 4	0.60	*4.0*	*0.49*	1.40	*6.9*	*0.84*	2.80	*10.6*	*1.29*	7.2	*19.7*	*2.40*	31.2	*64.2*	*7.96*
		1.6	2.4		3.5	3.4		6.7	3.9		15.8	3.9		60.3	3.9
(19,685) 6	0.60	*4.1*	0.62	1.40	*7.0*	*1.06*	2.80	*10.7*	*1.62*	7.2	*19.8*	*3.00*	31.2	*64.3*	*9.75*
		1.6	2.5		3.5	3.5		6.7	4.0		15.8	4.0		60.3	4.0
(26,246) 8	0.44	*2.9*	*0.55*	1.04	*5.1*	*0.97*	2.07	*7.8*	*1.48*	5.3	*14.7*	*2.80*	23.1	*48.5*	*9.24*
		1.2	1.7		2.7	2.4		5.1	2.7		12.0	2.7		45.8	2.7
(32,808) 10	0.31	*2.1*	*0.51*	0.71	*3.6*	*0.87*	1.43	*5.5*	*1.33*	3.7	*10.4*	*2.52*	15.9	*34.5*	*8.36*
		0.9	1.2		1.9	1.7		3.6	1.9		8.5	1.9		32.6	1.9
(39,370) 12	0.21	*1.4*	*0.45*	0.49	*2.5*	*0.80*	0.98	*3.9*	*1.25*	2.5	*7.4*	*2.38*	10.9	*24.4*	*7.85*
		0.6	0.8		1.4	1.1		2.6	.13		6.1	1.3		23.1	1.3
(45,931) 14	0.13	*0.9*	*0.40*	0.31	*1.6*	*0.70*	0.62	*2.5*	*1.10*	1.6	*4.8*	*2.12*	6.9	*15.9*	*7.01*
		0.4	0.5		0.9	0.7		1.7	0.8		4.0	0.8		15.1	0.8
(52,493) 16	0.07	*0.4*	*0.24*	0.15	*0.9*	*0.54*	0.31	*1.3*	*0.79*	0.8	*2.5*	*1.51*	3.4	*8.4*	*5.08*
		0.2	0.2		0.5	0.4		0.9	0.4		2.1	0.4		8.0	0.4
(59,054) 18	0.05	*0.3*	*0.25*	0.11	*0.5*	*0.41*	0.22	*0.8*	*0.66*	0.6	*1.7*	*1.41*	2.5	*6.1*	5.05
		0.2	0.1		0.4	0.1		0.7	0.1		1.6	0.1		6.0	0.1
(65,616) 20	0	*0*	*0*	0	*0*	*0*	0	*0*	*0*	0	*0*	*0*	0	*0*	*0*
		0	0		0	0		0	0		0	0		0	0

Notes: (1) All rain rates are surface equivalent intensities.

(2) Distributions are all liquid below 4.5 km, mostly liquid 4.5-6.0 km, and nearly all ice above 7.0 km.

(3) Cloud precipitation water division is at D= 100 μm. Cloud water includes ice with melted diameter D<100 μm.

Table 2-6

Some Maximum LWC Data Points Reported by Various Authors

LWC ($g\ m^{-3}$)	Location	Reference	Method of Obtaining Data
60	Maryland	2.11 2.13	1 min record rainrate converted to LWC using Reference 2.10
44	Oklahoma	2.6	LWC directly measured by aircraft
29	Florida	2.8	LWC directly measured at ground level
28	Colorado	2.25	LWC directly measured by aircraft
23	"	"	"
22	Florida	2.8	LWC directly measured at ground level

Table 2-7

LWC Profile Used in the Weather Threat Study

(after Reference 2.14)

Altitude (km MSL)	Ratio of LWC to maximum LWC
0	1.00
2	1.00
4	1.00
6	1.00
8	0.76
10	0.54
12	0.38
14	0.25
16	0.13
18	0.10
20	0.00

Table 2-8

Size of the ARC Data Base

(The numbers below indicate the number of data points from each year.)

Year	Maximum Hail Reflectivity	Hailshaft Equivalent Diameter
1983	178	1255
1984	117	750
1985	119	863
Total	414	2868

Table 2-9

AIA RECOMMENDED RAIN AND HAIL CERTIFICATION CRITERIA FOR HIGH-BYPASS COMMERCIAL ENGINES

Hazard	Maximum Threat Quantity		Maximum Altitude	Ambient W/A Ratio	Test Duration
	10^{-8} Probability	*Cert. Recom.			
Rain	18.9 gm^{-3}	20 gm^{-3}	6100 m (20,000 ft.)	3.06%	3 min
Hail	9.5 gm^{-3}	10 gm^{-3}	4600 m (15,000 ft.)	1.37%	30 sec

* Recommended certification water levels increased 5% to provide margin for minimum quality engines.

Table 2-10

DEFINITION OF ENVIRONMENT WATER THREAT

Phase of Water	Data Source	Uncertainty	Operational Impact	Comments
Humidity	MIL STD 210C	Low	Low	Altitude lapse based on model
Rain	Published literature	Low	High	
Hail	AIA (ARC & GNEFA)	High	High	From radar data

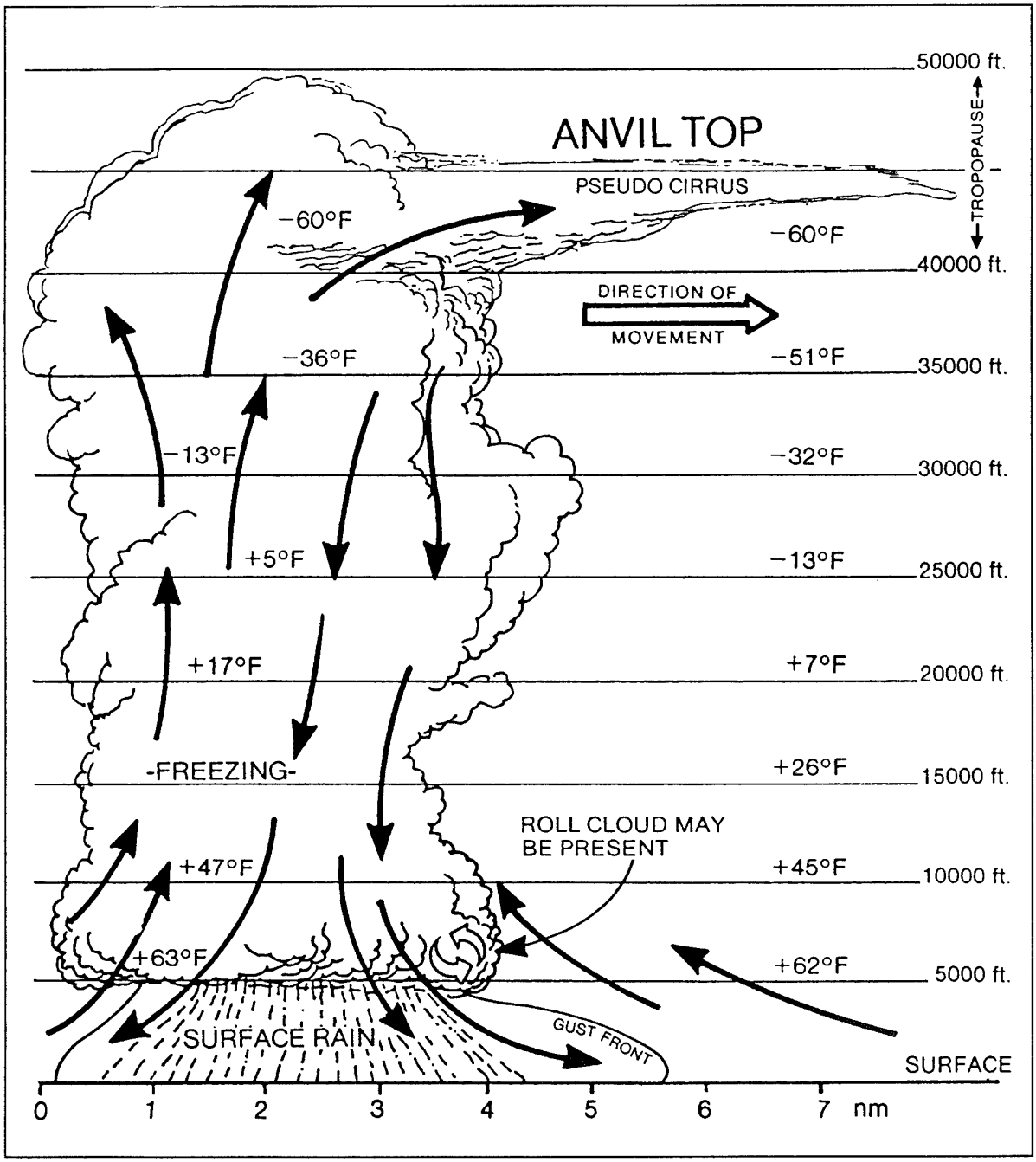

Figure 2-1

A Mature Thunderstorm Cell
(Courtesy of the United States Power Squadron)

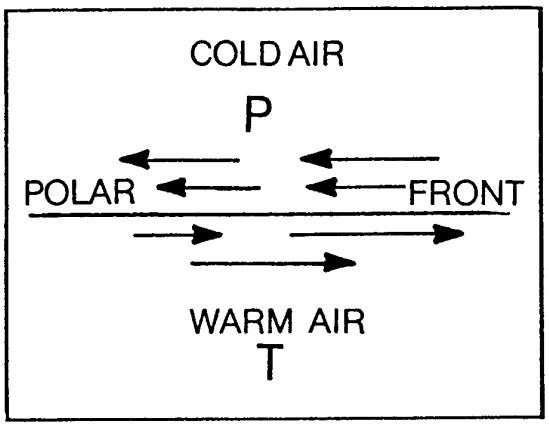

Figure 2-2(a) Polar Front

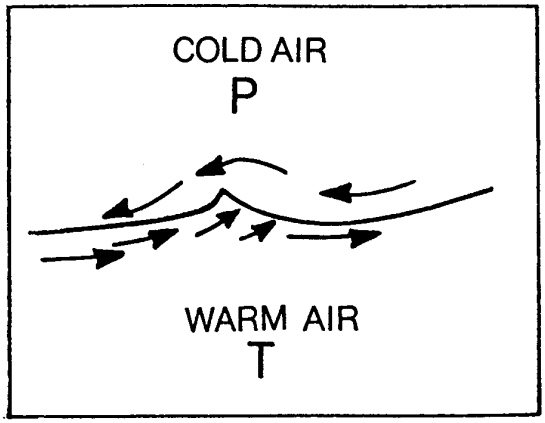

Figure 2-2(b) Cyclogenesis

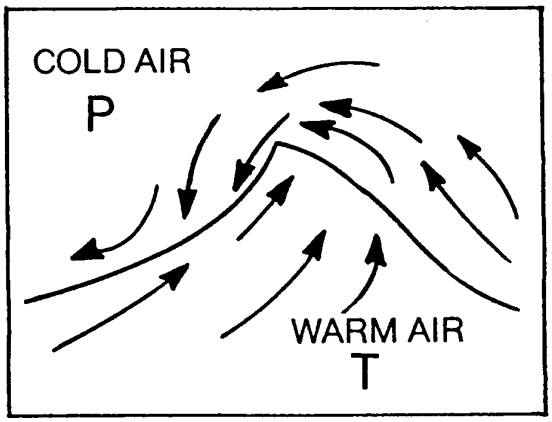

Figure 2-2(c) Development

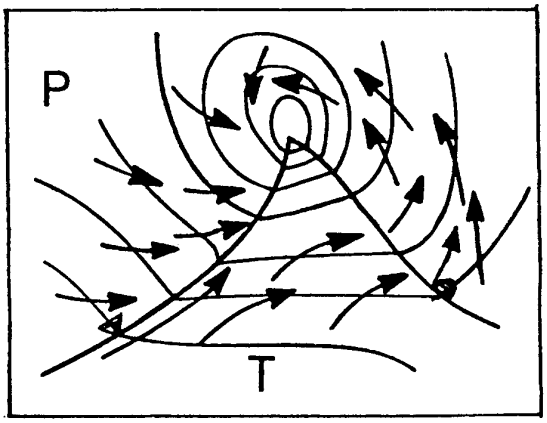

Figure 2-2(d) Mature Cyclone

Figure 2-2

Development of an Extratropical Cyclone
(Courtesy of the United States Power Squadron)

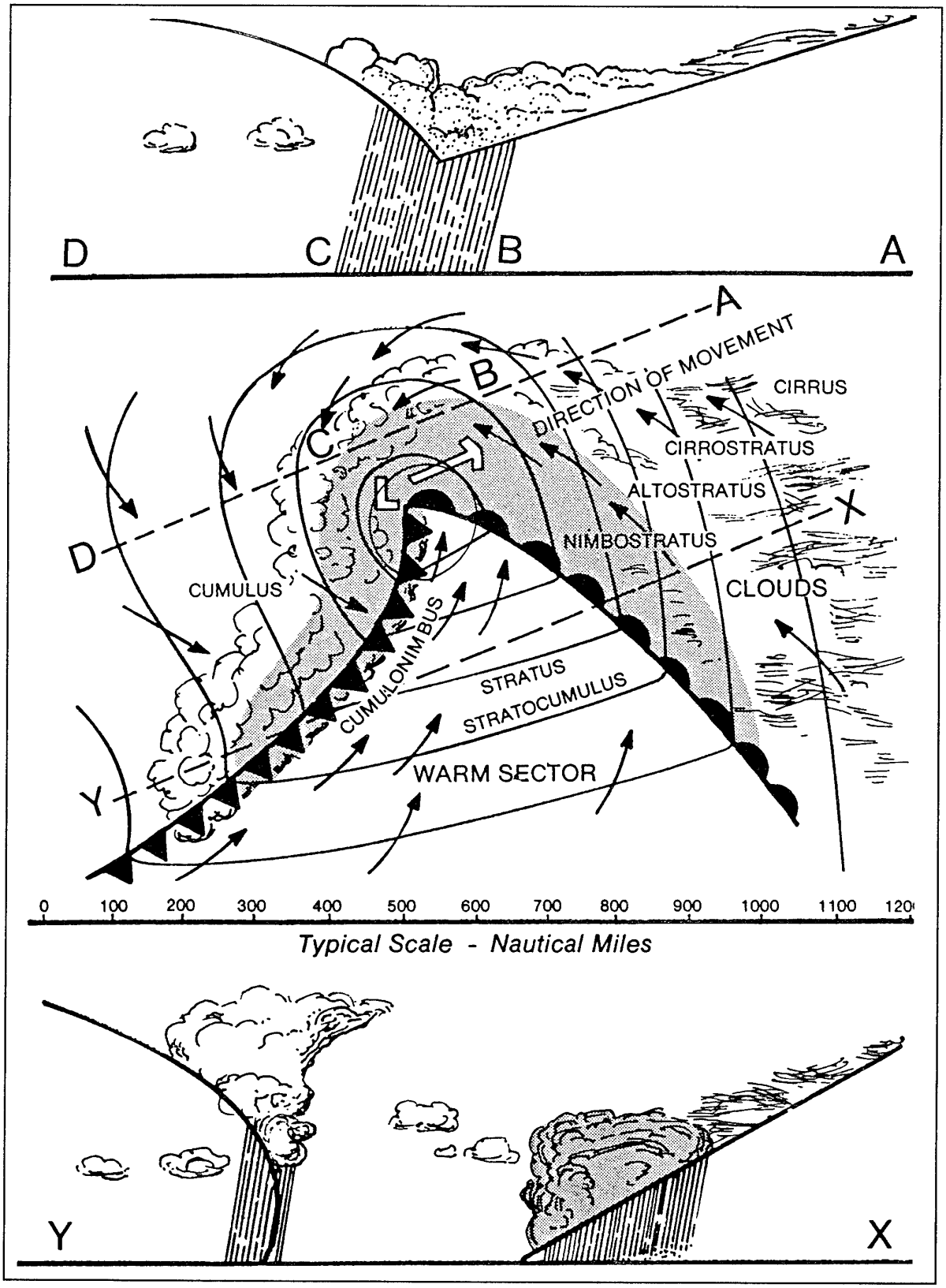

Figure 2-2(e) Guide to a Mature Extratropical Cyclone

Figure 2-2 Development of an Extratropical Cyclone
(Courtesy of the United States Power Squadron)

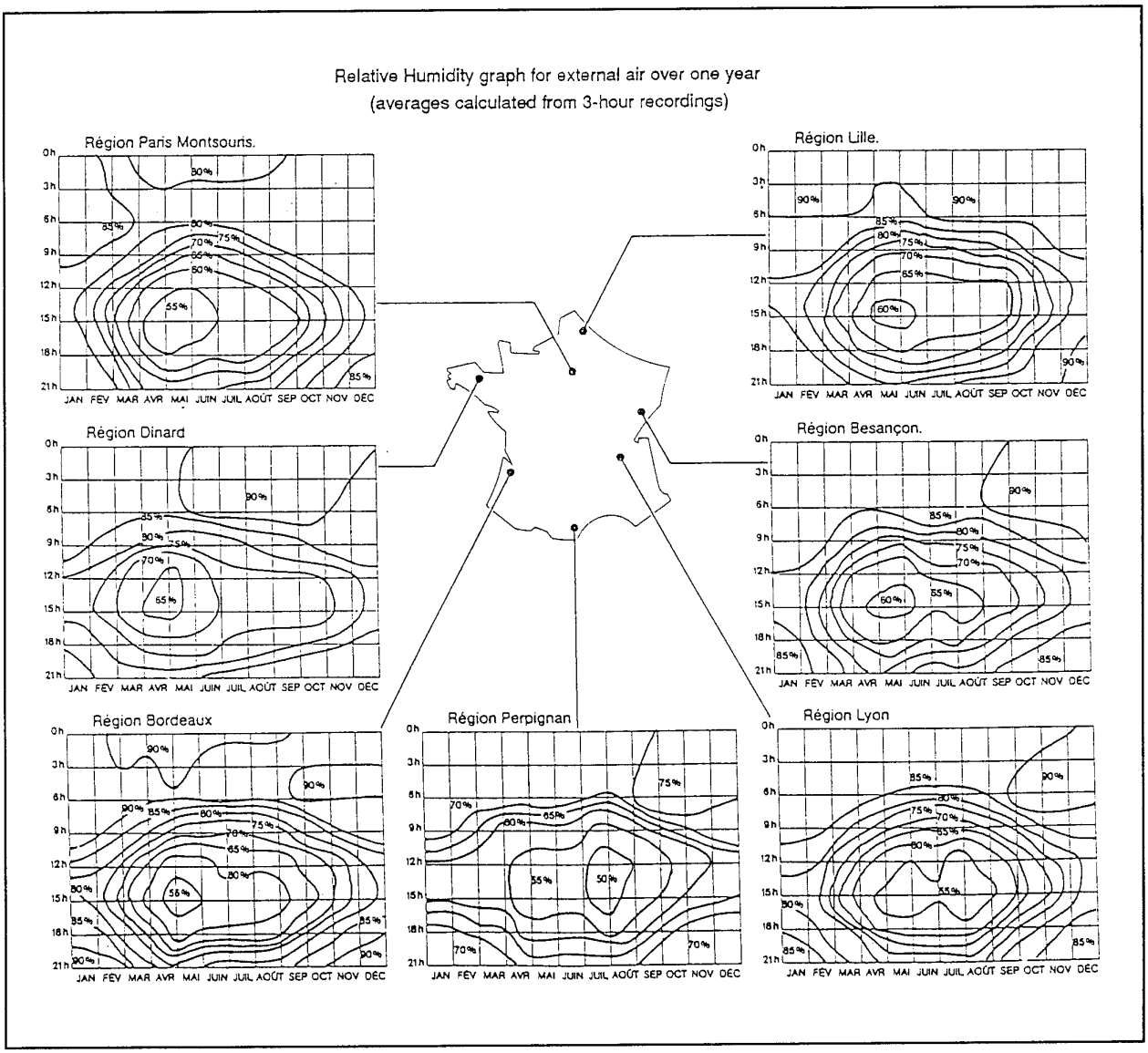

Figure 2-3

Annual Variation of Relative Humidity Levels for Seven Regions of France

(The analysis of Relative Humidity reveals that, for all areas, the average annual figure is always greater than 50 % and can reach 95 % or even 100 % (fog!).)

(courtesy of "MUNSTERS")

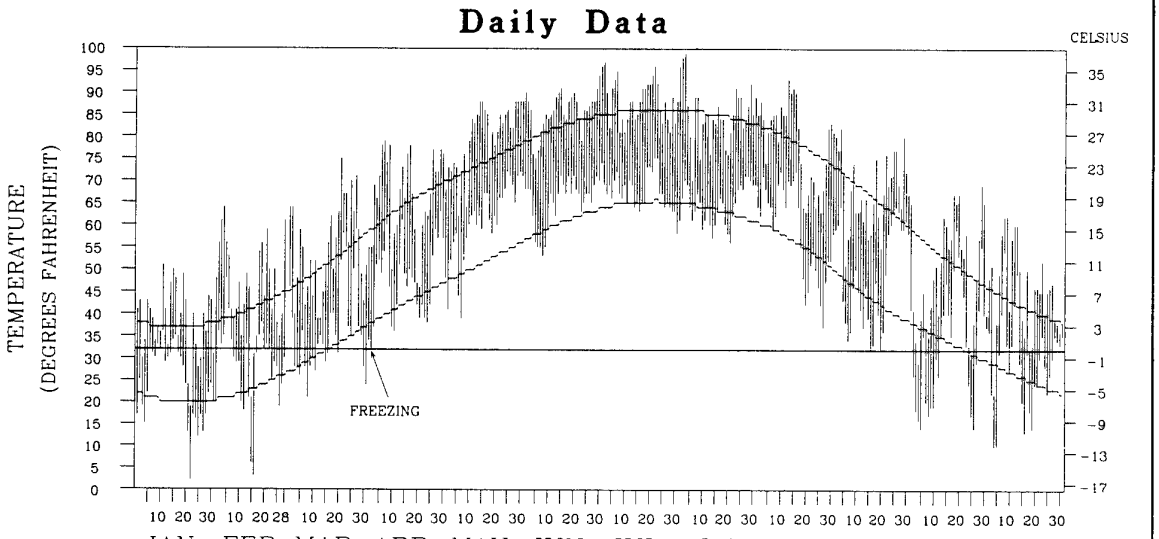

NORMALS, MEANS, AND EXTREMES

CINCINNATI. (GREATER CINCINNATI AIRPORT) OHIO

LATITUDE: 39°03'N LONGITUDE: 84°40' W ELEVATION: FT. GRND 869 BARO 888 TIME ZONE: EASTERN WBAN: 93814

	(a)	JAN	FEB	MAR	APR	MAY	JUNE	JULY	AUG	SEP	OCT	NOV	DEC	YEAR
RELATIVE HUMIDITY (%)														
Hour 01	29	75	74	72	71	77	80	83	84	82	78	75	76	77
Hour 07 (Local Time)	29	79	78	77	76	80	82	85	88	88	83	80	80	81
Hour 13 (Local Time)	29	67	64	59	53	55	56	57	57	57	55	63	69	59
Hour 19	29	69	65	60	55	58	59	61	63	66	65	68	72	63
PRECIPITATION (inches):														
Water Equivalent														
-Normal		3.13	2.73	3.95	3.58	3.84	4.09	4.28	2.97	2.91	2.54	3.12	3.00	40.14
-Maximum Monthly	44	9.43	6.72	12.18	7.19	9.48	7.36	8.36	7.71	8.61	8.60	7.51	7.90	12.18
-Year		1950	1955	1964	1970	1968	1977	1962	1982	1979	1983	1985	1990	MAR 1964
-Minimum Monthly	44	0.57	0.25	1.14	1.04	1.13	0.95	1.18	0.31	0.18	0.25	0.43	0.51	0.18
-Year		1981	1978	1960	1971	1964	1965	1951	1953	1963	1963	1949	1976	SEP 1963
-Maximum in 24 hrs	44	4.33	2.84	5.21	2.72	3.71	3.45	4.28	3.12	4.54	4.47	3.36	2.96	5.21
-Year		1959	1990	1964	1950	1956	1974	1988	1957	1979	1985	1948	1948	MAR 1964
Snow,Ice pellets,hail														
-Maximum Monthly	44	31.5	13.3	13.0	3.7	0.2	0.0	T	0.0	0.0	5.9	12.1	12.5	31.5
-Year		1978	1971	1968	1977	1989		1991			1989	1966	1989	JAN 1978
-Maximum in 24 hrs	44	8.1	9.3	9.8	3.6	0.2	0.0	T	0.0	0.0	5.0	9.0	7.5	9.8
-Year		1978	1966	1968	1977	1989		1991			1989	1966	1990	MAR 1968

Figure 2-4

Annual Variation of Temperature and Precipitation for Cincinnati, Ohio
(Source: US National Climatic Data Centre)

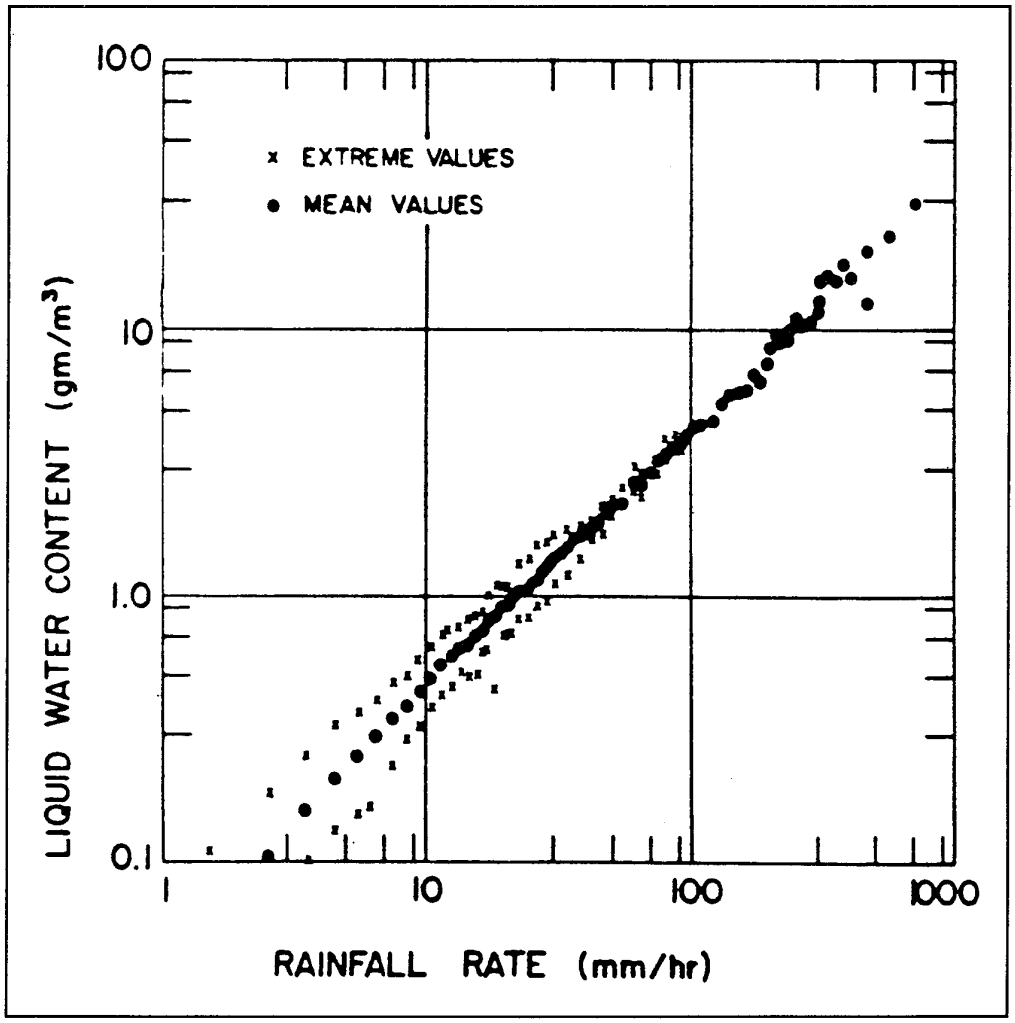

Figure 2-5
Example of a Scatter Plot of Liquid Water Content versus Rainfall Rate
for Miami
(from Reference 2.9)

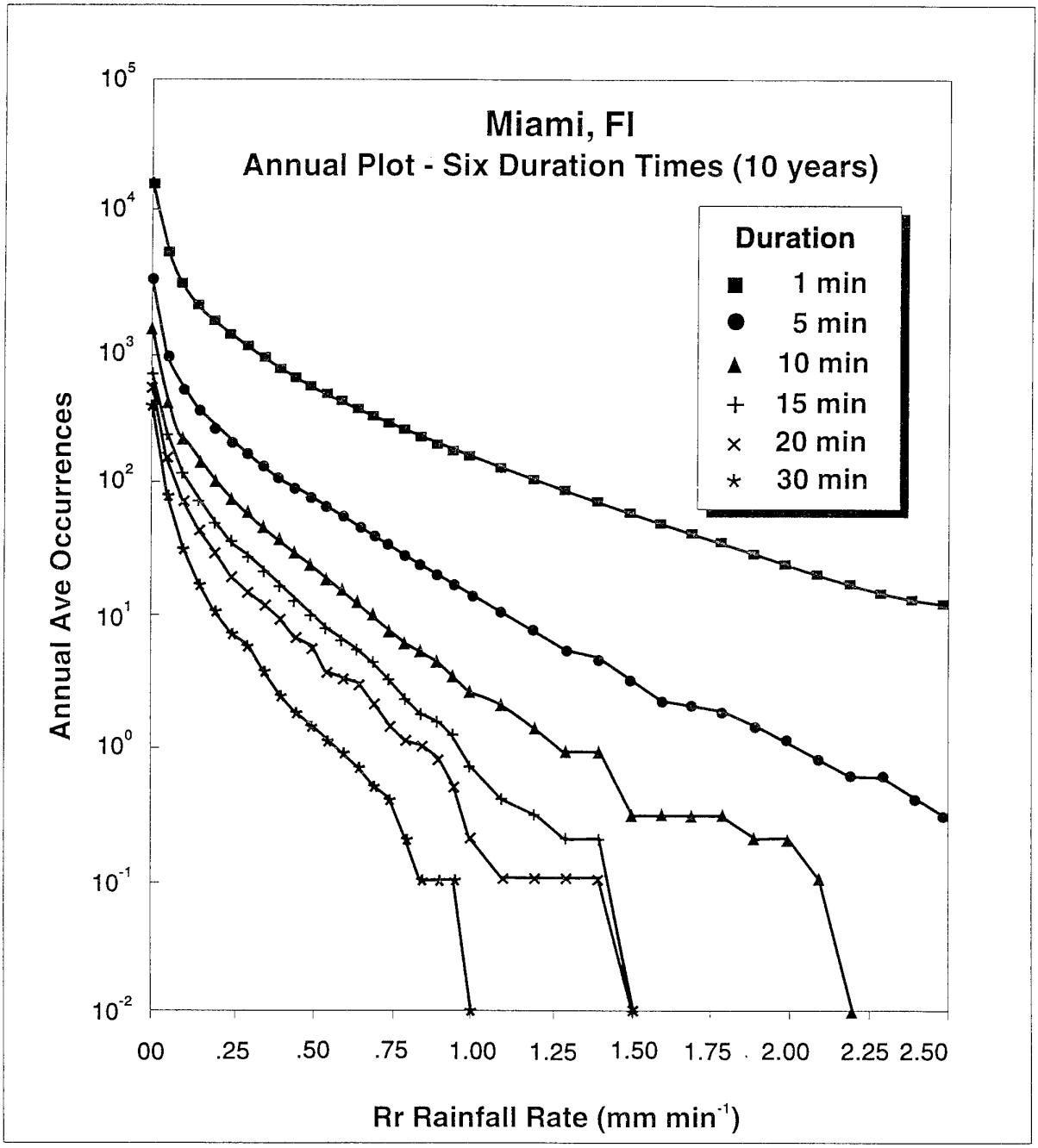

Figure 2-6

Annual Average Number of Occurrences of 1-min. Rain Rates for Six Duration Times at Miami, Florida. Rain Rates are those Equalled or Exceeded during Each Minute of the Specified Duration (from Reference 2.4)

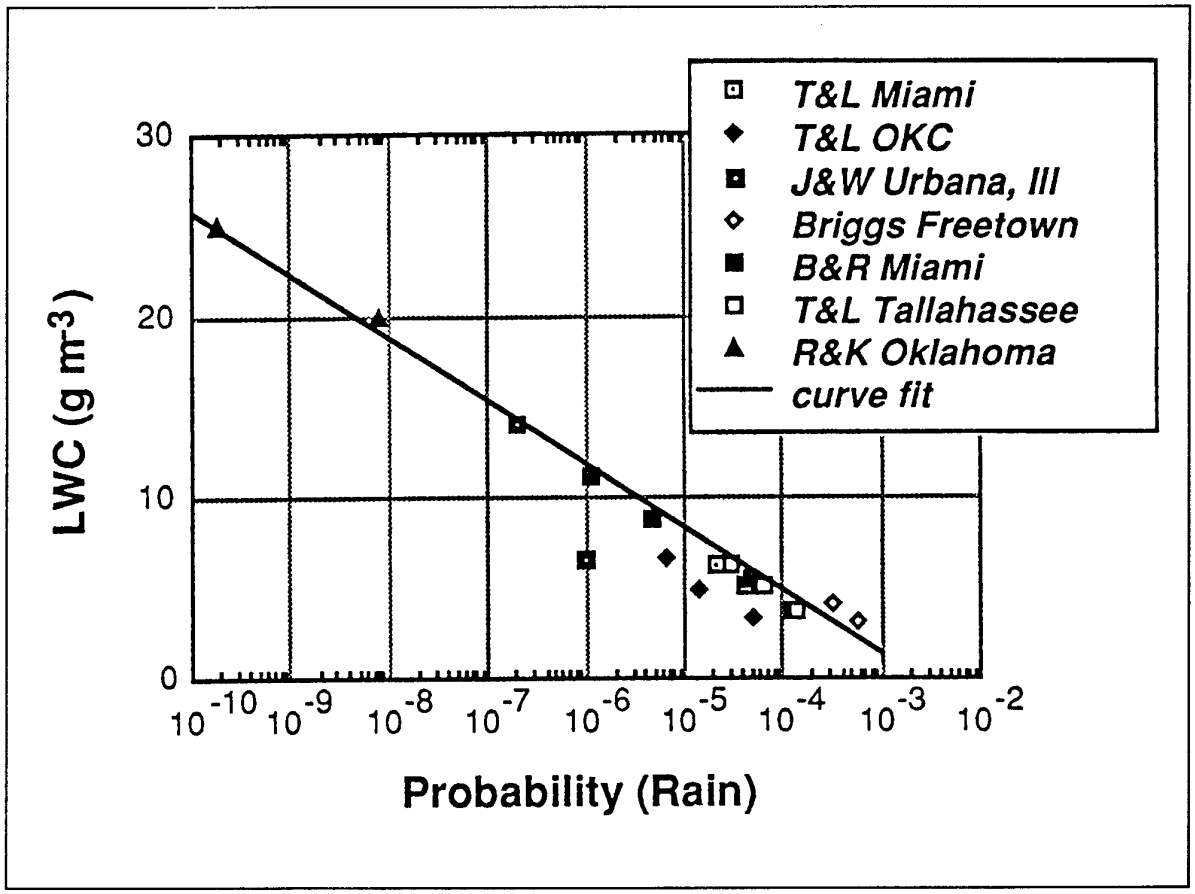

Figure 2-7

Probability of a given LWC Value being Equalled or Exceeded at a Point at any Random Instant in a Worst Case Location for Each Probability Level. Data points, as described in the text, are indicated. (Reference 2.3)

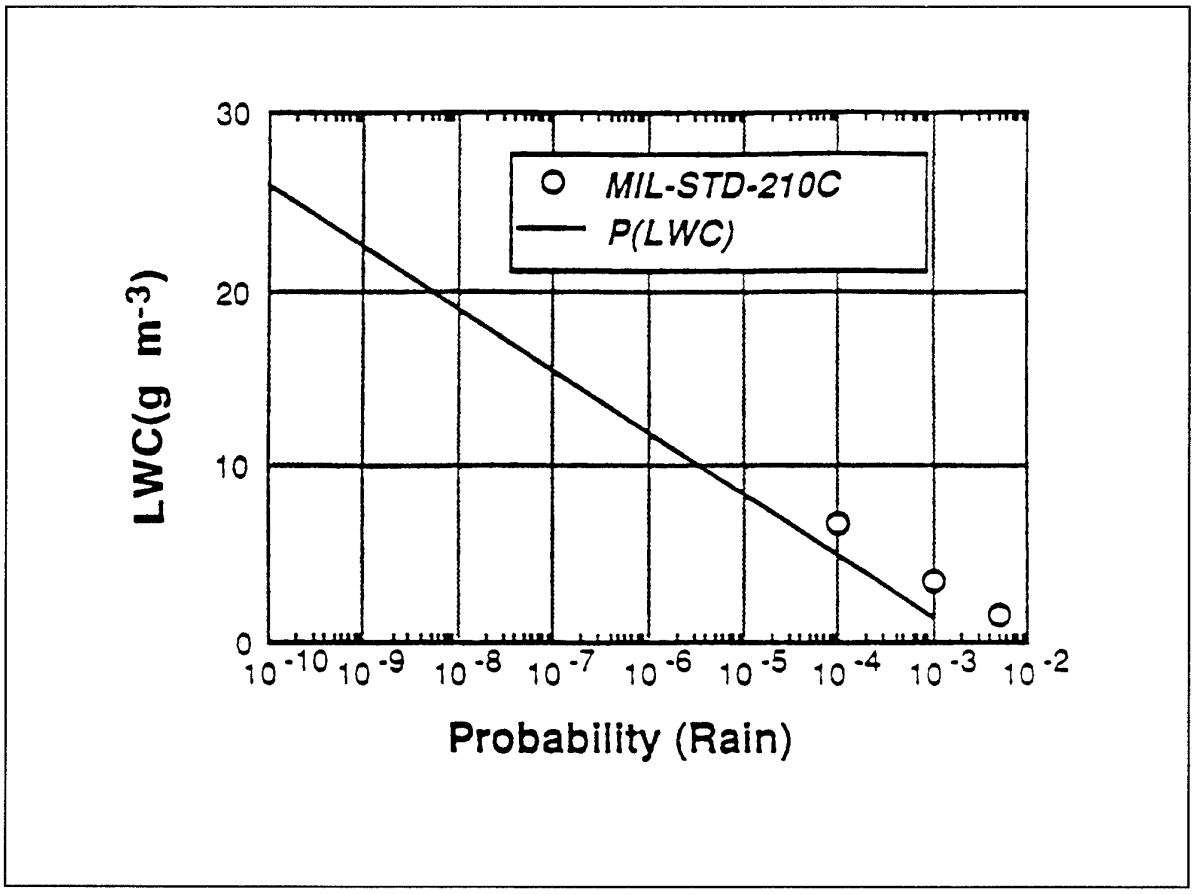

Figure 2-8

Rain Curve as in Figure 2-7 with the 0.5%, 0.1%, and 0.01%of time worst case, worse month data points from Reference 2.2

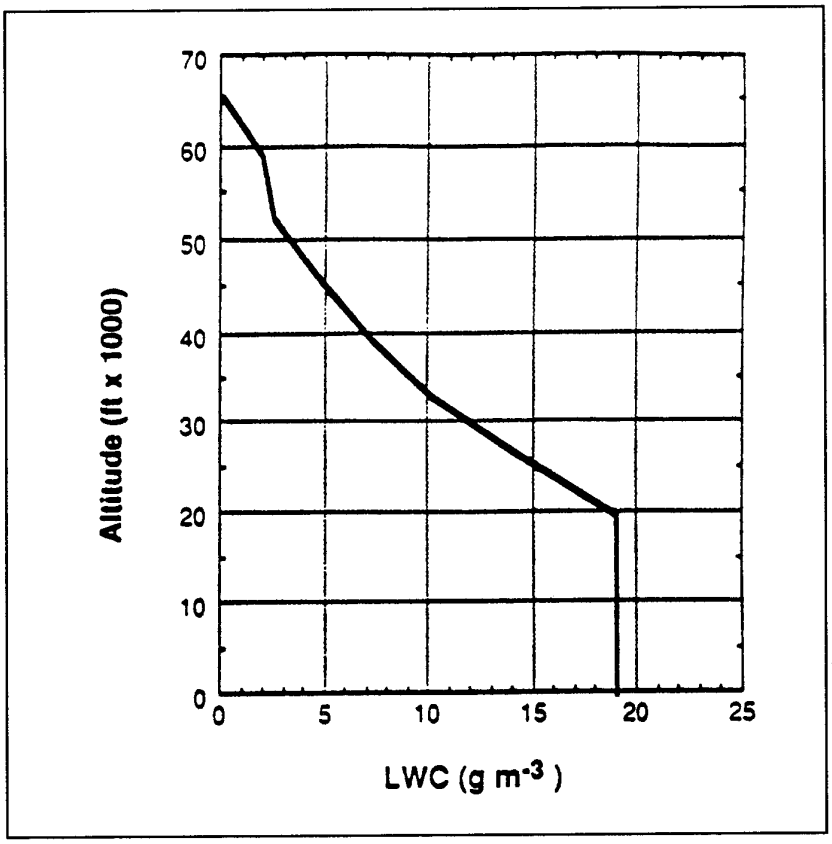

Figure 2-9

Vertical Profile of LWC for the 10^{-8} Probability LWC of 18.9 g m^{-3}

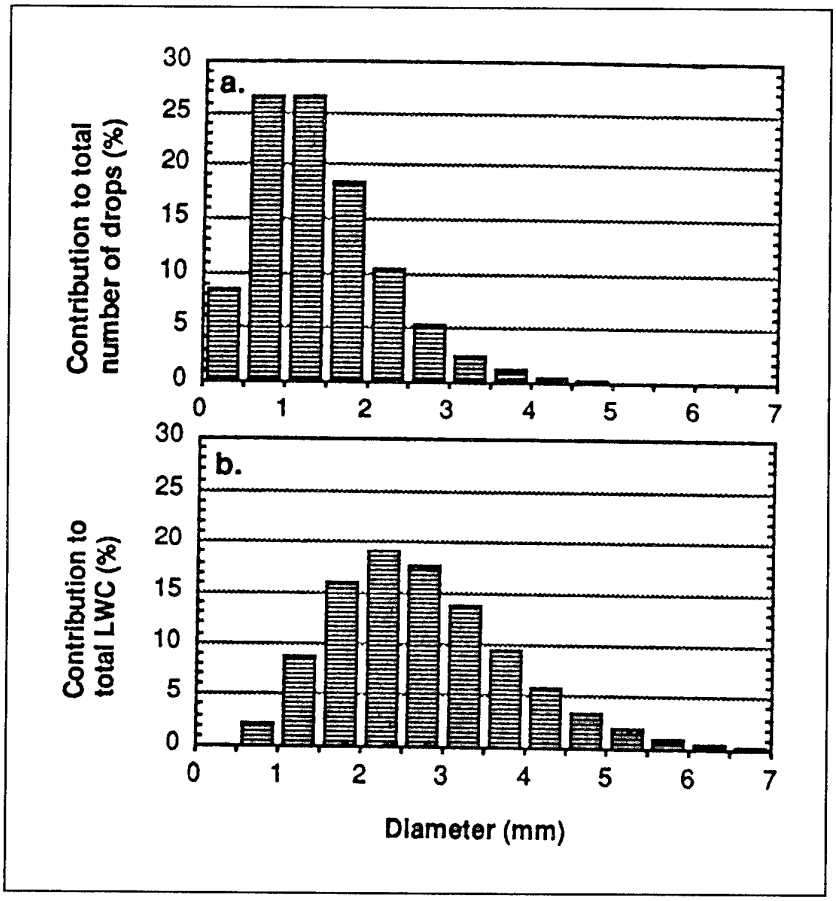

Figure 2-10

Raindrop Size Distribution
(a) Contribution to the Total Number of Raindrops from each 0.5 mm Diameter Interval
(b) Contribution to the Total LWC from each 0.5 mm Diameter Interval
(from Reference 2.14)

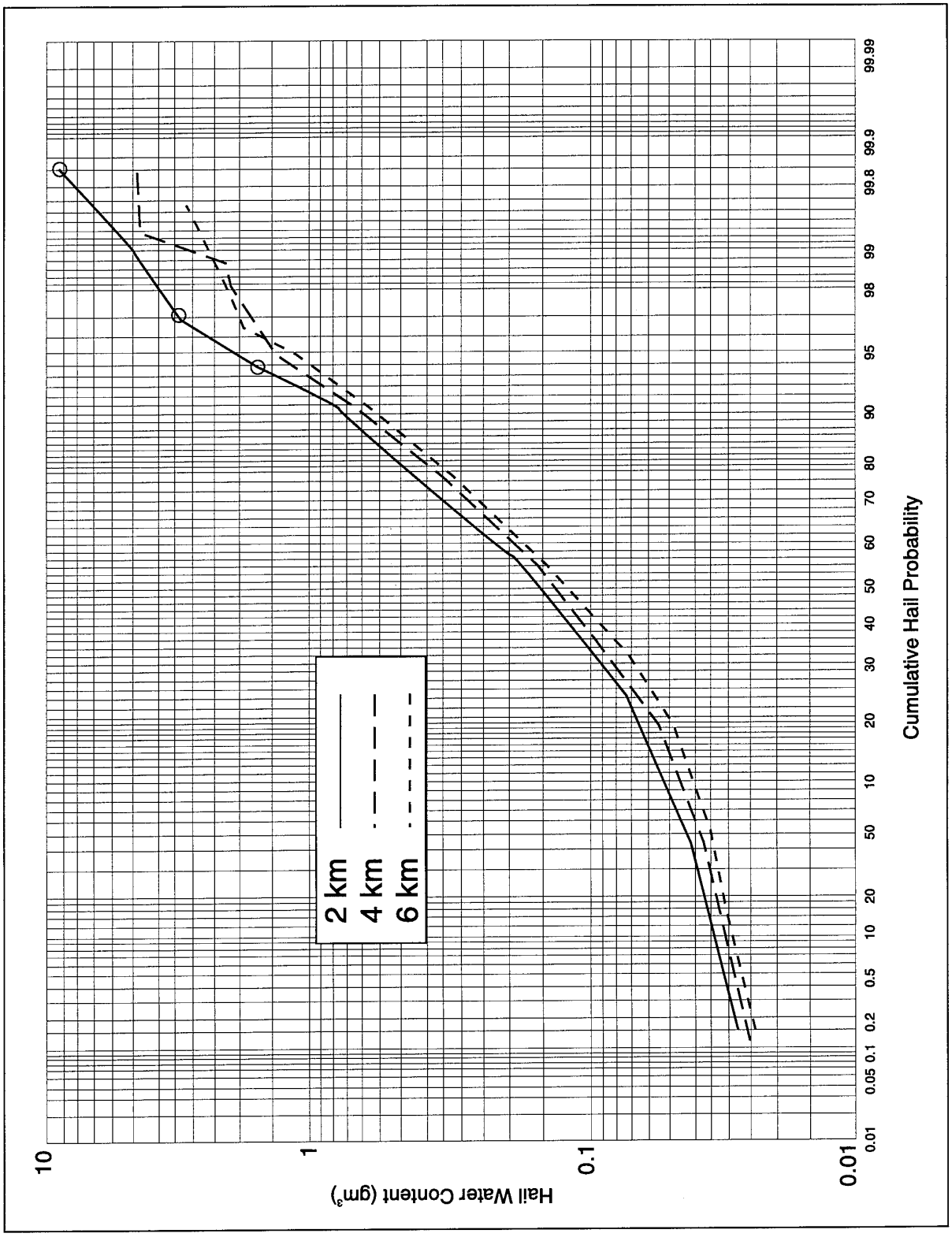

Figure 2-11

Cumulative HWC Distributions at 2, 4, and 6 km Above Ground Level, Derived from ARC Reflectivity Data

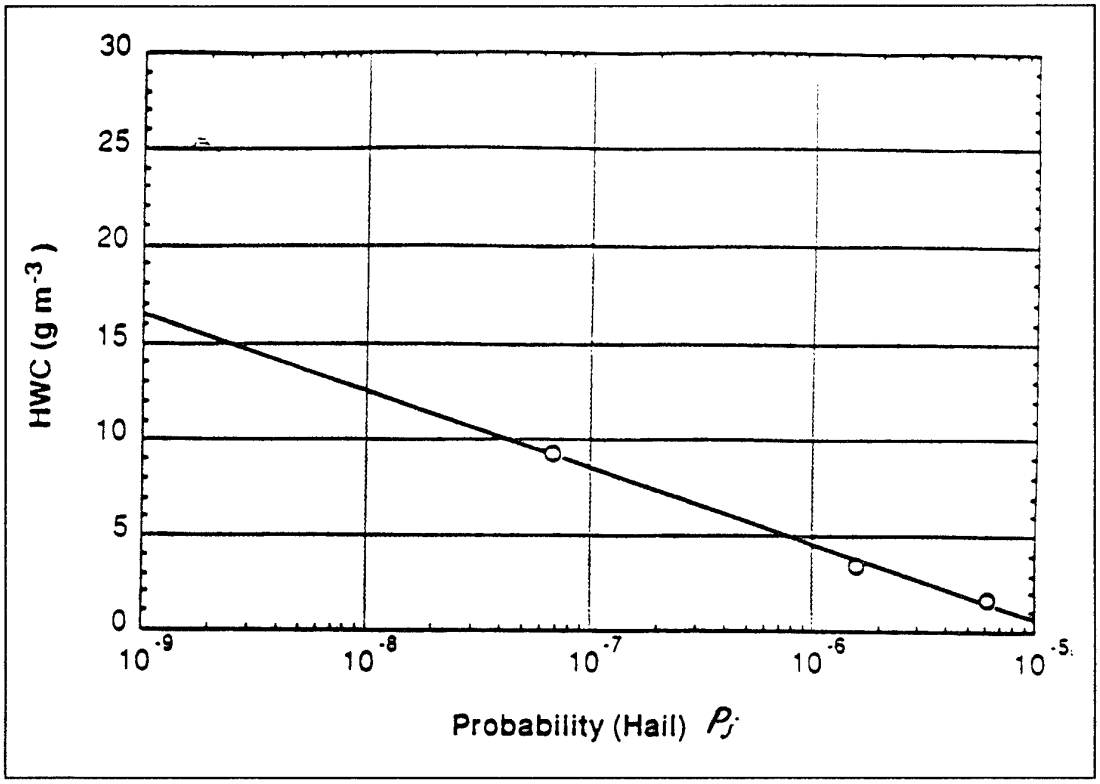

Figure 2-12

Boeing-derived Hail Curve with the Three Data Points used to Define the Curve Fit
(Reference 2.3)

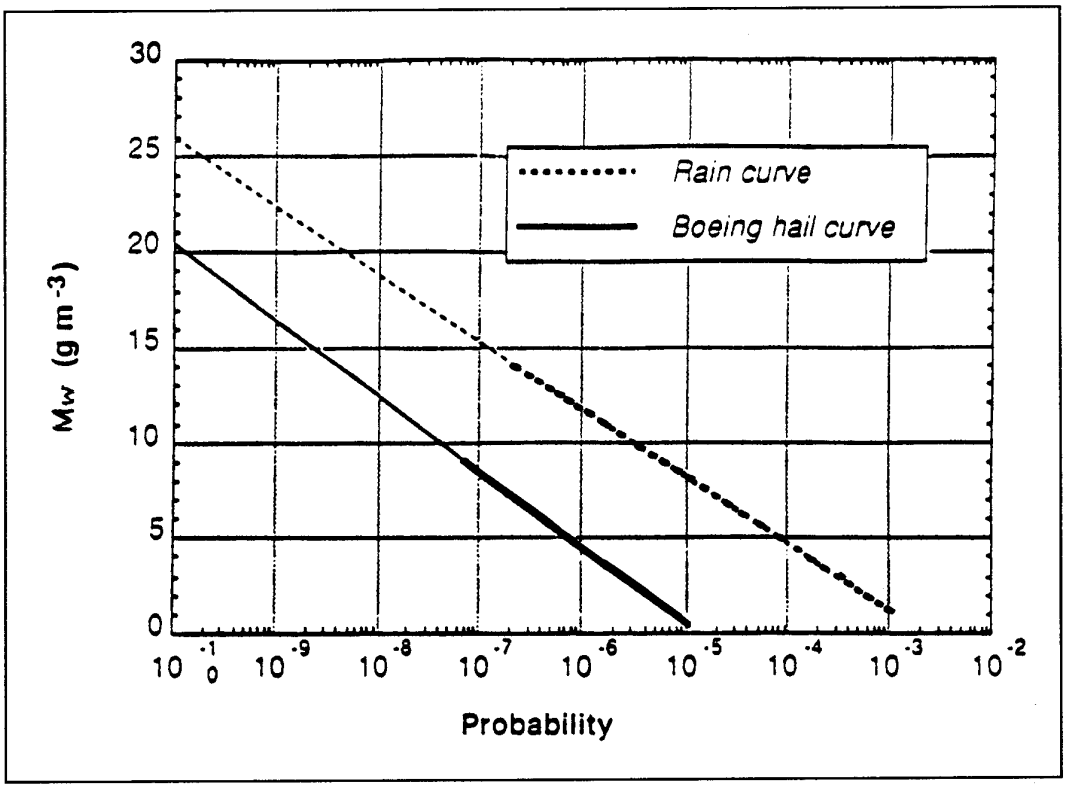

Figure 2-13

Comparison of the Rain Curve from Figure 2-8 and the Hail Curve from Figure 2-12.
Thin Portions of the Curves Indicate Extrapolated Data
(Reference 2.3)

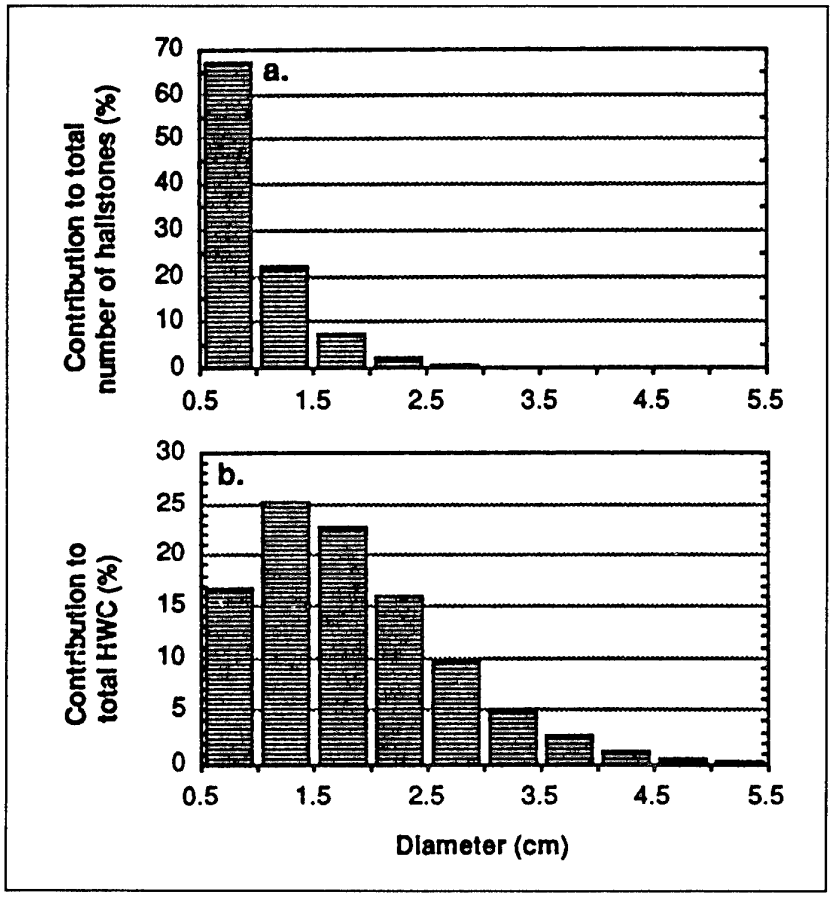

Figure 2-14

Hailstone Size Distribution
(a) Contribution to the Total Number of Hailstones from each 0.5 cm Diameter Interval
(b) Contribution to the Total HWC from each 0.5 cm Diameter Interval
(Reference 2.3)

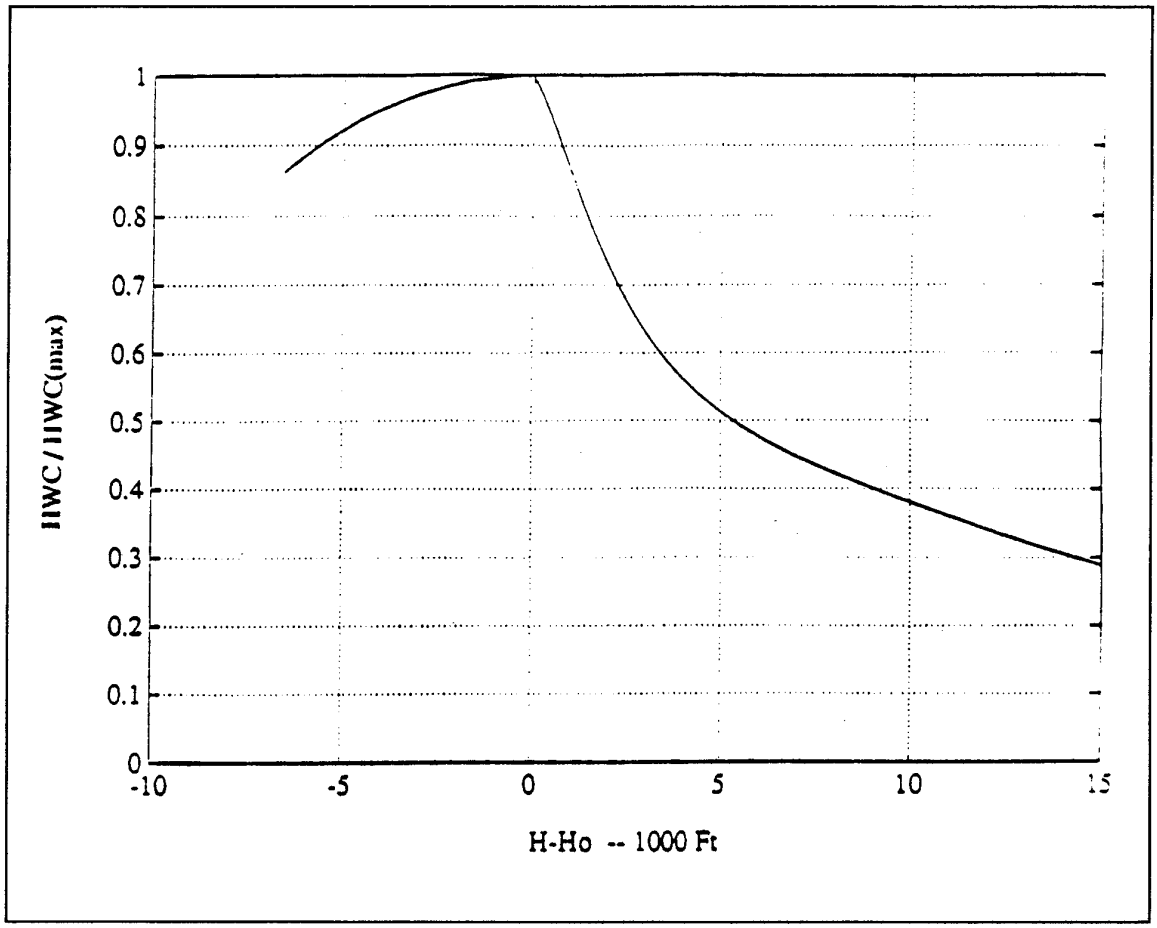

Figure 2-15

Normalized HWC as a Function of Height H above the Freezing Level Height Ho
(Reference 2.3)

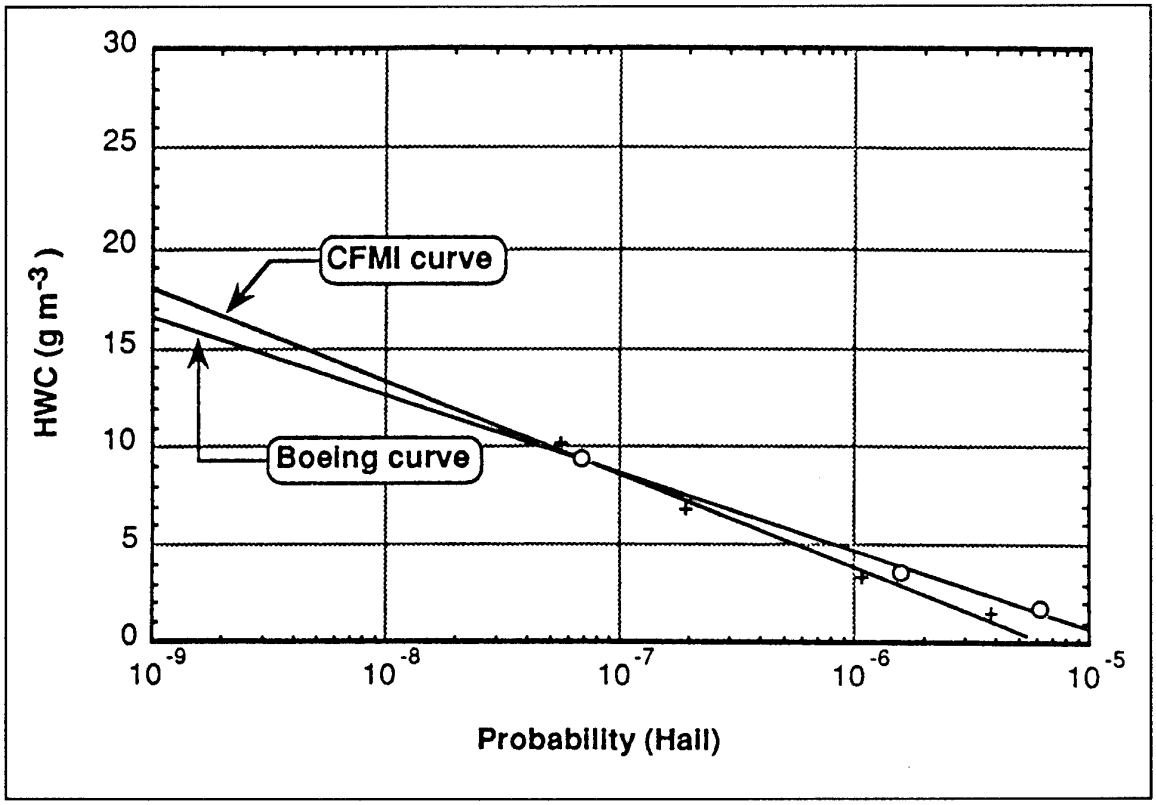

Figure 2-16

Comparison of the Boeing-Derived and CFMI-Derived Hail Curves
(Reference 2.3)

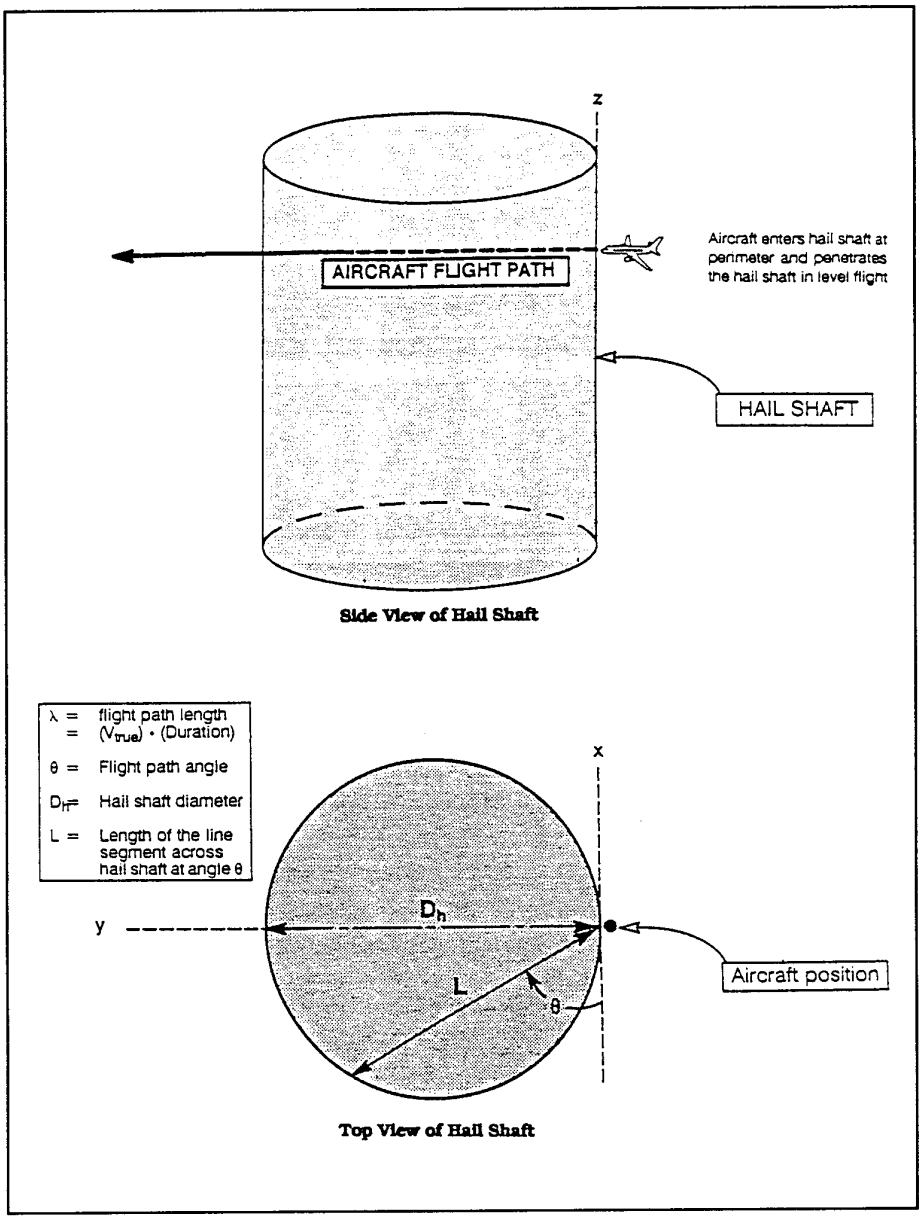

Figure 2-17

Aircraft Flight Path Through a Hail Shaft
(Reference 2.3)

2.17(a) Side View of Hail Shaft - This figure shows the aircraft entering a hail shaft The hail shaft is represented by a cylinder of constant HWC. The aircraft enters the side of the shaft at an angle relative to the tangent.

s-17(b) Top View of the Hail Shaft - This figure shows a top view of the hailshaft in in Figure 2-17(a). The aircraft passes through the hail shaft at an angle θ. L is the length of the line segment across the hail shaft at the angle θ. The hail shaft diameter is D_h.

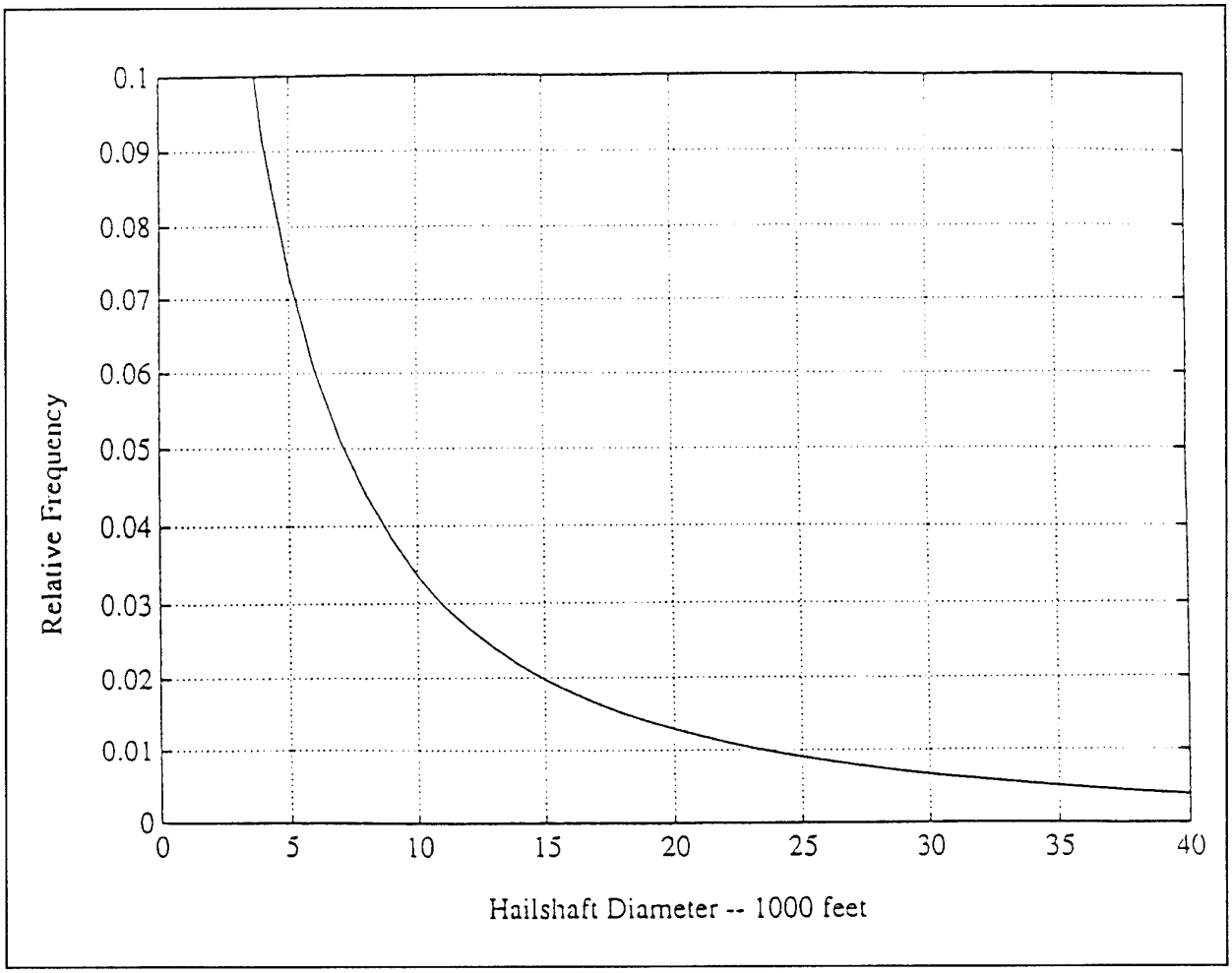

Figure 2-18

Relative Frequency Distribution of Equivalent Hailshaft Diameters Derived from Data Provided by ARC. The ARC Frequency Distribution was Derived from Dual-Polarization Radar Measurements
(Reference 2.3)

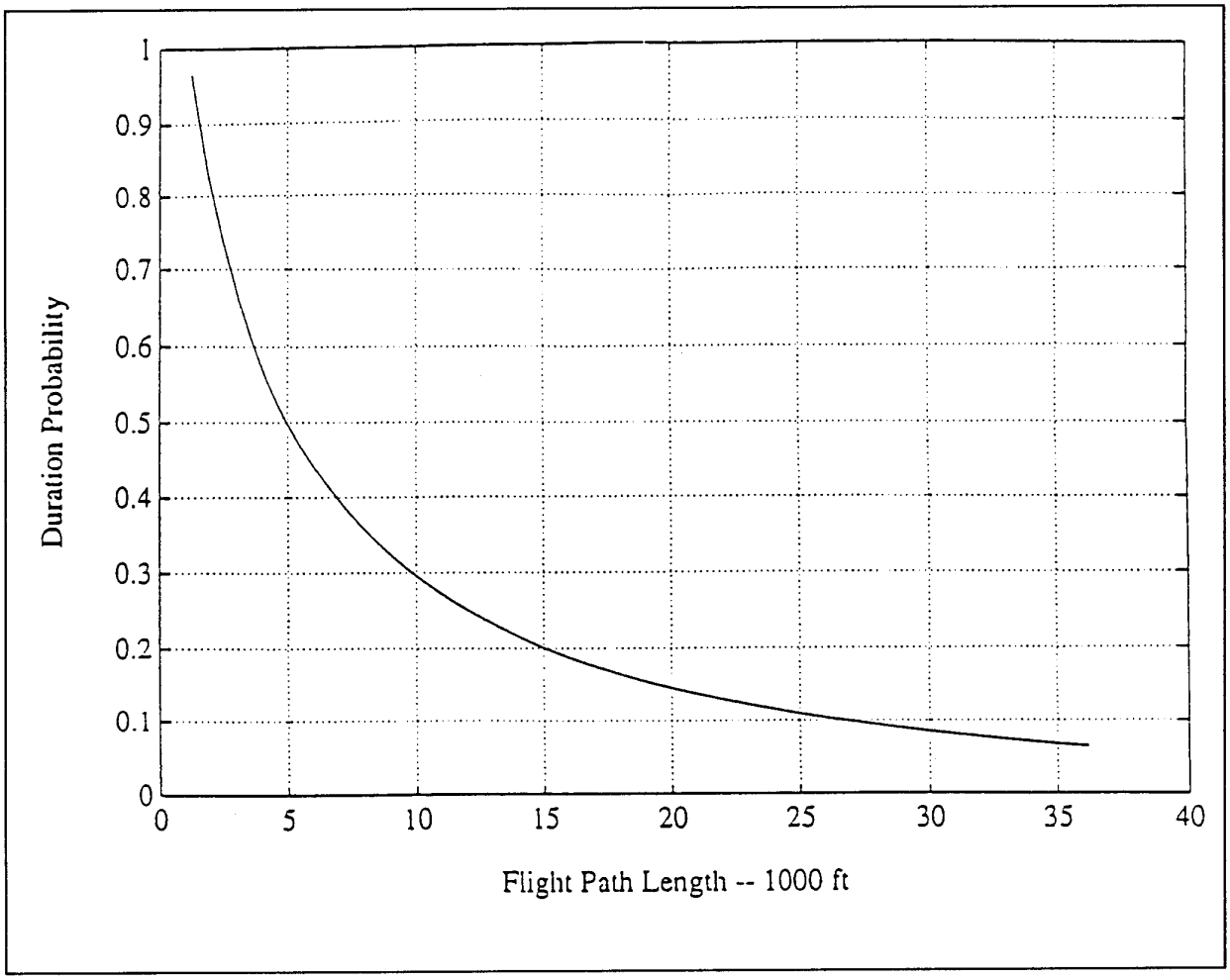

Figure 2-19

Duration Probability as a Function of Flight Path Length, from a Numerical Integration of Equation 2-23
(Reference 2.3)

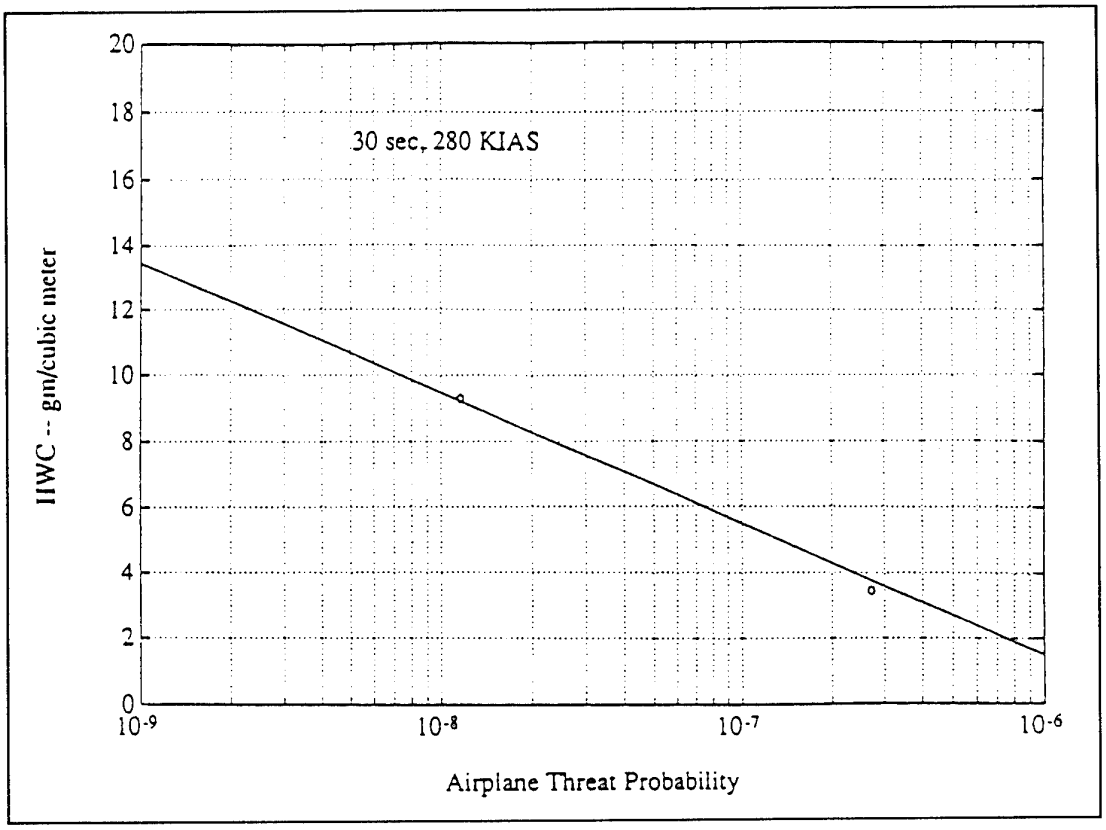

Figure 2-20

ARC Airplane Threat Curve for a 30 second Duration at 280 KIAS, 0°C T_{amb}.
This curve is applicable at an altitude of 4570 m (15,000 ft)
(Reference 2.3)

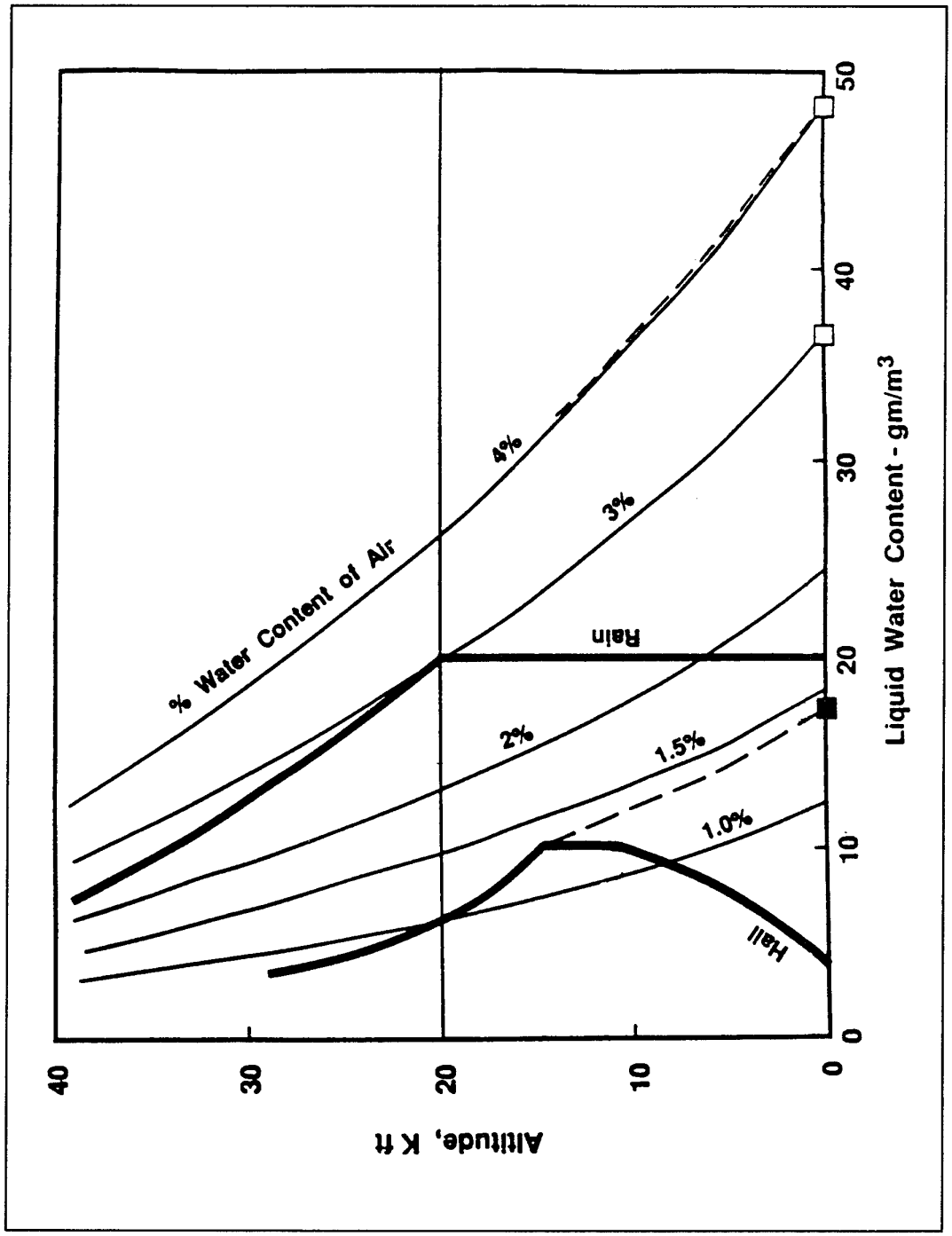

Figure 2-21

AIA Rain/Hail Requirements and Loci for Certification Tests

3. GASEOUS HUMIDITY: EFFECT ON COMPONENTS AND ENGINE PERFORMANCE [1]

3.1 INTRODUCTION

From the early beginnings of gas turbines, it was recognized that humidity in the inlet air could potentially affect their performance. Since, however, reliability and operability received more attention than performance, humidity effects were considered to be of secondary importance and were usually neglected in test data evaluation. With the commercial competition and the refinement of engine performance, driven by increasing fuel costs, attention has been focussed on humidity, as it shifts component and total engine performance curves.

To illustrate the order of magnitude of the effect of gaseous humidity on the principal engine performance parameters, Table 3-1 summarizes some parameter variations, referenced to dry conditions, for two moist ambient conditions and three engine operating conditions:

ambient conditions:

(i) moderate condition:
297 K, 75% RH,
war (water to dry air ratio) = 0.0143
(100 grains water /lb_mdry air)

(ii) severe condition:
303.15 K (ISA + 15 K), 100% RH,
war = 0.0272

engine operating conditions:

(i) constant LP corrected speed $N/\sqrt{(\gamma RT_s)}$

(ii) constant LP mechanical speed

(iii) constant EPR

In open cycle gas turbine engines, the processes of compression, combustion and expansion involve, as working fluid, a mixture composed of ambient air (dry air plus water vapour) and combustion gases. The performance of the engine components will be affected by the characteristics of the working fluid, and so by the presence of atmospheric water. The vapour phase of water can be present in the working fluid under certain conditions.

For fluid temperatures higher than 647.3 K, water exists only in the form of vapour and condensation cannot occur. At lower temperature levels, water vapour will be present, for equilibrium conditions, when the water vapour partial pressure is lower than the saturation pressure. The maximum water vapour concentration will be achieved when the partial pressure is equal to the saturation pressure. In non-equilibrium conditions, supersaturated states can occur.

When humid air is ingested into an engine component without condensation, its performance is altered, compared to that related to dry air, due to changes in

a) molecular weight,
b) the ratio of specific heats γ of the working fluid.

The contribution of the mixture molecular weight variation can be taken into account in a fundamental way and this effect on the engine component characteristics will constitute the major part of the correction.

The other remaining effect, generated by the variation of the specific heat ratio γ caused by the water vapour concentration, is actually part of the wider problem of taking into account the effect of the γ changes. The problem arises, on a larger scale, when transposing a component map measured on the partial test bench to the estimated characteristics map of the same component mounted on an engine, considering the range of supply conditions.

Transposing a component characteristic constitutes a real problem for the following reasons:

- From fundamental fluid mechanics, it is evident that complete fluid similarity would be very constraining. By considering all the physical equations which govern the flow, four conditions must be met in order that two flow patterns are similar:
  identity of Mach number
  identity of Reynolds number
  identity of Prandtl number
  identity of ratio of specific heats γ.
  It is impossible, in practice, to satisfy all these identities simultaneously. Simplifications in analyses must be made to get at least approximately similar flow patterns.
- It is a common practice to develop a thermodynamic model of the component (compressor, turbine), considered as a whole

[1] Tables and Figures for Chapter 3 begin on page 3-24

system. The component characteristic map is expressed by means of corrected parameters which include simplifications and approximations in order to reflect the various operating conditions.

This chapter, devoted to gaseous humidity, deals successively with the following items:

- description of the properties of the fluids involved,
- expression of the engine component characteristics,
- consequences on the engine performance.

3.2 FLUID PROPERTIES

3.2.1 Basic Effects

(i) Wet and dry air

The normal ambient fluid entering a gas turbine, both for dry air and air with gaseous humidity, consists of a mixture of gaseous constituents including nitrogen N_2, oxygen O_2, gaseous water H_2O, carbon dioxide CO_2, and argon Ar. Very small amounts of other constituents below a mass fraction of $2 \cdot 10^{-5}$ can be ignored for performance considerations (see definition of standard air, page xv, or Reference 3.1).

As the ingested air passes through the engine, the composition changes due to combustion with the injected fuel resulting in the addition of, mainly, CO_2 and H_2O.

By definition, dry air contains no H_2O, whereas humid air contains gaseous water, the amount depending on the degree of saturation and the ambient temperature. Humid air results in a higher amount of gaseous water throughout the engine, since starting with a water content at the engine inlet the water content downstream of the combustion chamber will be higher too, compared with combustion using dry air.

(ii) Fluid parameters affecting performance

The fluid parameters of humid air which have the largest effect on the performance of gas turbine engines are the gas constant R and the isentropic exponent γ (or, alternatively, the specific heat at constant pressure). These quantities are related to each other:

$$c_p = \frac{\gamma}{\gamma - 1} R \qquad 3\text{-}1$$

Since γ is a non-dimensional parameter, it has been preferred over expressions with c_p in most of the formulas of this chapter.

Other fluid parameters describing friction or heat transfer have a much smaller effect on gas turbine performance and are not considered here, as the variation with humidity is estimated to be negligible.

(iii) Variation of gas constant with humidity

The gas constant R of a single constituent, or of a mixture, is directly related to the universal gas constant $\Re$ and the molecular weight, M, according to:

$$R = \frac{\Re}{M} \qquad 3\text{-}2$$

The gas constant of a mixture can be obtained as the mass-averaged value of the gas constant of the constituents. This gives for the gas constant of a mixture

$$R_{mix} = \sum x_c \, R_c \qquad 3\text{-}3$$

where x_c is the mass fraction of a constituent ($\Sigma x_c = 1$). For standard dry air (page xv), the gas constant R = 287.05 J/(kg K). Since the gas constant of H_2O is as high as R = 461.5 J/(kg K), the gas constant of an air mixture with gaseous humidity is higher than that of dry air, depending on the fraction of H_2O.

Combustion generally varies the molecular weight and the gas constant, depending on the combustion products and, hence, on the fuel composition. For a fuel with 1.93 hydrogen/carbon (H/C) atom ratio, CO_2 and H_2O are produced in a ratio which gives a molecular weight and, therefore, gas constant closely the same as for dry air. Most aircraft kerosine fuels come fairly close to this composition, allowing an assumption of no change in gas constant due to combustion. When an engine is ingesting humid air, a change in gas constant due to combustion may also be neglected, but, due to the higher gas constant from the beginning, the gas constant downstream of the combustor is higher than with dry air at the inlet (Figure 3-1). The higher gas constant of humid air results in a lower density at a given pressure and temperature.

(iv) Isentropic exponent

The isentropic exponent is defined primarily by the number of atoms in a molecule, but it is affected also by the modes of excitation and, therefore, by the temperature. Air is a mixture of, principally, diatomic

gases resulting in an isentropic exponent $\gamma = 1.4$ at ambient temperatures. Since gaseous water, with tri-atomic molecules, has an isentropic exponent $\gamma = 1.33$ at ambient temperatures, the presence of humidity lowers the isentropic exponent of a mixture of humid air. Due to the temperature influence on isentropic exponent, the variation of this parameter has to be considered throughout the engine stations. Generally, for humid air the isentropic exponent is lower at all engine stations than for dry air (Figure 3-2).

(v) Specific Heat

For humid air, the specific heat is affected by the higher gas constant and the lower isentropic exponent (Equation 3-1), both influences resulting in an increase of specific heat (Figure 3-3).

(vi) Entropy Function

For exact calculations of isentropic compression and expansion processes, the entropy function is generally used. For a change in state of a perfect gas at constant entropy:

$$\frac{dP_S}{P_S} = \frac{c_p(T_S)}{R}\,\frac{dT_S}{T_S} \qquad 3\text{-}4$$

or, assuming R = constant:

$$\int_{P_{S1}}^{P_{S2}} \frac{dP_S}{P_S} = \frac{1}{R}\int_{T_{S1}}^{T_{S2}} \frac{c_p(T_S)}{T_S}\,dT_S \qquad 3\text{-}5$$

The entropy function is defined as

$$\Phi(T_S) = \frac{1}{R}\int_{T_{Sref}}^{T_S} \frac{c_p(T_S)}{T_S}\,dT_S \qquad 3\text{-}6$$

Then the following simple relationship can be used for isentropic changes in state

$$\Phi(T_{S1}) - \Phi(T_{S2}) = \ln\frac{P_{S1}}{P_{S2}} \qquad 3\text{-}7$$

The changes of gas constant R and specific heat c_p with water content have been described already. The effect of **war** on entropy function can be evaluated easily.

Alternatively to the use of entropy function, one can also calculate isentropic processes approximately using equivalent estimated values for specific heat or the isentropic exponent γ.

(vii) Gas dynamic parameters

For a given Mach number, some gas dynamic and aero engine parameters are affected by the isentropic exponent only and not by the gas constant, e.g.,

$$\frac{P_T}{P_S} \qquad \frac{T_T}{T_S} \qquad \frac{F}{(A\ P_T)}$$

Other parameters are affected by both gas constant and isentropic exponent, e.g.,

$$\frac{W\sqrt{T_T}}{P_T} \qquad \frac{\Delta H}{T_T} \qquad \frac{N}{\sqrt{T_T}} \qquad \frac{W_F}{\sqrt{T_T}P_T}$$

However, if RT_T is used instead of T_T in the latter parameters, these parameters depend on the isentropic exponent only. Gas dynamic parameters as $W\sqrt{T_T}/P_T$ etc. have to be corrected according to the ratio of the gas constants of humid and dry fluid.

The Mach numbers, pressure ratios and angles associated with shocks depend on the isentropic exponent γ only and do not depend on the gas constant R. However, as the effect of γ on the parameters mentioned is not strong, for the small γ changes associated with gaseous humidity the variations in shock parameters can normally be ignored.

3.2.2 Calculation Procedures

(i) Gas composition

For dry air, normally the standard composition is used [with 78.084 vol.% N_2, 20.948 vol.% O_2, 0.937 vol.% Ar and 0.032 vol.% CO_2 (page xv)]. The absolute humidity of humid air is given by the water to dry air ratio

$$\mathbf{war} = \frac{m_v}{m_{d,a}} \qquad 3\text{-}8$$

The water mass fraction of the humid air mixture (specific humidity) is given as

$$x_v = \frac{\mathbf{war}}{\mathbf{1} + \mathbf{war}} \qquad 3\text{-}9$$

For humid air with a mass fraction of gaseous water x_v, the mass fractions of all constituents except water are given by

$$x_c = \frac{x_{c\ d,a}}{1 + \mathbf{war}} \qquad 3\text{-}10$$

For combustion gases, the fraction of the constituents can be evaluated using the same algorithm as used for combustion with dry air, regarding the combustion products. For a fuel with carbon and hydrogen reacting with oxygen without dissociation (i.e. no CO and NO_x etc. taken into account), Equations 3-11 to 3-14 apply:

$$x_{O_2,o} = \frac{1}{m_i + m_F}[m_i x_{O_2,i} + m_F x_{O_2,F} - m_F M_{O_2}(\frac{x_{C,F}}{M_C} + \frac{x_{H,F}}{4M_H})] \qquad 3\text{-}11$$

$$x_{CO_2,o} = \frac{1}{m_i + m_F}[m_i x_{CO_2,i} + m_F x_{CO_2,F} + m_F M_{CO_2}\frac{x_{C,F}}{M_C}] \qquad 3\text{-}12$$

$$x_{H_2O,o} = \frac{1}{m_i + m_F}[m_i x_{H_2O,i} + m_F x_{H_2O,F} + m_F M_{H_2O}\frac{x_{H,F}}{2M_H}] \qquad 3\text{-}13$$

where i = combustor inlet,
o = combustor outlet
F = fuel.

The mass fraction of the remaining constituents is given by:

$$x_{c,o} = \frac{1}{m_i + m_F}[m_i x_{c,i} + m_F x_{c,F}] \qquad 3\text{-}14$$

(ii) Gas constant

As the gas constant is given by the composition of the fluid, it can be calculated using Equations 3-3 and 3-10. Figure 3-1 gives the gas constant R for dry air and the extreme **war** of 0.03 for different equivalence ratios. The latter is the ratio of the fuel to air ratio **far** to the stoichiometric fuel to air ratio $\mathbf{far}_{stoich}$.

(iii) Calorific quantities

For performance calculations, different methods are used to determine the enthalpy, specific heat, isentropic exponent or entropy function. An often applied method is to use enthalpy or specific heat data depending on temperature for dry air, and, for stoichiometric combustion, to use the properties of the gases resulting from dry air and fuel. The fluid properties for gases less than stoichiometric can be calculated as a mixture of air and stoichiometric gases. Additional fluid data are required for humid air and for stoichiometric combustion gases resulting from humid air. To handle different amounts of humidity the effect of humidity can be assumed to be linear.

When, alternatively, the fluid is modeled not for dry air and stoichiometric combustion gases, but for the constituents mentioned above, i. e. N_2, O_2, H_2O, CO_2 and Ar, no additional fluid data are required. In this case, the quantities of the mixture are calculated as mass averaged values of the quantities of the constituents directly. In the case of enthalpy,

$$h_{mix} = \sum x_c \; h_c \qquad 3\text{-}15$$

To handle gaseous humidity with this alternative method of fluid modelling, the only inputs required for the definition of the air are the x_c values for humid air. All the other calculations are done consistent with those for dry air. Therefore this alternative method may be preferred for its simplicity.

For temperatures exceeding 1800 K, dissociation should be taken into account. As dissociation depends on pressure, fluid data such as enthalpy and specific heat depend on both temperature and pressure at a given composition.

3.2.3 Amount of Gaseous Water

3.2.3.1 *Vapour Pressure and Partial Pressure*

The gaseous humidity is limited by the saturated vapour pressure of H_2O, which is a function of temperature only (see Figure 3-4). If the partial pressure of the water vapour in the air exceeds the vapour pressure, condensation will occur, i.e. the formation of liquid water at temperatures above the freezing point, or of ice at temperatures below freezing point. The partial pressure of any constituent is given by the ideal gas equation applied to the constituent, i. e.

$$P_{Sc} = \frac{m_c \; R_c \; T_S}{V} \qquad 3\text{-}16$$

For water, a higher vapour pressure will allow a higher partial pressure P_v and hence more mass of water m_v and a higher fraction of water without condensation. As the vapour pressure rises exponentially with temperature, condensation can occur only in the inlet components of a running engine, regardless of the production of H_2O and the resulting increase of vapour pressure downstream of a combustor.

3.2.3.2 *Water to Dry Air Mass Ratio*

The humidity of ambient air is often expressed by the degree of saturation

$$\varphi = \frac{\mathbf{war}}{\mathbf{war}_{sat}} \qquad 3\text{-}17$$

relating the actual content of water to the maximum content without condensation. For saturated air $P_v = P_{sat}$. Applying the ideal gas equation for dry air and gaseous water results in

$$\mathbf{war} = \frac{m_v}{m_{d,a}} = \frac{P_{Sv}}{P_{S\,d,a}} \frac{R_{d,a}}{R_w}$$

$$= \frac{P_{S\,sat}}{\frac{P_{S\,mix}}{RH} - P_{S\,sat}} \frac{R_{d,a}}{R_w} \qquad 3\text{-}18$$

Using the vapour pressure as a function of temperature, the water to dry air ratio of humid air can be determined depending on degree of saturation, pressure and temperature of the air. The water to dry air ratio of saturated air, $\mathbf{war}_{sat}$, is given in Figure 3-5. As the pressure effect on the product, ($\mathbf{war}_{sat}$ $P_{S\,mix}$), is small, for a given temperature the saturated water to dry air ratio increases with falling pressure, approximately reciprocal to the pressure. At altitude the temperature is much lower than at sea level and therefore the saturated water to dry air ratio is normally considerably lower than at sea level. For standard and non-standard atmosphere conditions, $\mathbf{war}_{sat}$ as a function of altitude is given in Figure 3-6. For evaluation of the water to dry air ratio for nonsaturated air, see Chapter 2 for degree of saturation.

Table 3-2 provides a summary of the relationships discussed in this section.

3.3 COMPONENT PERFORMANCE

3.3.1 Inlet

The maximum amount of water vapour in the air is shown as saturated water-air-ratio in Figure 3-6. One can see that, at low altitude and temperatures above ISA, a significant amount of water can be in the air. On the other hand, at altitudes above 6000 m (20000 ft), humidity will not be significant enough to cause any noticeable change in engine performance.

Simulated altitude conditions in an altitude test facility (ATF) can deviate with respect to humidity significantly from the real conditions, especially at ram conditions. The reason is that in the ATF the total temperature, not the static temperature, is produced in front of the test vehicle. Total temperatures are much higher and therefore the air can hold much more water. The saturated water-air-ratios for ram inlet total temperature and pressure are shown for a range of subsonic Mach numbers in Figure 3-7.

The amount of water in the air in a real test depends obviously on the outside air conditions in the case where there is no dryer in the ATF. The maximum amount of water in the outside air can be taken from Figure 3-6. For that purpose one can read the graph for the altitude of the ATF location and the actual outside air temperature. The relative humidity measured on the day gives then the real water-air-ratio of the airstream entering the ATF.

How is the engine inlet performance affected by humidity? Effects of gaseous humidity are

consequences of changes in gas constant and in isentropic exponent. As shown in Section 3.3.2.1 (Similarity Parameters), for incompressible flow there is no effect of the isentropic exponent on the flow field. The change in gas constant will have an effect on density, but not on the correlations between pressure ratio, temperature ratio and Mach number.

In compressible flow the isentropic exponent affects the flow field. That can be seen, for example, from the gas dynamic equations describing vertical and oblique shocks. Therefore, in principle, there will be an influence of humidity on engine inlet performance.

The flow capacity of the intake will also change with humidity. The corrected flow per unit area (assuming a blockage factor (the effective flow area divided by the geometrical area) of unity) is

$$\frac{W\sqrt{T_T}}{AP_T} = \sqrt{\frac{\gamma}{R}}\frac{Ma}{\left(1+\frac{\gamma-1}{2}Ma^2\right)^{\frac{\gamma+1}{2(\gamma-1)}}} \qquad 3\text{-}19$$

For critical conditions the relation of the flow capacities for dry air and a mixture of dry air with water vapour (neglecting changes of γ with temperature) is

$$\frac{\left(W\frac{\sqrt{T_T}}{P_T}\right)_{d,crit}}{\left(W\frac{\sqrt{T_T}}{P_T}\right)_{mix,crit}} = \sqrt{\frac{R_{mix}}{R_d}}\sqrt{\frac{\gamma_d}{\gamma_{mix}}}\frac{\left(\frac{\gamma_{mix}+1}{2}\right)^{\frac{\gamma_{mix}+1}{2(\gamma_{mix}-1)}}}{\left(\frac{\gamma_d+1}{2}\right)^{\frac{\gamma_d+1}{2(\gamma_d-1)}}} \qquad 3\text{-}20$$

In this formula the term $\sqrt{R_{mix}}/\sqrt{R_d}$ is numerically much more important than the terms with the isentopic exponent. Equation 3-20 is strictly valid only as long as the blockage factor is not affected by humidity.

Inlet pressure losses should be correlated with corrected flow, for example, as

$$\frac{\Delta P_T}{P_T} = f\left(\frac{\frac{W\sqrt{T_T}}{P_T}}{\left(\frac{W\sqrt{T_T}}{P_T}\right)_{crit}}\right) \qquad 3\text{-}21$$

By this procedure the effect of humidity can be described fairly accurately.

In a venturi the mass flow is measured indirectly. It is calculated from the total temperature T_T, effective area A_{ef}, total pressure P_T and static pressure P_S. If, in an actual test, the air is humid and the measured quantities are evaluated assuming dry air, then an error exists even for those cases where no condensation takes place. The error introduced by neglecting humidity depends on the water-air ratio war and the Mach number Ma.

The true static temperature T_S can be found from the entropy function

$$\Phi(T_S, \mathbf{war}) = \Phi(T_T, \mathbf{war}) - \ln\left(\frac{P_T}{P_S}\right) \qquad 3\text{-}22$$

The true velocity is

$$V = \sqrt{2\left[h(T_T, \mathbf{war}) - h(T_S, \mathbf{war})\right]} \qquad 3\text{-}23$$

The mass flow per unit area can then be calculated from

$$\frac{W}{A_{ef}} = \frac{P_S}{R_{mix}\,T_S}V \qquad 3\text{-}24$$

If humidity is neglected, i.e. assuming **war** = 0, the result is an incorrect flow per unit area. In Figure 3-8 the difference between real and calculated flow assuming zero humidity is shown in percent as a function of Mach number and water-air ratio. The significant error is introduced mainly by the change in gas constant R due to humidity.

3.3.2 Turbomachinery

3.3.2.1 *Similarity Parameters*

The performance of a turbomachine is usually described using so-called "similarity parameters". If the numbers for these parameters are the same for two different

operating conditions, then it is concluded that the flowfields are similar to each other.

What are similar flowfields? An initial condition is that the directions of all velocity vectors are the same. However, their magnitudes might be different. All the velocity triangles in all stages have the same shape for strictly similar operating conditions. Therefore at any point within the turbomachine, for two different operational conditions O1 and O2:

$$\left(\frac{V}{U}\right)_{O1} = \left(\frac{V}{U}\right)_{O2} \qquad 3\text{-}25$$

Consider typical velocity diagrams. At the inlet to a turbomachine, the ratio of axial velocity to circumferential velocity must be the same for similar operating conditions (see Figure 3-9):

$$\left(\frac{V_{ax,i}}{U_i}\right)_{dry} = \left(\frac{V_{ax,i}}{U_i}\right)_{mix} \qquad 3\text{-}26$$

The term V_{ax}/U is known as flow coefficient.

From Euler's law applied to a single stage we get the increase in total enthalpy:

$$\Delta h = \frac{PW}{W} = U_1 V_{U,1} - U_2 V_{U,2} \qquad 3\text{-}27$$

Normalized with U_1^2:

$$\frac{\Delta h}{U_1^2} = \frac{V_{U,1}}{U_1} - \frac{U_2}{U_1}\frac{V_{U,2}}{U_1} \qquad 3\text{-}28$$

$\Delta h/U_1^2$ is called the work coefficient. For similar operating conditions the work coefficient will be the same since $\Delta h/U_1^2$ can be calculated from velocity ratios only.

The flow will enter the blade rows with relative velocity W_k and the vane rows with the velocity V_j. Within the passages there will be losses and area changes, both of which affect the exit velocity.

Incompressible flow - In the case where the fluid is incompressible, any change in velocity is directly coupled with an area change. The losses are proportional to velocity squared:

$$\Delta h_{Loss} = \sum \zeta_j V_{j,1}^2 + \sum \zeta_k W_{k,1}^2 \qquad 3\text{-}29$$

The isentropic efficiency of a compressor can be defined as

$$\eta_{comp} = \frac{\Delta h - \Delta h_{Loss}}{\Delta h} \qquad 3\text{-}30$$

The isentropic turbine efficiency can be defined analogously.

Dividing Equation 3-30 by U_1^2 leads to

$$\eta_{comp} = \frac{\frac{\Delta h}{U_1^2} - \sum \zeta_j \frac{V_{j,1}^2}{U_1^2} - \sum \zeta_k \frac{W_{k,1}^2}{U_1^2}}{\frac{\Delta h}{U_1^2}} \qquad 3\text{-}31$$

As long as the loss coefficients ζ_j and ζ_k do not change, efficiency will be the same for similar operating conditions. In reality, the loss coefficients are dependent on Reynolds number, but, as in this discussion, it is generally assumed that humidity does not affect Reynolds number.

The pressure ratio can be calculated from the specific work and the efficiency. Since humid air has both a different gas constant R and isentropic exponent γ compared to dry air the pressure ratio for a given specific work will change with humidity:

$$\frac{P_{T2}}{P_{T1}} = \left(\frac{\eta_{comp}\,\Delta h}{\frac{\gamma_{equiv}}{\gamma_{equiv}-1} R T_{T1}} + 1\right)^{\frac{\gamma_{equiv}}{\gamma_{equiv}-1}} \qquad 3\text{-}32$$

Alternatively, one can use the entropy function to correlate pressure ratio with specific work.

Compressible flow - For compressible flow the velocity changes in a duct with variable area do not depend only on the area changes as in case of incompressible flow. Even for the simple case of isentropic flow the velocity ratio depends on the Mach number level:

$$\frac{V_1}{V_2} = \frac{A_2}{A_1}\left(\frac{1 + \frac{\gamma-1}{2} Ma_1^2}{1 + \frac{\gamma-1}{2} Ma_2^2}\right)^{\frac{1}{\gamma-1}} \qquad 3\text{-}33$$

Thus the isentropic exponent γ, which is dependent on humidity, has an impact on the velocity ratio.

The losses in a compressible flowfield depend not only on the velocity squared but also on the Mach number. In a supersonic flowfield the losses are dependent also on the isentropic exponent as can be seen from the formula describing a normal shock:

$$\frac{P_{T2}}{P_{T1}} = \left[\frac{1}{\left(\frac{\gamma-1}{\gamma+1} + \frac{2}{(\gamma-1)Ma_1^2} \right)^{\gamma} \left(\frac{2\gamma}{\gamma+1} Ma_1^2 - \frac{\gamma-1}{\gamma+1} \right)} \right]^{\frac{1}{\gamma-1}} \qquad 3\text{-}34$$

Therefore, full similarity of velocity triangles in a compressible flowfield requires

* geometric similarity (areas and blockage factors)
* equal V_{ax}/U
* Reynolds number has negligible effect
* Prandtl number has negligible effect, i.e. heat transfer effects on the flowfield do not change
* equal Mach number
* equal isentropic exponent

Component characteristics based on equal Mach numbers - In a real engine the geometry of a turbomachine changes slightly with operating conditions. Differences between the thermal expansion of casings and disks cause changes in tip clearance. There is some blade untwist, especially in the case of long fan blades. If variable geometry is used, then the positioning of vanes may be inaccurate.

In the following we ignore all these effects, and assume that the geometry does not change with operating conditions, i.e. geometric similarity is fulfilled, and Reynolds number and Prandtl number effects are negligible.

For similar operating conditions all velocity ratios and all Mach numbers must be the same. The velocity diagram parameters can easily be converted to Mach numbers:

$$\frac{V_{ax,1}}{U_1} = \frac{V_{ax,1}}{\sqrt{\gamma_1 RT_{S1}}} \frac{\sqrt{\gamma_1 RT_{S1}}}{U_1} = \frac{Ma_{V_{ax,1}}}{Ma_{U_1}} \qquad 3\text{-}35$$

$$\frac{\Delta h}{U_1^2} = \frac{\Delta h}{\gamma_1 RT_{S1}} \frac{\gamma_1 RT_{S1}}{U_1^2} =$$

$$\frac{\Delta h}{\gamma_1 RT_{T1}} \frac{1 + \frac{\gamma_1 - 1}{2} Ma^2_{V_{ax,1}}}{Ma^2_{U_1}} \qquad 3\text{-}36$$

If we keep the Mach numbers $Ma_{Vax,1}$ and $Ma_{U,1}$ constant and $\Delta h/\gamma_1 RT_{S1}$ constant then the velocity triangles are similar for a given isentropic exponent γ_1 and gas constant R.

In this development we assume that the flow at the inlet of the turbomachine is axial. The (axial) Mach number at the inlet can be correlated with the mass flow and the inlet total pressure and temperature:

$$\frac{W\sqrt{T_{T1}}}{P_{T1}} =$$

$$A_1 \sqrt{\frac{\gamma_1}{R}} \frac{Ma_{V_{ax,1}}}{\left(1 + \frac{\gamma_1 - 1}{2} Ma^2_{V_{ax,1}} \right)^{\frac{\gamma_1+1}{2(\gamma-1)}}} \qquad 3\text{-}37$$

Circumferential Mach number $Ma_{U,1}$ can be expressed as

$$Ma_{U_1} = \frac{U_1}{\sqrt{\gamma_1 RT_{S1}}} =$$

$$\frac{N}{\sqrt{\gamma_1 RT_{T1}}} k \sqrt{1 + \frac{\gamma_1 - 1}{2} Ma^2_{V_{ax,1}}} \qquad 3\text{-}38$$

where k is a unit conversion factor.

For given values of $W\sqrt{T_{T1}}/P_{T1}$ and $N/\sqrt{T_{T1}}$ from Equations 3-37 and 3-38, the Mach numbers $Ma_{V,ax,1}$ and $Ma_{U,1}$ can be calculated when γ_1 and R are known. Then $\Delta h/U^2_1$ can be found from $\Delta h/T_{T1}$ using Equation 3-36.

Compressor maps are often prepared using the parameters $W\sqrt{T_{T1}}/P_{T1}$, $N/\sqrt{T_{T1}}$ and $\Delta h/T_{T1}$. Such maps represent similar flowfields for a gas with given isentropic exponent and gas constant.

Effect of isentropic exponent and gas constant on characteristics - It was already mentioned that the velocity ratio of a compressible flow in a duct with area change depends not only on Mach numbers, but also on isentropic exponent, see Equation 3-33. That means that full flow similarity can only be achieved when the isentropic exponent of the gas does not change.

Note that the gas constant R does not appear in Equation 3-33, therefore similar flowfields are possible with gases having different gas constants.

When full similarity is not possible, one has to make simplifications. Arbitrarily, the mean Mach number at the inlet of the turbomachine can be kept constant when changing from one gas to another.

From Equation 3-38 there follows a relation between $N/\sqrt{T_{T1}}$ for dry and wet air:

$$\frac{\left(\frac{N}{\sqrt{T_T}}\right)_d}{\left(\frac{N}{\sqrt{T_T}}\right)_{mix}} = \sqrt{\frac{R_d}{R_{mix}}}\sqrt{\frac{\gamma_d}{\gamma_{mix}}\,\frac{1+\frac{\gamma_{mix}-1}{2}Ma_{V_{ax}}^2}{1+\frac{\gamma_d-1}{2}Ma_{V_{ax}}^2}} \qquad 3\text{-}39$$

The effect of the change in gas constant due to humidity can be evaluated easily. The influence of a change in isentropic exponent is related to the Mach number.

Figure 3-10 shows, term by term, numbers for different speed corrections evaluated for fairly wet air with 3% water vapour content. The effect of the isentropic exponent (second square root in Equation 3-39) is small compared to the effect of the gas constant.

The influence of humidity on corrected flow can be described by

$$\frac{\left(\frac{W\sqrt{T_T}}{P_T}\right)_d}{\left(\frac{W\sqrt{T_T}}{P_T}\right)_{mix}} = \sqrt{\frac{R_{mix}}{R_d}}\sqrt{\frac{\gamma_d}{\gamma_{mix}}}\,\frac{\left(1+\frac{\gamma_{mix}-1}{2}Ma_{V_{ax}}^2\right)^{\frac{\gamma_{mix}-1}{2(\gamma_{mix}-1)}}}{\left(1+\frac{\gamma_d-1}{2}Ma_{V_{ax}}^2\right)^{\frac{\gamma_d-1}{2(\gamma_d-1)}}} \qquad 3\text{-}40$$

In Figures 3-11 and 3-12 it can again be seen that the change in gas constant due to humidity dominates the change in corrected flow.

To include the effect of humidity on specific work, an additional assumption is required. To retain geometric similarity, the correlation for specific work is $\Delta h/U^2$=const. This assumption is also often made in procedures for Reynolds corrections on characteristics. From Equation 3-36 it follows that

$$\frac{\left(\frac{\Delta h}{T_T}\right)_d}{\left(\frac{\Delta h}{T_T}\right)_{mix}} = \frac{R_d}{R_{mix}}\,\frac{\gamma_d}{\gamma_{mix}}\,\frac{1+\frac{\gamma_{mix}-1}{2}Ma_{V_{ax}}^2}{1+\frac{\gamma_d-1}{2}Ma_{V_{ax}}^2} \qquad 3\text{-}41$$

This equation is similar to Equation 3-39; as might be expected, the correction for specific work is the correction for speed squared.

It is not possible to derive a general equation for efficiency changes due to humidity. Therefore, the assumption is made often that efficiency does not change with fluid properties. In reality, especially in multistage machines, a change in efficiency due to modified stage matching has to be expected. There is presently no general rule available to estimate the magnitude of an efficiency change with humidity.

In summary we have made the following assumptions for a humidity correction procedure for turbomachine characteristics:

* Mach numbers at the inlet to the turbomachine are retained

* $\Delta h/U^2$ does not change
* efficiency is not affected by humidity

Other assumptions will lead to different correlations. Whatever the assumptions are, there is some arbitrariness since full flow similarity is, in principle, not achievable with gases of different isentropic exponent.

3.3.2.2 *Compressors*

Various companies and research institutes use different map correction procedures for humidity. In the following, these procedures are compared against the method described in the previous section.

Method A: The speed correction is done according to

$$\frac{\left(\frac{N}{\sqrt{T_T}}\right)_d}{\left(\frac{N}{\sqrt{T_T}}\right)_{mix}} = \sqrt{\frac{\gamma_d \, R_d}{\gamma_{mix} \, R_{mix}}} \qquad 3\text{-}42$$

In comparison to Equation 3-39, the Mach number dependent terms are missing. This is equivalent to setting the Mach number to zero. As can be seen from Figure 3-10 this leads to slightly smaller corrections compared to the rigorous method which takes into account the actual Mach number and specific heat ratio at the inlet of the compressor.

The flow correction is of the same magnitude as the speed correction:

$$\frac{\left(\frac{W\sqrt{T_T}}{P_T}\right)_d}{\left(\frac{W\sqrt{T_T}}{P_T}\right)_{mix}} = \sqrt{\frac{\gamma_d \, R_{mix}}{\gamma_{mix} \, R_d}} \qquad 3\text{-}43$$

As in the case of the speed correction, the Mach number terms are left out (see Figures 3-11 and 3-12).

The specific work correction is the square of the speed correction:

$$\frac{\left(\frac{\Delta h}{T_T}\right)_d}{\left(\frac{\Delta h}{T_T}\right)_{mix}} = \frac{\gamma_d \, R_d}{\gamma_{mix} \, R_{mix}} \qquad 3\text{-}44$$

There is no correction applied to the efficiency. Pressure ratio can therefore be calculated from

$$\left(\frac{P_{T2}}{P_{T1}}\right)_d = \left[\frac{\left(\frac{P_{T2}}{P_{T1}}\right)_{mix}^{\frac{\gamma_{mix}-1}{\gamma_{mix}}} - 1}{\frac{R_{mix}}{R_d}\frac{\gamma_{mix}}{\gamma_d}\frac{c_{pd}}{c_{p\,mix}}} + 1\right]^{\frac{\gamma_d}{\gamma_d - 1}} \qquad 3\text{-}45$$

The entropy function, instead of the isentropic exponents, could be used in the above equation.

Method B: This method generalizes the compressor characteristic map to various supply conditions (temperature, humidity) that differ from the reference conditions by assuming the invariability of the four corrected parameters:

$$\frac{N}{\sqrt{\gamma R T_T}} \qquad \left(\frac{W}{W_{crit}}\right)_{inlet}$$

$$\left(\frac{W}{W_{crit}}\right)_{exit} \qquad \frac{\Delta h}{\gamma R T_T}$$

The corrections for the corrected speed and the specific work are identical to those described in Method A (Equations 3.42 and 44).

Method B differs from Method A by the selection of the two other invariants described by W/W_{crit} = the ratio of the actual mass flow to the critical mass flow, considered for the annulus inlet and exit areas. Assuming the invariability of these parameters means that the actual mass flow variation with humidity is in direct proportion to the associated change in the critical mass flow.

Compared to the expression of Equation 3-43,

$\frac{W\sqrt{T_T}}{P_T}\sqrt{\frac{R}{\gamma}}$, the expression

$$\frac{W}{W_{crit}} \quad \text{or} \quad \left(\frac{\frac{W\sqrt{T_T}}{P_T}}{\left(\frac{W\sqrt{T_T}}{P_T}\right)_{crit}} \right)$$

applied, for instance, to the annulus inlet compressor area, reduces the deviations when considering a constant axial inlet Mach number for different supply conditions (temperature, humidity), as described in Reference 3.2.

The expression $(W/W_{crit})_{exit}$ reflects the axial exit Mach number. When applying this generalized representation of compressor operation, two similar operating points are characterized by the identity of the two Mach numbers corresponding to the rotational speed and the axial exit velocity, the inlet Mach number and the specific work being deduced. It is postulated that the flow similarity, based on Mach number, can be applied to the overall operation of the compressor.

The compressor efficiency and pressure ratio are therefore determined on these bases. The compressor efficiency is slightly influenced by variations in the isentropic exponent and the fluid gas constant when considering different inlet conditions (temperature and humidity): the efficiency decreases slightly with water to dry air ratio **war**. The same trend is observed for the pressure ratio variation.

Method C: The speed correction is defined as

$$\frac{\left(\frac{N}{\sqrt{T_T}}\right)_d}{\left(\frac{N}{\sqrt{T_T}}\right)_{mix}} = \sqrt{\left(\frac{\gamma_d\, R_d}{\gamma_{mix}\, R_{mix}}\right)\left(\frac{\gamma_{mix}+3}{\gamma_d+3}\right)} \qquad 3\text{-}46$$

The term in the second bracket represents the Mach number term of the reference method for $Ma_{Vax}= 0.707$.

The flow correction is also formulated for Mach number equal to 0.707. This leads to

$$\frac{\left(W\frac{\sqrt{T_T}}{P_T}\right)_d}{\left(W\frac{\sqrt{T_T}}{P_T}\right)_{mix}} = \sqrt{\frac{\gamma_d}{\gamma_{mix}}\frac{R_{mix}}{R_d}}\left(\frac{4}{\gamma_d+3}\right)^{\frac{\gamma_d+1}{2(\gamma_d-1)}}\left(\frac{\gamma_{mix}+3}{4}\right)^{\frac{\gamma_{mix}-1}{2(\gamma_{mix}-1)}} \qquad 3\text{-}47$$

Instead of specific work, in this method the pressure ratio is corrected. It is postulated that the density ratio of the compressor remains the same for equivalent conditions. Using a polytropic efficiency of 0.9 leads to

$$\left(\frac{P_{T2}}{P_{T1}}\right)_{mix} = \left(\frac{P_{T2}}{P_{T1}}\right)_d^{\frac{\gamma_{mix}(1-0.1\gamma_d)}{\gamma_d(1-0.1\gamma_{mix})}} \qquad 3\text{-}48$$

Specific work can then be calculated from the corrected pressure ratio and an unchanged efficiency. If the specific work would be corrected, then the consequence would be a change in efficiency.

Method D: The speed correction factor is

$$\frac{\left(\frac{N}{\sqrt{T_T}}\right)_d}{\left(\frac{N}{\sqrt{T_T}}\right)_{mix}} = \sqrt{\frac{\gamma_d^{0.75} R_d}{\gamma_{mix}^{0.75} R_{mix}}} \qquad 3\text{-}49$$

By this method the Mach number term is approximated as shown in Figure 3-10. The corrected airflow is adjusted for humidity using

$$\frac{\left(W\frac{\sqrt{T_T}}{P_T}\right)_d}{\left(W\frac{\sqrt{T_T}}{P}\right)_{mix}} = \sqrt{\frac{\gamma_d^{0.65}}{\gamma_{mix}^{0.65}}\frac{R_{mix}}{R_d}} \qquad 3\text{-}50$$

For comparison with other mass flow corrections see Figures 3-11 and 3-12.

The correction for specific work is the square of the speed correction. Assuming efficiency is unchanged allows recalculation of the pressure ratio from

$$\left(\frac{P_{T2}}{P_{T1}}\right)_d = \left[\frac{\left(\frac{P_{T2}}{P_{T1}}\right)_{mix}^{\frac{\gamma_{mix}-1}{\gamma_{mix}}} - 1}{\frac{R_{mix}}{R_d}\frac{\gamma_{mix}^{0.75}}{\gamma_d^{0.75}}\frac{c_{pd}}{c_{pmix}}} + 1\right]^{\frac{\gamma_d}{\gamma_d - 1}} \qquad 3\text{-}51$$

Comparison of correction methods: The magnitude of the different correction factors can be read for some of the methods from Figures 3-10 to 3-12. The question remains, however, how well do these theoretical correlations agree with reality?

Generally the humidity corrections are small. It is practically impossible to check the procedures against measurements because the scatter in the measured data will most probably be much bigger than the differences between the humidity correction methods.

An alternative to measurements are calculated compressor maps or CFD results. Since CFD calculations are rather expensive they are normally not used for complete maps.

For comparison purposes two maps for a multistage compressor were calculated. The program used loss characteristics for each blade and vane row that were adjusted to compressor interstage measurements. The first map is valid for standard day inlet conditions (T_{T1} = 288.15 K, P_1 = 101.325 kPa, dry air). The second map was also calculated for dry air, but increased inlet temperature, T_{T1} = 500 K. Thus a lower isentropic exponent is implied. The inlet pressure was set to 200 kPa which results in the same Reynolds number basis for both maps.

The difference in inlet temperature between both maps results in an isentropic exponent change of 0.015. The same effect on isentropic exponent would be caused by the extremely high water-air ratio of **war** = 0.15. Thus the effect of humidity on isentropic exponent is exaggerated in the following discussion by a factor of approximately ten with respect to practical applications.

The change in gas constant due to humidity was not fed into the compressor map calculation program. This however does not invalidate the results. It has been shown in Section 3.3.2.1 that by use of the proper correlations the effect of gas constant can be taken into account correctly.

In Figure 3-13 the calculated data for 100% design speed are shown plotted as $\Delta h/\gamma RT_T$ against $W\sqrt{T_T}/P_T{}^*\sqrt{(R/\gamma)}$.
The speedlines are comparable because

$$\frac{N_1}{\sqrt{\gamma_1 RT_{T1}}} = \frac{N_2}{\sqrt{\gamma_2 RT_{T2}}}$$

It can be seen that neither efficiency nor specific work are the same. This is caused by rematching effects between the compressor stages.

The map parameters used in Figure 3-13 are consistent with the correction factors of Method A. Thus Figure 3-13 shows the limited validity of the assumptions that are the basis of Method A. If the parameters used are ideal, the lines will collapse. The differences between the curves for T_{T1} = 288 K and 500 K are caused by the change in isentropic exponent. In spite of keeping the compressor inlet velocity triangle (expressed in Mach numbers) the same, there are differences in the predicted compressor behaviour.

Figures 3-14 to 3-17 show the results for the different correction methods applied to the conventional format of a compressor characteristic. Note that, in the conventional compressor map format, $N/(\gamma RT_{T1})^{1/2}$ is replaced by $N/(T_{T1})^{1/2}$ and, analogously, the term for mass flow is simplified to $W(T_{T1})^{1/2}/P_{T1}$. It can be seen that none of the correction procedures yields the exact change in isentropic efficiency. However, it should be noted that the differences between the methods are generally small. For realistic humidity values in the range around **war** = 0.015 the effects of isentropic exponent are only one tenth of those shown in Figures 3-13 to 3-17.

The example shown may not be representative of all the different types of compressors that are used in gas turbines. This is a field for further theoretical study.

Correction procedures for surge line: In multistage compressors especially, the surge line may be affected by a change in isentropic exponent. Since the flowfields cannot be exactly similar for operation in gases with different isentropic exponents, the flow angles are not the same.

However, as already mentioned, the effect of water vapour in the air is mainly a change in gas constant; the change in isentropic exponent is secondary.

Compressor test analysis: On a compressor test bed, both at the inlet and the exit, the total

temperatures T_{T1} and T_{T2} as well as the total pressures P_{T1} and P_{T2} are measured. Ideal specific work Δh_{is} is calculated from inlet temperature and pressure ratio. Actual specific work Δh is found either from total temperatures or from torque measurement.

Compressor efficiency is

$$\eta_C = \frac{\Delta h_{is}}{\Delta h} \qquad 3\text{-}52$$

Ideal specific work is calculated from

$$\Phi(T_{T2,is}, \mathbf{war}) = \Phi(T_{T1}, \mathbf{war}) + \ln\left(\frac{P_{T2}}{P_{T1}}\right) \qquad 3\text{-}53$$

$$\Delta h_{is} = h(T_{T2,is}, \mathbf{war}) - h(T_{T1}, \mathbf{war}) \qquad 3\text{-}54$$

The actual specific work can be found directly from the measured total temperatures

$$\Delta h = h(T_{T2}, \mathbf{war}) - h(T_{T1}, \mathbf{war}) \qquad 3\text{-}55$$

If the air is humid and the actual and isentropic specific work are calculated assuming the air is dry (**war** = 0) then an incorrect value will be calculated for efficiency. The difference between true and (incorrectly) calculated efficiency depends mainly on pressure ratio and water-air ratio. Inlet temperature T_{T1} and efficiency level play a secondary role. Figure 3-18 was calculated for real efficiency = 0.9 and inlet temperature T_{T1} = 288.15 K. The deviation from the correct result is significant even for small water-air ratios.

In the case where the actual specific work is derived from the measured torque, a precise mass flow measurement is needed. In addition, windage and bearing losses must be taken into account. Figure 3-19 was prepared with the idealistic assumption that the actual specific work has been measured exactly and only the ideal specific work has been calculated incorrectly (i.e. assuming dry air). If the mass flow is derived from venturi measurements (and dry air has been assumed), the mass flow error may be determined as described in the previous section. The latter is transferred to the torque and decreases the errors shown in Figure 3-19. The resultant error for a venturi Mach number of 0.5 is shown in Figure 3-20.

3.3.2.3 *Turbines*

The methods in use for turbines differ somewhat from those used for compressors. They will be compared against the methods described in Section 3.3.2.2

Method A: The correction procedure described as Method A in Section 3.3.2.2 for compressors is also in use for turbines. The correction factors can be derived by setting the Mach number in the equations to zero.

Method B: This correction method proceeds from the same principles at Method B described in section 3.3.2.2 for compressors by assuming the invariability of the three corrected parameters

$$\frac{\dfrac{N}{\sqrt{\gamma R T_T}}}{\left(\dfrac{W}{W_{crit}}\right)_{exit}} \qquad \left(\frac{W}{W_{crit}}\right)_{inlet}$$

For an inlet Mach number of one, the selection of $(W/W_{crit})_{inlet}$ generates no deviation and the calculated value is independent of the component supply conditions.

This method used for turbine map representation differs from Method B related to compressors in that a correction to the specific work $\Delta h/(\gamma R T_T)$ is incorporated in order to express the invariability of the turbine efficiency whatever the upstream conditions, as usually postulated by the aerodynamicists.

Method C: This method differs from Method A by setting the Mach number to unity in all equations. Thus the speed correction factor is:

$$\frac{\left(\dfrac{N}{\sqrt{T_T}}\right)_d}{\left(\dfrac{N}{\sqrt{T_T}}\right)_{mix}} = \sqrt{\frac{R_d}{R_{mix}} \frac{\gamma_d}{\gamma_d + 1} \frac{\gamma_{mix} + 1}{\gamma_{mix}}}$$

For the flow the correction factor becomes

$$\frac{\left(W\frac{\sqrt{T_T}}{P_T}\right)_d}{\left(W\frac{\sqrt{T_T}}{P_T}\right)_{mix}} \qquad 3\text{-}57$$

$$\sqrt{\frac{\gamma_d}{\gamma_{mix}}\frac{R_{mix}}{R_d}}\left(\frac{2}{\gamma_d+1}\right)^{\frac{\gamma_d-1}{2(\gamma_d-1)}}\left(\frac{\gamma_{mix}+1}{2}\right)^{\frac{\gamma_{mix}-1}{2(\gamma_{mix}-1)}}$$

The specific work correction factor is the square of the speed correction factor:

$$\frac{\left(\frac{\Delta h}{T_T}\right)_d}{\left(\frac{\Delta h}{T_T}\right)_{mix}} = \frac{R_d}{R_{mix}}\,\frac{\gamma_d}{\gamma_d+1}\,\frac{\gamma_{mix}+1}{\gamma_{mix}} \qquad 3\text{-}58$$

Efficiency is assumed to remain constant as in case of Method A.

Comparison of correction methods: Corresponding to the case for compressors, for comparison purposes, maps of turbine characteristics have been calculated for isentropic exponents of $\gamma = 1.4$ and $\gamma = 1.3$. The change in γ has been highly exaggerated compared with the change due to humidity to make the effects evident. No Reynolds number effects have been taken into account for these calculations.

There are basic differences in the γ influence between purely subsonic flow and flow with choked cross section. For subsonic flow, flow direction and density are the important parameters. However, as soon as choking occurs, the Mach number becomes a governing parameter. In the choked cross section the Mach number is equal to one, and following a stream tube in the other locations the parameters are given by the pressure and temperature ratios and the cross section area ratio relative to the choked area. Also, the changes in flow direction and losses due to supersonic flow become significant.

For choked first stage vanes, the mass flow for various γ can be evaluated just from gas dynamic considerations, assuming no effect on total pressure losses between turbine inlet and choked area.

As long as sonic velocity is not exceeded, the calculated effect of γ on efficiency for the turbine was very small. This may be due to the fact that, under these conditions, γ has only a small effect on the flow parameters determining the losses. However, as choking occurs for different γ at different map points, due to the losses associated with choked flow there is some γ effect on efficiency for choked flow.

In Figures 3-21 and 3-22 the calculated mass flows and efficiencies are shown for $\gamma = 1.4$ and $\gamma = 1.3$ using conventional parameters. There are also shown the curves obtained by taking the $\gamma = 1.4$ values and correcting to $\gamma = 1.3$ applying the methods described. The turbine used for this comparison is a single stage turbine typical for HP application. For high values of $\Delta h/T$, the vane exit Mach number is slightly below one.

Figure 3-21 is for high $\Delta h/T_T$ and the γ change used shows a decrease in mass flow parameter of 2.4%, resulting in a corresponding error if no correction is applied. Method A overcorrects, resulting in too low a mass flow. This method is based on a constant Mach number in a large turbine inlet cross-sectional area, but in fact the inlet Mach number is decreasing for choked flow and lower γ, explaining the deviation. Method C is based on choked flow and therefore, for the turbine investigated, mass flow differences can be ignored. However, for turbines with low vane Mach number, a noticeable error would occur with Method C, and a smaller error with Method A, which is correct in the incompressible case. Method B is exact for the two extreme cases of choked/nil flow, and generates a small deviation for the intermediate regime.

Since even for a water-to-air ratio as high as 0.03 the change in γ is approximately 40 times less than that used for this comparison, the effect of γ due to humidity on turbine maps is very small. Compared with other uncertainties in performance calculations, the influence of γ can be ignored but the correction for R should be applied. Some more thoughts about the effect of γ on turbine maps can be found in Reference 3.20.

Turbine test analysis: The measurements on turbine test beds are the same as for compressors. The calculation procedures are analogous to the compressor case. Figure 3-23 shows the efficiency error when the actual specific work is derived from measured total temperatures for $T_{T1} = 1600$ K, fuel-air ratio = 0.02 and real efficiency = 0.9. The results for other test conditions are very similar.

Figure 3-24 is valid for the case where the actual specific work is calculated from the torque. This is an ideal case since any error in mass flow measurement is transferred directly to specific work and

decreases the total error as in the case of compressor testing. For the magnitude of mass flow errors in venturi measurements, see above.

3.3.3 Combustion

Humid air has a different chemical composition from dry air. As can be seen from the tabulated mole fractions of the constituents, there is less oxygen available for burning fuel in humid air:

	N_2	O_2	H_2O	Ar	CO_2
war =.03	74.491%	19.984%	4.601%	0.893%	0.03%
dry air	78.084%	20.948%	-	0.937%	0.032%

These data were taken from Reference 3.1, tables 1A and 17A.

The tables of Reference 3.1 present properties based on constant gaseous compositions, but at high fuel-air ratios and low pressures dissociation has to be taken into account. Then the composition of the gas is defined by chemical equilibrium conditions. As an example, representative for reheat operation at high altitude, the equilibrium compositions are shown in the next table for equivalence ratio 1, temperature 2000 K and 1 bar pressure:

	N_2	O_2	H_2O	Ar	CO_2	other
war =.03	69.617%	0.184%	16.605%	0.835%	12.117%	0.642%
dry air	72.762%	0.182%	12.895%	0.873%	12.662%	0.626%

In performance calculations, the chemical composition of the gases is only of secondary interest. It is, however, important to know which temperature rise one gets for an injected amount of fuel.

In the following table some data are given for the effect of a water-air ratio of 0.03 on the ideal temperature rise (efficiency = 1) in main burners. The temperature increase for a given far is lower in humid air.

far = 0.01	**far** = 0.02	**far** = 0.03
ΔT_{out} = -9.7 K	ΔT_{out} = -18.3 K	ΔT_{out} = -26.0 K

In reheat systems, dissociation plays a bigger role than for main burners since both the pressure levels are lower and the fuel-air ratios are higher. In the table below some typical data are given for the change in ideal temperature rise due to humidity (**war** = 0.03) in reheat systems.

	far = 0.04	**far** = 0.05	**far** = 0.06
T_{in} = 500 K	ΔT_{out} = -32.3 K	ΔT_{out} = -36.4 K	ΔT_{out} = -37.8 K
T_{in} = 700 K	ΔT_{out} = -32.0 K	ΔT_{out} = -34.9 K	ΔT_{out} = -36.2 K
T_{in} = 900 K	ΔT_{out} = -31.4 K	ΔT_{out} = -33.1 K	ΔT_{out} = -34.7 K

Note that the maximum temperature achievable (stoichiometric burning at fuel-air ratio approximately 0.07) in humid air is lower than in dry air.

The effect of humidity on the ideal burning process can be simulated easily within performance calculation computer programs. No additional problem is created since burner systems do not follow the Mach number similarity.

Since there is less oxygen available for burning in humid air one should expect an influence of water-air-ratio both on efficiency and blow-off limits.

Pollution is only a secondary topic within this report. There are some effects of humidity on combustion products. From chemical equilibrium calculations one can derive that NO_x is decreasing with increasing humidity. Generalized correction factors are presented in Reference 3.3.

3.3.4 Nozzles

Gross thrust of a nozzle is represented by:

$$F = W V + A (P_S - P_{amb}) \qquad 3\text{-}59$$

For the ideal case where the static pressure in the nozzle exit plane is equal to the ambient pressure, this equation can be expressed in terms of Mach number and isentropic exponent. Due to humidity, the isentropic exponent will decrease (Figure 3-2). The effect on thrust can be calculated from Equation 3-60.

$$\frac{\left(\frac{F}{A\ P_T}\right)_d}{\left(\frac{F}{A\ P_T}\right)_{mix}} = \frac{\gamma_d}{\gamma_{mix}} \frac{\left(1 + \frac{\gamma_{mix}-1}{2} Ma^2\right)^{\frac{\gamma_{mix}}{\gamma_{mix}-1}}}{\left(1 + \frac{\gamma_d-1}{2} Ma^2\right)^{\frac{\gamma_d}{\gamma_d-1}}} \qquad 3\text{-}60$$

In Figure 3-25 this equation was evaluated for a range of Mach numbers and changes in the isentropic exponent. In general, the impact of humidity on thrust is small. Note that, in contrast to many other humidity correction formulae, the Mach number level is important here. It is not justifiable to simplify the above formula to the ratio of γ_d/γ_{mix}.

3.4 ENGINE PERFORMANCE

The performance of the complete engine in humid conditions will be some superposition of the previously presented component effects. In addition, the control actions also may be affected. If the control system uses functional relationships with parameters affected by humidity, eg. corrected speed, then control actions will vary with humidity. This section presents a description of consistent analysis methods, followed by a presentation of available data to illustrate and validate the methods.

The gas dynamic analysis for humidity effects on compressor speed and airflow (Equations 3-39 and 3-40) can be extended to other parameters of importance for overall engine performance assessment. Samuels and Gale (1950) (Reference 3.4) have derived ratios of dry to moist air parameters for a single spool engine. Some details of that analysis are included here to allow comparisons to engine test data (engine station numbers are consistent with SAE ARP 755A). Engine fuel flow corrections were derived by defining the fuel flow as a function of combustor temperature rise:

$$\eta_b Q_L W_F = W c_p T_{T4} \left(1 - \frac{T_{T3}}{T_{T4}}\right) \qquad 3\text{-}61$$

By substituting Equation 3-43 for the airflow term, and considering the quantities T_{T4}/T_{T1} and

T_{T3}/T_{T4} as invariant with humidity, and constant inlet Mach number, the correction for fuel flow becomes:

$$\frac{W_{F,d}\ /\delta\sqrt{\Theta}}{W_{F,mix}\ /\delta\sqrt{\Theta}} = \frac{\sqrt{R_{mix}\ \gamma_d}}{\sqrt{R_d\ \gamma_{mix}}} \frac{c_{p\ b,d}}{c_{p\ b,mix}} \qquad 3\text{-}62$$

where the specific heat is to be calculated for the burner or combustor.

With turbine inlet temperature and component efficiency assumed to be invariant with humidity changes, Samuels and Gale (Reference 3.4) included a humidity correction for turbine exit temperature:

$$\frac{T_{T5,d}}{T_{T5,mix}} = \frac{1-\eta_t\left[1-\left(\frac{P_{T5}}{P_{T4}}\right)_d^{\Gamma_d}\right]}{1-\eta_t\left[1-\left(\frac{P_{T5}}{P_{T4}}\right)_{mix}^{\Gamma_{mix}}\right]} \qquad 3\text{-}63$$

where:

$$\Gamma_d = \frac{\gamma_d - 1}{\gamma_d}$$

and

$$\Gamma_{mix} = \frac{\gamma_{mix} - 1}{\gamma_{mix}}$$

The possible rematching of components with humidity variations is allowed for in the terms for the turbine pressure ratio. The authors also assumed that Reynolds numbers, effective flow areas, and flow coefficients were constant with changes in humidity. These analytical methods are useful to understand the general effects of humidity on overall engine performance. However, maintaining the various assumptions, ie. choked nozzles, while including the effects of the control system, limits the general application of these corrections.

3.4.1 Performance Parameter Correction Methods

There are two general methods for the estimation of humidity effects on overall engine performance. The first method uses an aerothermodynamic model of the engine cycle, coupled with a complete accounting of gas composition and thermodynamic properties for each component (Section 3.2.2). Water-to-air ratio or absolute humidity would be an input ambient condition so that the cycle calculations would implicitly include the effect of humidity.

It is also necessary to correct test data for ambient humidity. Current "analysis by synthesis" procedures available to manufacturers scale and adjust computer model parameters to match actual data for actual ambient (moist) conditions. This tuned model can then be run at the desired dry, reference condition for comparison purposes. An alternate method is to correct, individually, the data for each measured performance parameter. Ratios of dry to moist parameter values, eg. Equations 3-39 and 3-40, may be applied for correction directly. However, to use these corrections correctly requires the proper reference power setting, used in the derivation: constant inlet axial Mach number. Therefore, the effect of humidity could be directly calculated for inlet airflow, rotor speed, fuel flow, thrust, and turbine temperature, if data were available, or desired, at constant inlet Mach number.

A more usual reference performance parameter is the corrected inlet gas flow (water vapour and air) corrected for the variation in specific heat ratio and gas constant (Equation 3-40 and Lazalier et al, Reference 3.5). Data for other parameters, first corrected with the recommended factors from Sections 3.3 and 3.4, can then be cross-plotted, at constant corrected gas flow. Thus, performance analysis plots can be constructed while maintaining the reference condition used in the derivation of the humidity corrections.

3.4.2 Component Rematching and Control System Considerations

The actual application of the correction methods described above can be significantly influenced by component rematching and control system operation, as a result of operation in humid air. The corrections of Section 3.3 predict changes in corrected speed (Equation 3-39) and combustor temperature rise (Section 3.3.3) for comparisons at constant corrected (ambient temperature, pressure, and true gas properties) flow. This indicates that some component rematching may occur, dependent on the extent of the humidity change. For example, the change in corrected speed at constant corrected flow predicted for a fan implies a change in pressure ratio and temperature rise.

With humidity effects predicted for engine control parameters and component temperature rises, the selection of engine control modes could be affected. However, if the gas property accounting is carried out within a cycle deck, then the appropriate control functions will be selected automatically.

The control logic will have to be applied explicitly if the humidity corrections are used, following the approach of Section 3.4.1. Three typical control modes are considered here:

i) corrected speed control: since corrected speed would be altered with humidity changes (at constant Mach number / inlet gas flow), control scheduling or mode shifts may occur. The anticipated shifts should be small unless the humidity changes are extreme, or the engine is operating near a mode boundary.

ii) exhaust gas temperature control: the discussion of Section 3.4 implies a direct alteration of this temperature with changing humidity. If the engine is operating near the temperature control limit, the control mode could be altered.

iii) engine pressure ratio control: since no direct effect of humidity is predicted in Section 3.4, shifts in control mode will occur only if the re-matching of the engine components is sufficient to change the turbine exit pressure.

An example of these effects is available for a low bypass ratio mixed flow, military turbofan. With constant corrected fan speed control, the humidity correction for engine core fuel flow is shown in Figure 3-26 (with Samuels and Gale (Reference 3.4) and Fishbeyn and Pervyshin (Reference 3.6) as references). Corrections vary over the range of inlet temperatures shown because the corrected fan speed at the set point (military power) changes.

3.4.3 Validation of Correction Methods

Some engine data with humidity corrections have been compiled to validate the prediction methods of Sections 3.3 and 3.4.1. The Samuels and Gale (Reference 3.4) corrections for corrected parameters agree with the component corrections shown in Section 3.3: rotor speed (Equation 3-42), airflow (3-43), and thrust (3-60).

Fishbeyn and Pervyshin (Reference 3.6) applied theoretical corrections similar to those of Section 3.3 and Samuels and Gale, by incorporating the gas property accounting into a component-level, thermodynamic cycle deck or program. This model was run with varying humidity and power setting levels for cycles with bypass ratios of 0 to 4 and turbine inlet temperatures of 900 to 1400 K. The validation process for the model is not discussed. However, the correction factors derived by simulating changing humidity levels, at constant inlet Mach number, Ma_u, were in excellent agreement with those of Samuels and Gale. Fishbeyn and Pervyshin claimed that the single set of derived correction factors collapsed the model outputs to within 0.5 percent for the range of engine cycles and ambient conditions studied. These corrections were weak quadratic functions of absolute humidity (**war**):

Thrust: $C_X = 1 - 0.0826\ \mathbf{war} - 0.0021\ \mathbf{war}^2$

Fuel Flow: $C_F = 1 + 0.4882\ \mathbf{war} + 0.3828\ \mathbf{war}^2$

Airflow: $C_A = 1 - 0.3352\ \mathbf{war} - 0.4010\ \mathbf{war}^2$

Compressor Speed:
$C_N = 1 + 0.2607\ \mathbf{war} - 0.1538\ \mathbf{war}^2$

Turbine Inlet Temperature:
$C_T = 1 - 0.0845\ \mathbf{war} - 0.119\ \mathbf{war}^2$

where **war** has the units of mass ratio of water to air. These theoretical corrections are compared to empirical corrections in the next two sections.

3.4.3.1 *Experimental Validation*

a) Turbojet Engines with Centrifugal Compressors: For verification of their analytically-derived corrections, Samuels and Gale (Reference 3.4) conducted an experimental investigation with two engines operated at controlled humidity levels. One was a single-spool turbojet engine, with a centrifugal-type compressor and a single-stage axial-flow turbine. The other was also a turbojet engine, higher in thrust by 185% but of similar configuration.

In the initial comparative plot between theoretical and experimental corrections, the theoretical curves were calculated by assuming a constant compressor inlet Mach number, while the experimental data were based on engine operation at constant engine speed and inlet temperature (Reference 3.4). Thus, differences of between 0.7% for engine speed, and 1.8% for thrust, were ascribed to the different reference conditions. To verify this proposition, the theoretical curves were adjusted to a constant engine speed; the resulting curves for the theoretical and experimental approaches agreed within 0.5% up to absolute humidities of 0.03 (Figure 3-27). This finding points out the importance of the reference conditions in properly applying the humidity corrections. The authors concluded by suggesting that their approximate method could be used for humidity corrections, and that corrections determined for one engine could be applied to any engine of similar type. A more complete discussion of the assumptions and limitations of these two reports is given in Reference 3.7.

b) Turbojet Engine: Counts and Lazalier (Reference 3.8) studied performance test data with controlled humidity levels. Specific fuel consumption

results showed 1 and 2% increases at constant absolute humidity levels of 0.017 and 0.031, respectively. For the two specific points examined, the authors found excellent agreement with the theoretical method of Fishbeyn and Pervyshin. Their experimental and theoretical results agree with the prediction of Section 3.3 (Figure 3-28 with relative rather than absolute humidity).

c) Low Bypass Ratio Turbofan Engine: Similar controlled humidity tests were conducted with an F100 low-bypass-ratio fan engine (Lazalier et al, Reference 3.5). Tests at near-sea-level conditions used absolute humidities of 0.010, 0.016 and 0.020. The effects of variation in absolute humidity from 0.01 to 0.02 were:

i) engine pumping characteristic (engine pressure ratio vs engine temperature ratio) (Figure 3-29): negligible effect;

and at a high power setting (airflow of 90.4 kg/s (199.3 lbm/sec)):

i) corrected rotor speed at constant inlet Mach number (Figure 3-30): +0.20%. This agrees with the predicted value (Section 3.3.2.2) of 0.26%.

ii) corrected fuel flow at constant inlet Mach number (Figure 3-31): +0.49%, in agreement with the predicted value (Section 3.4) of 0.50%;

iii) corrected net thrust at constant inlet Mach number (Figure 3-32): no change, which agrees with the predicted value of -0.08%;

iv) corrected turbine inlet temperature at constant inlet Mach number (Figure 3-33): no change, which is consistent with the predicted correction of -0.08%;

v) corrected SFC at fixed corrected thrust (Figure 3-34): 0.5% increase at intermediate power, compared to the theoretical prediction, derived from combining the thrust and fuel flow corrections, of 0.6%.

The experimental data clearly verify the predictions when the comparisons are conducted in the proposed manner (Section 3.4.1), respecting the reference condition of the derivation.

Some limited data were also available for a TF41, an engine of slightly higher bypass ratio (Reference 3.9). Experimental data were gathered at sea-level-static conditions (304 K), at a fixed engine pressure ratio of 2.1, for absolute humidities of 0.0099 and 0.0175. The author concluded that the measured and predicted effects agreed to within 0.3 percent. However, Figure 3-35 shows significant differences for the corrections to ambient-corrected fuel flow and turbine exit temperature. The source of the predicted humidity effects is not known, but all of the predicted effects agree in magnitude and sign with those of Section 3.3. The deviations in fuel flow and turbine temperature may be caused by the noted shift in the engine airflow (at constant engine pressure ratio) which would cause the reference inlet Mach number to differ from the dry test condition. An improved comparison, using the method of Section 3.4.1 and Lazalier et al (Reference 3.5), would be appropriate, if the full data set was available.

d) High Bypass Ratio Turbofan Engine: Only limited data appear to be available to validate the predictions for high bypass ratio engine. Reference 3.10 provides data from production engine tests for the RB211-535. Humidity corrections according to Section 3.2 were applied to reduce scatter in the test data. Results presented show reductions in two sigma scatter, at take-off power, for:

i) SFC: from scatter of 0.944% in basic data to 0.779% after humidity corrections;

ii) Turbine gas temperature: from scatter of 8.02 K in basic data to 7.79 K after humidity corrections;

iii) Low rotor speed: from scatter of 0.82% in basic data to 0.72% after humidity corrections.

To correct data taken at humid conditions, Reference 3.10 found SFC and low rotor speed are reduced in value and turbine gas temperature is increased. These data offer a limited validation of the methods of Section 3.3 for high bypass ratio turbofans, since complete test data with controlled humidity levels have not become available.

3.4.3.2 *Engine Operator Corrections*

Gas turbine operators in ground test facilities or stationary installations are often provided with formulae by manufacturers to correct for humidity effects on engine performance. Without information from the suppliers, it is not possible to find out how these corrections were established and whether they are of theoretical or empirical origin. Most likely, they are a combination of both.

A limited survey of field humidity corrections yielded the following sample, taken mostly from test cell operation instructions and engine manuals. A list of their sources is given in References 3.11 to 3.18. The corrections from Samuels and Gale, and Fishbeyn and Pervyshin, have been included as reference points for these comparative examinations. The findings of this survey have previously been presented by Bird and Grabe (Reference 3.7). Reference Conditions, i.e. para-ameter(s) held constant for wet to dry comparisons were not available for GE T/C (Reference 3.16), JT9D

(Reference 3.14), and RB211 (Reference 3.15). For the CFM56 (Reference 3.13), no correction is applied to EPR.

a) Compressor Speed: Compressor speed was the most common engine parameter to be corrected for humidity. All correction curves but one had the same trend as the predictions, i.e. the compressor speed would be higher in moist air than in dry (Figure 3-36). For a representative test condition of 293 K and 80% RH, which yields an absolute humidity of 0.0118, the various sources would suggest a speed correction of 0.3 ±0.1 percent.

The sole exception was the correction given for the J79 engine specifically (Reference 3.11), which suggests a drop in compressor speed (hence not plotted in Figure 3-36). The correction was intended for use in collapsing test cell correlation results when plotted as a function of engine pressure ratio. Since this is the same apparent application and reference condition for the general corrections applicable to J85/J79 engines (Reference 3.12) plotted in Figure 3-36), the reasons for the differences are not evident.

It will be noted that for multi-spool engines, the available data for PW100 (constant SHP) and RB211 engines showed decreasing speed corrections for each spool of higher pressure.

b) Airflow: The general prediction was that with moisture in the air, the airflow decreases relative to the dry-air condition. Different corrections were given for the LM2500 stationary gas turbine, depending on the reference control mode. For constant shaft horsepower (SHP) and power turbine speed (NPT), the airflow correction is nearly twice the correction for the control mode of constant power turbine inlet total temperature (T54) and power turbine speed (NPT). This observation underscores the importance of considering the assumptions made and operating mode prevailing when correcting for humidity, as pointed out in Section 3.4.1.

c) Fuel Flow: All predictions agreed that fuel flow would increase with moist air (Figure 3-37). Depending on the operating modes, the humidity corrections for the LM2500 were the largest (T54 and NPT constant), as well as the smallest (SHP and NPT constant), among those corrections that were available. The correction is strongly affected by the reference condition and the control mode. It should be noted that for the selected ambient condition of 293 K/80% RH, the average correction would be about 0.5 percent. This is an important adjustment to fuel flow data in performance assessment.

d) Turbine Inlet and Outlet Temperatures: Turbine inlet or outlet temperatures can be expected to decrease with humidity (Figure 3-38). The apparent spread among correction curves can largely be attributed to differences in operating or reference modes (LM2500: SHP, NPT fixed versus NG, NPT fixed) and gas path station (PW100: HP turbine inlet (T4) versus HP turbine outlet (T6)). However, at an inlet condition of 293 K/80% RH, most corrections are relatively small, say less than 0.2%. At 1400 K, 0.2% represents only 2.8 K, an amount which would normally not be easily detected, given the uncertainty of most instrumentation.

e) Thrust or Power: The thrust or power corrections for humidity presented conflicting results (Figure 3-39). Two users, in three applications, followed the prediction trend that moisture in the inlet air would lead to a reduction in thrust. The LM2500 data (SHP, NPT fixed) and the J85/J79 (Reference 3.12) indicated somewhat greater thrust/power reductions from moisture than predicted from analysis. However, at 293 K/80% RH, corrections were only of the order of 0.15%. The third, the CFM56 corrections, were so small as to be virtually non-existent.

Two further data sources gave corrections with an opposite trend, ie. thrust/power *gains* from humidity (Figure 3-39). One was the LM2500 stationary gas turbine with T54, NPT fixed, and the other the J79 engine (Reference 3.11), which, by the way, also had the compressor speed corrections with an opposite trend. The LM2500 power humidity corrections were significantly larger than the J79 ones (0.6% vs. 0.3% at 293 K and 80% RH).

The differences in corrections for the two LM2500 reference modes (SHP, NPT fixed and T54, NPT fixed) may be explained using the airflow corrections. Moist airflow is predicted to be relatively greater for the constant temperature case, and so the power output should be relatively greater at these higher airflow levels.

f) Specific Fuel Consumption: Only the LM2500 data set included corrections for specific-fuel-consumption (SFC). While Fishbeyn and Pervyshin had given SFC curves in their report (1970), the curve for Samuel and Gale was derived from fuel flow and thrust data (Grabe and Bird, Reference 3.19). Compared to either of these humidity corrections, the LM2500 corrections for either control mode were small, about one third of the values estimated by the two theoretical/empirical methods. At 293 K and 80% RH (absolute humidity 0.0118), the LM2500 humidity correction would be approximately 0.2% for either mode.

3.4.4 Summary

Gas dynamic property corrections for water vapour in inlet air to gas turbines have been derived and shown to agree with several sets of test data. The predictions are reasonably well validated for low bypass ratio turbofans, with only a limited validation of turbojet and high bypass ratio engines, because of a dearth of test data. However, cycle studies suggest that the same methods should be valid for engines with bypass ratios up to 4 and turbine inlet temperatures of 1400 K (the range of the cycles studied).

The available test data from controlled humidity operations show that moderate to high levels of absolute humidity will affect most engine performance parameters by 0.1 to 1.0 percent. The magnitude and the sign of the changes are significantly altered by the choice of reference condition, i.e. dry air and which performance parameter is to be held constant. Corrected inlet gas flow or EPR showed low sensitivity to humidity at constant inlet Mach number. These may then also be considered for reference parameters.

A series of accessible, manufacturer-supplied, humidity corrections for the field data generally agreed in trend, if not in magnitude, with the predicted corrections. The published corrections for one particular gas turbine differed significantly between operating modes. This underscores the importance of recognizing reference conditions and operating modes in humidity corrections.

3.5 CONCLUSIONS AND RECOMMENDATIONS

Chapter 3 deals with gaseous water only, and all the statements apply only if there is truly no condensation.

The fluid properties of humid air can be described in a number of ways. The most correct way is to do all calculations for mixtures of the gases N_2, O_2, H_2O, CO_2, and Ar. That, however requires considerable computer power. Alternatively, one can describe the fluid properties using approximate methods (i.e. tabulations or polynomials) with water-air-ratio as an additional parameter.

Component performance is affected by humidity in two ways: the primary effect comes from the change in gas constant. This effect can be considered in a straightforward manner. The change in isentropic exponent due to humidity is not large but its effect cannot be described in a simple way.

The characteristics of compressors and turbines are based on Mach number similarity. A change in the isentropic exponent will not allow full similarity of flow fields. The effect of the isentropic exponent on the flow field can only be approximated and, as indicated above, there are different approximations in current use for humidity effects. A comparison with a compressor map calculation program showed that none of the correction methods described in this report is superior to the others. In fact, as yet, no method can predict the effects of the isentopic exponent in a fully satisfactory way.

Fortunately, with respect to the effect of gaseous humidity, it is not important to have extremely accurate methods for describing the effect of a change in the isentropic exponent. For simplification of the calculations, it is recommended that corrections for the change in the gas constant due to humidity be included, but the effect of humidity on the isentropic exponent may be ignored. The situation is more serious within the normal operating range of core compressors where the isentropic exponent changes much more due to inlet temperature than due to humidity. Another example where a knowledge of the isentropic exponent is important is in the transfer of component rig data to engine simulations, especially in the case of cold flow tests of turbines. This problem, however, is not part of this report. The effects of gaseous humidity on overall engine performance can be predicted using cycle calculation programs that have included appropriate component characteristics. For realistic answers it is necessary that the engine control system be described correctly. The reaction of an engine to a change in humidity depends on the controlling parameter. The effects for constant speed are different than those for constant pressure ratio, for example.

For the development of improved correction methods, it is necessary to enlarge the database of compressor and turbine map calculations. There may be a difference between single stage machines and multi-stage machines. Moreover, different map calculation programs may give different answers.

When no performance calculation program is available, humidity corrections can be applied that have been defined for specific engines by the manufacturer. The magnitude of the corrections is engine specific and cannot be applied, without risk, to other engines.

A summary of the effects of gaseous humidity on engine performance is given in Table 3-3.

3.6 REFERENCES

3.1 Gordon, Sanford, *Thermodynamic and Transport Combustion Properties of Hydrocarbons With Air*, NASA TP 1906, July 1982.

3.2 Duponchel, J.P., Loisy, J., Carrillo, R., *Steady and Transient Performance Prediction of Gas Turbine Engines*, AGARD LS 183, May 1992.

3.3 Donovan, P., and Cackette, T., *The Effects of Ambient Conditions on Gas Turbine Emissions - Generalized Correction Factors,* ASME 78-GT-87, 1978.

3.4 Samuels, J.C. and B.M. Gale, *Effects of Humidity on Performance of Turbojet Engines*, National Advisory Committee for Aeronautics, Washington, D.C., Tech. Note 2119, 1950.

3.5 Lazalier, G.R, J.D. Palmer and R.E. Harper, *Altitude Development of the F100-PW-100 Turbofan Engine Phase IX*, Arnold Engineering Development Center Technical Report. June 1975.

3.6 Fishbeyn, B.D. and N.V. Pervyshin, *Determination of the Effect of Atmospheric Humidity on the Characteristics of a Turbofan Engine*, Translation by Foreign Technology Division, Wright-Patterson AFB, OH, FTD-HT-23-290-68 (AD 715232), 1970.

3.7 Bird J. and W. Grabe, *Humidity Effects on Gas Turbine Performance*, ASME International Gas Turbine and Aeroengine Congress and Exposition, Orlando, FL, June 3-6, 1991, Paper No. 91-GT-329, 1991.

3.8 Counts, H.J. and G.R. Lazalier, *Baseline Performance of Newly Overhauled J75-P-17 Turbojet Engines*, Arnold Engineering Development Center Technical Report, February, 1978.

3.9 Anonymous. *Altitude Evaluation of An Overhauled TF41-A-1 Turbofan Engine (S/N 141683).* Arnold Engineering Development Center Technical Report. August 1977.

3.10 Rolls Royce, *Test Data for Validation of Humidity and Condensation Correction Methods*, Private Communication with C. Begley, 23 July 1993.

3.11 U.S. Air Force, *Operations, Maintenance Technical Manual and Parts Breakdown. Test Cell Correlation 33D4-6-261-1 Set*, T.O. 33D4-6-261-1. 1C3954G1 (General Electric), Published under Authority of the Secretary of the Air Force, 1 December 1966 (Change 1 - 30 April 1984).

3.12 U.S. Air Force, *General Engine Test and Technical Manual Test Cell Instructions. Turbojet, 2J-J1-10 Turbofan Aircraft Engines*, T.O. 2J-J1-10, Published under Authority of the Secretary of the Air Force, 16 September 1963.

3.13 Air Canada, *Air Canada Unit Overhaul Manual 901, Engine Testing CFM56. Testing 72-00-00 October 1985, January 1986, October 1988.* Air Canada, Dorval, Quebec, Canada, 1988.

3.14 Air Canada, *Air Canada Unit Overhaul Manual 901, Engine Testing, Effectivity: JT9D-7R4D "A" Package. 71-00-00 Testing. June 1984, June 1986, February 1988.* Air Canada, Dorval, Quebec, Canada, 1988.

3.15 Air Canada, *Air Canada Unit Overhaul Manual 901, RB211-524B4 Test Schedule, Testing 72-00-00, July 1981, February 1982, May 1983, November 1983, January 1987.* Air Canada, Dorval, Quebec, Canada, 1987.

3.16 General Electric Company, *Commercial Engine Test Cell Correlation Procedure,* Procedure Design Engineering Department, Mail Drop G40, 1 Neumann Way, Box 156301, Cincinnati, OH, 45215-6301, October, 1988.

3.17 General Electric Company, *LM2500-30 Marine Gas Turbine Performance Data,* Marine and Industrial Engine Division, Cincinnati, OH, General Electric MID-TD-2500-8, July, 1981.

3.18 Pratt & Whitney Canada, *PW100 Test Bed PW100 Correction Program Humidity Effects,* Paul R. Nutt, January 31, 1989.

3.19 Grabe, W.K. and J.W. Bird, *Humidity Effects on Gas Turbine Performance*, National Research Council of Canada, Institute for Mechanical Engineering, Ottawa Ontario, Technical Report TR-ENG-003, 1988.

3.20 Braig, W. and Riegler, C., *Berücksichtigung des Einflusses des Isentropenexponenkn auf die Kennfelder von Turbinen.* Forschung im Ingenieurwesen, September, 1994.

Table 3-1

EFFECT OF GASEOUS HUMIDITY ON ENGINE PERFORMANCE PARAMETERS

(Mean values for various engines ranging from $0 < BPR < 6$)

war = 0.0143	constant $N/\sqrt{\gamma RT_T}$	constant N	constant EPR
Compressor speed N	+ 0.34%	0	+ 0.4%
Air flow W_a	- 0.50%	- 0.9%	- 0.4%
Fuel flow W_F	+ 0.69%	- 0.7%	+0.7%
Thrust F	- 0.13%	- 1%	~ 0
SFC	+ 0.82%	+ 0.3%	+ 0.7%

war = 0.0272	constant $N/\sqrt{\gamma RT_T}$	constant N	constant EPR
Compressor speed N	+ 0.65%	0	+ 0.8%
Air flow W_a	- 0.96%	- 1.6%	- 0.8%
Fuel flow W_F	+ 1.31%	- 1.3%	+ 1.4%
Thrust F	- 0.25%	- 1.9%	~ 0
SFC	+ 1.56%	+ 0.6%	+ 1.4%

Table 3-2

SUMMARY OF RELATIONSHIPS

	dry air (d,a)	**water vapour** (v)	**mixture** (mix)
Mass fraction relative to dry air (Absolute humidity)	1	**war** $= x_v / x_{d,a}$ $= 0.622\ P_{Sv}/(P_{Smix} - P_{Sv})$	1 + **war**
Mass fraction relative to mixture (Specific humidity)	$x_{d,a} = 1/(1 + \mathbf{war})$	$x_v = \mathbf{war}/(1 + \mathbf{war})$	1
Density	$\rho_{d,a}$	$\rho_v = \mathbf{war} * \rho_{d,a}$	$\rho_{mix} = (1 + \mathbf{war})\ \rho_{d,a}$
Gas constant	$R_a = 287.05$ J/kg.K	$R_v = 461.52$ J/kg.K	$R_{mix} = \dfrac{287.06 + 461.52\mathbf{war}}{1 + \mathbf{war}}$
Temperature (equilibrium)	$T_{S\,d,a}$	$= T_{S\,v}$	$= T_{S\,mix}$
Pressure (Dalton's Law)	$P_{S\,d,a} = P_{S\,mix} - P_{S\,v}$ $P_{S\,d,a} = \dfrac{P_{S\,mix}}{(\mathbf{war}/0.622 + 1)}$	$P_{S\,v}$ $P_{S\,v} = \dfrac{P_{S\,mix}}{(0.622/\mathbf{war} + 1)}$	$P_{S\,mix}$

$$\text{Relative humidity} \qquad RH = \frac{P_{Sv}}{P_{Ssat}}$$

$$\text{Degree of saturation} \qquad \varphi = \frac{\mathbf{war}}{\mathbf{war}_{sat}}$$

$$\mathbf{war} = 0.622\ \frac{P_{Ssat}}{\dfrac{P_{Smix}}{RH} - P_{Ssat}}$$

$$\varphi = RH\ \frac{P_{Smix} - P_{Ssat}}{P_{S\,mix} - P_{Sv}}$$

For the range of temperatures considered here, the partial pressures $P_{S\,v}$ and $P_{S\,sat}$ are small compared to $P_{S\,mix}$ and therefore: $\varphi \approx RH$, indicating that the relative humidity RH is very close to the degree of saturation.

Table 3-3

CAPABILITY OF RECOMMENDED PRACTICES TO ASSESS THE EFFECTS OF GASEOUS HUMIDITY ON COMPONENT AND ENGINE PERFORMANCE

	ASSESSMENT METHOD	PERFORMANCE		OPERABILITY		COMMENTS
		Influence	Confidence	Influence	Confidence	
Components:						Measurement of gaseous humidity effects is important for tests where 1-2% difference in performance parameters is to be studied.
Inlet	A	M	H	L	H	
Fan/Splitter	A	M	H	L	H	
Compressor	A	M	H	L	H	
Combustor	A	M	H	L	H	
Turbine	A	M	H	L	H	
Nozzle: Core	A	L	H	L	H	
Nozzle: ByPass	A	L	H	L	H	
Engine:						
Controls	A	M	M	L	H	
Starting	A + T	N/A	N/A	L	M	
Power Transients	A	M	M	L	L	
Determining Core Water	N/A	N/A	N/A	N/A	N/A	

A - Analytical H - High M - Medium
T - Test L - Low N/A - Not Applicable

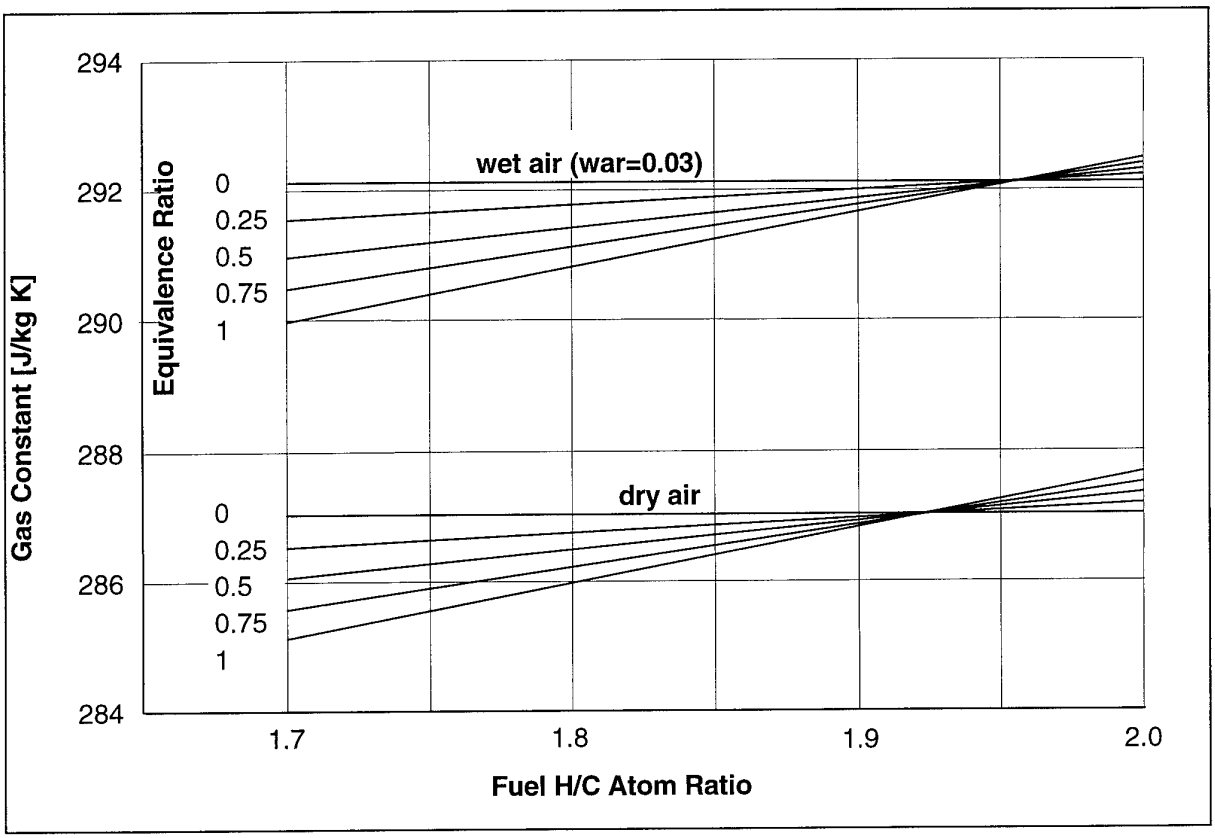

Figure 3-1

Gas Constant of Combustion Gases for Dry and Wet Air for Different
Fuel H/C Atom Ratios and Equivalence Ratios
(Reference 3.1 for Constant Composition)

Equivalence Ratio = **far** /**far**, stoich
far, stoich (dry air) = 0.06953 for H/C = 1.7
= 0.067628 for H/C = 2.0
far, stoich (wet air, war = 0.03) = 0.067624 for H/C = 1.7
= 0.065658 for H/C = 2.0

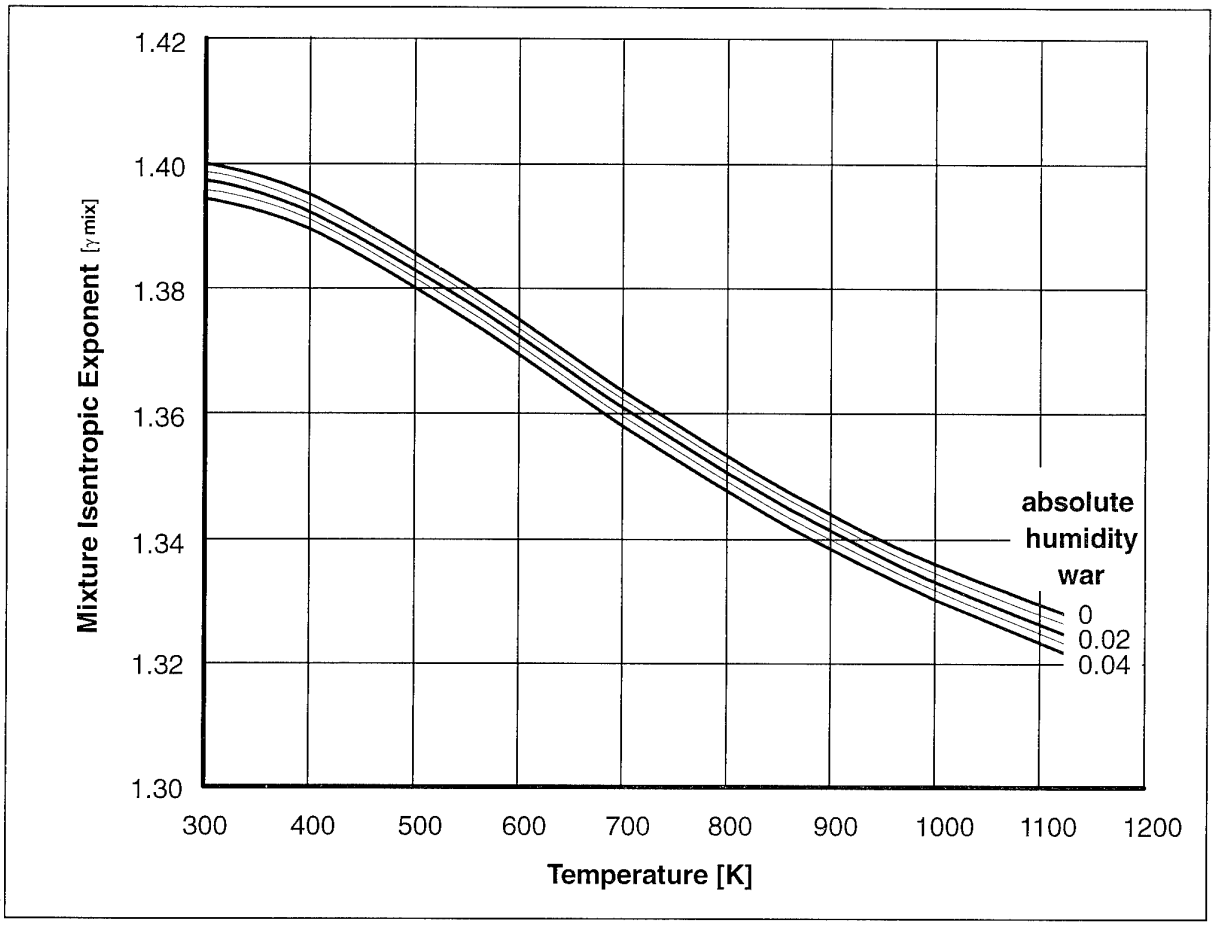

Figure 3-2

Isentropic Exponent for Dry and Wet Air

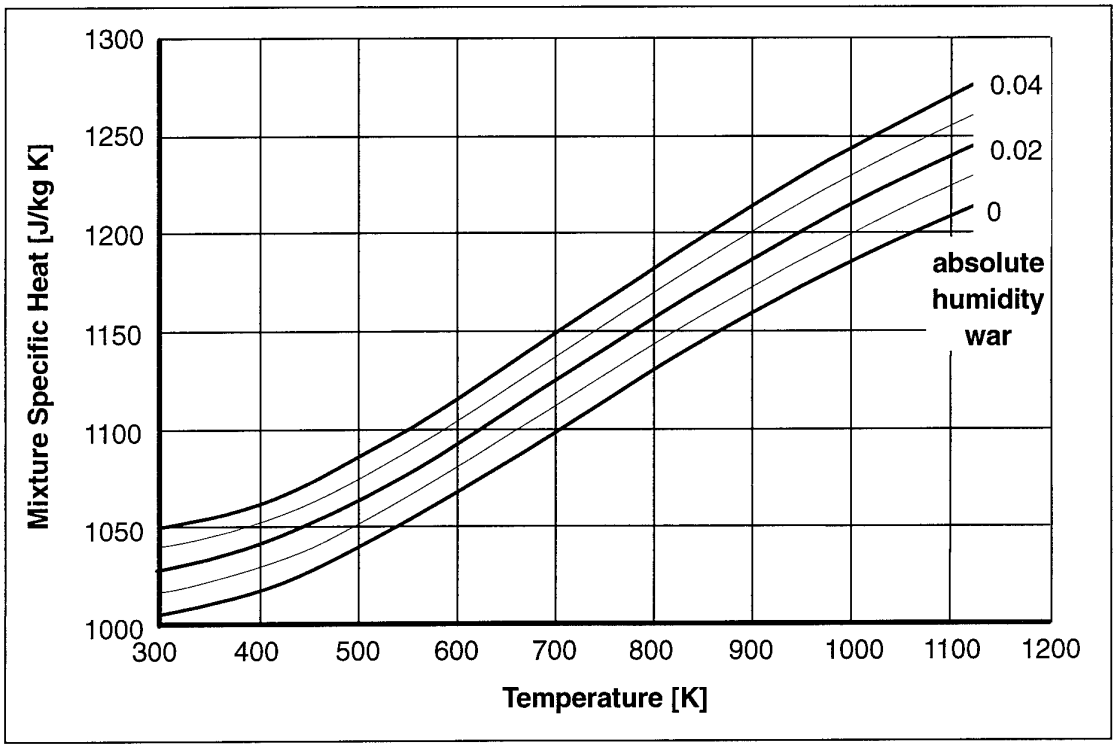

Figure 3-3

Specific Heat for Dry and Wet Air

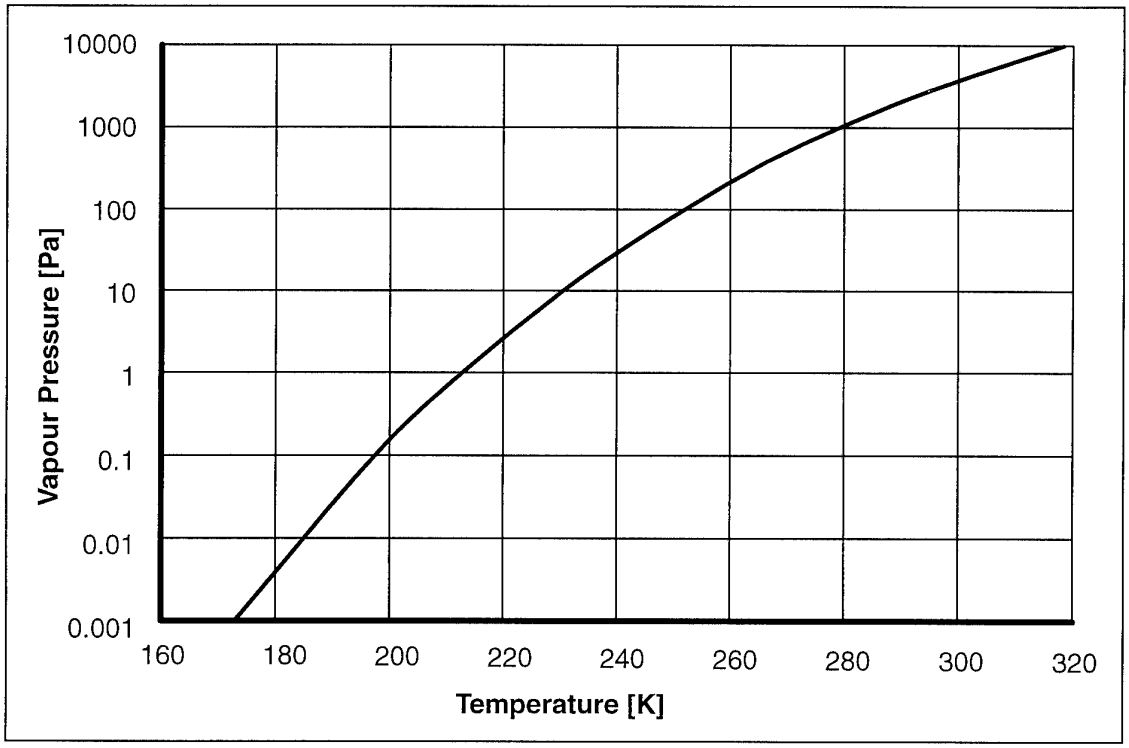

Figure 3-4

Vapour Pressure

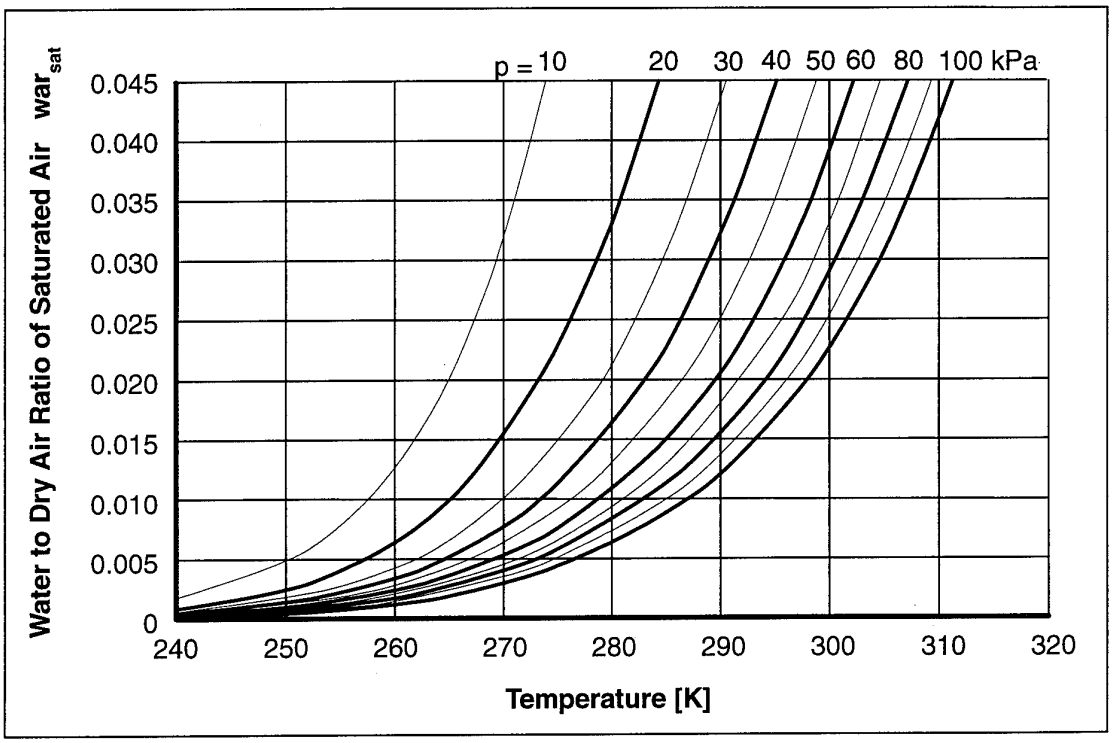

Figure 3-5

Saturated Water-Air-Ratio

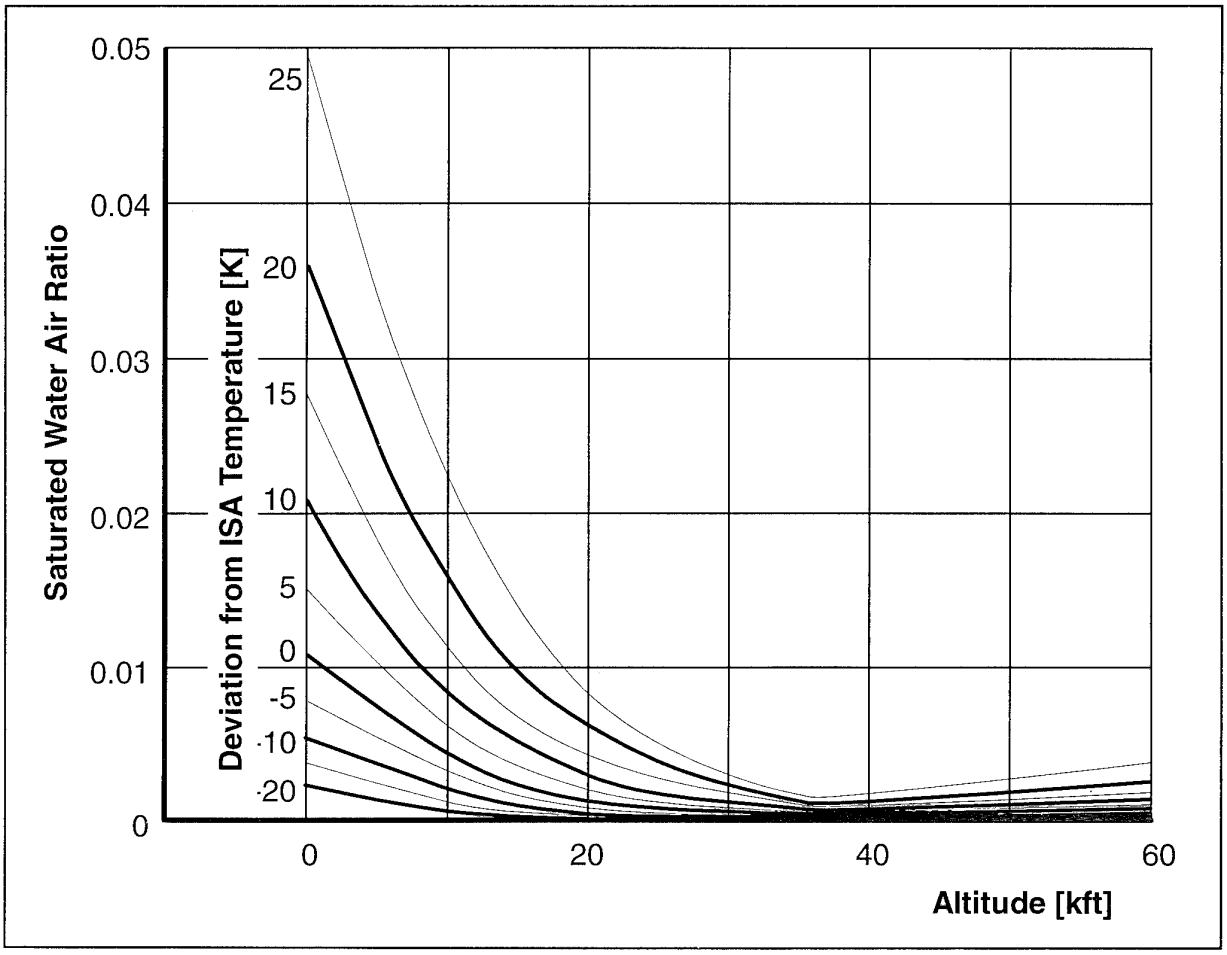

Figure 3-6

Water-Air-Ratio for Saturated Conditions as a Function of Altitude
and Deviation from ISA Conditions

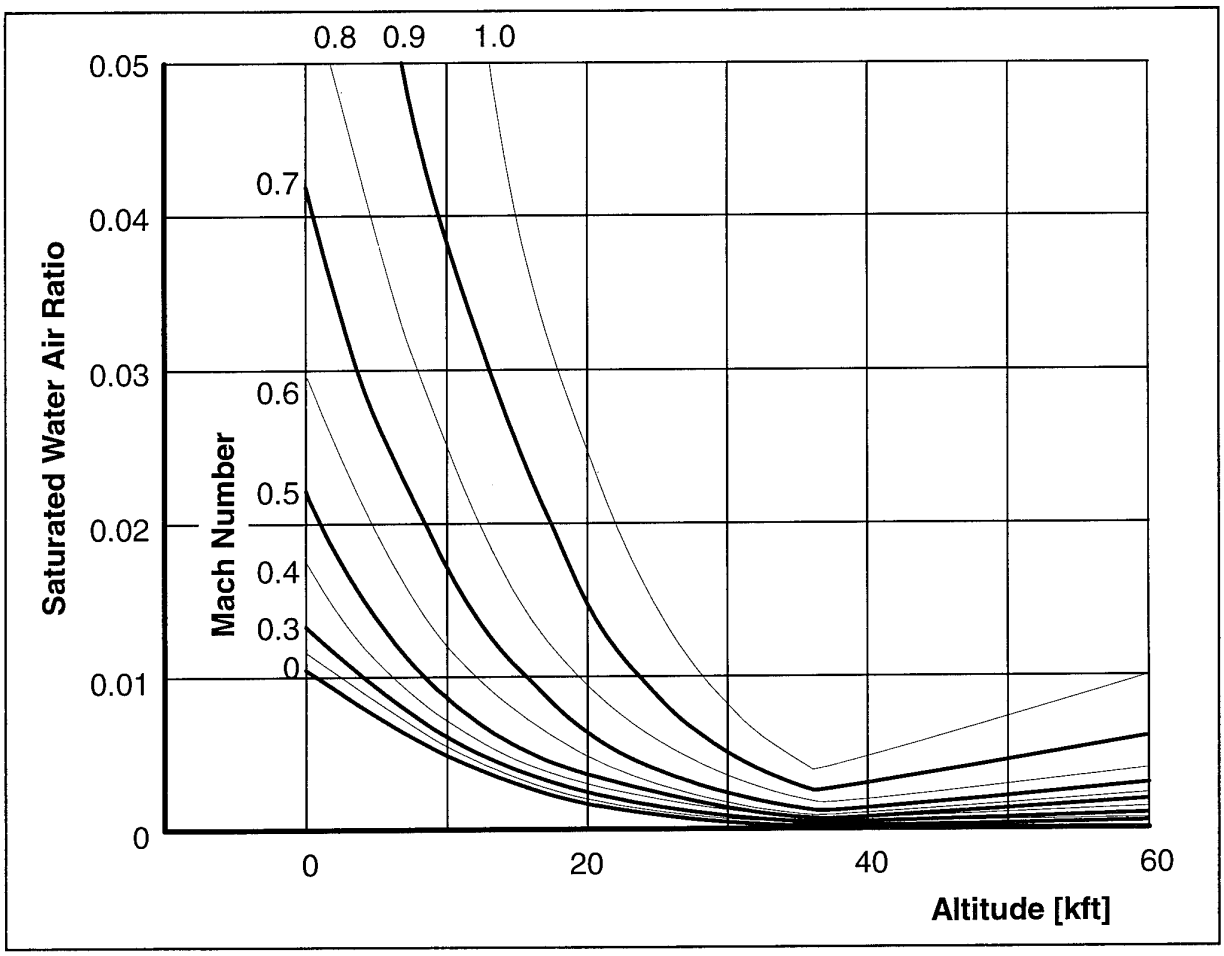

Figure 3-7

Water-Air-Ratio for Saturated Conditions During ATF Tests
as a Function of Altitude and Simulated Flight Mach Number

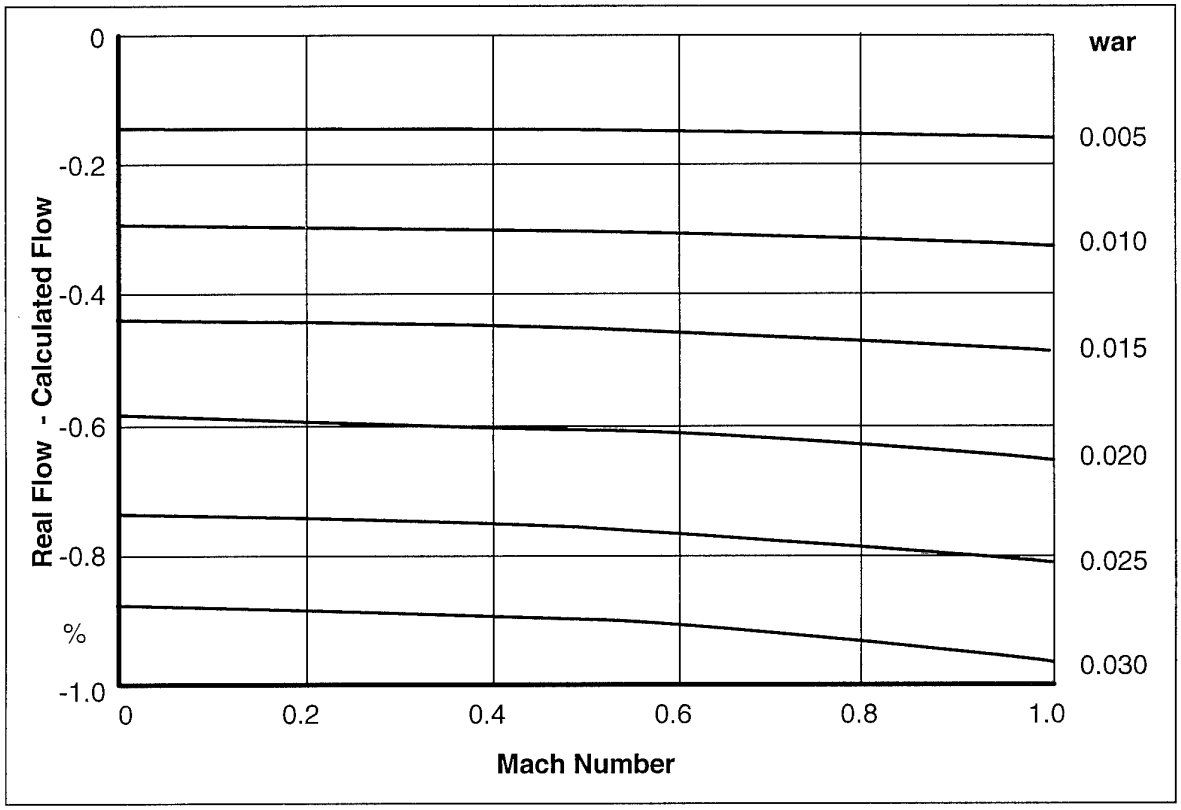

Figure 3-8

Mass Flow Error if Humidity is Neglected in Evaluation of Venturi Measurements

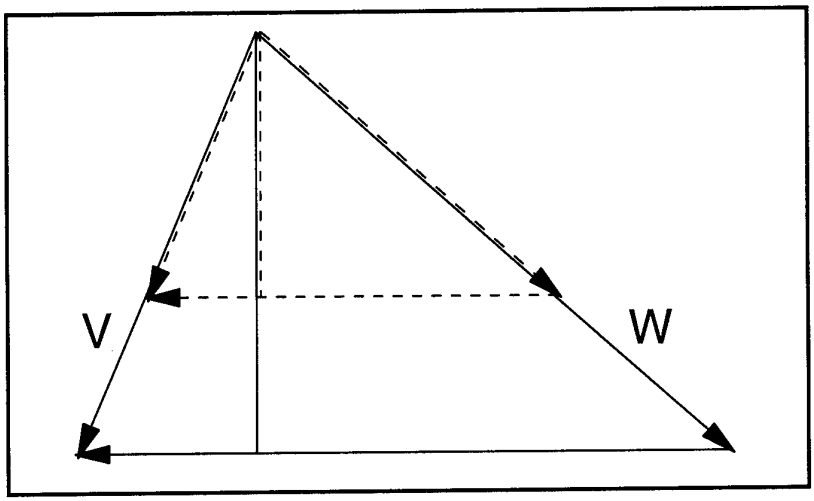

Figure 3.9

Similar Operating Conditions

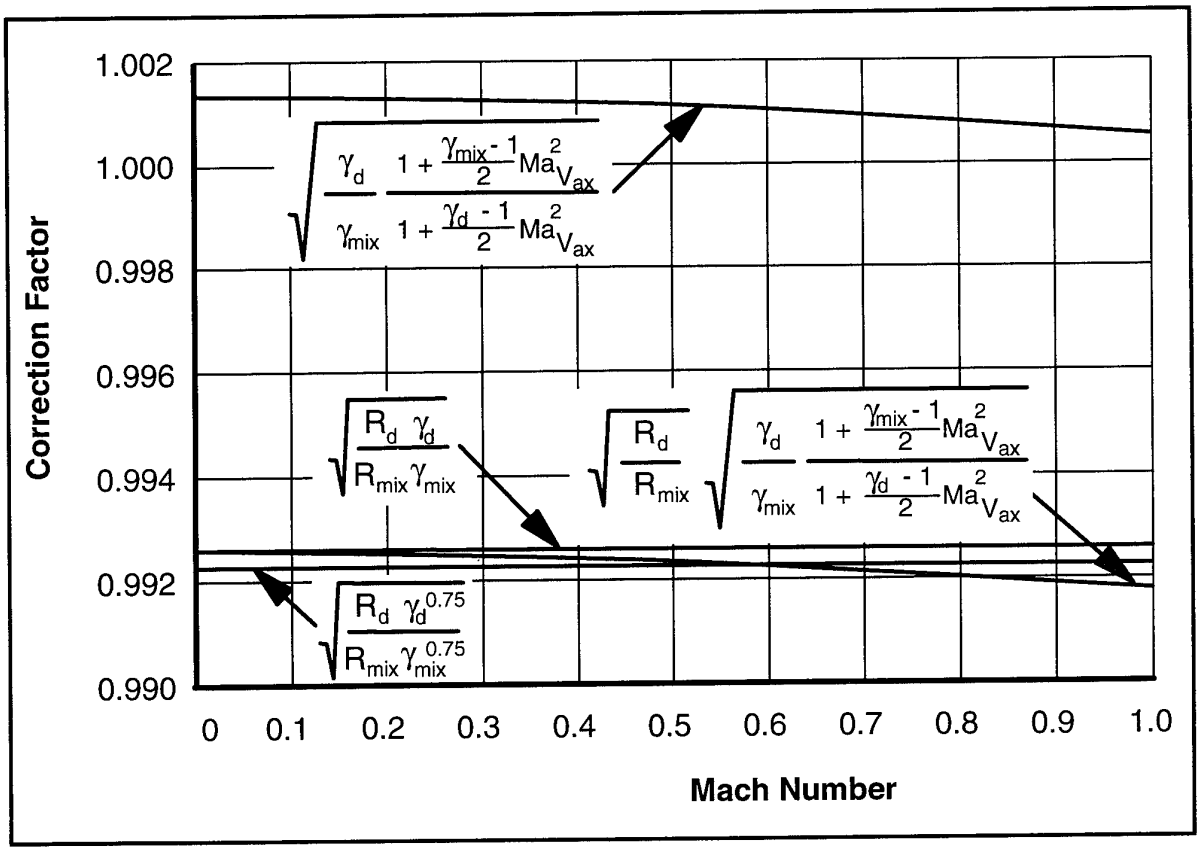

Figure 3-10

Speed Correction for **war** = 0.03

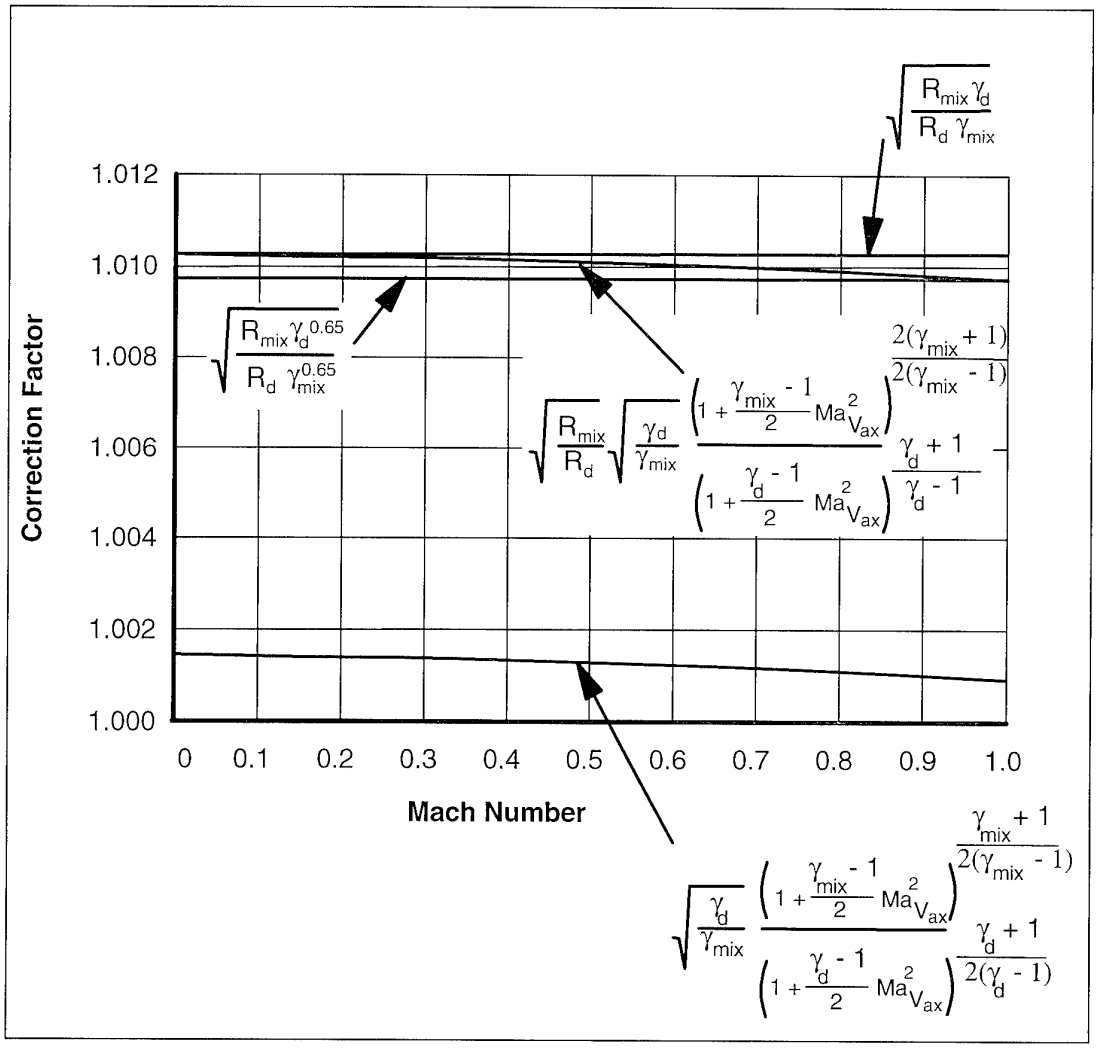

Figure 3-11

Mass Flow Correction for **war** = 0.03 (T = 288 K, **far** = 0)

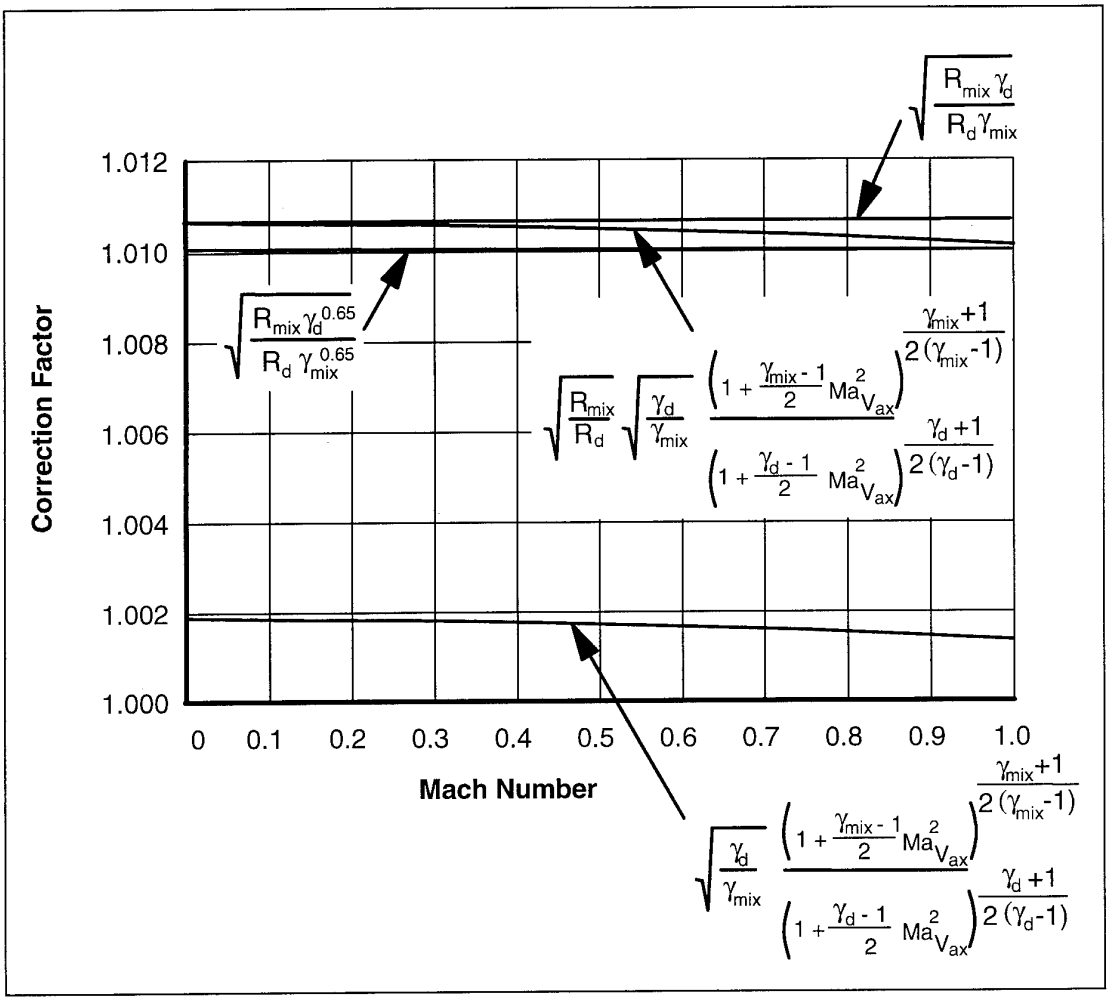

Figure 3-12

Mass Flow Correction for **war** = 0.03 (T = 1400 K, **far** = 0.02)

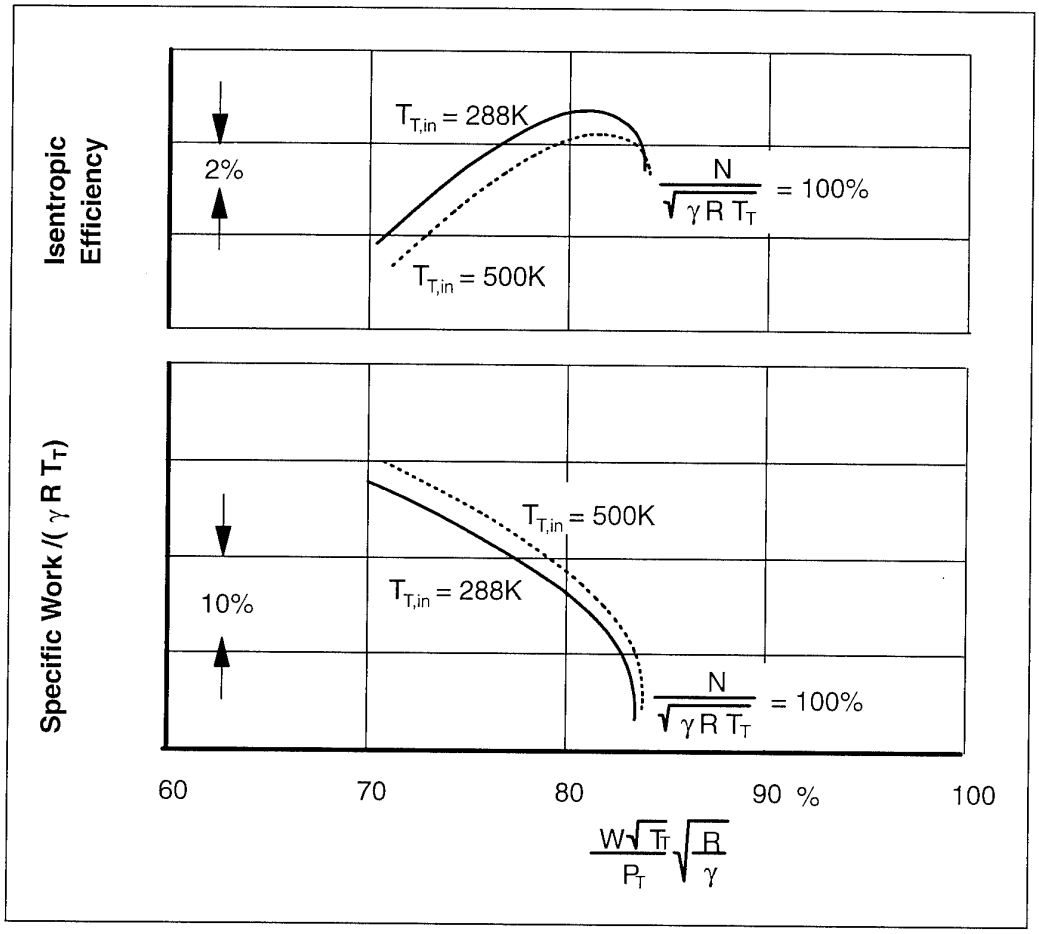

Figure 3-13

Effect of Change in Isentropic Exponent Due to Increase of Compressor Inlet Temperature from 288 K to 500 K on Compressor Characteristics (Note that Typical Humidity Effect is Only 1/10 of the Effect Shown)

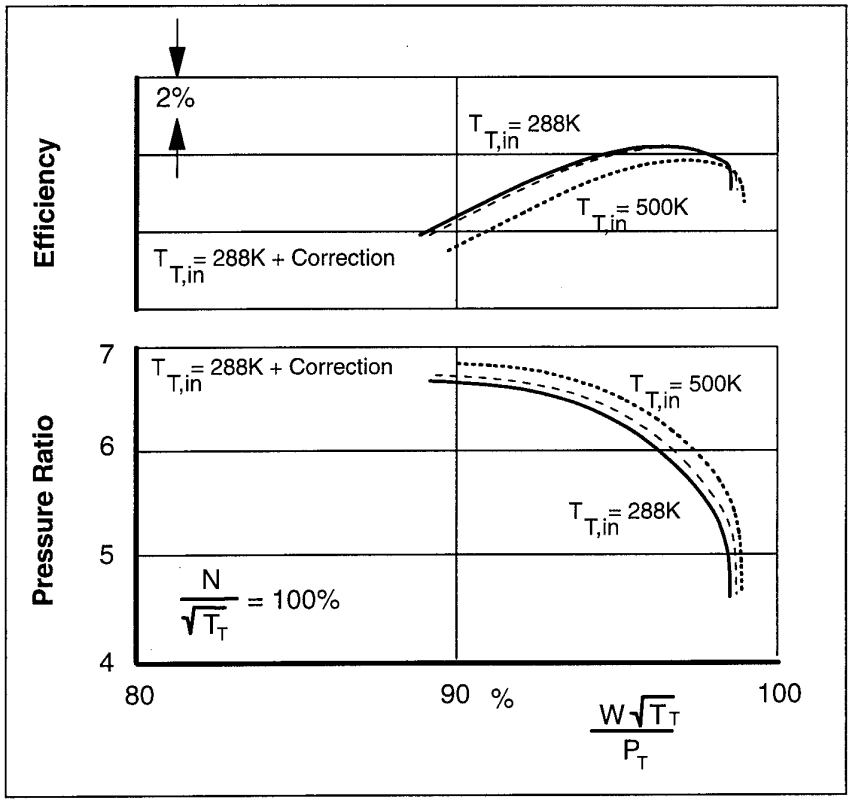

Figure 3-14

Effect of isentropic exponent compared to correction method A

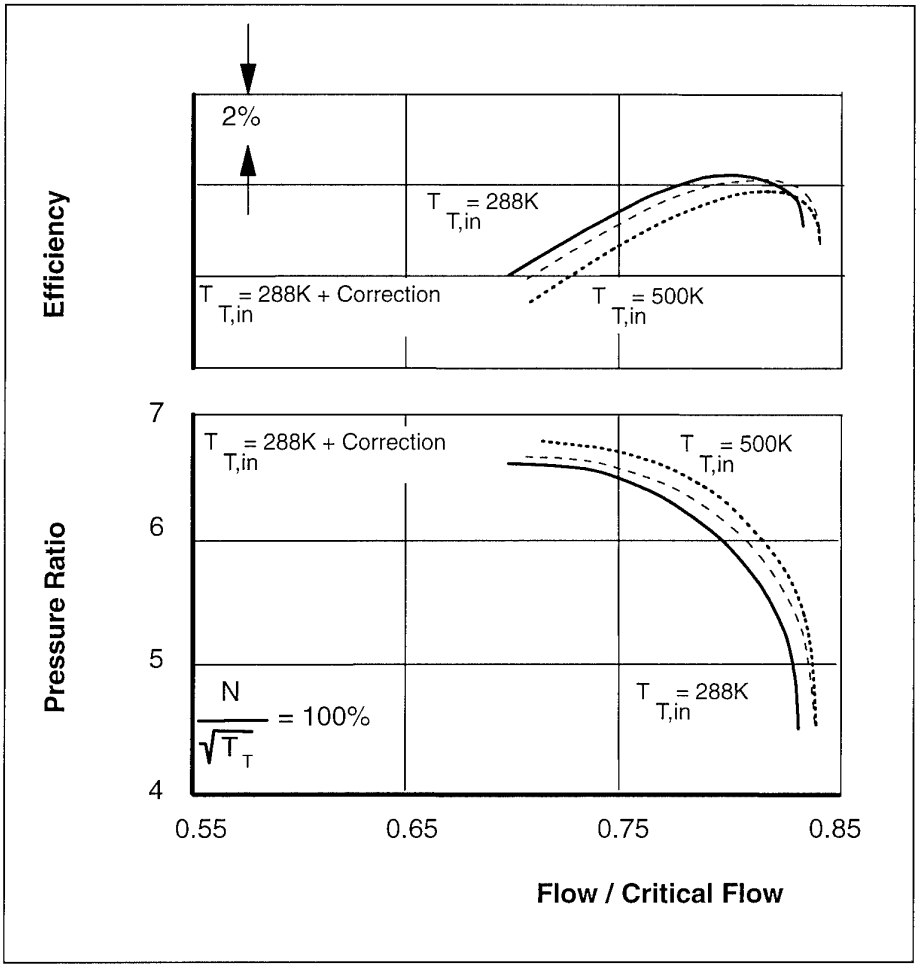

Figure 3-15

Effect of Isentropic Exponent Compared to Correction Method B

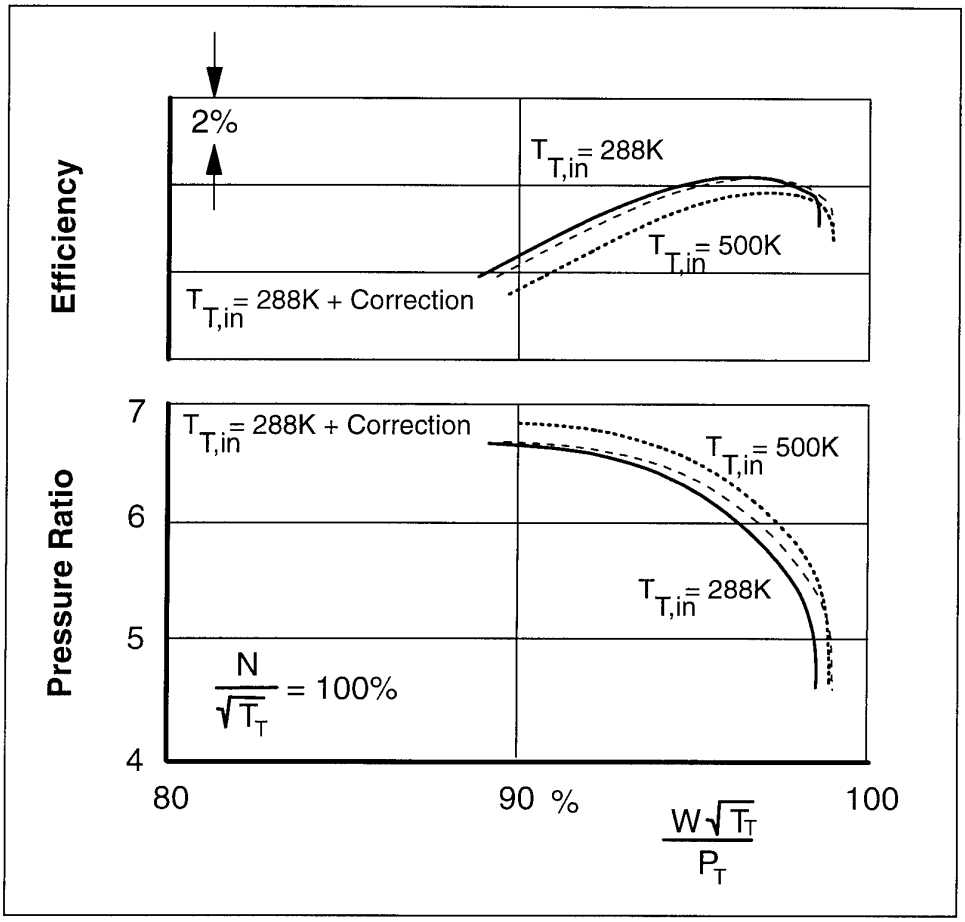

Figure 3-16

Effect of Isentropic Exponent Compared to Correction Method C

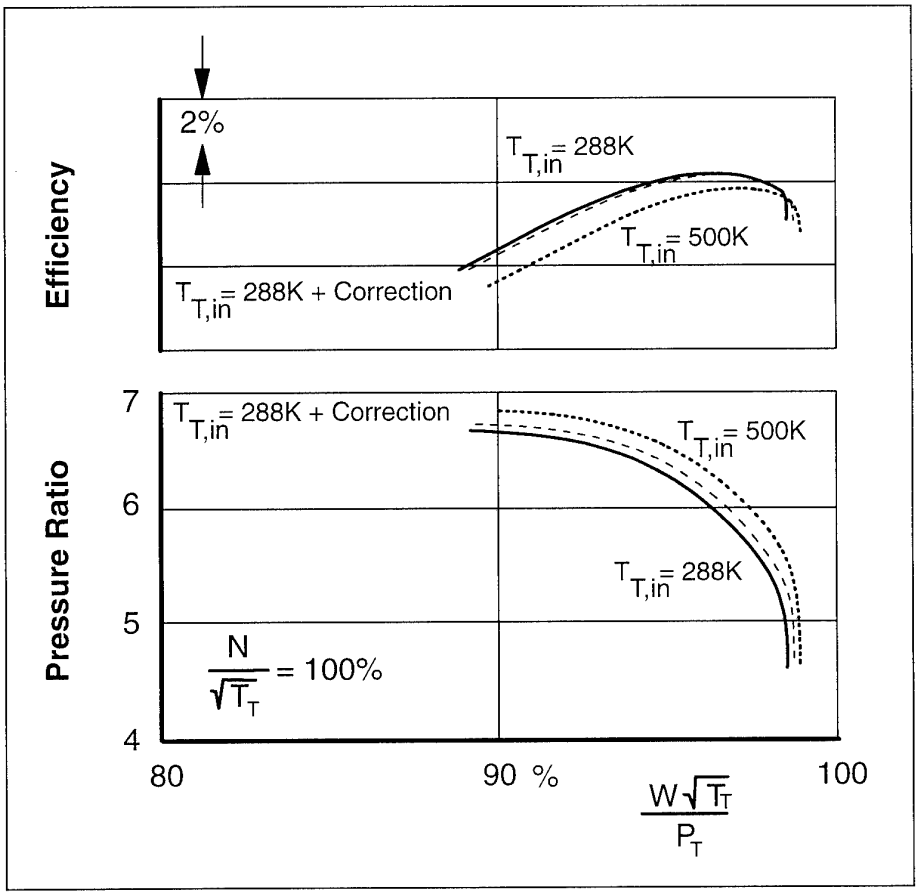

Figure 3-17

Effect of Isentropic Exponent Compared to Correction Method D

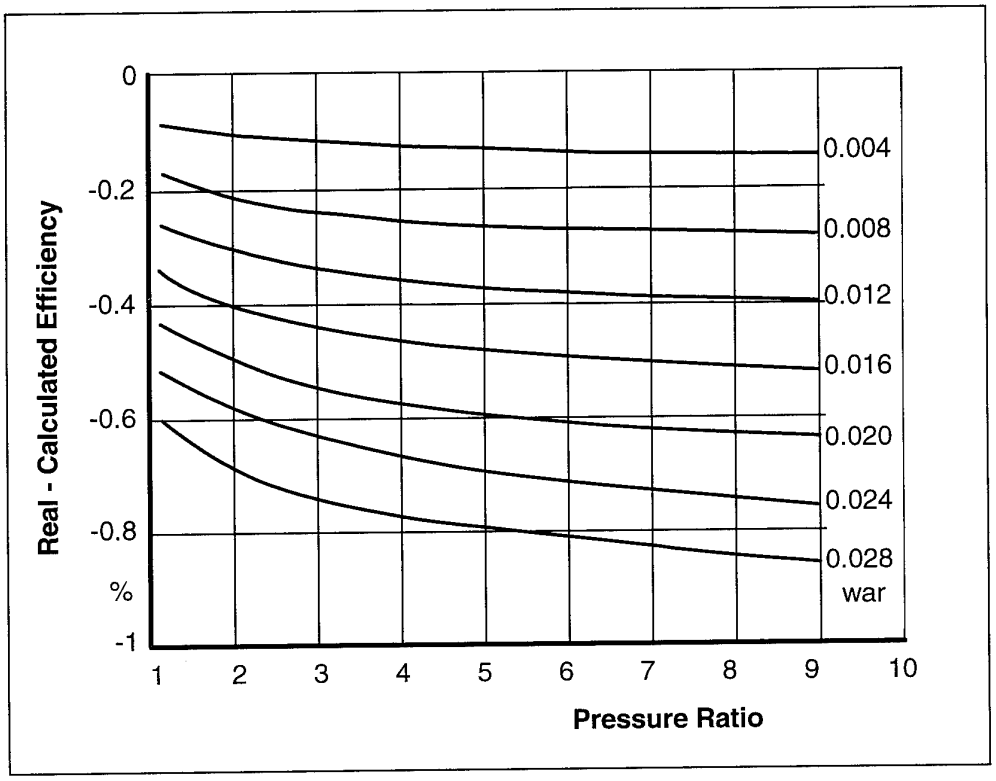

Figure 3-18

Isentropic Compressor Efficiency Error if Humidity is Neglected
(T = 288 K, η = 0.9, Δh from Measured Temperatures)

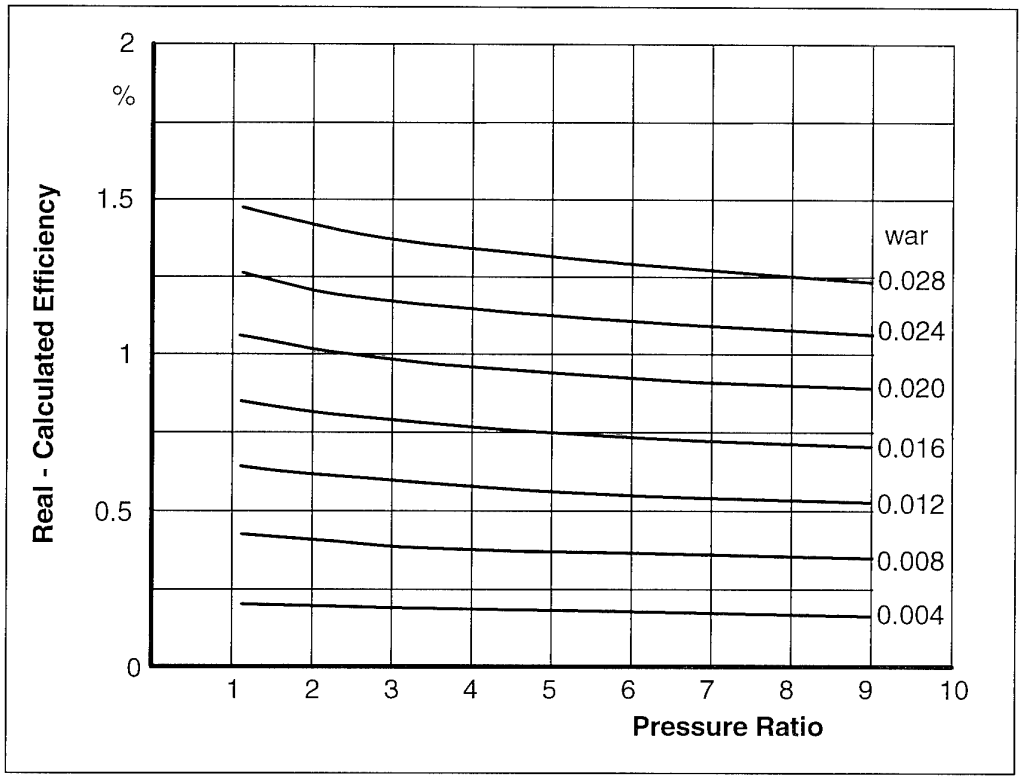

Figure 3-19

Isentropic Compressor Efficiency Error if Humidity is Neglected
(T = 288 K, η = 0.9, Δh From Measured Torque, No Mass Flow Error)

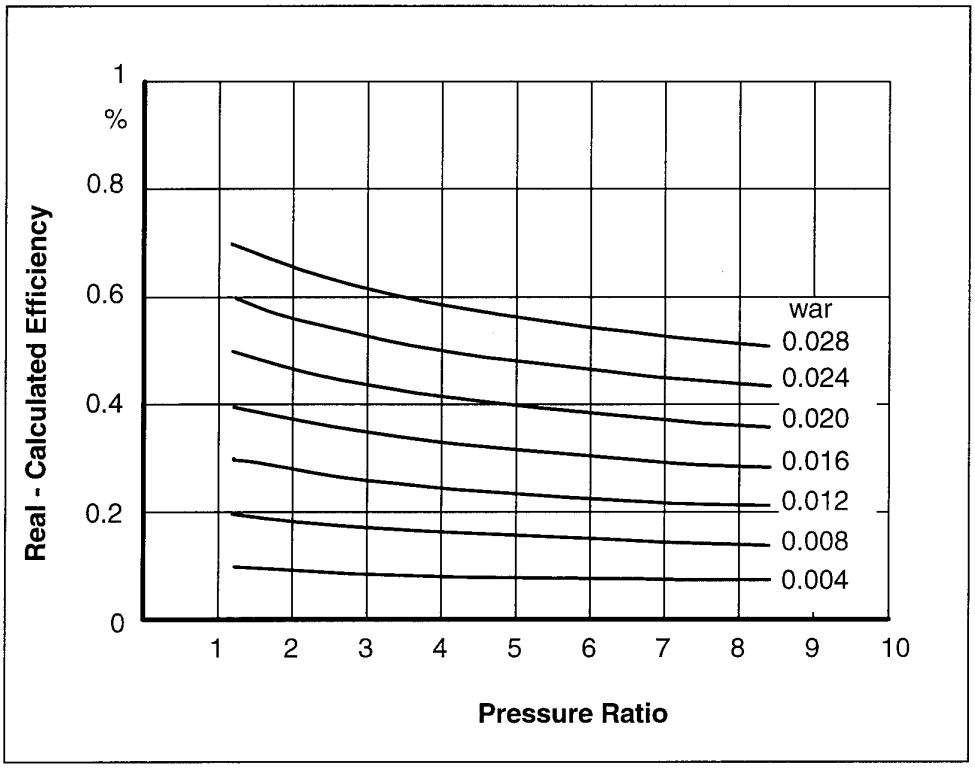

Figure 3-20

Isentropic Compressor Efficiency Error if Humidity is Neglected
(T = 288 K, η = 0.9, Δh from Measured Torque,
Mass Flow Error in Venturi for Ma = 0.5)

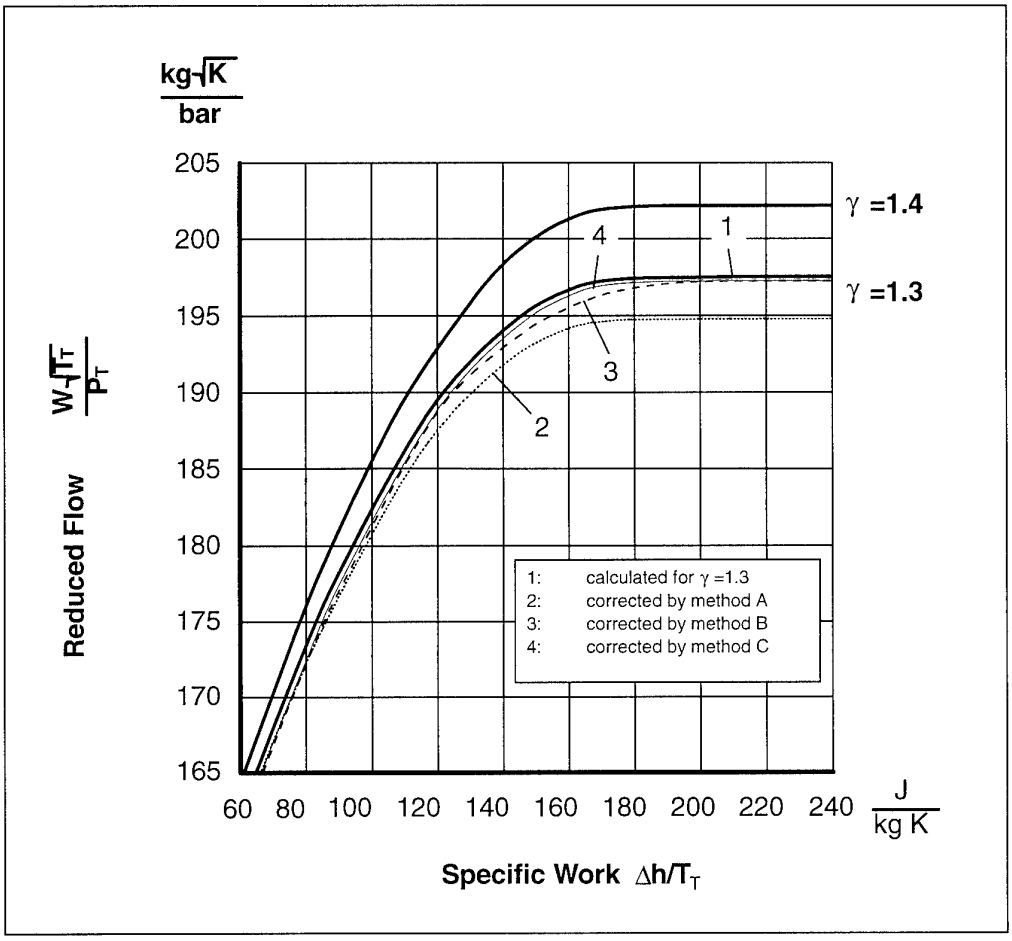

Figure 3-21

Correction Methods for Turbine Corrected Flow

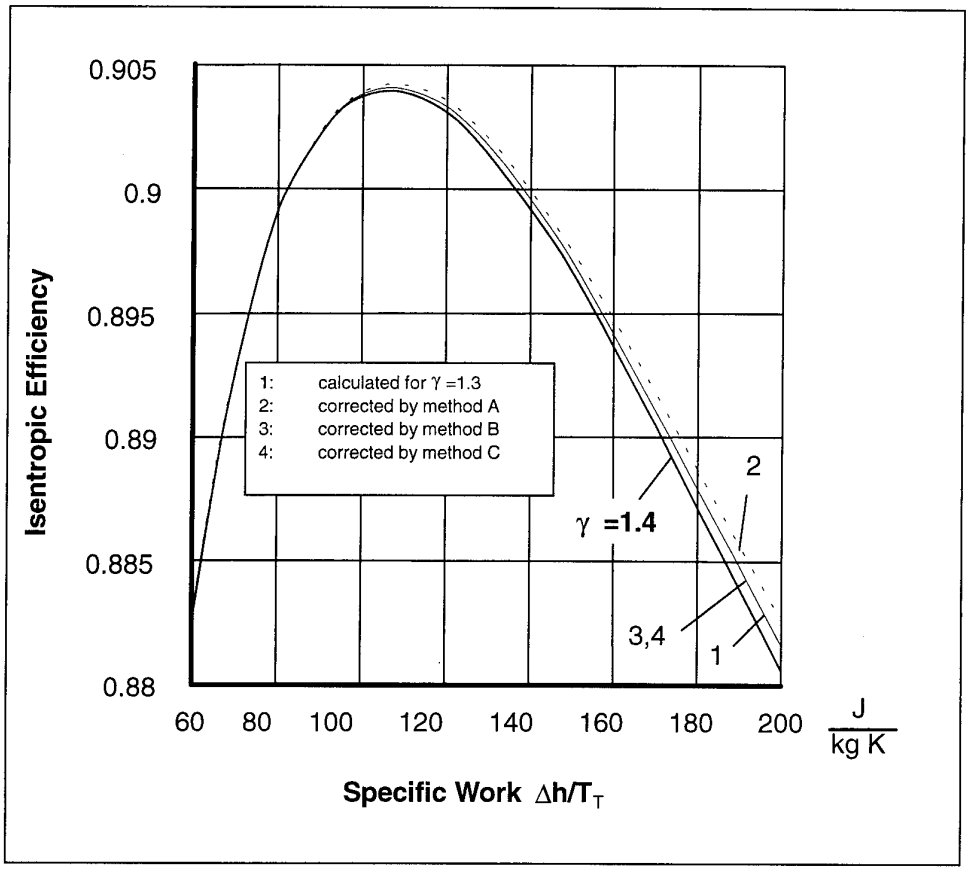

Figure 3-22

Correction Methods for Turbine Efficiency

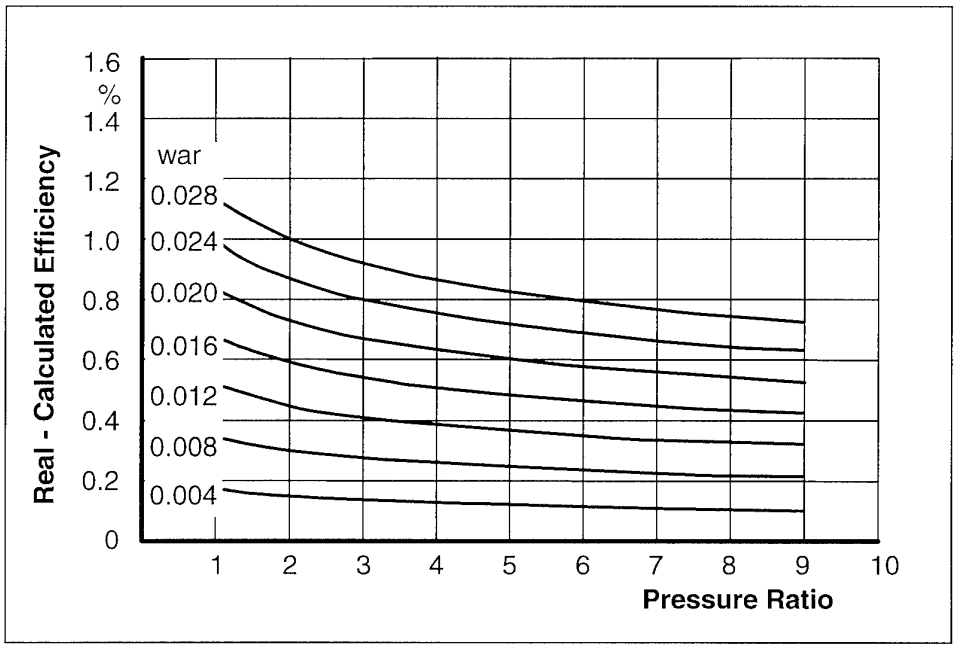

Figure 3-23

Isentropic Turbine Efficiency Error if Humidity is Neglected
(T = 1600 K, **far** = 0.025, η = 0.9, Δh from Measured Temperatures)

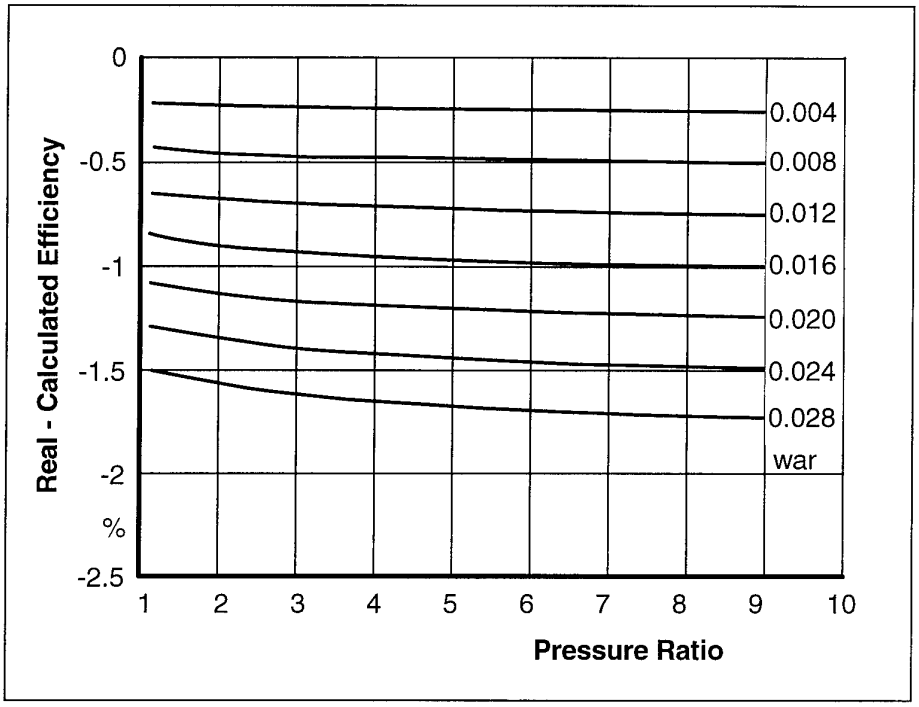

Figure 3-24

Turbine Efficiency Error if Humidity is Neglected
(T = 1600 K, **far** = 0.025, η = 0.9, Δh from Measured Torque, no Mass Flow Error)

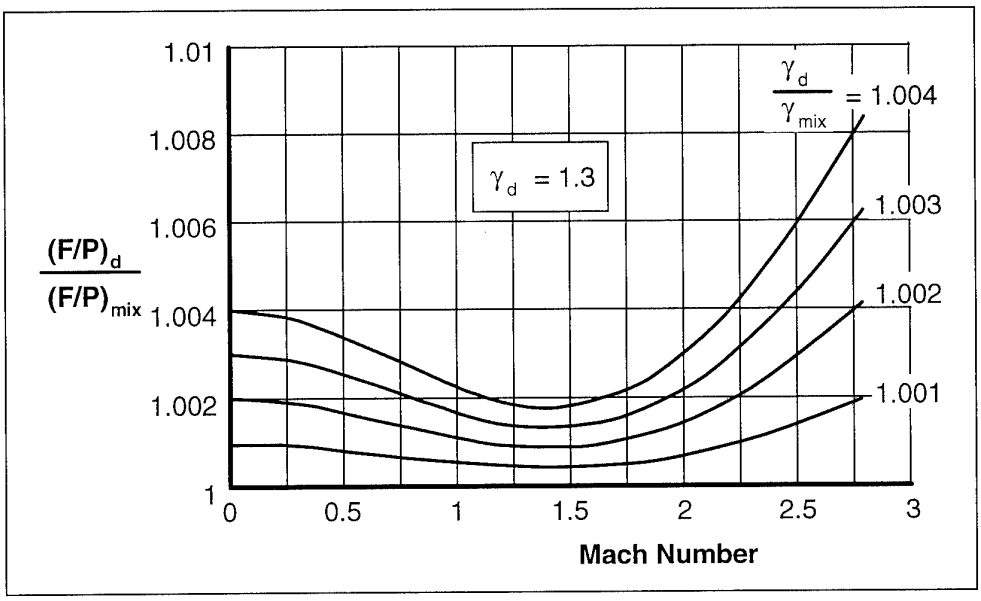

Figure 3-25

Impact of Isentropic Exponent on Thrust of a Fully Expanded Nozzle

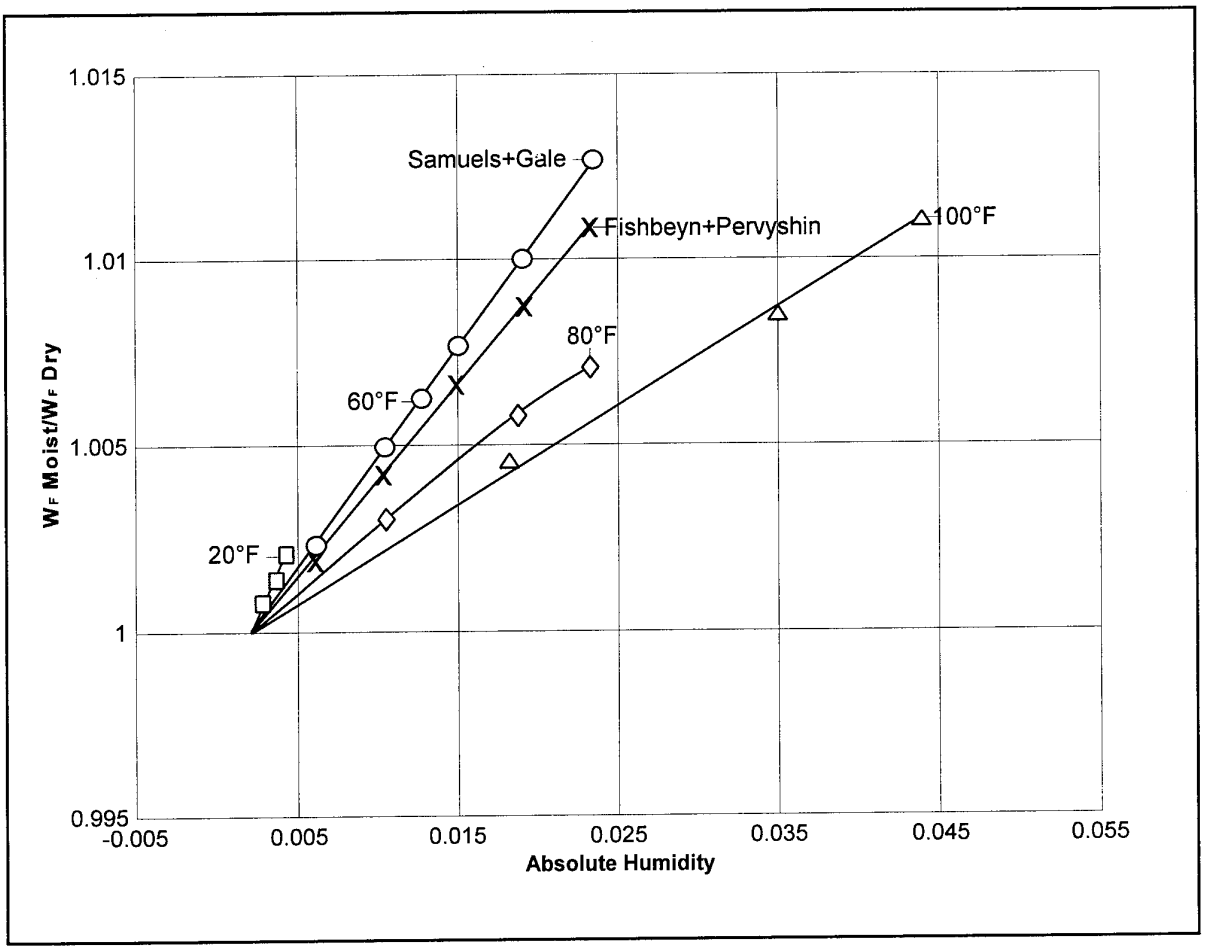

Figure 3-26

Humidity Corrections for Fuel Flow at Fixed Military Power Lever Angle
at 20, 60, 80, 100°F and Reference Methods (Constant Inlet Mach)

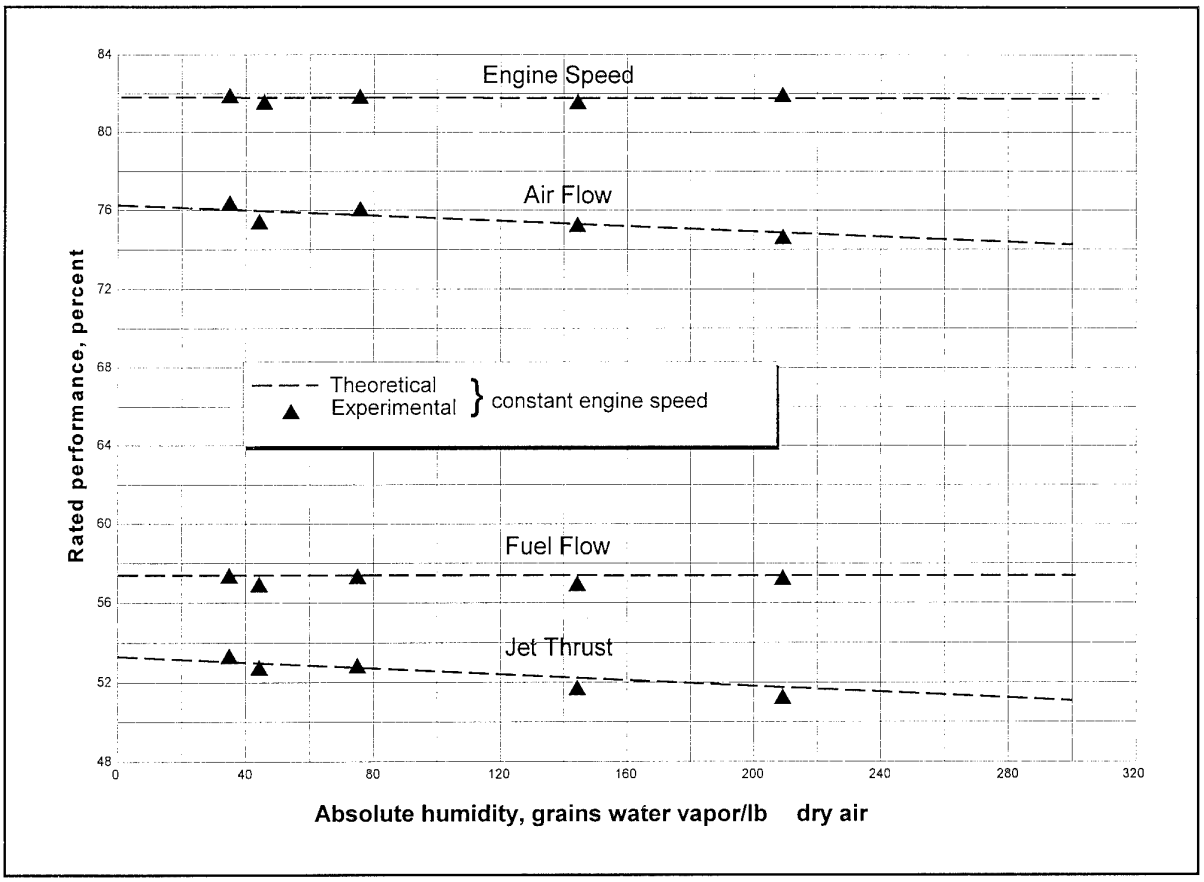

Figure 3-27

Effect of Humidity on Engine Performance. Sea-level, Ram Pressure Ratio, 1.1; inlet temperature 110°F
[**war** = 0.03 corresponds to 210 grains water vapour/lb dry air]
(Reproduced from Reference 3.4)

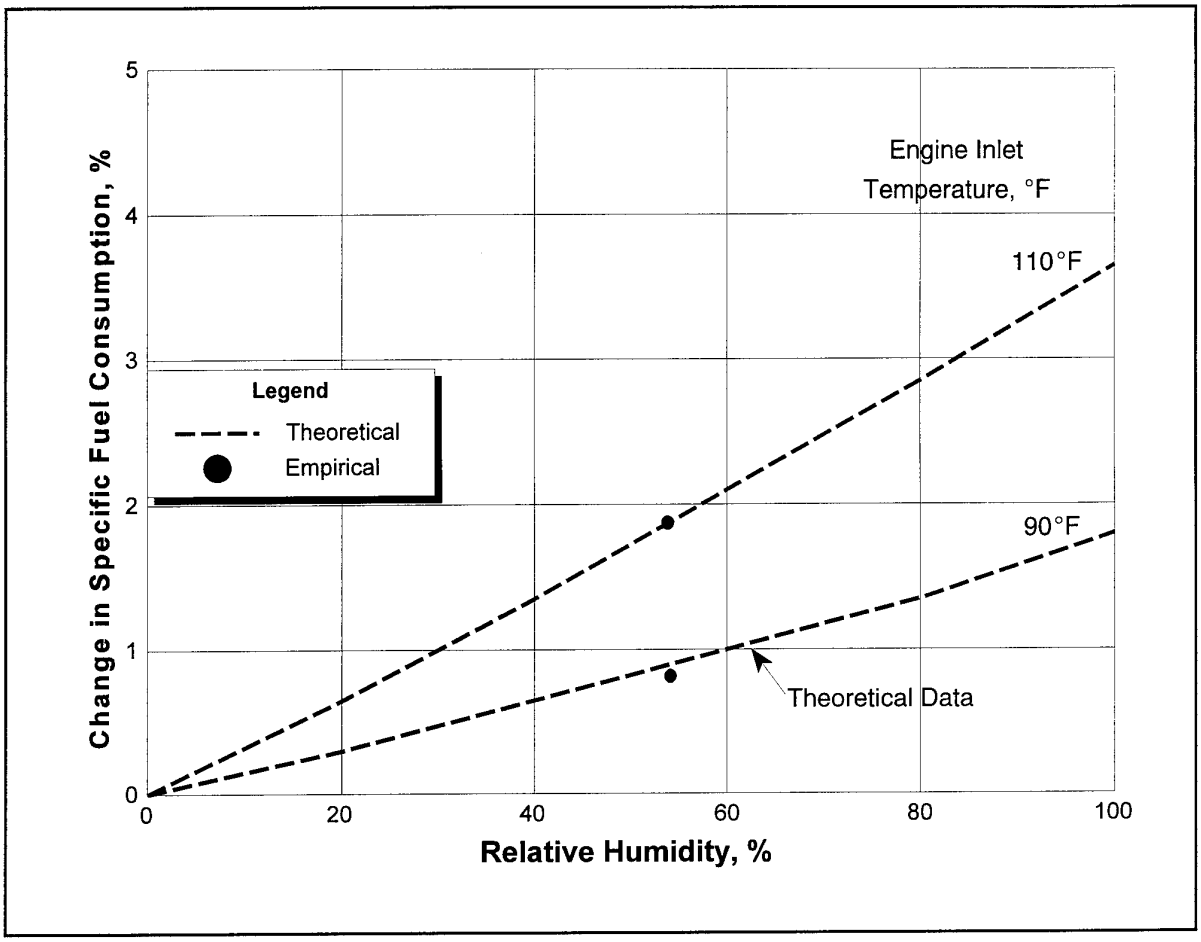

Figure 3-28

Humidity Effects on Engine Performance at Sea-Level Static Conditions
(Reproduced from Reference 3.8)

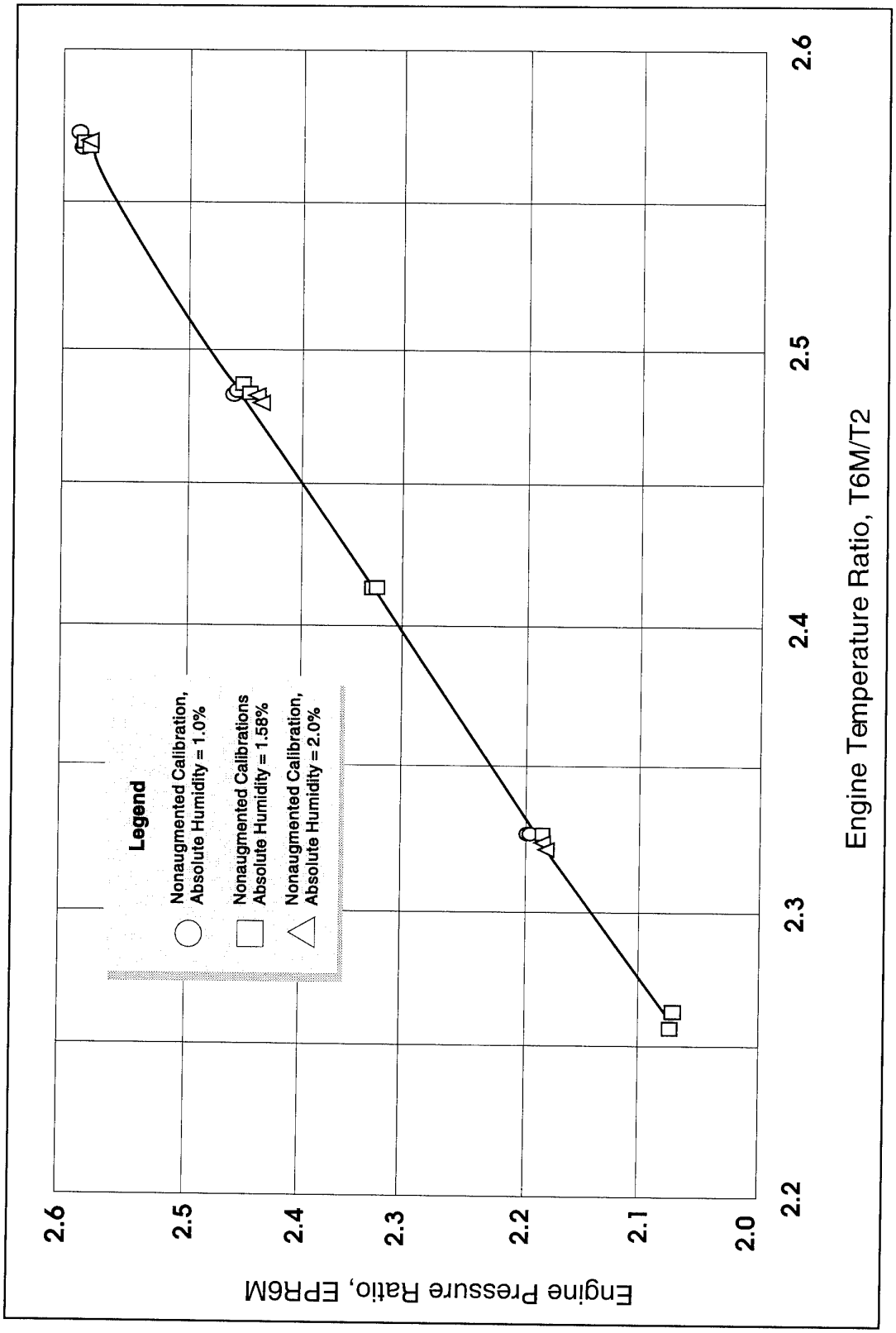

Figure 3-29

Engine Pumping Characteristics at Near Sea-level-static Conditions
(Reproduced from Reference 3.5)

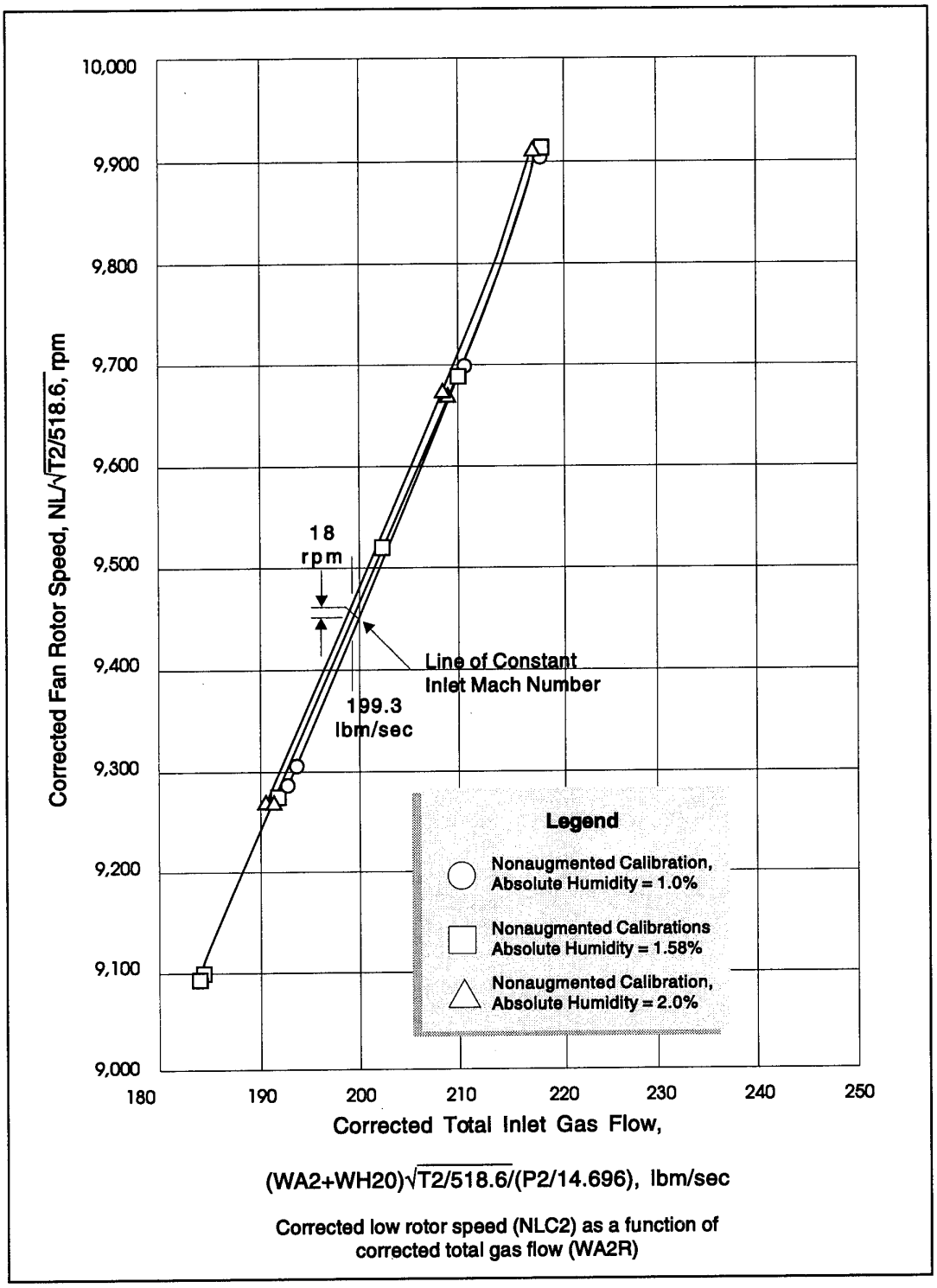

Figure 3-30

Effects of Variable Inlet Humidity on Corrected Rotor Speed
at Near Sea-level Static Conditions
(Reproduced from Reference 3.5)

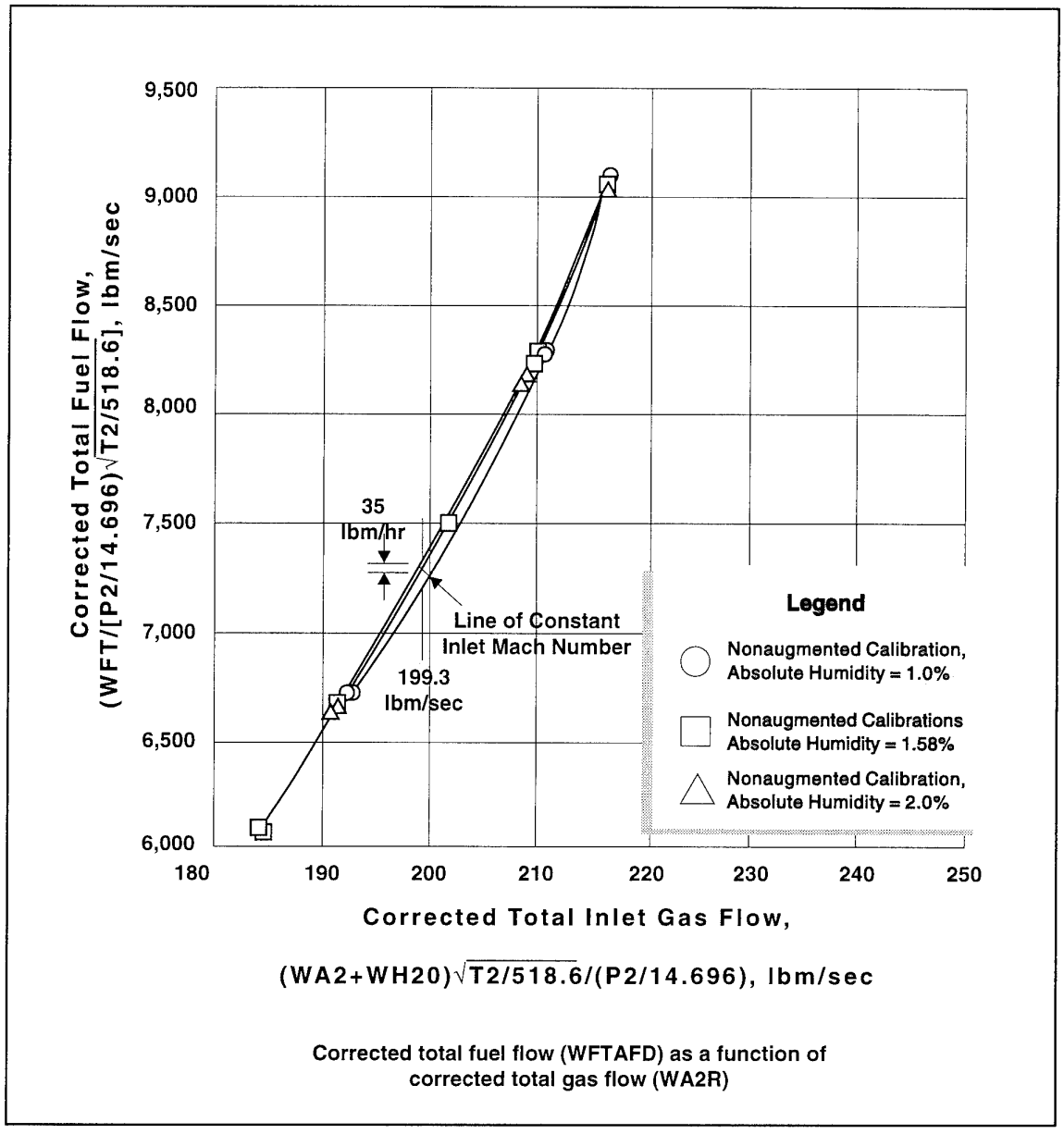

Figure 3-31

Effects of Variable Inlet Humidity on Corrected Total Fuel Flow
at Near Sea-level Static Conditions
(Reproduced from Reference 3.5)

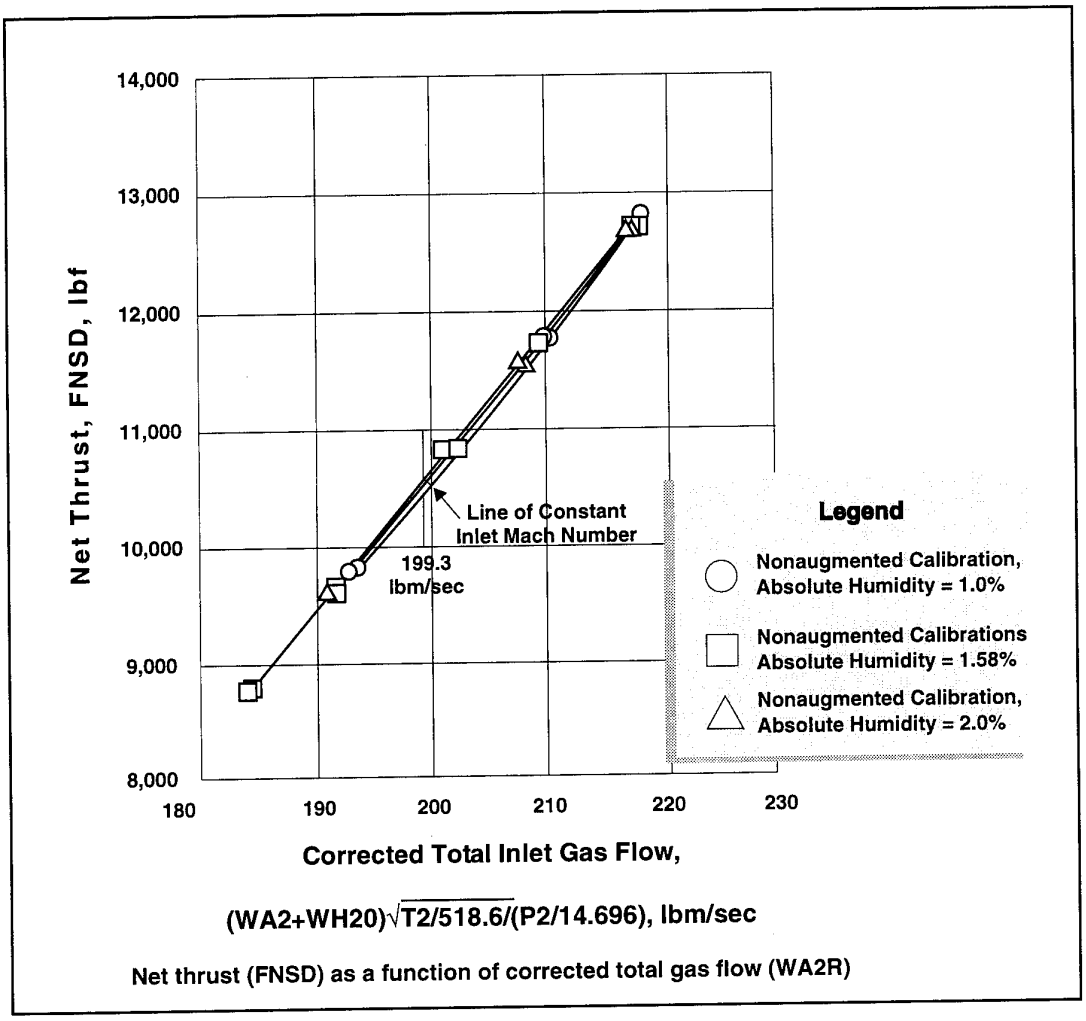

Figure 3-32

Effects of Variable Inlet Humidity on Net Thrust
at Near Sea-level Static Conditions
(Reproduced from Reference 3.5)

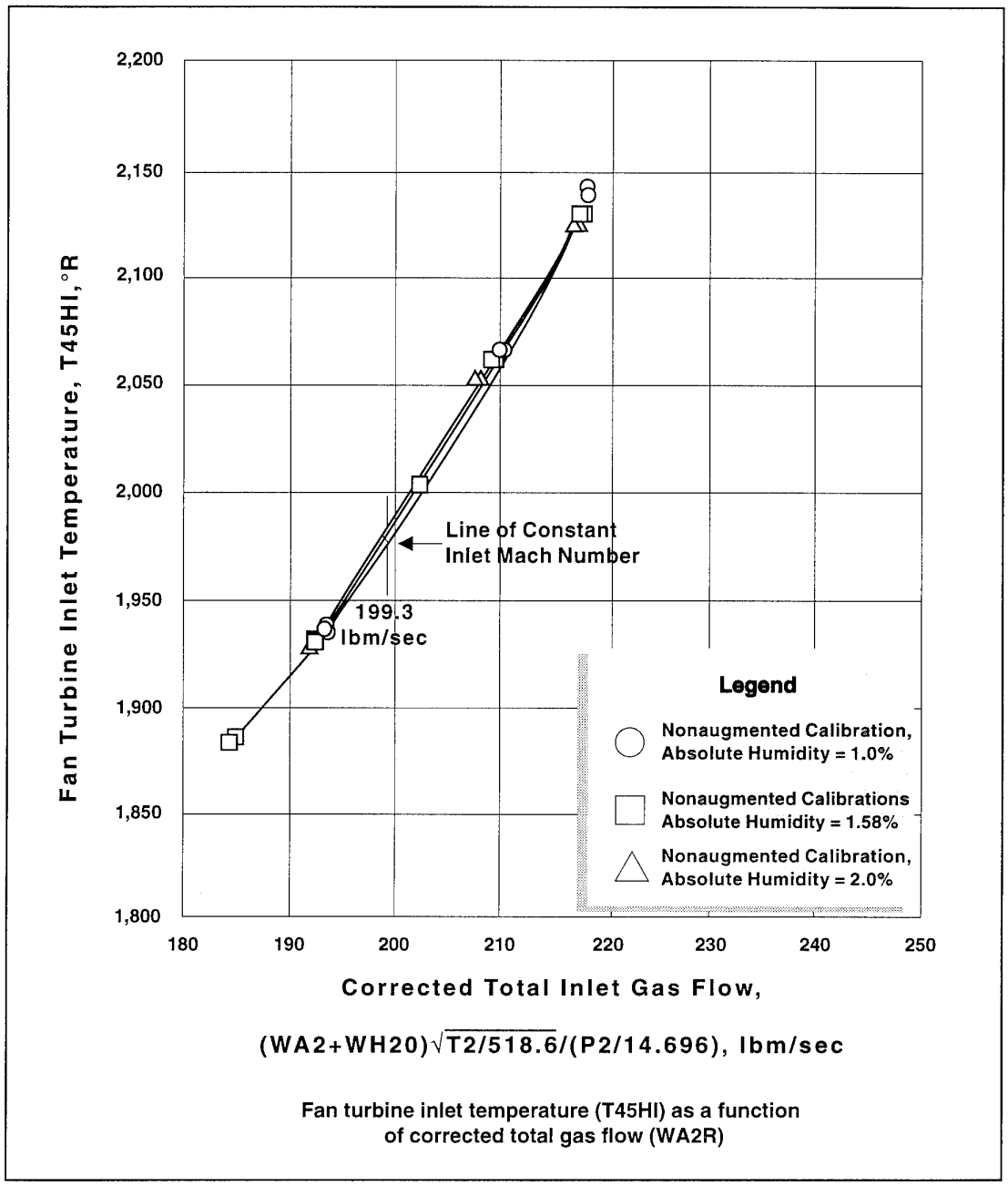

Figure 3-33

Effects of Variable Inlet Humidity on Fan Turbine Inlet Temperature
at Near Sea-level Static Conditions
(Reproduced from Reference 3.5)

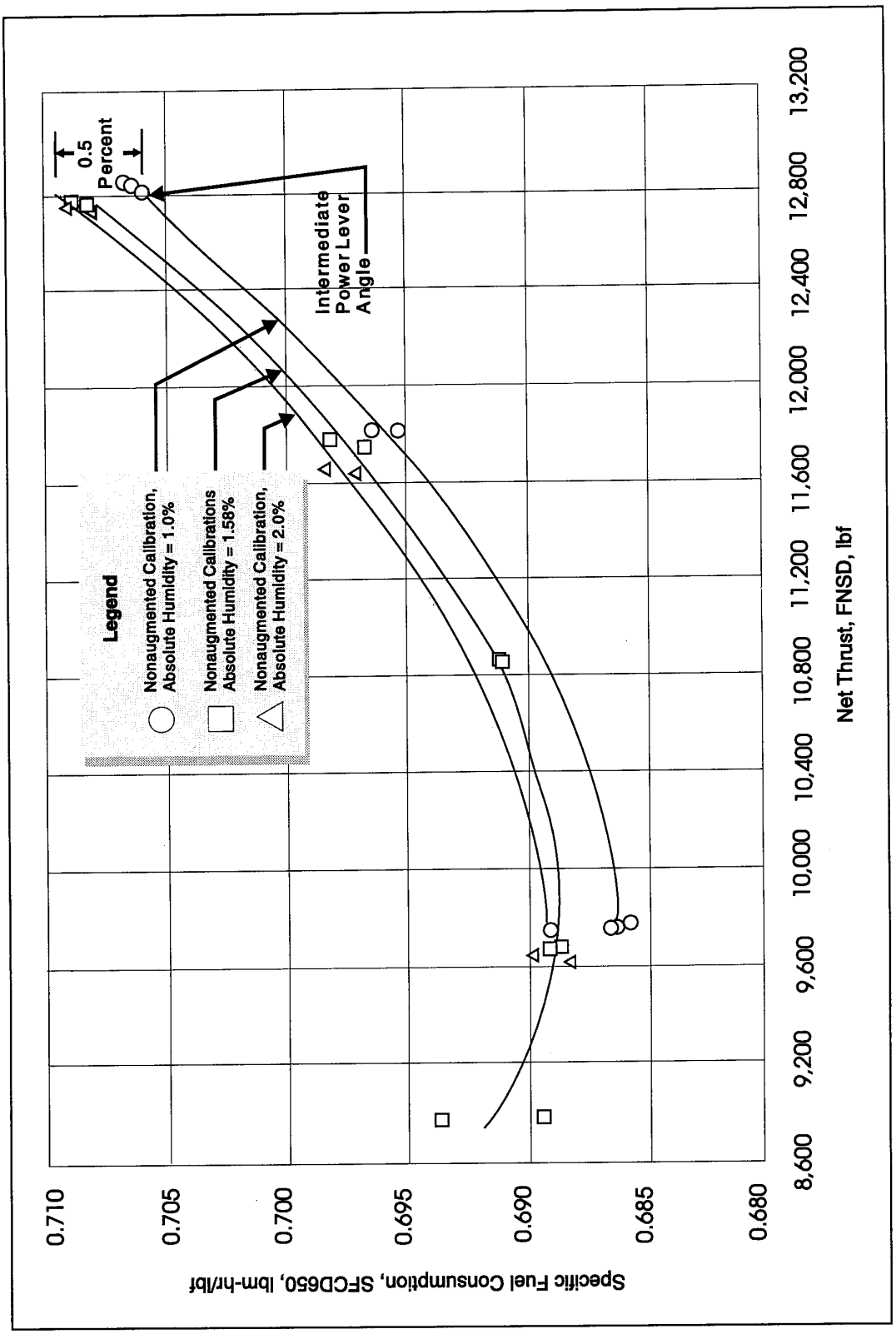

Figure 3-34

Specific Fuel Consumption as a function of Net Thrust at Near Sea-Level -Static Conditions with Variable Inlet Humidity (Reproduced from Reference 3.5)

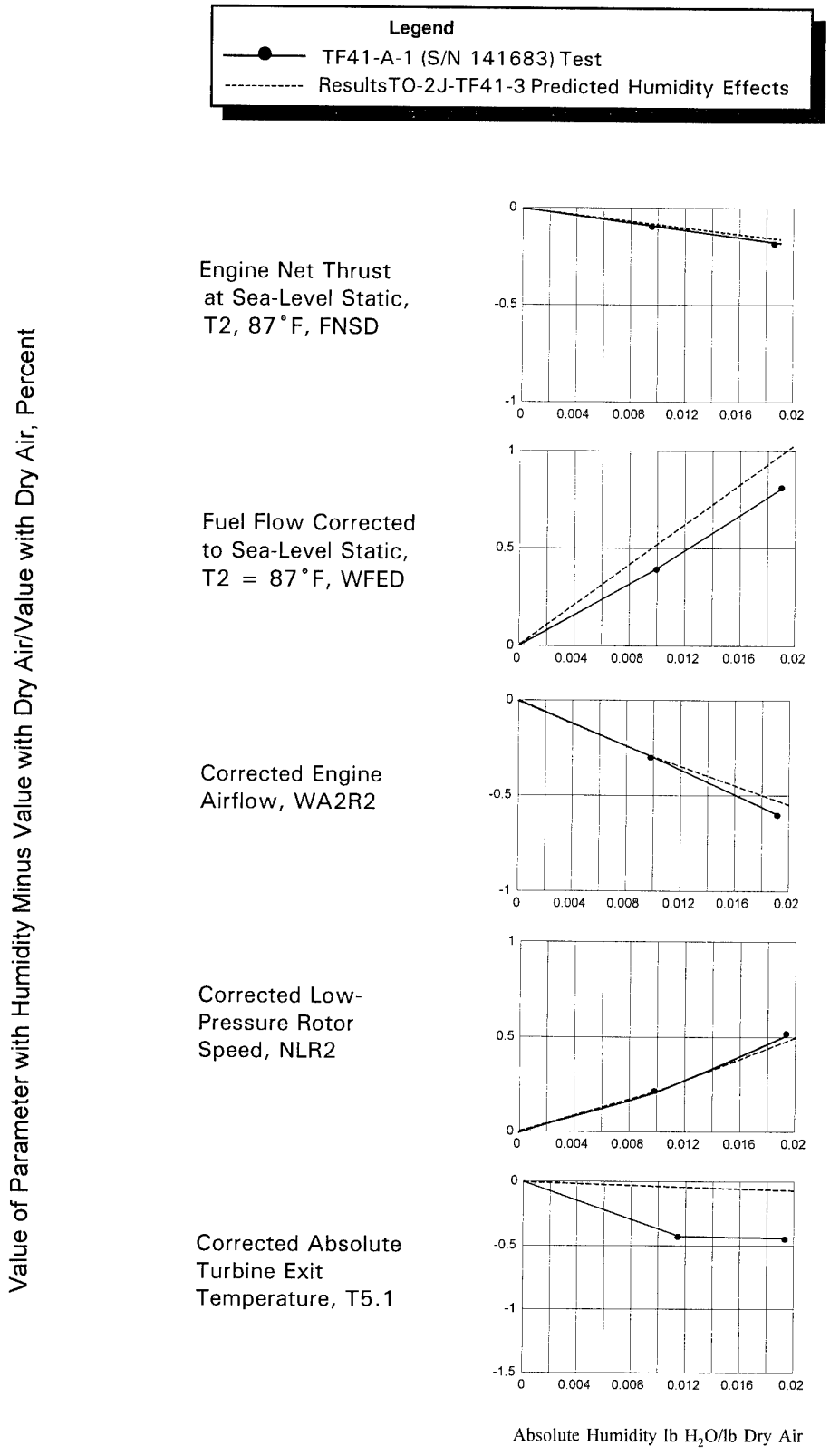

Figure 3-35
Comparison of actual and predicted effects of humidity on TF41-A-1 engine (S/N 141683) performance at near sea-level-static conditions (P2 = PSO = 10.0 psia, T2 = 87°F) at engine pressure ratio of 2.1 (Reproduced from Reference 3.9)

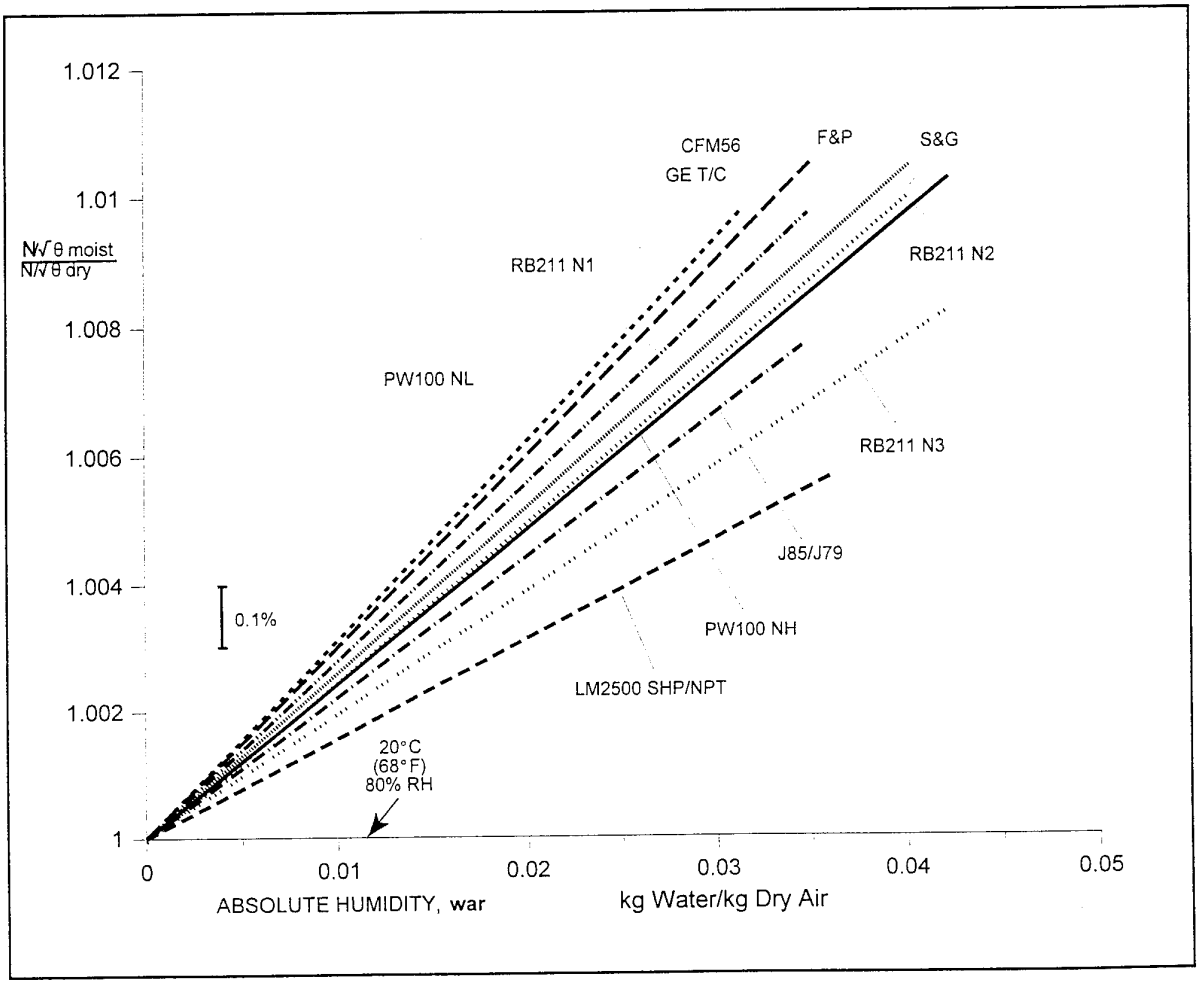

Figure 3-36

Comparison of Speed Correction Factors for Absolute Humidity
(Reference 3.7)

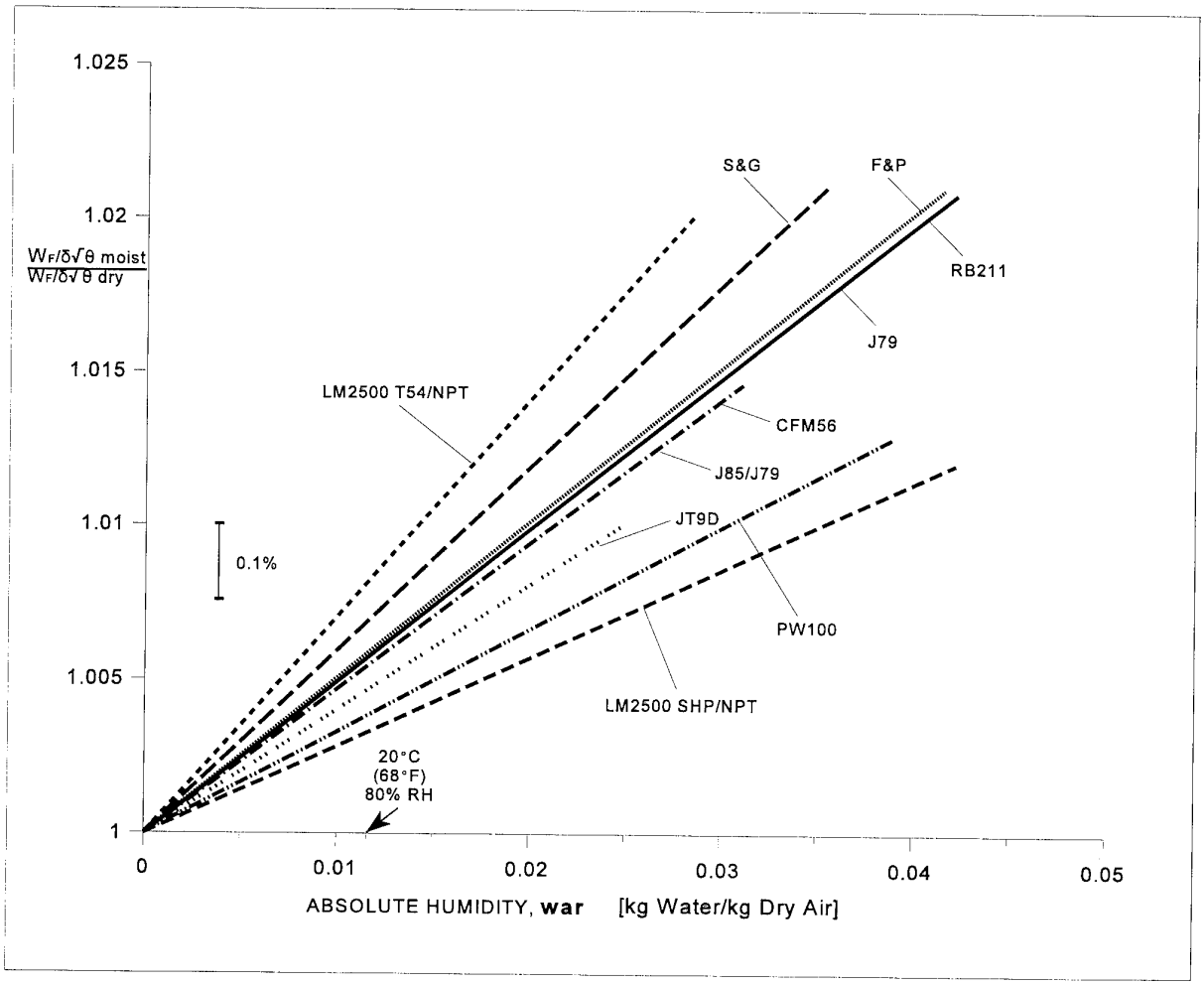

Figure 3-37

Comparison of Fuel Flow Correction Factors for Absolute Humidity
(Reference 3.7)

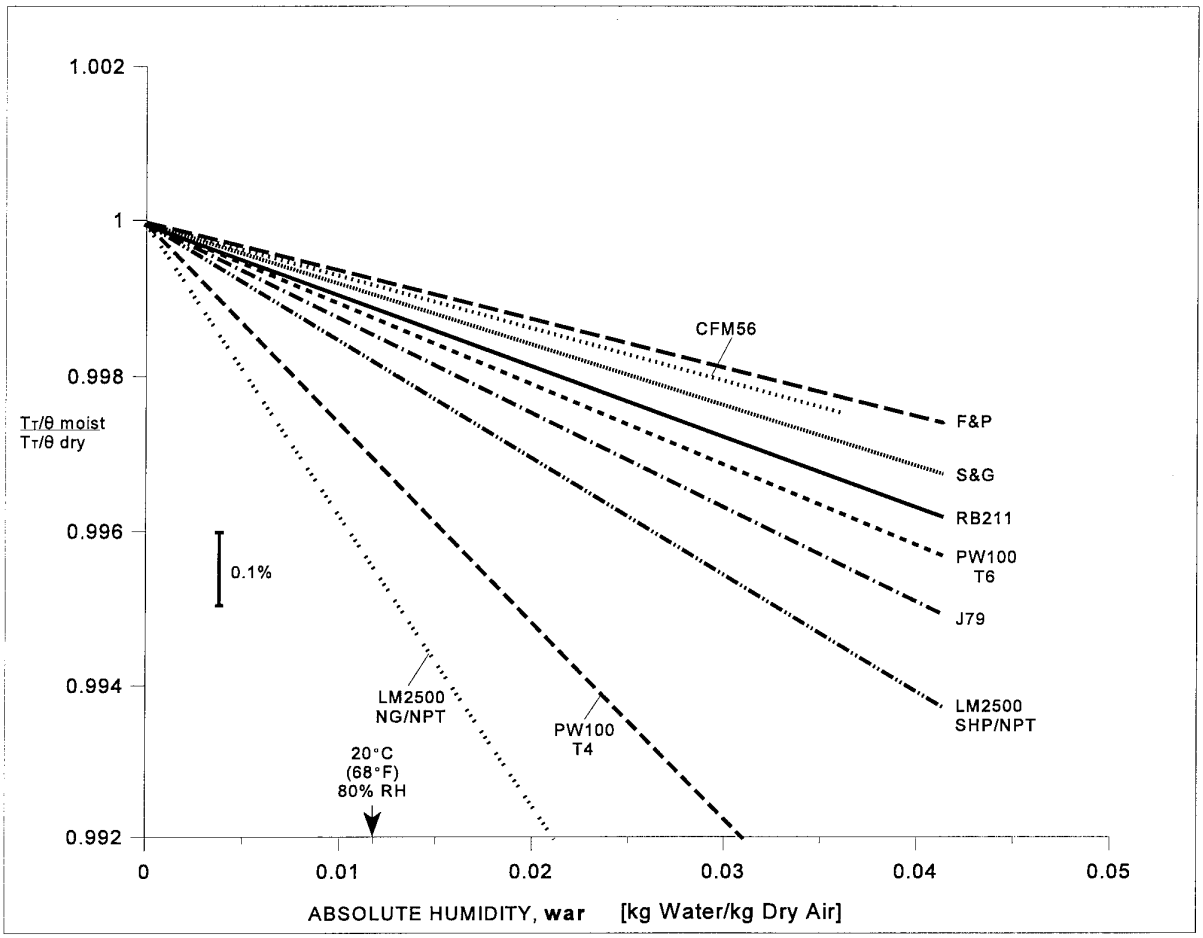

Figure 3-38

Comparison of Turbine Inlet or Outlet Temperature Correction Factors for Absolute Humidity
(Reference 3.7)

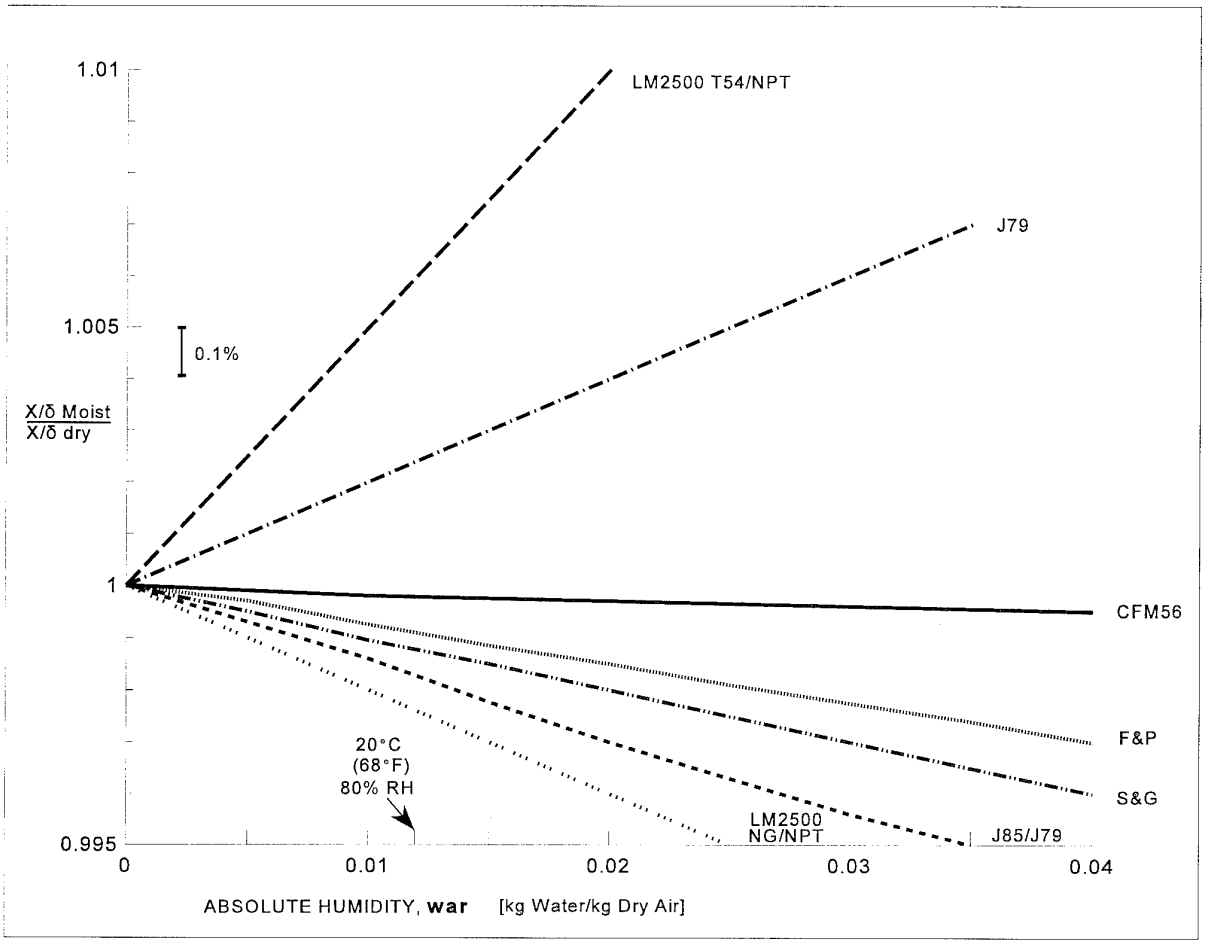

Figure 3-39

Comparison of Thrust or Power Correction Factors for Absolute Humidity
(Reference 3.7)

4. CONDENSATION: EFFECT ON COMPONENTS AND ENGINE PERFORMANCE[1]

4.1 INTRODUCTION

The effects of air inlet condensation on gas turbine engine performance have received increasing attention from aero-engine manufacturers over the last 25 years, particularly in North America where climate and ground test inlet design have combined to emphasize the effects. An increase of 2% in specific fuel consumption due to condensation can occur during an American summer compared to less than 1% in central Europe. More recently however, changes in ground inlet design and more stringent production engine acceptance margins have necessitated engine manufacturers to adopt condensation correction procedures.

When A7 aircraft powered by TF30-P6 and P8 engines were first used in South East Asia, excessive engine military power trims on the fuel control schedule were reported, resulting in turbine entry temperature increases of up to 50 K. However, when the A7 aircraft aboard a carrier reached the Sea of Japan, with lower levels of ambient temperature and ambient relative humidity, incidents of repeated engine military trimming ceased. Engine trim variations were also noted with A7 aircraft operating between Jacksonville, Florida, (NAS - Cecil Field) and Yuma, Arizona (MCAS). Investigation by Spencer and Archer (Reference 4.1) indicated the primary cause of variations in engine trim to be the result of condensation occurring in the aircraft's inlet duct during operation in a high relative humidity environment.

Over a period of several years, JT9D engine test data showed unexplained cyclic variations in specific fuel consumption. The variations correlated with seasonal changes in ambient conditions even though corrections were made for ambient temperature and specific humidity. Analysis by Blake (Reference 4.2) showed that condensation was theoretically possible at the levels of humidity occurring in the Hartford area. Subsequent testing using a laser photo-sensor system detected the presence of condensation within the relatively short, bellmouth test inlet. It was concluded that the effects of inlet condensation could be as high as +0.7% SFC with high humidity conditions.

When humid air - an equilibrium mixture of dry air and water vapour - is induced into the subsonic air inlet system of a gas turbine engine, the increase in velocity of this air which occurs in the inlet duct, and the associated reduction in its static temperature and static pressure, can result in the condensation of water droplets. This change of state and the consequent release of latent heat increases the total temperature and reduces total pressure of the final gaseous mixture, adversely affecting the performance of the engine.

The effect of condensation on engine performance during stationary operation can occur during performance acceptance testing of production engines prior to delivery and during development performance or back-to-back testing. The results of such testing may easily be confused by the condensation effects which have proved difficult to quantify due to the problems of ascertaining the extent to which the condensation has occurred and the point in the engine at which the subsequent re-evaporation is completed. These problems are discussed in more detail later in this chapter.

In normal service operating conditions, inlet condensation does not appear to be a significant factor. Inlet condensation does not occur, for example, at cruise because the aircraft Mach number is higher than the local Mach number in the engine inlet, which results in the static temperature and pressure of the air increasing as it enters the inlet, precluding condensation. During production pass-off acceptance testing, failure to account for inlet condensation may lead to reduced margins on SFC, TGT and NL (e.g. up to 0.6% increase in TGT) .

This chapter deals with particles small enough to follow the flow; large particles are covered in Chapter 5.0.

Investigations into the condensation phenomenon have centred upon two particular directions:

(i) The calculation of condensation temperature

[1] Tables and Figures for Chapter 4 begin on page 4-23

rise by an analytical model of the flow process into the air inlet.

(ii) The correlation of measured engine performance changes against the associated amount of condensation measured or calculated by an analytical model.

The former has highlighted the importance of dust/particle concentration in the condensation process. The latter activity has highlighted the difficulty of reliably quantifying by observation or measurement the extent to which the condensation process has occurred by the time the mixture of air, water vapour and water droplets reach the engine face. Any intrusive measurement in the inlet duct, such as that from a temperature or pressure probe has the disadvantages of being a local measurement only, in a flow which is significantly different from any one dimensional average concept. In addition, the probe may cause changes in the flow due to its own presence. Alternatively, any non-intrusive measurements are generally either too remote, too unrepresentative or too impractical to be of significant use.

Aero-engine manufacturers have used empirically derived corrections based on correlations of measured engine performance changes against the maximum ideal temperature rise due to condensation. These corrections are generally accepted by the Certifying Authorities and by aircraft manufacturers as being appropriate for the correction of production engine acceptance data. The engine manufacturers use the corrections to guide them in specifying environmental test limits and understanding the test data from engine development testing.

4.2 CONDENSATION IN FLOWING HUMID AIR

This section describes the main physical phenomena involved with condensation in flowing humid air.

4.2.1 States of Water

Water as a pure substance can exist in one of three phases: solid (i.e. ice), liquid or gas, depending on its temperature and pressure. Under certain conditions the liquid and gaseous (vapour) phases can exist simultaneously in equilibrium. Figure 4-1 shows that liquid and vapour can exist in equilibrium only along a single temperature/pressure line. This line is commonly referred to as the saturation line and the saturation pressure is a unique function of temperature.

When the temperature drops below 0°C, icing can occur (at normal and low pressures). As with liquid and vapour, ice and vapour can exist in equilibrium only along a single temperature/pressure line on a P,T diagram (Figures 4-1 and 7-1).

The states of the water can be represented by: pure steam (i.e. vapour or gas), pure liquid, pure ice (i.e. solid), liquid + vapour, liquid + ice, vapour + ice, liquid + ice + vapour (triple point).

Water can also exist in non-equilibrium states (also called metastable states) of subcooled steam and subcooled water. For example, a mass of water under P and T conditions "normally" in the form of water can exist temporarily in the form of a gas when the flow is accelerated. Subcooled water, that is water in the form of liquid instead of ice, is more commonly encountered in nature and the subcooling may reach high values, for example 30°C, for very pure water. Metastable states play an important role in the process of condensation and depend on the rate of the pressure and temperature changes and on the purity of the water.

When water vapour is mixed with air, the phase equilibrium relationships remain essentially unchanged. It is important to note that the determinant pressure is the partial pressure of the water vapour and not the total system pressure.

4.2.2 The Condensation Process

As humid air is accelerated through a nozzle (e.g. in an engine inlet), its Mach number (Ma) increases, resulting in a reduction in the static temperature (T_S) and static pressure (P_S) of the mixture in accordance with the following relationships:

$$\frac{T_T}{T_S} = 1 + \frac{(\gamma-1)(Ma)^2}{2} \qquad 4\text{-}1$$

$$\frac{P_T}{P_S} = \left[1 + \frac{(\gamma-1)(Ma)^2}{2}\right]^{\frac{\gamma}{\gamma-1}} \qquad 4\text{-}2$$

As the temperature and pressure of the mixture are reduced, the temperature and pressure of

the water vapour also reduce in accordance with the following relationships:

$$T_{Sv} = T_{Smix} \qquad 4\text{-}3(a)$$

$$\frac{P_{Smix}}{P_{Sv}} = \frac{0.622}{\mathbf{war}} + 1 \qquad 4\text{-}3(b)$$

where **war** is the absolute humidity of the mixture and 0.622 is the ratio of the molecular weights of water and air.

As long as no condensation occurs, **war** remains constant and the expansion can be expressed, in the P,T diagram, by the classical formula for a perfect gas

$$\frac{P_S}{T_S^{\frac{\gamma}{\gamma-1}}} = \text{constant} \qquad 4\text{-}4$$

for both the mixture and the vapour phase.

The relationships between T and P are shown in Figure 4-1 which shows that the saturation pressure decreases at a much faster rate than the vapour partial pressure with increasing Mach number. As the Mach number increases, the condition of the water vapour changes from ambient (1) and approaches the saturation line to condition (2), after which condensation in an equilibrium state should occur to condition (3).

As is well-known in wind-tunnel flows (especially with "clean humid air"), the liquid phase does not appear immediately after crossing the saturation line (equilibrium state) but after residing a certain time in a "non-equilibrium state" in the nozzle and in the form of a fog composed of submicronic particles.

This "condensation delay" results when there are rapid changes in temperature and pressure. In these transient processes, time may be insufficient for an equilibrium of phases to occur because condensation involves heat transfer, the rate of which is limited by various factors.

Departures from equilibrium are represented in terms of either the degree of subcooling ΔT or the supersaturation ratio S. The subcooling is defined by

$$\Delta T = T_{sat(P_v)} - T_S \qquad 4\text{-}5(a)$$

where $T_{sat(Pv)}$ is the saturation temperature corresponding to the prevailing partial pressure P_v, and T_S is the actual static temperature. (Note that $\Delta T < 0$ for superheated, equilibrium states, and $\Delta T > 0$ for subcooled, metastable states.) The supersaturation ratio is defined by

$$S = \frac{P_v}{P_{sat(T_s)}} \qquad 4\text{-}5(b)$$

where P_v is the actual partial pressure of the water vapour and $P_{sat(Ts)}$ is the saturation pressure corresponding to the local static temperature T_S. (Note that $S < 1$ for superheated states, and $S > 1$ for subcooled, metastable states.) Downstream of the condensation zone, where thermodynamic equilibrium is assumed, $\Delta T = 0$, and $S = 1$.

The net amount of subcooling is the result of two opposite processes:

$$\Delta T = \Delta Te - \Delta Tr \qquad 4\text{-}6$$

where ΔTe = subcooling due to air expansion in the nozzle, and
ΔTr = reheating due to the latent heat released by condensation.

In a rapid expansion, where subcooling occurs, the air/water condition varies along a line represented typically by 1-2′-3 of Figure 4-1. At 2, the air condition crosses the saturation line and enters a region of subcooling. If no condensation occurred, the air condition would reach point 2″ due to isentropic expansion. However, condensation begins at a point 2′ (the actual point depending on the cleanliness of the air and the speed of expansion) and then the static temperature reduction due to expansion is offset, to a degree, by the reheating due to the latent heat released by the condensing vapour. The mixture condition thus follows a line from 2′ to 3 as shown in Figure 4-1. At point 3 a quasi-equilibrium state is reached, and further cooling (expansion) is along the saturation line. The heat release due to condensation (leading to an increase in total temperature ΔT), is one of the major effects

related to condensing flow, because this changes the inlet flow conditions of the compressor. The ideal ΔT (T3-T2") is calculated when the condensation process takes place in equilibrium (line 1-2-3 in Figure 4-1).

A characteristic of condensation is that the process is thermodynamically irreversible and results in an increase in entropy and loss of total pressure. The ideal temperature rise and pressure drop due to condensation are shown in Figure 4-2. The temperature rise is determined by an energy balance of the gas, vapour and liquid phases between inlet entry and exit. The pressure loss associated with the temperature rise is calculated based on conservation of momentum.

Spencer and Archer (Reference 4.1), examined the effect of a number of variables on condensate level. The temperature rise was expressed as a function of the condensate flow ratio (Wr_f) and the specific enthalpy of evaporation (h_{fg}).

$$T_T = T_{amb} + \frac{Wr_f \, h_{fg}}{c_{p\ mix}} \qquad 4\text{-}7$$

To determine the condensate flow ratio, equilibrium conditions were assumed, and the four equations 4-1, 4-2, 4-7 and 4-8 (below) solved at engine face Mach number.

$$Wr_f = \mathbf{war}_{amb} - \mathbf{war}_{local} \qquad 4\text{-}8(a)$$

or

$$Wr_f = \mathbf{war}_{amb} - \frac{P_{sat} \, R_{d,a}}{(P_S - P_{sat}) \, R_w} \qquad 4\text{-}8(b)$$

where **war** is the absolute humidity, and

P_{sat} (saturated vapour pressure) is determined at T_S using saturated steam tables.

Examination of the four equations shows that there are five variables which determine the level of condensate:

(1) Relative humidity
(2) Ambient temperature
(3) Ambient pressure
(4) Inlet duct flow Mach number (dependent on duct area and engine mass flow)
(5) Inlet duct total pressure recovery.

The influence of these variables on condensate level at equilibrium conditions is shown in Figures 4-3 to 4-7, which assumes that the condensation process occurs at a Mach number equal to the compressor face Mach number to simplify the momentum pressure loss calculations.

Spencer and Archer also postulated that the same potential exists for condensation to occur with the engine behind a bellmouth or long inlet duct since the static conditions at the fan face are similar. The potential is described as the degree of supersaturation of the water vapour within the inlet configuration. Observations of bellmouth inlets at the time showed no signs of condensation. It was therefore concluded that water vapour was present in the bellmouth in a supersaturated state due to the lack of time for nucleation sites (Section 4.2.3) to form. It was demonstrated that in a long inlet duct the visible condensate occurs at a higher local relative humidity and further along the duct length than the total bellmouth length as shown in Figure 4-8. Once the nucleation sites formed, the air-water mixture quickly approached equilibrium, validating the assumption of equilibrium at the compressor face.

Figure 4-9 shows the envelope of ambient relative humidity versus inlet Mach number necessary for inlet condensation to occur at equilibrium conditions. It is assumed that there is adequate time and conditions favourable for the formation of droplets to occur.

The psychrometric chart indicating the relationship between relative humidity, absolute humidity and dry bulb temperature at sea level barometric pressure is shown in Figure 4-10.

4.2.3 Methods of Condensation

Two methods of condensation have been identified, homogeneous and heterogeneous. Homogeneous condensation describes a process whereby the water vapour spontaneously forms very small droplets (each drop containing fewer than 50 molecules). Much research has been done on this process as it commonly occurs in wind tunnels. Analysis (References 4.3, 4.4 and 4.5) has shown it to occur in significant amounts only when the supersaturation ratio is greater than 4.0, which is only likely to occur in engine inlets when the inlet Mach number is supersonic.

Heterogeneous condensation describes a process whereby the water vapour condenses out onto submicron particulate matter called condensing nuclei which exist in the air. "Large particles" are defined as covering a range of diameters from 0.1 - 2.0 μm (microns), while particles with diameters smaller than 0.1 μm are referred to as "Aitken" nuclei.

Heterogeneous condensation has received a lot of research as it is the process that forms clouds. The degree to which any condensing nuclei will result in water condensing onto them is dependent upon the particle size and shape and its electrical charge (both sign and amount). The process occurs in significant amounts at lower supersaturation ratios (less than 2.0) than homogeneous condensation and so is the dominant mechanism in engine inlets where the Mach number is typically in the region of 0.5 to 0.8 at high engine powers. Both methods are discussed in more detail in Section 4.7.

The particles can be sea salts, dust, pollen, combustion products, smog and ions. They are generally in the size range 0.01 to 0.1 μm. The concentration in the atmosphere varies with geographic location, elevation, season and weather conditions. During July at the South Pole it is around 10 parts per cubic centimetre (cc), while in January it is around 100 parts/cc (Reference 4.6). Concentrations of around 10^3 parts/cc occur over the ocean and 10^6 parts/cc in polluted urban air (Reference 4.7). Samples taken near an express way in Denver, Colorado, had around 6.1 x 10^5 nuclei/cc with a mean particle size of 0.032 μm (Reference 4.8). The formation rate of atmospheric aerosol particles is shown in Table 4-1.

Whilst the above discussion appears to be relevant for both engine test and simulated flight situations, the presence of nucleating particles in the air has a significant impact. This may lead to homogeneous condensation in cleaner atmospheres or where particles have been separated in the conditioning process in altitude chambers. In ground test plants, and in less clean regions of the world, heterogeneous condensation will play a larger role.

4.2.4 The Mechanism of Droplet Growth

Both methods of condensation create very small drops, and only a small amount of latent heat. Most of the heat is released in the subsequent growth of the drops which can end up being more than 10 times the original diameter (or 1000 times the volume). Research by Zerkle, Colley and Doel (Reference 4.9), and References 4.3, 4.10 and 4.11, has shown that there is a critical drop radius that determines whether a drop will grow or shrink when it is in supersaturated vapour. If the drop is smaller than the critical radius it will shrink, if it is larger it will grow.

The critical radius is mainly a function of $1/\ell n\ S$. At low Mach number, if the vapour is just saturated (relative humidity = 100%, supersaturation ratio = 1.0) then $1/\ell n\ S$ = infinity. If the supersaturation ratio = 2.0, then the critical radius is calculated to be 0.0017 μm which is smaller than nearly all of the particles present in air. Thus water will condense out onto all of the particles at the start of the duct, but as the water vapour condenses the supersaturation ratio will fall and the critical radius will rise so water may stop condensing onto the smallest particles.

The rate at which the drops grow depends on the size of the drops relative to the mean free path of the gas molecules. The mean free path varies most strongly with the increase of static pressure of the air. It does not vary greatly over the normal range of ambient pressure and temperature at sea level and the Mach numbers associated with engine inlets. An average value is 0.2 μm which is in the middle of the range for particle sizes in air.

If the drop radius is less than the mean free path of the gas (air and water vapour) molecules, then the growth rate depends on the relative kinetic energy of molecules striking the drop surface.

If the drop radius is greater than the mean free path of the gas molecules, then the growth rate depends on the rate at which heat can be transferred away from the surface of the drop. The latent heat released is assumed to first raise the temperature of the surface of the drop. Heat then conducts into the drop and transfers out into the gas, where it tends to increase the temperature, reducing the subcooling and re-establishing equilibrium. If the surface temperature of the drop remains high (i.e. heat transfer is low) then water molecules at the surface of the drop will tend to evaporate, so absorbing latent heat and lowering the surface temperature of the drop.

If the engine inlet is long enough, then an equilibrium is reached where the growth rates have fallen to zero and the supersaturation ratio has fallen close to 1.0.

4.3 COMPONENTS

4.3.1 Inlets

4.3.1.1 *Engine Inlets*

The rules governing the flow into a subsonic inlet of an engine follow closely the description given in Section 4.2.2. The conditions delivered to the compressor face will depend on the geometry of the inlet with longer

inlet arrangements providing more potential for condensation and shorter inlet configurations providing greater degrees of supersaturation. The actual engine inlet configuration will be determined by the airframe, with wing mounted engines generally having short inlets and fuselage mounted engines longer inlets, the latter generally incurring more problems. At altitude, condensation in inlets is less likely to be a problem because of the reduced water content in the air.

Supersonic inlets have the added complexity of shock systems and considerable scope for generating condensation which is not necessarily in equilibrium with its surrounding conditions. Generally, longer inlets will generate compressor face conditions in which the degree of supersaturation is minimised. However, the actual degree of condensation is also a function of the number of nucleating particles present (and therefore ambient conditions) as well as inlet geometry.

Inertial Particle Separators (IPS) are now often used in helicopter engines and, although subsonic, will potentially suffer severe problems due to longer flow paths and extended regions of accelerated flow.

Filters could also introduce further complexities with the flow (which is possibly already supersaturated) as it passes through moisture laden fabric, as this could precipitate condensation and separate it from the flow. In a continuous flow process this water will be re-injected into the mainstream, probably not as homogenously distributed particulate but as surface water and large droplets (see Chapter 5).

The actual air pressure and temperature at the fan face is generally not known because measurement of these parameters is made upstream of the condensation process. Condensation affects temperature instrumentation by droplets impinging on the thermocouple head. If the conditions are right for re-evaporation, heat transfer will take place between the thermocouple head and the droplet as the latent heat needed for re-evaporation is drawn from the thermocouple head. This artificially reduces the measured temperature below its actual value.

Practical evidence of condensation within an A7 aircraft inlet duct on installed turbofan engine performance was investigated by Spencer and Archer (Reference 4.1). Three variables were identified as possible causes of fuel control schedule trim variations (Section 4.4.2) required to achieve the engine's design thrust:

(1) Ambient temperature
(2) Ambient relative humidity
(3) Ambient specific humidity

Comparison of day versus night operation, with different levels of ambient temperature and ambient relative humidity but constant specific humidity, also showed large shifts in the power trim. It was therefore concluded that specific humidity was not the contributing factor.

On-site testing (NAS, Cecil Field) also indicated different power trims between day and night with low and high levels of relative humidity respectively. It was postulated that either the characteristics of the inlet duct or the engine's internal matching had changed between these conditions. Since changes in relative humidity did not affect engine performance when installed with a bellmouth inlet, it was concluded that any changes in engine performance when operating behind an aircraft inlet duct must be caused by phenomenon within the inlet duct itself.

Engine operation in a high relative humidity environment resulted in water droplets being observed to condense out of the air in the inlet duct. Performance shifts (Section 4.4.2) correlated closely with analytical estimates (Section 4.2.2). Spencer and Archer concluded that the same analytical assessment could not necessarily be applied to every inlet configuration, since duct length and geometry are influencing factors in initiating nucleation. An inlet duct of shorter length or more constant flow area may not provide sufficient time or potential for condensation to occur.

An engine test with varying relative humidity levels was conducted in an out-door test cell with a TF30-P8 experimental engine and full scale simulated A7 aircraft inlet duct. During testing, the 'dry air' total temperature was measured with a special probe to record actual air temperature. A conventional probe restagnates the air locally and re-evaporates the condensate, returning the air to ambient conditions. The probe design forced the air to make two sharp turns prior to stagnation. This caused the liquid water droplets to be removed from the sampled air. The probe, located at the compressor face recorded a temperature 5.6 K higher than the ambient temperature, supporting the theory of a higher total temperature in the presence of condensation.

4.3.1.2 *Inlet Shock Waves*

The occurrence, position and strength of shock structures are functions of the gas composition. Therefore changes in gas composition resulting in changes to the gas content and ratio of specific heat would be expected to modify the shock structure in the inlet and on the blading of transonic/supersonic stages.

Shocks invoke very rapid velocity gradients, and particles which generally follow the Stokes drag

relation will not be able to follow the rapid transient leading to an imbalance between the flow and particle quantities behind the shock. This is most obviously the case for velocity but will also be the case for temperature. On the downstream side of the shock this will lead to quantity exchanges between the particles and gas leading to both an apparent smearing of the shock and an increase in the associated losses. The extent of the changes in shock structure and losses is difficult to generalise because they will depend on the 'dry' flow conditions and the characteristics of the particulate.

It is of interest to note that during pitot-traverse drag measurements on isolated aerofoils in wind tunnels by Pearcey (Reference 4.12), the results at Mach numbers near and above the shock-stall have failed to repeat from day to day. During such tests there was considerable variation in the Mach number at which the drag began to rise rapidly and therefore very large changes in the values of drag coefficient, C_D, at Mach numbers above this. Such results demonstrate a definite correlation between the observed variations in C_D and the variation in atmospheric humidity, as shown in Figure 4-11 in which the Mach number where C_D exceeds 0.01 (Ma_{crit}) is plotted against the initial relative humidity. Since the shock-stalling speed at 1 deg should be very similar to that at 0 deg, values for both incidences are included and show a roughly linear relationship between this Ma_{crit} and the relative humidity.

It has also been noted, Reference 4.12, that clouds of condensed moisture are often visible at the sides of aerofoil wakes at Mach numbers below those which produce extensive condensation in the free stream. A sketch of the extent of visible condensation in a typical case for a 30.5 cm (1-ft) chord model is reproduced in Figure 4-12. For the speed just above the shock-stall at which this sketch was obtained, condensation apparently commenced at a point on each surface immediately ahead of the shock wave and spread out laterally as it moved downstream, so that at the position of traverse (0.5*c* behind the trailing edge), it extended over a considerable distance in this direction. For the tests during which the above sketch was made, a little condensation was noticed at a speed slightly below that at which the shock wave was first visible. If, as may justifiably be expected, this condensation leads to a drop in the total head, the readings in the normal wake will be affected and the 'effective' wake, or the region in which the total head pressures are below the free-stream value, will be extended in width. The measured loss in momentum, and hence the measured C_D, will consequently be much too large. Although this report is for isolated aerofoil data it appears reasonable to suggest that turbo-machinery blading will respond similarly.

4.3.1.3 *Engine Test Facility Inlets*

Blake (Reference 4.2) conducted an analysis of condensation effects in a JT9D turbofan engine operating behind a bellmouth test inlet. A condensation detection system was used, consisting of a helium neon laser which projected a beam of red light across the inlet of the engine, and a photo multiplier which was positioned on the opposite side of the inlet and offset from the beam as shown in Figure 4-13. In this way, the photo multiplier responded only to light which was scattered by water droplets towards the photo multiplier.

Figure 4-14 shows the results of the laser system installed in two experimental engines, with the output voltage increasing with Mach number and relative humidity. Figure 4-15 shows that condensation occurred only when the critical Mach number predicted by theory was obtained.

During another series of engine tests, photographs of the engine inlet were taken over a range of engine power levels and ambient conditions. At low humidities and/or low engine power levels, where no condensation is predicted, the laser beam was not visible because no light was scattered towards the camera. At higher power levels and humidity conditions, where condensation is predicted by theory, the laser beam was clearly visible. In addition, the visible intensity of the laser beam was seen to vary with engine power and humidity. Photographs where the laser beam was visible were in the condensation portion of Figure 4-15.

This analysis of condensation was limited to one-dimensional flow, although some photographs indicated a two-dimensional flow regime showing more condensation occurring near the walls of the inlet rather than the centre. In a two-dimensional flow field, the streamlines near the wall achieve a higher Mach number than those in the centre and therefore increase the propensity for condensation.

4.3.2 Compressors (Fans)

The compressor or fan is the first active component of the gas turbine engine to encounter the potentially particulate laden flow delivered by the inlet. This flow enters the compressor and receives further acceleration over the suction surface of the first set of blades. This may, or may not, be associated with a shock structure although, increasingly, with the adoption of transonic

stages and fans, this will be the case. The initial local flow conditions are therefore analogous to those in the inlet as described above, although the region over the blade suction surface is very restricted. As the flow accelerates and passes through shocks, it is likely that in moist conditions some degree of supersaturation will occur but the degree of condensation will depend on many factors, including stage geometry, inlet conditions and nucleation particles.

As the flow passes further into the compressor the air is heated by the work expended upon it. This will gradually cause re-evaporation, eventually creating dry conditions somewhere within the compressor if the temperature rise is great enough. The temperature rise across the first stage of modern gas turbines is typically 50 K which, under most conditions, would be sufficient to re-evaporate any condensate created in the inlet. However, where large water droplets (rain, etc.) enter the compressor, quite extensive regions of the compressor may operate with liquid present. The rate of evaporation is complicated and depends on the heat transfer which is a function of the relative velocities and the temperature of the air and droplet. The evaporation rate increases rapidly once the boiling point of the liquid is reached. (The boiling temperature increases through the compressor due to the increasing pressure.)

The condensation process could be relatively well defined if it were not for the uncertainty of the particle size spectra and evaporation times. Indeed, psychometric charts exist to aid the calculation but these assume equilibrium between the condensate and flow which appears most unlikely in view of the short dwell times involved. The results of such a calculation, however, are provided in Section 4.3.2.1 in order to demonstrate the magnitude of the effect.

The net effect of inlet condensate in the flow is to increase the total mass flow (and available gaseous flow) for a particular non-dimensional operating condition (inlet incidence and blade speed). These inlet conditions, however, no longer define the incidence distribution throughout the compressor as the re-evaporating flow modifies the volume flow and consequently the incidence distribution. If the stage matching has been optimised for dry air, the condensing and re-evaporation process will cause stage mismatch, possibly resulting in reduced efficiency and/or flow range.

It appears that the general influence will be that evaporation (or re-evaporation) within the compressor will have the effect of increasing the mass of gaseous flow but the evaporation process absorbs heat so the flow has a lower temperature. The increase in gaseous mass flow rate will tend to increase the velocity (and flow coefficient) while the reduced temperature will increase density which tends to reduce the volume flow rate (reducing flow coefficent). The reduced temperature also increases the corrected operating speed, thereby increasing the stage pressure rise and density (reducing the axial velocity and flow coefficient) towards the outlet. Furthermore, the presence of evaporation tends to make the compression process more isothermal and so increase the pressure rise for a specific work input, further increasing density and reducing the stage flow coefficient.

If the compressor is operating at design conditions, the rear stages will operate near peak efficiency in dry conditions. The influence of condensation at the inlet, and re-evaporation within the compressor, appears to cause these rear stages to rematch at reduced flow coefficients (i.e. towards stall). As surge is approached at high speed, it is usually the stalling of the rear stage(s) which prompts surge. The influence of condensation in the inlet and subsequent re-evaporation will tend to advance this process by rematching these stages closer to stall, thus providing a narrower operating range.

At low speeds the picture is somewhat different, as in this case, where the flow rate is reduced (operation towards surge), it is usually the front stage which stalls, causing surge, and, as the volumetric flow rate through these stages is largely unaltered (little re-evaporation has occurred), the surge condition would remain largely the same. A schematic diagram of this is shown in Figures 4-16 and 17. The net effect of stage matching appears to be significant. Our understanding of this rematching phenomena could be significantly improved by the use of stage stacking models able to simulate re-evaporation. Some work in this area is discussed in References 4.13 and 4.14.

4.3.2.1 *Sample Equilibrium Calculations for a Multistage Compressor with Large Scale Water Ingestion*

The following calculations assume that the water is perfectly mixed with the airflow and both are in equilibrium. These simplifications are clearly limiting and the calculation presented here is presented merely for scoping the magnitude of the problem. Such calculations were undertaken by various parties interested in thrust augmentation on early engines, Reference 4.15. It should be emphasized that the amount of water ingested in these calculations exceeds that available from condensation, but the example is presented here to illustrate the effect.

The table below summarizes the results of calculations of compressor-outlet conditions when various amounts of water are ingested at the compressor inlet.

The following conditions are assumed:

Ambient static temperature, T_{Samb}	288.15 K
Ambient static pressure, P_{Samb}	101.325 kPa
Flight Mach No.	0.85
Compressor adiabatic efficiency, η_{comp}	0.80
Compressor enthalpy rise, Δh_{comp}	198.4 kJ/kg
Air mass flow, W_a	36.59 kg/s

Condition (Sufficient water exists at the inlet for the following conditions)	Amount of water evaporated (kg water/kg air)	Outlet pressure P3 (kPa)	Outlet temperature T3 (K)
No water	0	596	526
Air saturated at compressor inlet	0.0113	658	497
Air saturated through one-half of work input process	0.0384	745	432
Air saturated up to compressor outlet	0.0565	822	368

These calculations have involved only the simplest correction for changes in compressor efficiency and assume equilibrium between water content and air. However, they do serve to illustrate that the effects can be very large, radically changing both delivery pressure and temperature.

4.3.3 Combustors

Although the combustion performance will be influenced by the presence of condensation and water droplets in the inlet air, these conditions would rarely occur as the inlet air is pressurised and any water will be removed as part of the compression process. As water will influence the process, however, care should always be taken to avoid water being introduced to the flow from inlet ducting. Most testing is completed at elevated temperature and this further reduces the influence of condensation.

4.3.4 Turbines

The process of condensation in turbines is the reverse of that in compressors in that it is likely to influence the turbine outlet (rather than the compressor inlet). The air inlet conditions for a turbine, however, are usually controlled (unlike those of a compressor) and the action therefore is to avoid condensation by ensuring an appropriate inlet temperature which gives an outlet temperature above the dewpoint.

Condensation is a very major problem in the final stages of steam turbines and extensive literature for this exists - see, for example, Moore et al., Bakhtar and Tochai, Kleitz et al., Guha and Young, (References 4.16 to 4.19, respectively). This work, however, is not truly applicable to the testing of gas turbines where such conditions should be avoided during calibration testing.

An indication of how condensation can be avoided during rig testing, follows. The parameters relevant in this respect are the water to air ratio of the air ducted to the turbine and the static temperature/pressure combinations existing at the turbine stations. Figure 3-5 gives the saturated water to air ratio depending on temperature and pressure, where condensation does not occur. Under normal turbine operating conditions, the limiting conditions are reached at the turbine exit first.

Example:

The static conditions expected at the turbine exit are:

$T_S = 280$ K

$P_S = 80$ kPa

The air ducted to the turbine is taken from the atmosphere at an ambient temperature of 300 K, a pressure of 100 kPa and a relative humidity RH=60%.

From Figure 3-5, the water-air ratio of the mixture is:

$$\mathbf{war} = RH\ \mathbf{war}_{sat} = 0.0135.$$

According to the conditions at the turbine exit, from Figure 3-5 the saturated water to air ratio is:

$$\mathbf{war}_{sat} = 0.0075.$$

To be sure that no condensation occurs, the air has to be dried not to exceed $\mathbf{war}_{sat}$.

Alternatively, the inlet temperature of the turbine can be raised to get a higher turbine exit temperature. According to Figure 3-5, a turbine exit temperature of 288 K is required to exclude condensation at a water-to-air ratio of 0.0135 and a pressure of 80 kPa.

4.3.5 Nozzles

The effect of condensation in a converging - diverging nozzle is shown in Figure 4-18. At low values of relative humidity, condensation occurs in the divergent part of the nozzle producing an increase of pressure. At high values of relative humidity, condensation occurs in the convergent subsonic zone, which causes a decrease of pressure.

The effect of shock waves, from a typical experimental result at low relative humidity, is shown in Figure 4-19. Homogeneous condensation occurs in the divergent part, producing an increase of pressure, and the droplets evaporate at the crossing of the first aerodynamic shock wave, re-accelerating the flow. (The second aerodynamic shock wave, which adjusts the flow to the atmospheric exhaust pressure, is not represented in this figure.)

The term "onset of condensation" is often used to describe homogeneous nucleation because of the sudden appearance of the condensation fog (Section 4.2.2).

4.4 WHOLE ENGINE RELATED EFFECTS

4.4.1 General Effects

Condensation causes a change in state of the inlet duct flow by changes in the following parameters entering the engine:

(1) Increasing total temperature
(2) Decreasing total pressure (subsonic flow)
(3) Converting some of the vapour into liquid water

In addition, velocity and Mach number increase, while static pressure, density and local humidity decrease. The change in state, when not accounted for, will appear as shifts in corrected engine performance. These apparent shifts are primarily the result of correcting the engine's operating parameters from conditions not representative of those at the compressor face. Accounting for the temperature rise and pressure loss in the inlet for the measured engine performance, together with changes in the engine's internal matching due to water ingestion would remove the apparent shift in corrected performance.

Both temperature increase and pressure reduction degrade engine performance. Analysis of the pressure loss by Blake (Reference 4.2) indicated that the loss in total pressure is very small. Furthermore, a similar momentum effect associated with the re-evaporation process during compression offsets the pressure loss. The effect of the temperature increase on measured engine performance is shown in Figure 4-20. Two compression processes are indicated, one without inlet condensation (1, 2), and one with inlet condensation (1, 3, 4, 5). Only the properties of the air portion of the mixture are considered, not the changes in entropy of the water vapour or liquid portions of the mixture. The figure assumes re-evaporation after the compression process is complete. Comparison of the final two states shows the final temperature after condensation is higher. The resultant increase in fan work to achieve the same pressure ratio requires more fuel flow and hence higher SFC. The figure also shows that the magnitude of the work increase is dependent on when re-evaporation takes place.

Blake conducted an experimental test program using a JT9D-7 engine to establish empirically the effect of inlet condensation on specific fuel consumption. In addition to this engine, data from several other JT9D experimental engines were used resulting in a total of 47 engine calibrations over a range of ambient conditions as shown in Figure 4-21. To minimise the possible effects of engine performance deterioration, all engine data were compared on a back to back basis. The percentage change in specific fuel consumption during engine testing was compared to the analytically derived ideal temperature rise in the inlet due to condensation as shown in Figure 4-22.

Due to the limitations in instrumentation accuracy and the relatively small shifts in performance being measured, a large data sample was required together with the use of statistical methods to increase confidence in the results. The solid line is a first degree least squares fit which takes account of random SFC measurements. The dashed lines represent a 95% confidence band, or ± 2 standard deviation scatter from the mean, indicated by statistical analysis. The correlation shows a penalty of +0.34% SFC on a typical summer's day in the Hartford area with an ideal inlet temperature rise of 4 K.

An analytical model was constructed by Blake with the following assumptions:

(1) Equilibrium conditions upstream of the fan
(2) Negligible momentum or heat transfer pressure loss
(3) Constant compressor adiabatic efficiency
(4) Re-evaporation downstream of the fan rotor and midway in the low pressure compressor.

The model predicted a change in SFC of +0.7% with an inlet temperature rise of 4 K.

The measured effect of condensation on performance is therefore around half of that predicted by the analytical model. This difference was attributed by Blake to the following factors:

(1) Equilibrium conditions may not have been reached in the bellmouth inlet, due to low residence time, resulting in a temperature rise lower than predicted.
(2) A large amount of the condensate may re-evaporate within the fan rotor, and reduce the impact on fan performance.
(3) The simplification of one-dimensional flow may give substantial errors relative to the real two dimensional flow field.

Blake concluded that the effects of inlet geometry, fan aerodynamics and engine thermodynamic cycle were unknown and therefore the SFC correlation was considered applicable only to the particular test engine/inlet configuration.

During the analysis, the thrust/engine pressure ratio (EPR) relationship was examined. No change in this relationship was noted with inlet condensation, so it was concluded that no loss in take off thrust would be expected on the JT9D engine due to condensation.

4.4.2 Controls

Investigations into the effect of condensation on the TF30 non-afterburning engine control system was conducted by Spencer and Archer (Reference 4.1) and is summarised below.

TF30-P6 and P8 engines installed in A7 aircraft showed significant variations in military trim level with changes in relative humidity levels of the ambient atmosphere. In addition, engines trimmed in high relative humidity conditions had higher turbine entry temperatures (+50 K) than those trimmed in a low relative humidity environment. From an operability viewpoint, these variations needed a large amount of aircraft downtime to maintain engine trim,while the higher turbine inlet temperature reduced engine life.

The fuel control system enables the engine's design thrust to be achieved at the maximum power lever angle. This is performed on the TF30 engine by scheduling the HP rotor speed as a function of compressor inlet total temperature. To compensate for variations in the thrust vs HP speed relationship between engines, the fuel control schedule can be trimmed. A trim chart is used showing the relationship of $P7/P_{amb}$ to ambient temperature consistent with the design thrust of the engine. Trimming is performed by adjusting the fuel schedule so that the engine produces the level of $P7/P_{amb}$ indicated on the trim chart at the ambient temperature. Once trimmed, the fuel control schedules an HP rotor speed at the maximum power position which varies only with compressor inlet total temperature. Since the fuel control's T2 sensor stagnates the air, the sensed temperature at sea level static conditions remains at ambient regardless of the degree of condensation.

The correlation between the fuel control parameter ($NH/\sqrt{\Theta_{amb}}$) and trim parameter ($P7/P_{amb}$) is assumed to be unique in the derivation of the charts. However, on-site tests (NAS, Cecil Field) showed a shift between the fuel control parameter and trim parameter with low and high relative humidity as shown in Figure 4-23. Ambient conditions were used to correct the data, therefore variations in inlet duct temperature due to condensation appear as shifts in gas-generator corrected performance (Section 4.4.1).

The effect of condensation on trim is shown in Figure 4-24, for the same ambient temperature and different levels of relative humidity. Since the fuel control senses ambient temperature, it schedules the same HP rotor speed and hence the same $NH/\sqrt{\Theta_{amb}}$ as indicated in Figure 4-24. However, since the $P7/P_{amb}$ is different at the two conditions, the relative humidity trim corrections shown in Figure 4-25 were designed to compensate for the variation in $P7/P_{amb}$.

Spencer and Archer noted that even if the fuel control's T2 sensor was capable of measuring dry air

total temperature rather than ambient temperature, trim corrections would still be necessary. For example, if the HP rotor speed schedule remains constant with inlet temperature, Figure 4-24 is still applicable.

Without the relative humidity trim corrections, an engine trimmed at high relative humidity would be trimmed to the same $P7/P_{amb}$ as for low relative humidity and would operate at higher HP rotor speed and turbine temperature levels. The implication of applying trim corrections at high relative humidity is a reduction in take-off thrusts.

An engine trimmed to the same parameter as being scheduled by the fuel control system would not require trim corrections. However, variations in thrust would still occur if the parameter was corrected using inlet temperature.

4.5 CURRENT PRACTICES

4.5.1 Component Testing

The presence and process of condensation and re-evaporation can influence the thermal performance of components. Furthermore, many of the concepts of enthalpy change across a component and its operating efficiency involve an assumed flow process where the physical properties of the gas are known and condensation/re-evaporation does not exist. As a separate issue, condensation/re-evaporation influences instrumentation; this is discussed in Chapter 7.

The treatment of condensation/re-evaporation in component testing is largely inadequate as little account is taken of the process (considerably less account than for the testing of whole engines, Section 4.5.3). The considerations largely involve avoidance and association of any inconsistent result with the probable occurrence of condensation. Certain precautionary procedures are adopted and these are discussed below.

4.5.1.1 *Inlets*

The procedure here is very largely to avoid problems. For high speed inlets this can be a significant problem unless control of the inlet air conditions is possible as in some Altitude Facilities. Detection largely involves visual observation.

4.5.1.2 *Compressors (Fans)*

Condensation can be a problem particularly in the first few stages. The procedure is again largely one of avoidance. Detection can be a problem as many facilities involve "closed" ducting and visual inspection is not possible. Furthermore it is very uncommon to test compressors in altitude test facilities. The problem is made worse by the common practice of testing at low inlet pressures to reduce power consumption. There is a fairly clear need to improve condensation detection instrumentation for such testing. The situation is worse for fans than for compressors as the former usually have a smaller temperature rise and are more susceptible to the effects of condensation. For this reason, some organisations restrict the testing of fans to ambient conditions within defined humidity limits (Section 4.5.2).

4.5.1.3 *Combustors*

Before combustion, the inlet pressure is increased and therefore the process is unlikely to be compromised by the presence of condensation. In the combustion process considerable heat is added, further drying the air. If care is not taken, however, and condensation or droplets from inlet ducting enter the combustion chamber, this can considerably influence the combustion process. Therefore, care should always be taken in considering combustor inlet conditions.

4.5.1.4 *Turbines*

Turbines are normally tested with warm inlet air and, so long as care is taken not to let the outlet temperature fall below the dewpoint, there should be no problem. Once again, what is required is some detection process for the presence of condensate at turbine outlet.

4.5.2. Engine Humidity Limits

Grabe and Bird (Reference 4.20) reported that during a cell correlation program, using a GE F404 turbofan engine, the following psychrometric conditions were specified by the engine manufacturer:

(1) Relative humidity less than 75%
(2) Absolute humidity less than 0.01428 kg water/kg dry air
(3) No visible moisture in the air.

Condition (3) would normally be avoided if (1) and (2) are adhered to. The absolute and relative humidities specified occur at a temperature of 297 K (shown in Figure 4-10). With an inlet Mach number of 0.44 and a temperature of 297 K, Figure 4-9 shows a saturation limit around 50% relative humidity. The limit of 75% relative humidity therefore exhibits a supersaturation level of 150% with no condensation. This was justified by Grabe and Bird as a condition free of condensation on the grounds that a short bellmouth inlet has a small

dwell time. In addition, Spencer and Archer claimed that a supersaturation ratio of 220% was condensation free (Figure 4-8). The limits which were adopted by the authors of Reference 4.20 are shown in Figure 4-26. Grabe and Bird concluded that, in the absence of agreed procedures for the correction of gas turbine performance for the effects of condensation, the best solution was the avoidance of condensation. The alternative of artificially drying the air is an expensive process.

The engine manufacturer has revised its test limits, from those quoted above, to be based on the ideal temperature rise in the inlet rather than relative and absolute humidity. This results in more testing being performed during cold periods when condensation is low, even at high relative humidity. The revised humidity limits allow an ideal temperature rise (TRISE) of 7.2 K for most performance testing and 2.8 K for fan mapping. Figure 4-27 shows the relative humidity/inlet temperature envelopes using both the old and revised humidity limits, together with average winter and summer daily variations. It shows that the revised limits are expanded at low temperatures and low airflow rates. The use of $W\sqrt{\Theta}/\delta$ in the revised humidity limits means they are valid only for a particular inlet geometry configuration. In addition, some companies utilise a laser condensation detection system in the inlet to permit a run/no run decision beyond the TRISE limitations.

The need to have good but workable humidity limits is considered important to enable good quality performance data to be obtained with the minimum of testing interruption. During RB211 development engine testing, humidity limits were used to reduce the possibility of condensation formation within the inlet, as shown in Figure 4-28.

The humidity limits were verified using fan delivery and inlet temperatures. Figure 4-29 shows the difference between fan root delivery temperature and extended airmeter inlet temperature, over a range of engine power levels for different environmental conditions. The high humidity conditions result in an artificially reduced measured temperature at fan delivery caused by re-evaporation of water droplets from the thermocouple head. The relative humidity and ambient temperature combinations that result in condensation, shown in Figure 4-29, exceed the humidity limits in Figure 4-28 for an extended airmeter, validating the humidity limits.

4.5.3 Engine Empirical Condensation Corrections

Because of the difficulty of reliably quantifying by observation or measurement the extent to which the condensation process has occurred at the engine face, aero-engine manufacturers have attempted to correct engine test data for the effects of condensation by using empirically derived corrections based on correlations of measured engine performance changes against the ideal temperature rise due to condensation.

If the pressure, temperature, velocity and humidity are known for the mixture, the ideal stagnation pressure and temperature of the gas phase with condensation can be determined. The rise in gas-phase stagnation temperature from ambient is TRISE. The relationship between TRISE and ideal or equilibrium TRISE is shown in Figure 4-30 for the condensation process following an isentropic expansion. The ambient condition is represented by point T_{amb}. The state of the mixture following rapid isentropic expansion in the inlet is represented by points IA for air, IL for liquid and IV for water vapour. As the supersaturated mixture flows through the inlet duct, the two-phase mixture moves towards the equilibrium state represented by points EA, EL and EV. Note that for the air and vapour, temperature rises during the condensation process while the liquid temperature decreases towards the equilibrium temperature of the mixture.

The ideal temperature rise referred to is that which would be reached if the condensation process proceeded to complete thermodynamic equilibrium along the liquid/vapour saturation line assuming the following:

(1) The inlet flow is one dimensional.
(2) Residence time in the inlet is adequate.
(3) Particle concentration is adequate.

(1) and (2) are principally related to inlet geometry and can therefore be correlated empirically for a given engine/inlet combination. However, (3) is effectively random due to the difficulty of counting and sizing the particles together with determining their activity. With normal engine inlet geometry, condensation can be completely inhibited by too low a particle concentration. This makes empirical corrections based on ideal condensation temperature rise completely independent of the unknown particle contribution, which could result in errors of corrected engine test data.

The condensation corrections used for the RB211-535 production pass-off engines were derived during the RB211/CF6 risk and revenue sharing agreement between RR and GE. It was assumed that the RB211-535 and CF6-50 engines and test bed inlet configurations were similar enough for the transfer of

correction factors. The correction factors were derived to enable the "wet" data (no correction for inlet condensation) to "dry" data (corrected for inlet condensation) correction to occur in a single equation:

$$DRY = WET \times (1 + ['K\ FACTOR' * TRISE]) \quad 4\text{-}9$$

where TRISE is the ideal temperature rise due to condensation, determined knowing the engine inlet conditions and configuration. The 'K FACTOR' is shown in Figure 4-31 as a function of thrust. It shows that the correction factors for fuel flow, fan speed and exhaust gas temperature (inter-turbine) reduce to zero at an intermediate power condition. These were the only parameters which varied significantly with condensation. Table 4-2 shows the effect of applying these correction factors at 178 kN thrust and 5 K TRISE.

Engine/inlet condensation correlations can be derived by analysing production engine data at specific thrust levels. For each thrust level, the data are corrected for the effects of humidity and plotted against TRISE. The major assumption is that any variation of humidity-corrected SFC with TRISE is caused solely by condensation effects. Figure 4-32 shows the SFC data from 44 RB211-524 production engines at take-off thrust. A best fit straight line through the data has a slope (% SFC/K temperature rise) which, with the opposite sign and divided by 100, is the condensation correction 'K FACTOR'. The statistical significance of the correlation was confirmed by examination of the linear correlation coefficient (>95%) which is described below:

The extent to which N points $(x_i,y_i) \rightarrow (x_n, y_n)$ fit a straight line is indicated by the linear correlation coefficient (lcc):

$$lcc = \frac{\Sigma(x_i-\bar{x})(y_i-\bar{y})}{[\Sigma(x_i-\bar{x})^2\ \Sigma(y_i-\bar{y})^2]^{1/2}} \quad 4\text{-}10$$

which lies in the interval $-1 \leq lcc \leq 1$. Values of lcc close to ± 1 indicate a good linear correlation, values close to 0 indicate little or no correlation.

Examination of the 2 x standard deviation ÷ mean value, expressed as a percentage for no correction, humidity corrected and humidity plus condensation corrected SFC data, in Table 4-3, shows the degree of scatter to progressively reduce. This is to be expected if the correction procedure is valid, since an increase in the scatter of SFC after the application of any form of correction would indicate that either the correction gradient is wrong or that the physical nature of the correction is false. The improvements in SFC scatter are small but this is the result of the number of other factors involved in the total scatter rather than a fault in the correction itself. This can be demonstrated by considering a basic SFC scatter of 0.8% and considering it to be made up of the following elements of scatter at the 95% confidence level (i.e. two standard deviations).

SFC variation	
Engine build variation	± 0.4%
Test measurement accuracy	± 0.4%
Humidity effect (uncorrected)	± 0.4%
Condensation effect (uncorrected)	± 0.4%
Total root sum square (RSS)	± 0.8%

It should be noted that these figures are illustrative only. If a humidity correction was applied which completely eliminated the scatter due to this element, the total scatter would then become $(3 \times 0.4^2)^{1/2} = \pm 0.693\%$ compared to the original level of $\pm 0.8\%$, i.e. an improvement of less than 0.11%.

A further correction for condensation effects would then improve the scatter to $(2 \times 0.4^2)^{1/2} = \pm 0.566\%$, i.e. a further improvement of 0.13%. This explains the relatively small improvements in scatter shown in Table 4-3.

Analysis of RB211 engine data also indicated a statistically significant condensation correlation for the low pressure compressor speed, turbine gas temperature (TGT) and, additionally, intermediate pressure compressor speed.

Engine/inlet condensation corrections can also be obtained by repeatedly testing a single engine over a wide range of humidity conditions. An assessment of the engine deterioration would then have to be made and all the results corrected accordingly.

4.6 ENGINE STUDIES AND RECENT WORK

4.6.1 Analytical Assessment

4.6.1.1 *Zerkle, Colley and Doel Analysis*

Zerkle, Colley and Doel presented details of an analytical model of moisture condensation in engine inlet ducts at an ASME symposium in 1982 (Reference 4.9). It was considered by the authors that an exact model of the inlet condensation process was not feasible, therefore a reasonably accurate model incorporating the most important factors influencing the inlet flow properties was developed. Only heterogeneous condensation (Section 4.2.3) was considered, where supersaturated water vapour condenses onto nucleation particles in the gas which are assumed to be spherical, wetted and chemically inert. Input parameters include ambient nuclei concentration, size distribution and inlet geometry. A summary of the parametric study conducted by Zerkle, Colley and Doel is given below.

The effects of inlet duct Mach number and ambient relative humidity on equilibrium or ideal inlet temperature rise using the 'Zerkle' computer code are shown in Figure 4-33. The ideal temperature rise assumes thermodynamic equilibrium including saturation, complete condensation and droplet growth. The analytical model showed that only inlet duct Mach number (mass flux), ambient air pressure, temperature and relative humidity affected the ideal temperature rise.

The non-equilibrium or actual condensation process is also affected by the concentration and size distribution of condensing nuclei in the air as well as the residence time in the inlet. The effect of inlet duct Mach number and ambient relative humidity on critical nuclei diameter is shown in Figure 4-34. The mechanism of droplet growth is such that if the drop is smaller than the critical size it will shrink, if it is larger it will grow (Section 4.2.4). Figure 4-34 shows that for an inlet Mach number greater than 0.5 and an ambient relative humidity above 75%, supersaturated vapour will condense on nuclei larger than about 0.005 μm. This represents more than 95% of the nuclei being activated. A particle size distribution suggested by Fuchs (Reference 4.21) for condensing nuclei is shown in Figure 4-35, with a median size of 0.032 μm.

The effect of duct length on inlet condensation is shown in Figure 4-36, assuming a constant area duct, 100% ambient relative humidity, nuclei concentration of 6.1 x 10^5 particles/cm^3 (cc) and a reference particle size distribution approximating Figure 4-35. The calculations to produce Figure 4-36 were repeated with a uniform particle size having a median value of 0.032 μm which gave nearly identical results.

The effect of nuclei concentration on inlet condensation is shown in Figure 4-37. Ambient air is expanded in a converging duct up to 102 cm, followed by a straight duct up to 203 cm, then a diverging duct symmetrical to the converging duct up to 305 cm. The figure shows that the temperature rise curve for 10^7 nuclei/cc closely follows the equilibrium/ideal curve. It should be noted that supersaturation and condensation exist when the TRISE curves (dashed) are below the equilibrium TRISE curve (solid), while evaporation occurs when the TRISE curves are above the equilibrium curve.

Zerkle, Colley and Doel concluded the following:

(1) Condensation occurred on submicron particles called condensing nuclei present in the air.

(2) Ambient relative humidity and particle concentration are the most significant parameters affecting the condensation process.

(3) Condensing nuclei counters accurate to particle sizes as small as 0.002 μm are required.

(4) The analytical model requires experimental verification before it can be used with confidence for engine evaluation.

4.6.1.2 *MD11 and Long Inlets*

The effects of condensation in the MD-11 centre duct inlet have been investigated using a program based on the paper produced by Zerkle, Colley and Doel to predict the actual temperature rise (Section 4.6.1.1).

An outline drawing of the full scale MD-11 centre duct inlet is shown in Figure 4-38. The condensation temperature rise along the inlet duct with 90% ambient relative humidity and 0.5 Mach number in the parallel section of the duct, is shown in Figure 4-39 for varying values of nuclei count. The particle size distribution approximates that suggested by Fuchs (Figures 4-35 and 4-36). Particle concentrations of 10^7/cc and 10^6/cc reach the maximum level of condensation early in the duct while 10^5/cc reaches the maximum level towards the end of the duct. Concentrations of 10^4/cc and 10^3/cc have a very small effect. The effect of ambient relative humidity, inlet Mach number and ambient temperature on the maximum values of equilibrium temperature rise in the inlet is shown in Table 4-4.

Figure 4-40 shows the influence of particle concentration on the ratio of actual temperature

rise/equilibrium temperature rise at the last point in the inlet, adjacent to the fan, for the range of inlet Mach number and relative humidity shown in Table 4-4. The critical range of particle concentration is 10^4 to 10^5/cc, with 10^4/cc producing around 20% of the equilibrium temperature rise while 10^5/cc achieves 100%. A particle concentration of 5 x 10^4/cc is required for 80% of the full equilibrium temperature rise to be attained.

Young (Reference 4.22) conducted a theoretical analysis on the effects of homogeneous and heterogeneous nucleation of water vapour in long inlet ducts during stationary operation on the ground. It was indicated that because phase change proceeds at a certain rate, the effects of condensation are determined by absolute time scales, and therefore depend on both local Mach number and its rate of change. Figure 4-41 shows, for a straight inlet duct with diameter 2.4 m and length 8.5 m, that the rate of expansion near the cowling wall is much higher than along the centre-line of the duct. Young concluded the following:

1. Homogeneous condensation of water vapour is unlikely to occur in the core flow of the inlet (at Mach numbers of 0.8) except for extreme conditions of very high inlet temperature and relative humidity. However, homogeneous condensation could occur in a narrow annulus adjacent to the inlet cowling where the high curvature of the streamlines results in an over-expansion to Mach numbers of about 1.0-1.1. The condensation in this region while independent of the inlet length is influenced by the geometry and may therefore occur in short inlets designed for wing-mounted engines as well as in long ducts designed for tailmounting. These results have been confirmed by visual observation during stationary engine tests.
2. Heterogeneous condensation, unlike that of homogeneous condensation is not well understood and at present no satisfactory theory exists. Atmospheric particles are not spherical, are of varied composition, and may or may not be water soluble. Using a simple model, it was shown that heterogeneous condensation in tail-mounted engines with very long inlet ducts can be substantial for particle concentrations found near industrialised areas.
3. At subsonic Mach numbers, condensation accelerates the flow in the inlet. Calculations in a parallel duct at Mach numbers of 0.8 have shown that reversion to equilibrium may be sufficient to thermally choke the flow (assuming constant mass flow rate). Measured increases in fan rotational speed during engine testing when condensation occurred is consistent with an increase in flow velocity approaching the engine.

4.6.1.3 *CF6 Inlet*

The effects of condensation within the inlet duct of a CF6 engine have been investigated using the "Zerkle" computer code (Section 4.6.1.1).

A drawing of the inlet duct is shown in Figure 4-42. Streamtube mass flow/area characteristics were taken from an axisymmetric calculation of the inviscid flow through the inlet using a streamtube curvature computer program. The streamlines range from $\psi = 0$ at the axial centre line to $\psi = 8$ at the bellmouth outer boundary. Streamline $\psi = 4$ lies on a stream surface encompassing 50% of the total mass flow.

The effect of ambient relative humidity on ideal and actual condensation temperature rise in a CF6-80A engine-mounted bellmouth inlet with two-dimensional flow effects is shown in Figures 4-43 and 4-44 respectively. The actual TRISE curves have fewer fluctuations than the ideal TRISE curves because droplet growth effects lag behind equilibrium.

4.6.2 Particle Concentration Measurement

Measurements of particle concentration have been made using a Differential Mobility Particle Size Analyser (DMPSA) which measures airborne particle distributions in the 0.02-0.9 μm diameter range with high resolution. The DMPSA consists primarily of a Differential Mobility Analyser (DMA) which removes a narrow range of particle sizes from an aerosol stream and a Condensation Nucleus Counter (CNC) which measures the concentration of particles in the narrow size range. All the particles larger than 0.9 μm are removed by an impactor at the aerosol inlet to the DMA. Particles which do not pass through the slot, no longer play a role in the measurement. The electrical mobility of particles is proportional to the diameter or size. The DMPSA is described in more detail in Section 7.3.1.1.

A survey of the number and distribution of sub-micron particles present in the ambient air was conducted during engine testing at a facility in Derby, England, in the month of April. Figure 4-45 shows the ambient particle levels during a nine hour period. The periods of higher particle concentration can be linked to engine or rig operation on site. The mean value of particle concentration is 7 x 10^3/cc with a mean diameter varying from 0.0422 μm at 16.15 hours to 0.0885 μm at 9.15 hours, exhibiting an overall mean of 0.067 μm.

The diameter of particles which can form the nucleus of a water droplet range from around 0.005 μm to around 0.3 μm (Figure 4-35). However, the DMPSA only counts particles with diameters between 0.02 and 0.9 μm so it could be excluding around 30% of the condensing particles - smaller than 0.02 μm.

Experience by one engine manufacturer has suggested that the particle count inside the test cell may be substantially higher than outside the cell due to recirculation of combustion products and other particles within the cell.

4.6.3 Concept of Particle Activity Factor

Section 4.6.1.2 predicts that particle concentrations of around 5 x 10^4/cc are required to achieve a significant temperature rise due to condensation, while Section 4.6.2 quotes typical measured particle concentrations of around 7 x 10^3/cc. These data suggest that condensation is unlikely to occur in engine inlets due to too low a particle count. However, the 'Zerkle' analytical method assumes that the particles are both electrically and chemically inert (i.e. insoluble). The particle concentration input to the analytical model requires the measured data to be factored around ten times, from 7 x 10^3 to 5 x 10^4/cc, to predict significant condensation, in the longer inlet ducts, under the appropriate environmental conditions.

Work conducted at an engine manufacturer in Atlanta, USA, where predictions from a 'Zerkle' condensation program were compared with actual observations of condensation in model inlets, also required a program particle concentration input of around ten times greater than was actually measured before it could predict the observed condensation adequately.

In the natural world, the majority of small particles are known to be active to some extent, which would be expected to enhance their power as condensing nuclei. The particle concentration enhancement factor can be regarded as a particle 'activity factor' which is currently not accounted for in the analytical model.

A model, calibrated to account for the particle activity could be used to predict the temperature rise in the inlet of an engine during testing. This method is particularly useful since it may not be necessary to develop performance corrections for every engine/inlet family, but only to determine the actual temperature at the fan face for any given test. If there is a significant effect on turbomachinery (in addition to knowing actual fan face temperature), a performance correction correlated against actual temperature rise, rather than ideal temperature rise, should reduce the magnitude of the correction and result in a smaller scatter band in corrected data.

4.6.4 Condensation Assessment Using an Analog Inlet Duct

In the absence of nucleation and droplet growth models (Section 4.7), an analog of the engine inlet can be used. The Condensibility Meter or 'Sonic Duct' is a device developed by one engine manufacturer to assess the amount of condensation occurring in engine inlets during sea level testing. It consists essentially of a miniature duct 0.0254 m diameter and 0.3048 m long, operated choked, and sampling air from the test bed vicinity which is intended to act as an analog of the engine inlet. The duct is preceded by an inlet flare of constant radius, and exhausts through a diffuser to a centrifugal compressor driven by an electric motor. If the quality of the air entering the engine is such that a large proportion of condensation will occur, then condensation should also occur in the 'Sonic Duct'. The condensation temperature rise occurring in the duct is deduced from two static pressure measurements in the duct walls together with inlet total pressure, and an empirical relationship derived from a one-dimensional numerical model which assumes the duct flow to be an approximation of a Rayleigh flow with condensation providing the heat input. The condensibility meter should provide a measure of the propensity of the air to condense in the inlet.

The condensibility meter could be used for production pass-off testing to provide a better parameter against which to correlate performance (Section 4.5.3), that is, to replace the ideal temperature rise due to condensation with the temperature rise measured with the condensibility meter. This may reduce the scatter in production pass-off test data still further but would not help in development testing where the historical data to produce empirically derived corrections does not exist.

This method has been investigated during pass-off testing for a series of RB211-524 engines. The results show that correlating SFC and Intermediate Pressure Compressor Speed with condensibility meter temperature rise reduces data scatter compared to the normal ideal temperature rise based correlation.

4.7 MODELLING

To calculate flow with condensation, numerical codes have to solve a set of equations describing:

- the mechanical balances of the flow (mass, energy, momentum),
- the state equation of the fluid (gaseous mixture: air + water vapour),
- the condensed water flow rate (droplet rate formation and droplet growth).

4.7.1 Droplet Rate Formation

4.7.1.1 *Homogeneous Condensation*

Modelling this process of phase transition is related, in the classical theory, to the following two criteria:

(a) **critical radius** of a stable water embryon in a subcooled medium (Kelvin-Helmholtz equation):

$$r_{crit} = \frac{2\sigma}{\rho_w R_w T \ln S} = f(\Delta T) \qquad 4\text{-}11$$

where σ = surface tension,
ρ_w = density of liquid water,
R_w = gas constant of the water vapour phase, and
S = supersaturation ratio.

Equation 4-12 shows that the equilibrium vapour pressure of a small drop of radius r is greater than $P_{sat(Ts)}$:

$$P_{S,r} = P_{sat} \exp\left(\frac{2\sigma}{r \rho_w R_w T}\right) \qquad 4\text{-}12$$

As discussed in Section 4.2.4, a condensing nucleus exposed to supersaturated vapour is expected to grow if its radius is greater than $r_{crit.}$

The table below gives typical values of r_{crit} relating to the subcooling ΔT or to the supersaturation S:

r (μm)	1	0.1	0.01	0.001
ΔT K	0.02	0.17	1.7	17
$S=P_v/P_{sat(Ts)}$	1.001	1.01	1.105	2.32

(b) **Nucleation Rate J**

$$J = K_c N_c \qquad 4\text{-}13(a)$$

with

$$N_c = N_0 \exp\left(-\frac{\Delta G_c}{KT}\right) \qquad 4\text{-}13(b)$$

$$\Delta G_c = \frac{4}{3}\pi r_{crit}^2 \sigma \qquad 4\text{-}13(c)$$

with K = Boltzmann constant,
N_0 = number of water molecules per kg,
N_c = number of clusters of critical radius r_{crit} deduced from the statistical Maxwell's law,
ΔG_c = a potential barrier that clusters have to overcome to become stable,
K_c = a parameter whose complexity depends on the physical model adopted to describe the formation of a droplet of water from a "cluster".

The classical theory of homogeneous nucleation is given by the Volmer-Frenkel equation:

$$J = \sqrt{\frac{2\sigma}{\pi M_w^3}} \frac{\rho_v^2}{\rho_w} \exp\left(-\frac{\Delta G_c}{KT}\right) \qquad 4\text{-}14$$

where M_w = mass of one water molecule, (2.99×10^{-26} kg),
ρ_v = density of water vapour.

Typical values of J at maximum subcooling ($\Delta T_{max} \approx$ 25/35 K) are of the order of 10^{20} to 10^{25} [m^{-3} s^{-1}].

Because the rate of droplet formation is highly exponential, the fog can be treated as a monodispersed medium composed of droplets formed at the end of the nucleating process ($\Delta T = \Delta T_{max}$).

A number of corrections and amendments to the classical theory have been proposed in the past. Experiments indicate (Reference 4.22) that, in the present context where the water vapour content is low, Equation 4-14 is probably a fairly accurate representation of reality.

4.7.1.2 *Heterogeneous Condensation*

The simplest model assumes that each foreign particle acts as a condensation nucleus as soon as its radius r becomes greater than the critical radius of the subcooled medium given by Equation 4-11. As shown in Figures 4-35 and 4-46, the smaller the size of the particles, the higher their concentration. Thus the number of active condensation nuclei will grow as the subcooling increases.

The model should be corrected by taking into account the chemical nature of each foreign particle. Two categories of impurities can be considered (Reference 4.23):

(a) Water soluble nuclei - These nuclei decrease the supersaturation necessary for germ formation.

(b) Insoluble particles (wettable or partially wettable) - Account has to be taken of the influence of the substrate of the foreign catalyst on which the embryon develops. For certain species, condensation can occur before the saturation line.

4.7.2 Droplet Growth

Nuclei that emerge from the nucleation process (homogeneous or heterogeneous) will grow further by condensation of vapour molecules on their surface. The rate of condensation on a drop is governed by two factors:

(a) the rate at which the latent heat can be carried away from the surface into the surrounding humid air (heat absorbed by the droplet itself being negligible), and

(b) the mass balance (the diffusion of water molecules through air).

The laws describing these phenomena depend on the pressure levels (vapour and mixture) and the size of the droplets. For very small submicronic droplets in a low pressure environment, the continuum model is no longer appropriate because the molecular structure of the gas becomes significant. Purely molecular heat and mass transfer must be considered. For example, the molecular heat transfer coefficient α can be expressed using Knudsen number Kn:

$$Kn = \frac{\text{mean free path of gas molecules}}{\text{diameter of droplet}} = \frac{1.5\,\mu\sqrt{RT_S}}{2r\,P_S} \qquad 4\text{-}15$$

where μ = absolute viscosity, and
R = gas constant of the gaseous phase (air + vapour).

4.8 SENSITIVITY FACTORS

In Section 4.5.3, the condensation corrections that were used for the CF6-50 engines were derived empirically at constant corrected fan speed and expressed as a function of corrected inlet flow. The corrections that were used for the RB211-535 engine were applied at constant thrust and expressed as a function of constant corrected thrust. The latter approach represents more closely the physics of the inlet condensation process.

The corrections indicate that accounting for condensation reduces the levels of SFC, exhaust gas temperature (EGT) and NL. These parameters are more sensitive to condensation at higher thrusts due to the increased Mach number in the airmeter. Applying the corrections at high thrust and 5 K ideal inlet temperature rise, changes engine parameters by -1.1% SFC, -0.6%EGT and -0.6% NL.

An analytical assessment of the ideal or equilibrium temperature rise caused by heterogeneous condensation in an MD11 inlet at 90% relative humidity and 293 K inlet temperature indicated a rise of 6 K at 0.5 Mach number - within the inlet - and 17 K at 0.8 Mach number, which indicates the powerful effect of inlet geometry on condensation temperature rise.

At particle concentrations less than 10^3/cc, the ideal temperature rise is negligible.

4.9 CONCLUSIONS AND RECOMMENDATIONS

The inability to account for the effects of inlet condensation can incur cost penalties during development, compliance and production pass-off testing. The practice of restricting engine development testing during periods of high relative humidity to avoid inlet condensation will increase engine certification timescales. During compliance testing, an increase in SFC caused by inlet condensation may result in guarantee payments to the customer, while, during production pass-off testing, an engine failing to meet limits on SFC and other performance parameters will be rejected for rework.

Because of the difficulty of reliably quantifying by observation or measurement the extent to which the condensation process has occurred at the engine face, aero-engine manufacturers have attempted to correct engine test data for the effects of condensation by using empirically derived corrections based on correlations of measured engine performance changes against the ideal temperature rise due to condensation. However, no account is taken of the particle concentration, which, if low enough, will completely inhibit condensation. In addition, it is necessary to develop performance corrections for every engine/inlet combination, since condensation is also affected by inlet geometry.

In circumstances where compliance engines are wrongly corrected to dry conditions by condensation corrections which are not merited (i.e. the compliance engines are not affected by condensation and are already producing their best performance), the effect would be to penalise all other engines by demanding from them a performance improvement equal to the falsely applied condensation correction.

The shift in **corrected** engine performance when condensation has occurred during engine testing is largely the result of not accounting for the temperature rise in the engine inlet. The ability to predict the temperature rise in the inlet would therefore greatly improve the current situation. The effects of condensation on engine performance could then be predicted for an engine in a test cell environment fitted with a bell mouth inlet, as well as for the engine fully installed in an airframe with a different inlet configuration. Furthermore, while condensation may be avoided on test, it cannot be avoided in an operational environment.

A model to predict the onset of heterogeneous condensation in engine inlets was developed by Zerkle, Colley and Doel (Reference 4.9). Experimental validation of the analytical model suggests it may under-predict the inlet temperature rise. This may be caused by the assumptions of one-dimensional flow, spherical particles and particles which are chemically inert and wetted (i.e. insoluble).

The use of humidity limits to restrict engine testing and avoid condensation, as used by some manufacturers, takes no account of inlet geometry or particle concentration. An alternative to humidity limits is a measurement system capable of identifying when condensation has occurred. One manufacturer has used a laser system in the inlet to make run/no-run decisions and to allow decisions to be made regarding testing beyond the normal test limits. There is a real need to know if condensation is occurring and, although it is not commonly adopted, it appears reasonable to suggest that video images be used. These could be cheap and, where installed (usually for other purposes) they have indicated the presence of condensation together with a measure of the extent. The images available also indicate the unsteady and local nature of inlet condensation.

Engines which are trimmed in high humidity conditions may have higher turbine entry temperatures, thereby reducing engine life, while changes in ambient humidity levels may influence operability by requiring more aircraft downtime to maintain engine trim.

The theoretical analysis conducted by Young (Reference 4.22) has indicated that homogeneous condensation could occur in a narrow annulus adjacent to the inlet cowling where the high curvature of the streamlines results in an over-expansion to Mach numbers of about 1.0-1.1. Both homogeneous and heterogeneous condensation may therefore need to be accounted for in the inlet-temperature-rise model. Two-dimensional effects can be taken into account using an axisymmetric calculation of the inviscid flow using a streamtube curvature computer program. Two-dimensional calculation schemes for condensing flow in moist air have been reported by Schnerr and Dohrmann (Reference 4.24), but they are a major undertaking and not commonplace.

The treatment of condensation/re-evaporation in component testing is largely inadequate as little account is taken, with avoidance being the main consideration. Methods need to be developed for modelling the influence of condensation (and re-evaporation) on engine components, and, in particular, the stage matching and stage performance within multistage axial flow compressors.

Table 4-5 shows the influence of condensation

and the confidence of the assessment method for both performance and operability on individual components and the engine. The areas where the influence is high, i.e. inlet, compressor and engine control, are those where the confidence of assessment is low, demonstrating that condensation is still not well understood.

4.10 REFERENCES

4.1 Spencer, James H., and Archer, David C., *The Effect of Condensation within an Aircraft Inlet Duct on Installed Turbofan Engine Performance*, Proceedings of the Tenth National Conference on Environmental Effects on Aircraft and Propulsion systems, Philadelphia, May 1971.

4.2 Blake, J.C., *Effects of Condensation in the JT9D Turbofan Engine Bellmouth Inlet*, AIAA Paper No. 75-1325, AIAA/SAE 11th Propulsion Conference, Anaheim, California, September 29 - October 1, 1975.

4.3 Wegener, P.P. and Mack, L.M., *Condensation in Supersonic and Hypersonic Wind Tunnels.*, Advances in Applied Mechanics, Vol 5, H L Dryden and Th.von Karman, editors, Academic Press, New York, 1958 pp 304-447.

4.4 Wegener, P.P., *Gas Dynamics of Expansion Flows With Condensation, and Homogeneous Nucleation of Water Vapour*, Gas Dynamics Series, Vol 1, Non-equilibrium Flows, part I, P.P. Wegener, editor, Marcel Dekker, New York, 1969 pp 163-243.

4.5 Colley, W.C. and Doel, D.L., *Analysis of Moisture Condensation in Engine Inlet Ducts*, General Electric TM77-666, Evendale, 1977.

4.6 Bodhaine, B.A. and Murphy, M.E., *Calibration of an Automatic Condensation Counter at the South Pole.*, Journal of Aerosol Science, Vol 11, 1980, pp 305-312.

4.7 Ross, R.D., *Air Pollution and Industry*, Van Nostrand Reinhold, New York 1972.

4.8 Willeke, K., and Whitby, K.T., *Atmospheric Aerosols: Size Distribution Interpretation.*, Journal of the Air Pollution Control Association, Vol 25, No 5, 1975, pp 529-534.

4.9 Zerkle, R.D., Colley, W.C., and Doel, D.L., *Analysis of Moisture Condensation in Engine Inlet Ducts.*, General Electric Company, Proceedings of the Symposium of Particulate Laden Flows in Turbomachinery, ASME, New York 1982.

4.10 Stever, H.G., *Condensation Phenomena in High Speed Flows.*, High Speed Aerodynamics and Jet Propulsion Series, Vol 3, Fundamentals of Gas Dynamics., H.W. Emmons, Editor, Princeton University Press, Princeton, 1958, pp 526-573.

4.11 McDonald, J.E., *Homogeneous Nucleation of Vapour Condensation, Part I: Thermodynamic Aspects, Part II: Kinetic Aspects*, Am. J. Physics, Part I, Vol.30, 1962, pp 870-877, Part II, Vol.31, 1963, pp 31-41.

4.12 Pearcey, H.H., *The Effect of the Condensation of Atmospheric Water Vapour on Total Head and Other Measurements in the NPL High Speed Tunnels*, Aeronautical Research Report, 1951

4.13 Murthy, S.N.B., Reese, B.A., Arcangeli, G.T., Tsuchiya, T., *Analysis of Water Ingestion Effects in Axial Flow Compressors*, Technical Report AFAPL-TR-78-35, September 1976-November 1977. Air Force Aeropropulsion Laboratory, Wright-Patterson Air Force Base, Ohio 45433.

4.14 Ludorf, R.K. and Elder, R.L., *Effects of Droplet Evaporation on Compressor Stability*, Paper B20, European Conference on Turbomachinery - Fluid Dynamic and Thermodynamic Aspects, VDI, Germany, March, 1995.

4.15 Wilcox, E. Clinton, and Trout, A.M., *Analysis of Thrust Augmentation of Turbojet Engines by Water Injection at Compressor Inlet Including Charts for Calculating Compression Processes with Water Injection*, National Advisory Committee for Aeronautics, 1951.

4.16 Moore, M.J., Jackson, R., Wood, N.B., Langford, R.W., Keeley, K.R. and Walters, P.T., *Method of Measuring Stage Efficiency in Operational Wet Steam Turbines*, I.Mech.E. Conference on Steam Turbines for the 1980's, I.Mech.E. Conference Publications 1979-12.

4.17 Bakhtar, F. and Mohammadi Tochai, M.T., *An Investigation of Two-dimensional Flows of Nucleating and Wet Steam by the Time-Marching Method*, Int. J. Heat and Fluid Flow, 1980, Vol. 2(1), pp5-18.

4.18 Kleitz, A., Laali, A.R. and Courant, J.J., *Droplet Size Measurement and Calculation in Wet Steam Turbines*, Technology of Turbine Plant Operating with Wet Steam, BNES, London, 1988.

4.19 Guha, A. and Young, J.B., *Time-Marching Prediction of Unsteady Condensation Phenomena Due to Supercritical Heat Addition*, I.Mech.E. C423/057, 1991.

4.20 Grabe, W., and Bird, J., *Humidity Effects on Gas Turbine Performance*, National Research Council Canada, Technical Report TR-ENG-003, NRC No 30241, December 1988.

4.21 Fuchs, N.A., *The Mechanics of Aerosols*, Pergamon Press, New York, 1964 pp 5-14.

4.22 Young, J.B., *Condensation in Jet Engine Intake Ducts during Stationary Operation*, ASME Paper 93-GT-5, International Gas Turbine and Aeroengine Congress and Exposition, Cincinnati, USA, May 24-27, 1993.

4.23 Götz, G., Meszarosn, E., Vali, G., *Atmospheric Particles and Nuclei*, Akadémiai Kiadó, Budapest, 1991.

4.24 Schnerr, G., and Dohrmann, U., *Theoretical and Experimental Investigation of 2-D Diabatic Transonic and Supersonic Flowfields*, IUTAM Symp. Transonicum III, Gottingen, 1988, Springer-Verlag 1989, pp 132-140.

Table 4-1

FORMATION RATE OF ATMOSPHERIC AEROSOL PARTICLES

(Reference 4.23)
(Courtesy MIT Press)

(in Tg yr^{-1} units)

Reference	SMIC (1971) <20 μm	Prospero (1984)
Natural Aerosol Sources		
Soil and rock debris*	100 - 500	60 - 360
Forest fires & slash burning*	3 -150	-
Sea salt	(300)	1000 - 2000
Volcanic debris	25 - 150	4 - 90
Particles formed from gases		
Sulfate	130 - 200	40 - 400
Ammonium salts from NH_3	80 - 270	-
Nitrate from NO_x	60 - 430	60 - 620
Hydrocarbons from plants	75 - 200	75 - 1100
Subtotal	773 - 2200	1239 - 4570
Man-made Aerosol Sources		
Particles (direct emission)	10 - 90	6 - 100
Particles formed from gases		
Sulfate from SO_2	130 - 200	100 - 200
Nitrate from NO_x	30 - 35	23 - 35
Hydrocarbons	15 - 90	15 - 27
Subtotal	185 - 415	144 - 362
Total	958 - 2615	1383 - 4932

Note: Asterik denotes unknown amounts of indirect man-made contributions. The parenthesis in the case of sea salt (SMIC) means that only particles transported over long distances are taken into account.

Table 4-2

INLET CONDENSATION CORRECTION - RB 211-535

Influence of Applying Correction at 178 kN thrust and 5 K TRISE

Parameter	K Factor	% Change
NL (fan speed)	-0.00127	-0.6 %
W_F (fuel flow)	-0.00213	-1.1 %
EGT (exhaust gas temperature)	-0.00127	-0.6 %

Table 4-3

INLET CONDENSATION CORRECTION - RB 211-524

$\frac{\text{2 standard deviations}}{\text{mean value}}$ (%) at take-off thrust

	No correction	Humidity correction only	Humidity and condensation correction
SFC	1.22	1.16	0.952

Table 4-4

ANALYTICAL ASSESSMENT OF EQUILIBRIUM TEMPERATURE RISE IN MD11 INLET

Maximum Equilibrium Temperature Rise K

		Ambient Temperature K	Relative Humidity		
			50 %	90 %	100 %
Inlet Mach number (parallel section)	0.5	283.15	-	5	-
		293.15	-	6.4	-
	0.8	283.15	5.8	11.4	12.8
		293.15	-	16.7	-

Table 4-5

CAPABILITY OF RECOMMENDED PRACTICES TO ASSESS THE EFFECTS OF INGESTED CONDENSING FLOW

	ASSESSMENT METHOD	PERFORMANCE		OPERABILITY		COMMENTS
		Influence	Confidence	Influence	Confidence	
Components:						Assessment is restricted to ground testing of complete engines only. Not applicable to rig tests or to airframe/engine installations.
Inlet	A + T	H	L	L	H	
Fan/Splitter	A + T	H	L	H	L	
Compressor	A + T	H	L	H	L	
Combustor	T	M	H	L	H	
Turbine	A + T	M	H	L	H	
Nozzle: Core	A + T	L	H	L	H	
Nozzle: ByPass	A + T	L	H	L	H	
Engine:						
Controls (Sensors and Logic)	A + T	M	M	L	H	
Starting	T	N/A	N/A	L	M	
Power Transients	T	M	M	L	L	
Determining Core Water	N/A	N/A	N/A	N/A	N/A	

A - Analytical H - High M - Medium
T - Test L - Low N/A - Not Applicable

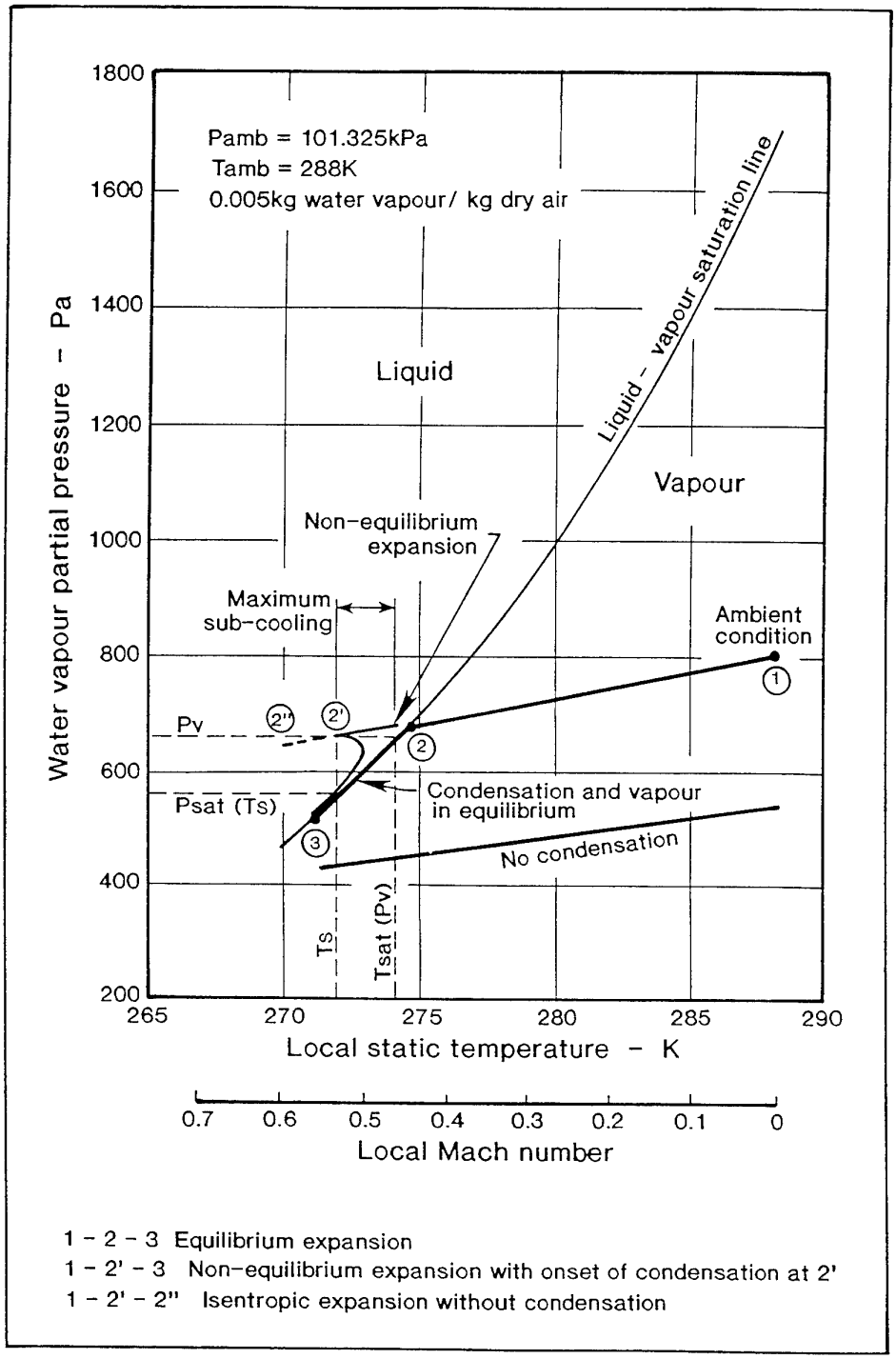

Figure 4-1

Phase Diagram for Water and the Condensation Process

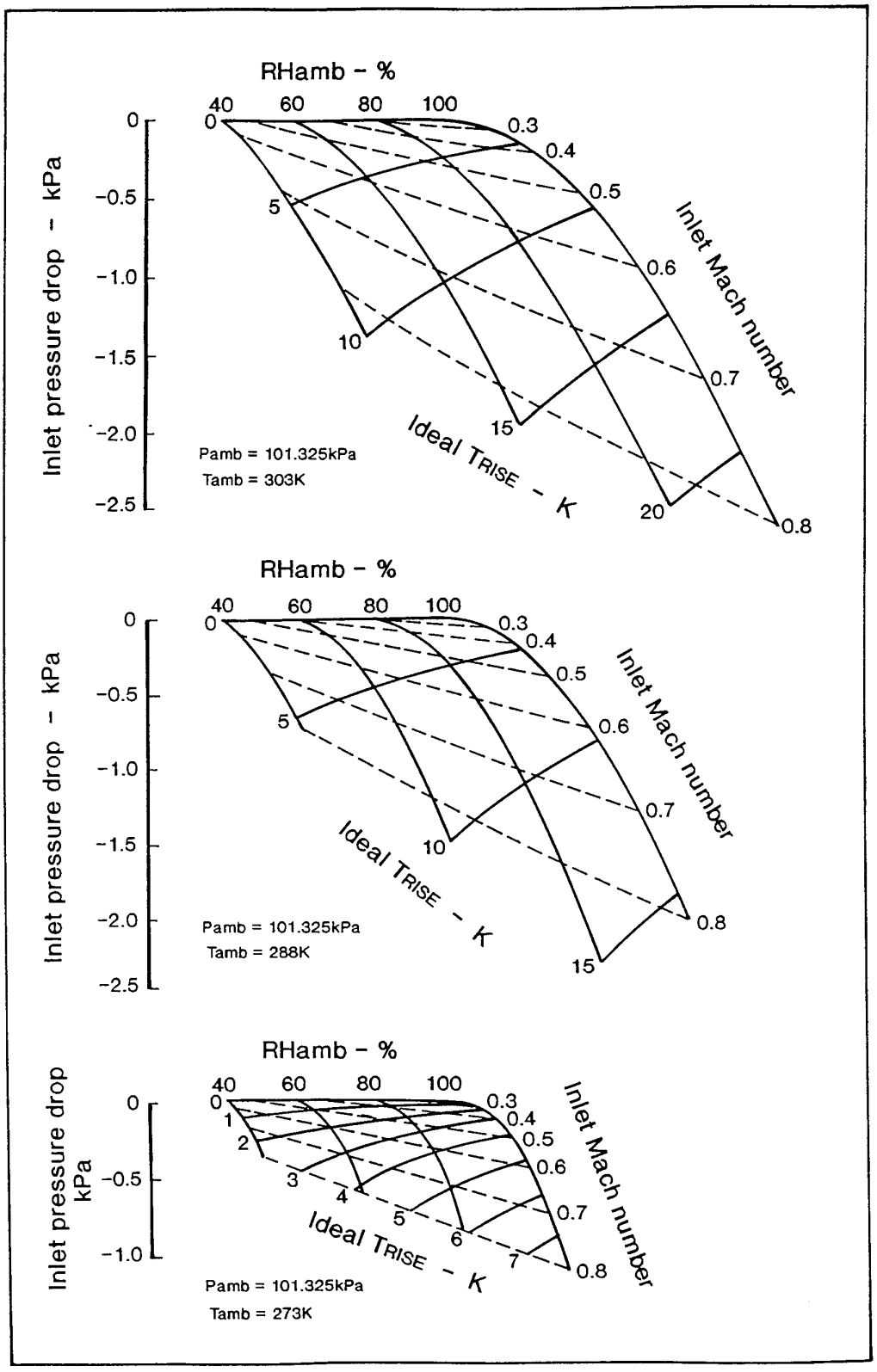

Figure 4-2

Ideal Temperature Rise and Pressure Drop due to Inlet Condensation

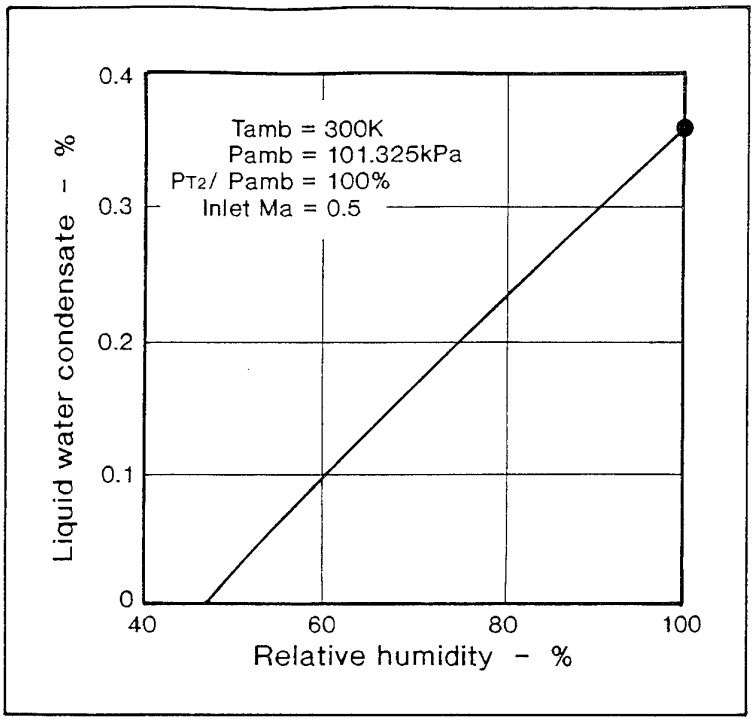

Figure 4-3

Effect of Relative Humidity on Water Condensate Levels
in an Inlet Duct

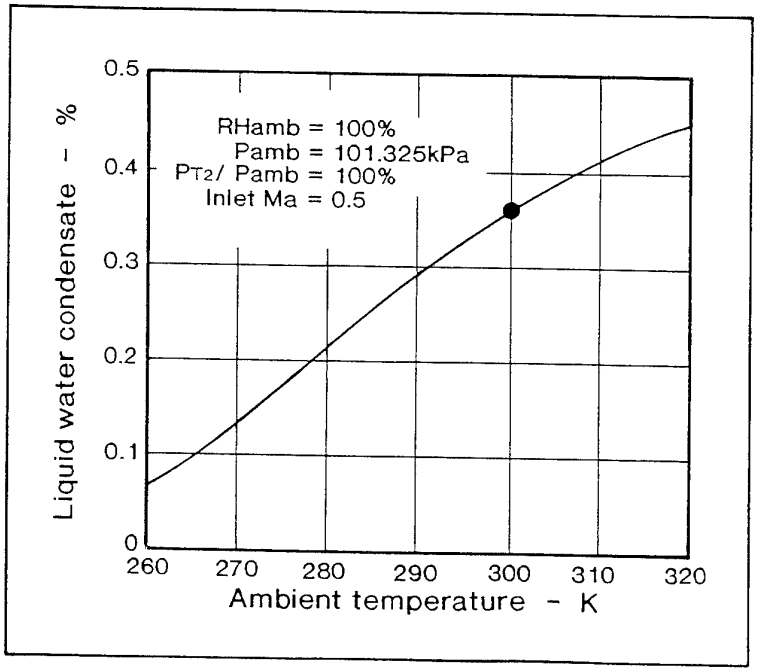

Figure 4-4

Effect of Ambient Temperature on Water Condensate Levels
in an Inlet Duct

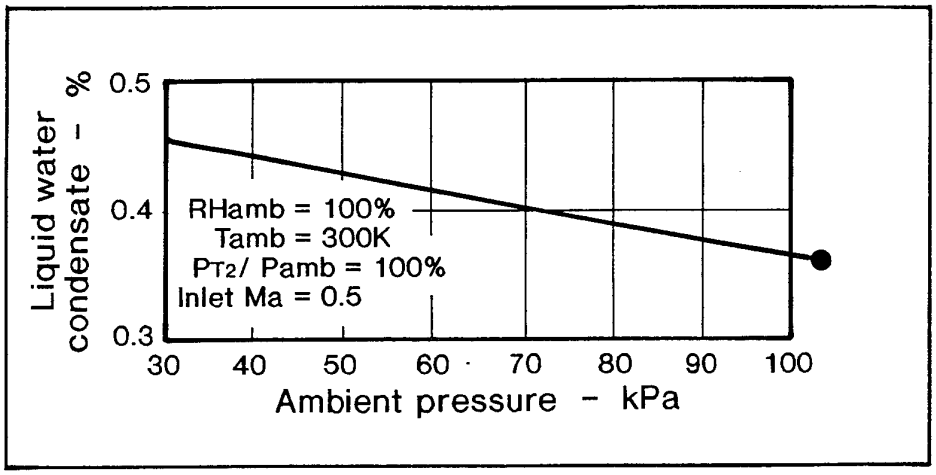

Figure 4-5

Effect of Ambient Pressure on Water Condensate Levels
in an Inlet Duct

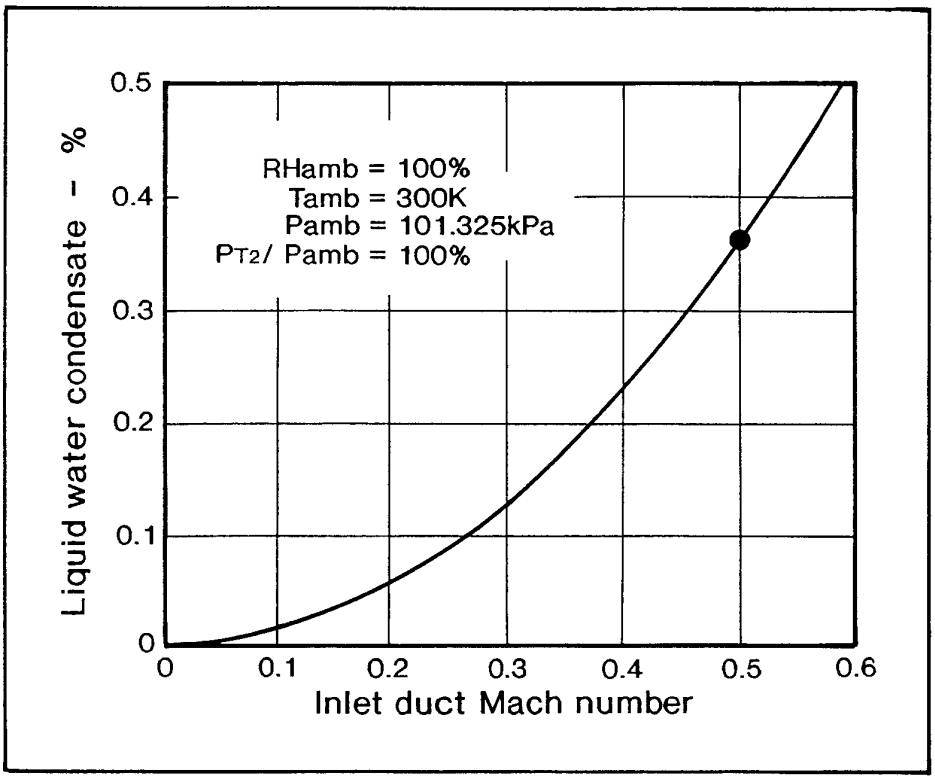

Figure 4-6

Effect of Inlet Duct Mach Number on Water Condensate Levels
in an Inlet Duct

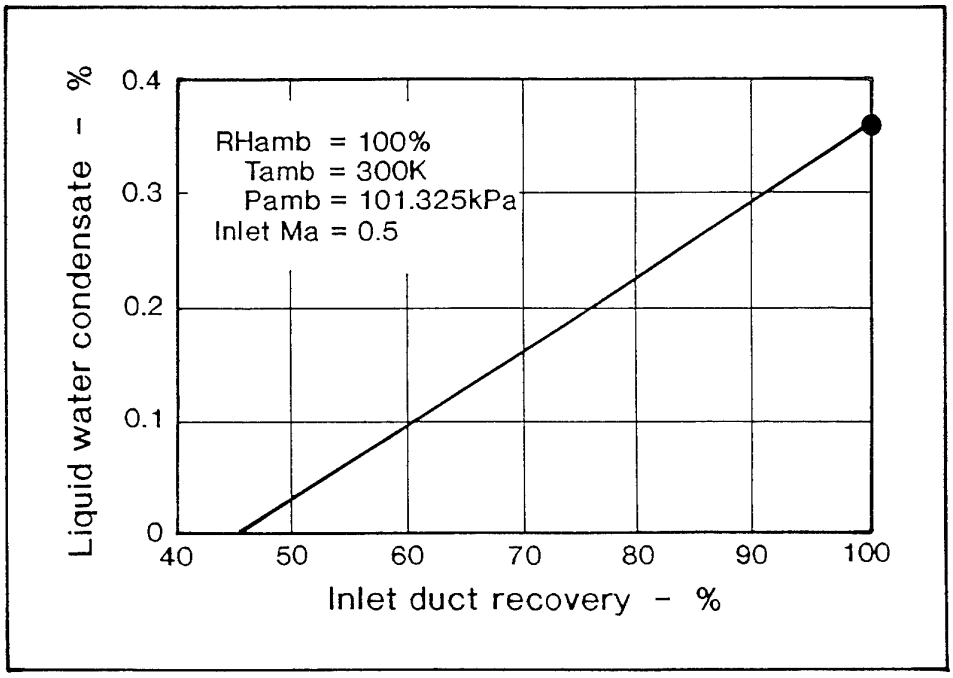

Figure 4-7

Effect of Inlet Duct Recovery on Water Condensate Levels
in an Inlet Duct

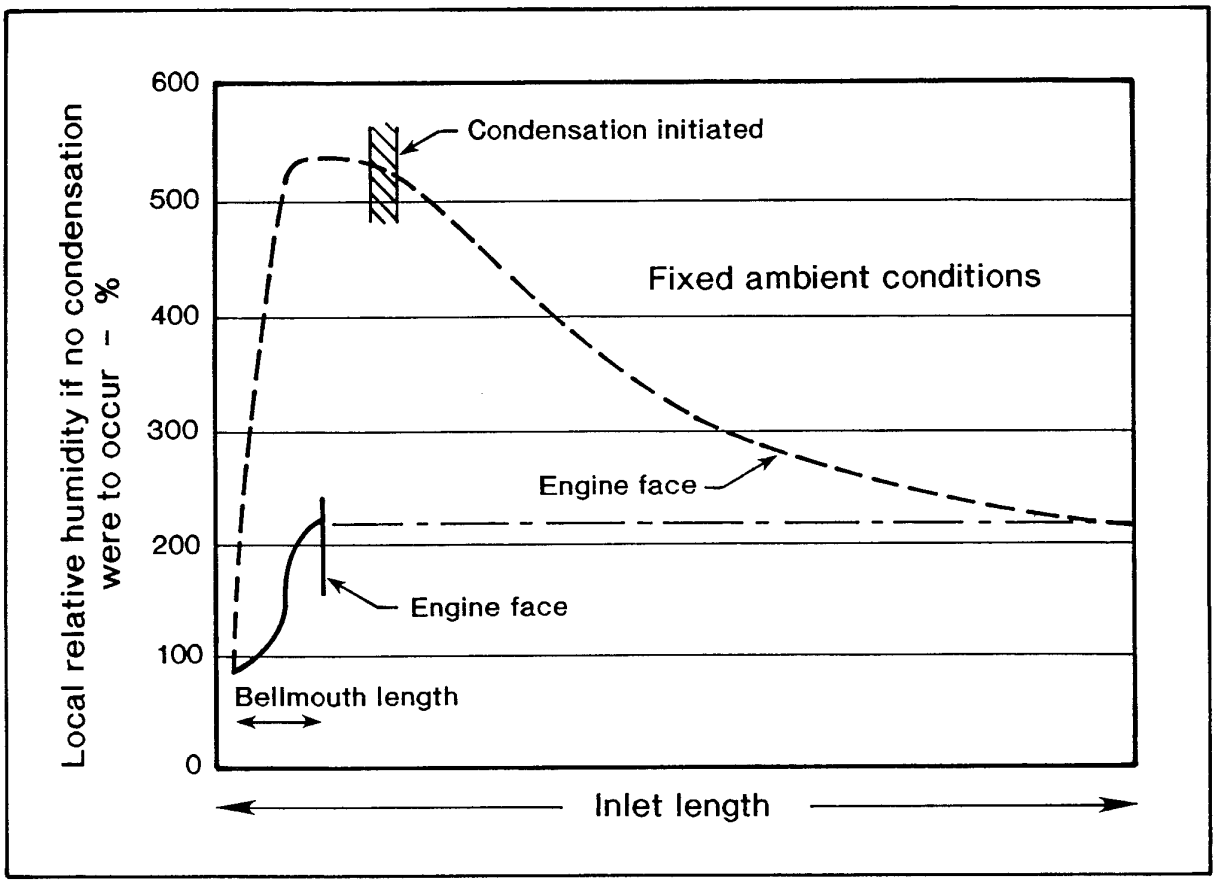

Figure 4-8

Condensation Potentials within an Inlet Duct and Bellmouth

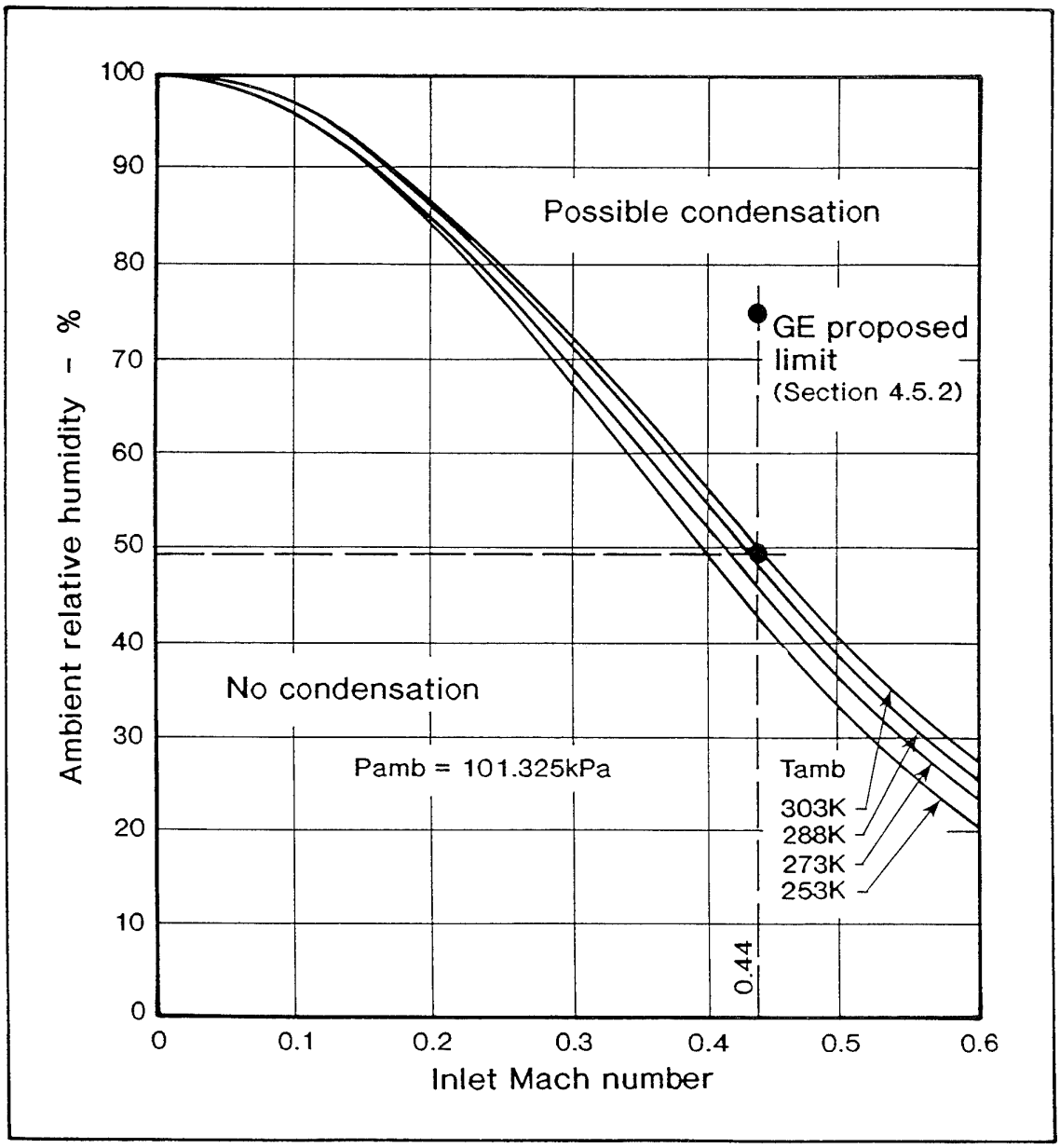

Figure 4-9

Theoretical Limits for Condensation

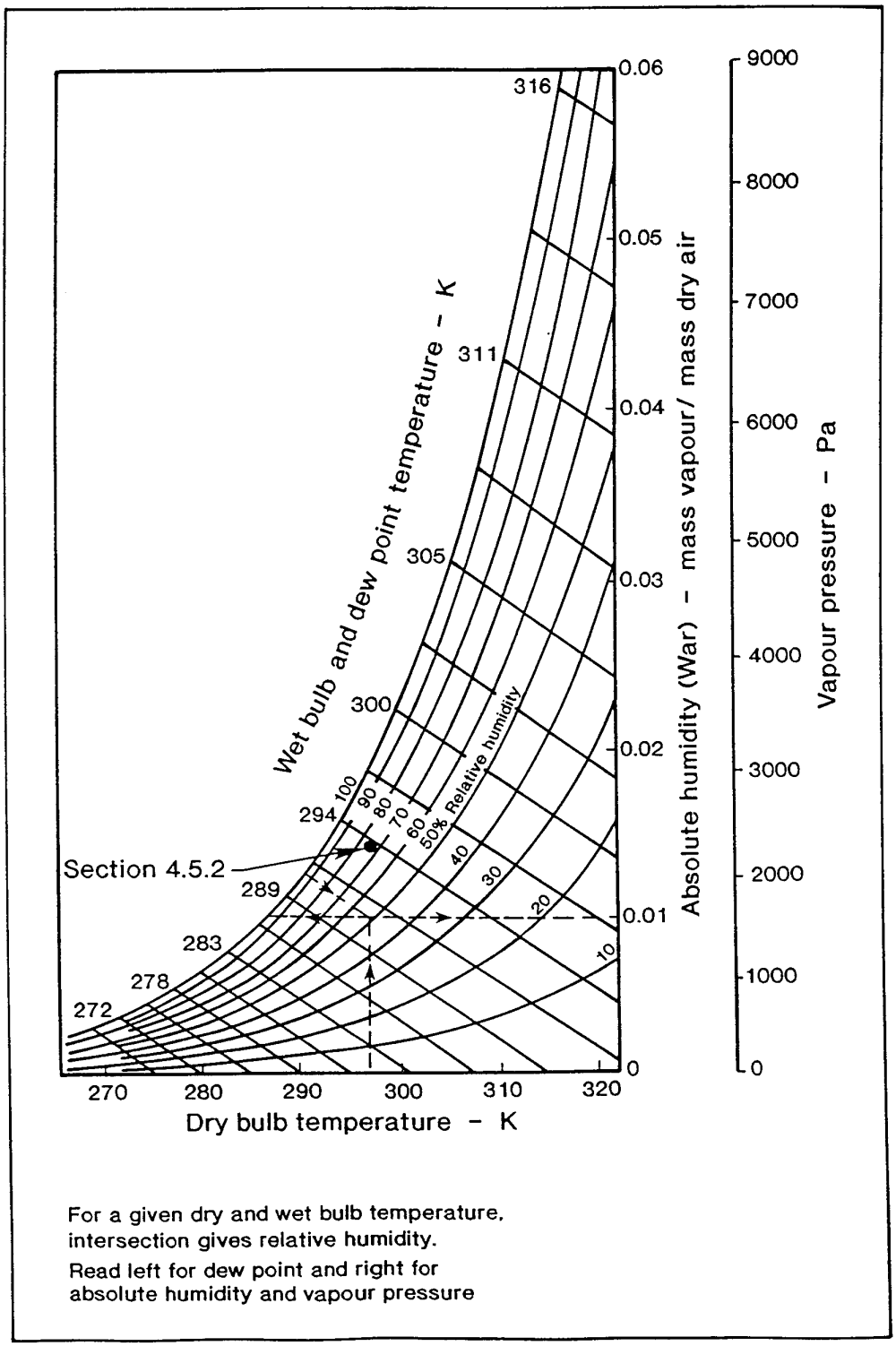

Figure 4-10

Psychrometric Chart

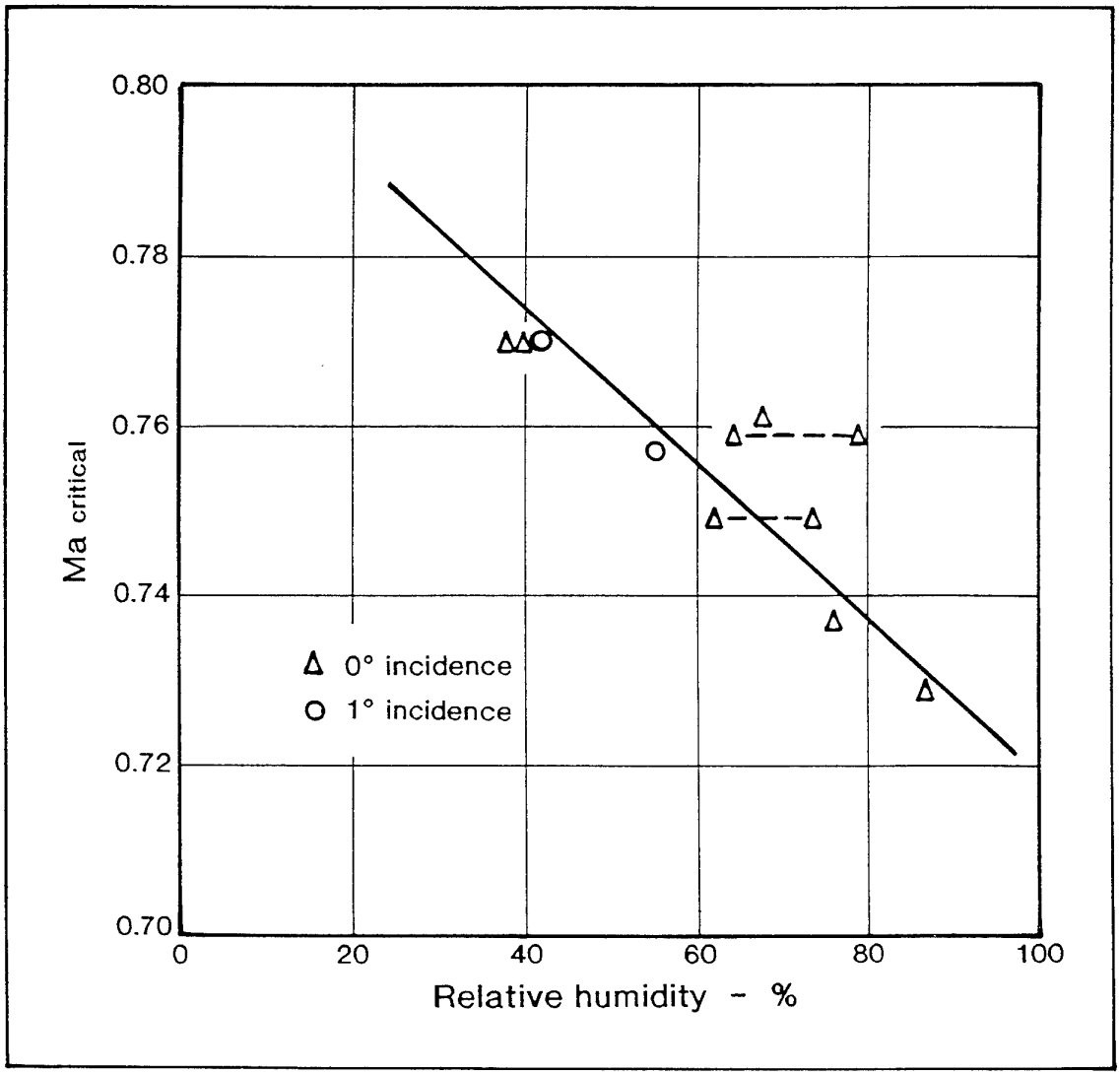

Figure 4-11

Variation of Ma_{crit} (Mach Number at which $C_D > 0.01$) with Humidity
for an Isolated Aerofoil
(Reference 4.12)

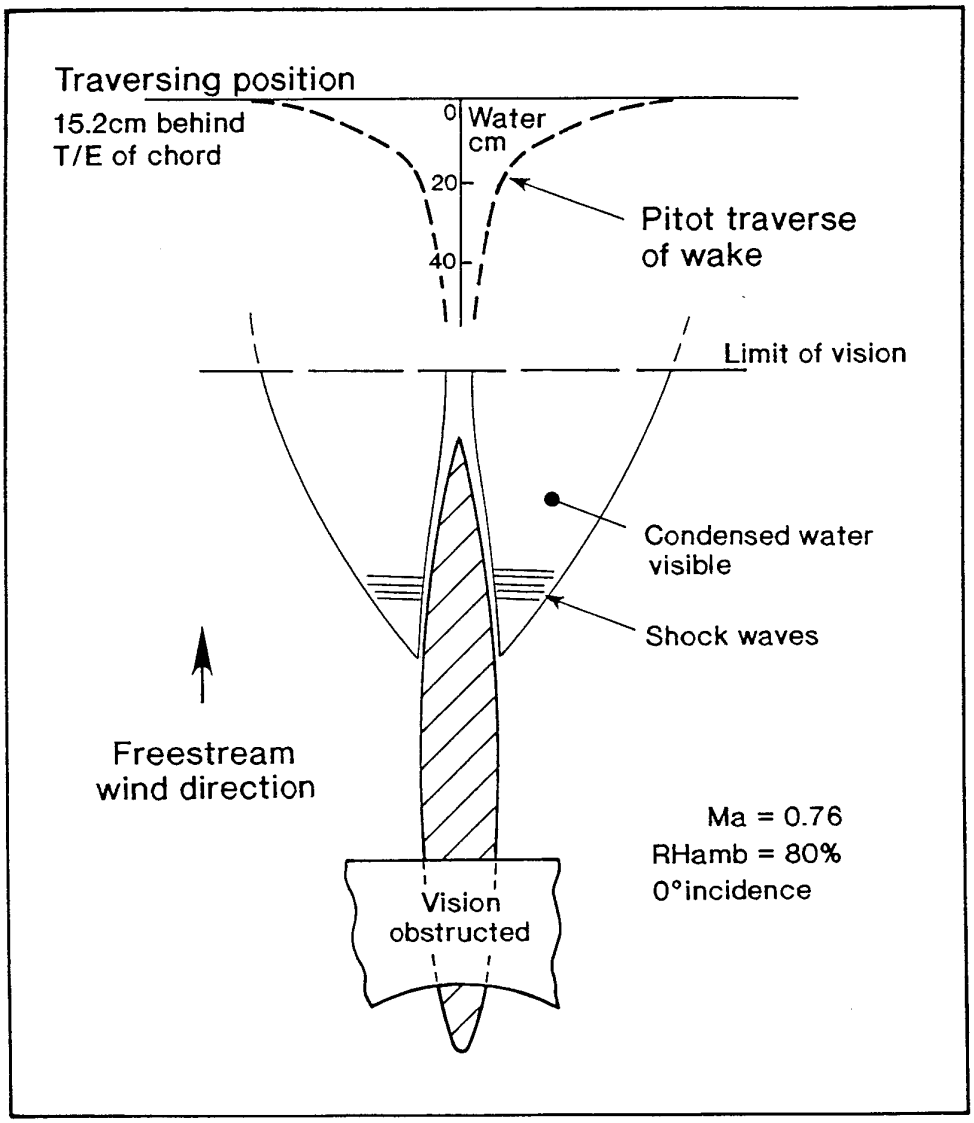

Figure 4-12

Visible Condensation for a 30.5 cm (1 ft) Chord Model Aerofoil
(Reference 4.12)

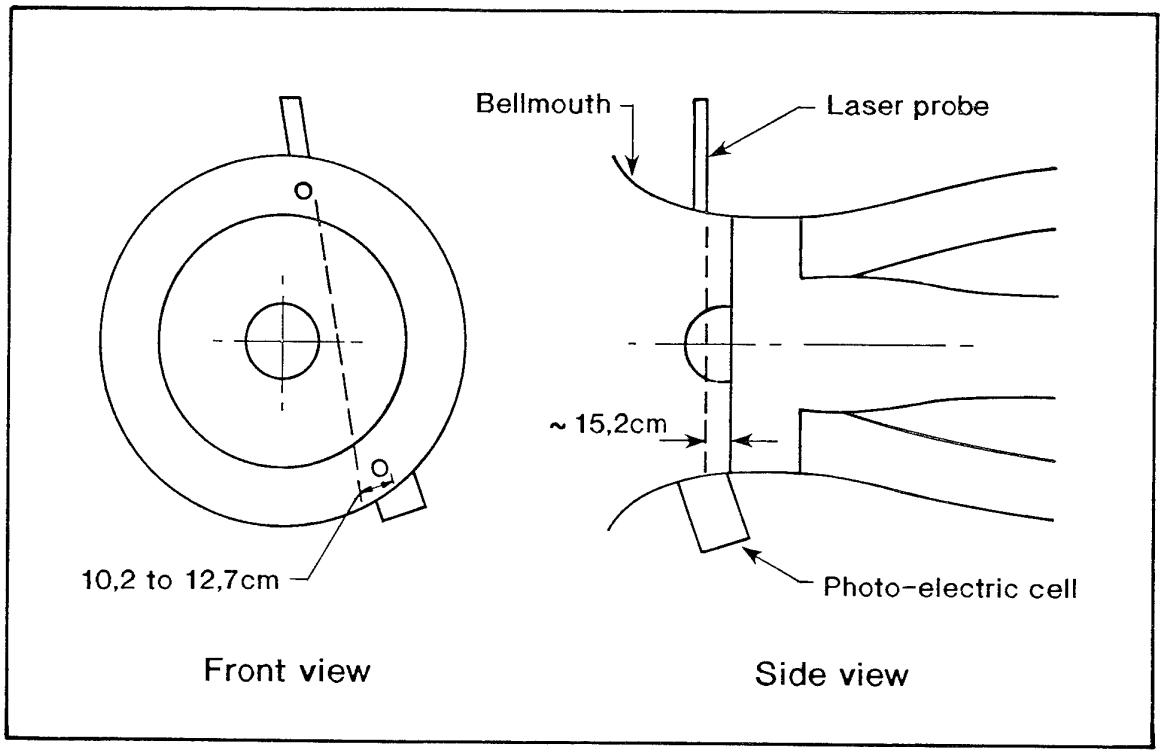

Figure 4-13

Laser Condensation Detection System Installation

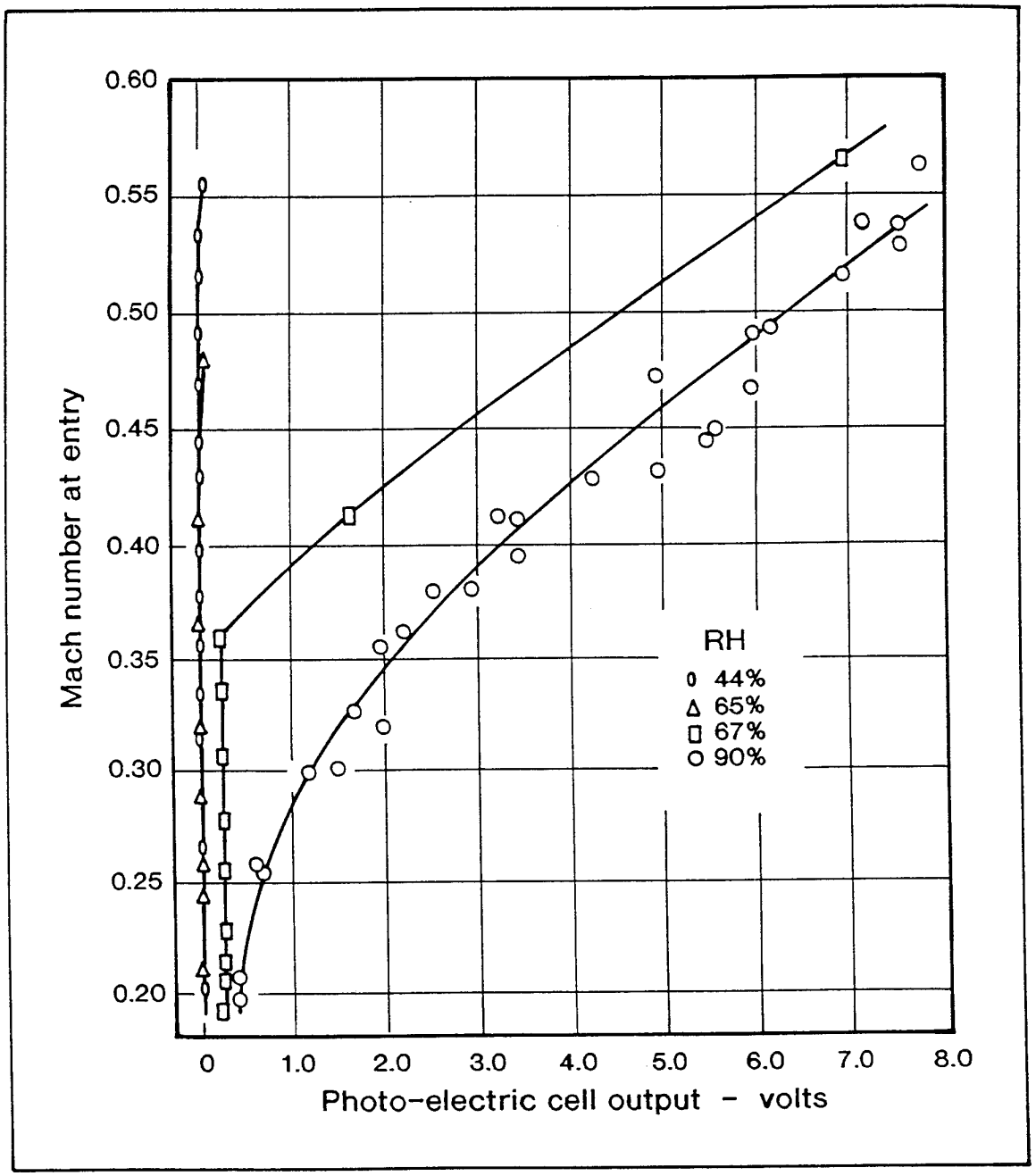

Figure 4-14

Laser Photomultiplier Results

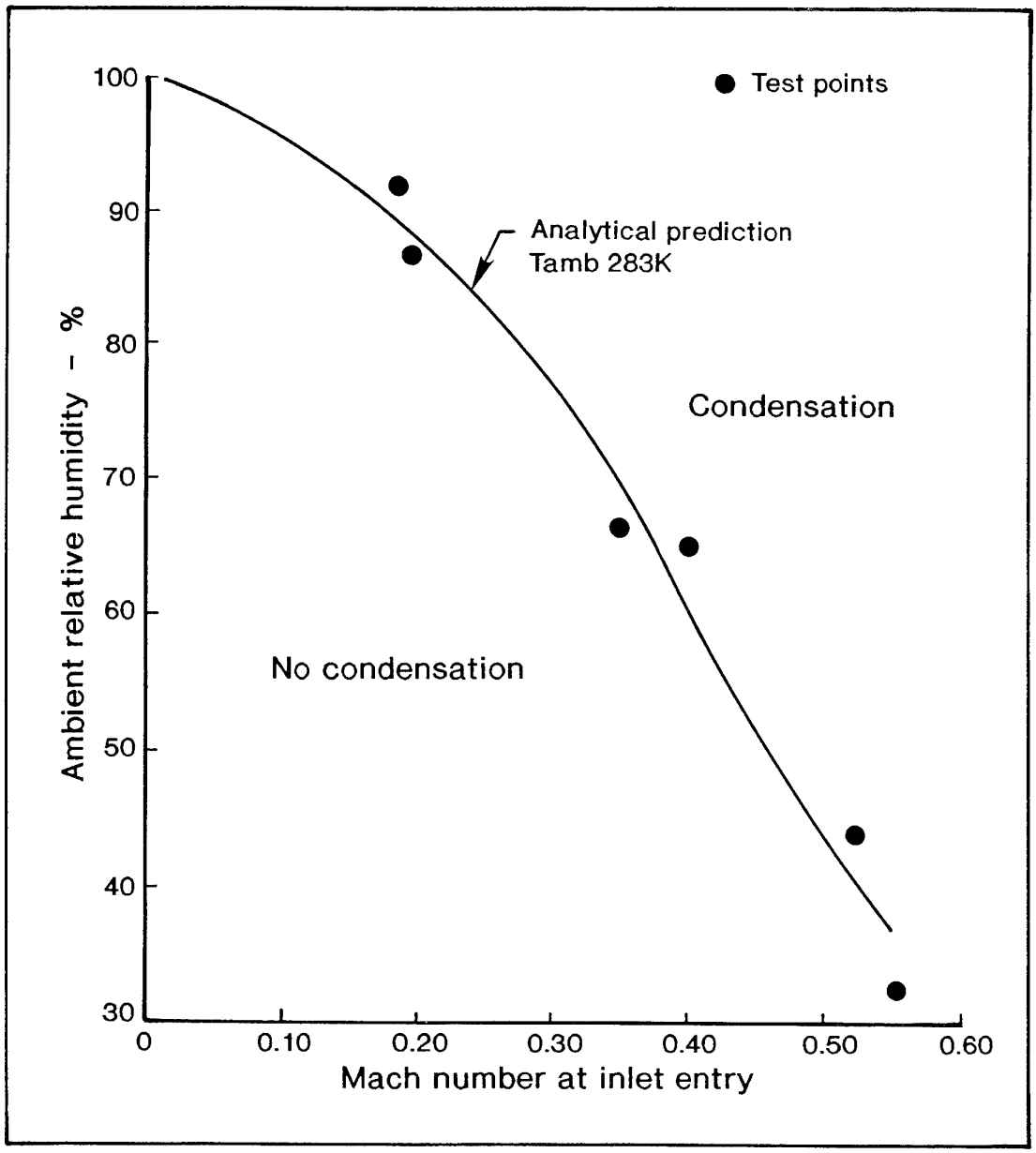

Figure 4-15

Actual Limits for Condensation

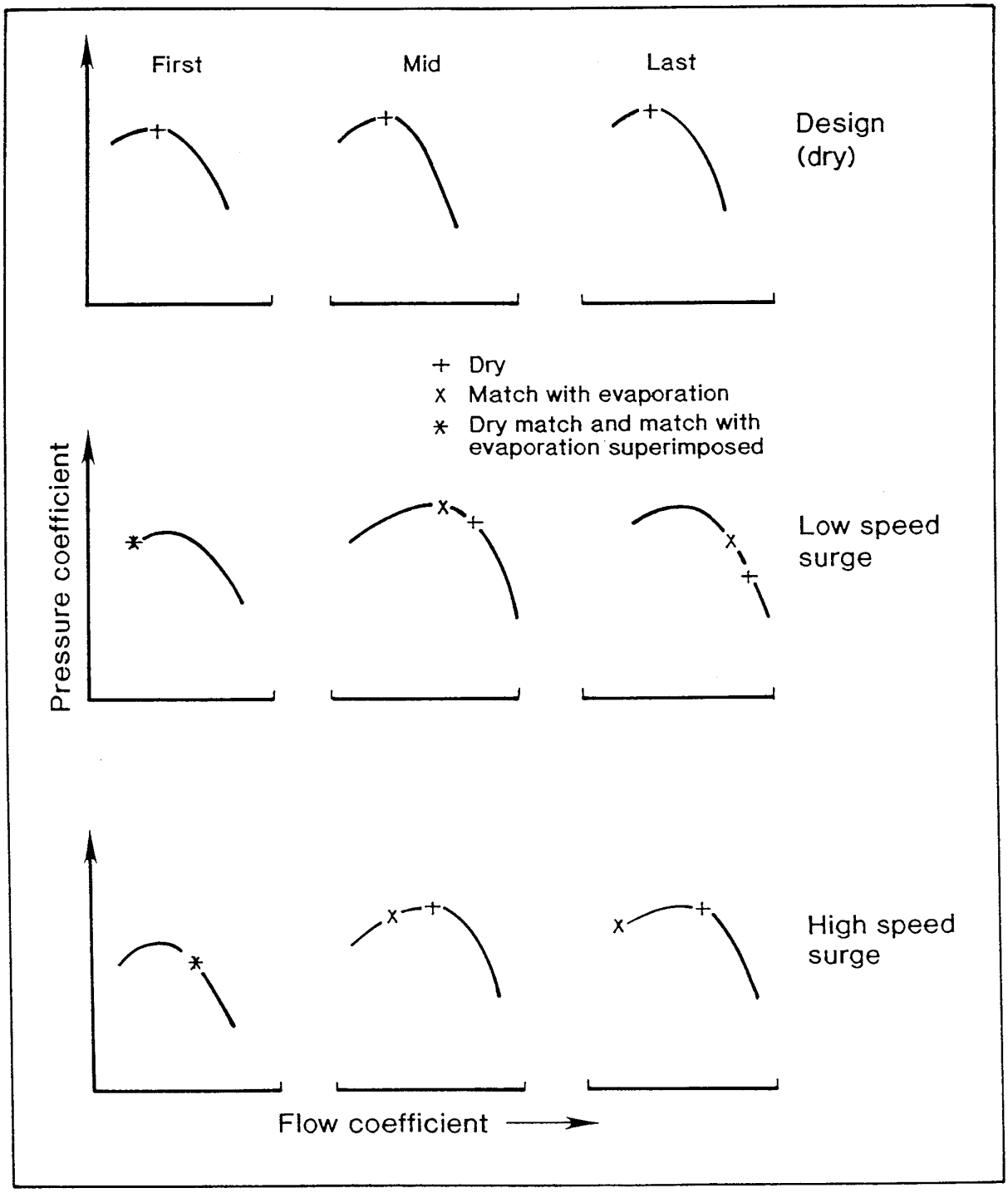

Figure 4-16

Estimated Effect of Evaporation on Stage Matching

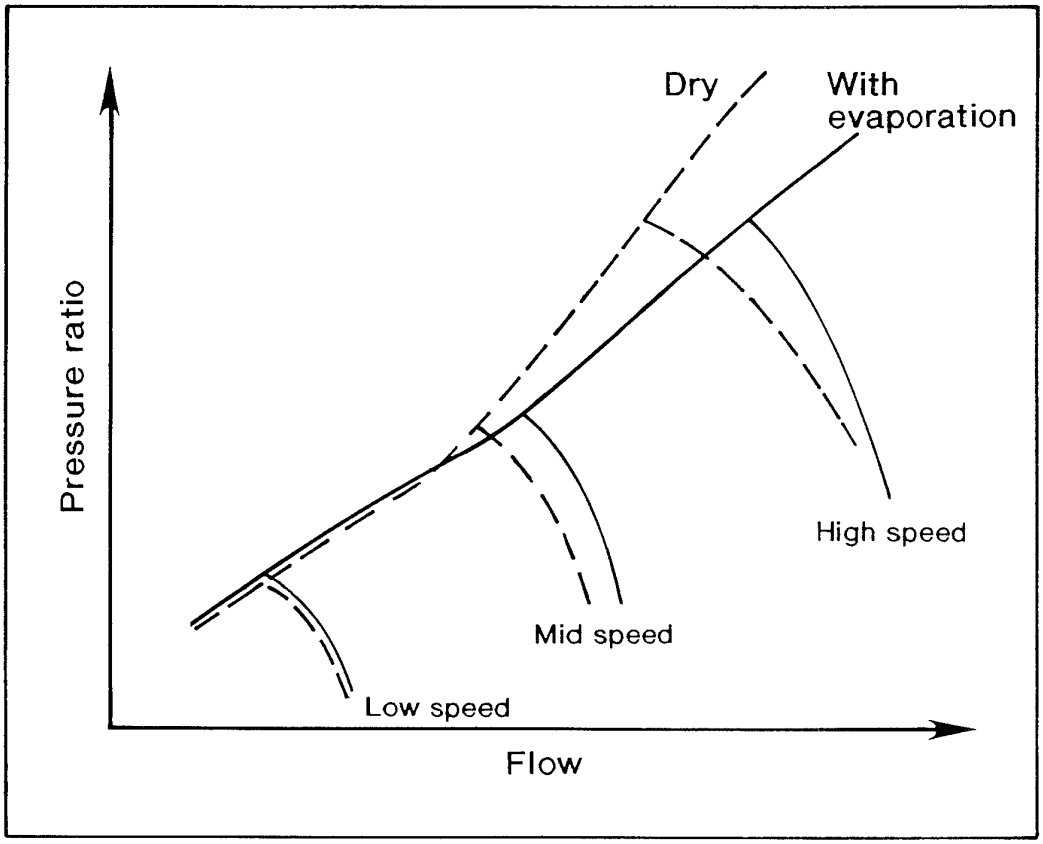

Figure 4-17

Estimated Influence of Evaporation within an Axial Flow Compressor
(Effects amplified for clarity)

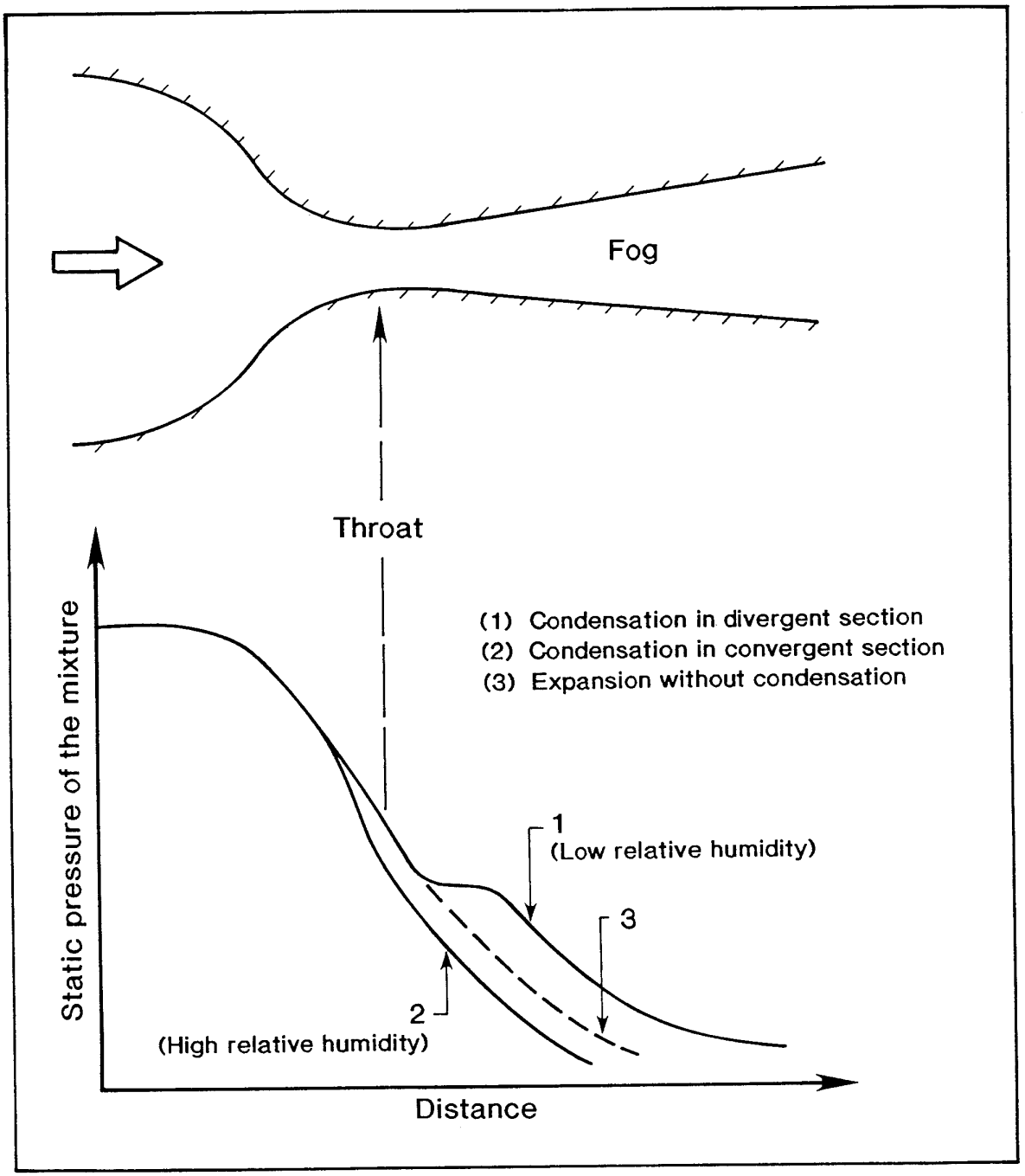

Figure 4-18

Effect of Condensation in a Converging-Diverging Nozzle

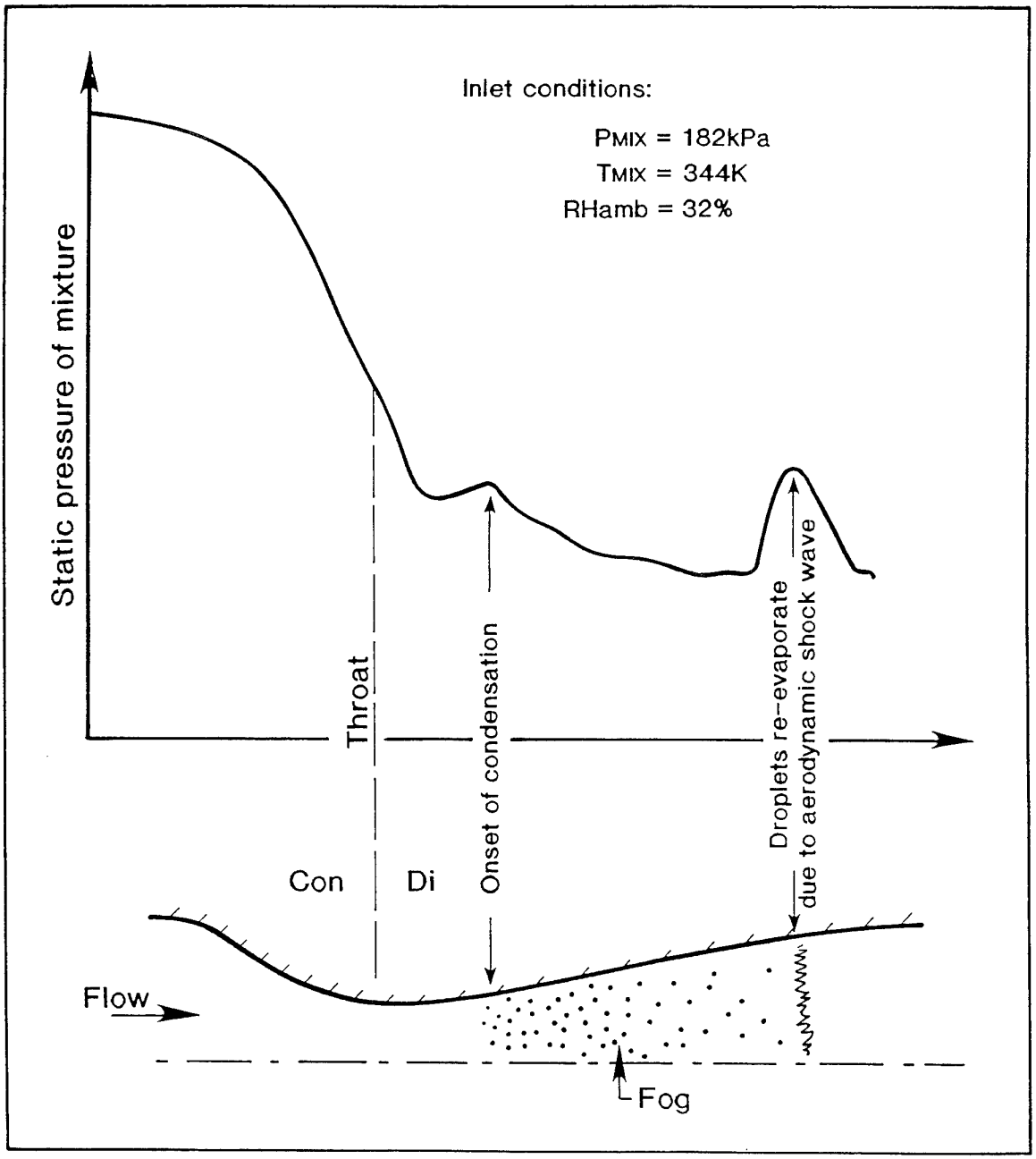

Figure 4-19

Typical Converging-Diverging Nozzle Experimental Result

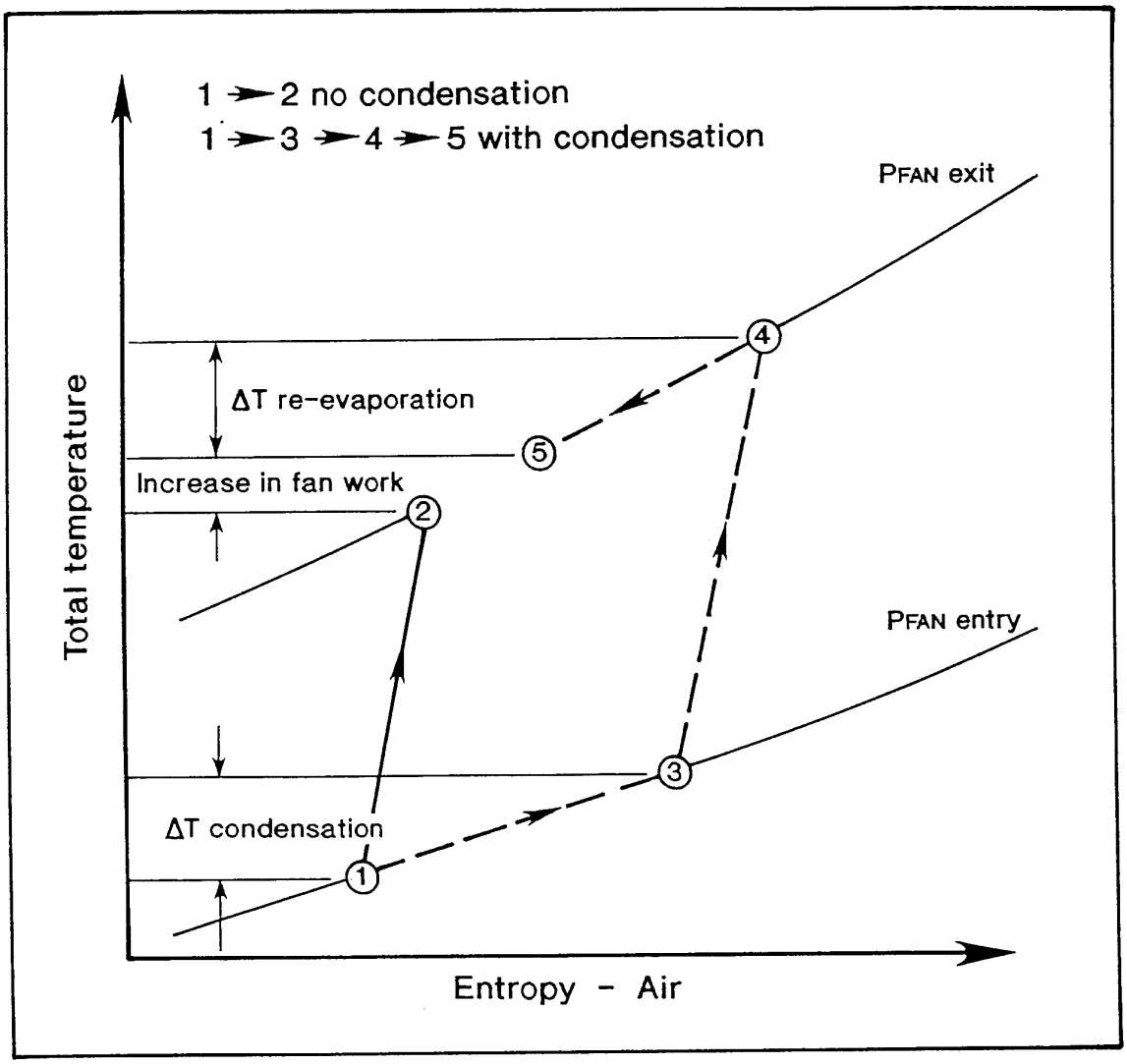

Figure 4-20

Effect of Condensation on Compression

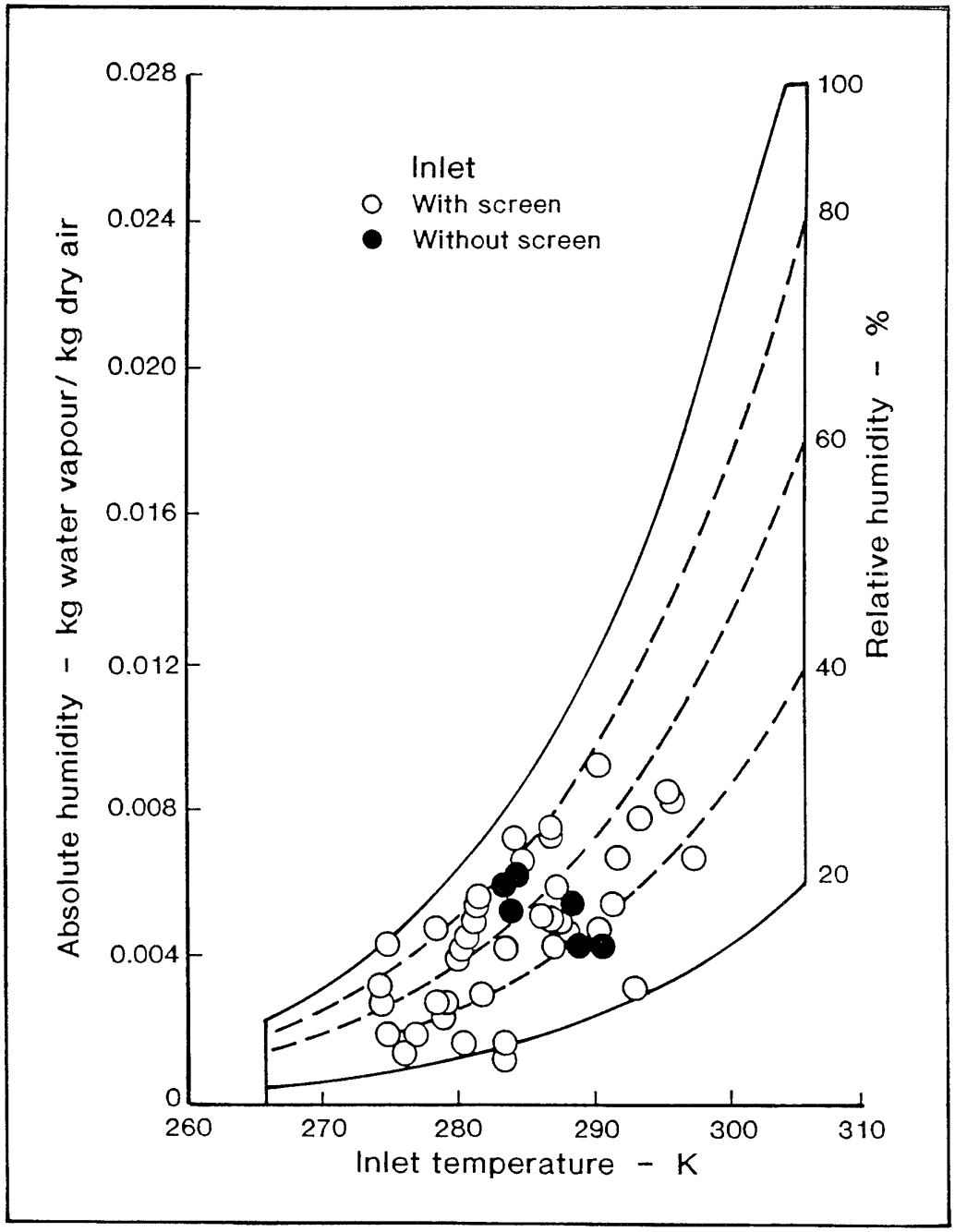

Figure 4-21

Range of Test Data for JT9D Experimental Test Program

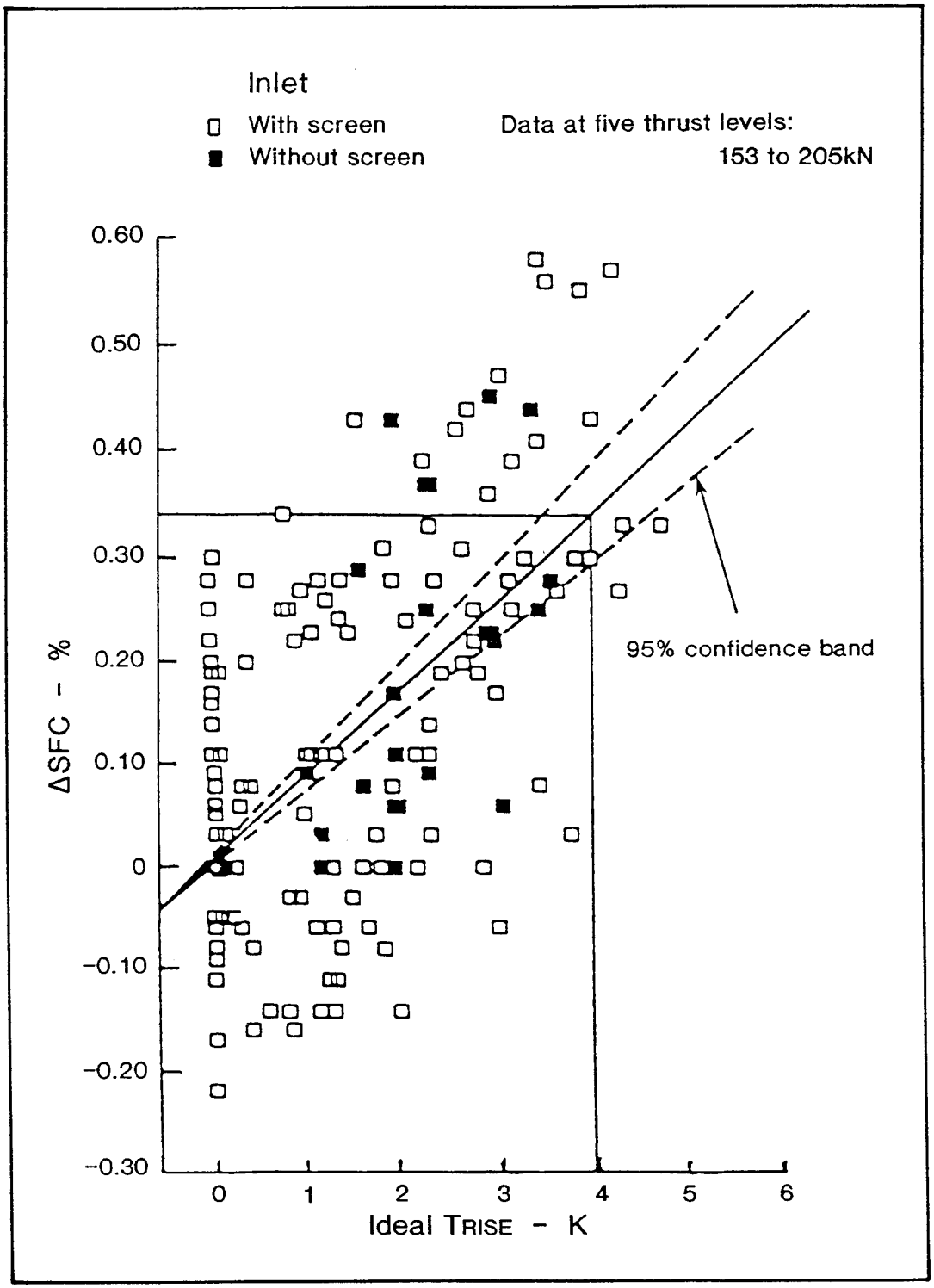

Figure 4-22

Correlation of JT9D Test Data

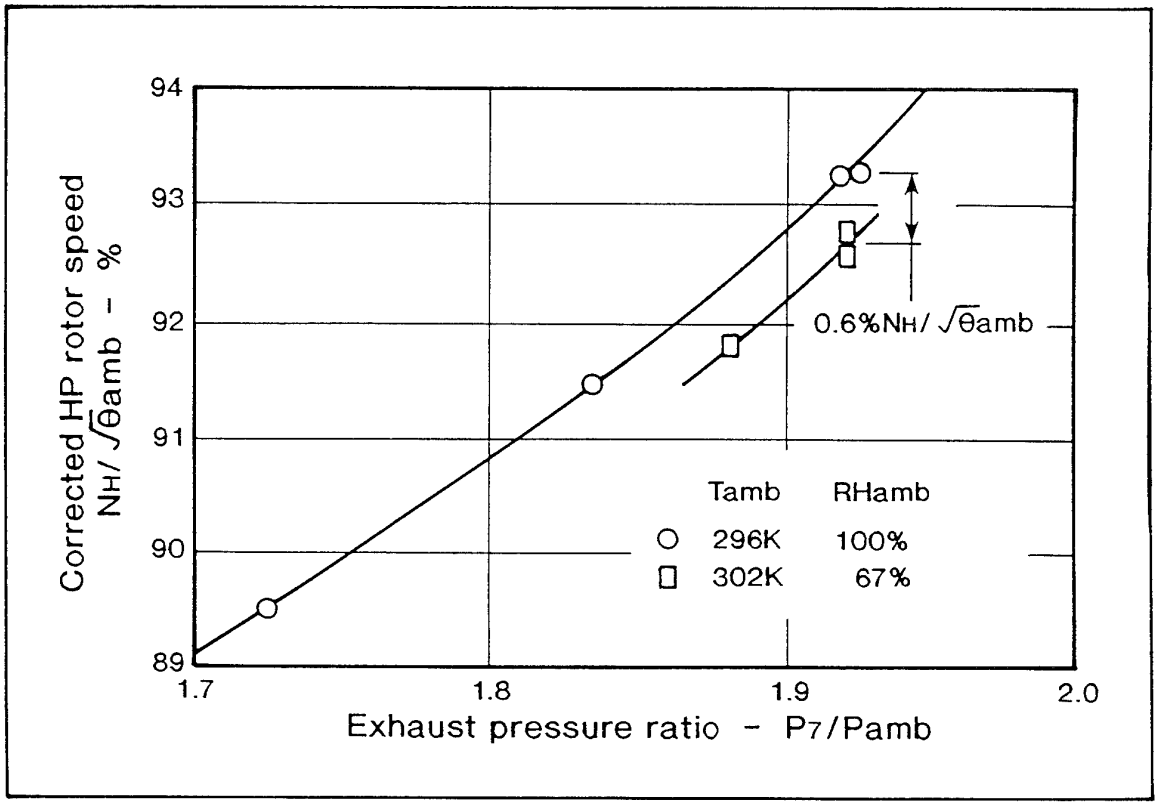

Figure 4-23

TF30 Gas Generator Performance Shift due to Inlet Condensation

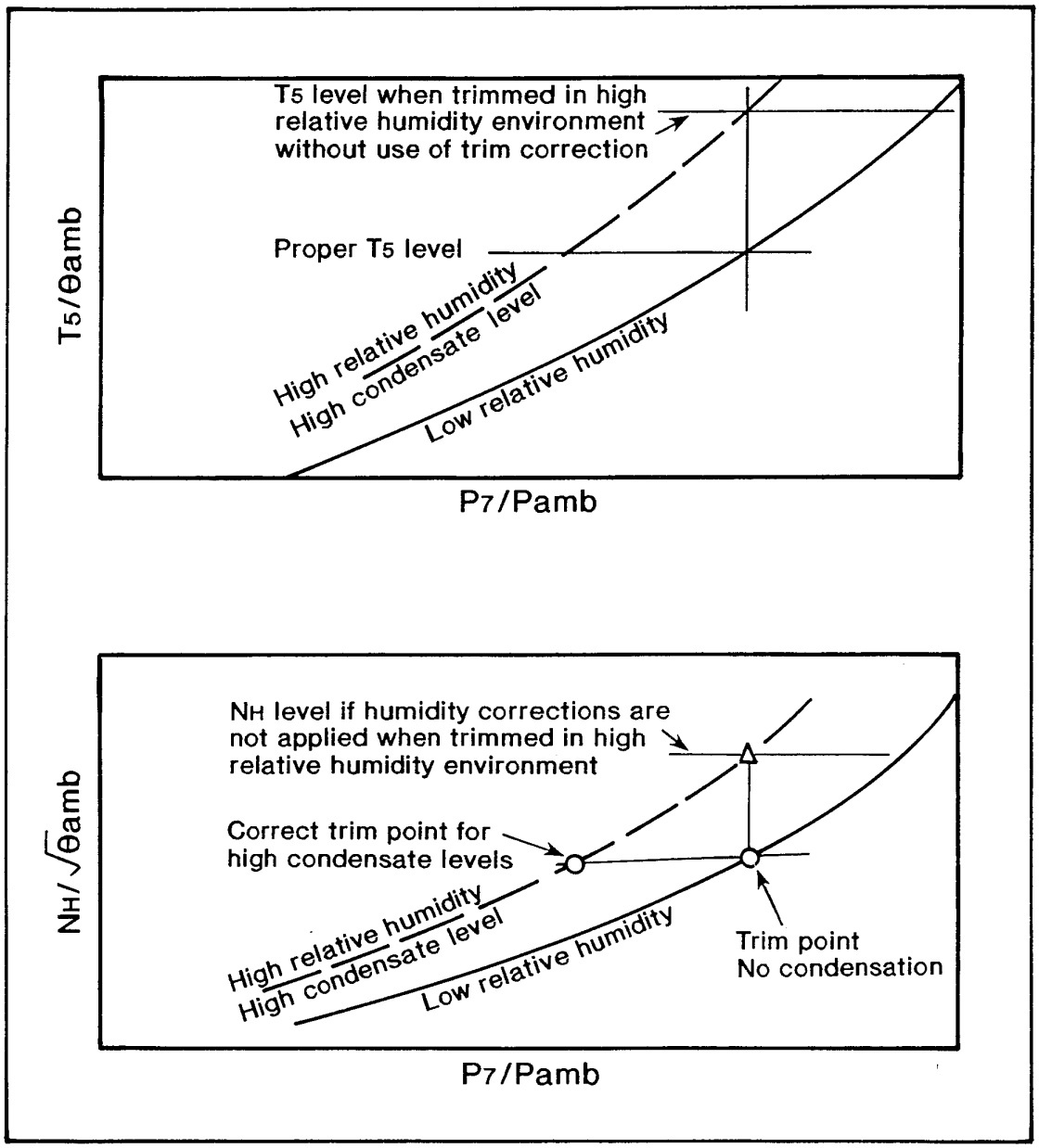

Figure 4-24

Effect of Condensation on TF30 Military Power Trim
at Constant Ambient Temperature

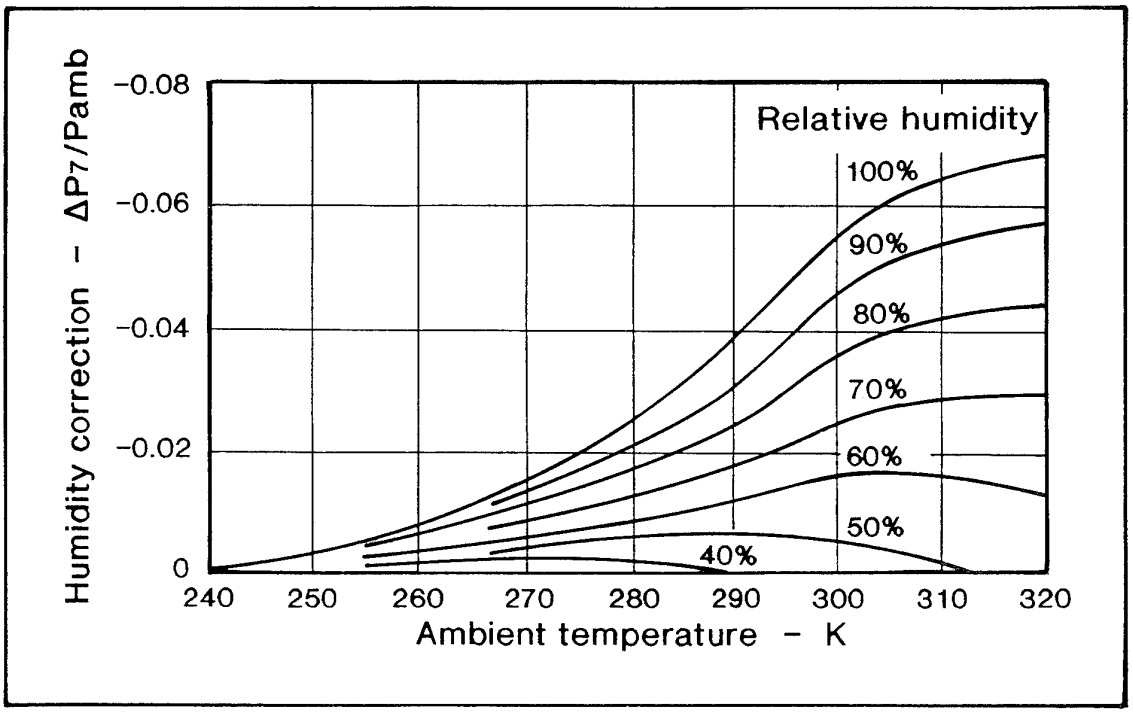

Figure 4-25

TF30 Relative Humidity Trim Corrections

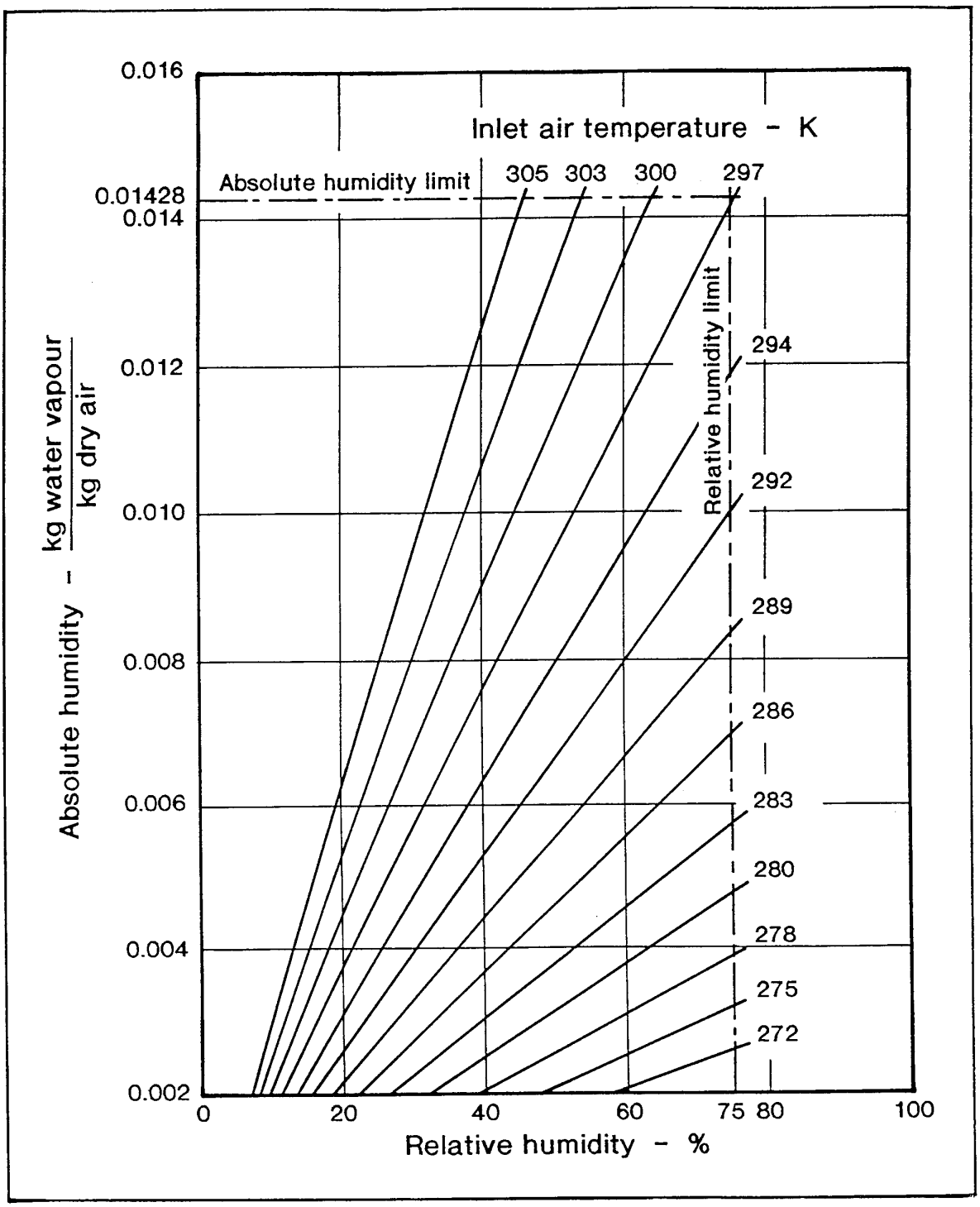

Figure 4-26

Operational Limits for Inlet Air Humidity

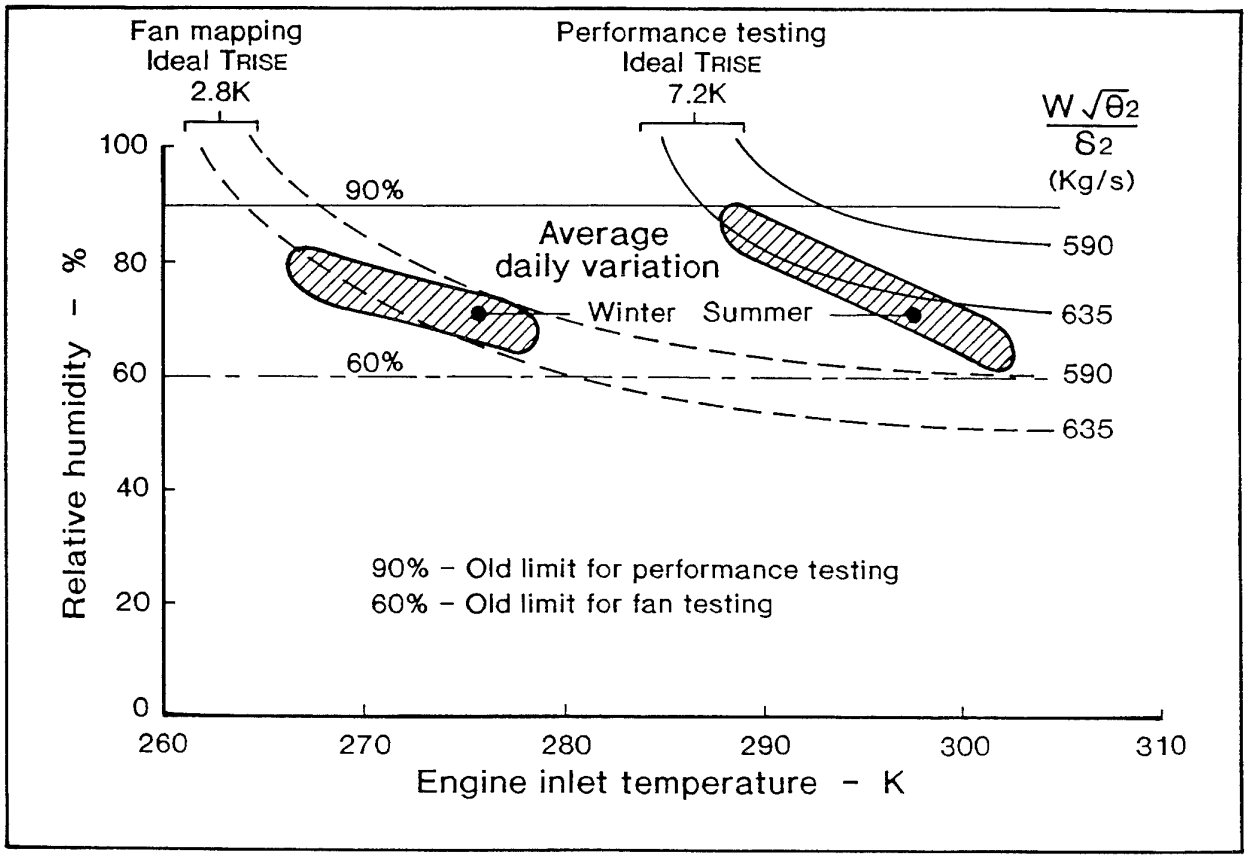

Figure 4-27

Relative Humidity Limits for CF6-80A Engine Testing with Bellmouth

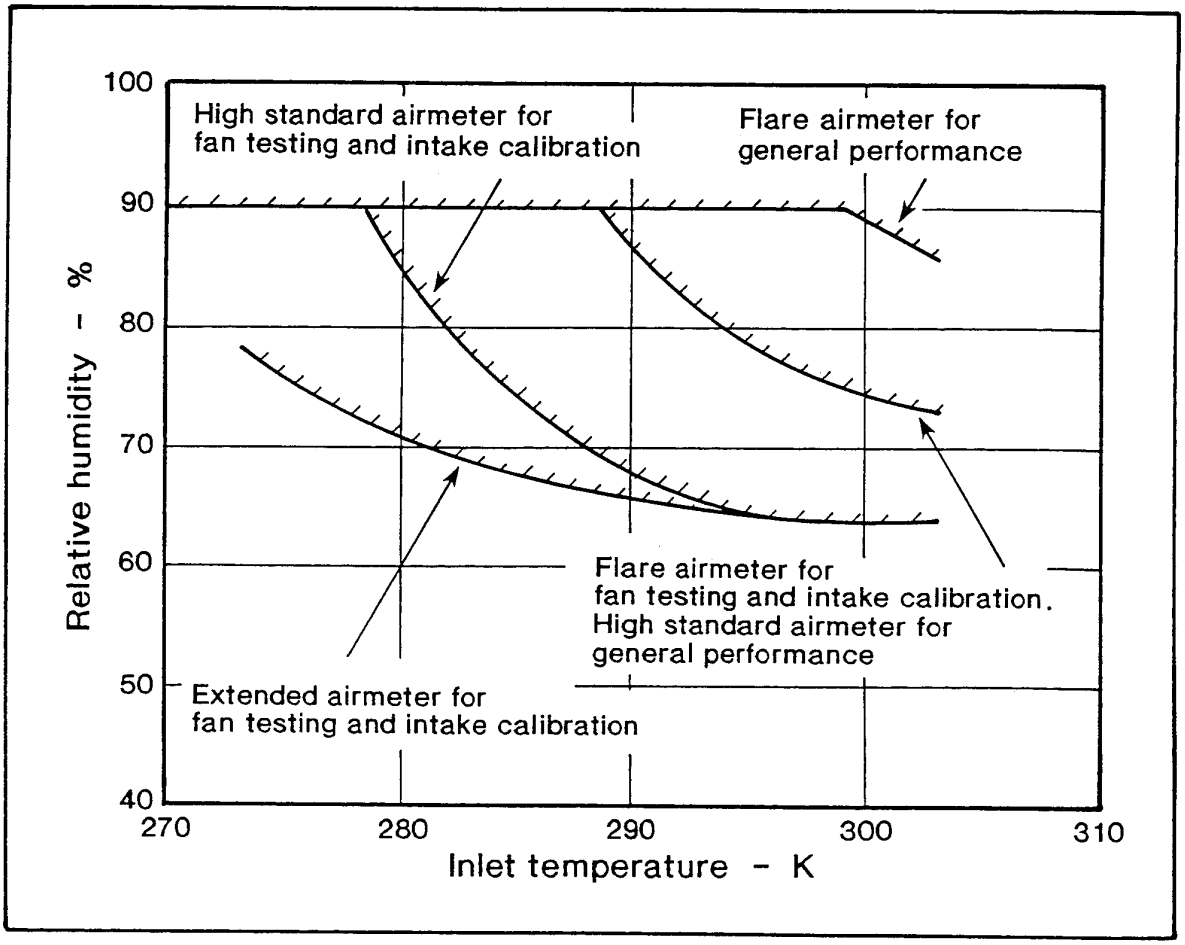

Figure 4-28

Relative Humidity Limits for RB211 Development Engine Testing

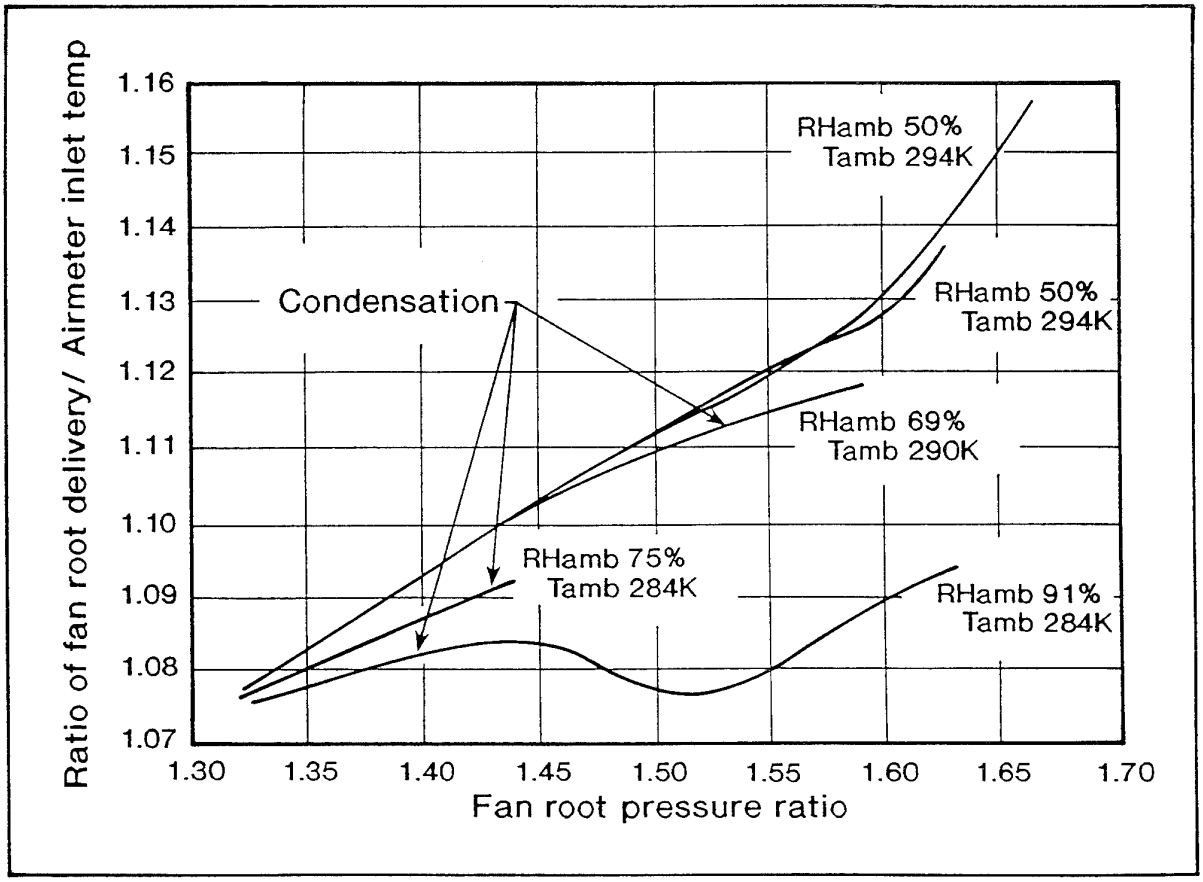

Figure 4-29

Effect of Inlet Condensation on Fan Root Delivery Temperature

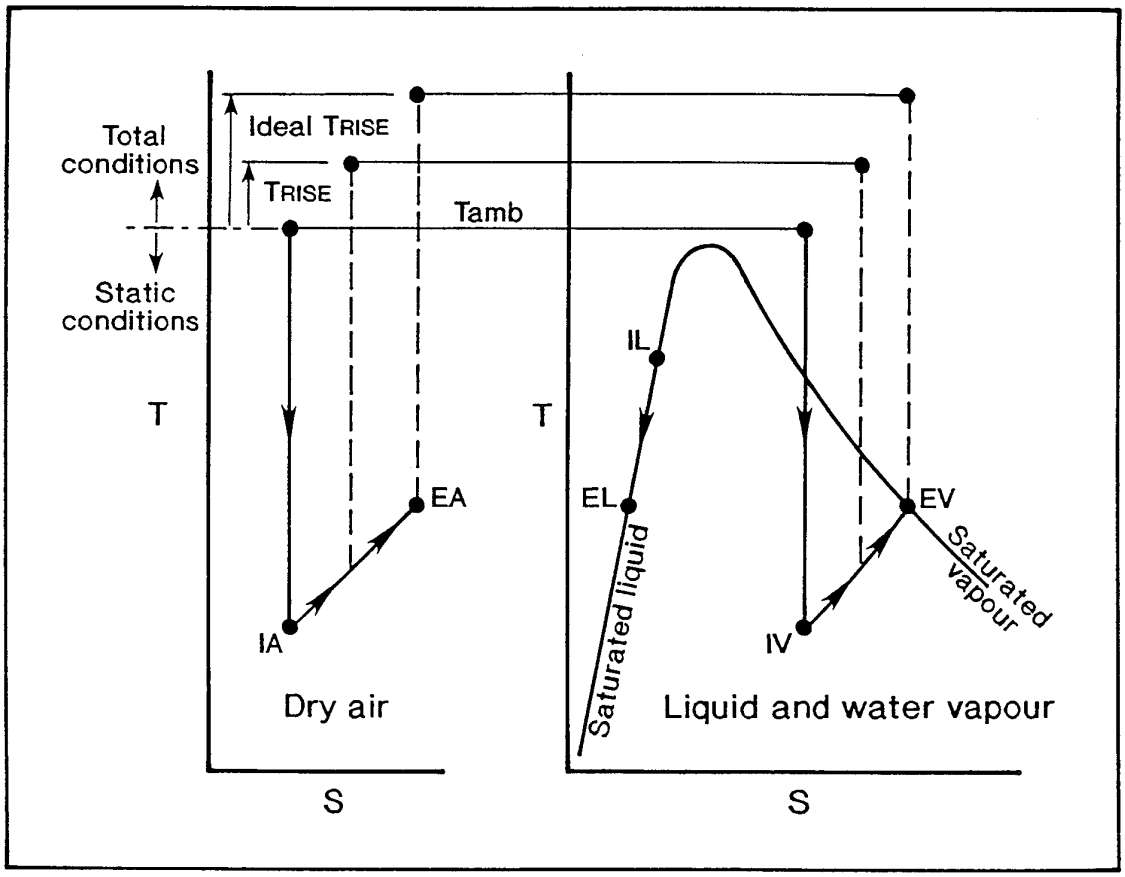

Figure 4-30

Temperature - Entropy Diagram with Condensation

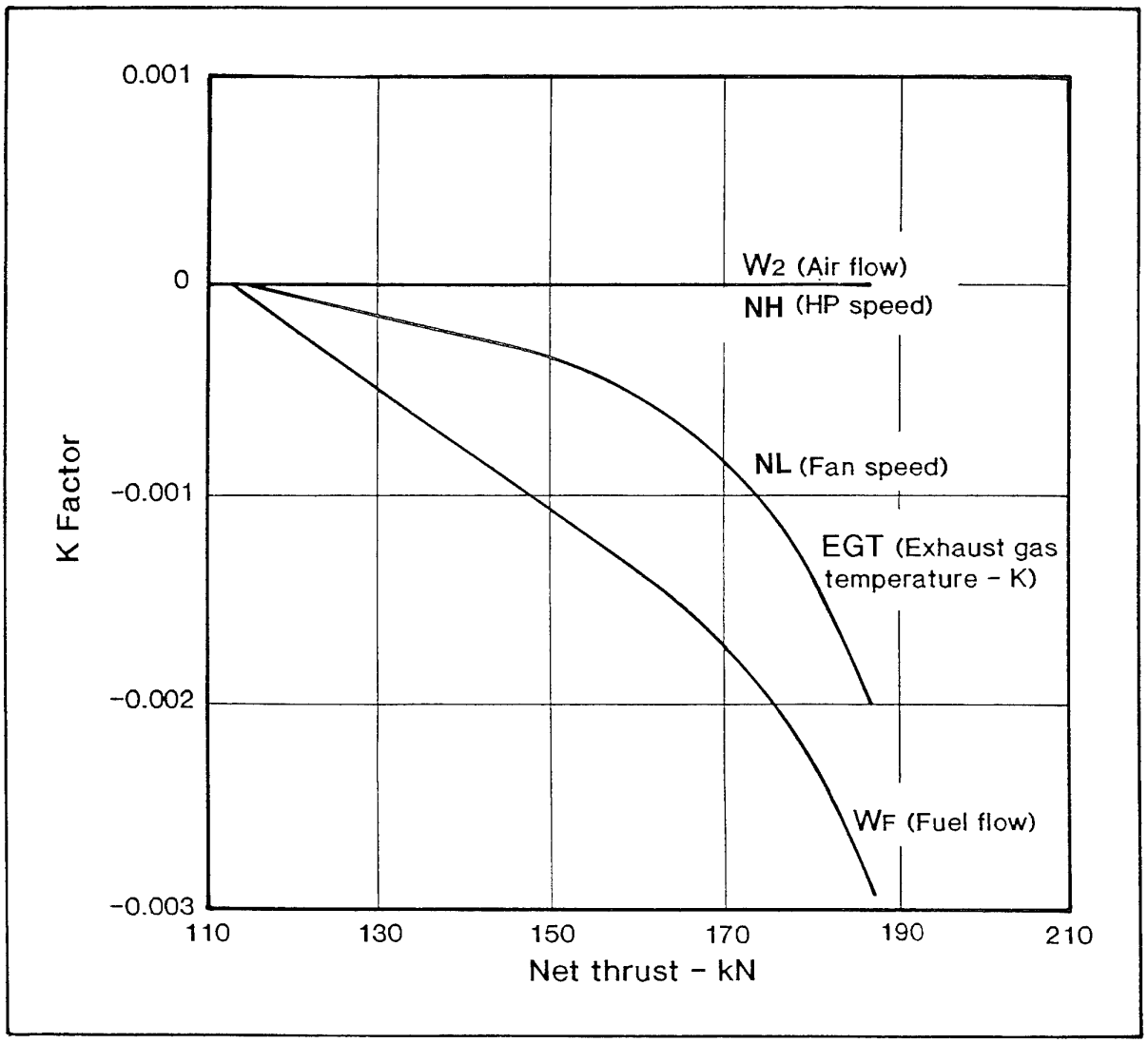

Figure 4-31

RB211-535 Inlet Condensation Correction Factors at Constant Thrust

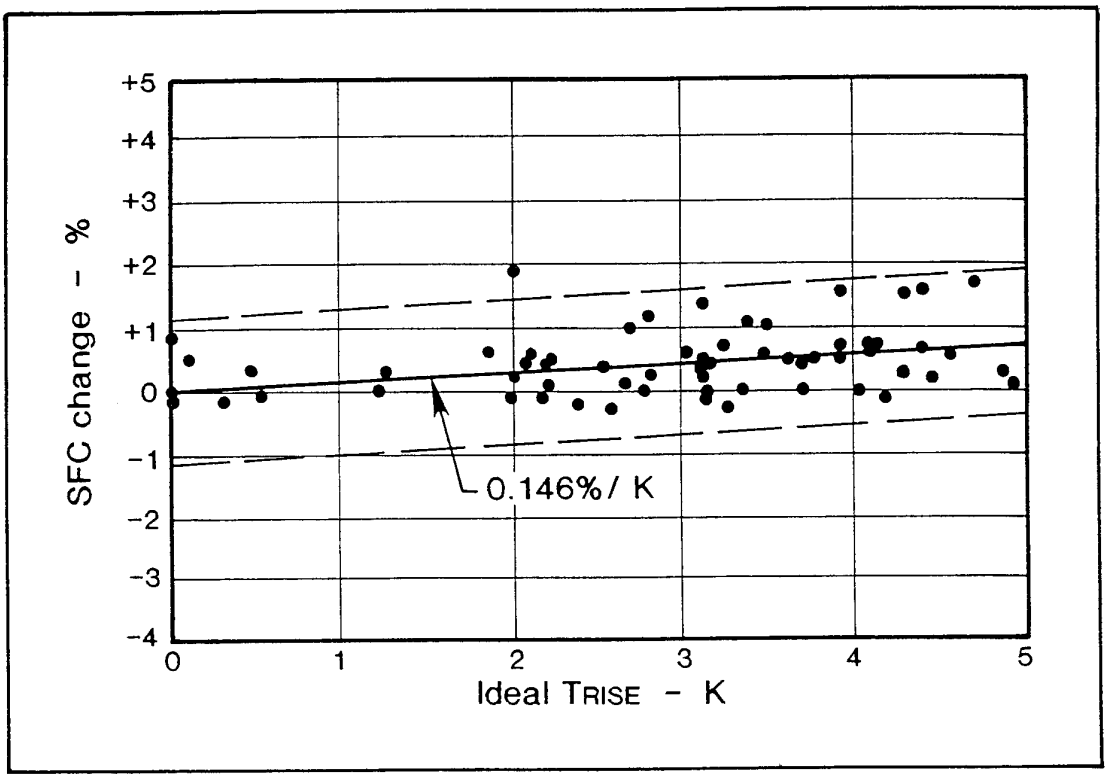

Figure 4-32

RB211-524 SFC versus Ideal Temperature Rise at Take-off Thrust

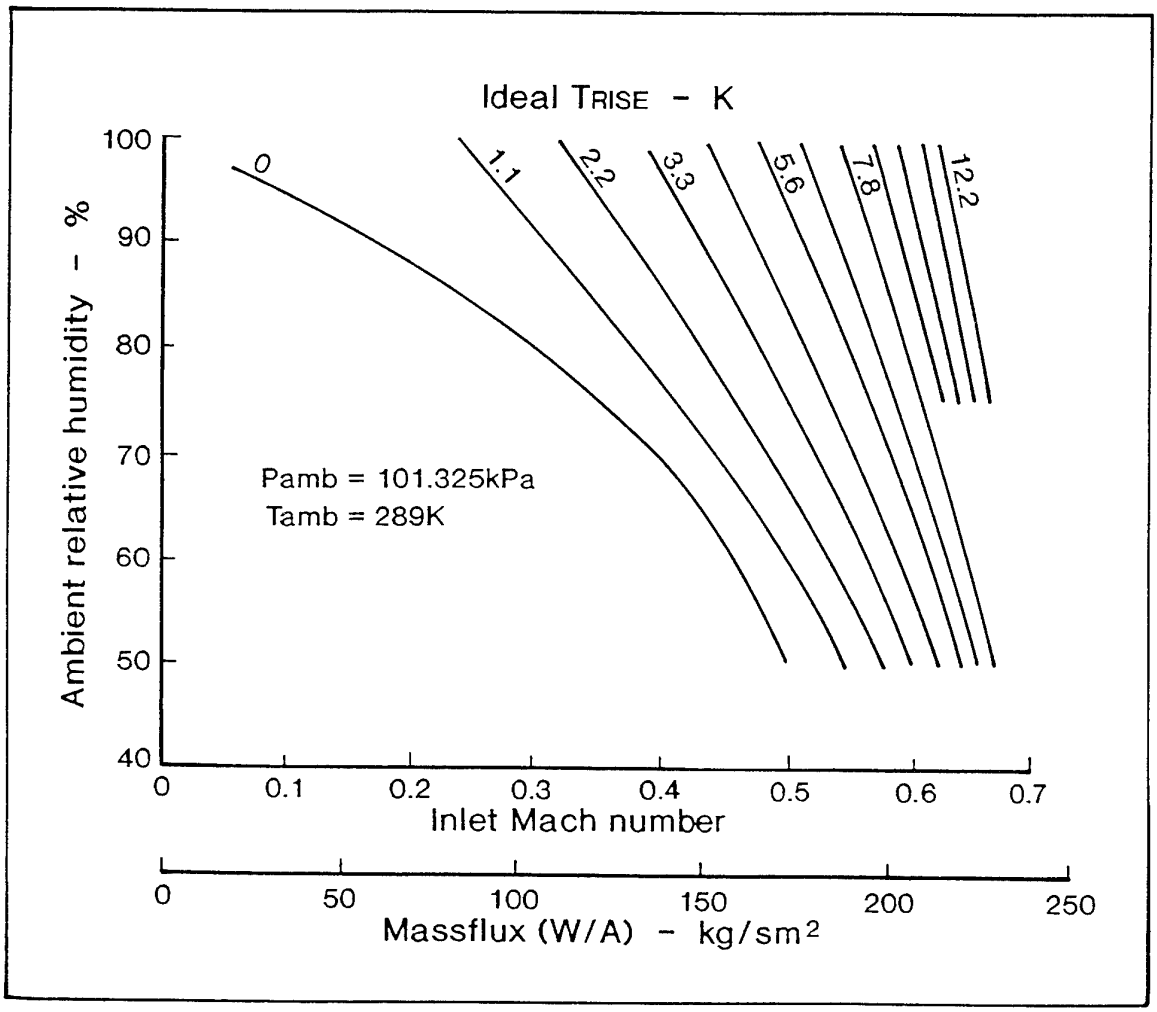

Figure 4-33

Effect of Inlet Duct Mach Number and Relative Humidity
on Ideal Temperature Rise

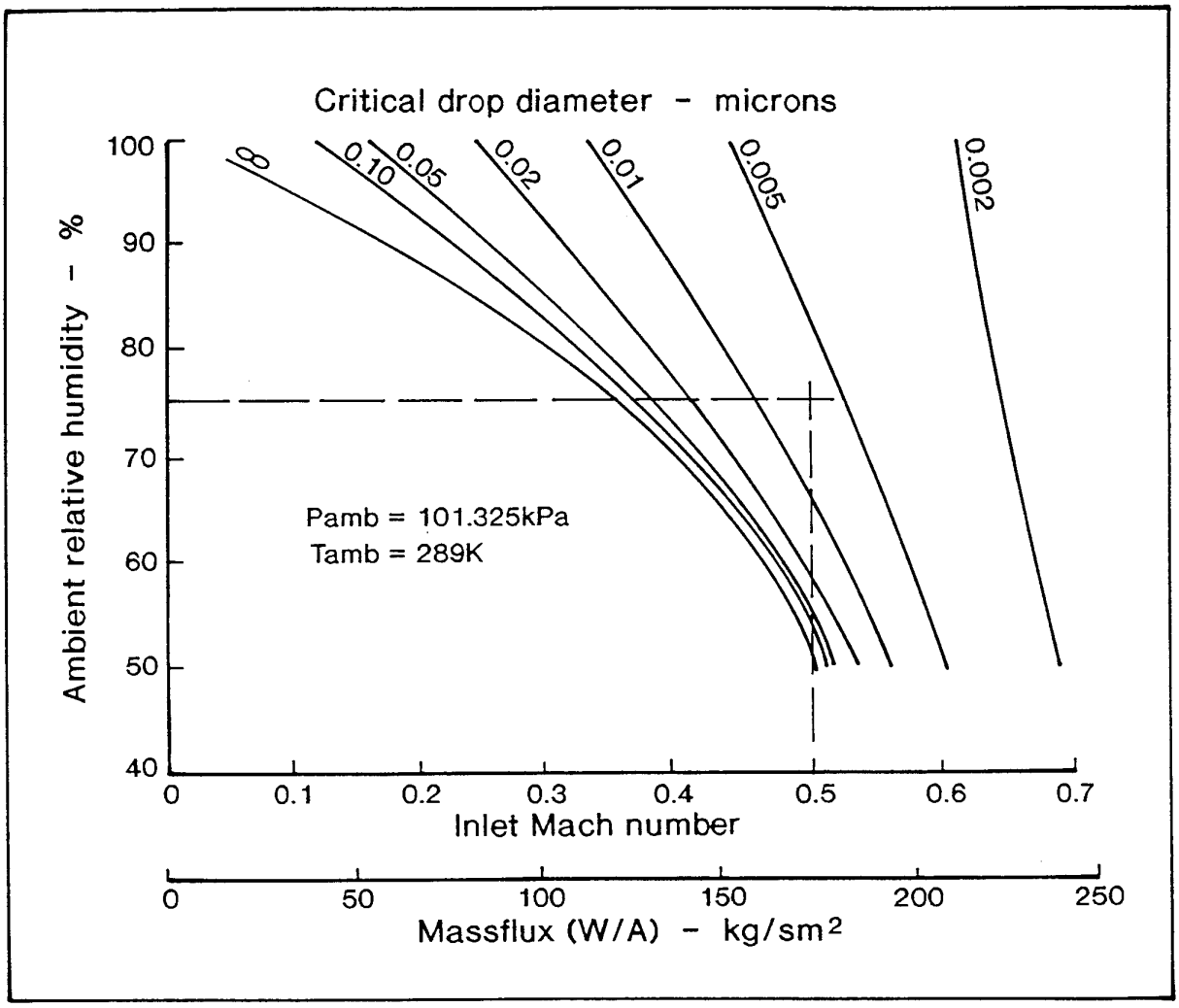

Figure 4-34

Effect of Inlet Duct Mach Number and Relative Humidity
on Critical Nuclei Diameter

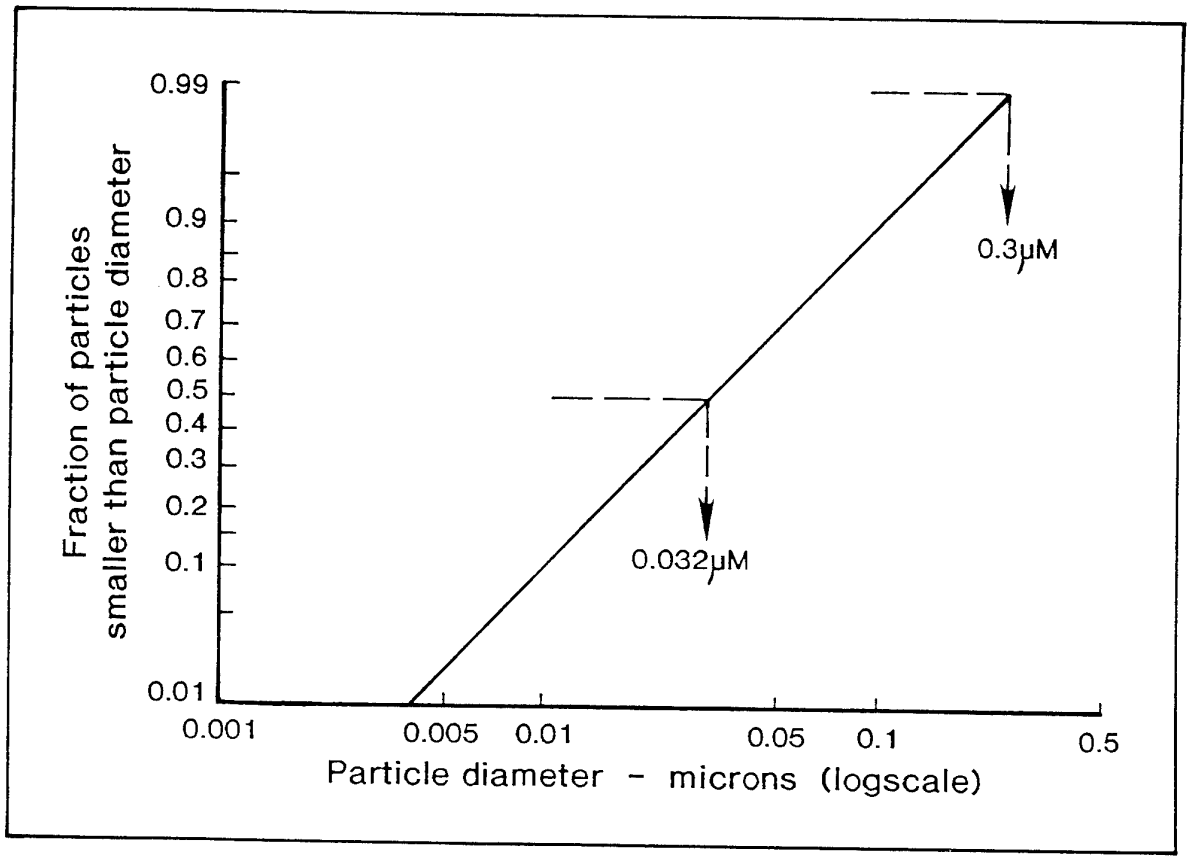

Figure 4-35

Particle Size Distribution for Condensing Nuclei

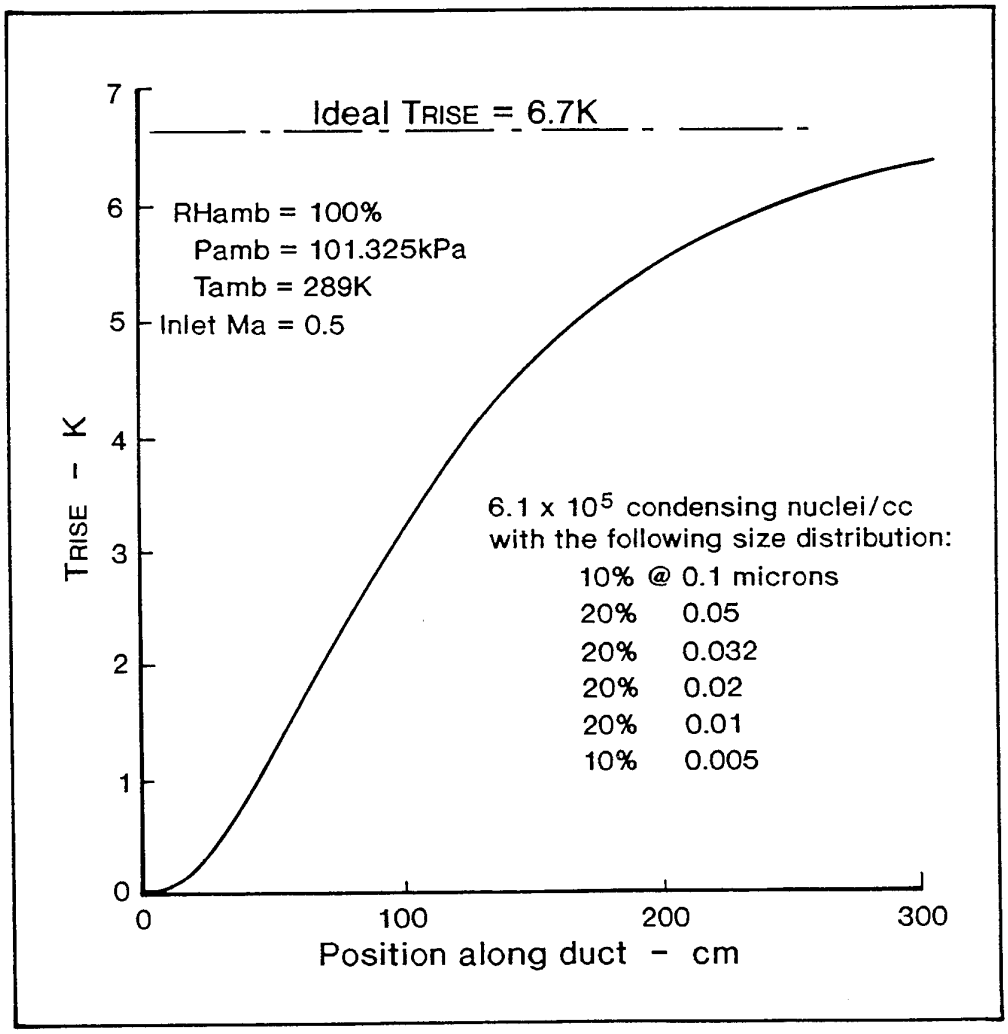

Figure 4-36

Condensation Temperature Rise Along a Constant Area Inlet Duct

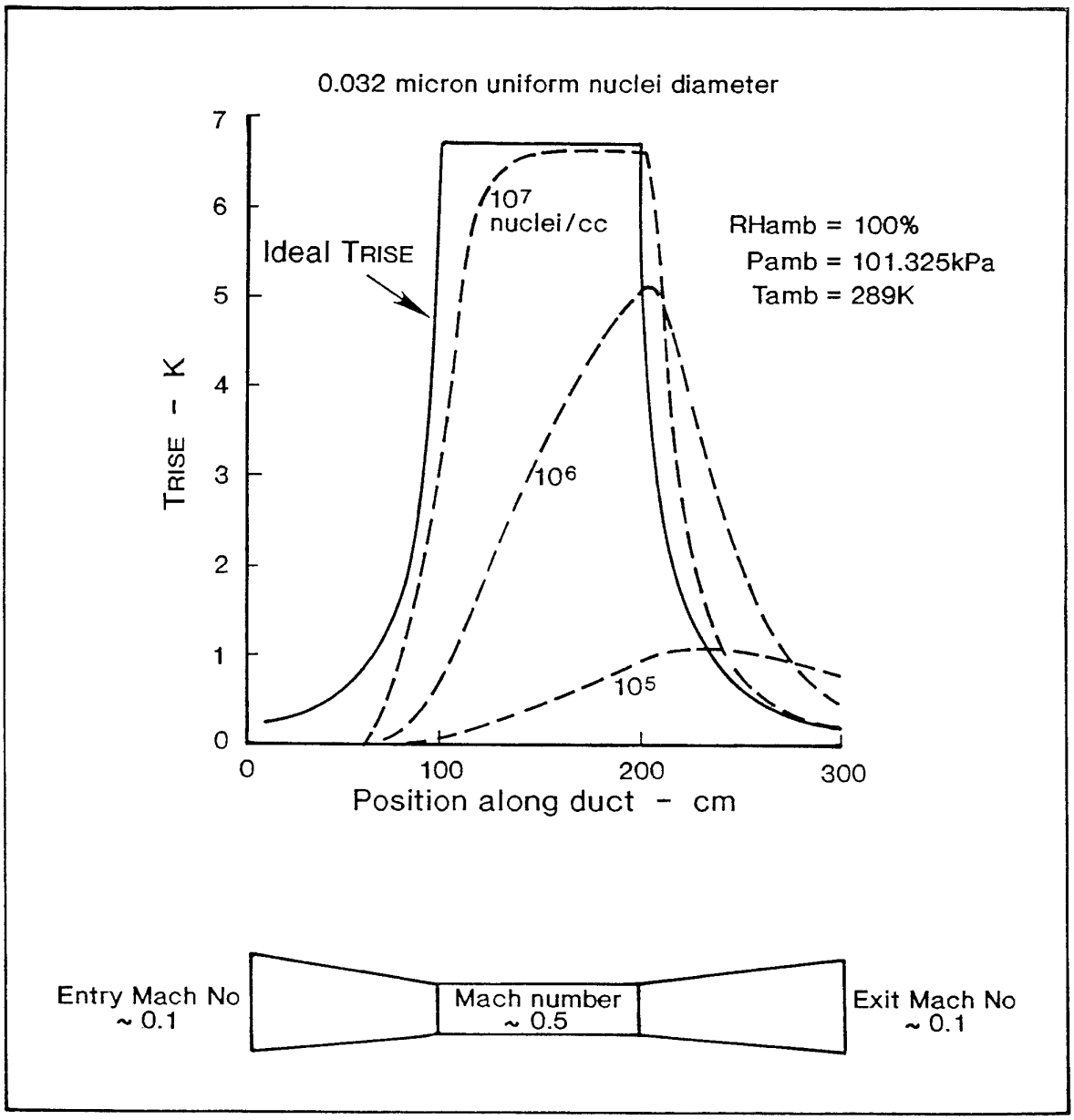

Figure 4-37

Effect of Nuclei Concentration on Inlet Condensation

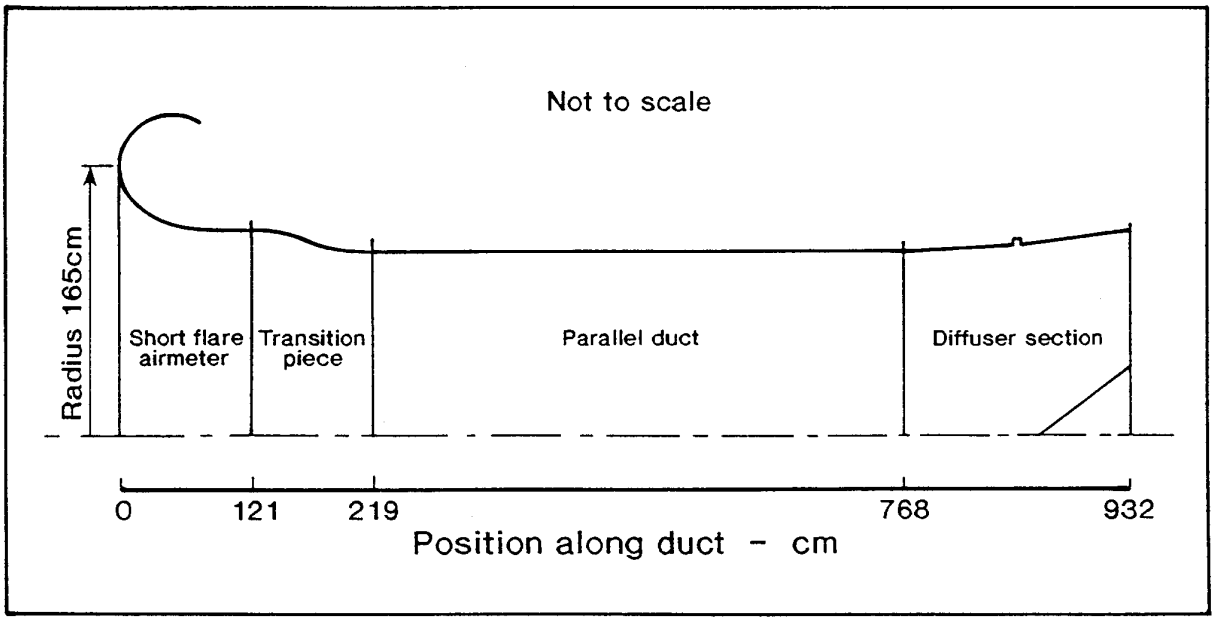

Figure 4-38

MD-11 Centre Duct Inlet

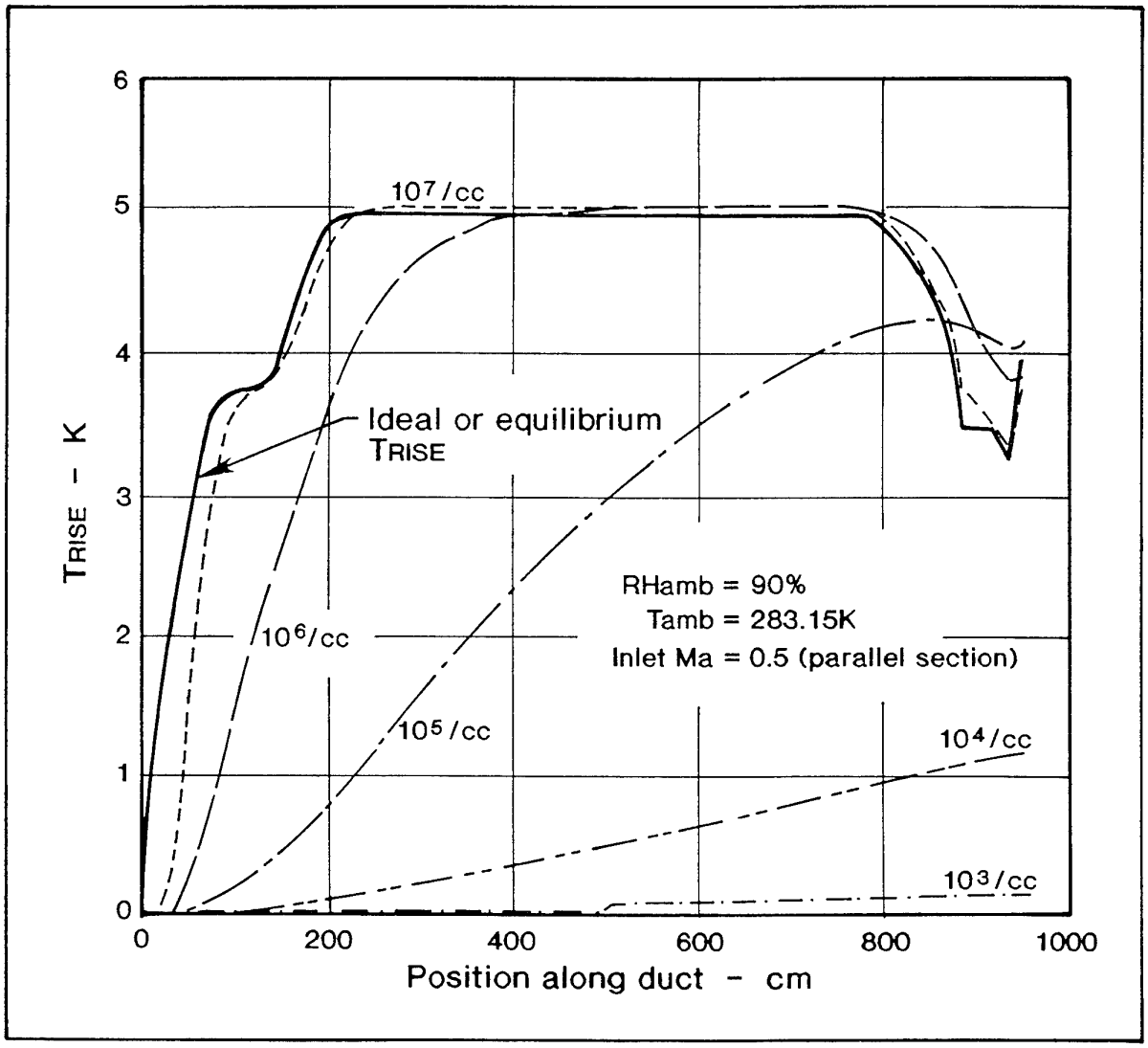

Figure 4-39

Condensation Temperature Rise Along an MD-11 Centre Duct Inlet

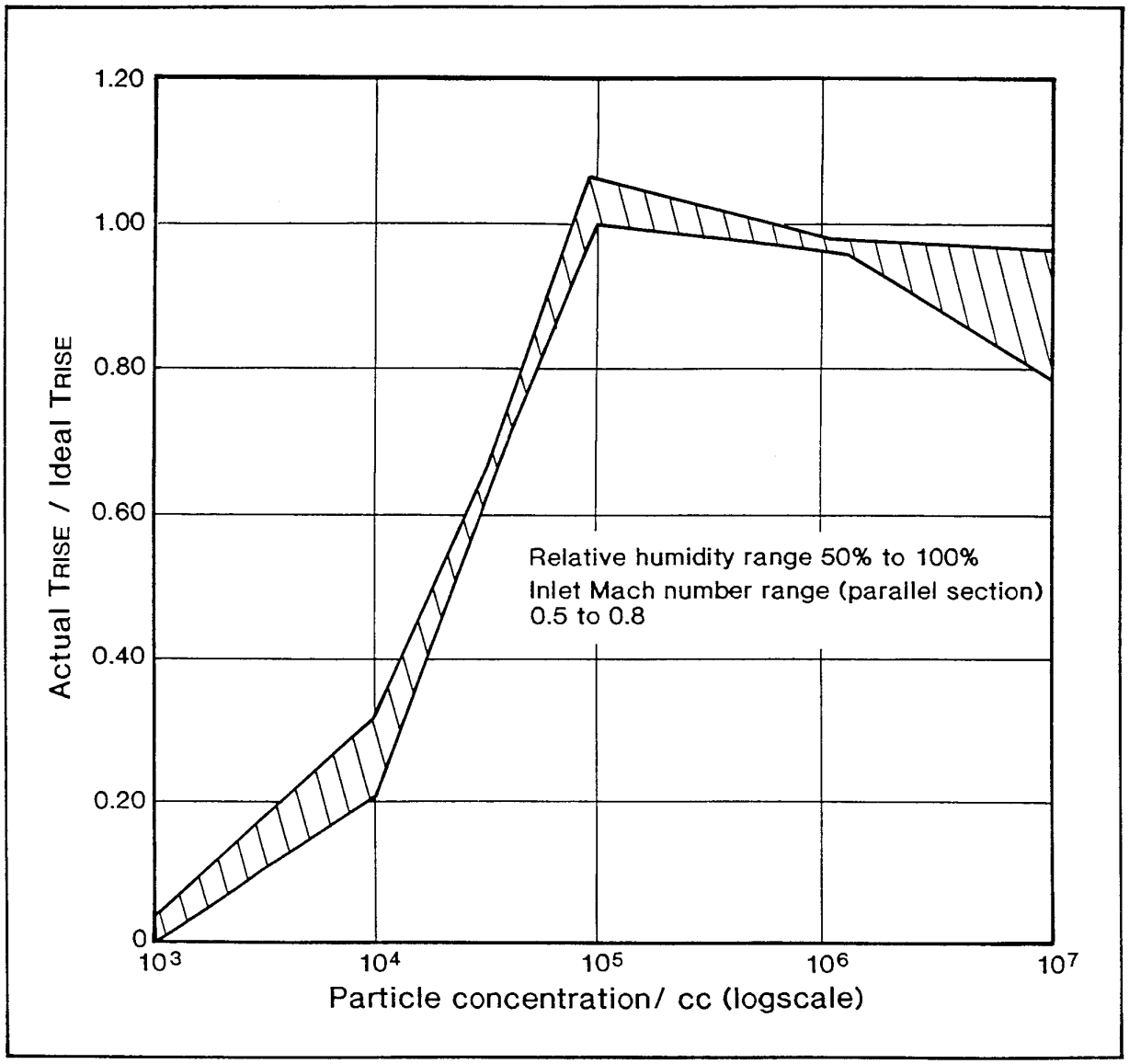

Figure 4-40

Influence of Particle Concentration on Actual/Ideal Temperature Rise
at Exit to an MD-11 Centre Duct Inlet

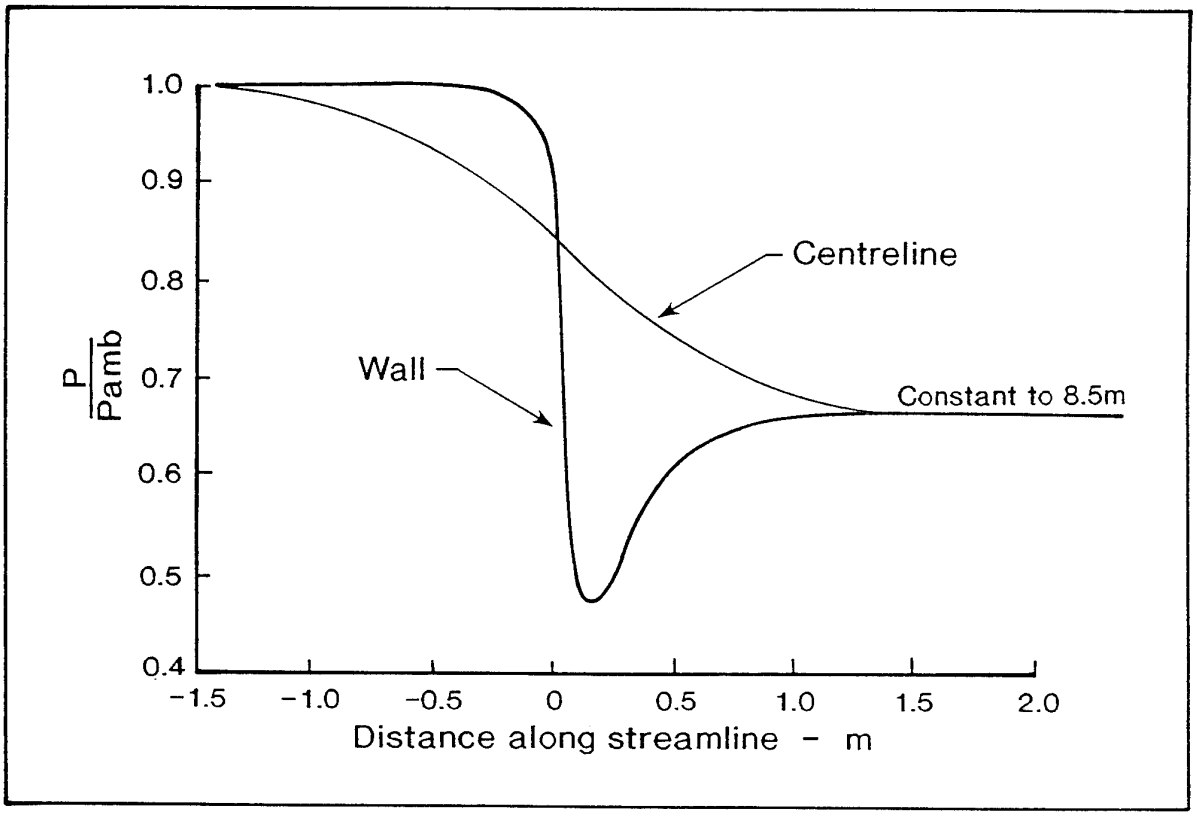

Figure 4-41

Engine Inlet Pressure Distributions

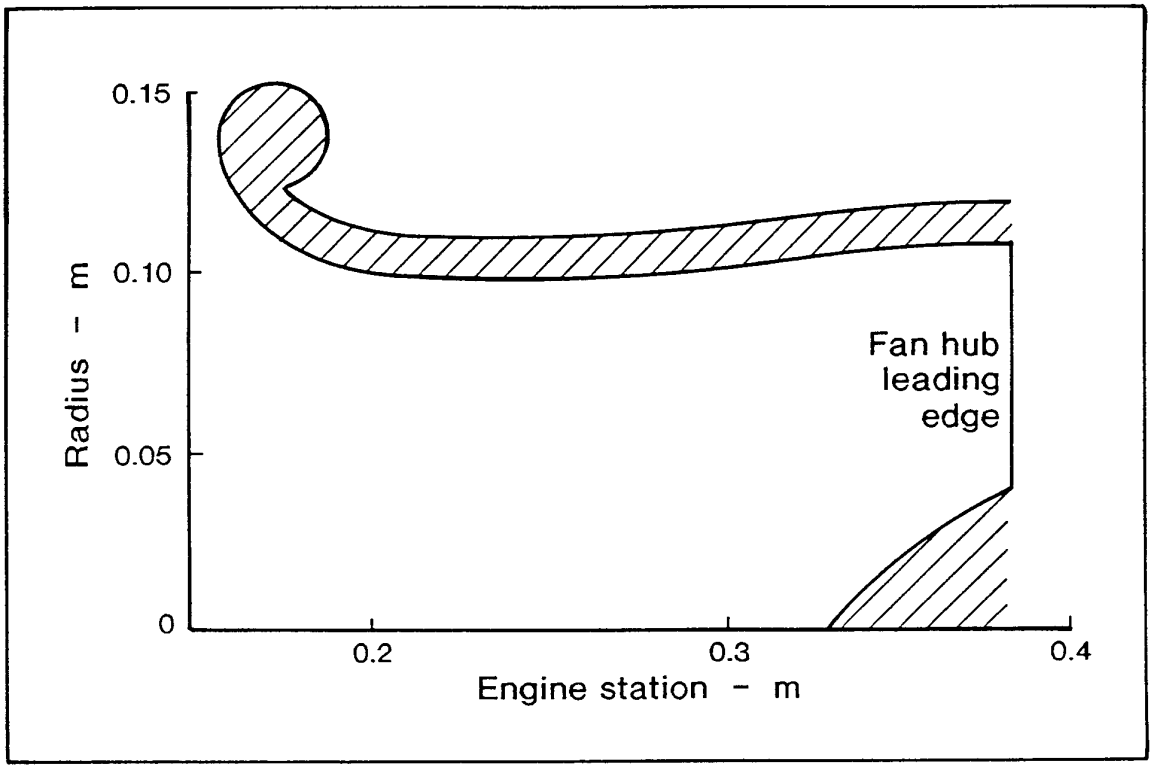

Figure 4-42

CF6-80A Engine-mounted Bellmouth Inlet

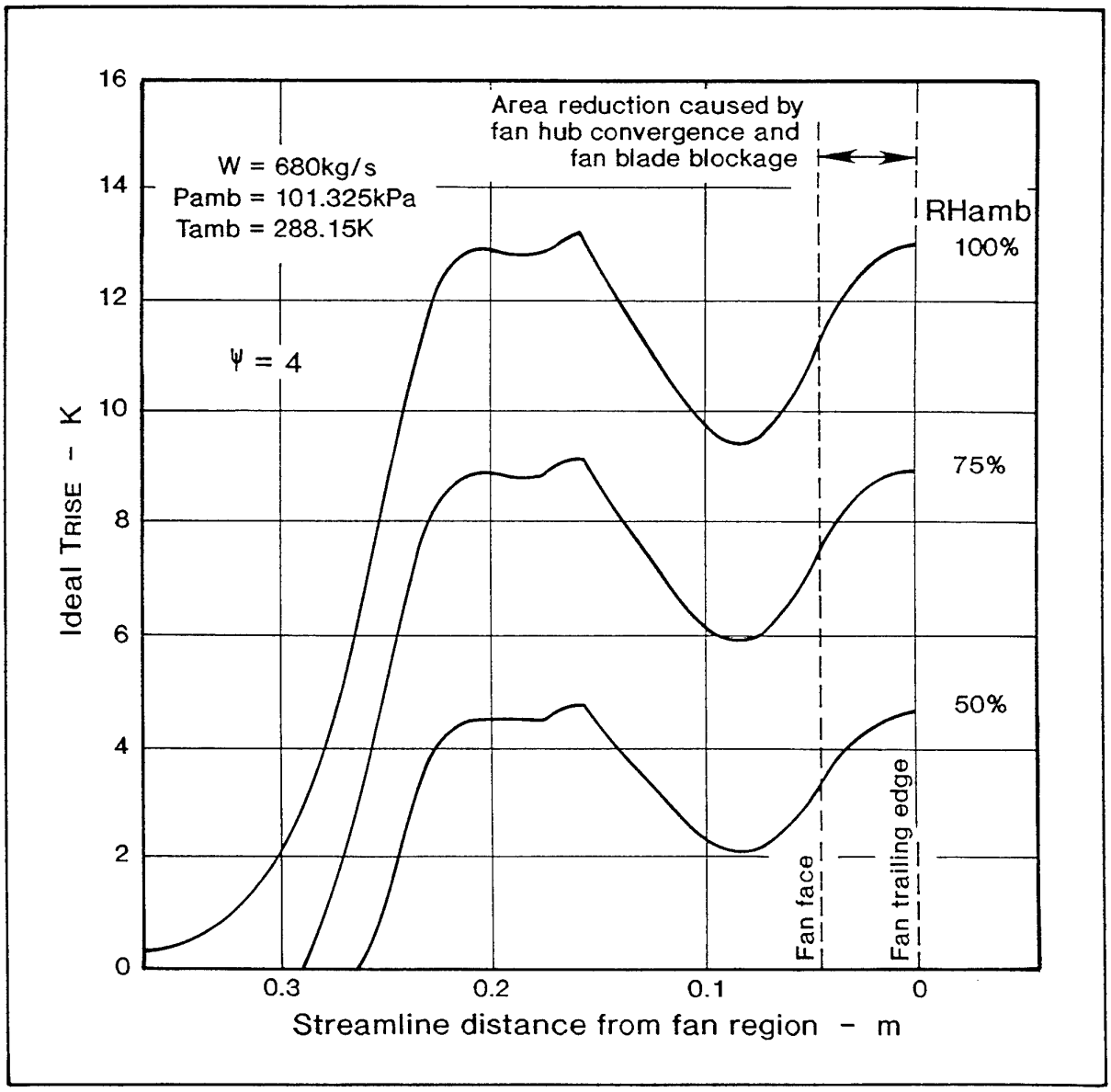

Figure 4-43

Effect of Ambient Relative Humidity on Ideal Condensation Temperature Rise
in a CF6-80A Engine-mounted Bellmouth Inlet

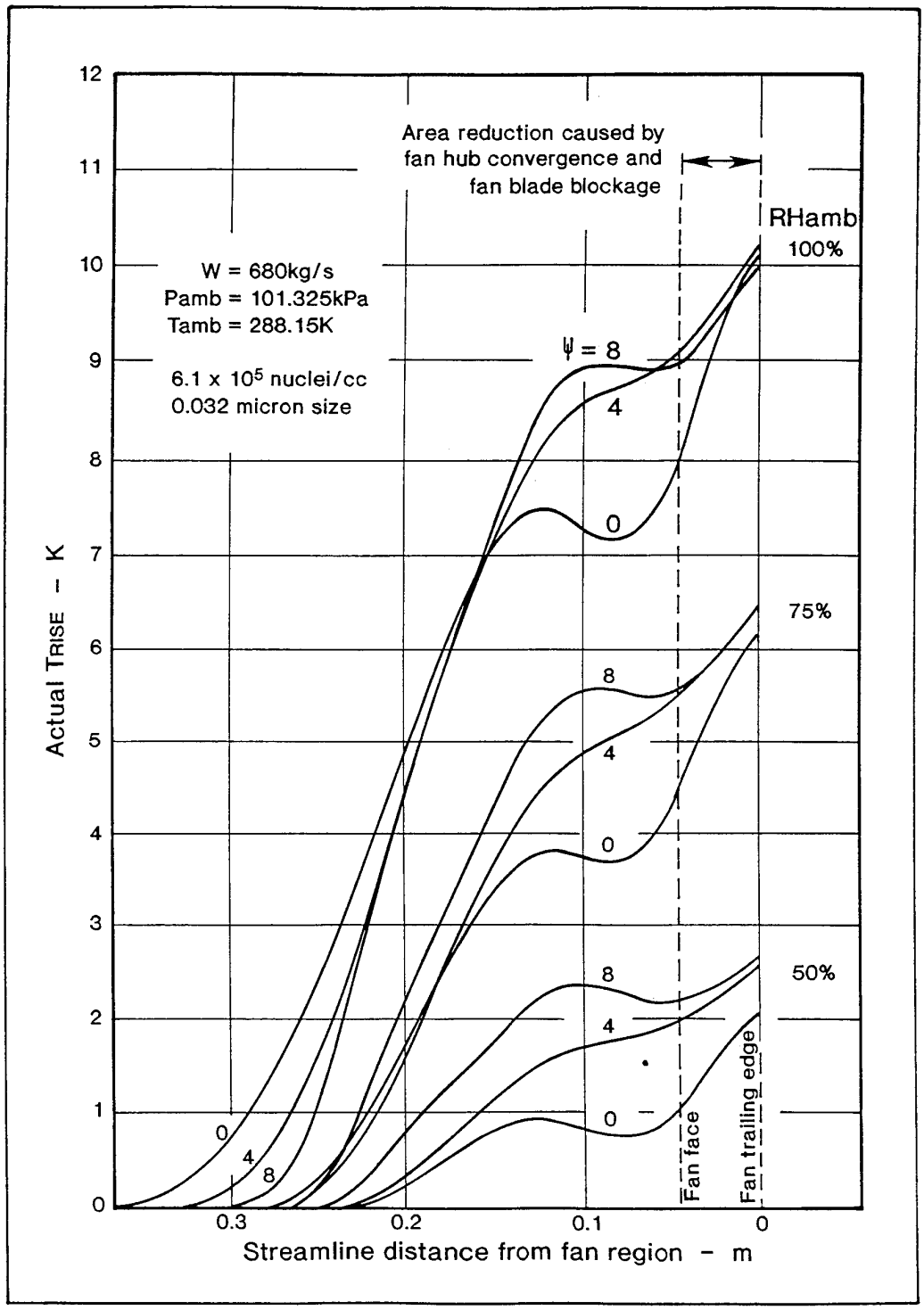

Figure 4-44

Effect of Ambient Relative Humidity on Actual Condensation Temperature Rise
in a CF6-80A Engine-mounted Bellmouth Inlet

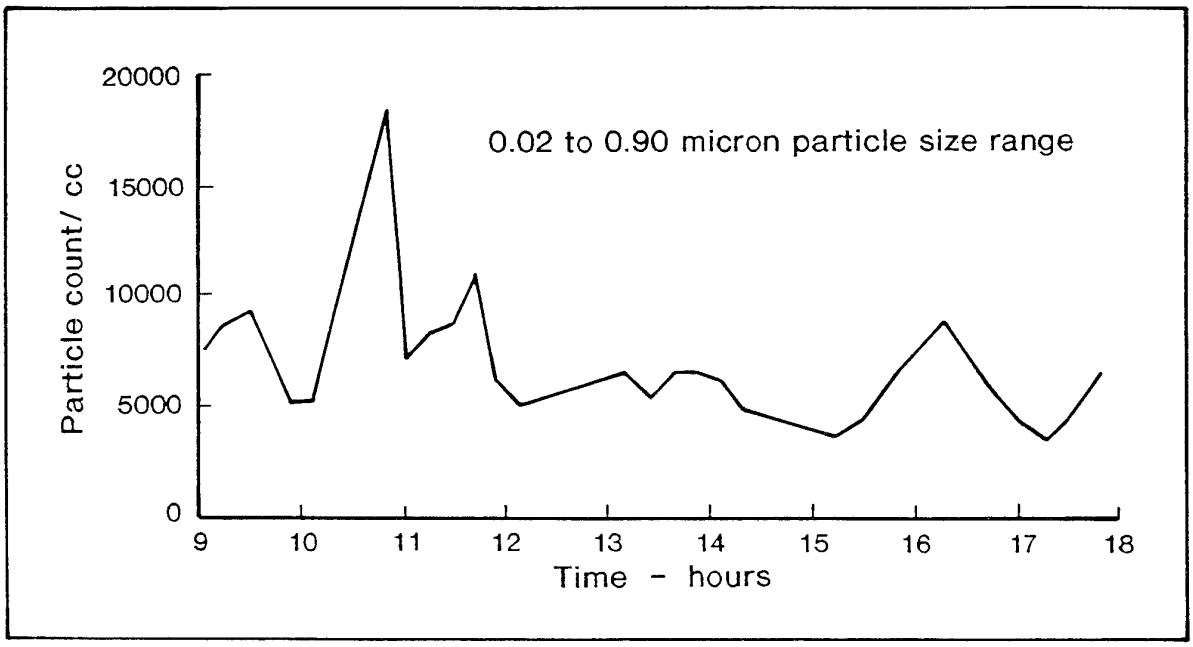

Figure 4-45

Ambient Particle Levels During Engine Testing at Derby, England

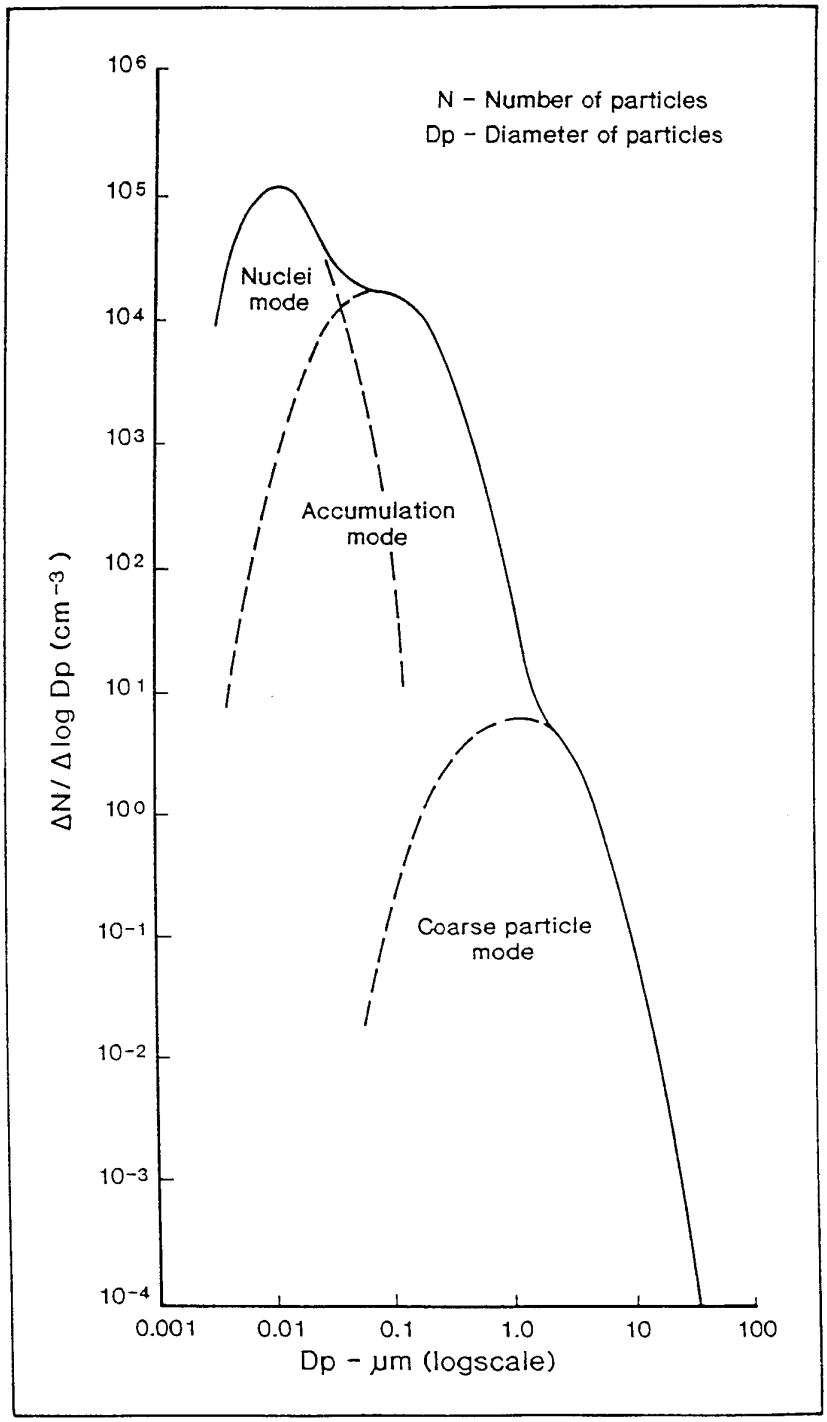

Figure 4-46

Number/Size Distribution of Aerosol Particles under Urban Conditions
According to Whitby (1978) - Reference 4.23
(Courtesy of Pergamon Press)

5. LIQUID WATER, SNOW AND HAIL: EFFECTS ON COMPONENTS AND ENGINE PERFORMANCE/OPERABILITY[1]

5.1 INTRODUCTION

The ingestion of large quantities of water, snow and hail into the inlet of a gas turbine engine during flight has been a growing concern of the aircraft engine industry. The problem is four-fold: (1) definition of the threat, (2) determination of the effects of water ingestion on engine operation, (3) development of engine designs and/or operational procedures that can circumvent serious adverse effects of in-flight water/hail ingestion and (4) determination of certification and test requirements. Being a matter of safety, and a potential problem generic to all gas turbine engines, the effects of water and/or hail are of vital concern to both military and civilian interests.

Water and ice have long been recognized as having potentially damaging effects on turbine engines. FAA certification and military qualification procedures require bird, water and ice ingestion testing for each new engine design before it can enter service. While these precautions to prevent catastrophic consequences of water ingestion have been generally successful, there have been several instances in commercial service where engines have lost power in rain storm or hail conditions. This power loss is a result of a burner flameout, rollback with loss of rotor speed to below idle conditions, or compressor stall, all of which can result in an engine shutdown in flight.

The case histories for the following two events which occurred in 1987 and 1988 on Boeing 737-300 aircraft powered by CFM56-3 engines illustrate the potential for dual engine flameout descent in severe inclement weather and provide an insight as to the causes and effects (Reference 5.1).

First Event:

A Boeing 737-300 equipped with CFM56-3 engines experienced a dual engine flameout in heavy rain and hail while descending into Salonika, Greece, in August, 1987. The flight recorder showed that both engines had flamed out simultaneously at 2700 m (8900 feet), 289 KIAS, 15°C TAT, at idle descent power. Both engines were restarted without difficulty, and the aircraft descended and landed normally.

Flight reports showed heavy rain and hail, with moderate turbulence and with lightning in the vicinity. Based on the crew report, the hail shower was one of the most violent ever encountered by the captain.

Ground inspection revealed that the airplane horizontal stabilizer had been dented from numerous large diameter hailstones. The anti-collision light was broken, and the paint had been removed from the radome. There was no damage to the wing leading edges and no damage to the engines. Engine and related system checks conducted on the ground showed all aircraft and engine systems to be normal.

Second Event:

A Boeing 737-300 equipped with CFM56-3 engines experienced a dual engine flameout while in descent from 10670 m (35,000 feet) into New Orleans in May, 1988. Icing conditions were detected and cowl anti-ice was on. The crew reported severe rain and hail and lightning, with severe turbulence and high aircraft vibrations at 5030 m (16,500 feet), 267 KIAS, -29°C TAT.

The crew reported light icing until about 30 seconds before the power loss. At that time they reported a sudden encounter with heavy hail, heavy rain, with moderate turbulence and with lightning in the vicinity. The weather service reported that the storm system included level 5 and 6 activity (level 6 is the highest classification) (Table 5-1).

The crew was unable to restore power on either engine. The aircraft landed safely on a grass levee near the intercoastal waterway. There was no landing damage and no injuries.

This was a new aircraft that had entered service only 11 days earlier. System checks conducted on the ground showed the engine and aircraft systems to be normal. Engine number 2 had overtemperature

---

[1] Tables and Figures for Chapter 5 begin on page 5-18.

damage in the turbine, from the unsuccessful in-flight start attempts in the rain and hail. Engine number 2 was replaced and the aircraft was flown to the New Orleans airport.

Engine number 1 was removed and run in a CFMI test cell, where it demonstrated normal operation and normal flameout margin.

This chapter will address the effects of water/hail ingestion on engine component/overall performance and operability. A methodology will be developed that will assist in determining analytically the water content in various engine components during rain and hail-storms, and the resulting impact on performance and operability. The engine and rig tests conducted to calibrate the analytical model will also be discussed.

The primary area of interest will be low power (descent idle) operating conditions at altitudes between 1500 and 6000 m (5000 and 20000 feet), because it is here that the atmospheric water/hail-to-air ratio is greatest (Chapter 2), and because the engine effectively concentrates ingested water in the core at low speed/low power operating conditions. There is also less excess energy at low power to process the water in the compressor and combustor before exceeding operating limits.

5.1.1 Engine Rundown (Rollback)

The energy required for the engine to run at a given speed is directly influenced by water ingested, accessory load and the engine component efficiencies. Figure 5-1 illustrates the effect of water/hail ingestion on engine control characteristics. The dashed operating lines represent fuel required for various rates of water ingestion. As the water-air ratio is increased, the operating line moves upward toward the acceleration schedule because of the increased fuel required to evaporate/melt the water/ice. The higher the operating line, the more fuel is required to run steady-state. If the steady-state requirements of the engine exceed the acceleration schedule, the engine will rollback (run-down) resulting in a thrust loss. This will cause a lack of throttle response and may cause operation below idle, leading to a rollback causing engine shutdown. Surge or combustor blow out may also occur.

5.1.2 Combustor Flameaout

Water/ice ingestion into the combustor will result in decreased burner efficiency and will eventually lead to flameout.

5.1.3 Compressor Surge

Ingestion of water will cause a loss in surge margin because of increased compressor operating line, Figure 5-2. The increase in operating line occurs because the water/hail evaporated in the combustor displaces air and acts like a throttle on the compressor. There may also be limited rematching due to energy transfer from the compressor blades to the water/hail in the compressor itself. Engine testing results have shown that the compressor surge line itself is not significantly altered by water ingestion at descent idle conditions.

5.2 PARTICLE BEHAVIOUR

5.2.1 Particle Trajectories - General Principles

This section deals very briefly with the trajectory of particles in the flow field. The flow fields within a gas turbine intake can be closely approximated using computational methods, and conventional or optical instrumentation (e.g. laser velocimetry, phase doppler particle analysis). Within this flowfield, particles enter the gas turbine and, depending on their size, either tend to follow the airflow (small particles) or behave ballistically (large particles).

Particles of interest in this study typically have the following formats:

Liquid: Raindrops, Clouds and Fog

Raindrops - can be considered as spherical (Size: from 20 μm to several mm, although in the intake they are usually broken up and smaller particles dominate);

Clouds - may contain smaller droplets and droplets in subcooled state;

Fog - is formed of submicron and micron sized droplets (see also Chapter 4).

Solid: Snow, Hail, Graupel

Snow - If the freezing is slow and gradual, ice is in crystalline form, more or less regular and complex (see Figure 5-3). Snow can be "dry" or "wet" (containing some liquid).

Hail, Graupel - If the solidification is fast (or from subcooled droplets), ice is in the form of an amorphous mass, with sometimes

crystalline tails (see Figures 5-3 and 7-15). Size: from 0.5 to several cm.

5.2.1.1 ***Small drops (condensation fog)***

These droplets are submicronic and closely follow the air flow. Only a few of them are captured by the curved surface of blades (see Figures 5-4 and 5-5).

5.2.1.2 ***Large particles (drops, hail)***

In the domain of interest for gas turbine applications, the motion of a particle (mass m) is governed by the classical law - Equation 5-1. (For very large particles, gravity must be taken into account.)

$$F_D = m \frac{dV_p}{dt} \qquad 5\text{-}1$$

where F_D = drag force exerted by the surrounding medium,
V_p = relative velocity of the particle.

The drag force F_D may be expressed in terms of a drag coefficient C_D:

$$F_D = \frac{1}{2} C_D \pi \frac{D_w^2}{4} \rho_a (V_a - V_w)^2 \qquad 5\text{-}2$$

where V_a = air velocity,
V_w = droplet velocity
ρ_a = density of air.
D_w = diameter of drop

C_D depends on a number of factors. In case of spherical drops bigger than 10 μm in air, C_D is sufficiently well approximated, depending on Reynolds number (Re) of the droplet, by the following relations:

$$C_D = 24 / Re \qquad Re < 1 \text{ (Stokes law)} \qquad 5\text{-}3$$

$$C_D = (21.64/Re) + 2.36 \qquad 1 < Re < 10 \qquad 5\text{-}4$$

$$C_D = (21.942/Re^{.718}) + .324 \qquad Re > 10 \qquad 5\text{-}5$$

$$\text{where} \quad Re = \frac{\rho_a V_p D_w}{\mu_a}$$

The effect of droplet distortion due to aerodynamic forces can be approximated by multiplying C_D in Equation 5-2 by (Reference 5.2):

$$1 \quad \text{for} \quad We/\sqrt{Re} = 0$$

and $$1.7 \quad \text{for} \quad We/\sqrt{Re} = 0.79$$

with linear interpolation between these values.

The droplet trajectories can then be calculated by solving the equation of motion once the flow field (V_a) is obtained. These methods ignore the influence of the droplets on the airflow, which is reasonable when the droplet mass flow is considerably less than that of the airflow.

The knowledge of droplet trajectories helps to predict the deposition rate on internal surfaces and the efficiency of internal separators. Two examples are given in Figure 5-4 which show that droplets bigger than 70 μm are captured by blades and form liquid films. Part of the liquid films formed by the deposition are thrown off in the air flow, for example at the trailing edge of blades, in the form of bigger drops ($>$ 20 μm) (Figure 5-5), but the major part of the liquid water will be found in the form of films at the inner casing. Because the heat exchange and mass transfer between the air and the liquid surface are low compared to the resident time (fraction of second), it is possible that a large part of the liquid will pass through the compressor and into the combustion chamber, where it can be responsible for flameout in the case of heavy rain (concentrations $>$ 5 - 10 g/m^3).

External flow calculations have been carried out to predict the water concentration zones. This knowledge allows improved design of de-icing and anti-icing devices as well as the positioning of the measuring probes (temperature and pressure) in areas of the engine less affected by water shedding.

5.2.2 Rain Droplet Disintegration

The aerodynamic process for droplets and air entering the inlet results in a relative velocity between the droplets and the air. The relative velocity causes a viscous drag force which tends to break the original droplets into smaller droplets when the shear force becomes sufficiently large to overcome the surface tension force holding a droplet together. The general droplet break up model also includes another mode whereby internal viscous forces, due to droplet deformation, exceed surface tension forces causing rupture. (see e.g. References 5.3 to 5.22)

5.2.2.1 ***Droplet Breakup Model*** - The rain droplet breakup model is based on the experimental

quantification of the hypothesis that break-up during flight conditions occurs due to external viscous drag forces overcoming surface tension forces. Internal viscous forces, tending to disintegrate the droplets do not play a major role in the break-up process because long times are required. A functional expression of this hypothesis appears in Equation 5-6:

$$\frac{\text{Drag Force}}{\text{Surface Tension Force}} = \frac{C_D \rho_a (V_a - V_w)^2 A_w}{2\sigma_w \pi D_w} = \frac{C_D}{8} We \qquad 5\text{-}6$$

where

C_D = drag coefficient of water droplet
ρ_a = density of air
V_a = velocity of air
V_w = velocity of water droplet
A_w = cross sectional area of water droplet
σ_w = surface tension of water
D_w = diameter of water droplet
We = Weber Number
= $\rho_a(V_a-V_w)^2 D_w/\sigma_w$

It is noted that C_D is a function of Re for uniform drops in an airstream (e.g. Equations 5-3 to 5-5 for spherical droplets).

5.2.2.2 ***Experimental Calibration*** - To test and calibrate the rain droplet breakup model a facility was constructed at the United Technologies Research Centre (UTRC) (Reference 5.3) in which liquid water droplets were subjected to inertial and viscous forces simulating descent idle in flight conditions (Figure 5-6). The walls of the rig were designed so that the airflow would accelerate and produce a V_a-V_w for the injected droplets of the same magnitude and at the same rate as would be encountered in flight. A centrifugal compressor was used to supply airflow through the convergent test section generating velocities up to 124 m/s (408 ft/sec) at the throat. Individual water droplets were injected at the entrance to the convergent section using calibrated syringes and a pump system.

The relative velocities and rates of change in the convergent section simulated the relative velocities and the Weber numbers encountered at in-flight descent idle conditions. Photographic and video techniques were used to document and understand the breakup process qualitatively and quantitatively. A photograph and schematic of this system are shown in Figures 5-7 and 5-8. A television camera synchronized to a stroboscopic lighting system was used to photograph the droplet breakup process at specific stations along the test section. A time delay generator was used to illuminate the droplet after a precisely known time interval to enable calculation of the droplet velocity. The air velocity was measured using pitot/static pressure probes. Recorded video images, freeze frame Polaroid photographs, and an image enhancement computer system were used in the analysis.

Droplets with diameters ranging from 500 to 3000 microns were generated in the rig with throat velocities ranging from 21 to 124 m/s (70 to 408 ft/sec). The droplet position and velocity at breakup were measured as were the particle size distributions after breakup. The droplet diameter and velocity range tested encompassed most of that which would be encountered in the atmosphere during severe storms at in flight descent idle power.

5.2.2.3 ***Droplet Breakup Mechanism*** - A rapid "shear" droplet breakup process occurred for droplet diameters greater than ~ 600 microns over the entire idle descent power range. A slower shear breakup process characterized by a "bag" or "hat" formation was observed at throat velocities on the order of 45 m/s (150 ft/sec) (Figure 5-9). The shear breakup mode, depicted in Figure 5-9, and typical for inflight descent conditions, was characterized by a gradual deformation of the drop from a sphere to an irregular disk. The sides of the disk were ripped off giving the impression of a series of strings being pulled off the disk. At this stage, the mass appeared to explode into a mist of fine droplets. The measured time of the shear breakup process was on the order of 2 milliseconds. The shear breakup process observed was similar to the shear breakup process reported in the literature (References 5.3 and 5.4).

The breakup process observed during these tests was correlated with $We/\sqrt{Re}$. Figure 5-10 shows a plot of $We/\sqrt{Re}$ as a function of throat velocity. Shear type breakup occurred when $We/\sqrt{Re}$ was approximately 0.79 or greater. (Hat type breakup or no breakup occurred at much lower $We/\sqrt{Re}$ values as indicated in Figure 5-10.) It was observed that, in order for the shear type breakup to occur, it was necessary for the time rate of change of $We/\sqrt{Re}$ to be greater than approximately 30, which is exceeded in typical in-flight descent conditions.

It was noted that the 'hat' breakup mode, which occurred with lower airflow and throat velocities at $We/\sqrt{Re}$ of approximately 0.4, was more complicated and took relatively longer compared to the shear type, and only occurred when the rate of change

of $We/\sqrt{Re}$ was <30. The hat mode breakup process, shown in Figure 5-9, usually led to three large droplets with average diameters of about $D_w/3$, droplets with an average diameter of about $D_w/6$, and a spray of fine droplets.

For flight inlets, under typical rain ingestion conditions at descent idle, the rate of change of air to droplet relative velocity and $We/\sqrt{Re}$ will be such (i.e $We/\sqrt{Re} \geq 0.79$ and $\Delta(We/\sqrt{Re})/\Delta t > 30$) as to produce rapid shear breakup. Therefore the resulting smaller droplets (smaller than would result from hat mode breakup) will yield relatively lower scoop factors (see Section 5.3).

5.2.2.4 ***Droplet Velocities*** - The single droplet test data permit calculation of both the position along the duct at which breakup occurs and the droplet velocity. The droplet velocities were measured for various droplet sizes. The initial spherical droplets were deformed into disks. An appropriate drag coefficient, greater than the value for a sphere, and an adjusted diameter, to allow for the drop distortion, were calculated from the experimental data. A new drag law was derived based on these data, and was used in the CFD code to calculate the droplet Weber Number. The droplets or disks break up at the critical $We/\sqrt{Re}$ value of 0.79. The theoretical breakup distances and $We/\sqrt{Re}$ were very close to the experimental values (Figure 5-11).

5.2.2.5 ***Mean Droplet Diameter After Breakup*** - Once the condition of droplet breakup is known, one must determine the resulting droplet sizes. This can be done using the approach developed by Wolfe and Anderson (References 5.4 and 5.5) in which they use an empirical correlation for the mass mean diameter (D_{wm}):

$$D_{wm} = \left[\frac{136\, \mu_w \sigma_w^{3/2} D_w^{1/2}}{\rho_a^2 \rho_w^{1/2} (V_a - V_w)^4} \right]^{1/3} \qquad 5\text{-}7$$

The initial droplet size (D_w) is known, and the air (V_a) and water (V_w) velocities have been previously determined. The UTRC experimentally determined D_{wm} agreed well with the results of Wolfe and Anderson.

5.2.2.6 ***Droplet Size Distribution After Breakup*** - The Rosin-Rammler mean diameter ($\overline{X}$) can be determined from the mass mean diameter:

$$\overline{X} = 1.96\, D_{wm} \qquad 5\text{-}8$$

Hence, knowing $\overline{X}$ one can calculate the resulting spray distribution after breakup from the Rosin-Rammler distribution function given by:

$$v = 1 - \exp[-(D/\overline{X})^N] \qquad 5\text{-}9$$

where:

- v = mass fraction contained in diameters less than (D)
- $\overline{X}$ = Rosin-Rammler mean diameter = mean diameter at $v = 0.632$
- N = Rosin-Rammler width parameter $\cong 3.0$ based on UTRC experimental data.

Sample distributions are illustrated in Figure 5-12. The maximum droplet diameter after breakup, as determined from video images obtained from the single droplet facility, agrees very closely with the theoretical 99 percent droplet size. A flow diagram of this procedure for calculating the water droplet velocity and sizes approaching a gas turbine is included in Figure 5-13.

In summary, hat-type breakup is not typical of inflight operation at idle descent and only occurred during the test at very low speeds of less than 46 m/s (150 ft/sec) and low rates of change of $We/\sqrt{Re}$ (i.e. < 30). Shear breakup occurred at typical in-flight descent conditions, and the resulting smaller droplets are influenced to a greater extent by the aerodynamic forces imparted by the air. Therefore, concentration due to scooping during in-flight operation will be reduced. This effect is in contrast to the process of hail ingestion. Hail will not disintegrate until it hits a solid surface and the aerodynamic forces to slow it down will be much less effective. This process will result in much higher concentration factors for hail particles as they enter the inlet of the engine in flight.

5.2.3 Hail Disintegration

The analytical model which calculates trajectories and centrifuging of ingested hail requires a quantitative definition of the process of hail disintegration upon impact with a solid engine surface such as the inlet spinner or fan/compressor surface. Detailed knowledge of ice particle diameters, velocity vectors and rebound angles are necessary (References 5.23 to 5.26).

5.2.3.1 ***Experimental Quantification of Disintegration Process*** - An air cannon (Figure 5-14) has been designed by Pratt & Whitney in the USA to accelerate ice projectiles to velocities that would occur when ice is ingested into an engine in-flight. The high velocity ice particles disintegrate upon impact with a solid

surface and the process was photographed with a high speed motion picture camera; velocity of the disintegrated particles and angle of bounce were determined by analysis of the motion pictures, Figure 5-15. High resolution still camera photographs using a stop motion strobe technique were used to determine particle size distributions (References 5.24 and 5.25).

The test matrix covered the range of hail parameters expected to be encountered in flight during severe storms:

- hail size - 12.5 to 50 mm (1/2" to 2") diameter
- hail temperature - -20 to 0 °C
- velocity - 75 to 275 m/s (250 to 900 ft/sec)
- impact angle - 0 to 90°
- surface - wet, dry, rough, smooth
- engine spinner, fan blade

Different types of ice, including a layered formation (onion skin), ice with diffused air (party ice), and hard solid ice balls, were tested. The disintegration process upon initial impact, second impact and third impact was also photographed and quantified, Figure 5-16. Typical photographs of the disintegration process are shown in the following figures. Figure 5-17 depicts 90° impact on a spinner. Figure 5-18 shows a 25 mm (1 in) ice ball at 40° impact angle with views parallel and perpendicular to the plane of impact.

5.2.3.2 ***Size Distribution After Impact*** - The hail disintegration process can be characterized by the Rosin-Rammler distribution function. This function (Equation 5-9) has been commonly used to define spray droplet distributions. It has been found also to provide a very good representation of the size distribution of disintegrated ice.

Statistical correlation of the experimental data provide:

$$\frac{D_{max}}{Do} = 1.2647 + 0.16001 \ln\left(\frac{1}{V_N}\right) - 0.0796\,(Do - 1) \qquad 5\text{-}10$$

$$\frac{\overline{X}}{Do} = -0.19422 + 1.05\left(\frac{D_{max}}{Do}\right) \qquad 5\text{-}11$$

$$N = 0.40729 \exp\left(\frac{2.326\,\overline{X}}{D_{max}}\right) \qquad 5\text{-}12$$

where:

D_{max} = the maximum post impact particle size (diameter or largest lateral dimension),

Do = particle size prior to impact (diameter or largest lateral dimension),

V_N = component of impact velocity normal to surface = $V_{in} \sin \beta_{in}$,

N = Rosin-Rammler mean diameter (see Equation 5-9).

Particle size distribution effects due to all of the experimental variables were investigated. Most of the experimental parameters were not found to have a statistically significant effect. Hail size distributions were found to be primarily dependent on initial hail particle diameter and normal component of impact velocity. Analysis of the high speed motion photographs has shown that the disintegrated hail particles retained nearly all of their velocity component parallel to the impacted surface, while losing all of the normal component. This results in nearly all the energy associated with the normal impact velocity component contributing to the disintegration of the incoming particle. This effect is borne out in the statistical correlation of all the data, Equations 5-10 to 5-12, in which only the normal impact velocity and particle size are parameters.

Although particle size distributions were obtained for primary, secondary and tertiary impact data for the cannon rig tests, Equations 5-10, 5-11 and 5-12 were correlated based on the primary impact data, i.e. impacts with only a single plate.

The correlation based on a single impact can also be used to model the secondary and tertiary impact disintegration results, verifying the theoretical model regarding normal impact velocity as the energy source which disintegrates the hail particles. Figure 5-19(a to e) shows experimental data and statistical correlations of 13 mm (1/2"), 25 mm (1") and 50 mm (2") diameter hail balls impacting with various impact angles and initial velocities on primary, secondary and tertiary plates. Typical values for the size of fragments of disintegrated particles are 5.8 mm (0.23 in) for a 13 mm (1/2-in) diameter ball impacting a surface at 20 degrees at 183 m/s (600 ft/sec) (Figure 19(b)), and 10 mm (0.40 in) for a 51 mm (2-in) diameter ball at the same impact angle and velocity, (Figure 19(d)). The

comparison of the experimental data and the correlation predictions are excellent.[2]

5.2.3.3 ***Post Impact Particle Kinetics*** (References 5.25 and 5.26) - Analysis of high speed photographs from this hail cannon test showed that the disintegration process was essentially inelastic, with the rebound angle being on the order of $1^{o} \pm 1^{o}$, Figure 5-20. The shattered ice expands in a circular pattern in the reference frame moving with the ice ball. The expansion process can be evaluated from continuity considerations as ice debris on the surface is forced outward from the point of impact by the remaining portion of the ice which is still approaching the surface. Empirical results show that this is a reasonable basis for modelling the phenomenon except at the very beginning of the process. During the initial phase the surface geometry of the ice ball adds additional impulsive acceleration to the ice debris. The ice expansion velocity, (V_{exp}), in Figures 5-21(a) and 5-21(b), has been determined from geometric and continuity considerations correlated to test data:

$$V_{exp} = \frac{dr}{dt} = \left[\frac{-3V_N Y}{\sqrt{r^2 - Y^2}}\right] \qquad 5\text{-}13$$

$$\text{or} = \left[\frac{1.5 V_N r_{local}}{2a}\right]$$

whichever is larger, and where the variables are defined in Figure 5-21(a) and 5-21(b). The thickness of the debris (a) is a function of the initial ice diameter and normal velocity and, from regression analysis of test data, may be approximated by a relationship illustrated in Figure 21(c). A curve fit of available data yielded the solid curve shown in this figure. Typical values for a are 5.8 mm (.23 in.) for a 13 mm (1/2 in.) diameter ball impacting the surface at 20 degrees at 183 m/s (600 ft/sec) and 9 mm (.35 in.) for a 50 mm (2 in.) diameter ball at the same impact angle and velocity.

---

[2] Work done at Loughborough University in England confirms the small bounce angle of shattered ice, the usefulness of the Rosin-Rammler distribution function to characterize the shattered particles, and the primary importance of the initial size and normal impact velocity on the disintegrated particle distribution. (Reference 5.23)

In the stationary frame of reference, the disintegrated debris spreads out in a cone pattern dependent on the velocity of the hail stone parallel to the surface and the radial velocities of the fragments (Figure 5-21(d)). The angle of the particle trajectory in this frame of reference is determined from geometry:

$$\theta = \arctan\left[\frac{\dot{r}\sin\psi}{V_P\gamma_R + \dot{r}\cos\psi}\right] \qquad 5\text{-}14$$

where γ_R = restitution ratio = 1 for smooth surfaces.

The "spread angle" is defined as the maximum value of θ, which occurs at the maximum value of the above arctangent function, i.e.:

$$\theta_{max} = \arctan\left[\frac{\dot{r}\sin\left\{\cos^{-1}\left(-\frac{\dot{r}}{V_P\gamma_R}\right)\right\}}{V_P\gamma_R - \frac{\dot{r}^2}{V_P\gamma_R}}\right] \qquad 5\text{-}15$$

Applying the simplifying condition of uniform circumferential distribution of mass, the variation with θ can be shown to be:

$$\frac{dm}{d\theta} = \frac{\rho a r^2 \pi}{360 D_0}\left(\frac{b^2 + 2b\cos\psi + 1}{b\cos\psi + 1}\right) \qquad 5\text{-}16$$

where $b = (V_{tan}\gamma_R)/\dot{r}$

V_{tan} = velocity component parallel to surface

a/D_0 – from Figure 5-21(c)

ρ = density of ice

This relationship is plotted and compared with test data in Figures 5-21(e) and 5-21(f).

5.2.3.4 ***Low Velocity Post-Impact Bounce Angle***

At very low impact velocities ice particles and hail have been observed to "bounce". This regime occurs when the energy in the normal velocity component is not sufficient to shatter the ice (Reference 5.26).

An experiment was conducted to ascertain the conditions for which ice did bounce after impact. In this experiment hail balls were dropped from various

heights. The results of this experiment indicated that at low impact velocities, in the range of 3-6 m/s (10-20 ft/sec), ice bounced and did not shatter. At velocities above this range ice shattered (Figure 5-22).

A mathematical model has been constructed based on the experimental data and following hypotheses:

- the impact energy must exceed a certain level to shatter the ice particle,
- the impact energy is distributed across the particle surface area,
- the kinetic energy/area is proportional to ((the normal impact velocity) / dia)^2.

The velocity above which ice shatters and below which it bounces is characterized by Equation 5-17.

$$Vc^2 D_o = 18.23 \qquad 5\text{-}17$$

where Vc = velocity below which ice will bounce.

A plot of Equation 5-17 is shown in Figure 5-23 over a broader range of particle size and velocity. The slope of the curve in Figure 5-23 can be derived on the basis that the kinetic energy required to break the bonds holding the ice together is proportional to the cross sectional area of the ice particle.

The ice drop tests also provided data to determine the ratio of rebound to impact velocity and bounce angle for instances where ice did not shatter. The coefficient of restitution is defined as:

$$COR = f[(V_N, \text{rebound})/(V_N, \text{impact})] \qquad 5\text{-}18$$

and is characterized by a normal distribution about an average value defined by Equation 5-19, Figure 5-24.

$$\log COR = -10.0\,(V_N/Vc) \qquad 5\text{-}19(a)$$

$$\text{for } .1 > V_N/Vc > 0$$

$$\log COR = -2.50\,(V_N/Vc) - 0.75 \qquad 5\text{-}19(b)$$

$$\text{for } 0.5 > V_N/Vc > 0.1$$

$$\log COR = -2.0 \qquad 5\text{-}19(c)$$

$$\text{for } V_N/Vc > 0.5$$

The hail breakup model is used in trajectory and centrifuging calculations for the inlet spinner and fan/compressor to determine the path of ingested hail and disintegrated particles as they progress into the engine core.

5.3 COMPONENTS

5.3.1 Inlet

5.3.1.1 *Scoop Factor*

Turbojet and turbofan inlets are designed to provide minimum inlet air spillage and inlet cowl drag at cruise conditions. For subsonic transport aircraft, this requires that the inlet area be sized to provide a mass flow ratio, Ao/Ai, Figure 5-25(a), of approximately 0.8 to 1.0 in the cruise operating region. At lower power conditions, the engine flow is reduced and the air will undergo a larger diffusion process to enter the inlet. This process proceeds according to the requirements of fluid dynamics and potential flow theory. The resulting change in the entering streamline is shown in Figure 5-25(b) for a high power design condition relative to a descent idle condition in a high bypass turbofan. The descent idle mass flow ratio is approximately 0.4 for a typical 5:1 bypass ratio design.

Rain and hail entering the engine inlet during flight will do so ballistically while the air will enter according to the laws of aerodynamics. Velocities in the flow field are calculated using a 3-D potential flow solver considering engine geometry, flight condition and engine power setting (airflow). The rain and hail particle trajectories are determined by solving the equation of motion, Equation 5-2 above, once the flow field has been determined. Drag coefficients vary with particle Reynolds number as discussed in Section 5.2.1 above. The inlet capture area of the water will be the geometric area of the inlet. A concentration effect or "scooping" occurs because the relative capture area of the water/hail (Ai) is larger than that of the airflow (Ao) (typical condition during subsonic cruise descent). The concentration effect becomes larger at reduced power (Figure 5-25).

Military aircraft and some commercial transport aircraft operate both subsonically and supersonically. The description of subsonic flow just above adequately describes a typical military transport. However, for transport, tactical, and strategic aircraft which operate both subsonically and supersonically the

characteristics of the inlet effects on flow are somewhat different.

Consider the simplified F-15 inlet configuration in Figure 5-26(a). The inlet may be considered to be designed for operation over an angle-of-attack (α) range from less than 0 to greater than 45-degrees and for operation up to Mach number 2.5. The scoop factor at low subsonic, high α conditions for such an inlet (Figure 5-26(b)) is different from (and generally larger than) that of the subsonic transport. Further, the presence of inlet bleeds and bypasses and a long inlet duct (approximately 10 engine diameters) provides a qualitative and quantitative change from the subsonic transport case by providing surfaces to impact and channel/remove the incident water.

When an inlet is operated at supersonic speeds, whether internally or externally, shock waves will generally be present. Velocity downstream of a shock wave will be lower than upstream. Static pressure will be higher and, if the shock wave is oblique, the direction of the velocity vector will undergo a virtually instantaneous change. The resultant differential velocity between a droplet and the airflow will then operate to deform and disintegrate the drop via the mechanism discussed above.

Effect of engine rating and flight velocity on scoop factor - One of the primary reasons why the greatest threat to engine operation during inclement weather occurs at low power conditions, particularly descent idle, is the increased concentration effect. Typical effects of power, aircraft velocity and altitude on "scoop factor" are shown in Figure 5-27(a) for a representative high bypass engine at descent idle conditions. Decreasing the speed of the aircraft and/ or increasing engine power reduces the scoop factor.

5.3.1.2 *Water Collection on the Spinner*

Water impacting the spinner will form a film which will move in response to aerodynamic and centrifuging (if the spinner rotates) forces on the film, Figure 5-27(b). These effects and methods for quantification are discussed later in this chapter.

5.3.1.3 *Hail*

The cowl inlet lip and the spinner geometry also have important effects on core water concentration for hail ingestion because of modified trajectories of disintegrated hail particles after impact. Bounce angles of disintegrated hail particles are generally low (see Section 5.2.3.3); inlet lip and spinner shape can have a significant impact on whether the particles are "bounced" into the core or harmlessly into the bypass duct.

5.3.2 Fan and Splitter

5.3.2.1 *Overall Inlet/Fan Scoop Factor*

Hail particles in severe hail storms are quite large and are influenced very little by local air velocities. Thus their trajectories are almost ballistic and nearly all hail particles inside the splitter radius could be scooped through the fan and into the engine core. See Figure 5-28.

Rain droplets behave differently. First, they are generally smaller than hailstones and therefore somewhat susceptible to air motion. Secondly, as they approach the engine they experience drag forces which tend to flatten the droplets into disks making them even more susceptible to air motion. Thirdly, as drag forces increase, most droplets break up into many smaller droplets which are significantly affected by air motion. This process is depicted in Figure 5-28 where the water droplet moves almost ballistically until the breakup point. It then disintegrates and tends to flow towards the outer fan radius and into the fan bypass duct. The path shown after breakup in this example represents an average droplet. The trajectory/centrifuge model discussed in this chapter actually tracks a large number of droplets, one at a time, from the breakup point. Figure 5-28 defines a total inlet/fan core scoop factor which is a measure of how much the ambient water/air ratio is concentrated at the inlet to the low pressure compressor. This parameter does not account for the effects of fan and spinner centrifuging and the bouncing of hail which will be discussed below.

Hail is much more likely to penetrate into the engine core than rain. Several factors contribute to this. First, more hail is scooped into the core initially. Secondly, hail is not slowed significantly by the air as it enters the engine which gives it a much better chance of passing through the fan blades, an effect due to the relative velocities of the hail particle and the rotating fan blade. Finally, even if the hail strikes the fan, it does not centrifuge radially outward to the bypass duct nearly as quickly as water because hail maintains its axial velocity (component parallel to the surface). Most of the rain forms a liquid film on the fan surface and loses most of its axial velocity. The fan imparts about the same tangential velocity to both rain and hail, so water which moves slower axially is more likely to centrifuge into the duct.

An effective way to remove a sizable amount of hail from the core is to optimize the spinner shape to deflect hail upon impact directly towards the fan duct. Engine designs where the LPC inlet is completely "hidden" behind the spinner provide a natural ballistic path for hail to take into the fan bypass duct.

5.3.2.2 ***Fan Centrifuging***

The relative angle of rain or hail particles approaching the fan (or any compressor blade) is most important for centrifuging effects, Figure 5-29. This is the angle of the water or hail particle approaching the fan as seen by an observer on the fan blade itself. This angle determines the likelihood of the particles hitting the fan or passing through. Particles with high axial velocities, such as hail which has not been slowed down by air drag, are more likely to pass through the fan without being struck by the blade surface.

The forces imparted to the rain/hail particles by the fan are shown in Figure 5-30. Part of the rain striking the surface will form a film. The film will move radially outward along the blade under the influence of a centrifugal force component. Its axial velocity will be slowed by a surface drag component. There will be a Coriolis force component which tends to move the film toward the rear of the blade. The force balance is defined in Equation 5-20.

$$F_{\text{Acting on the Film Element}} = F_{\text{Centrifugal}} + F_{\text{Surface Drag}} + F_{\text{Coriolis}} + F_{\text{Air Drag}} \qquad 5\text{-}20(a)$$

$$F_{\text{Film}} = \left(\rho_w \delta_{\text{Film}} \text{Surface Area} \frac{U^2}{r}\right) - \left(C_D \text{Surface Area} \frac{\rho_w V^2_{\text{Film}}}{2}\right) \qquad 5\text{-}20(b)$$

$$A_{\text{Film}} \cong \frac{U^2}{r} - \frac{C_D}{\delta_{\text{Film}}} V^2_{\text{Film}} \qquad 5\text{-}21$$

where:

ρ_w	=	film density
A_{Film}	=	film acceleration
V_{Film}	=	film velocity
r	=	radius of fan element
U	=	fan surface rotational velocity
C_D	=	drag coefficient of water on plate
δ_{Film}	=	film thickness which will be calibrated from engine experimental testing with water ingestion.

$$C_D/\delta_{\text{Film}} = \text{film thickness parameter} \qquad 5\text{-}22$$

For hail, the surface drag is $\cong$ 0, and

$$A_{\text{Ice}} \cong U^2/r \qquad 5\text{-}23$$

5.3.2.3 ***Engine Tests to Calibrate Fan Centrifuging***

Water ingestion tests were run with a 289 kN (65,000 lb) thrust class high bypass ratio engine to determine the effects of ingesting large amounts of water on engine operability (Reference 5.27). Information obtained for these tests was used to help calibrate trajectory/centrifuging/and engine cycle match mathematical models. In addition to the basic engine performance and operability characteristics with water ingestion, the test program was designed to supply modelers with needed information for determining the following:

1. The effectiveness of the spinner in centrifuging water.
2. The effectiveness of the fan in centrifuging water.
3. The effectiveness of the LPC splitter spacing (axial) on the amount of water ingested into the core.
4. The effectiveness of the LPC stability bleeds in moving water out of the core.
5. The effectiveness of spray nozzle experimental configuration to deliver water to the engine core.

The water rig used for this test included 17 spray nozzles directing measured quantities of water into the inner and outer diameters of the fan (Figure 5-31). Emissions probes at the primary exit and chemical analysis of the exit gas flow, were used to determine core water content. Videos of the water film development on the fan blades were taken through windows in the outer fan case.

Analysis of the test data indicated that approximately two-thirds of the water entering the inlet was centrifuged into the fan duct at descent power levels (more at higher power) (Figure 5-32).

Analysis of the emission and photographic data led to the following conclusions:

1. Approximately 70% of the water impacting the fan blade formed a film; 30% "bounced" at low angles of approximately 1° (Approximately the same as hail in Figure 5-20).
2. The film thickness parameter (C_D/δ) is a function of the available surface for the film formation as shown in Figure 5-33.
3. The film left the fan trailing edge in droplets greater than 2500 microns.

5.3.2.4 ***Effect of Splitter Gap Spacing***

Water centrifuged by the fan will tend to leave the fan

trailing edge moving radially outward toward the bypass duct. Very close proximity of the LPC splitter to the fan trailing edge can reduce the capability of the fan to centrifuge water into the bypass duct, but typically it is remote enough to have little to no influence.

For the engine research program described here, testing was done with the splitter 62.7 mm (2.47 in) and 26.7 mm (1.05 in) from the fan trailing edge, as shown in Figure 5-34. This change had no impact on the amount of water entering the engine core as determined by measurement of core water exiting the turbine and use of turbine exit chemistry. A gap between fan and splitter of less than 25 mm (1") can be expected to increase core water air ratio because centrifuged water leaving the fan trailing edge will impact the splitter and not enter the bypass duct.

5.3.3 Low and High Pressure Compressors

5.3.3.1 *Compressors*

Trajectories of rain and hail through the low and high pressure compressors are governed by the same physical and geometric considerations described previously for the fan. Engine processing of rain and hail is primarily a mechanical phenomenon until a phase change takes place.

Computation of rain and hail trajectories through the fan and low compressor may be done using a model which contains information regarding geometry and operating conditions of the engine, and applies rain/hail disintegration effects described earlier in this chapter. A representative plot, showing computed trajectories of ingested hail particles, is shown in Figure 5-35 (Reference 5.2).

At descent idle operating conditions, most of the rain/hail ingested into the core, which is not ejected through the stability bleed ports, will pass through the compressor without vaporizing. The mechanical processing of the ice/water by the compressor system will not cause significant changes in dry compressor aerodynamic efficiency or surge line. Figure 5-36 shows a comparison of measured high compressor operating line shift for an engine test of water ingestion with the calculated shift from a cycle match computer simulation for water vaporized in the combustor. The measured data are in agreement with the calculation confirming that most of the water passed through the compressor and evaporated in the combustor.

Compressor surge margin during rain/hail ingestion at descent operating conditions can be determined on the basis of ordinary steady-state dry compressor maps and matching effect due to vaporizing water/hail in the burner.[3]

5.3.3.2 *Stability Bleed Ports*

Large amounts of rain/hail which pass through the low compressor are ejected from the core through open stability bleed ports at descent idle conditions. Engine and rig tests were run to quantify the effectiveness of the bleed ports to remove rain and hail and to ensure that blockage of the ports by icing did not occur or interfere with bleed effectiveness.

5.3.3.2.1 *Water Removal Through Bleed Ports*

The effectiveness of the bleed system to remove water from the core was quantified for a high bypass engine. The bleed design is fully annular and modulated between the fully open and closed position depending on power.

Engine water ingestion tests were run with the bleed closed and open various amounts. The amount of water exiting through the bleed was determined by measurement of the difference in water entering and exiting the core. The test results indicate that the bleed was very effective in removing water from the core, Figure 5-37. Much of the water entering the low compressor was centrifuged to the outer radius and left the core when the stability bleed is partially opened.

5.3.3.2.2 *Hail Removal Through Bleed Ports*

Similar engine testing as described above for liquid water can also be done using injected ice to determine

---

[3] At conditions (particularly high power) it has been reported (Reference 5.28) on the basis of test data analysis that sufficient energy can be imparted by the compression system (mechanical and aerodynamic) to evaporate much of the water/hail before it reached the combustor. The conditions may be significant during a transient accel maneuver and may result in changes in compressor stage matching and adverse time dependent heat transfer phenomena.

During the period required for the compressor to reach thermal equilibrium with the ingested water/ice (on the order of 30 seconds) the temperature of the compressor case declines and the portion of water/ice evaporated in the compressor is reduced which causes more fuel to be required to maintain power. This effect has been cited to be a potential cause of engine shutdown due to rollback if required to run fuel margins are insufficient or to burner blowout if combustor efficiency margins are insufficient.

In any case, successful operation of the engine for a period of approximately one minute subsequent to a slam accel and decel with water ingestion clears the engine of problems due to above described effects.

the effectiveness of the engine in removing hail through the bleed ports. An improved understanding of the physics of the process and an equally valid certification of a particular bleed system design can be obtained using rig testing in conjunction with trajectory and hail disintegration modeling.

A rig was constructed to deliver crushed ice to the engine bleed and manifold system hardware in a similar manner as would occur in the engine operating in-flight at descent idle power. A schematic of the rig is shown in Figure 5-38. A centrifugal ice crusher/ accelerator supplied the required quantities of ice to the rig. The ice particles were further accelerated by an aerodynamic ejector system to velocities which would occur at the bleed location in the engine. Air was introduced into the bleed manifold test section to simulate air relative to ice velocities. A vacuum source was used to simulate the pressure drop across the bleed manifold as would occur in flight. The tested bleed manifolds were sections of actual engine hardware.

Tests were run with the bleed rig to determine the effectiveness of the bleed system to remove ice particles traveling along the bleed case wall. The rate of hail ingestion was varied over a range simulating approximately 0.6 to 2.3 times the amount to be expected in the engine during a 10 gm/m^3 hail storm. The measured effectiveness of the bleed system to remove hail remained constant at about 72%, Figure 5-39. This result demonstrated that particle to particle interaction was not significant. The tests were run with ice particles and air conditions similar to those which would occur in the engine at descent idle during severe storms with no bleed clogging (Reference 5.26).

5.3.4 Combustor

Nearly all of the water or hail ingested into the core/HPC at descent idle conditions will pass into the combustor in liquid or solid phase. Fuel requirements measured during engine test are consistent with evaporation of water and measured reduction of combustor efficiency (Figure 5-40(a) and Reference 5.29). The ice and water will approach the flame region in the burner and be evaporated. This process will cause a decrease in flame temperature which decreases combustion efficiency. Sufficiently large amounts of water will cause the burner to "blow out".

The effect of water evaporation in the combustor was measured during water ingestion engine testing. Combustion efficiency decreased with increasing water concentration as shown in Figure 5-40(b). Data from combustor rig testing with water, also shown on Figure 5-40(b), demonstrate that flameout is associated with reductions in burner efficiencies of approximately 40%. This efficiency level at flameout is consistent with typical dry combustor operating limits. Hail would be processed similarly except it would require more energy for the same weight of water because of the additional heat of fusion required for melting the ice particles.

5.3.5 Turbines and Nozzles

Core water and ice are evaporated in the combustor. They pass through the turbines and nozzles as water vapour. The effects on the engine operability and performance due to processing by these components is benign and is best evaluated by treating the water vapour as an additional component in the gas mixture as described in Chapter 3 of this report.

5.4 ENGINE

5.4.1 Controls

The impact of rain entering the engine can be significant. References 5.30 and 5.31 detail the results of an investigation of compressor stalls which occurred while climbing during rainstorms. The in-service flight data showed a shift in the fan-to-core speed relationship just prior to a stall. During subsequent water ingestion testing it was discovered that engine stalls occurred only at low water flow rates, corresponding to light rain conditions, and much high water flow rates were tolerated easily. The fan-to-core speed shift was explained when it was discovered that the variable compressor stator vanes were tracking substantially more open than the desired schedule which resulted in a loss of stall margin. See Figure 5-41.

This stator tracking problem was traced to errors from the compressor inlet temperature sensor as a result of water droplets impinging on its coils. The resulting temperature error was often in excess of 22°C (40°F) relative to the air temperature at the compressor inlet. This caused an open shift in the variable stator position which, in turn, resulted in a stall. At the higher water flow rates the booster discharge air was cooled by evaporation so that the difference between the wet sensor temperature and booster air temperature was relatively small. At lower water flow rates the

booster discharge air was cooled very little so the difference between the wet sensor and booster discharge air temperatures was large, see Figure 5-42.

The problem was solved by designing a rain shield to reduce the amount of rain droplets impinging on the temperature sensor.

Other problems with engine controls have resulted from the blocking of pressure sensors and lines with water or ice. In order to prevent these types of problems experience has shown that careful attention is required in the design and placement of the control sensors and the associated sense lines.

Because of their destabilizing effect, rapid throttle transients should be avoided when operating during conditions of severe water ingestion. In many instances, aircraft systems which provide feedback to the engine throttle may lead to severe engine transients. Such systems might include the use of the aircraft auto throttle system to control airspeed, particularly under severe inclement weather conditions, or the use of an automatic terrain-following control system during low level penetration missions. In both of these systems rapid throttle dithering occurs. When the throttle advances, the engine operates on the acceleration fuel schedule consuming a considerable amount of stall margin. This can result in an engine stall if the ingested water has affected the compressor stage matching or stator scheduling. Likewise, when the throttle is retarded there is a rapid reduction of combustor fuel flow, pressure and temperature, all of which aggravate burner stability and, when combined with the adverse effects of water ingestion, can result in burner blowout.

Control features that lead to favorable operation during water ingestion are:

1. Increasing engine speed during descent, which results in higher engine airflow thereby reducing the ingested water-air ratio. This often happens automatically by activating the anti-icing system.
2. Increasing the quantity of compressor bypass bleed airflow, which is an effective way of removing core water.
3. Sector burning in the combustor, which increases the local temperature rise at the active fuel nozzles. This improves the combustor resistance to blowout as well as reducing harmful emissions.
4. Activating a continuous ignition system, which facilitates the automatic relight sequence if the engine does blow out.

5.4.2 Starting

Inflight airstarts are often a problem when the engine is ingesting water. This is particularly true in modern high-bypass-ratio engines where a considerable amount of core stream energy is used to drive the bypass stream. Figure 5-43 shows the impact of increasing amounts of water ingestion on engine starting characteristics. The effect of ingesting even a low quantity of water is to increase significantly the time required to start an engine. A moderate amount of ingested water often results in hung starts which can only be cleared by reducing the water flow rate. Increasing the quantity of ingested water even further will create conditions where no combustor ignition is achieved. Sometimes with a hung start the compressor is operating with a rotating stall and will not accelerate after the water is shut off. When this happens, the exhaust gas temperature rapidly increases and will severely overtemperature the turbines. This situation requires rapid shut off of the engine fuel supply to prevent extensive engine damage.

5.4.3 Time Dependency

While an engine's tolerance to rain ingestion does not appear to be significantly time dependent, the same may not be true for hail ingestion. Figure 5-44 shows a comparison of the water ingestion capability for rain and hail (Reference 5.32). Because of the vastly improved effectiveness of the fan in centrifuging rain water into the bypass stream, the engine will tolerate two to six times more rain than hail. As explained in Section 5.3.2, most of the rain will impact on the spinner or the fan, while a significant amount of hail will pass between the fan blades. This figure also shows that the hail ingestion capability can be a time dependent phenomenon which results if ice builds up in the bleed air passages and cavities. The ice accumulation is a function of engine geometry, ambient temperature, fan and boost temperature rise, and exposure time. This figure shows hail ingestion capability can be dependent on ambient temperature, probably because the warmer ice produces more slush with a greater tendency to clog the passage ways.

5.4.4 Thrust Change

No measurable reduction in thrust during operation with rain/hail ingestion relative to dry operations at similar engine pressure ratio (EPR) has been observed or would be expected. Other control modes which result in an EPR change would also result in a commensurate thrust change (see Table 5-2).

5.4.5 Process to Determine Engine Core Water Concentration and Operability Characteristics

Analytical models calibrated by engine and rig test

results are employed to predict the in-flight rain/hail effects of engine designs so that an engine will meet qualification requirements.

The water/hail concentration model is assembled using the ideas, algorithms, and data described earlier in this section. The model is a Monte Carlo simulation that tracks individual particles as they enter the engine, pass through the fan and enter the engine core or fan bypass duct. It also calculates the fraction of water/hail residue eliminated from the core through the various bleeds. Engine altitudes, flight Mach number, power setting and mechanical configuration are simulated to determine their effects on water concentration in the core. Particles are tracked one at a time. The solution is complete when water concentration converges to a constant value. A cycle match simulation is used to calculate engine performance and component match shifts due to aerothermodynamic effects of core water processing.

The various components of the model are shown schematically in the Process Chart, Figure 5-45, and are described below.

1. Atmospheric Conditions (Threat)

Concentrations of rain and hail in the atmosphere which would occur once in 100,000,000 flights have been estimated and are presented in Chapter 2 of this document (References 5.17, 5.33 and 5.34). The operating conditions for maximum vulnerability for turbofan engines in a rain storm occur at 6000 m (20,000 ft) under idle power during descent with 20 gm/cubic metre in the atmosphere. For hail, the maximum vulnerability condition occurs at 4500 m (15,000 ft) with 10 grams/cubic metre hail in the atmosphere.

Statistical distribution functions for rain droplet diameters and hail particle diameters are also provided in Chapter 2.

2. Entry Stream Tube

The capture stream tube for the flow entering the engine is calculated using a 3-D potential flow solver considering engine size, inlet geometry, flight altitude and Mach number and engine power setting/airflow.

3. Fan/Spinner Aerodynamics

The fan-spinner aerodynamics are computed using an axisymmetric 2-D analysis which accounts for capture stream tube geometry, engine nacelle geometry, fan geometry, rotor speed, airflow and bypass ratio.

4. Rain and Hail Trajectories

Rain/hail particle velocities are tracked as they enter the inlet stream tube and go into the engine. The velocities relative to the air are calculated using appropriate drag coefficients, see Section 5.2.1. Disintegration of the rain into smaller droplets will occur and is governed according to the algorithm discussed in Section 5.2.2. No disintegration of hail will occur until a particle impacts a solid surface. Having calculated the rain/hail particle trajectories in the inlet the model proceeds to calculate the relative fractions of rain or hail impacting the fan or passing through.

5. Centrifuging

When rain impacts the fan or spinner it tends to form a film and be pumped radially outward. The centrifuge model is described in Section 5.3.2.2 and accounts for centrifugal, air drag and surface drag forces on the water film to calculate its trajectory and thereby the portion of the film centrifuged into the bypass duct.

When hail impacts a surface it disintegrates into small particles which lose nearly all of their velocity normal to the solid surface. The disintegrated residue proceeds along the surface at an average velocity nearly equal to the component parallel to the surface at impact. Therefore, much less centrifuging of hail into the bypass duct, relative to water, occurs. Algorithms to quantify and calculate the hail disintegration process, including small bounce and spread angles, are presented in Sections 5.2.3 and 5.3.2.2.

6. Trajectories through the Low Compressor/Fan Booster

Calculation of trajectories through the low compressor fan booster are handled in a similar way as through the fan.

7. Water Fraction Entering Core

The model calculates the fraction of rain/hail entering the engine core from the low compressor considering splitter geometry.

8. Bleed Port Effectiveness

Much of the rain/hail which enters the core will be concentrated near the flowpath outside diameter along the case walls. A significant portion of the rain and hail will be ejected from the core into the bypass duct through open intercompressor stability bleed ports. The amount of rain/hail ejected from the core bleed ports is design dependent, and hence engine model specific, and must be determined by engine and/or rig test.

Engine and rig calibration results for typical bleed designs are provided in Section 5.3.3.2.

At this point the model will have calculated the total water concentration entering the high compressor.

9. Effect of Water in Core

Computation of the water/ice behaviour in the

core compressor follows the principles applied in the low compressor. Some water/ice is ejected through the high compressor bleeds and is calculated based on engine test calibrations. Some water/ice may evaporate in the rear of the high compressor but the amount is small at low power and determined from engine calibration. Computation is repeated for individual particles; the solution is complete when water/ice concentrations at given engine stations reach a non-time dependent value.

Engine testing must be done to ensure that the engine can tolerate with margin the calculated levels entering the core.

The analytical model has been used to calculate core water concentration for engines with various bypass ratios at in-flight operating conditions. A plot of core-to-ambient water concentration ratio vs. engine design bypass ratio is shown in Figure 5-46 for both rain and hail ingestion. There is a general trend of increased core water concentration with increasing bypass ratio. The core concentration of hail is 2 to 3 time larger than for rain. These results are illustrative only and the core concentration for a particular engine will be greatly dependent on specific design features.

Figure 5-47 shows relative core-to-ambient water concentration as a function of power setting for a mid-bypass ratio engine. Fan centrifuge capability is decreased at low power. Hail is 2 to 3 times more concentrated in the core than rain at all power levels.

5.5 CONCLUSIONS AND RECOMMENDATIONS

Engine power loss events have occurred in gas turbine engines during operation in severe rain and hail storms. To guard against this type of event occurring in the future, procedures relating to design, analysis and test are recommended to ensure the engine is capable of acceptable operation throughout its flight operating envelope when subjected to maximum rain and hail concentrations expected to occur as defined in Chapter 2.

(i) Critical Point Analysis - Evaluation of engine operation throughout its flight envelope should be done to determine operating conditions for which minimum margins will exist during rain/hail ingestion. This analysis should address atmospheric conditions (see Chapter 2), water concentration in the engine core (analytical/test methods described earlier in this chapter), and required engine operating levels including power setting, bleed/horsepower off-takes and control logic. Among operability conditions to consider are margin for rollback, compressor surge, combustor blowout and margin for acceleration.

(ii) Analysis - Two types of analytical model are recommended for the analysis:

1. a cycle match analytical model capable of calculating engine aerothermodynamic and performance parameters throughout the flight envelope,
2. a trajectory/centrifuge model which calculates the concentration of rain and hail at various stations within the engine and core as the engine passes through a rain/hail storm. This is a quasi-steady model regarding engine performance and employs a Monte Carlo technique to converge on a solution for core water concentration.

(iii) Engine/Rig Test - Both models in (ii) must be calibrated for a particular engine by means of engine testing. Methods to calibrate cycle match analytical models are well known and have not been discussed here. Transient models can be useful, however they are not necessary if the ingestion testing is of sufficient time duration so that the engine reaches a steady operating condition and transient testing is done to verify acceleration capability.

The trajectory/centrifuge model is calibrated using data from rig and engine ingestion tests. A full scale engine water ingestion test must be run to calibrate the model. An engine hail ingestion test can also be run, however alternate equivalent methods employing rigs described earlier in this chapter may be used. These methods quantify differences in how the engine processes hail relative to rain, e.g. shattering upon impact, post impact trajectory, ejection through bleed ports.

(iv) Engine Testing to Assure Operability Margins - The particular engine model must be tested with water/hail ingestion to ensure that sufficient margins exist to preclude adverse operability events in-flight at critical points. Sea level testing to determine rollback margin, compressor surge margin, combustor blowout margin, and acceleration capability must be done. Rig testing can provide an alternate equivalent method to quantify differences for hail as above. The measured margins at sea level are extrapolated to critical point

flight conditions using the cycle match and trajectory/centrifuge models. Sufficient margins must exist at the critical in-flight operating conditions to preclude adverse operability events for the atmospheric threat weather conditions defined in Chapter 2.

Table 5-3 summarizes the capabilities of currently recommended practices to measure the effects of rain and hail on engine performance and operability. Although analytical methods are combined with physical testing to ensure high confidence operability, there are still several areas in which the confidence on the assessment of performance effects is low. Recommendations that could lead to improvements in assessment practices are given in Chapter 9.

5.6 REFERENCES

5.1 Alge, T.L., and Moehring, J.T., *Modern Transport Engine Experience with Environmental Ingestion Effects*, AGARD Conference Proceedings 558, pp.9-1-9-8, November, 1994.

5.2 Pratt & Whitney Internal Research by Kent Lyons.

5.3 Kennedy, J.B. and Roberts, J., *Rain Ingestion in a Gas Turbine Engine*, Presented at ILASS-AMERICAS Institute of Liquid Atomization and Spray Systems, 4th Annual Conference, Hartford, USA, pp 154-186, May, 1990.

5.4 Wolfe, H.E., and Anderson, W.H., *Kinetics Mechanism and Resultant Droplet Sizes for the Aerodynamic Breakup of Liquid Drops*, Aerojet-General Corporation Report 0395-04(18)SP, April, 1964.

5.5 Anderson, W.H., and Wolfe, H.E., *Aerodynamic Breakup of Liquid Drops, Part 1, Theoretical*, Proceedings of 5th International Shock Tube Symposium, White Oak, pp 1145-1152, 1965.

5.6 Dickerson, R.A. and Coultas, R.A. *Breakup of Droplets in an Accelerating Gas Flow*, AIAA 66-611, June 13-17, 1966.

5.7 Howarth, L., *Modern Developments in Fluid Dynamics, High Speed Flow*, Vol.2, p.722, Oxford University Press, 1953.

5.8 Bond, W.N. and Newton, D.A., *Bubbles, Drops and Stoke's Law*, Phil. Mag., Vol. 5, p. 794, 1928. Phil Mag. Vol.5, p.794, 1928.

5.9 Hanson, A.R., Domich, F.G., and Adams, H.S., *An Experimental Investigation of Impact and Shock Wave Breakup of Liquid Drops*, Report 125 U. of Minnesota, June, 1956; also Phys. Fluids, Vol.6, p.1070, 1963.

5.10 Hanson,A.R. and Domich, F.G., *The Effect of Liquid Viscosity on the Breakup of Droplets by Air Blasts - A Shock Tube Study*, Report 130, U. of Minnesota, June 1956; also Phys. Fluids, Vol.6, p.1070, 1963.

5.11 Ingebo, R.D., *Drag Coefficients for Droplets and Solid Spheres in Clouds Accelerating in Airstreams*, NACA TN 3762, Sept. 1956.

5.12 Institute of High Speed Mechanics, Reports of the Inst. of High Speed Mechanics, Tohoku, University Sendai, Japan, Vol.53, ISSN 0370-5315, 1987.

5.13 Kissel, G.J., *Rain and Hail Extremes at Altitude*, AIAA 79-0529, presented at the AIAA 15th Annual Meeting and Technical Display, Washington, USA, Feb. 6-8, 1979.

5.14 Lane, W.R., *Shattering of Drops in Streams of Air*, Ind. Eng. Chem., Vol.43, p.1312, 1951.

5.15 Morrell, G., *Critical Conditions for Drop and Jet Shattering*, NASA TN-D-677, Nov., 1960.

5.16 Mugele, R.A. and Evans, H.D., *Droplet Size Distributions in Sprays*, Ind. Eng. Chem., Vol.43, p.1317, 1951.

5.17 Murthy, S.N.B. (Assisted by A.J. Mullican), *Effect of Heavy Rain on Aviation Engines*, AIAA 89-0799, presented at the 27th Aerospace Sciences Meeting, Reno, Nevada, USA, Jan. 9-12, 1989.

5.18 Rabin, E. and Lawhead, R., *The Motion and Shattering of Burning and Non-Burning Propellant Droplets*, AFOSR TN-59-129, Rocketdyne, March 1959.

5.19 Kennedy, J. B., *High Weber number SMD Correlations for Pressure Atomizers*, ASME Paper 85-GT-37, July 15, 1985.

5.20 Weiss, M.A. and Worsham, C.H., *Atomization of High Velocity Airstreams*, ARS Jrl., Vol.29, p.252, 1959.

5.21 Royal Aircraft Establishment, *Rain Erosion and Associated Phenomena*, 1967.

5.22 Simpkins, P.G. and Bales, E.L., *Water-Drop Response to Sudden Accelerations*, J. Fluid Mechanics, Vol.55, Part 4, pp 629-639, 1972.

5.23 Sherwood, M. and Riley, S.J. *Studies into the Hail Ingestion Characteristics of Turbofan Engines*, AIAA/SAE/ASME/ASEE 29th Joint Propulsion Conference, Paper AIAA 93-2174, June 28-30, 1993.

5.24 United Technologies Research Center Research by Jan Kennedy

5.25 Pratt & Whitney Internal Research by Christopher Demers.

5.26 Pratt & Whitney Internal Research by William Colleti, Christopher Laurello and Steven Wojciechowski.

5.27 Pratt & Whitney Internal Research by Timothy Anderson.

5.28 McDonald, P.W., *Transient Engine Simulation and Analysis of an Ice Ingestion Test*, von Karman Institute for Fluid Dynamics, 1992-1993 Lecture Series "Gas Turbine Engine Transient Behaviour"' 10-12 May 1993.

5.29 Pratt & Whitney Internal Research by R.S. Mazzawy

5.30 Volk, L., *Engine Power Loss in Inclement Weather*, Unpublished work presented to AIA, September 13-14, 1966.

5.31 Russell, R.E., and Victor, I.W., *Evaluation and Correction of the the Adverse Effects of (i) Inlet Turbulence and (ii) Rain Ingestion on High Bypass Engines*, AIAA Paper 94-1984, 1984.

5.32 General Electric Company Internal Research Results

5.33 Byers, H.R., *General Meteorology*, McGraw-Hill, 1974.

5.34 Angot, A., *Traité de Météorologie*, Ed. Gauthier-Villars, Paris, 1944.

5.35 Marchik, E.A., *Motion of Condensed Phase in the Blade Passage of an Axial Gas Turbine Stage*, Teploenergetika, Vol. 12, No. 10, 1965.

Table 5-1

NATIONAL WEATHER SERVICE
RADAR-IDENTIFIED INTENSITY LEVELS OF PRECIPITATION

- based on S-band pulse doppler surface radar
- S-band same as X-band for rain. They differ for hail

LEVEL	PRECIPITATION CATEGORY	SURFACE RATE
		mm/min
1	Light	< 0.083
2	Moderate	0.083 - 0.47
3	Heavy	0.47 - 0.93
4	Very Heavy	0.93 - 1.90
5	Intense	1.90 - 3.0
6	Extreme	> 3.0

Table 5-2

EFFECT OF 0.01 ABSOLUTE HUMIDITY

ENGINE TYPE	PRIMARY CONTROL MODEL	THRUST IMPACT
High Bypass Ratio Commercial Engines	Pressure Ratio Fan Speed	0.0 % -0.2 %
Low Bypass Ratio Military Engines	Turbine Temperature Fan Speed	+0.9 % -1.0 %

Table 5-3

CAPABILITIES OF RECOMMENDED PRACTICES TO ASSESS THE EFFECTS OF LIQUID WATER (RAIN) AND HAIL

	ASSESSMENT METHOD	PERFORMANCE		OPERABILITY		COMMENTS
		Influence	Confidence	Influence	Confidence[2]	
Components:						
Inlet	A + T[1]	L	L	M	M	
Fan/Splitter	A + T[1]	L	L	M	M	
Compressor	A + T[1]	M	L	H	M	
Combustor	A + T[1]	H	M	H	L-M	
Turbine	A	M	L	L	H	
Nozzle: Core	A	L	H	L	H	
Nozzle: ByPass	A	L	H	L	H	
Engine:						
Controls (Sensors and Logic)	A + T[1]	H	N/K	H	M	
Starting	A + T[1]	N/A	N/A	H	L	
Power Transients	A + T[1]	N/K	N/K	H	M	
Determining Core Water	A + T[1]	L	M	L	M	

1 Analysis: Required to establish engine inlet environment transformed from atmospheric environment.
Test: Required to measure effect of water/hail ingestion.

2 Required Analytical and Test Procedures are defined so that confidence in Engine Capability is very high.

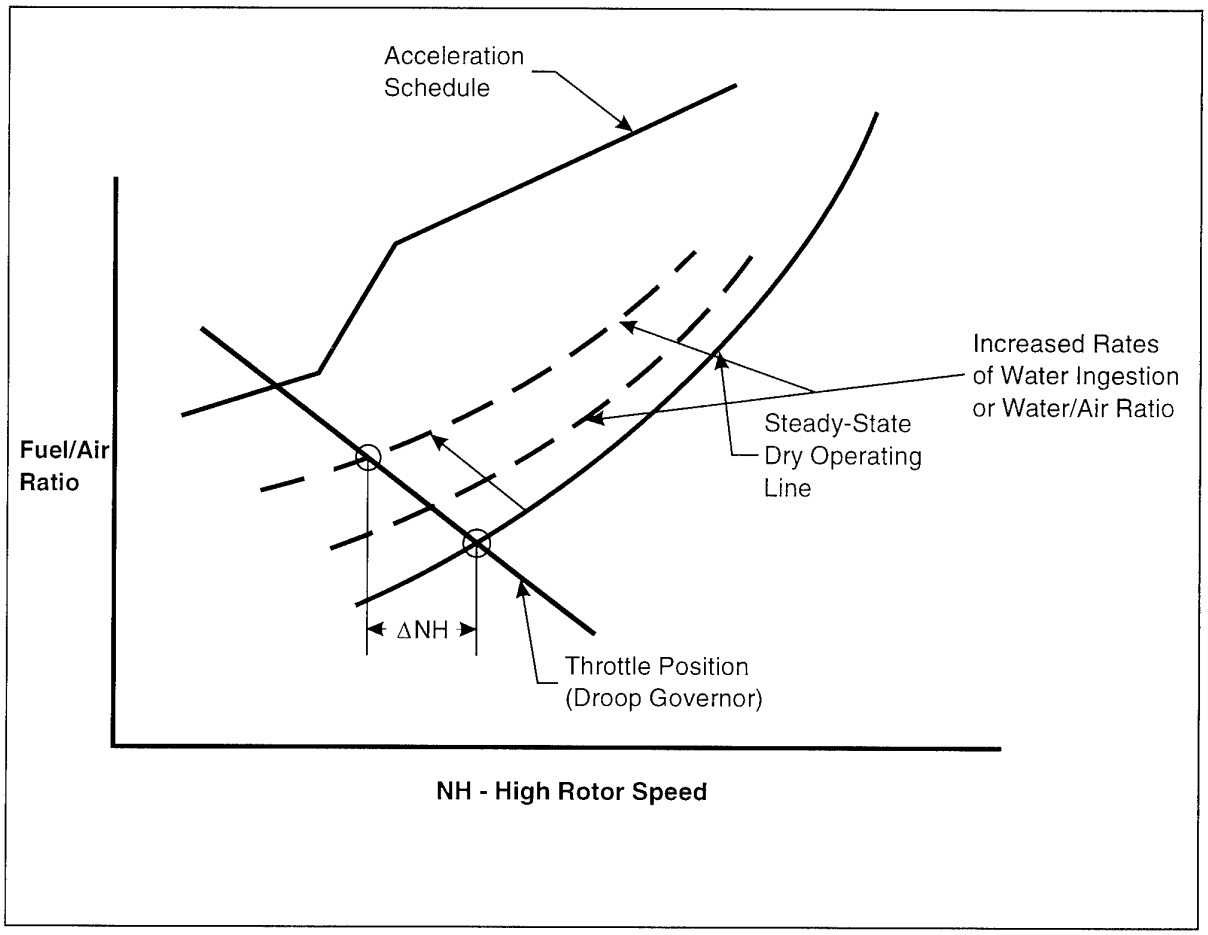

Figure 5-1

Typical Engine Control Characteristics

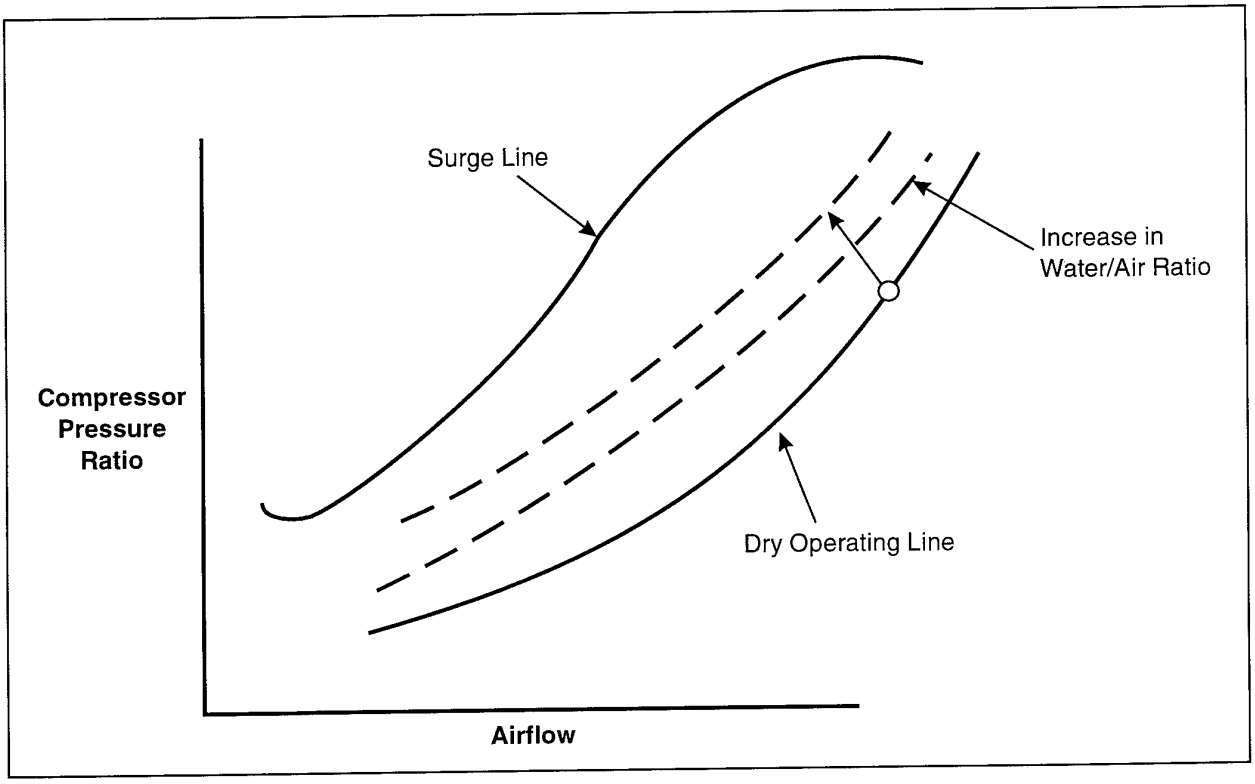

Figure 5-2

High Pressure Compressor

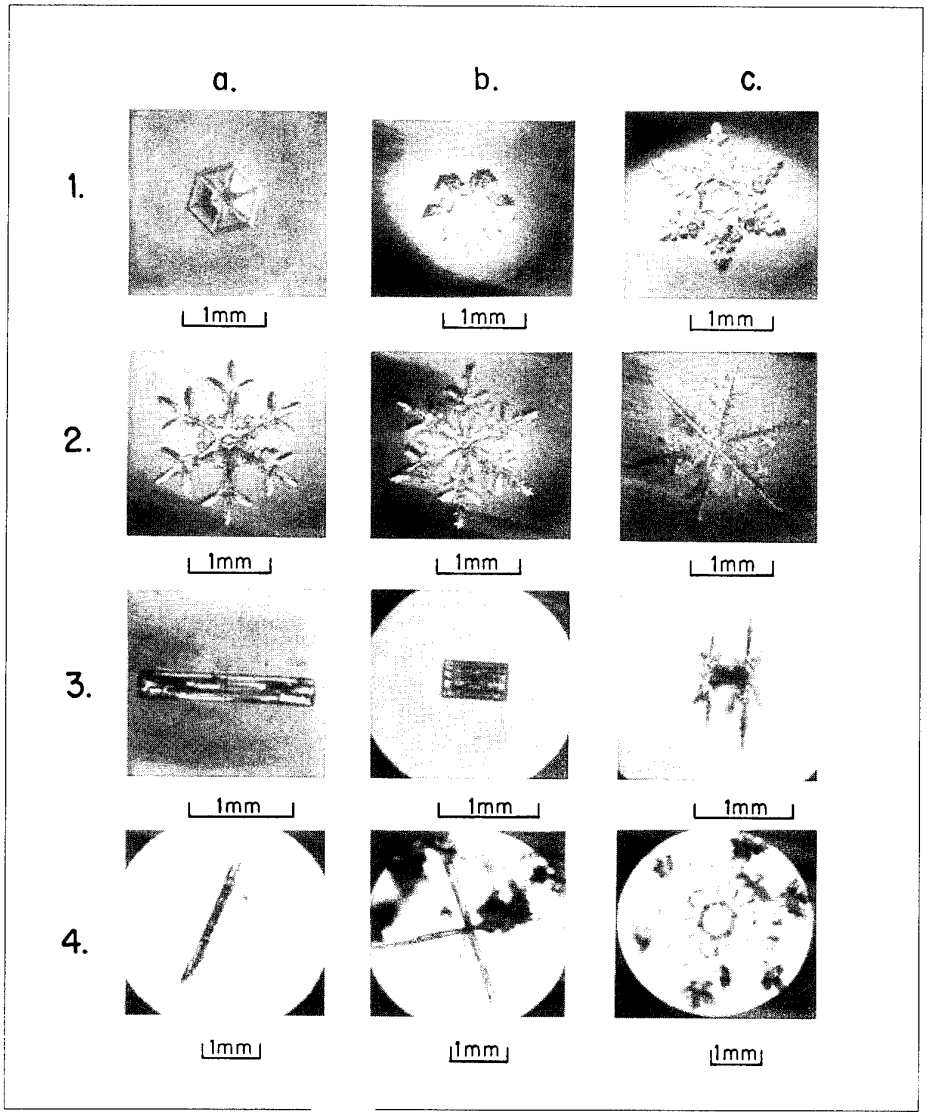

Figure 5-3

Microphotographs of Some of the Elementary Forms of Ice Crystals:

1a, b, c - Hexagonal Plates Showing Some Growth at Corners in b & c;
2a, b, c - Dentritic Forms;
3a, b - Columns; 3c - Capped Column, Shown in End View in 4c;
4a, b - Needles
(Reference 5.33)

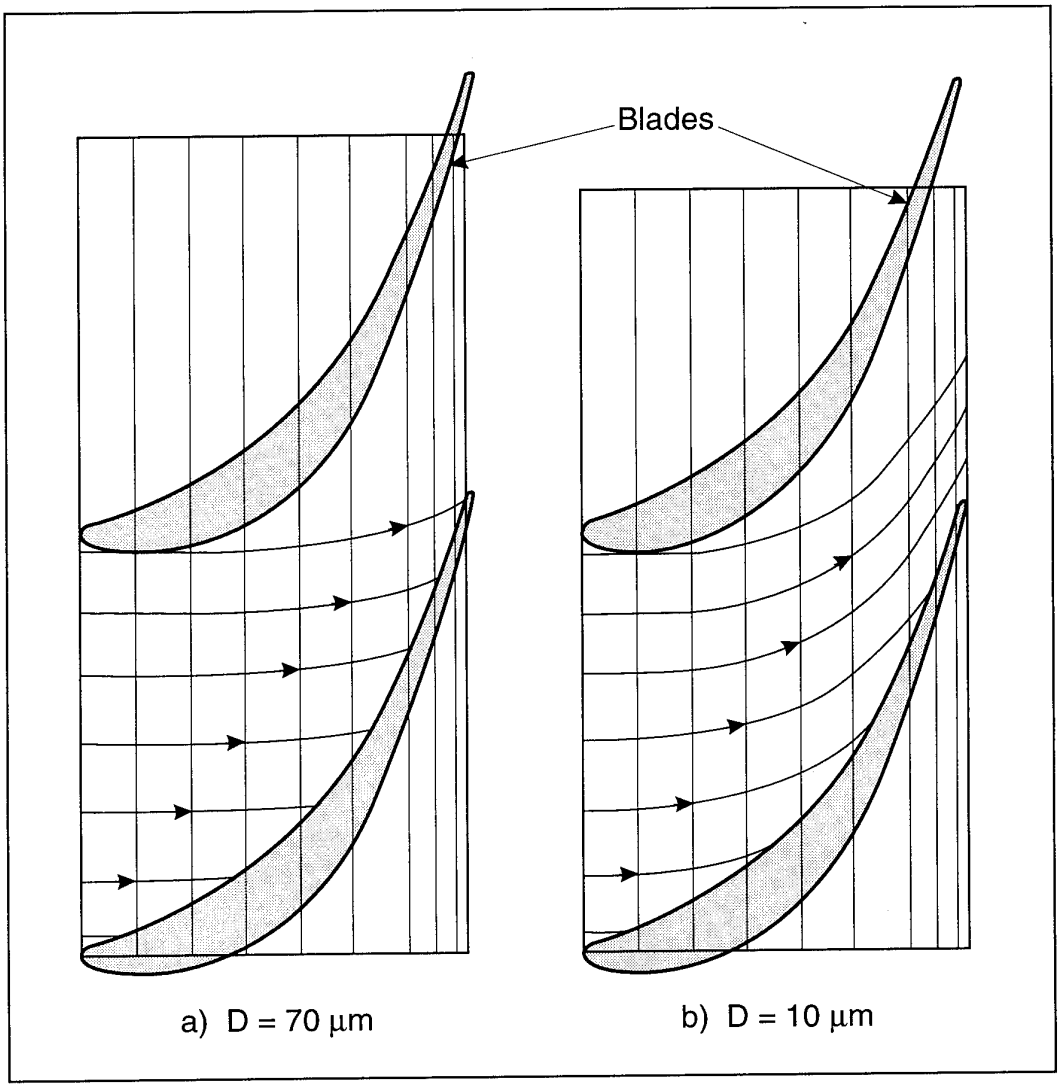

Figure 5-4

2-D Droplet Trajectory Calculations
(Reference 5.35)

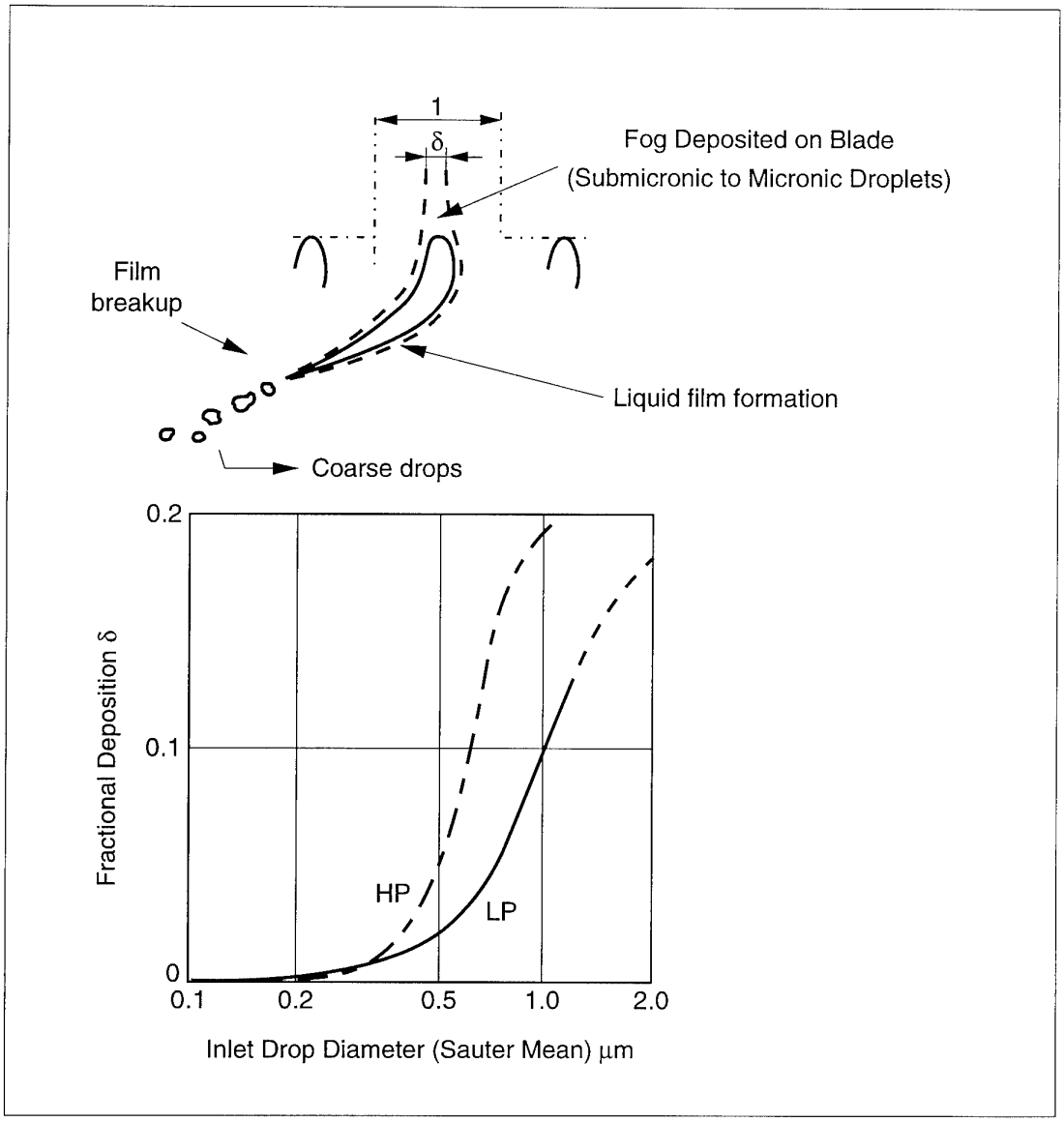

Figure 5-5

Micronic Droplet Deposition and Coarse Drop Formation
(Reference 7.8)

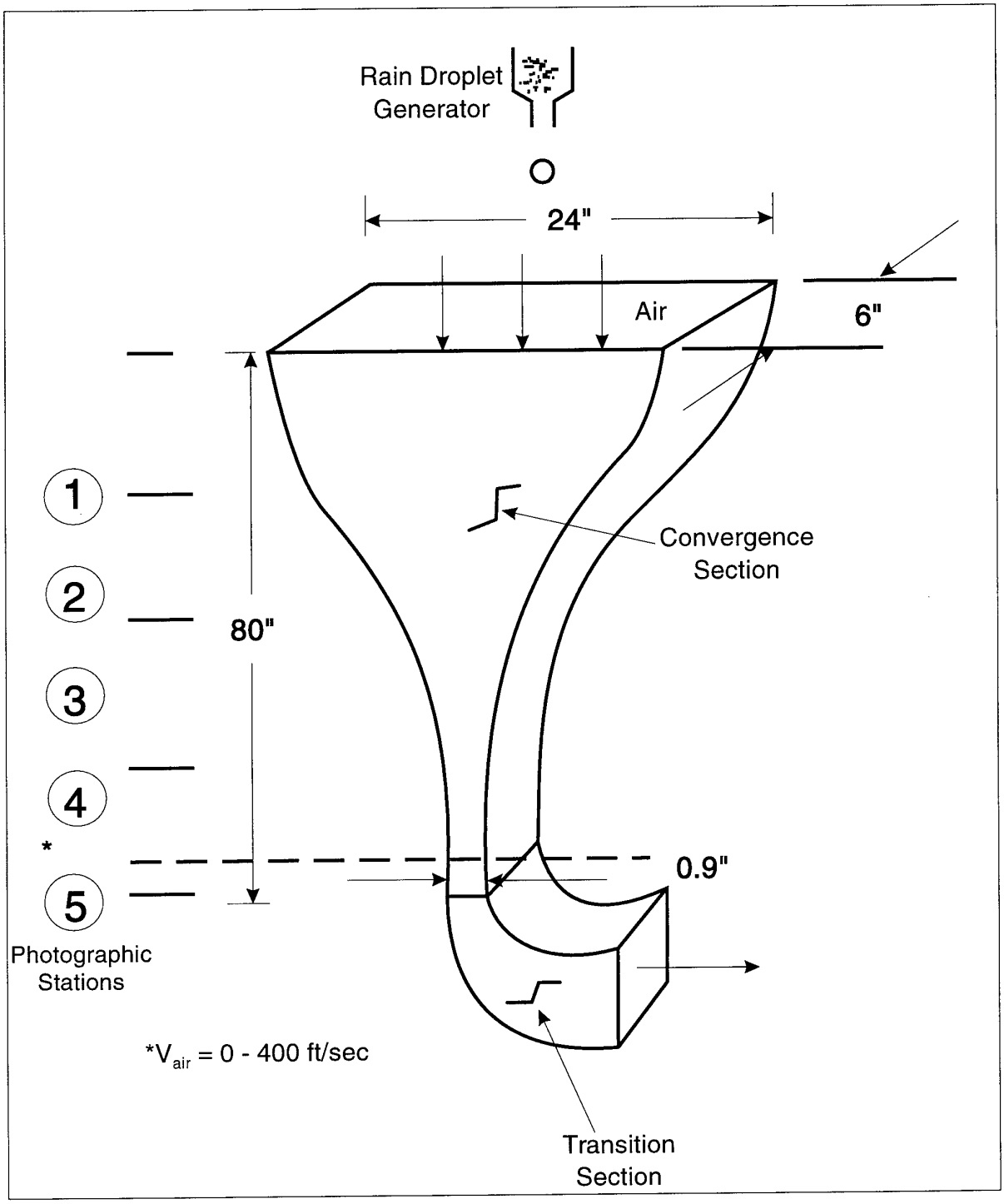

Figure 5-6

Rain Droplet Breakup Facility
(Reference 5.3)

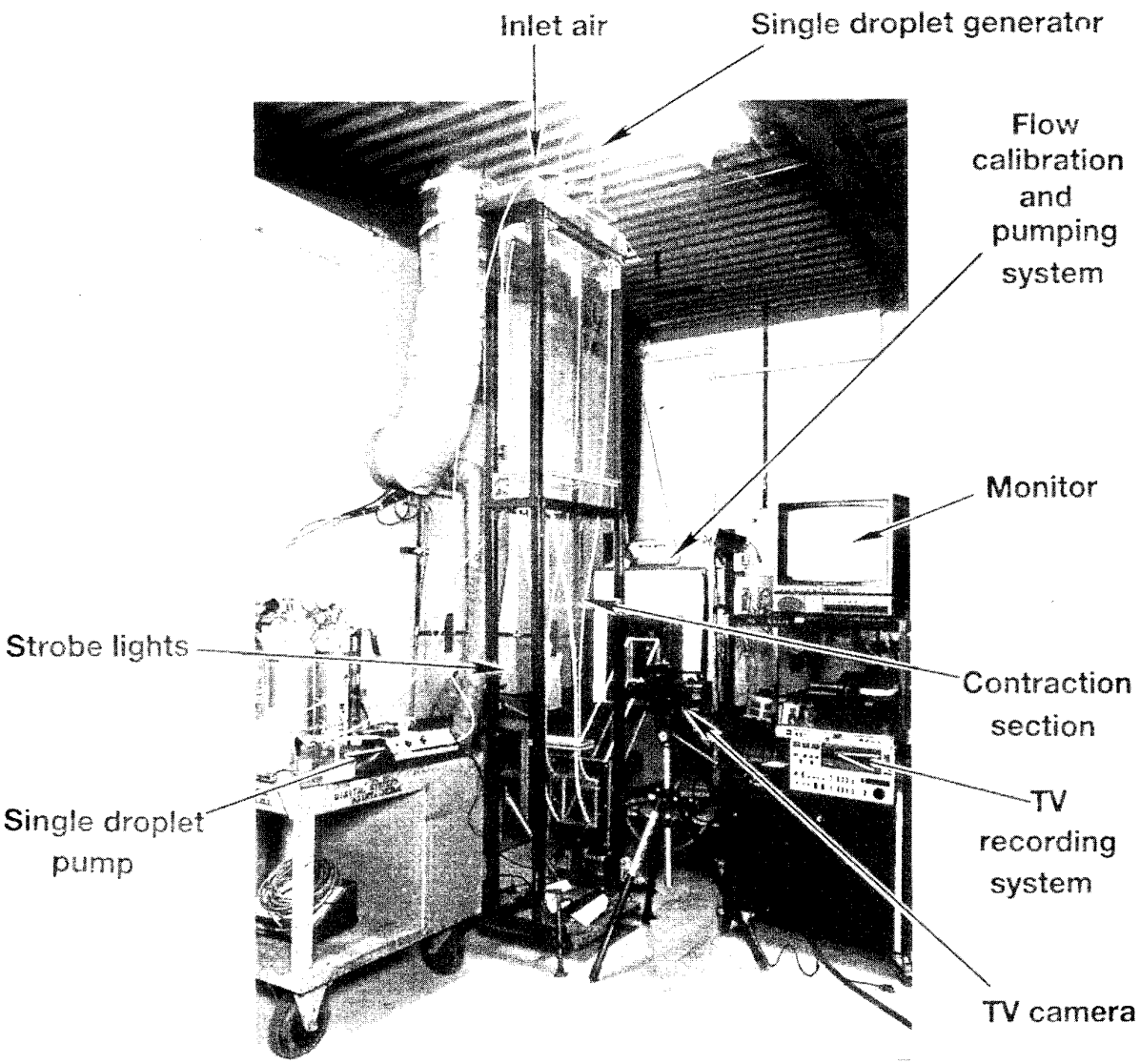

Figure 5-7

Single Droplet Facility

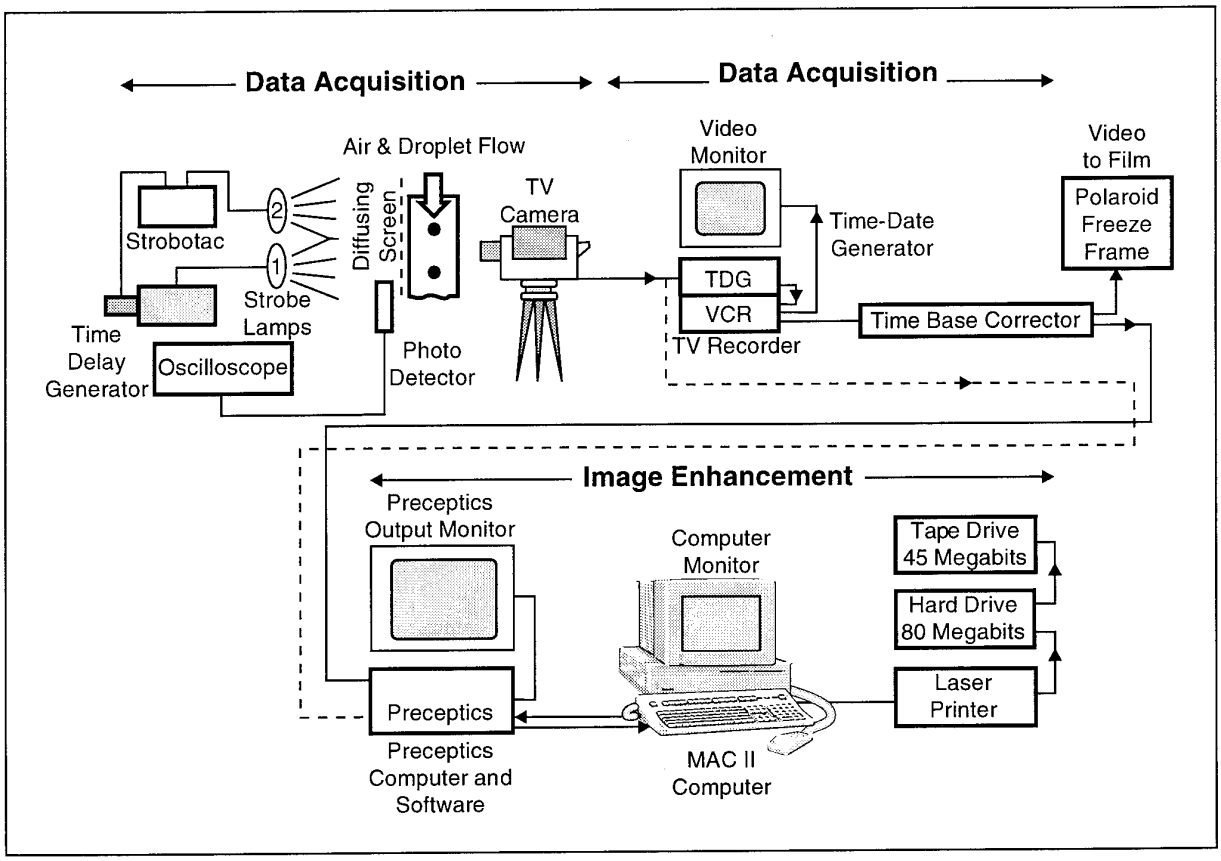

Figure 5-8

Image Acquisition System
(Reference 5.3)

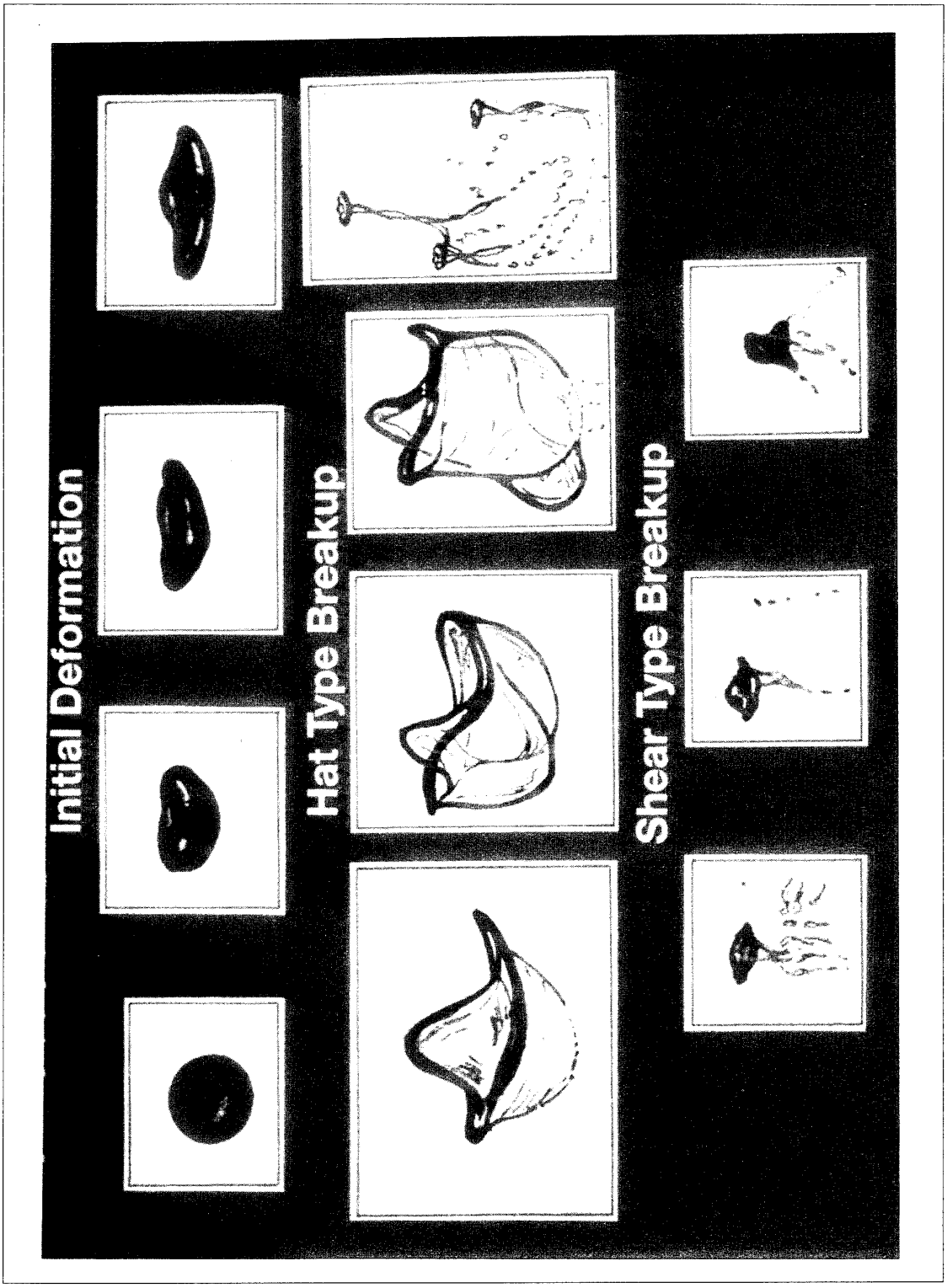

Figure 5-9

Droplet Breakup
(Reference 5.3)

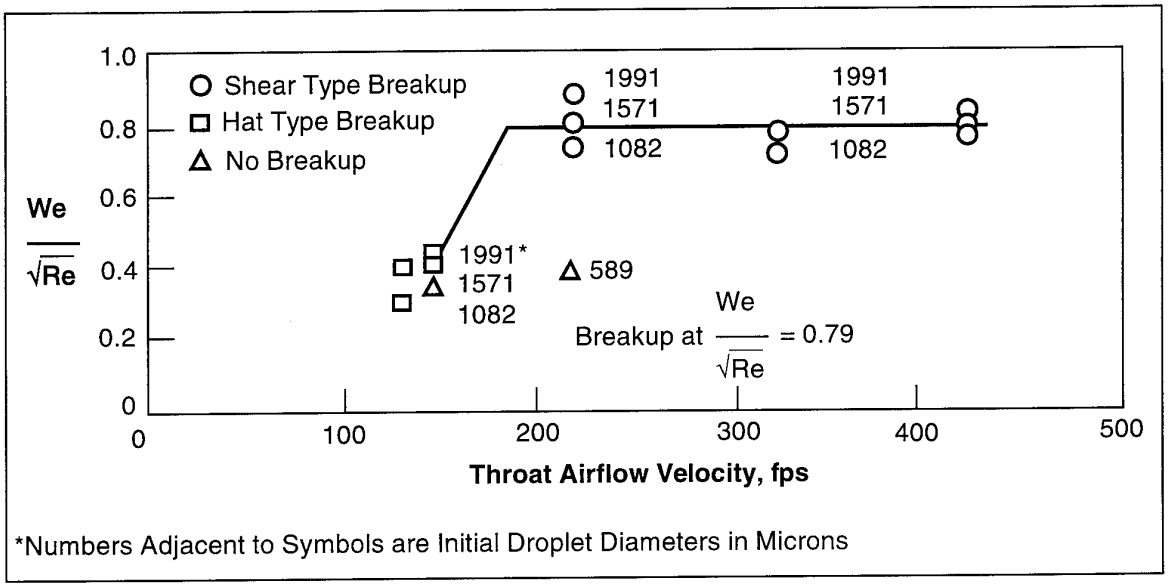

Figure 5-10

Droplet Breakup Criteria - Descent Idle Rain Ingestion
(Reference 5.3)

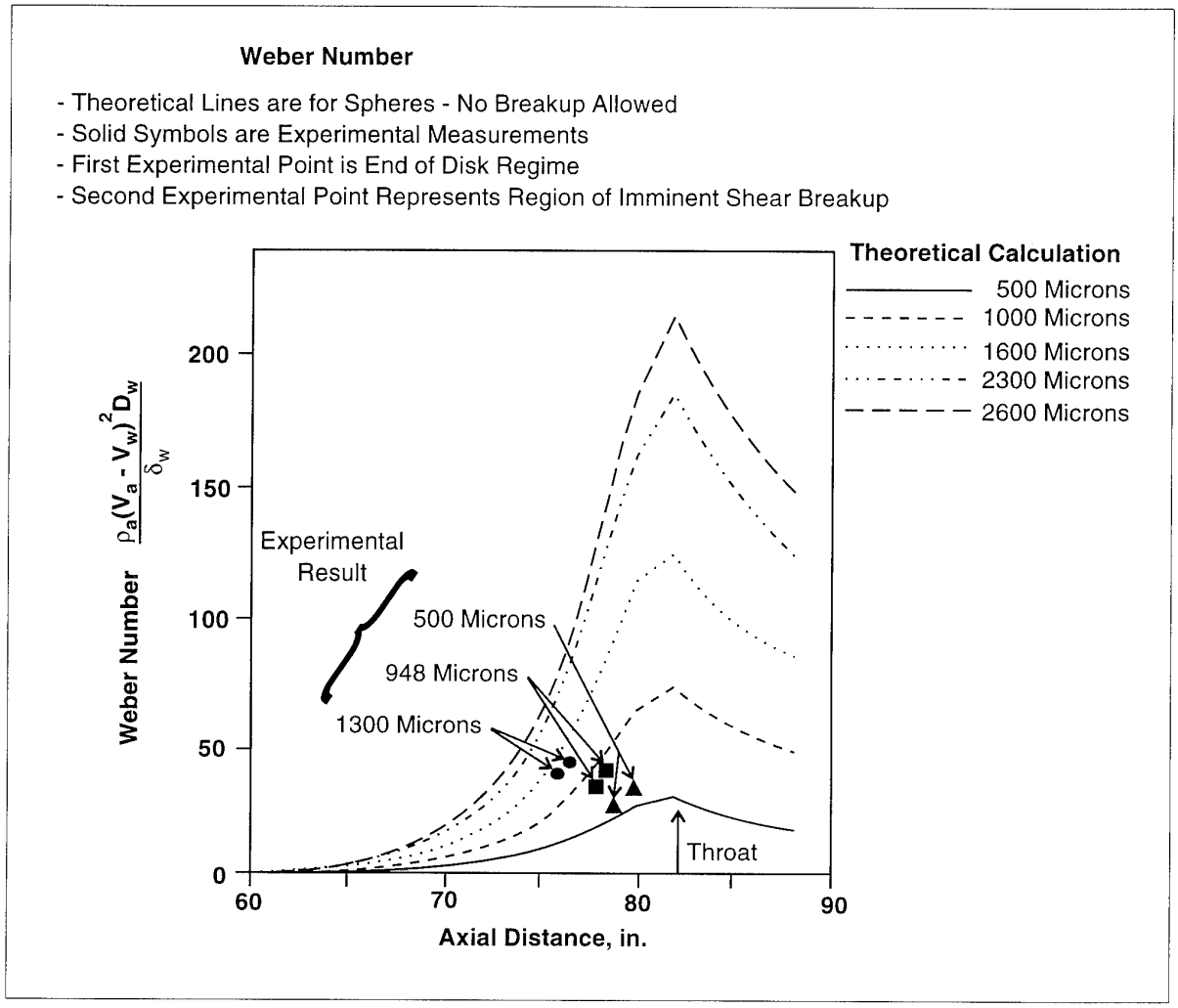

Figure 5-11

Theoretical and Measured Weber Numbers
Versus Axial Distance for Various Droplet Sizes
(Reference 5.3)

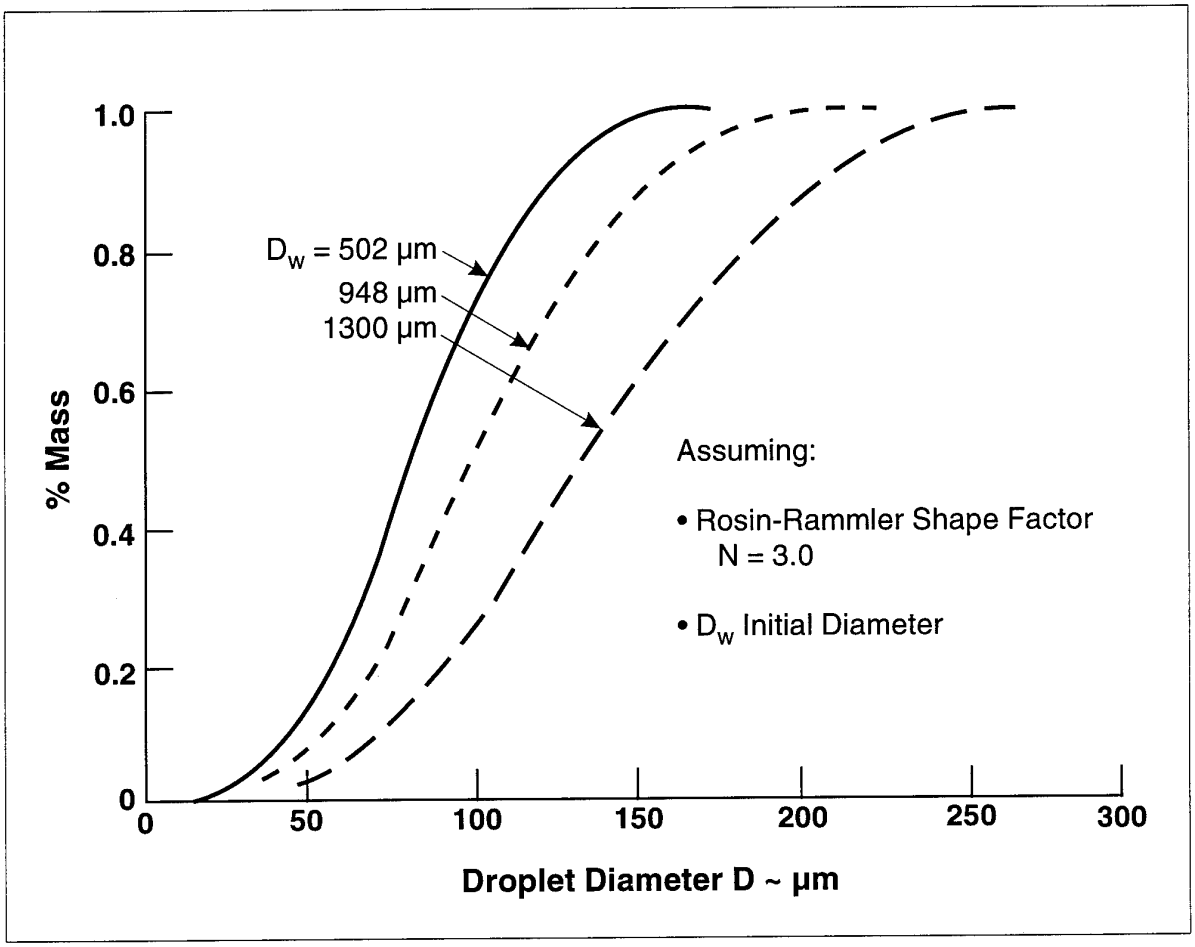

Figure 5-12

Droplet Distributions After Breakup

1) Specify Free Stream to Inlet Streamlines and Model Air Velocities

2) Select Rain Droplet Sizes 3000 - 500 μm

3) Calculate Rain Velocity Using Modified Drag Law to Account for Change From Sphere to Disc

See Equations 5-3 to 5-5.

4) Drop Breakup Occurs When

$$\frac{We}{\sqrt{Re}} = 0.79$$

For Shear Type Breakup Va > 150 fps

and $$\frac{d\left[\frac{We}{\sqrt{Re}}\right]}{dt} > 30$$

5) Breakup Distribution is Defined by Mass Mean Diameter

$$D_{wm} = \left[\frac{136\mu_w \ \sigma_w^{3/2} \ D_w^{1/2}}{\rho_a^2 \ \rho_w^{1/2}(V_a - V_w)^4}\right]^{1/3}$$

6) Based on Extensive Water Spray Data at Idle Descent Condition, the Distribution Fits Rosin Rammler Distribution and

$$N \approx 3.0$$

$$1 - v = \exp\left[-\left(\frac{D}{\bar{X}}\right)^N\right]$$

Where $\bar{X} = 1.96 \ D_{wm}$

Figure 5-13

Flow Diagram to Determine Rain Droplet Sizes and Velocities Entering a Gas Turbine Engine

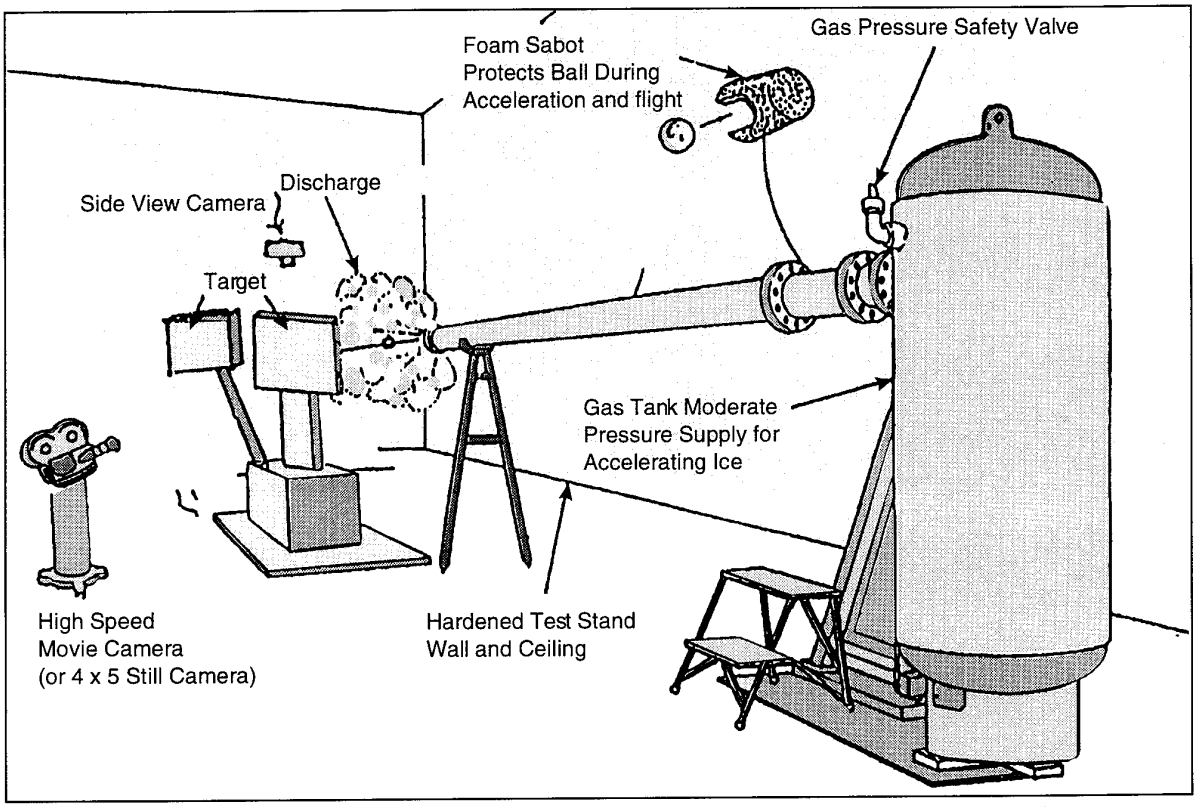

Figure 5-14

P&W Hail Impact Rig Schematic

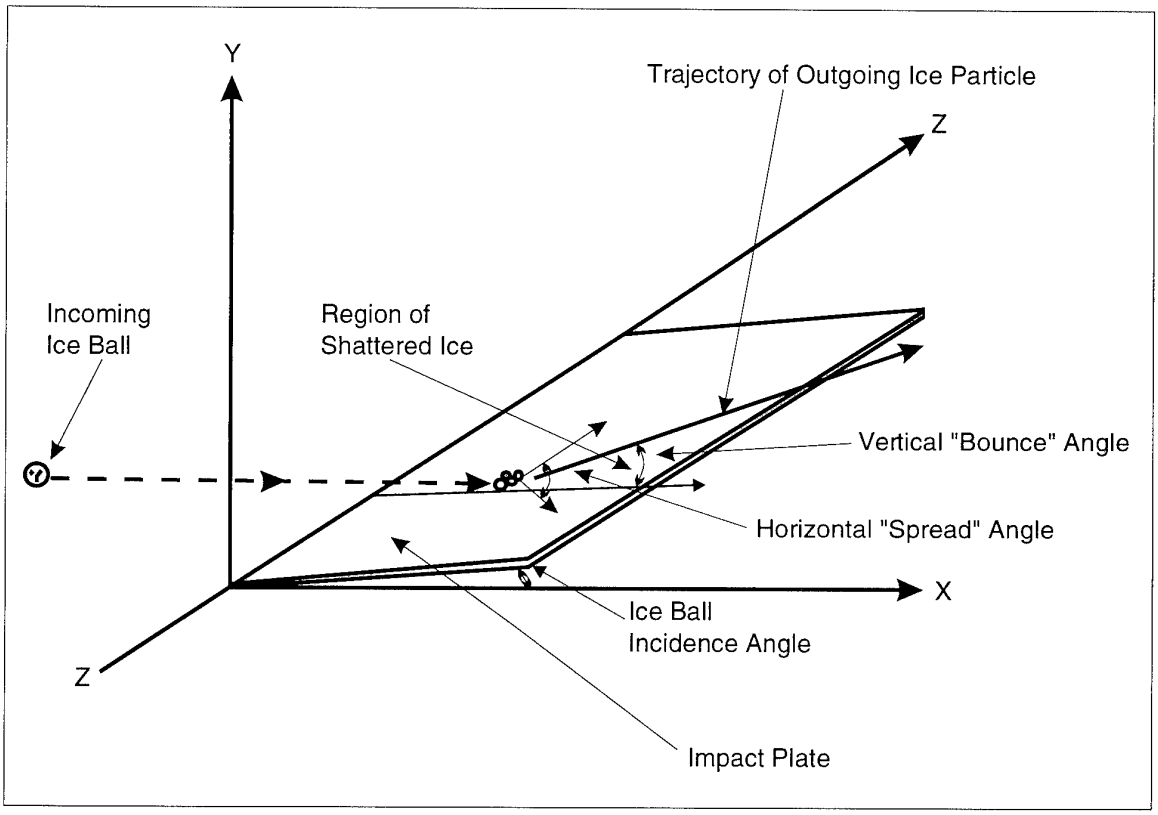

Figure 5-15

P&W Hail Impact Rig Velocity Vector Definitions

- Single impact testing provided basic correlating parameters for broad range of parameters:

  Hail size, velocity and angle:

• Hail size	1/2 - 2 inch dia.
• Hail temperature	-20 - 0° C
• Velocity	250 - 900 ft/sec
• Impact angle	0 - 90 degrees
• Surface	Wet, dry, rough smooth

- Multiple ice impact test results utilized to validate the correlations.

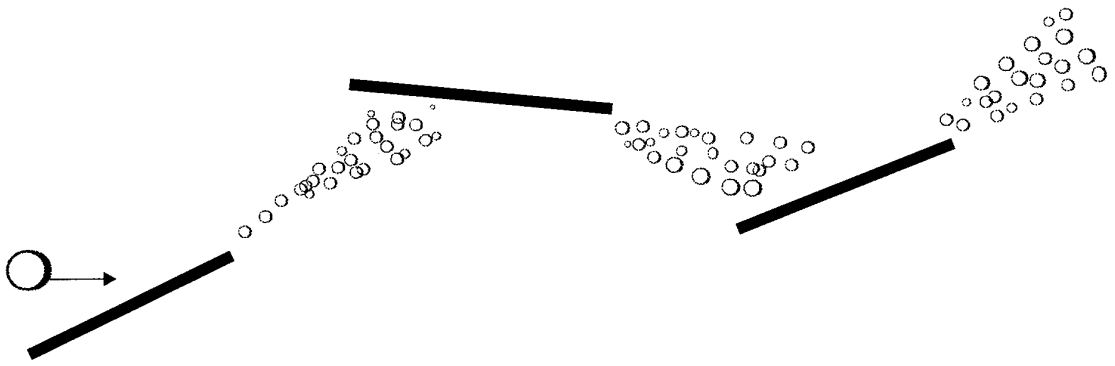

Figure 5-16

Extensive Hail Impact Test Data Base

Figure 5-17

90° Impact of Hail Ball on Spinner

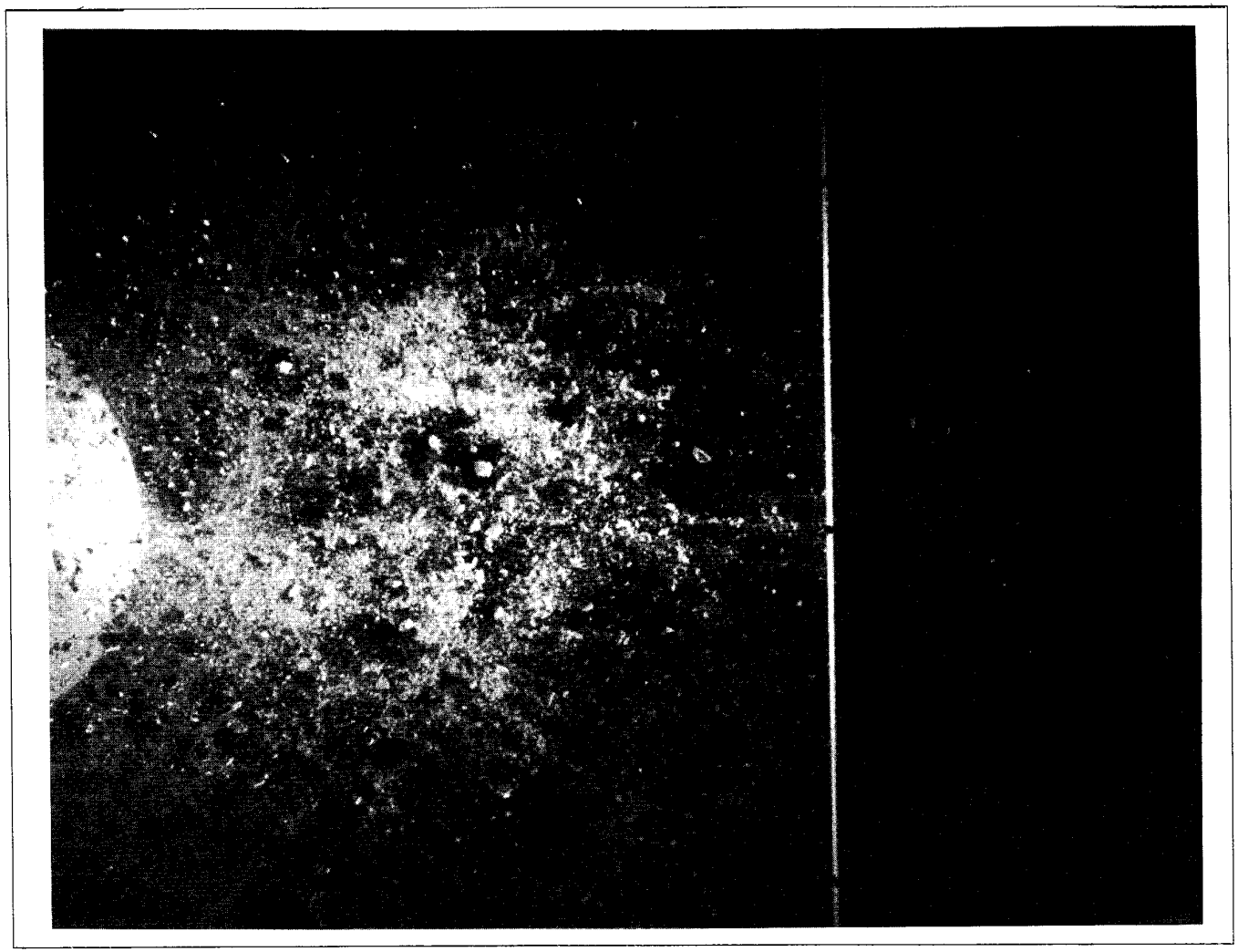

Figure 5-18(a)

Impact of 1-inch ice ball at 40° impact angle
(View from vertically above impact plane)

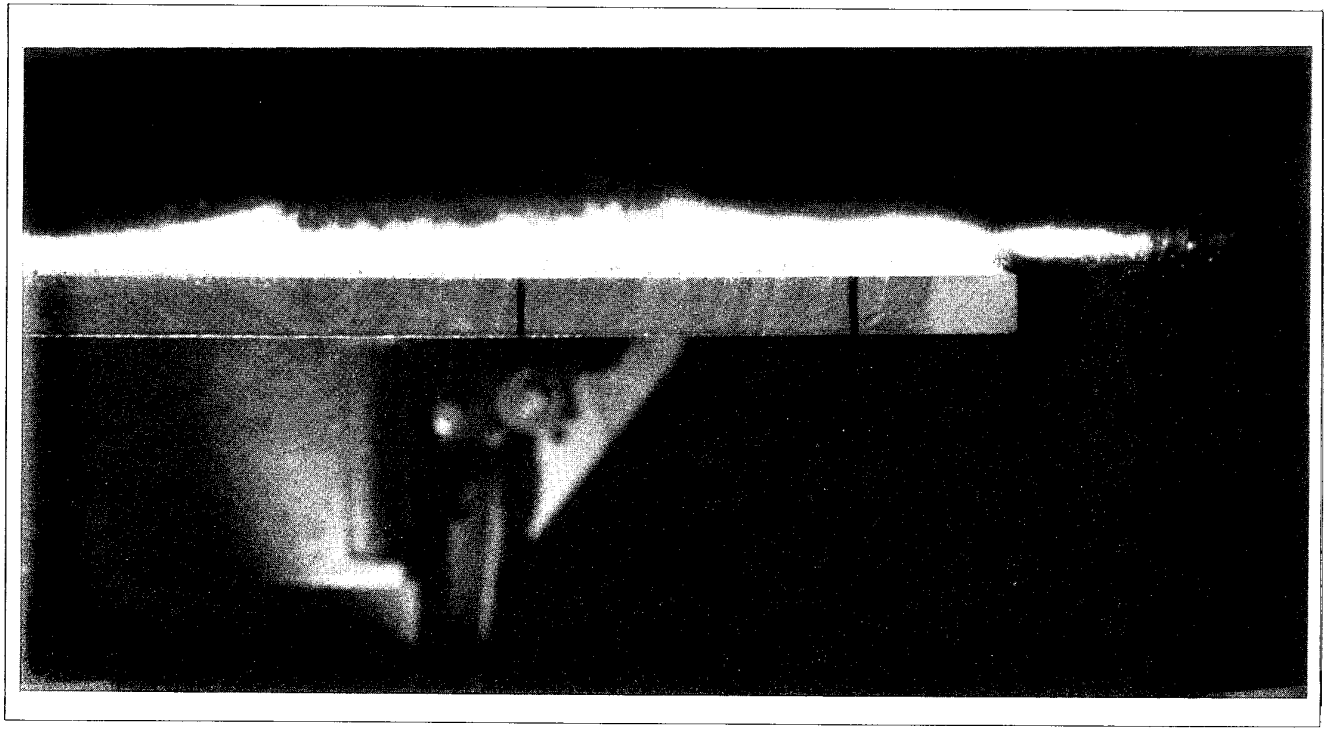

Figure 5-18(b)

Impact of 1-inch ice ball at 40° impact angle
(View parallel to impact plane)

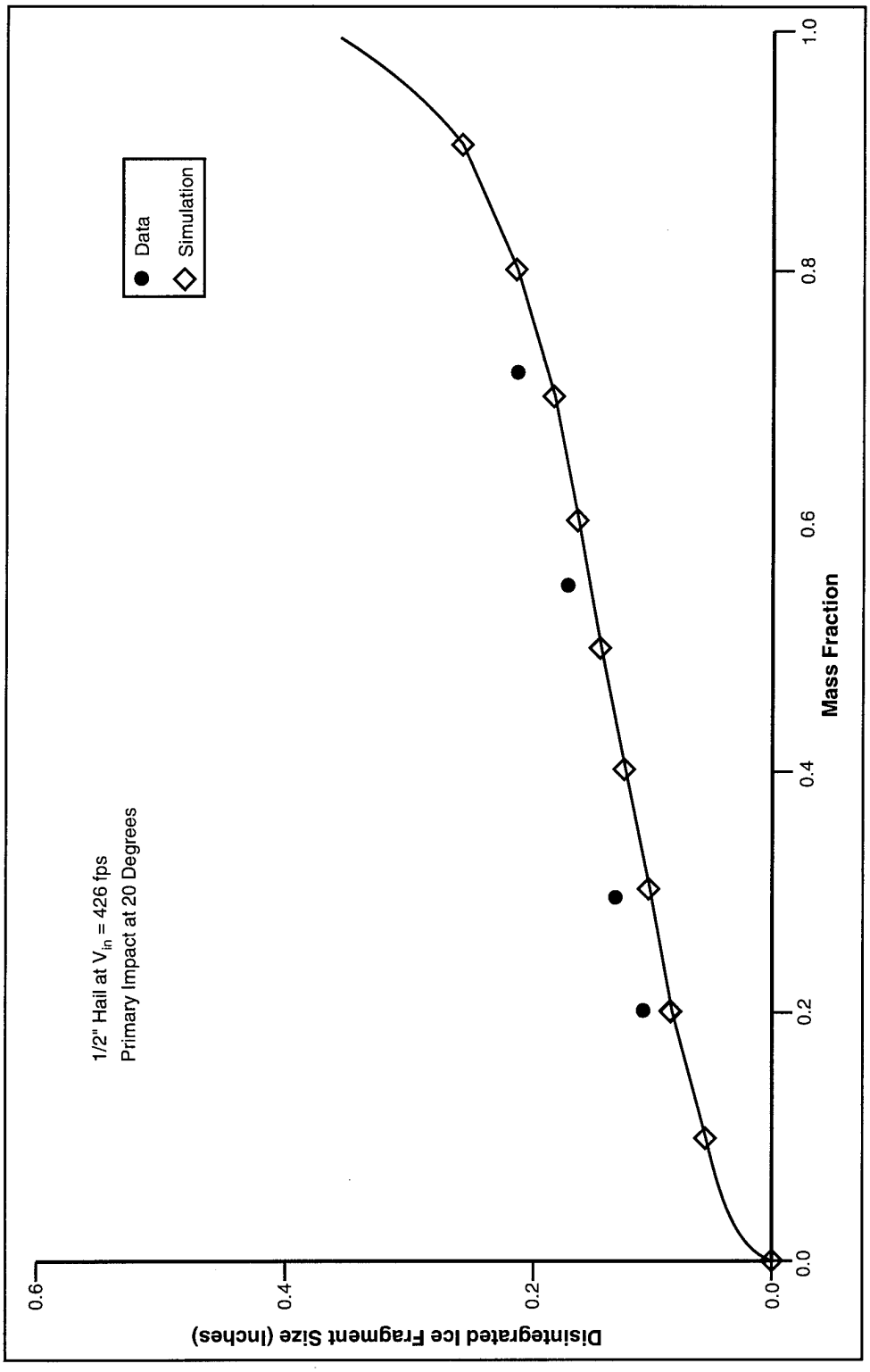

Figure 5-19(a)

Disintegrated Particle Size vs. Mass Fraction

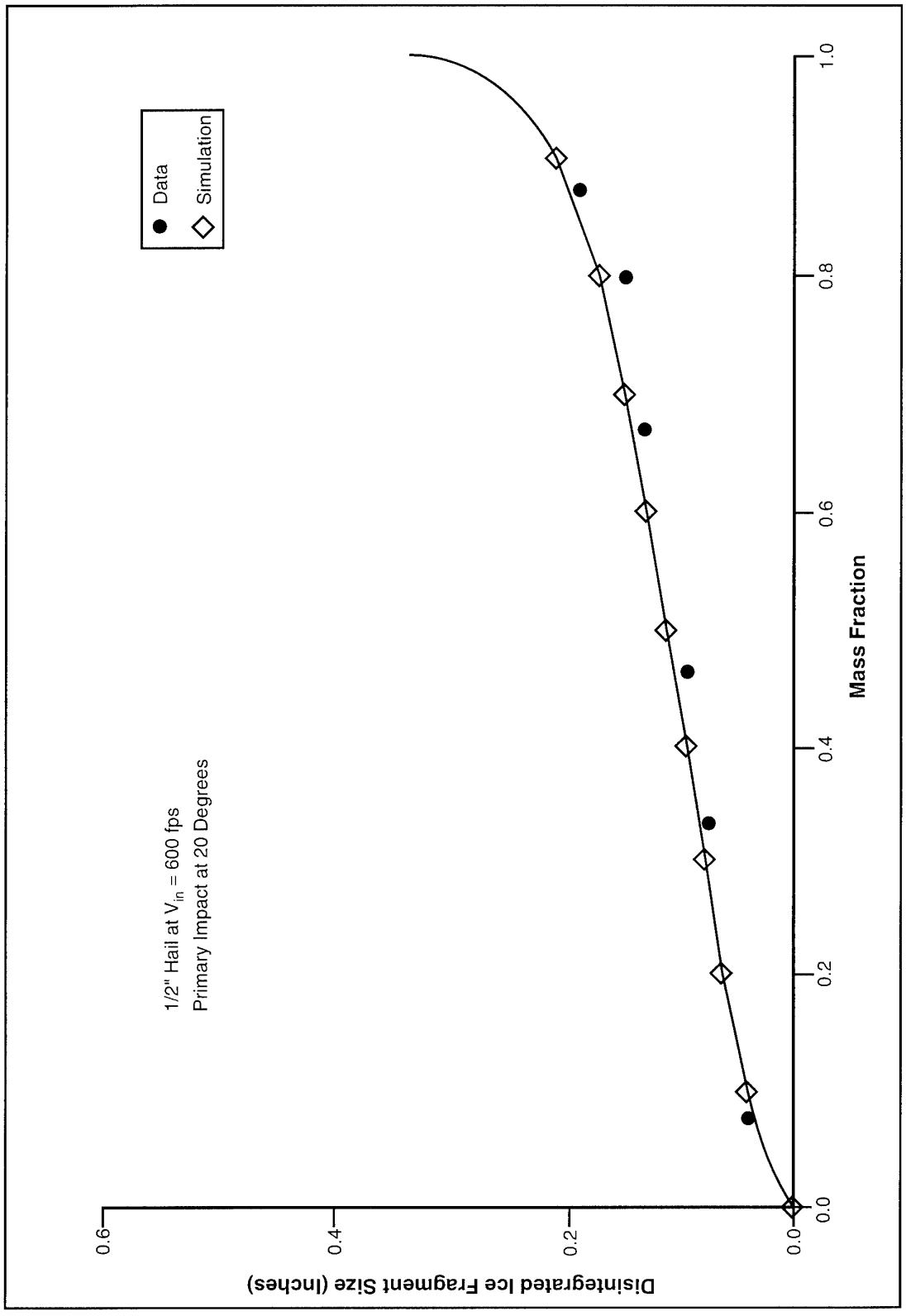

Figure 5-19(b)

Disintegrated Particle Size vs. Mass Fraction

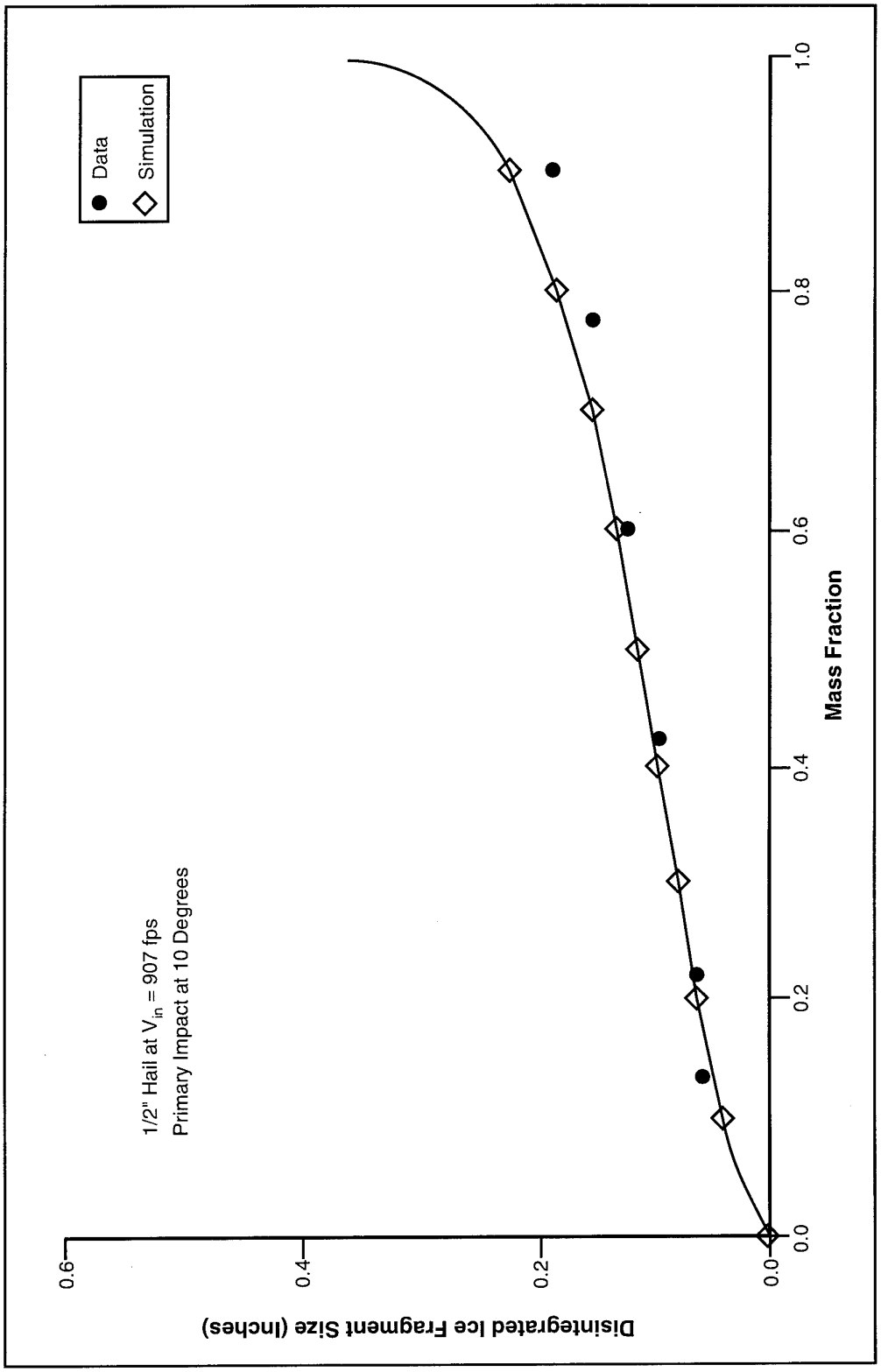

Figure 5-19(c)

Disintegrated Particle Size vs. Mass Fraction

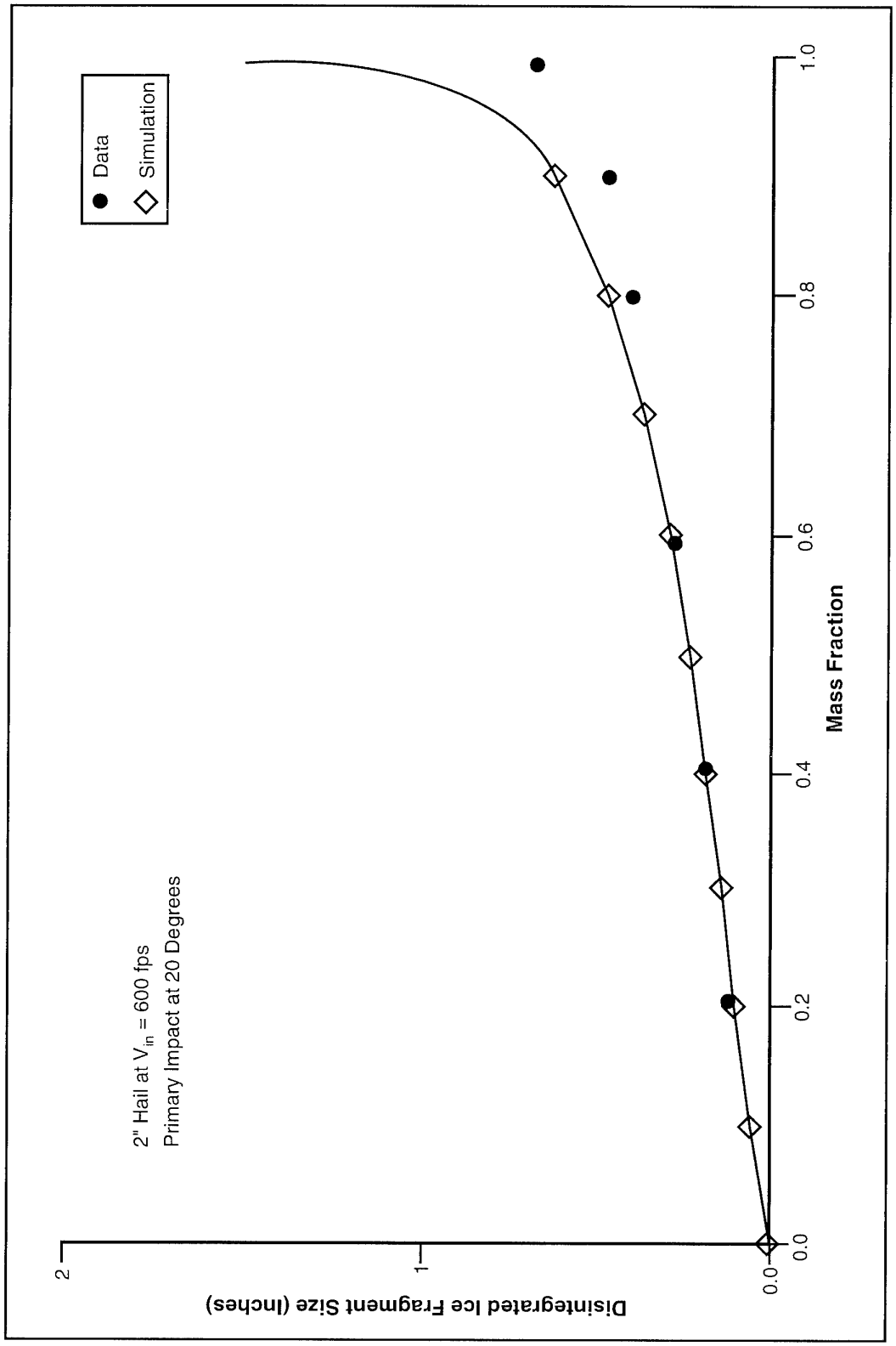

Figure 5-19(d)

Disintegrated Particle Size vs. Mass Fraction

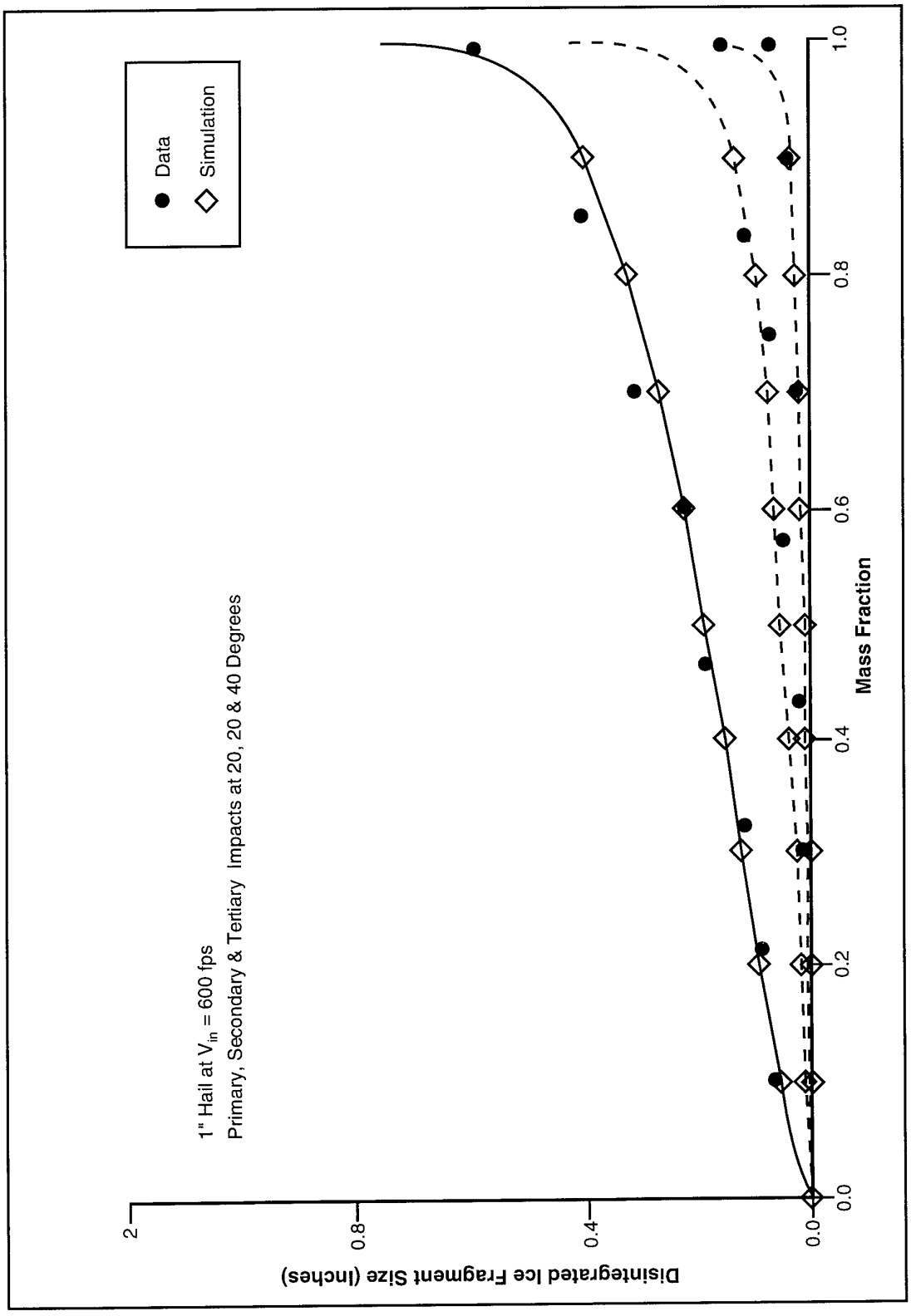

Figure 5-19(e)

Disintegrated Particle Size vs. Mass Fraction

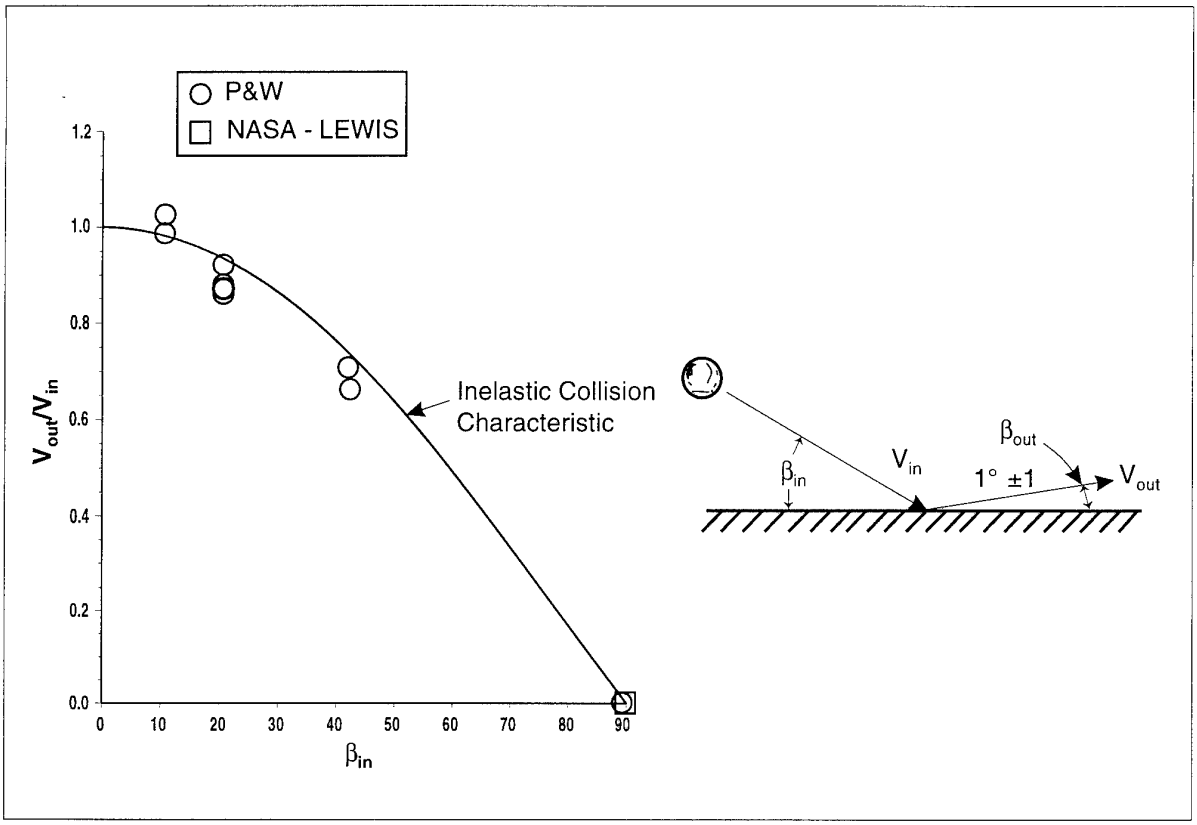

Figure 5-20

High Speed Photography of Impact Testing
Validates that Collisions are Inelastic

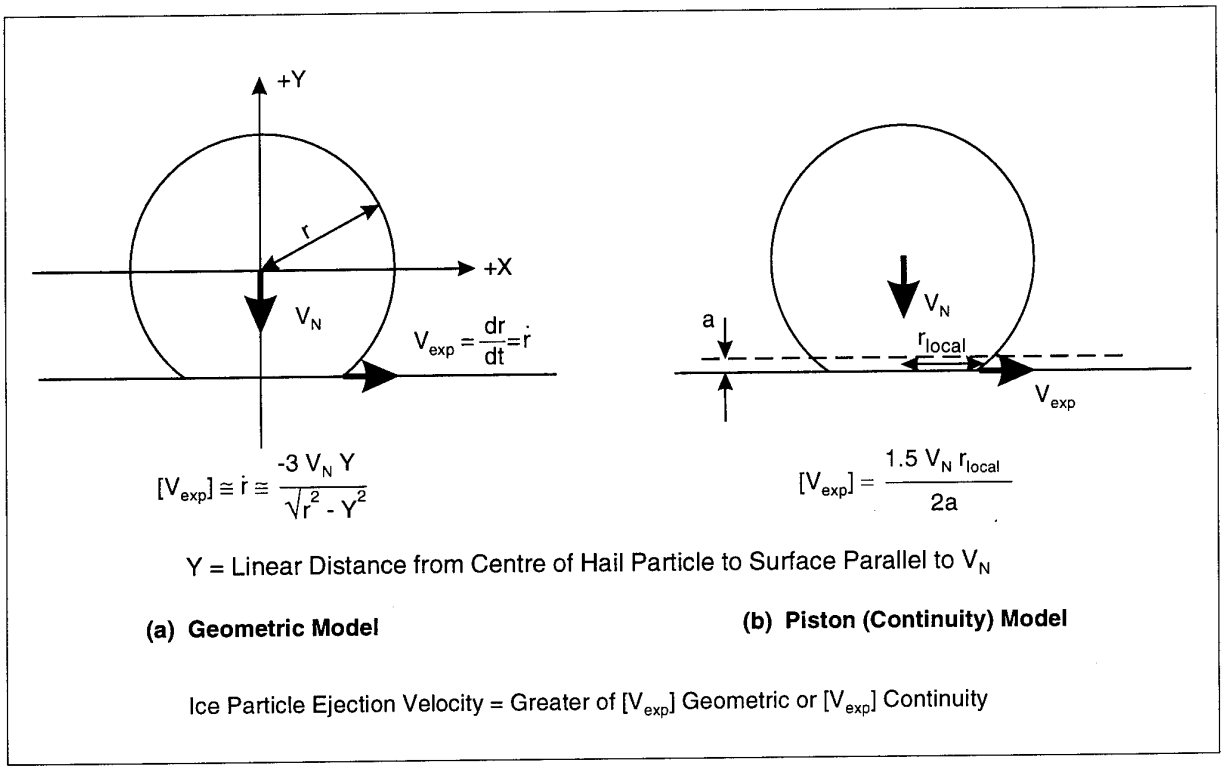

Figure 5-21(a,b)

Schematic of Hailstone Disintegration Model

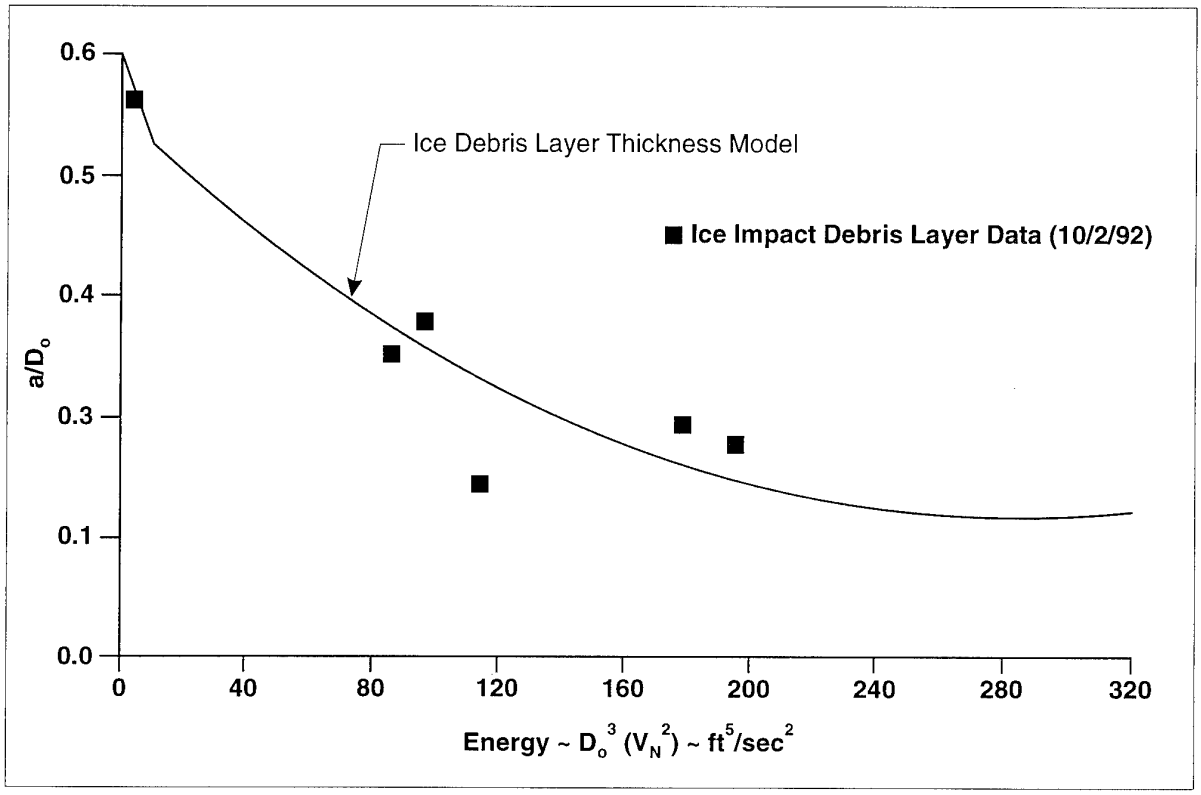

Figure 5-21 (c)

Ice Impact Debris Layer Thickness Model

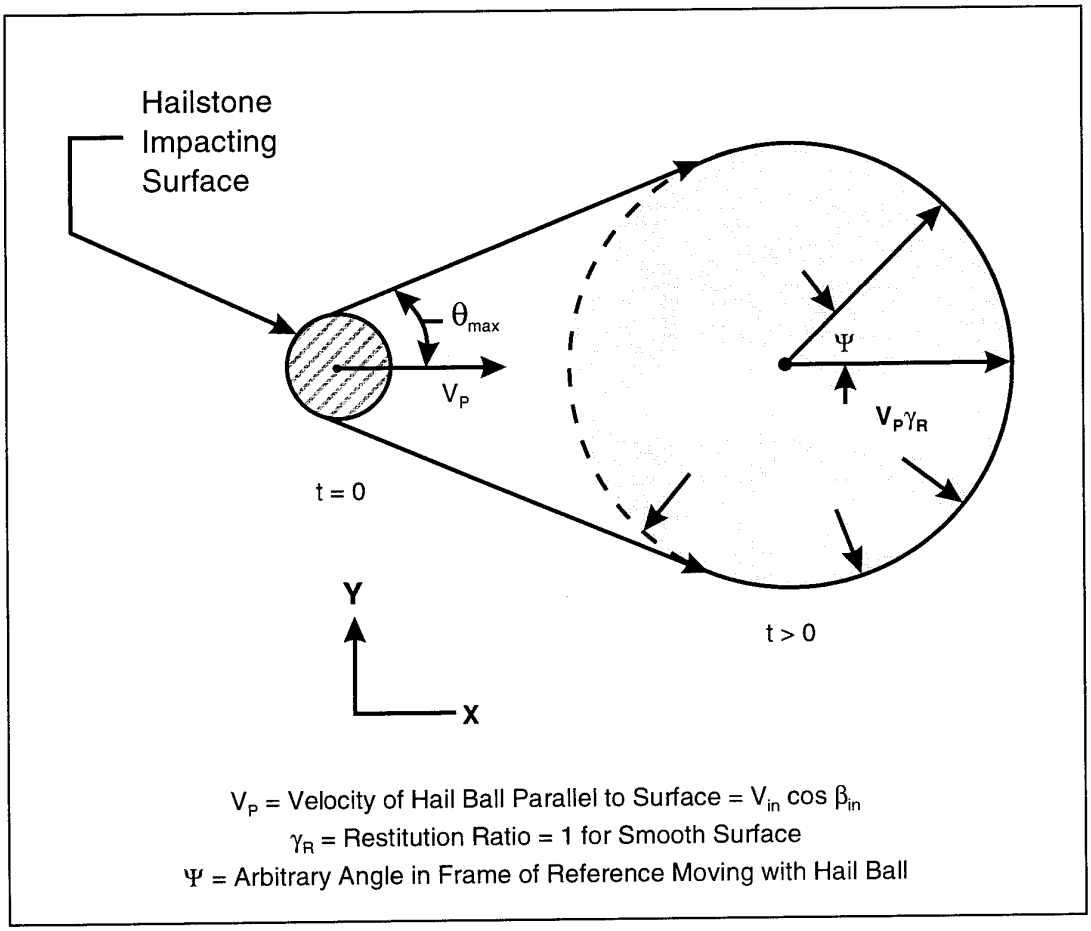

Figure 5-21(d)

Schematic of Hailstone Debris Spreading Process

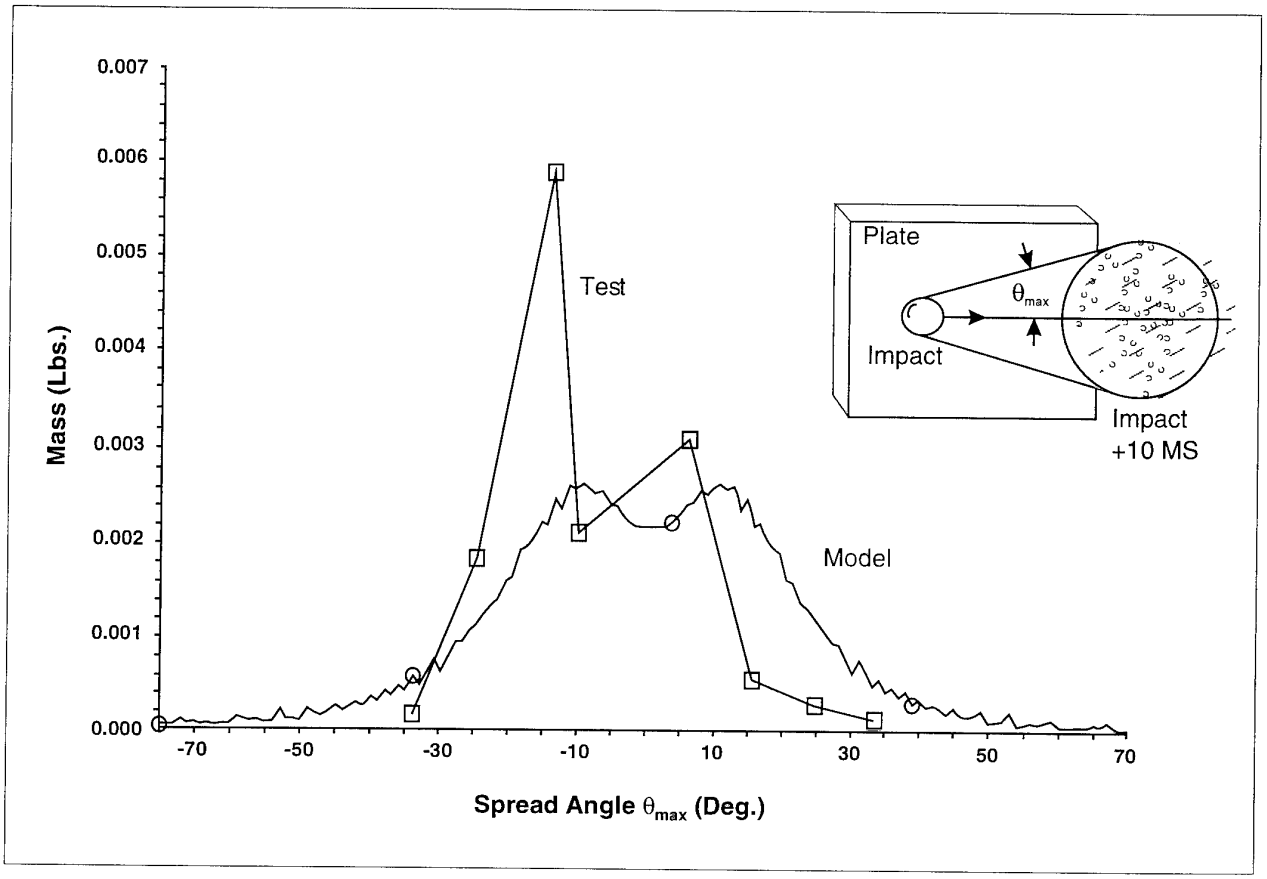

Figure 5-21 (e)

Spread Angle - Analytical Model & Test Data

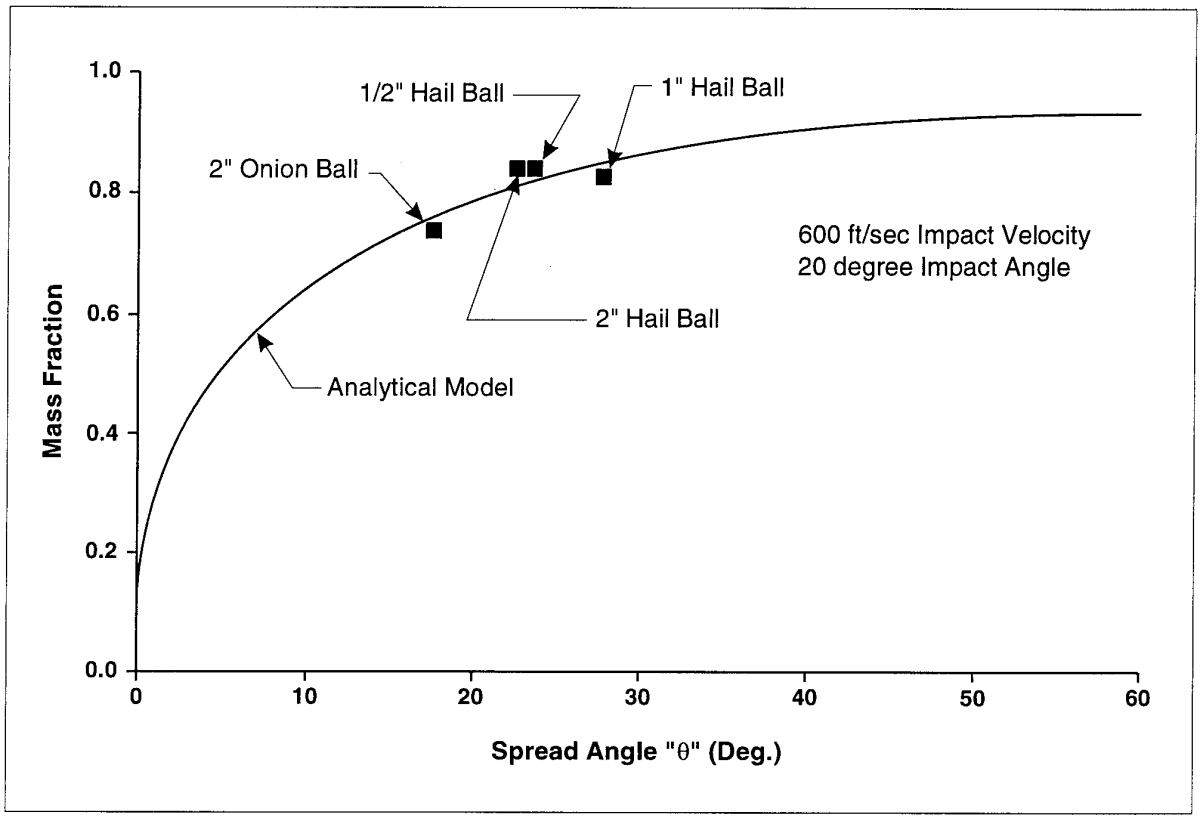

Figure 5-21 (f)

Spread Angle - Analytical Model & Test Data

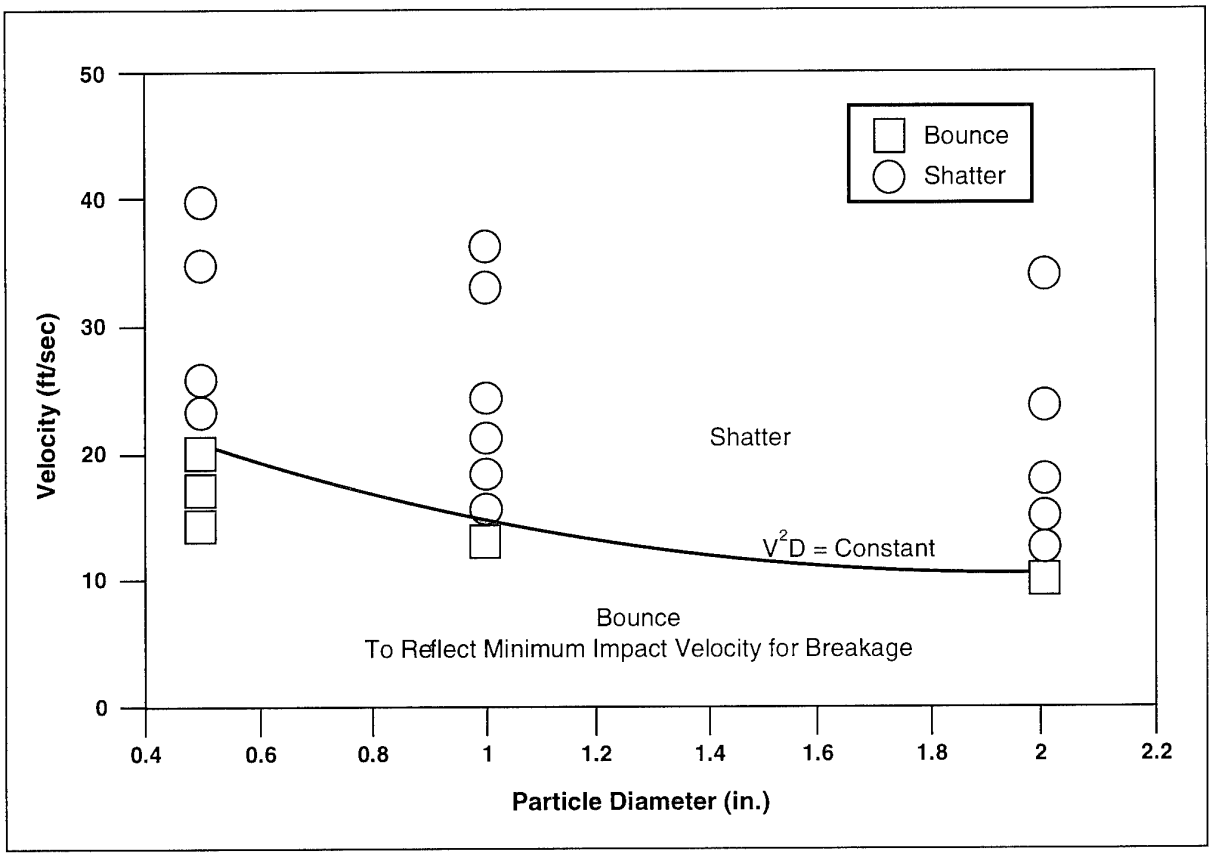

Figure 5-22

Shatter - Bounce Boundary

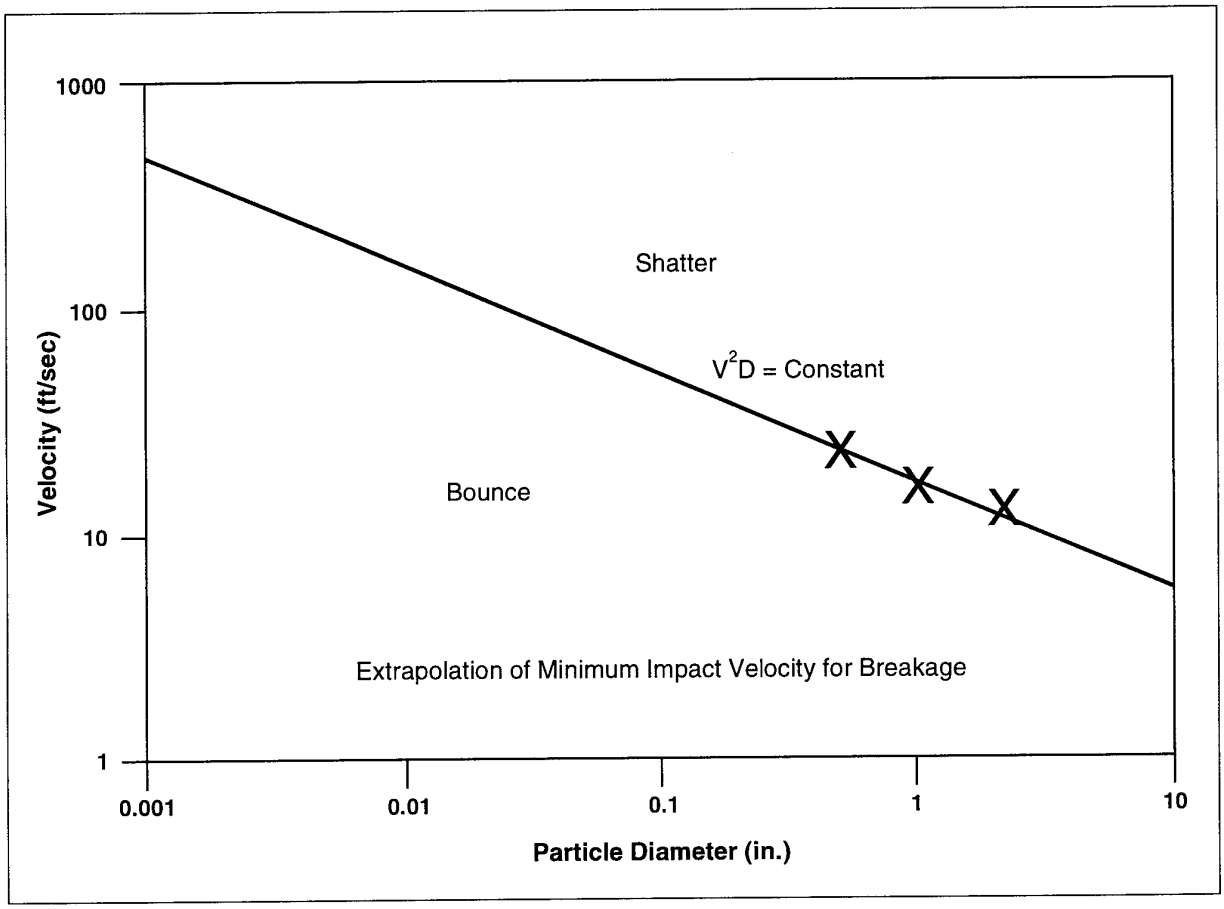

Figure 5-23

Shatter - Bounce Boundary

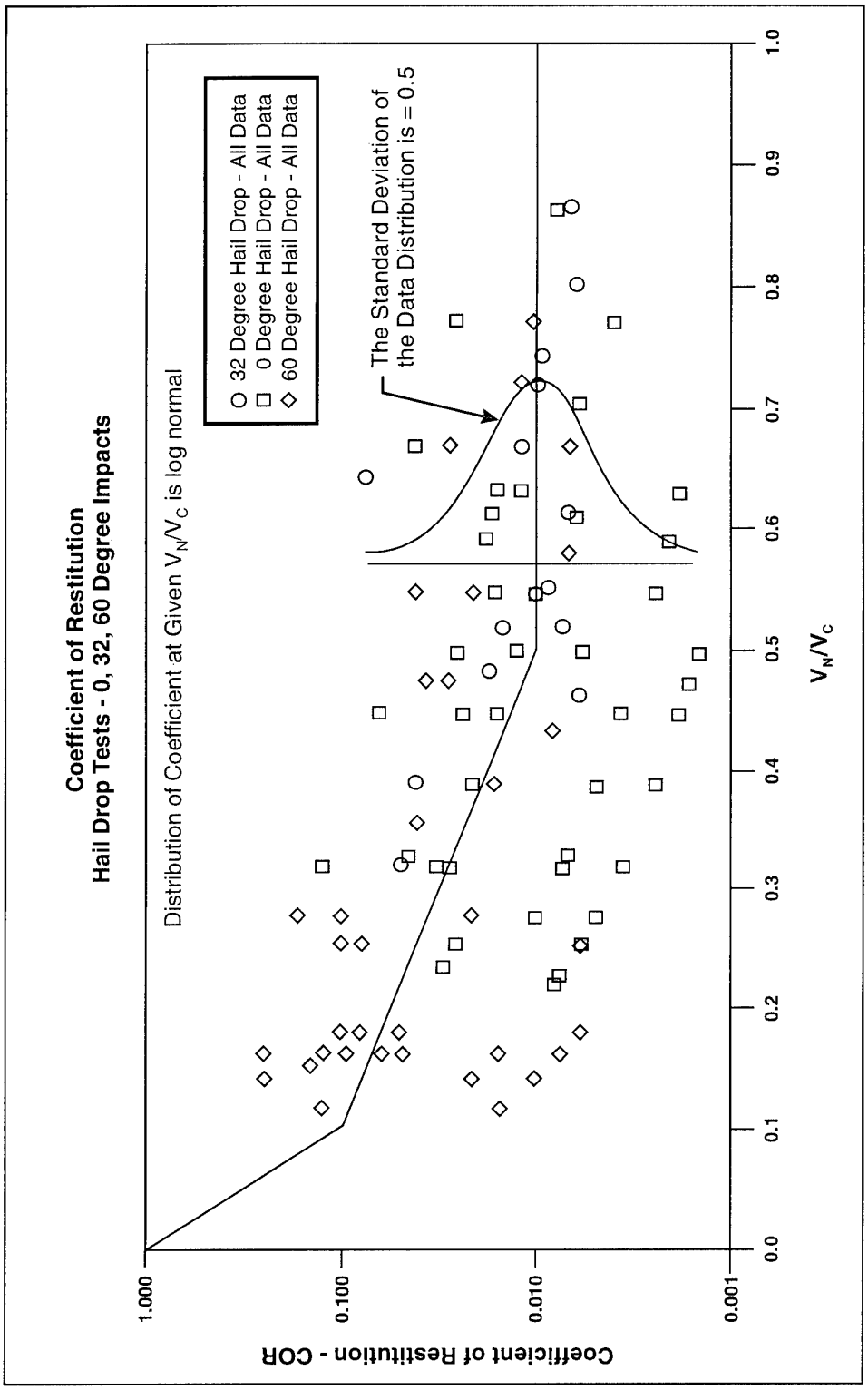

Figure 5-24

Correlation of Coefficient of Restitution

a) Inlet Air Spillage at Low Engine RPM/High Aircraft Speed Increases Engine Face Water/Air Ratio

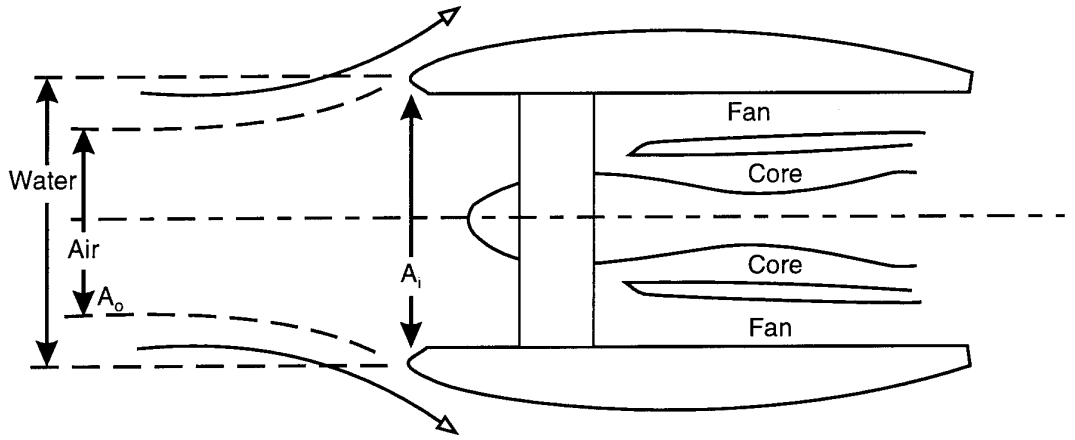

b) High Engine RPM/Low Aircraft Speed Decreases Engine Face Water/Air ratio by Reducing Air Spillage

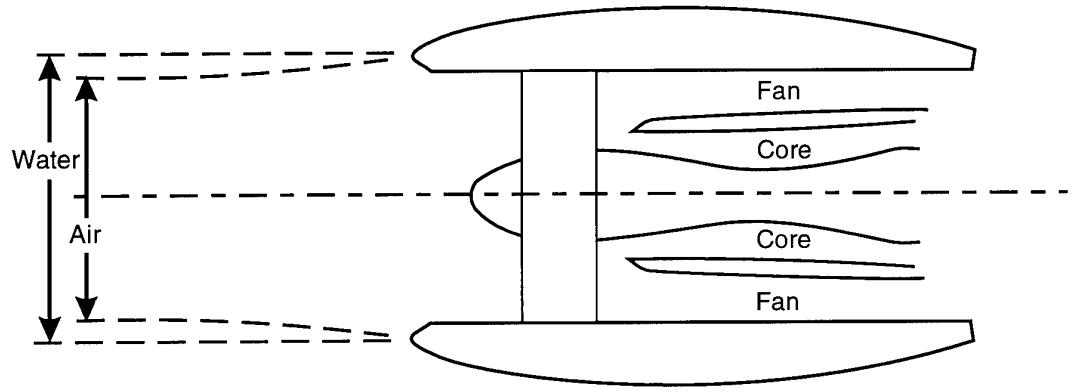

Figure 5-25

Scoop Factor

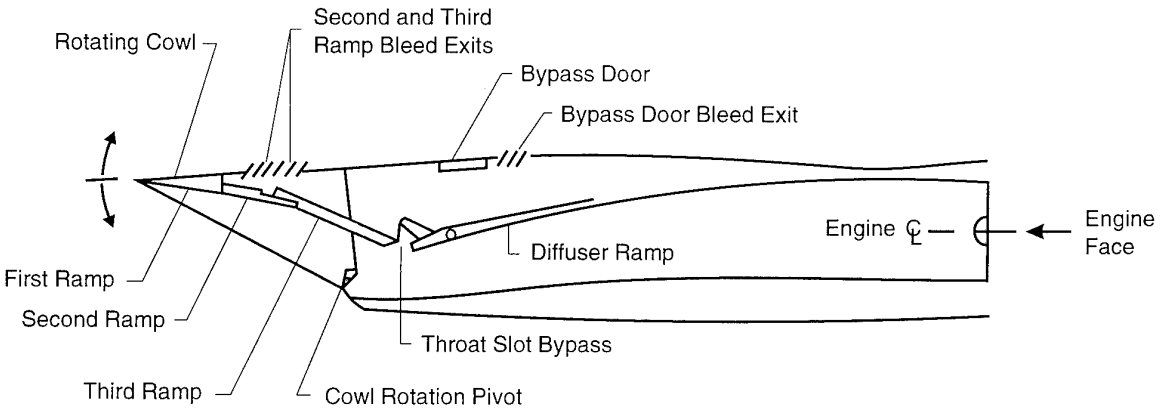

(From AIAA 8-12438 "Recent Propulsion System Flight Tests at NASA Dryden Flight Reearch Center by F.W. Burcham, L.P. Meyers, J. Nugent, P. Lasagna, and L.D. Webb, NASA Dryden Flight Research Center, Edwards AFB, CA)

Figure 5-26(a)

Diagram of the F-15 Inlet

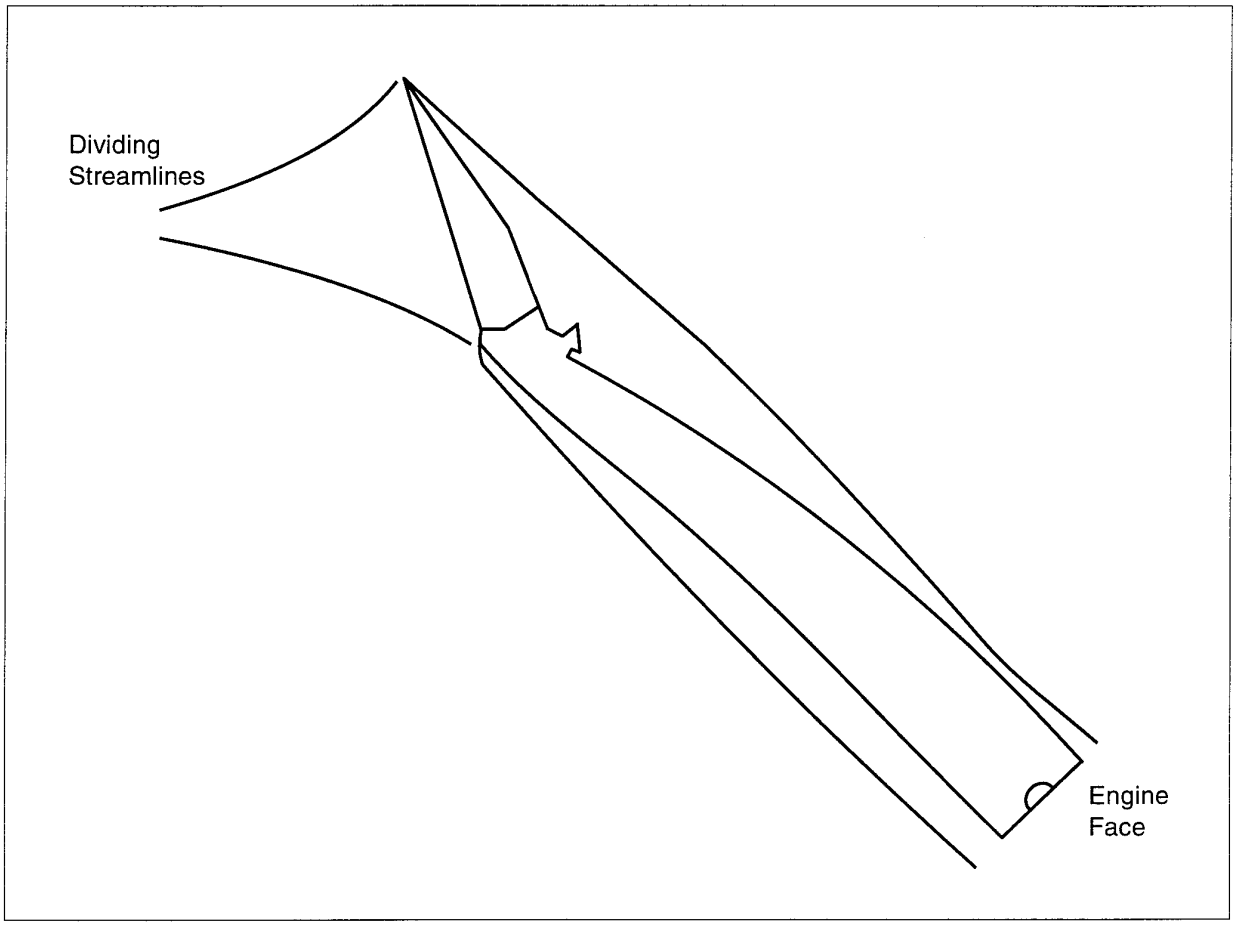

Figure 5-26(b)

Scoop Factor Schematic at High Angle-of-Attack

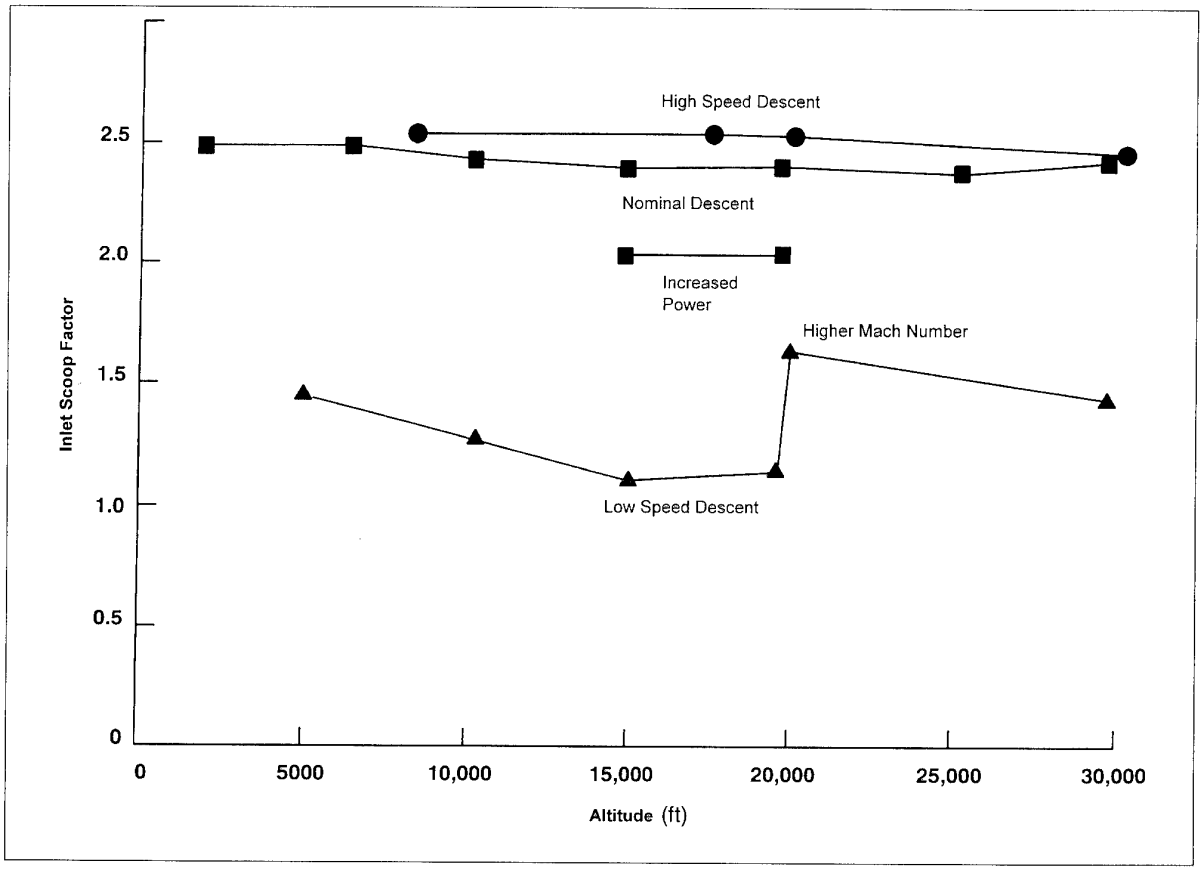

Figure 5-27(a)

Typical Idle Descent Inlet Scoop Factor

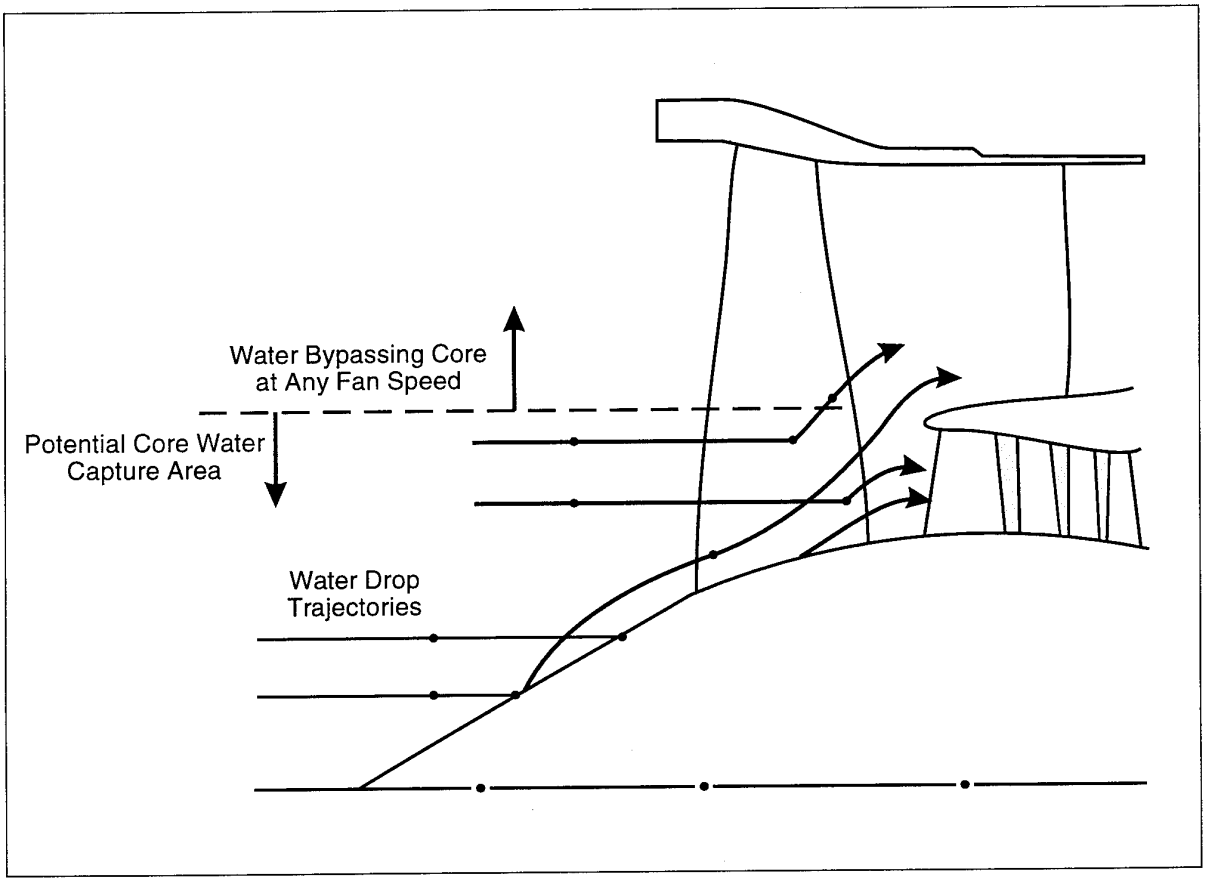

Figure 5-27(b)

Fan Centrifuges Water From Core

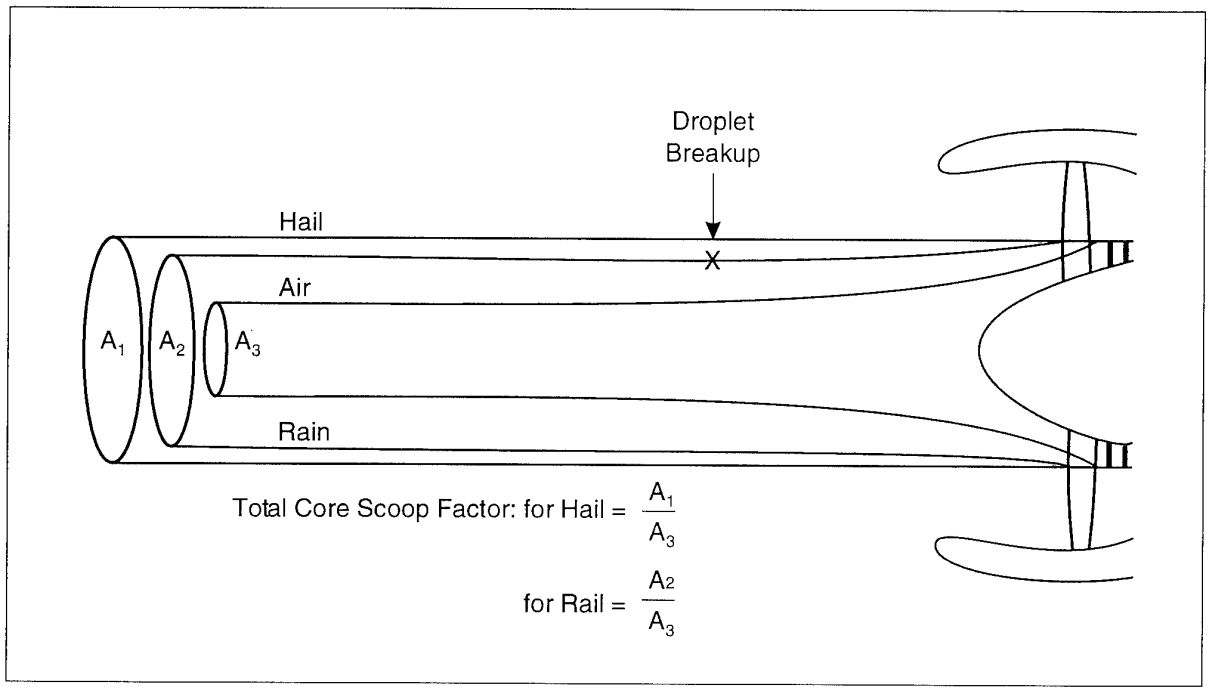

Figure 5-28

Core Capture Areas for Air, Rain and Hail - Typical
High - Bypass - Ratio Engine, 20,000 ft. Nominal Descent

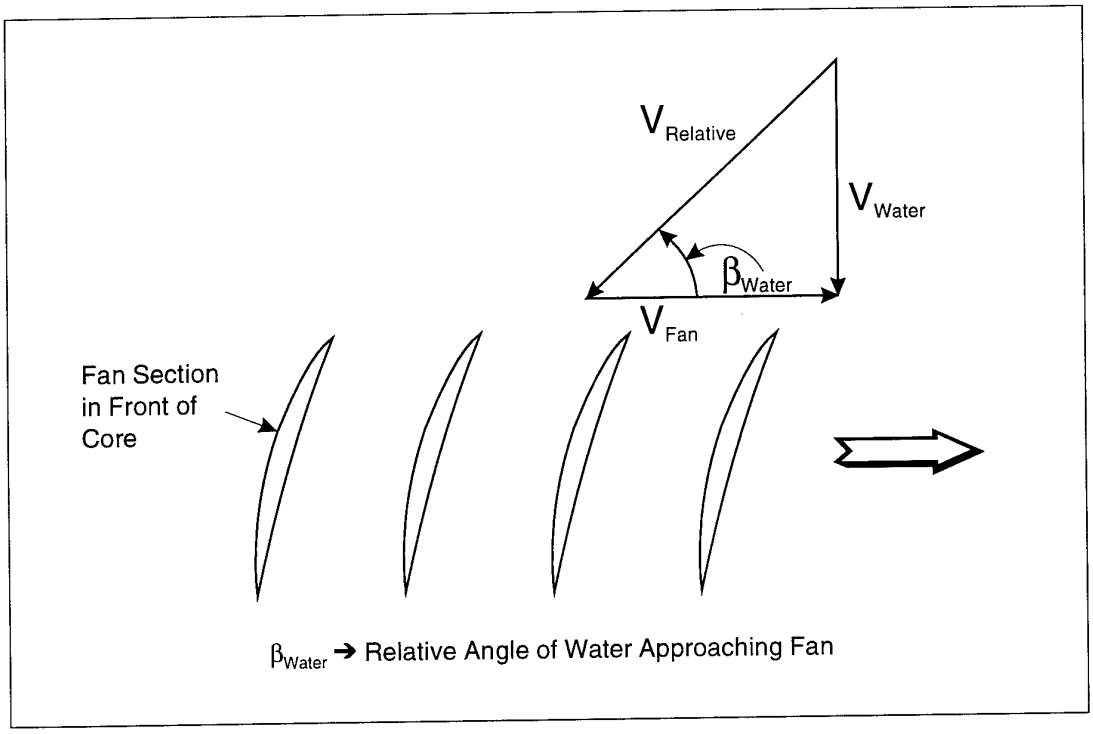

Figure 5-29

Effect of Water Velocity on Relative Inflow Angle

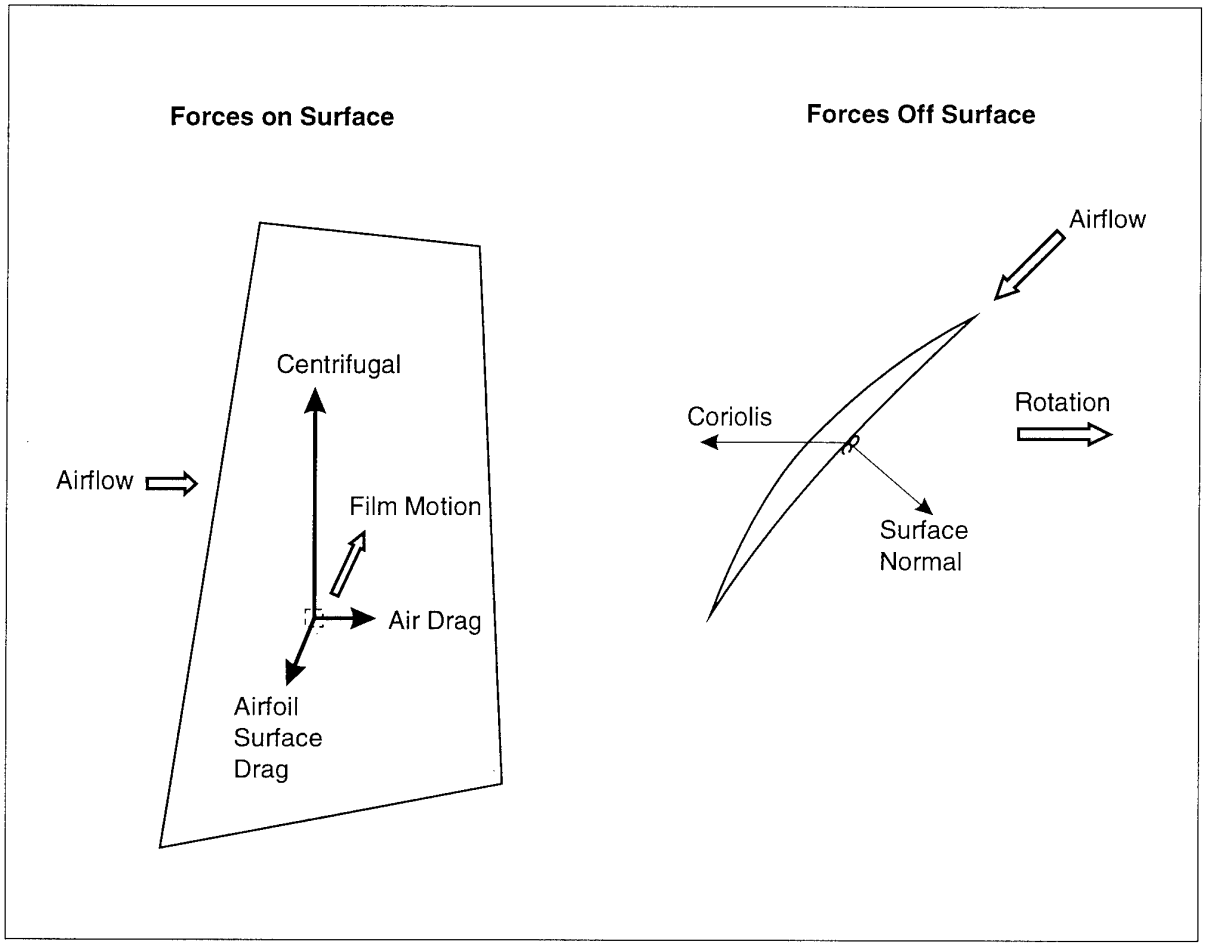

Figure 5-30

Forces of Water on Film

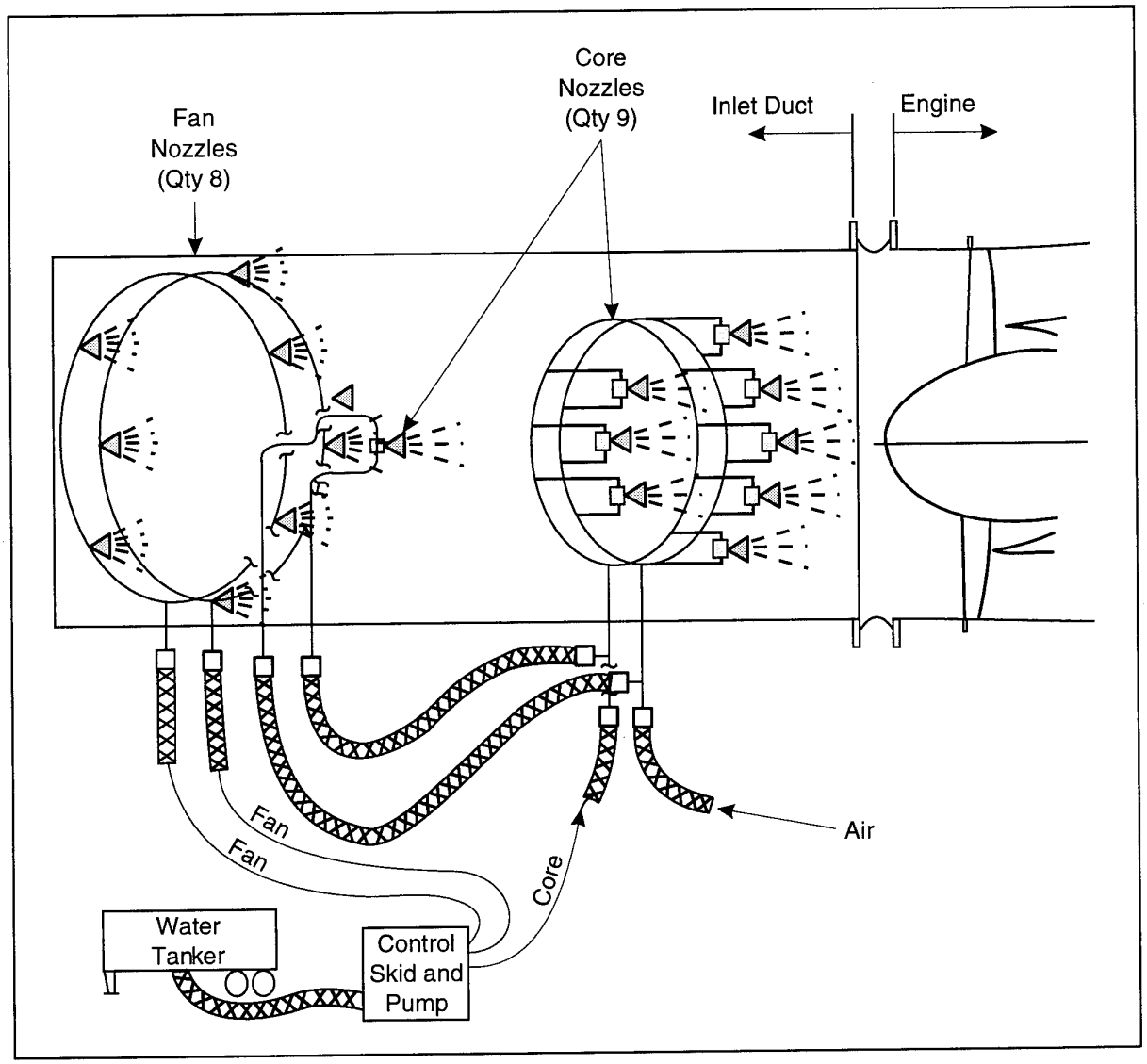

Figure 5-31

Schematic of Spray System Test Installation Configuration

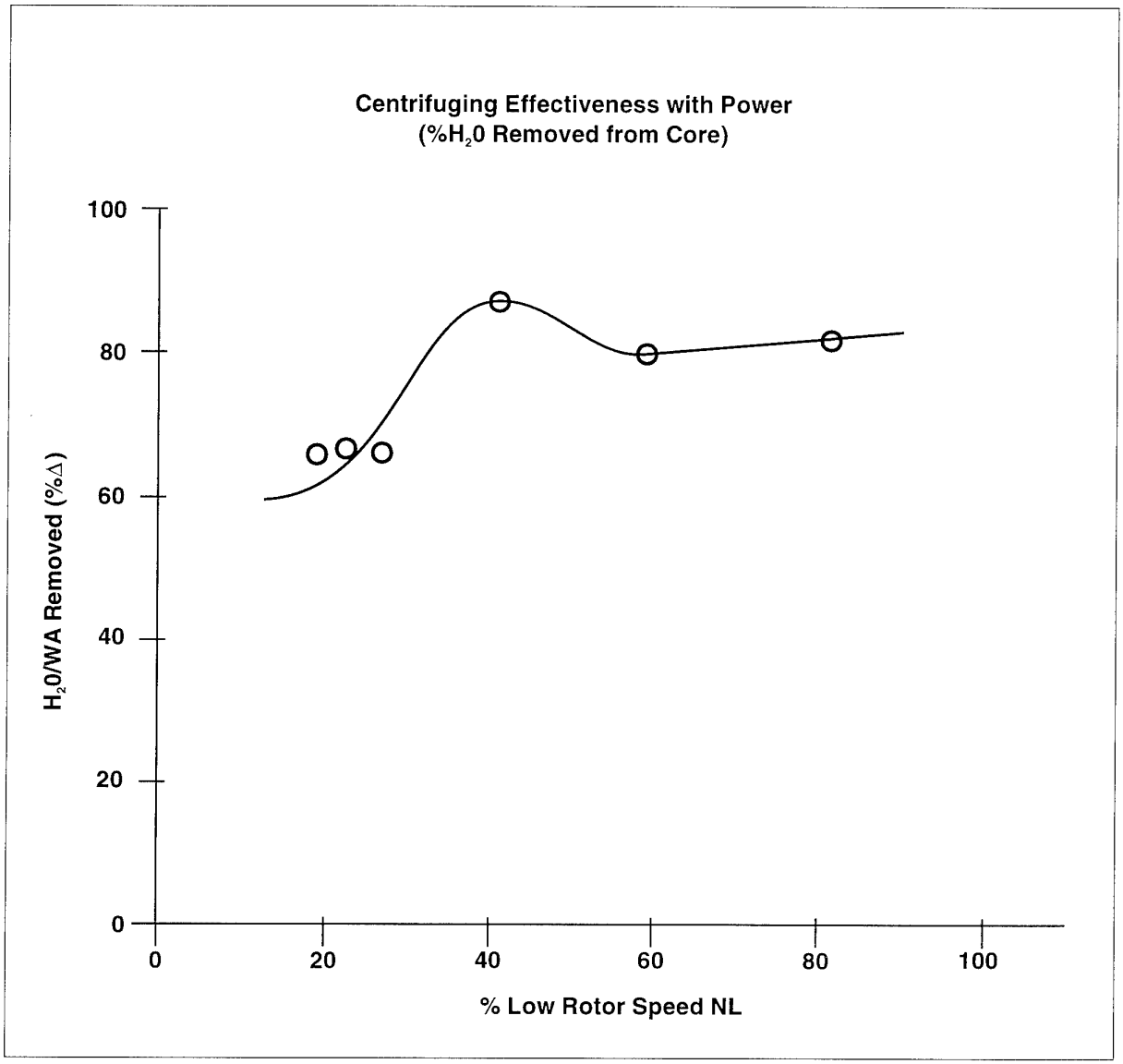

Figure 5-32

Engine Centrifuging Characteristics

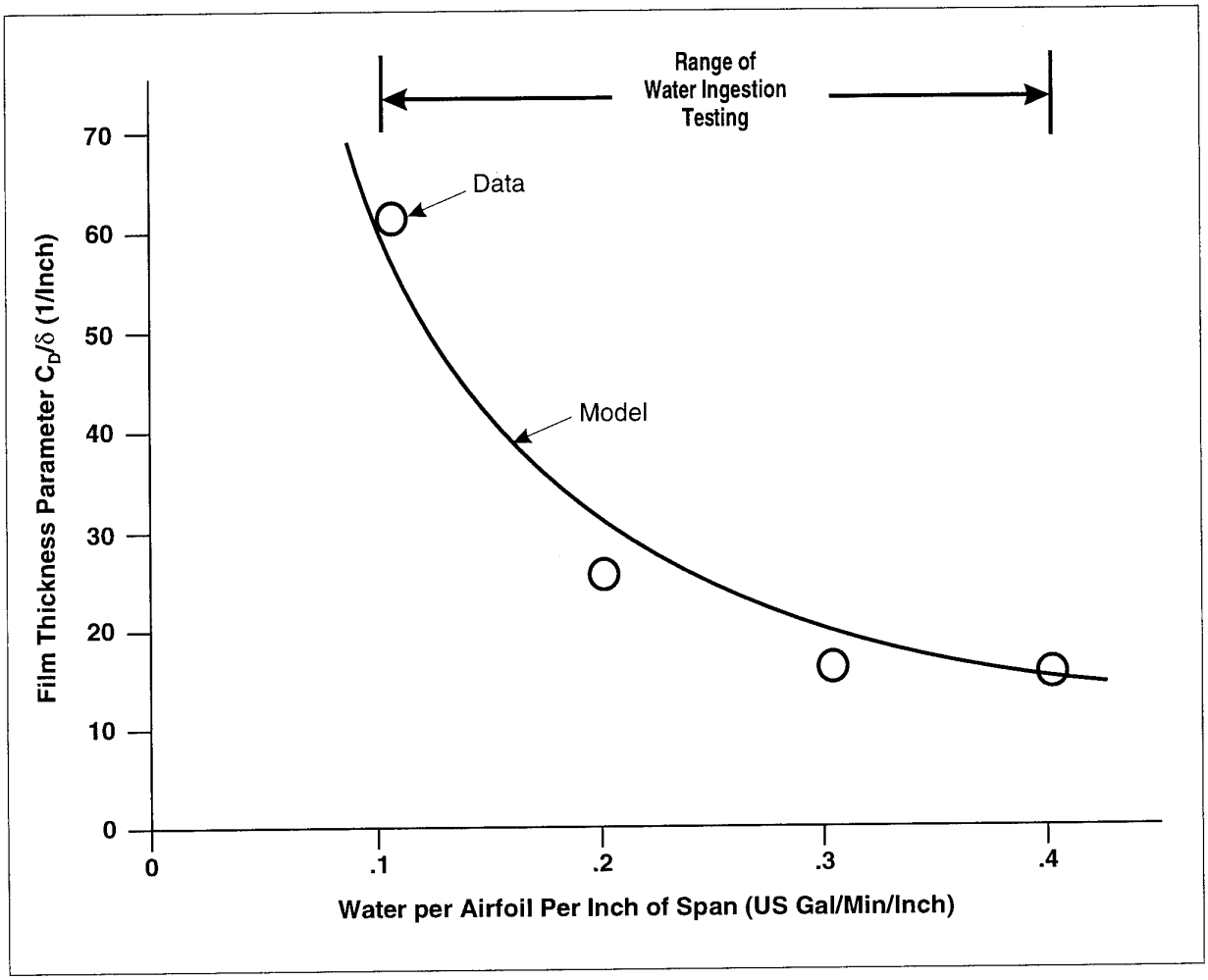

Figure 5-33

Model for Film Thickness Parameter

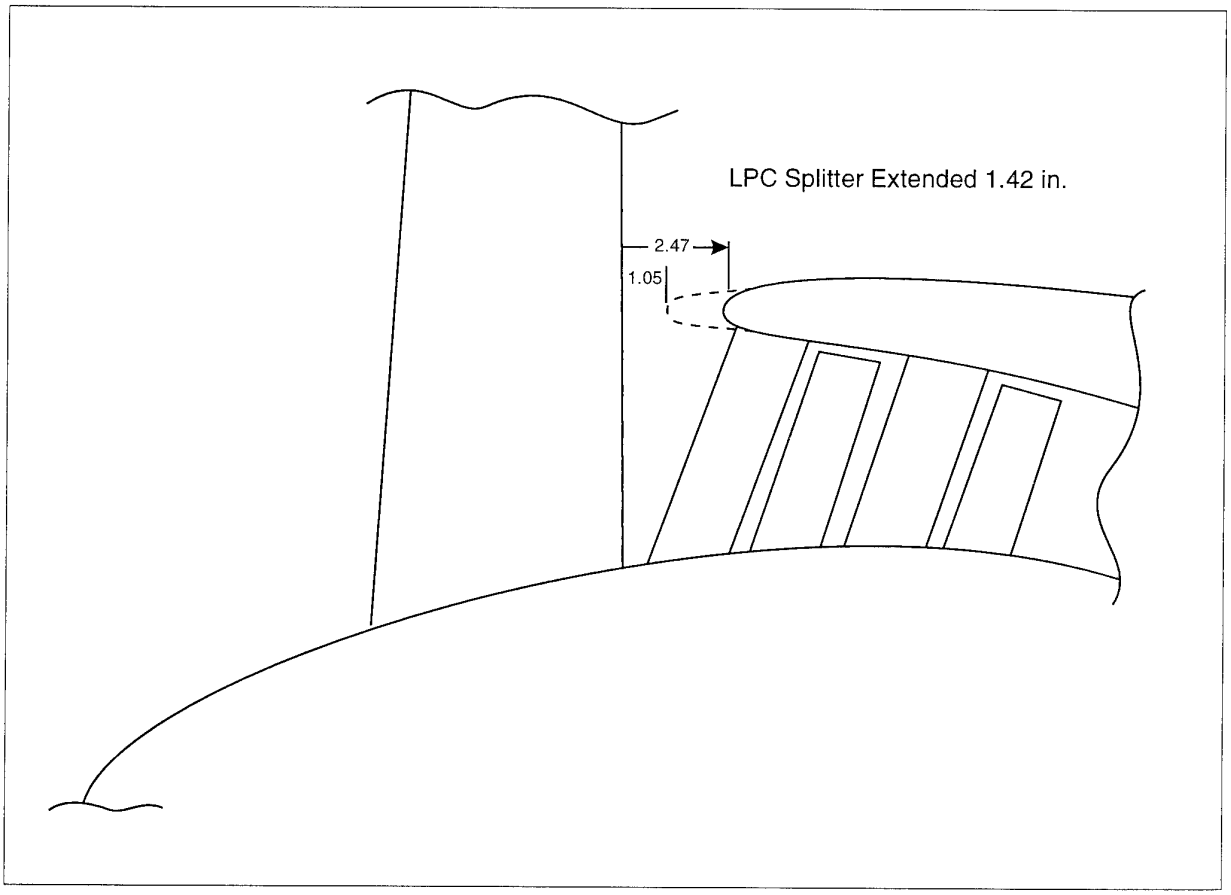

Figure 5-34

Schematic of Extended LPC Splitter Test Configuration

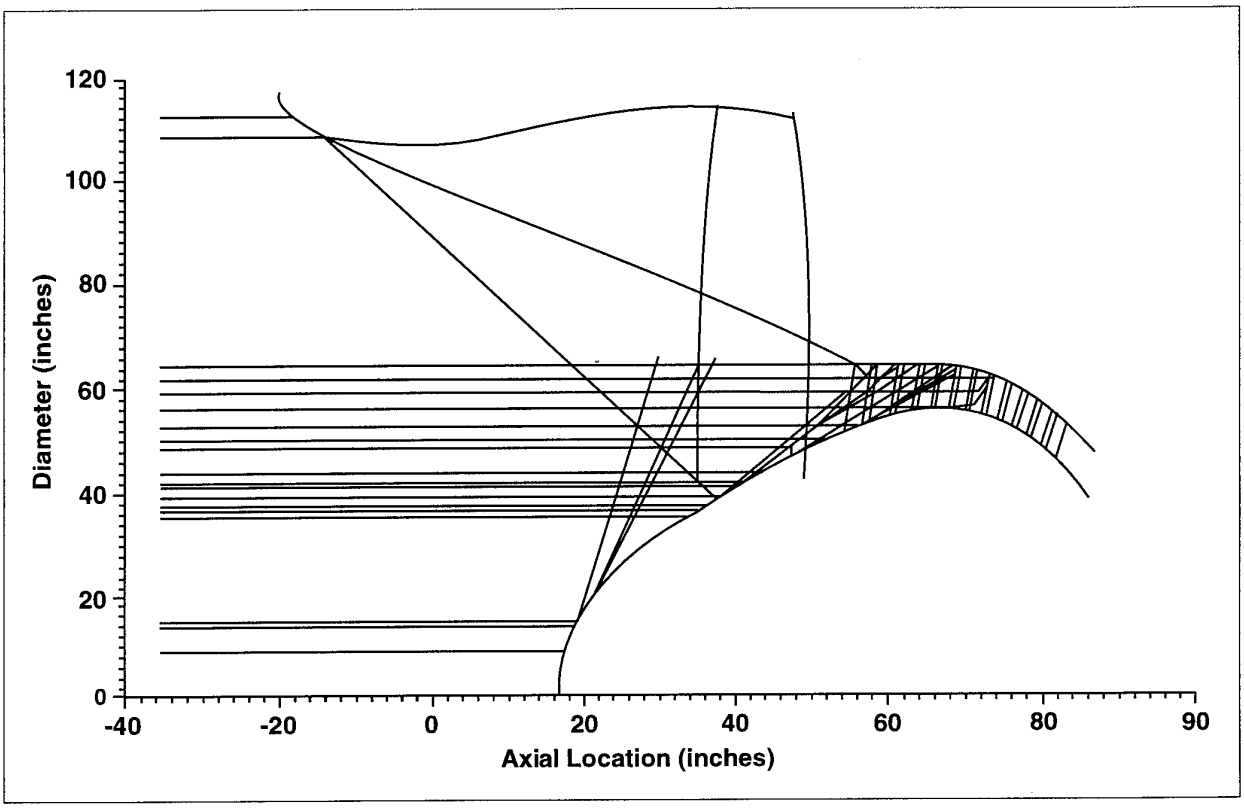

Figure 5-35

Hail Ingestion
(Typical Particle Tracks)

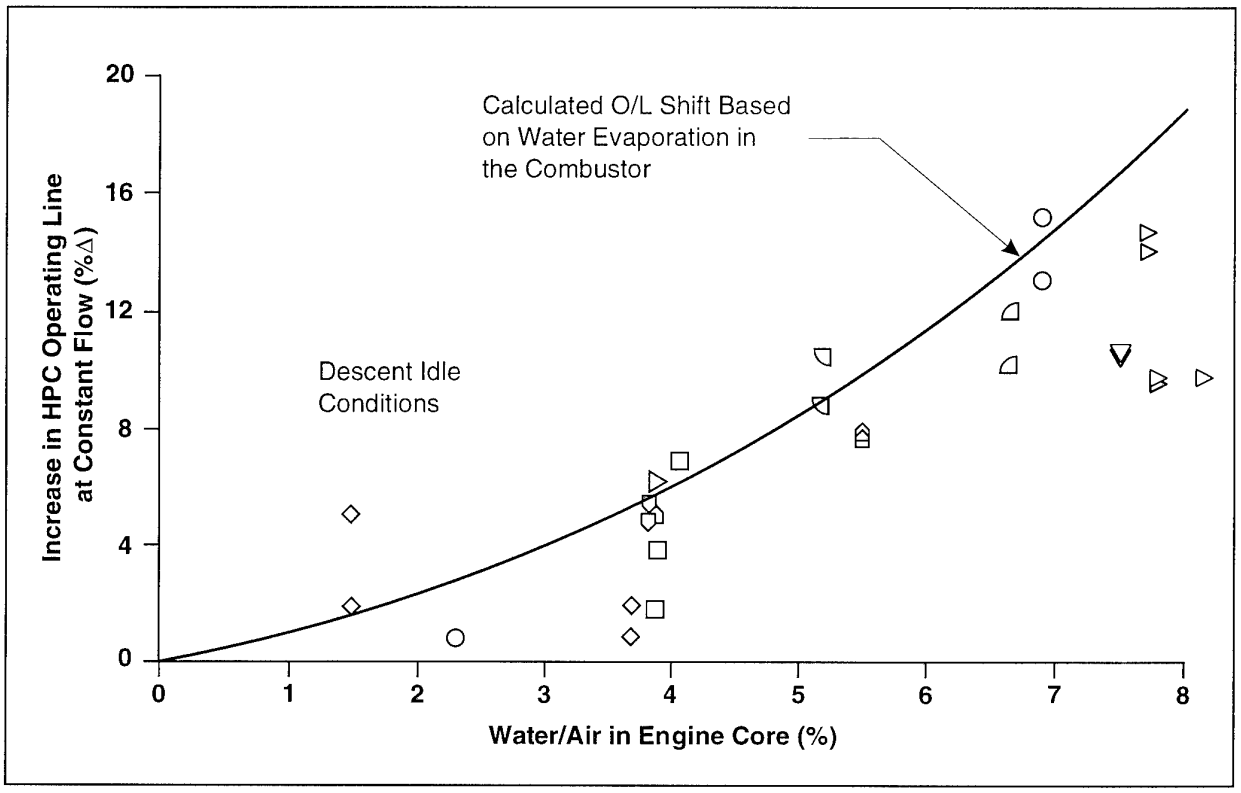

Figure 5-36

HPC Operating Line Shift is Consistent with Evaporation of Water in Combustor

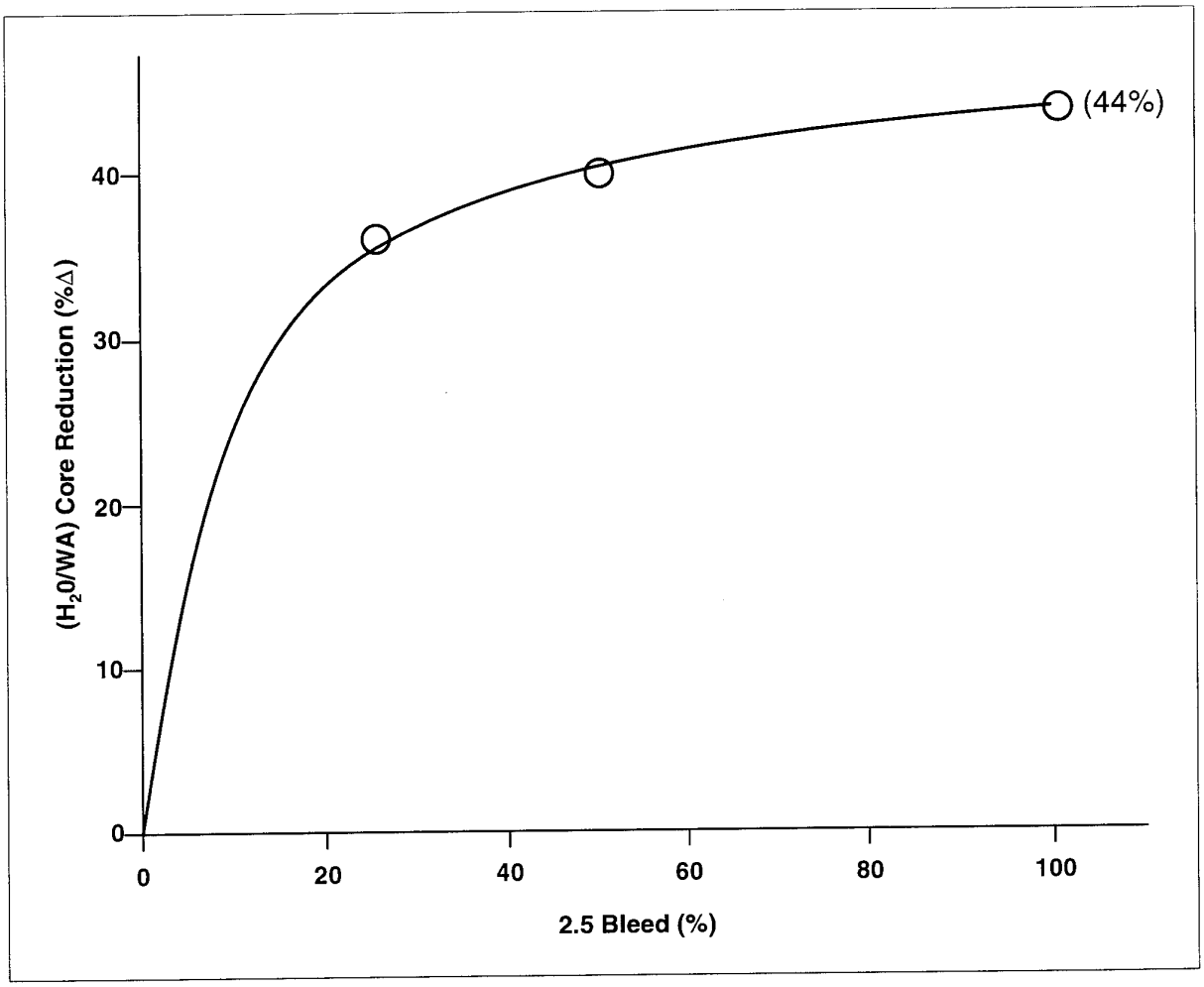

Figure 5-37

Effect of LPC Stability Bleed
(% H_20 Exiting LPC)

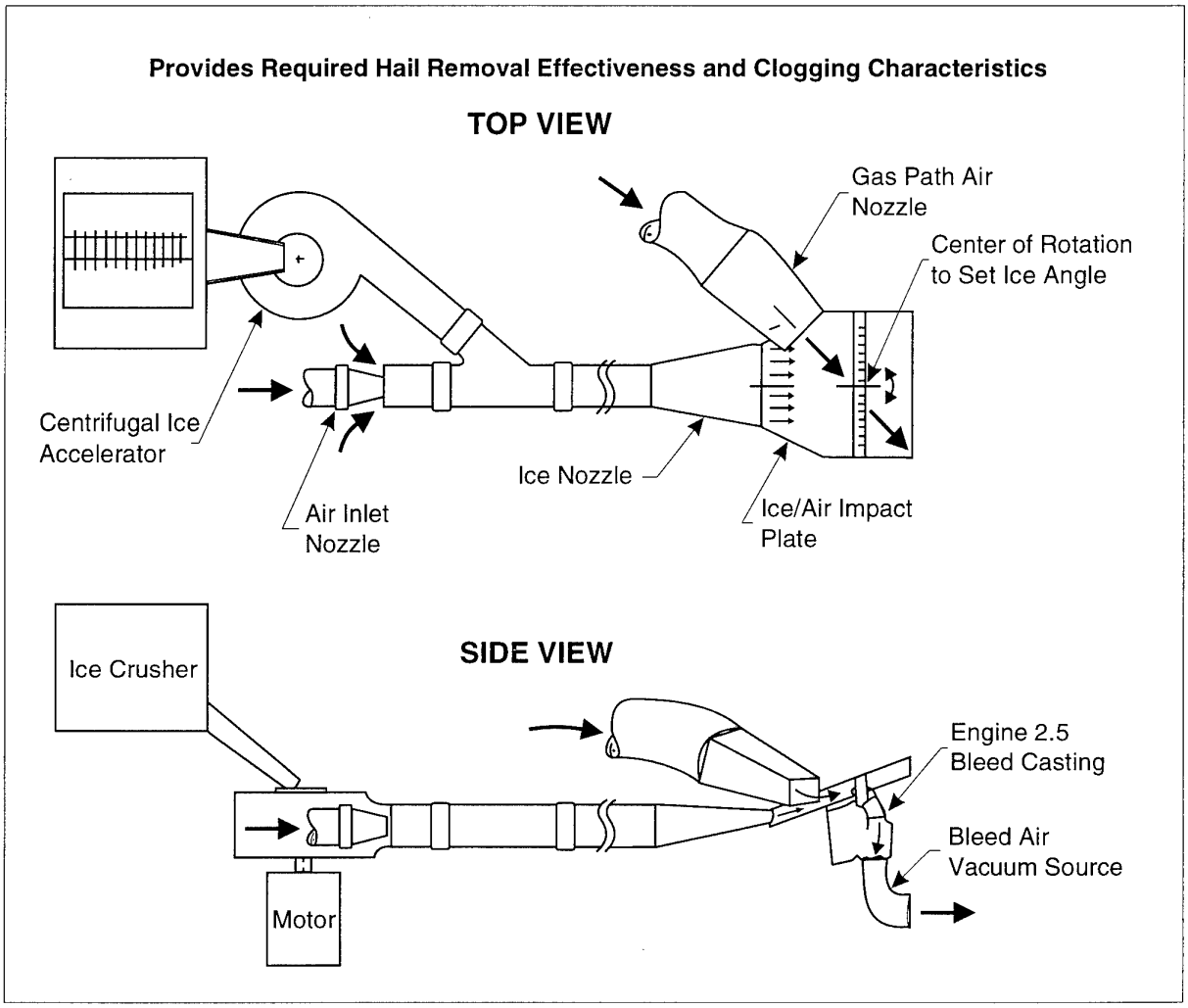

Figure 5-38

Bleed Rig Schematic

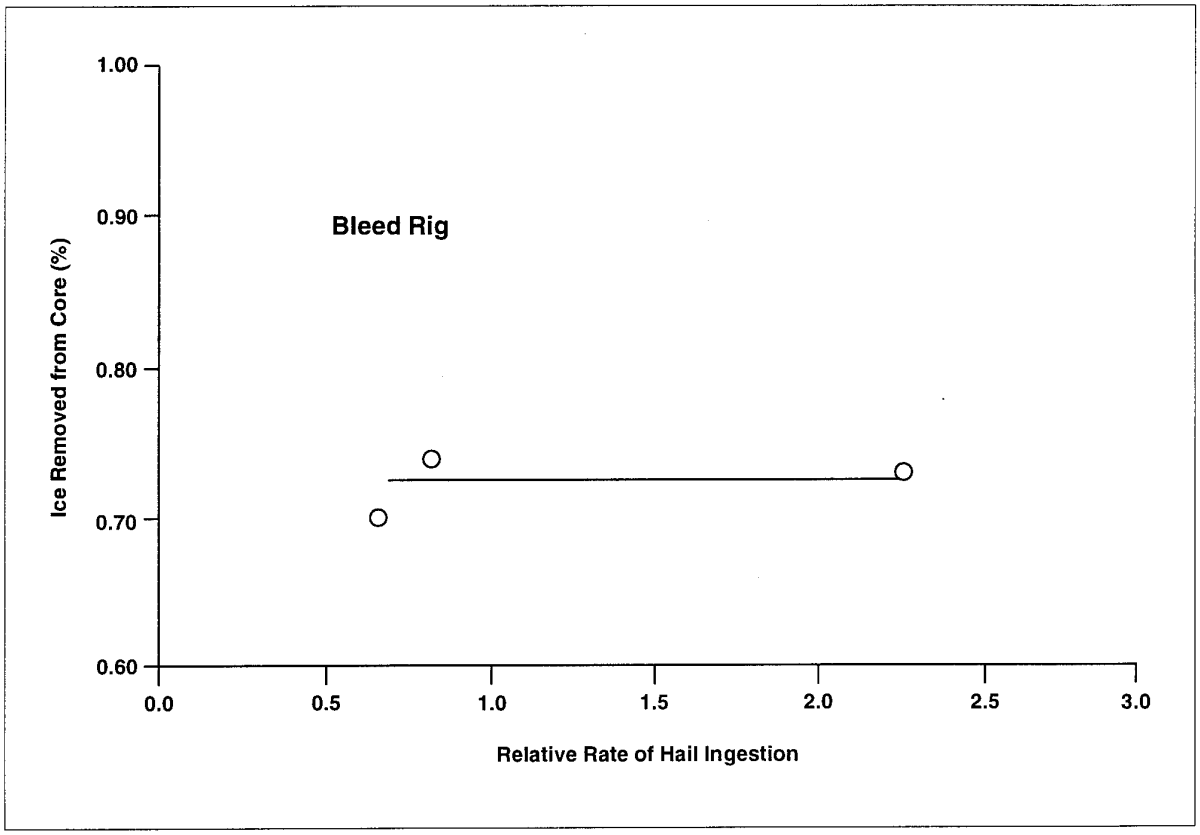

Figure 5-39

Ice Rate Sensitivity in Ice Ejection Effectiveness

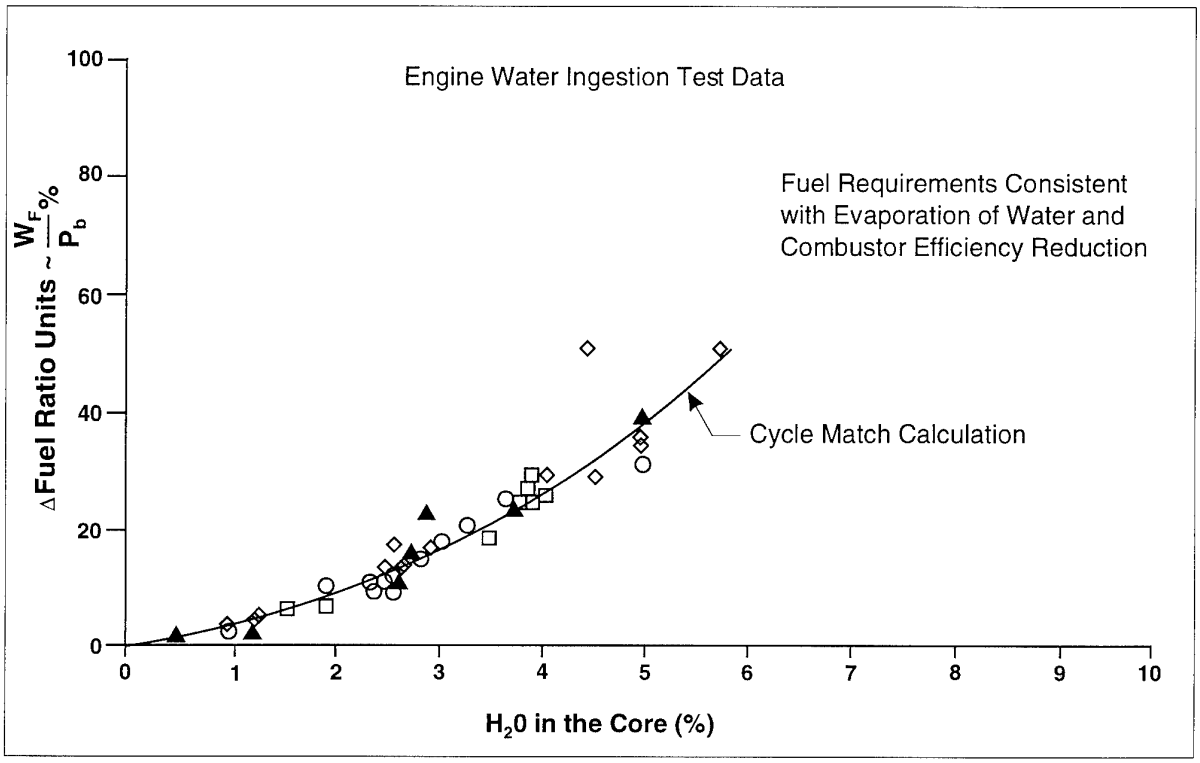

Figure 5-40(a)

Increased Fuel Requirements with Water Ingestion

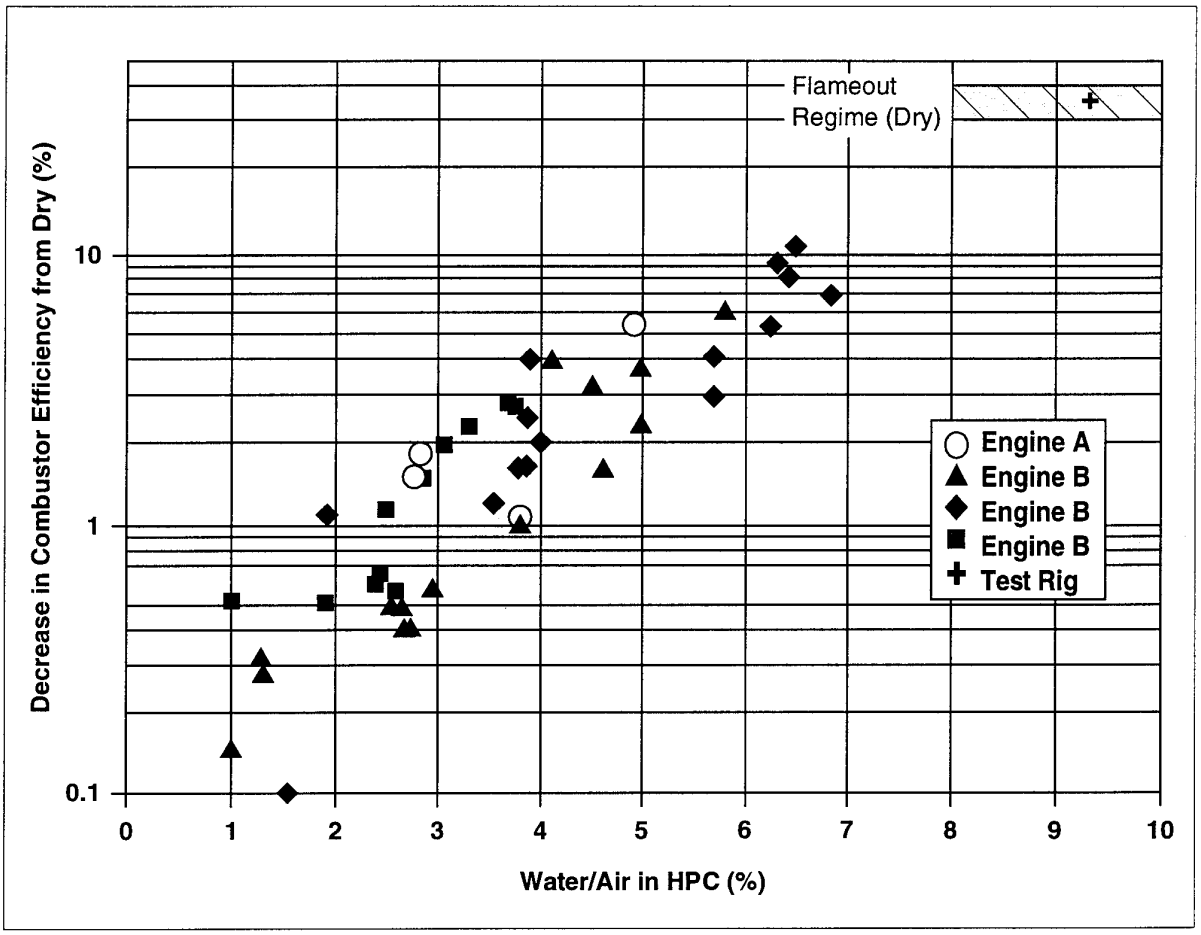

Figure 5-40(b)

Burner Efficiency vs. Water/Air in Core

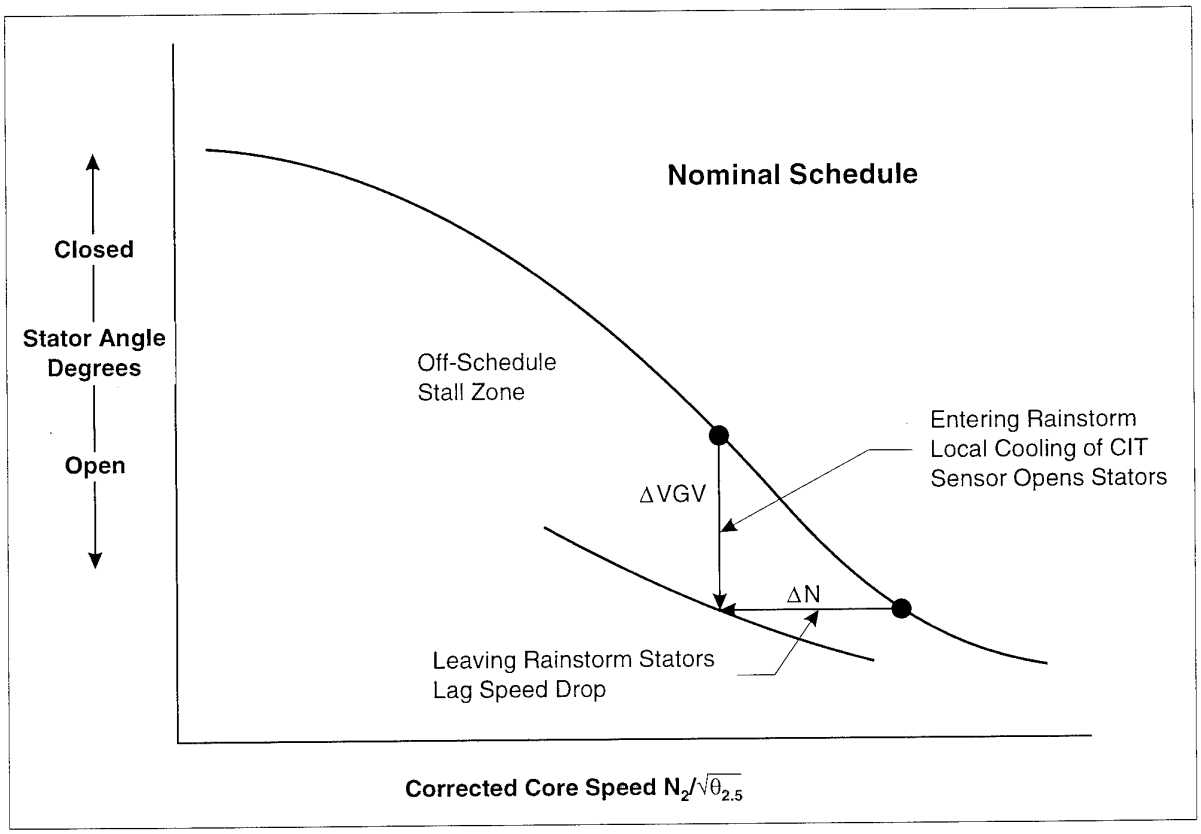

Figure 5-41

Rain Induced Stator Schedule Errors

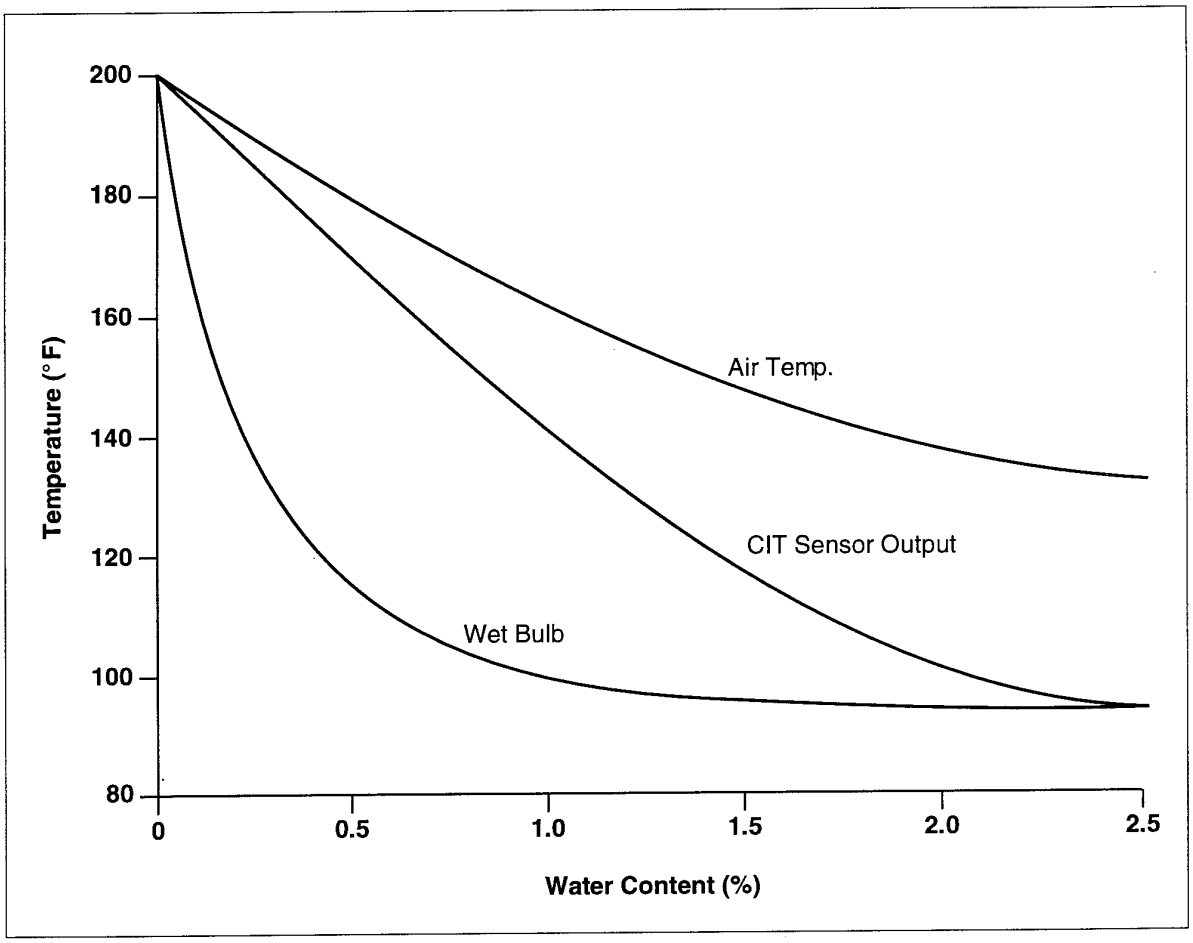

Figure 5-42

Effect of Airflow on CIT Sensor Measurement

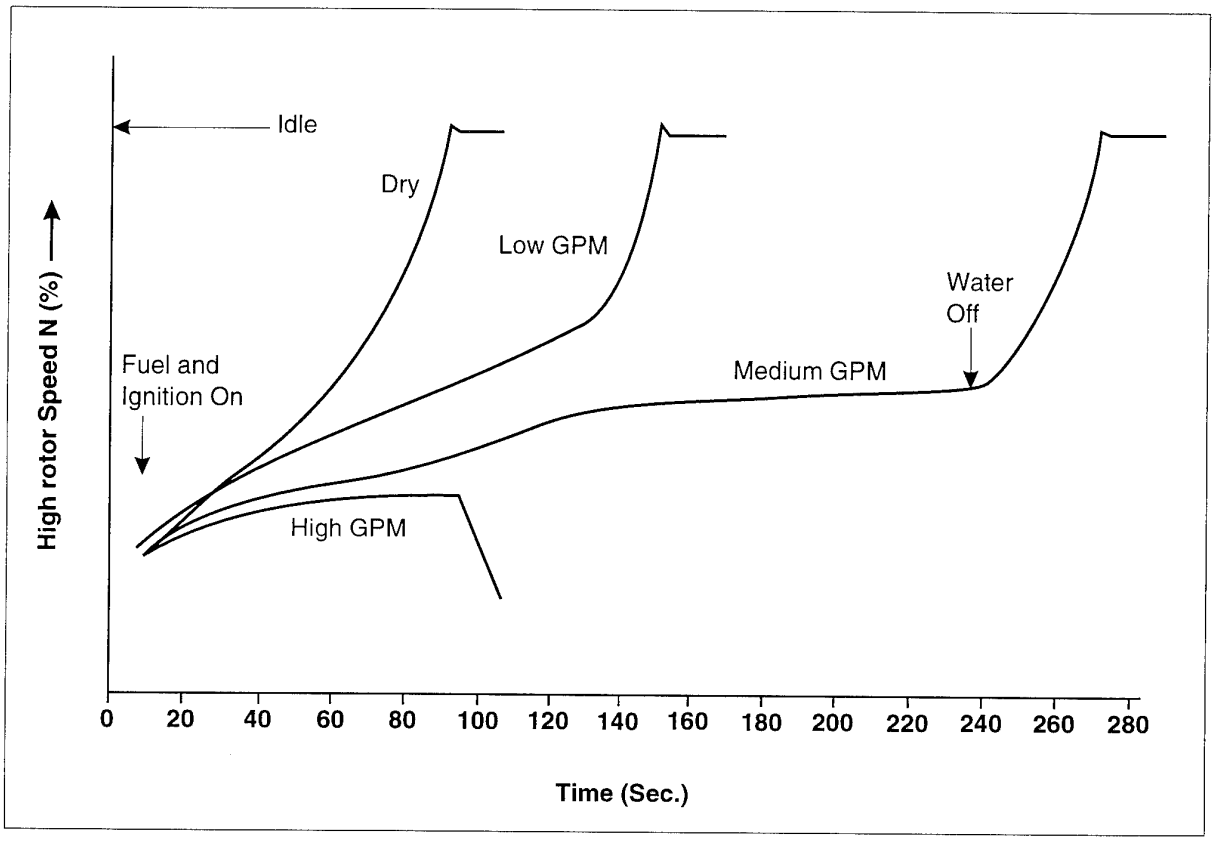

Figure 5-43

Effect of Water Ingestion on Engine Start

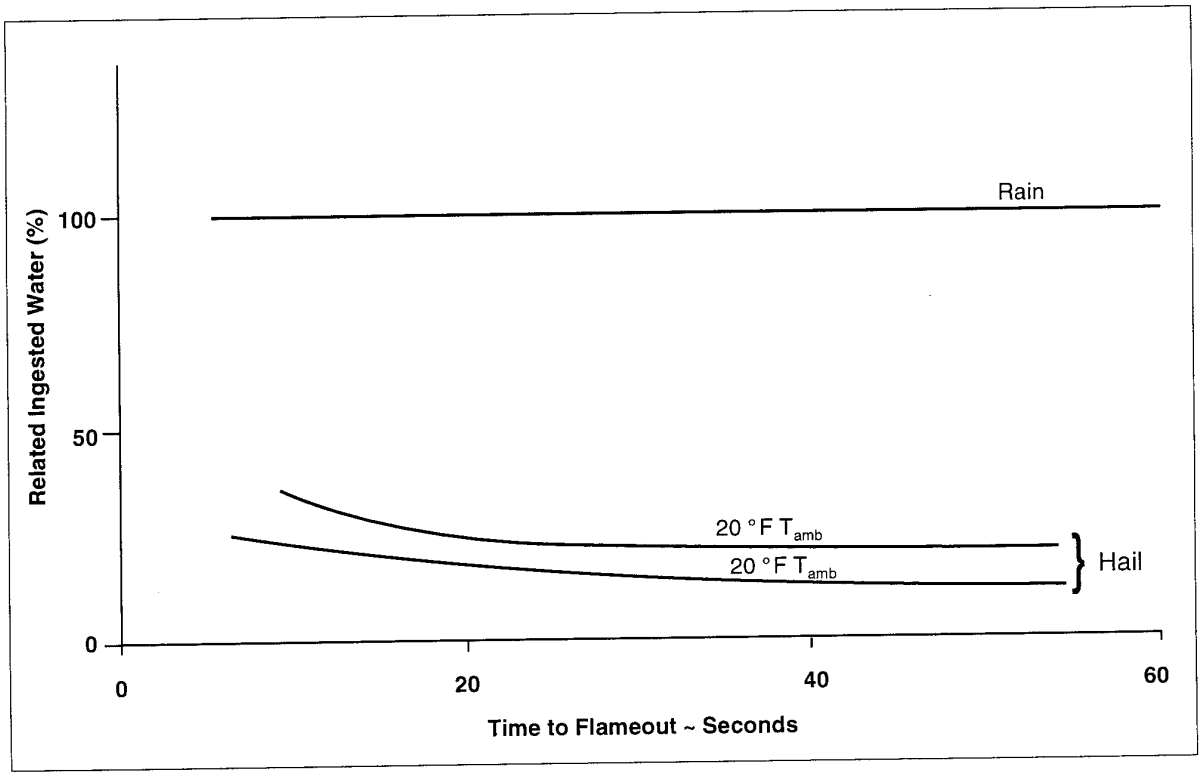

Figure 5-44

Water Ingestion Capability Tested for a High Bypass Ratio Engine

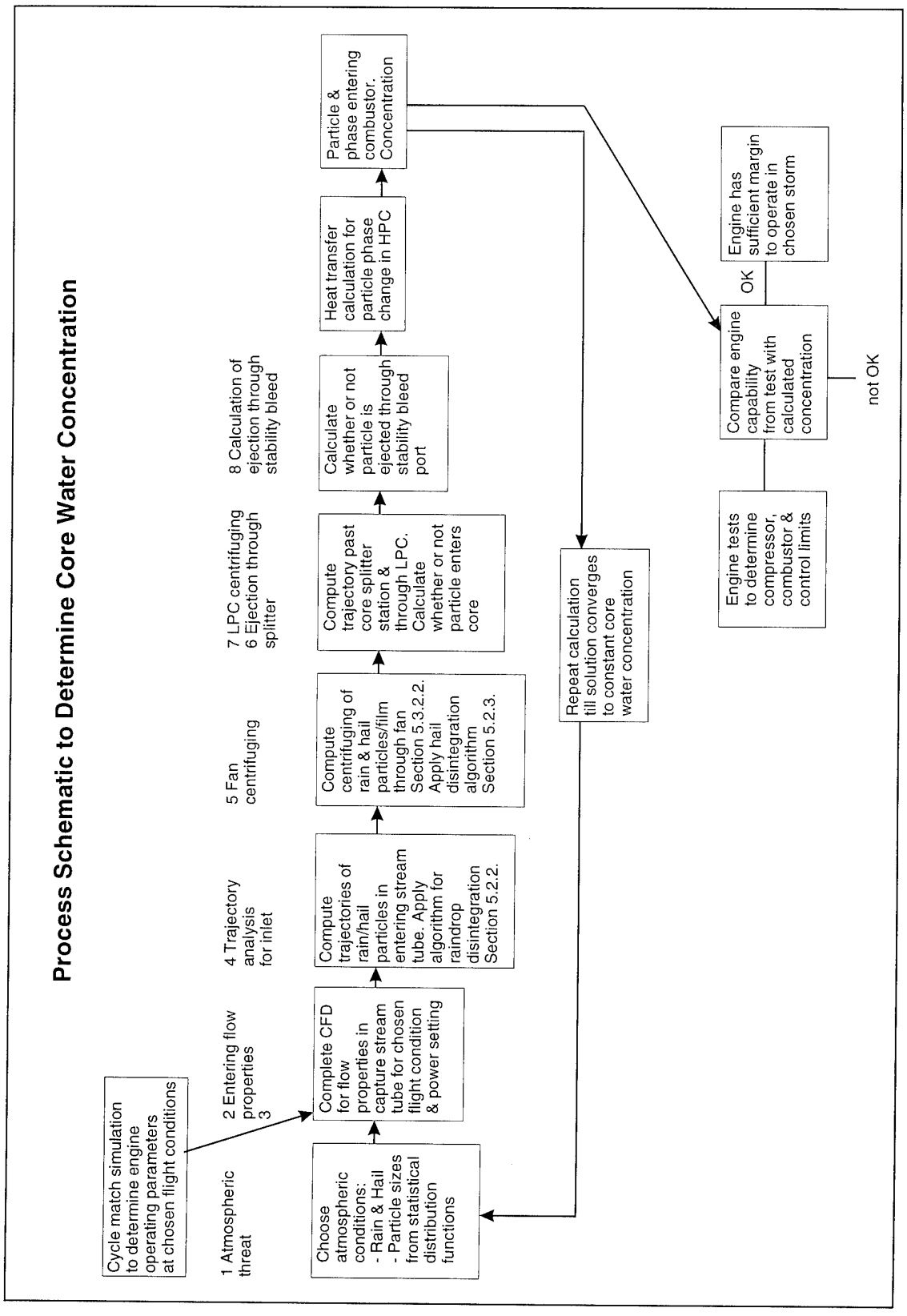
Process Schematic to Determine Core Water Concentration
Cycle match simulation to determine engine operating parameters at chosen flight conditions
1 Atmospheric threat
2 Entering flow properties
3
4 Trajectory analysis for inlet
5 Fan centrifuging
7 LPC centrifuging
6 Ejection through splitter
8 Calculation of ejection through stability bleed
Choose atmospheric conditions:
- Rain & Hail
- Particle sizes from statistical distribution functions
Complete CFD for flow properties in capture stream tube for chosen flight condition & power setting
Compute trajectories of rain/hail particles in entering stream tube. Apply algorithm for raindrop disintegration Section 5.2.2.
Compute centrifuging of rain & hail particles/film through fan Section 5.3.2.2. Apply hail disintegration algorithm Section 5.2.3.
Compute trajectory past core splitter station & through LPC. Calculate whether or not particle enters core
Calculate whether or not particle is ejected through stability bleed port
Heat transfer calculation for particle phase change in HPC
Particle & phase entering combustor. Concentration
Repeat calculation till solution converges to constant core water concentration
Engine tests to determine compressor, combustor & control limits
Compare engine capability from test with calculated concentration
OK
not OK
Engine has sufficient margin to operate in chosen storm

Figure 5-45

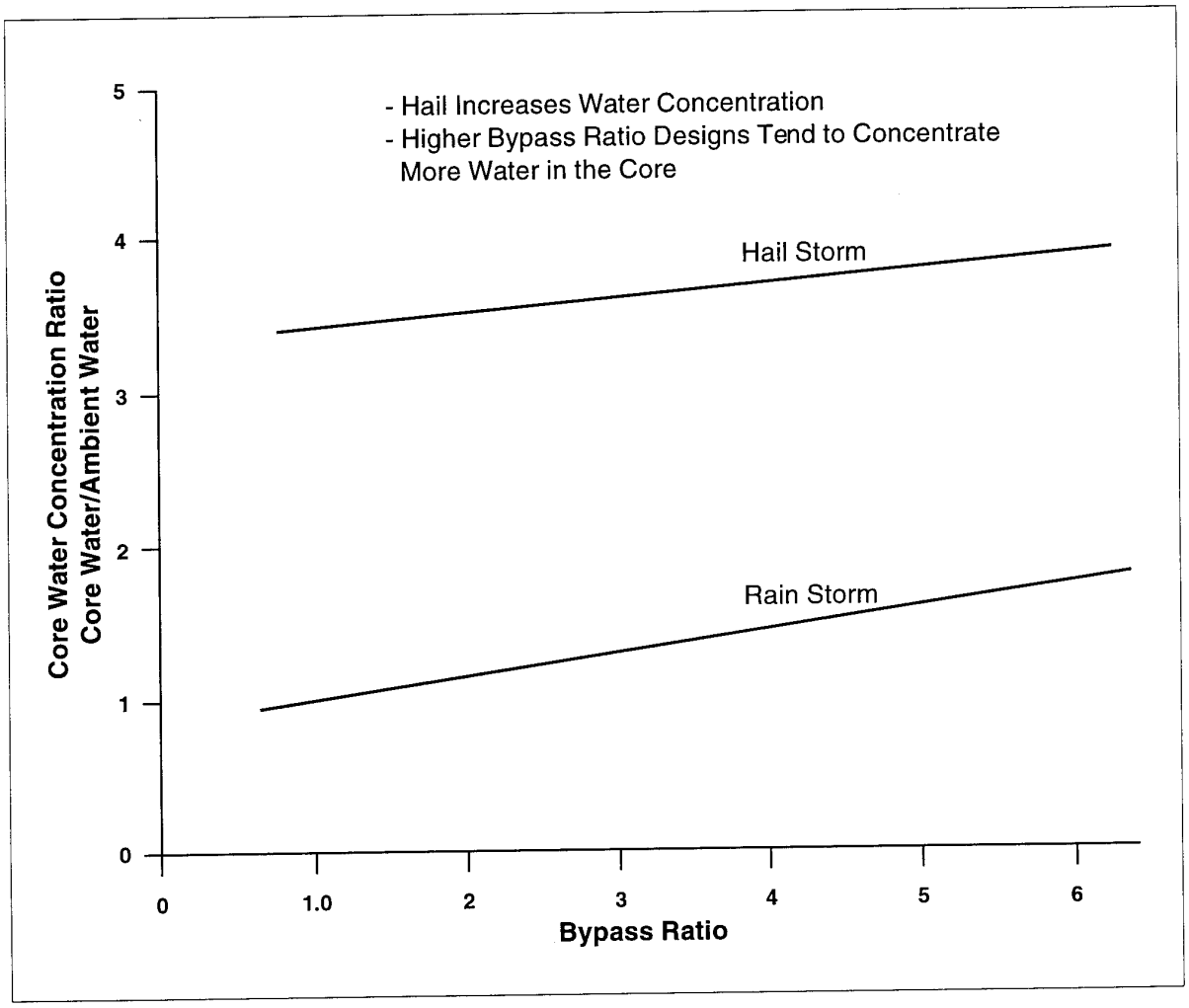

Figure 5-46

Bypass Ratio Effects on Core Rain/Hail Concentration

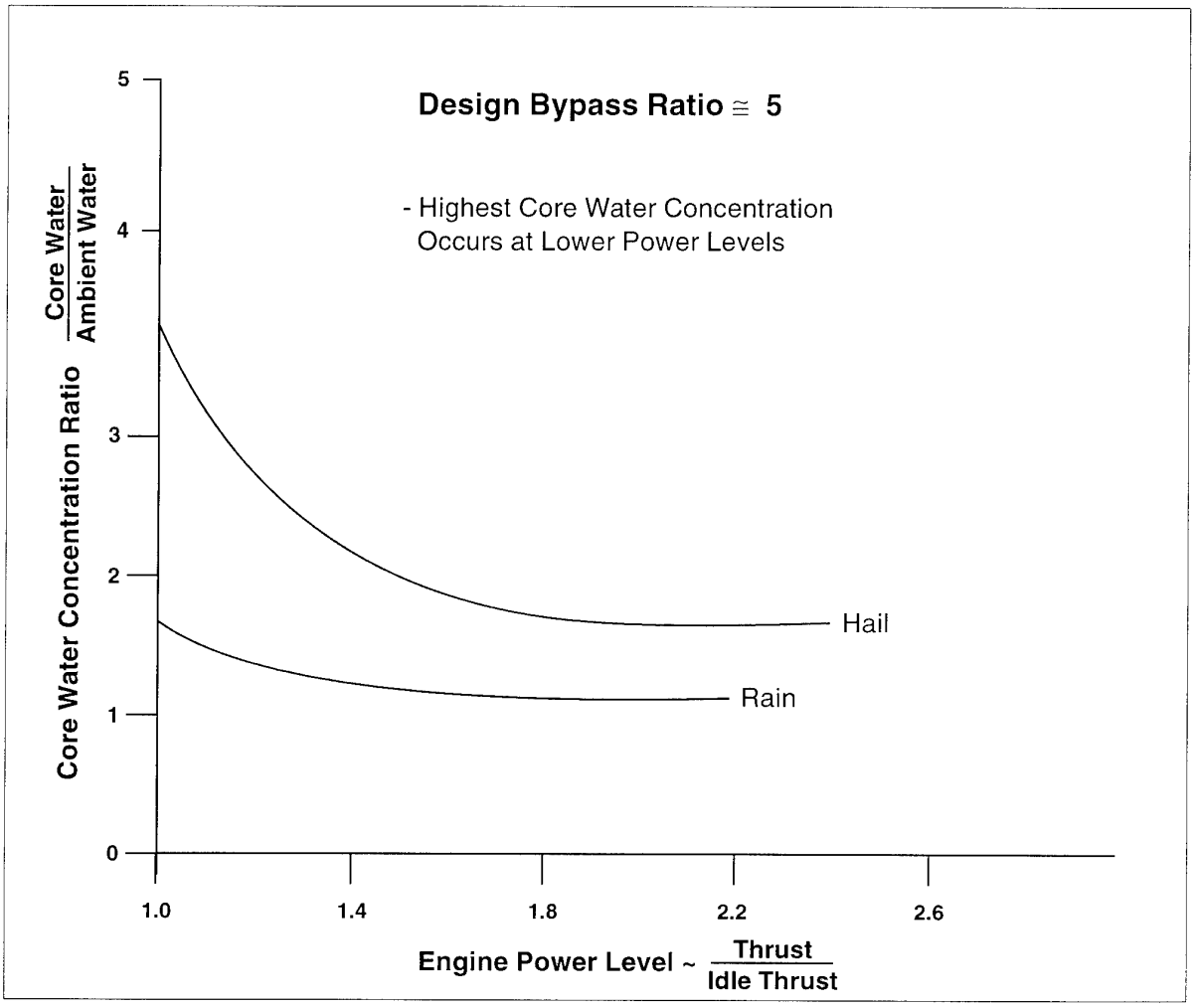

Figure 5-47

Engine Power Level Effect on Core Water Concentration

6. SPECIFICATIONS AND TEST REQUIREMENTS[1]

6.1 INTRODUCTION

A survey of acceptance specifications, dealing with hazards which fall within the scope of this publication, has been carried out. The scope embraces the estimation of the "effects of ingested water vapour, inlet condensation, rain, snow and hail on engine performance... and on engine operability...". The information extracted may not be up-to-date, and will, in all likelihood, not be complete. A conscious effort has been made not to include specifications treating hazards to aircraft which border on those within the stated scope, e.g. icing, salt water, birds, steam (carrier operation), rocket gases, sand and dust, and other foreign objects. In many cases, especially in that of icing, the separation was not possible, because some specifications tended to combine icing with, say, snow or ice crystal ingestion problems. Extracts from specifications will be quoted verbatim in all cases, and will be identifiable by indentation throughout the text. For that reason, units have not been edited to conform with the current SI practice. Key figures or tables from the references have been included (Tables 6-1 to 6-4 and Figures 6-1 and 6-2).

It should be noted, that all references in this chapter are for information purposes only and that the original and most current texts of specifications should be consulted for actual working applications. The following specifications and requirements have been found to contain relevant information for this survey:

- Military Specifications:
  - United States MIL-E-008593E(AS)
  - United States MIL-E-5007D
  - United Kingdom Defence Standard 00-971
- Civil Regulations:
  - Federal Aviation Regulations (US):
    - FAR 25, 29 and 33
  - British Civil Airworthiness Requirements:
    - Sections C and D
  - Joint Airworthiness Requirements:
    - JAR-E and JAR-25

The presentation of civil regulations first gives the applicable, general or aircraft/installation references followed by the engine specific sections.

6.2 MILITARY SPECIFICATION (United States)

6.2.1 MIL-E-008593E(AS): Turboshaft and Turboprop Aircraft Engines

The Military Specification MIL-E-008593E(AS), 1 March 1984, outlines "The General Specification for Engines, Aircraft, Turboshaft and Turboprop". A note indicates that the specification is approved for use within the Department of the Navy only. Prepared by the Naval Air Propulsion Center (PE21) for the Naval Air Systems Command (AIR-5360D), it is to be used in lieu of MIL-E-8593A, 15 October 1975, and it supersedes NAPC-E-80002, 7 November 1980. This specification is an update of one with a wider approval, MIL-E-008593D, but is believed to be representative for the purposes of this section.

3.2.5.4 Humidity Resistance. The engine components shall be resistant to malfunction and deterioration when subjected to 95 percent or higher humidity conditions for extended periods.

3.2.5.6.3 Ice Ingestion. The engine shall be capable of ingesting hail and sheet ice (3.0 inches x 9.0 inches x 0.25 inch) without flameout, lengthy power recovery, sustained power loss exceeding 10 percent of the power at the operating condition or major structural damage which would cause the engine to fail. The time for power recovery shall be specified in the engine specification. This capability shall be demonstrated in the ice ingestion test of 4.6.4.6.

3.2.5.6.5 Atmospheric Liquid Water Ingestion. The engine shall operate satisfactorily throughout the complete operating envelope up to 45,000 feet altitude or the maximum altitude of Figure 7, [Figure 6-1], whichever is lower, at power settings from idle to maximum power with up to 5.0 percent of the total airflow weight in the form of water (liquid or vapour) and with 50 percent of the liquid water entering the engine inlet through a segment equivalent to one-third of the capture area of the engine inlet.

---

[1] Tables and Figures for Chapter 6 begin on page 6-13.

4.6.4.6 Ice Ingestion Tests. The test engine shall be subjected to an ice ingestion test to demonstrate compliance with the requirements of 3.2.5.6.3. The type of ice and the conditions for ingestion shall be as follows:
a. One 2.0 inch diameter hailstone and two 1.0 inch diameter hailstones for each 400 square inches, or less, of the capture area at the engine inlet and for each additional fractional area larger than 50 percent thereof; shall be introduced into the engine inlet for typical takeoff, cruise and descent conditions. The hailstones shall be of 0.80 to 0.90 specific gravity.
b. Sheet ice of 0.80 to 0.90 specific gravity; one piece of sheet ice sized 3.0 inches x 9.0 inches x 0.25 inch shall be introduced into the engine inlet for typical takeoff and cruise conditions.

The procedures to be used for introduction of the hailstones and sheet ice at the engine inlet and the engine power settings and speed at which the hailstones and sheet ice are to be ingested shall be specified in the pre-test data of 4.3.5.1. The time for engine power recovery shall be recorded. During the tests, high speed photographic coverage of the inlet is required. The test will be considered to be satisfactorily completed when, in the judgment of the Using Service, the criteria of 3.2.5.6.3 have been met.

6.2.2 MIL-E-5007D: Turbojet and Turbofan Aircraft Engines

This specification agrees in essence with the previous one for turboshaft and turboprop engines. Identical specifications are included as: humidity resistance (section 3.2.5.4), ice ingestion (3.2.5.6.3), atmospheric liquid water ingestion (3.2.5.6.5) and ice ingestion tests (4.6.4.6).

6.3 MILITARY SPECIFICATION (United Kingdom)

6.3.1 DEFENCE STANDARD 00-971

GENERAL SPECIFICATION FOR AIRCRAFT GAS TURBINE ENGINES

The Defence Standard (29 May 1987) replaces:

D Eng RD 2100 Issue No.5, dated 27 January 1967, General Specification for the Test Requirements for Gas Turbine Aero Engines and

D Eng RD 2300 Issue No.3, dated 28 July 1967, General Specifications for the Design and Manufacture of Gas Turbine Aero Engines and Jet Pipes.

SECTION TWO. TECHNICAL REQUIREMENTS

8 Functional Characteristics

8.2 Operating Envelope. The engine shall be capable of continuous operation, free from stall or surge, throughout the operating envelope as specified in the engine specification. The operating envelope shall be defined in terms of an engine inlet pressure versus engine inlet temperature envelope from which shall be derived an altitude versus flight Mach number envelope. The envelope shall be based on the ICAO standard atmosphere of Def Stan 00-970, Volume 1, Chapter 101, Leaflet 101/2 and take into account the requirements of Def Stan 00-970 Volume 1, Chapter 101, Para.1.2.1, in respect of maximum and minimum atmospheric temperatures. Any pressure recovery factors and thermodynamic data (specific heats etc) assumed in deriving the altitude versus flight Mach number envelope are to be defined in the engine specifications. (Figure 1 of Def Stan 00-970 Volume 1, Chapter 101 is reproduced in this specification as Figure 1 [Figure 6-2]).

9 Environmental Conditions

9.6 Hail and ice ingestion. The engine shall be capable of ingesting hail and sheet ice, as specified at (a) and (b) below, without flame-out, lengthy power recovery or sustained loss of engine performance and/or handling characteristics, over the full range of engine operating conditions throughout the operating envelope of **8.2.** The time limit applicable to performance recovery shall be stated in the engine specification.

(a) Hailstones
- (i) Density - 0.8 to 0.9 kg/l.
- (ii) Size - 25mm and 50mm diameter.
- (iii) Quantity - 8 x 25mm and 4 x 50mm diameter stones per m^2 of representative intake area. A minimum of one stone of each size except where precluded by aircraft or intake configuration or size.

(b) Sheet ice
- (i) Density - 0.8 to 0.9 kg/l.
- (ii) Size and quantity - typical sizes, forms, thickness and quantities likely to form on the aircraft and be ingested by the engine.

9.7 Water ingestion. The engine shall be capable of functioning satisfactorily at all thrust/power levels throughout the operating envelope required by **8.2** but up to a maximum altitude of 13700m, when 4% of the total intake mass flow is water.

13 Engine systems

Requirements for all engine systems shall be defined in the engine specification and will cover the general requirements of **13.1** to **13.11.4** and be compatible with all relevant requirements for the engine. The engine contractor shall be responsible for the preparation and provision of specifications governing the detailed design and qualification requirements for any engine accessories contained within these systems. These accessory specifications shall conform with requirements of the engine specification and such other specifications referenced therein.

13.1 Anti-icing system. All parts of the engine susceptible to ice accretion during engine operation shall be provided with a means of anti-icing capable of enabling the engine operating and performance requirements of **9.2** to be achieved. A description of the system shall be included in the engine

specification.

13.1.1 Anti-icing system operation. If an anti-icing system is fitted it shall be capable of continuous operation throughout the performance/operating range of the engine without causing damage.

SECTION THREE. QUALIFICATION TEST REQUIREMENTS

19 Supplementary Tests

19.1.1.3 Endurance in continuous maximum/intermittent maximum icing conditions. A separate test shall be conducted at each temperature/altitude condition of Table P [Table 6-1], the test being made up of the cycle:
28 km horizontal extent in the liquid water content conditions of table PD column (a) appropriate to the test temperature followed by 5 km of liquid water content conditions of table P column (b) appropriate to the test temperature.

[Note: A "table PD" can not be found in the table section. It appears that this is an error and that "table PD" should read "table P" column (a).]

Each test shall be run at the minimum power for which satisfactory operation in icing conditions is claimed in the aircraft installation for which the test is being carried out and the total duration of each test shall be a minimum of 30 minutes. At the conclusion of each test the engine shall be run up to the maximum (unreheated) thrust/power condition as indicated in **19.1.1.8** to demonstrate any effects of ice shedding. If considered necessary by the Approval Authority an additional test at the -30°C condition of table P shall be carried out at the highest engine speed (up to maximum continuous thrust/power) at which appreciable ice could, when shed, enter the engine combustion chamber.

19.1.1.7 Testing in ice crystal and ice crystal/free water conditions. Where required by the Approval Authority to satisfy the requirements of safe engine operation in ice crystal or ice crystal/free water conditions the tests at **19.1.1.7.1** and **19.1.1.7.2** shall be conducted first with the anti-icing system 'ON' and then repeated with the anti-icing system 'OFF'.

19.1.1.7.1 Ice crystal conditions. A separate test shall be carried out at each of the temperature/altitude conditions shown in table Q [Table 6-2], each test consisting of repetitions of the test cycle shown in the table. The duration of the test cycle shall be derived from the flight profile and speed of the specific engine application in icing conditions and the horizontal extents shown in the table, but need not exceed 30 minutes.

19.1.1.7.2 Ice crystal/free water condition. A test shall be carried out at the temperature/altitude conditions shown in table R [Table 6-3] consisting of repetitive tests at each of the three ice crystal/free water concentrations shown in the table. The duration of each test shall be derived from the flight profile and speed of the specific engine application in icing conditions and the horizontal extent shown in the table but need not exceed 30 minutes.

19.1.4 Hail and ice ingestion. The tests of **19.1.4.1** and **19.1.4.2** shall be carried out to show that the engine meets the hail and ice ingestion requirements of **9.6.**

19.1.4.1 Hail ingestion. The following test conditions shall apply:
(a) Hail stone density, sizes and quantities shall be as at **9.5**(a)

[Note: This reference is wrong; it should read "**9.6**(a)", (see above).]

(b) The hailstones shall be dispersed over the engine or aircraft intake face or agreed simulation thereof.
(c) The duration of ingestion of the hailstones shall not exceed 5 seconds.
(d) The hailstone ingestion velocity and engine operating conditions shall be such as to simulate the most arduous conditions with respect to the ingestion within the relevant part of the flight envelope as agreed by the Approval Authority.
(e) During the test high speed photographic coverage will be required.

19.1.4.2 Sheet ice ingestion. The following test conditions shall apply:
(a) Sheet ice density, size and quantity shall be as at **9.6** (b) and agreed by the Approval Authority.
(b) Sheet ice ingestion velocity shall be representative of that which occurs after break-away during typical operational conditions for ice formation on the aircraft.
(c) During the test high speed photographic coverage will be required.

19.1.5 Water ingestion. The test at **19.1.5.1** and **19.1.5.2** shall be carried out to show that the engine meets the water ingestion requirements of **9.7**. During the test there should be no permanent performance deterioration. Sufficient measurements shall be taken before, during and after the test to demonstrate compliance with this requirement. Where there is a requirement to simulate the ingestion of runway water, a special test agreed by the Approval Authority will be necessary.

19.1.5.1 Test conditions
(a) The test may be performed at ambient temperature but account shall be taken of the effect which air inlet temperature would have on compressor clearances. Similarly the effect on clearances of the maximum 'g' load shall be taken into account. Evidence of these effects on clearances shall be supplied to the Approval Authority.
(b) A total water flow rate equal to 4% of weight of the intake air mass-flow shall be sprayed into the engine with a random distribution of droplets not exceeding 2 mm diameter whilst the engine is run successively at the following ratings for the times stipulated.
(i) Flight idle - 3 mins - water on.
(ii) Maximum take-off (no reheat) - 2 mins - water off.
(iii) Maximum take-off (no reheat) - 3 mins - water on.

19.1.5.2 Engine inspection. The engine shall be stripped after the test and examined for rubbing or other failures in the compressor. Approval of the engine will be based on an assessment of its condition and the extent of any rubbing and the provisions made in design to accommodate this.

6.4 FEDERAL AVIATION REGULATIONS (United States)

6.4.1 Part 25: Transport Category Airplanes

INDUCTION SYSTEM

§ 25.1091 Air induction.

(d)(2) The airplane must be designed to prevent water or slush on the runway, taxiway, or other airport operating surfaces from being directed into the engine or auxiliary power unit air inlet ducts in hazardous quantities, and the air inlet ducts must be located or protected so as to minimize the ingestion of foreign matter during takeoff, landing, and taxiing.

§ 25.1093 Induction system icing protection.

(b) *Turbine engines.* (1) Each turbine engine must operate throughout the flight power range of the engine (including idling), without the accumulation of ice on the engine, inlet system components, or air frame components that would adversely affect engine operation or cause a serious loss of power or thrust-

(i) Under the icing conditions specified in Appendix C, and

(ii) In falling and blowing snow within the limitations established for the airplane for such operation.

[Note: The test specifications for turbine engines given in the subsequent Sub-section 2 deal exclusively with a super-cooled water icing environment, without any mention of a snow test condition.]

6.4.2 Part 29: Transport Category Rotorcraft

INDUCTION SYSTEM

§ 29.1091 Air induction.

(e) Each alternate air intake must be located to prevent the entrance of rain, ice, or other foreign matter.

(f)(2) The air inlet ducts must be located or protected so as to minimize the ingestion of foreign matter during takeoff, landing, and taxiing.

§ 29.1093 Induction system icing protection.

(b) *Turbine engines.* (1) It must be shown that each turbine engine and its air inlet system can operate throughout the flight power range of the engine (including idling)-

(i) Without accumulating ice on the engine or inlet system components that would adversely affect engine operation or cause a serious loss of power under the icing conditions specified in Appendix C of this part; and

(ii) In snow, both falling and blowing, without adverse effect on engine operation within the limitations established for the rotorcraft.

6.4.3 Part 33: Aircraft Engines

§ 33.77 Foreign ob ect ingestion.

(c) Ingestion of water, ice, or hail, under the conditions prescribed in paragraph (e) of this section, may not cause a sustained power or thrust loss or require the engine to be shut down. It must be demonstrated that the engine can accelerate and decelerate safely while inducting a mixture of at least 4 percent water by weight of engine airflow following stabilized operation at both flight idle and takeoff power settings with at least a 4 percent water-to-air ratio.

(d) For an engine that incorporates a protection device, compliance with this section need not be demonstrated with respect to foreign objects to be ingested under the conditions prescribed in paragraph (e) of this section if it is shown that-

(1) Such foreign objects are of a size that will not pass through the protective device;

(2) The protective device will withstand the impact of the foreign objects; and

(3) The foreign object, or objects, stopped by the protective device will not obstruct the flow of induction air into the engine with a resultant sustained reduction in power or thrust greater than those values required by paragraphs (b) and (c) of this section.

[Note: Paragraphs (a) and (b) of this section deal exclusively with the ingestion of birds.]

(e) Compliance with paragraphs (a), (b), and (c) of this section must be shown by engine test under the following ingestion conditions:

Foreign Object	Test quantity	Speed of foreign object	Engine operation	Ingestion
ICE:	Maximum accumulation on a typical inlet cowl and engine face resulting from a 2-minute delay in actuating anti-icing system, or a slab of ice which is comparable in weight or thickness for that size engine.	Sucked in...	Maximum... cruise.	To simulate a continuous maximum icing encounter at 25°F.

Continued..

Foreign Object	Test quantity	Speed of foreign object	Engine operation	Ingestion
HAIL:(0.8 to 0.9 specific	For all engines: With inlet area of not more than 100 square inches: 1-inch hailstone. With inlet area of more than 100 square inches: one 1-inch and one 2-inch hailstone for each 150 square inches of inlet area or fraction therefor.	Rough air flight speed of typical aircraft.	Maximum cruise at 15,000 feet	In a volley to simulate a hailstone encounter. One-half the number of hailstones aimed at random area over the face of the inlet and the other half aimed at the critical face area.
	For supersonic engines (in addition): 3 hailstones each having a diameter equal to that in a straight line variation from 1 inch at 35,000 feet ito 1/4 inch at 60,000 feet using diameter corresponding to the lowest supersonic cruise altitude expected.	Supersonic cruise velocity. Alternatively, use subsonic velocities with larger hailstones to give equivalent kinetic energy.	Maximum cruise	Aimed at critical engine face area.
WATER:	At least 4 percent of engine airflow by weight.	Sucked in.....	Flight idle, acceleration, takeoff, deceleration.	For 3 minutes each at idle and take-off, and during acceleration and deceleration in spray to simulate rain.

6.4.4 Part 33: Water and Hail Ingestion Standard

In conjunction with members of an international inclement weather task group, the FAA has drawn up a draft Notice of Proposed Rulemaking (NPRM), with proposed changes to the water and hail ingestion standards for aircraft turbine engines (see Sections 2.3.3 and 2.3.4 respectively). The notice, entitled Airworthiness Standards; Water and Hail Ingestion Standards, has the preliminary identifying code: [4910-13]; 14 CFR Part 33. Other airworthiness agencies are considering similar changes based on the same study.

6.5 BRITISH CIVIL AVIATION REGULATIONS (United Kingdom)

Before the advent of the JAR, the BCAR were in effect for the UK. New engines developed or certified in the U.K. are expected to be certified according to the JAR (Begley, 1993). Any engine modifications leading to a change in engine mark are likely to be certified against the new JAR. However, minor modification packages on older engines are expected still to be certified using the BCAR, although major modifications may be certified along the JAR's.

6.5.1 Sub-Section D1 - General Definitions

Chapter D1-2 Definitions

GENERAL

1.5 Atmospheric Conditions

NOTE: The definitions of this paragraph 1.5 are not necessarily an accurate representation of meteorological data. The defined conditions are intended to provide an acceptable basis for the purposes of design for flight in atmospheric icing, hail and ice crystal cloud conditions.

1.5.2 Ice Crystal Cloud. The conditions in respect of ice crystals and water tabulated in Table 4 (D1-2) [Table 6-4] which are assumed to be encountered for the specific horizontal distances.

1.5.3 Hail. Hailstones the characteristics of which are in accordance with (a) to (d)-

(a) Maximum size 5 cm (2.0 in) mean diameter.

(b) Specific gravity 0.9.

(c) Encountered throughout the altitude range 0 to 12 000 m (40,000 ft) for a horizontal distance of 1 km (0.5 n mile).

(d) The number of stones encountered is assumed

as 20.0/m^2 (2.0/ft^2) of frontal area or 1.0 stones, whichever is the greater number.

6.5.2 Sub-Section D5 - Power Plant Installations

Chapter D5-5 Air Intake Systems

2. LOCATION OF ENGINE AIR INTAKES

2.1 General. Engine air intakes shall be located or protected and/or operating procedures shall be determined so that, in all normal conditions of operation compliance with the requirements of this paragraph **2** can be demonstrated.

2.2 Take-off from Precipitation-covered Runways[2]. Except where it is obvious, by inspection or other means, that precipitation on the runway would not enter engine air intakes during the take-off run, compliance shall be shown with the requirements of 2.2.1 or 2.2.2, as appropriate.

2.2.1 **Airplanes Certificated from Precipitation-covered Runways.** It shall be demonstrated that when the aeroplane is taking-off and traverses areas of precipitation up to whichever is the greater of 19 mm (0.75 in) depth or the precipitation depth for which take-off data are to be scheduled, the Power-units operate satisfactorily without unacceptable loss of power at all aeroplane speeds up to that at which the transition to climbing flight is completed and in the attitudes likely to be used in this speed range (see also **D2-2** App. No.1, 1.6). Compliance with this requirement may be shown either by means of complete take-offs in the specified precipitation conditions or by means of a series of demonstrations in areas of precipitation, the length of which is agreed by the CAA to be sufficient both to determine the effects on aeroplane performance and on engine behaviour and response, and to establish the stabilized spray pattern.

NOTE: Any special aeroplane handling techniques necessary to ensure compliance with this requirement should still comply with **D2-2,** 6.4.

2.2.2 **Aeroplanes not Certified for Take-off from Precipitation-covered Runways.** It shall be demonstrated that when the aeroplane is taking-off and traverses areas of precipitation up to 19 mm (0.75 in) in depth and not less than 91.5 m (300 ft) in length in the direction of the take-off, the Power-units operate satisfactorily without unacceptable loss of power at all speeds up to that at which the transition to climbing flight is completed and in all attitudes likely to be used in the specified speed range.

NOTES: (1) The CAA should be consulted where there is difficulty in meeting this requirement, in which case the CAA may agree with the Applicant suitable operational limitations to ensure satisfactory operation from a runway on which there are areas of slush and water, even though the runway is nominally clear.

(2) An aeroplane may be accepted as complying with this requirement even if the possibility of serious power reduction is found to exist in specific circumstances; for example, where the possibility of power reduction arises only at the point from which a take-off could safely be abandoned (even in adverse braking conditions) and no unacceptable damage is caused to the Power-units.

[2] For the purpose of this paragraph, "precipitation" means standing water, e.g. resulting from heavy rain, slush and snow, and "runway" means a concrete, paved or similar surface; for other surfaces, such as grass and gravel, reference should be made to the CAA.

3 ATMOSPHERIC CONDITIONS

3.1 **General.** The complete Power-unit as installed in the aeroplane and including the propeller shall be capable of functioning satisfactorily without unacceptable damage or unacceptable loss of power when operated in those atmospheric conditions of precipitation (hail) and cloud (super-cooled liquid and ice crystals)defined in **D1-2,** 1.5. In addition, consideration shall be given to flight in other forms of precipitation.

NOTE: See also **D4-1, 5** for requirements affecting the aeroplane as a whole.

3.1.1 After a descent through icing conditions, it shall be possible to perform a balked landing with satisfactory Power-unit response and handling, including recovery of power (see **D5-5** App. No.2, 1.1.2 (b)).

3.3 **Turbine Engines** (see **D5-5** App. No.2, **1**). Acceptable methods of providing evidence that the requirement of 3.1 is met shall be agreed with the CAA. An acceptable programme of testing for flight in ice-forming conditions is contained in **D5-5** App.No.2, **1.**

NOTES: (1) Where the use of any protection system has an adverse effect on the performance of the aeroplane, such effects will have to be determined and scheduled in accordance with **D2-2,3.**

(2) Where there is reason to believe that a Power-unit is susceptible to atmospheric conditions other than super-cooled cloud, the CAA will require to be satisfied that 3.1 is met in such conditions.

3.3.1 Means shall be provided to indicate (both on the ground and in flight) the functioning of any selectable protection system which is installed for compliance with 3.1.

3.3.2 Where a protection system involves the use of an expendable fluid, the duration of the fluid under all conditions of system operation shall be determined and included in the Flight Manual.

[Note: "Appendix No.2 To Chapter D5-5, Turbine Engines-Flight in Ice-forming Conditions" outlines a complete series of icing tests. These details are outside the scope of this publication. The following excerpt may, however, be of interest:]

TESTS (b) At the conclusion of each 30 minute test of (a) an acceleration from the test engine power to maximum power conditions should be carried out to demonstrate the effect of ice shedding.

NOTES: (1) Where the available test facilities are inadequate to test the complete engine, intake (and propeller if fitted) each item may be tested separately subject to the CAA being satisfied that adequate precautions have been taken to ensure that an equivalence of compliance has been established, e.g. the CAA has to be satisfied that the engine can satisfactorily absorb any ice that is likely to be shed from the intake (or propeller) if fitted.

6.5.3 Sub-Section C-3 - Turbine Engines

C3-3 5 Performance Corrections

5.1 All performance results shall be corrected to the following assumed conditions of atmospheric pressure and temperature at mean sea-level-

5.1.1.	Pressure	1013.25 mbar (14.7 lbf/in^2 abs).
5.1.2.	Temperature.	15°C (288 K).
5.1.3.	Atmosphere.	Dry air (if correction is significant).

5.2 **Correction for Humidity.** Unless otherwise prescribed by the Authority, no correction for humidity of the air supply shall be made to the power obtained. Humidity corrections appropriate to high atmospheric temperatures, at altitudes up to 4500 m (15,000 ft) shall be established, however, for each type of turbine Engine, for use in the assessment of aircraft performance in these conditions.

[Note: A section similar to Section 6.5.3 is found in Chapter C4-3 describing test conditions for turbine engines in rotorcraft.]

C3-4 21 Ingestion of Rain and Hail
Except where the Authority agrees that the Engine installation in a particular aeroplane will preclude such ingestion occurring, it shall be established that no hazardous condition can arise to the aeroplane as a result of ingestion into the Engine of rain or hail.
NOTE: Where the Authority is satisfied that the particular installation precludes ingestion and compliance with this requirement is established on that basis, the Engine approval will be endorsed accordingly.
21.1 Ingestion of Rain (see **C3-4** App., 7). It shall be established that ingestion of rain into the Engine will not result in unacceptable mechanical damage, e.g. as would occur from the sudden contraction of the Engine casing, or cause an unacceptable reduction of performance.
21.2 Ingestion of Hail (see **C3-4** App., 8). It shall be established that ingestion of hail will not hazard the aeroplane as a result of damage that may be caused, e.g. unacceptable immediate or subsequent loss of Engine performance, serious increase of Engine operating temperatures or deterioration of Engine handling characteristics over the full range of Engine operating conditions or dangerous mechanical damage.

Appendix 7: Rain Ingestion (see C3-4, 21.1) It is acceptable to establish compliance with the requirement of **C3-4**, 21.1 for rain ingestion by carrying out a test in the following conditions:
Water Concentration.
4% by weight of the intake air mass-flow during the test.
Droplet Size.
Not exceeding 2 mm.
Altitude.
Sea-Level.
Power.
(a) 3 minutes a flight idling speed with ingestion.
(b) 2 minutes at Maximum Take-off Power, without ingestion, to heat soak the Engine.
(c) 3 minutes at Maximum Take-off Power with ingestion.
Speed of Ingestion.
Not Relevant

Appendix 8: Hail Ingestion (see **C3-4**, 21.2) It is acceptable to establish compliance with the requirement of C3-4, 21.2 for hail ingestion by carrying out a test in the following conditions:-
Size of Hail Stones.
25mm (1 in) and 50 mm (2 in) diameter.
Specific Gravity.
0.8 to 0.9.
Number.
Ten 25 mm and ten 50 mm stones per m^2 of intake area (one 1 in and one 2 in per 150 in^2).
Duration of Ingestion.
Not more than 5 seconds.
Speed of Ingestion.
The maximum Rough Air Speed (T.A.S.), up to 4500 m (15,000 ft), of a representative aeroplane.
Engine Conditions.
Maximum Continuous Power.

NOTE: If after the test it is found that damage has occurred, further running or other evidence may be required to show that subsequent failures resulting from the damage are unlikely to occur. If the loss of Engine performance at take-off conditions is found to exceed 25% the Engine may not be suitable for installation in some types of aeroplanes.

6.6 JOINT AVIATION REGULATIONS (Europe)

The Joint Airworthiness Requirements - Engines (JAR-E) have been developed to harmonize national regulations in Europe covering the design, manufacture, test, maintenance and operation of aircraft (Stimpson, 1988). The JAR-E has been accepted as the sole national code by the United Kingdom and France. These regulations have also been accepted as an acceptable alternative for imported and domestic engines by: Germany, Netherlands, Belgium, Denmark, Finland, Norway, Sweden and Switzerland.

6.6.1 JAR-E Section 1 - Sub-Section D Turbine Engines; Design and Construction

JAR-E-540 INGESTION OF FOREIGN MATTER
(a) The engine shall be designed so that the ingestion of foreign matter that is likely to affect more than one Engine in multi-engined aircraft in any one flight, (e.g. rain, hail, ice, gravel, sand, small birds) is not likely to hazard the aircraft as a consequence of-
(1) Immediate or subsequent loss of performance, or
(2) Unacceptable deterioration of Engine handling characteristics during the flight.

6.6.2 JAR-E Section 1 - Sub-Section E Turbine Engines Type Substantiation

JAR-E-780 TESTS IN ICE-FORMING CONDITIONS
(d) Where the engine is considered to be vulnerable to operation in ice crystal cloud conditions, in mixed ice crystals and liquid water conditions, or in snow, such additional tests as may be necessary to establish satisfactory operation in these conditions shall be made.

JAR-E-790 INGESTION OF RAIN AND HAIL
(a) Except where the authorities agree that the Engine installation in a particular aircraft will preclude such ingestion occurring it shall be established that no hazardous condition can arise to the aircraft as a result of ingestion into the Engine of rain or hail. When the authority is satisfied that the particular installation precludes ingestion and compliance with this requirement is established on that basis, the Engine approval will be endorsed accordingly.

(b) *Ingestion of Rain.* It shall be established that the ingestion of rain in the Engine will not result in unacceptable mechanical damage (e.g. as would occur from the sudden contraction of the Engine casing), or cause an unacceptable loss of Engine performance. (See ACJ E 790(b).)

(c) *Ingestion of Hail.* It shall be established that the ingestion of hail into the Engine will not hazard the aircraft as a result of damage that may be caused, e.g. unacceptable loss of Engine performance, serious increase of

Engine operating temperatures or deterioration of Engine handling characteristics over the full range of Engine operating conditions or dangerous mechanical damage. (See ACJ E 790(c).)

(d) *Tests.* Where compliance is established by test-

(1) Where a retractable guard is fitted, the guard shall be in the extended position during the test. Unless it is also established that the requirements are met with the guard retracted, the Engine approval will be endorsed to the effect that compliance with the requirements has only been established with the guard in position.

(2) Where a fixed guard is fitted, compliance with the requirements shall be established with the guard in position.

(3) The effects on the Engine of operating with the guard in position shall be fully evaluated from the mechanical and the performance points of view.

(e) When it is necessary to carry out the tests of (b) and (c), the power and/or thrust of the Engine should be at least 75% of Take-off or Maximum Continuous Power and/or Thrust as appropriate. There should be no adjustment of the Engine controls within the first 15 seconds.

6.6.3 JAR-25 Section 1 Sub-Section E: Air Intake System

JAR 25.1091 AIR INTAKE

(d) (2) The aeroplane must be designed to prevent water or slush on the runway, taxiway, or other airport operating surfaces from being directed into the engine air intake ducts in hazardous quantities, and the air intake ducts must be located or protected so as to minimise the ingestion of foreign matter during take-off, landing and taxying. (See ACJ 25.1091 (d) (2).)

(e) If the engine air intake system contains parts or components that could be damaged by foreign objects entering the air intake, it must be shown by tests or, if appropriate, by analysis that the air intake system design can withstand the foreign object ingestion test conditions of JAR-E, C3-4, paragraphs 20 and 21 without failure of parts or components that could create a hazard. (See ACJ 25.1091 (e).)

6.7 APPLICATION OF REQUIREMENTS

An examination of these specifications and test requirements shows some interpretation of the wording would be needed in an actual application. For example, what is the definition of "acceptable damage" or "unacceptable loss of performance". Aspects of the actual certification tests are typically negotiated between the certificating agency and the manufacturer, who will usually certificate the product in several countries. In response, regulatory authorities have established some reciprocal procedures where specifications are comparable. The actions to "harmonize" the JAR's and FAR's are evidence of this trend.

To gain an understanding of the practical applications of the specifications and requirements, the existing certificating practices have been examined. Both the frequency of events and significance of performance changes are of interest. The BCAR provides some quantitative guidance for frequency of occurrence of effects to the complete aircraft:

a) Reasonably Probable: probability of 10^{-3} to 10^{-5} per hour of flight;

b) Remote: probability of 10^{-5} to 10^{-7} per hour of flight; and

c) Extremely Remote: probability of 10^{-7} to 10^{-9} per hour of flight.

References to acceptable performance loss include: BCAR Chapter 3-4 App. 8 which notes that performances losses of greater than 25%, with hail ingestion, may preclude the use of the engine in certain applications; and MIL-E-008593E which allows a power loss of up to 10% with hail and ice ingestion. However, the JAR and FAR refer to: serious loss of power or thrust (FAR 25.1093) and unacceptable loss of engine performance or serious increase of engine operating temperature (JAR-E-790).

It appears that these qualitative assessments are judged on a case by case basis. No general guidelines were available except that aircraft controllability and performance are always to be maintained. Therefore, the tolerance of degradation in engine performance or operability will depend on defining critical points in the aircraft's operations and the associated power and response requirements.

6.8 SUMMARY OF REGULATIONS AND SPECIFICATIONS BY HAZARD

A very brief summary of the material in Section 6.0 is being provided, organized by hazard, rather than by agency or specification, to facilitate comparisons between the various requirements. Similarities and significant differences are highlighted.

6.8.1 Surface Water and Slush

The FAA (Part 25), the JAA (JAR-25), and the CAA (Subsection D5) regulations establish design requirements for an air induction system to prevent water, slush, and other foreign objects from entering in hazardous amounts during take-off, landing, and taxiing. The rotorcraft regulations (FAR-27) require location and protection of the inlets to minimize ingestion.

6.8.2 Non-Condensating Moisture

The reference condition for performance results is typically specified to include dry air, eg. BCAR C3-3 5. The same BCAR regulations prescribe that no corrections to engine power are normally to be made for humidity of the air supply. However, humidity corrections for high atmospheric temperatures are to be established for use in the assessment of aircraft performance in these conditions. US Military specifications (6.2.1 and 6.2.2) require that engine components be resistant to malfunction and deterioration when subjected to high levels of relative humidity for extended periods.

6.8.3 Liquid Water

The US Military Specifications (6.2.1 and 6.2.2) call for satisfactory operation in atmospheric liquid water of up to 5 percent of total airflow, throughout the complete flight envelope. The civil regulations (FAA Standards Part 33, CAA Section 3-4) and the Defence Standard 00-971 specify a 4 percent water-to-air ratio, at flight idle and take-off power settings, and throughout the operating envelope, respectively. The JAA regulations require that no mechanical damage or loss of engine performance occur. Section 2.3.3 describes the proposed water content, droplet size and duration changes to FAR and JAR.

6.8.4 Hail and Sheet Ice

The requirements for ingesting hailstones, without causing damage or affecting engine health have been compared based on size, density and "normalized ingestion volume": volume of ice per unit of inlet area. Table 6-5 has been prepared to compare the requirements. The US MIL specifications describe hailstone sizes (diameters of 25 and 51 mm [1 and 2 inches]) which should not cause any damage or operational difficulty when ingested at a given rate (Sec.6.2). Defence Standard 00-971 identifies hailstones similarly in size and specific gravity, but requires a much higher ingestion volume. The proposed revisions to the JAR and FAR are described in section 2.3.4: most notable are the longer duration of the hail ingestion and the distribution of hail particle sizes.

The FAA Part 33 standards also specify hailstones of the same size, at an ingestion rate more or less severe than that of the MIL specification, depending on inlet size (Sec. 6.4). The JAA requirements demand that hail not cause damage or affect engine operation or performance. The CAA requirements give details of an atmospheric hail condition, in extent and environmental density not unlike those above (50 mm maximum diameter, 0.9 specific gravity), but at apparently the highest normalized ingestion volume (volume of ice per unit inlet area) of all (see Table 6-5). The engine is to operate safely, without unacceptable power loss, under these conditions.

The duration of exposure to hail specified in the regulations is from a few seconds, ie. FAR 33 volley, to 5 seconds (Def Stan 00-971) or more, eg. BCAR D1-2: exposure for the required 1 km for a 520 km/hr (280 knot) would be 6.9 seconds. This longest duration corresponds to the highest normalized ingestion volume (Table 6-5).

Ice accretions from inlet or aircraft parts are to be safely ingested. The US MIL specifications require ingestion of a sheet of ice (76 mm x 229 mm x 6 mm [3 inches x 9 inches x 0.25 inch]. The sheet ice for the Defence Standard 00-971 is identified by density, but size and quantity are to be related to what may be produced in the actual installation from any aircraft source. The FAR's derive the amount of ice from a 2 minute build-up only on the engine cowl and inlet.

6.8.5 Snow and Ice Crystals

The JAA requirements (JAR-E-780) identify ice crystals and snow as a potential hazard, and suggest testing as necessary to ensure satisfactory operation under these conditions. The CAA defines ice crystal clouds for different air temperatures and altitude ranges (Table 6-4); a footnote also describes mixed conditions of ice crystals and liquid water. The extent of storms (in kilometres) are given for water contents of 1,2,5

and 8 g/m^3, with typical particle sizes of 1 mm. A test program for these elements would be tailored to an aircraft's operating regime, i.e. flight speed, altitude, and inlet configuration. The Defence Standard 00-971 gives similar water content ranges but shorter durations. This standard also specifies ice crystal and mixed (ice crystal/liquid water) conditions, not unlike those of the CAA, with suggestions for test development.

6.9 COMPARISON OF OBSERVED ATMOSPHERIC WATER TO SPECIFIED HAZARDS

The incidences of water observed in the atmosphere are regularly assessed to define the threat to aircraft safety and to incorporate test and/or design requirements into regulations and specifications. The forms of atmospheric water have been described in Chapter 2 and MIL-STD-210C for various worst case scenarios. This section compares typical and worst case occurrences to the test and design descriptions found in the regulations and specifications, as summarized in section 6.8. In addition, the proposed revisions to the hail and liquid water sections (FAA NPRM) are included. A summary of the comparison is shown in Table 6-6.

6.9.1 Non-Condensing Moisture

The highest recorded absolute humidity was a water to air ratio of 2.18% (MIL-STD-210C). None of the regulations or specifications refer to such a hazard except to note that performance data should be corrected to dry conditions, if the corrections are significant.

6.9.2 Liquid Water

The existing MIL-STD-210C shows the water content of rain storms to range from 1.6 to 6.7 g/m^3, varying with altitude, for expected incidences of 0.5, 0.1 and 0.01 percent of the time. More recent AIA studies (Chapter 2) show liquid water contents up to 25 g/m^3 but with a probability of occurrence (an encounter of 3 minutes or more, per flight hour) of about 10^{-10}. Figure 2-19 shows the AIA-derived threat of 3.06 percent water air ratio at 6100 m (20,000 feet). Tests at sea level would require nearly 40 g/m^3 to maintain this percentage water with air of sea level density. The existing regulation test requirements are 4 percent water air ratio. The proposed, revision (FAA NPRM) to the regulations is expected to reflect the AIA findings and proposals.

Observed rain drop diameters are typically 1 to 2 mm with large drops at 5-8 mm (Section 2.1.3). Only one regulation specifies size as less than 2 mm. The AIA study shows diameters from 0.5 to 7 mm.

The duration of the AIA-defined threat (Section 2.5.2) is 3 minutes which corresponds to the duration of the BCAR tests, and the revision (FAA NPRM).

6.9.3 Hail

Hail water contents observed (Section 2.1.4) is in the range 2-9 g/m^3 for the most severe storms and an AIA-derived HWC corresponding to 1.37 percent water content of air. The regulations show a wide range of 0.3 to 1.03 x 10^{-3} m^3 of ice per m^2 of inlet area. For a given flight velocity and hail duration, this range of ingested hail may be converted to a percent water content. Following the example of section 2.5.1, at a flight velocity of 519 km/hr (280 knots) at 4600 m (15000 ft) the range of regulation-specified hail water content would be 0.04 to 0.15 per cent.

The regulations call for tests with 25 and 50 mm hail stones. Observed sizes are typically 5 to 30 mm (Section 2.1.4) with likely extremes described by MIL-STD-210C as 21 to 67 mm depending on altitude, for occurrences 1% and 0.1 percent of the time, respectively.

The duration of exposure to hail specified in the regulations is from a few seconds to ten seconds (Section 6.8.4) for aircraft velocities above 360 km/hr (200 knots), or a horizontal extent of 1 km. The AIA-derived hazard and proposed revision to the FAR and JAR include a duration of 30 seconds.

6.9.4 Sheet Ice

Sheet ice accumulations in MIL-STD-210C are really only relevant to long term accretion at heights below 125 m and velocities less than 230 km/hr (123 knots). Ice thicknesses of 18 to 35 mm are considered as design guidelines. The sheet ice regulations, when specific, call for 6 mm (0.25 inches), and require an amount of ice of fixed size or to depend on the installation (Section 6.8.4).

6.9.5 Snow and Ice Crystals

Ice crystal water contents of 0.1 to 1.2 g/m^3 are described in Section 2.1.4. The specifications include tests for 1 to 8 g/m^3, depending on the duration of exposure from 500 to 1 km, respectively. Particle sizes

of 1 mm are specified. Atmospheric observances of snow have shown a wide range of water contents (0.1 to 1.2 g/m^3) but storm extents are not described in MIL-STD-210C.

6.10 CONCLUSIONS AND RECOMMENDATIONS

Applicable specifications and test requirements have been reviewed for both military and civilian applications. Operational capability and safety of flight are the key goals. Similarities and differences were observed between the civil and military specifications.

Within the NATO countries, the existing engine specifications and test requirements for gaseous humidity are generally consistent with the maximum levels likely to be encountered in civil or military operations. However, recent analyses of meterological data have prompted a revision of the severity and duration of rain and hail hazards. In response, harmonized efforts by the FAA, JAA and other civilregulators are underway to change certification requirements and possibly to specify an allowable performance loss, following ingestion. There appears to be no corresponding review of military specifications.

These adverse weather requirements are particularly important to military operations with joint forces and to foreign military sales. These same requirements are also relevant to industrial joint-venture and consortium arrangements. Consequently, it appears desirable for responsible military and civil organizations, like NATO and ICAO to undertake the reconciliation of the differences in adverse weather requirements, for engine certification.

It should be noted that while general regulations do exist, application of these regulations for particular aircraft may vary. Therefore, it is recommended that contact be made with the appropriate certification agency for final requirements definition.

6.11 SOURCE DOCUMENTS

The versions or amendments of the regulations and specifications used to prepare section 6 are listed in this section. The most current version of relevant regulation or specification should be consulted.

1. Naval Air Systems Command. 1984. Military Specification Engines, Aircraft, Turboshaft and Turboprop, General Specification for. MIL-E-008593E(AS). 1 March 1984.

2. U.S. Department of Defence. MIL-E-5007D: Military Specification: Engines, Aircraft, Turbojet and Turbofan, General Specification for. 15 October 1973.

3. U.K. Ministry of Defence. 1987. DEFENCE STANDARD 00-971. General Specification for Aircraft Gas Turbine Engines. 29 May 1987

4. United States Federal Aviation Agency. 1990. Airworthiness Standards: Transport Category Airplanes - Part 25. Ch. 29 Amendment 25-72. August 20, 1990.

5. United States Federal Aviation Agency. 1991. Airworthiness Standards: Transport Category Rotorcraft - Part 29. Ch.25 Amendment 29-32. September 9, 1991.

6. United States Federal Aviation Agency. 1984. Airworthiness Standards: Aircraft Engines - Part 33. Ch 5 Amendment 33-10. March 26, 1984.

7. U.K. Civil Aviation Authority. 1981. British Civil Airworthiness Requirements: Sub-section D1 - General Definitions. Issued 16 December 1981

8. U.K. Civil Aviation Authority. 1972. British Civil Airworthiness Requirements: Sub-section D2 - Flight. Issued 16 October 1972.

9. U.K. Civil Aviation Authority. 1974. British Civil Airworthiness Requirements: Sub-section D5 - Power Plant Installations. Revised 30 August 1974.

10. U.K. Civil Aviation Authority. 1971. British Civil Airworthiness Requirements: Sub-section D4 - Design and Construction. Revised 15 November 1971.

11. Joint Aviation Authority. 1990. Joint Airworthiness Requirements: JAR-E. Change 8. 4 May 1990.

12. Joint Aviation Authority. 1989. Joint Airworthiness Requirements: JAR-25. Change 13. 5 October 1989.

13. U.S. Department of Defense, 1987: Military Standard, *Climatic Information to Determine Design and Test Requirements for Military Systems and Equipment,* MIL-STD-210C, 9 January 1987, Office of the Under Secretary of Defence, Research and Engineering, Washington, D.C.

14. Federal Aviation Administration. 1993. Notice of Proposed Rule Making (NPRM) 4910-13. 14 CFR Part 33. Note: Similar revisions are proposed by the JAA for JAR-E 790.

6.12 REFERENCES

6.1 Private Communication with C.Begley, Rolls Royce, 1993.

6.2 Stimpson, R., *The Gas Turbine Engine and its Certification*, United Kingdom Airworthiness Course, University of Kent, Canterbury, U.K. Rolls Royce Reprint PNR90496, NASA STI ETN-89-93690, 1988.

Table 6-1

Conditions for Tests in Continuous Maximum/Intermittent Maximum Icing Conditions (Reproduced from Table P, Def. Std. 00-971)

Ambient Air Temperature K	Altitude m	Liquid Water Content		Droplet Volume Mean Diameter μm
		(a)	(b)	
263.15	4500	0.6	2.2	20
253.15	6000	0.3	1.7	20
243.15	7500	0.2	1.0	20

Table 6-2

Conditions for Tests in Ice Crystal Conditions (Reproduced from Table Q, Def. Std. 00-971)

Ambient Air Temperature K	Altitude m	Test Cycle		Ice Crystal Mean Diameter mm
		Ice Crystal Concentration g/m^3	Horizontal Extent km	
263.15	4500	1 2 5	150 80 5	1
253.15	6000	1 2 5	150 50 5	1
243.15	10000	1 2 5	80 20 5	1

Table 6-3

Conditions for Tests in Mixed Ice Crystals/Free Water Conditions (Reproduced from Table R, Def. Std. 00-971)

Altitude m	Temperature K	Ice Crystal Concentration g/m^3	Free Water Concentration g/m^3	Extent km	Volume Mean Diameter μm
6000	263.15	1/2 1 4	1/2 1 1	150 80 5	Ice crystals, 1000 Water droplets, 20

Table 6-4
(Based on Table 4 (D1-2), BCAR)

Air Temp. K	Altitude Range		Max. Ice Crystal Content (g/m^3)	Horizontal Extent		Mean Particle Diameter (mm)
	($m \times 10^3$)	($ft \times 10^3$)		(n mile)	(km)	
273.15 to 253.15	3.0 - 9.0	10.0 - 30.0	8.0 5.0 2.0 1.0	0.5 2.5 50.0 300.0	1.0 5.0 100.0 500.0	1
253.15 to 233.15	4.5 - 12.0	15.0 - 40.0	5.0 2.0 1.0 0.5	2.5 10.0 50.0 300.0	5.0 20.0 100.0 500.0	

Note: In the temperature range 273.15 to 263.15 K the ice crystals are likely to be mixed with water droplets (with a maximum diameter of 2 mm) up to a content of 1 g/m^3 or half the total content, whichever is the lesser; the total content remaining numerically equal to Table 6-4.

Table 6-5

Relative Hail Ingestion Requirements

Agency/Spec	No./Size of Hail mm	Equiv. Vol. m^3	Frontal Area m^2	Vol./Area m
MIL-E-008593E	1 - 50mm & 2 - 25mm	7.72×10^{-5}	.258	$.30 \times 10^{-3}$
FAR Part 33	1 - 25mm ($<.0645$ m^2)	1.29×10^{-5}	.0645	$.20 \times 10^{-3}$
	1 - 25mm ($>.0645$ m^2) 1 - 50mm ($>.0645$ m^2)	6.44×10^{-5}	.0968	$.67 \times 10^{-3}$
CAA D-1	20 - 50mm	103.0×10^{-5}	1.0	1.03×10^{-3}
DEFSTAN 00-971	8 - 25mm & 4 - 50mm	30.9×10^{-5}	1.0	$.31 \times 10^{-3}$

Table 6-6

Water Form	Atmospheric Levels		Specification/Regulation	
	Typical Design Level	Maximum Observed	Existing	Revision[a] (FAA NPRM)
GASEOUS				
Amount (% W/A)	-	2.18	Correct if significant	-
LIQUID WATER				
Amount (g/m^3)	1.6-6.7[b]	25[c]		20[c]
(% W/A)		3.06[c]	4-5	3.06[c]
Size (mm)	1-2	8	<2	0.5 to 7
Duration (s)		180	180	180
HAIL				
Amount (g/m^3)	2-9[b]	10[d]		-
(% W/A)		1.37	[0.04-0.15]	1.37
Size (mm)	5-30	21-67	25, 50	5-60
Duration (km)	-	-	1	-
(s)	-	30	few-5 [5-10]	30
SHEET ICE				
Amount (mm)	-	-	76 x 229 or actual	-
Thickness (mm)		{18-35}	6	-
Duration (s)	-	-	Sucked in	-
SNOW ICE CRYSTALS				
Amount (g/m^3)	0.1-1.2	-	1-8	-
Size (mm)	-	-	1	-
Duration (km)	-	-	1-500	-

{ } only reference is for ice accumulation, near the ground, over long periods
[ ] calculation for example conditions using specification/regulation criteria

Notes: a. FAR/JAR NPRM Proposal (see reference list)
b. Depending on altitude
c. Altitude of 6100 m (20,000 ft)
d. Altitude of 4600 m (15,000 ft)

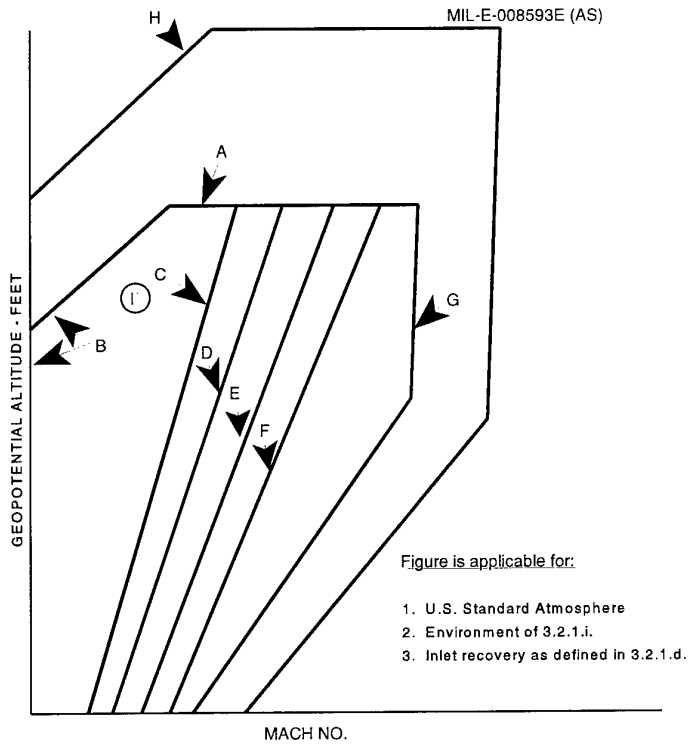

A. Maximum starting altitude.
B. Minimum Mach No. for starter assisted starting.
C. Minimum Mach No. for starting without starter assist, no customer power extraction, no customer bleed air extraction.
D. Minimum Mach No. for starting without starter assist, maximum customer power extraction, no customer bleed air extraction.
E. Minimum Mach No. for starting without starter assist, no customer power extraction, maximum customer bleed air extraction.
F. Minimum Mach No. for starting wiithout starter assist, maximum customer power extraction, maximum customer bleed air extraction.
G. Maximum Mach No. for starting air extraction.
H. Operating envelope.
I. Post-loiter starting point.

Figure 6-1

Engine Starting and Operating Limits
(Reference 3.2.1.4.1, 3.2.1.4.2, 3.2.1.4.4, 3.2.5.1, 6.2.1.38, 6.2.1.39, Figure 19)
(Reproduced from MIL-E-008593E(AS))

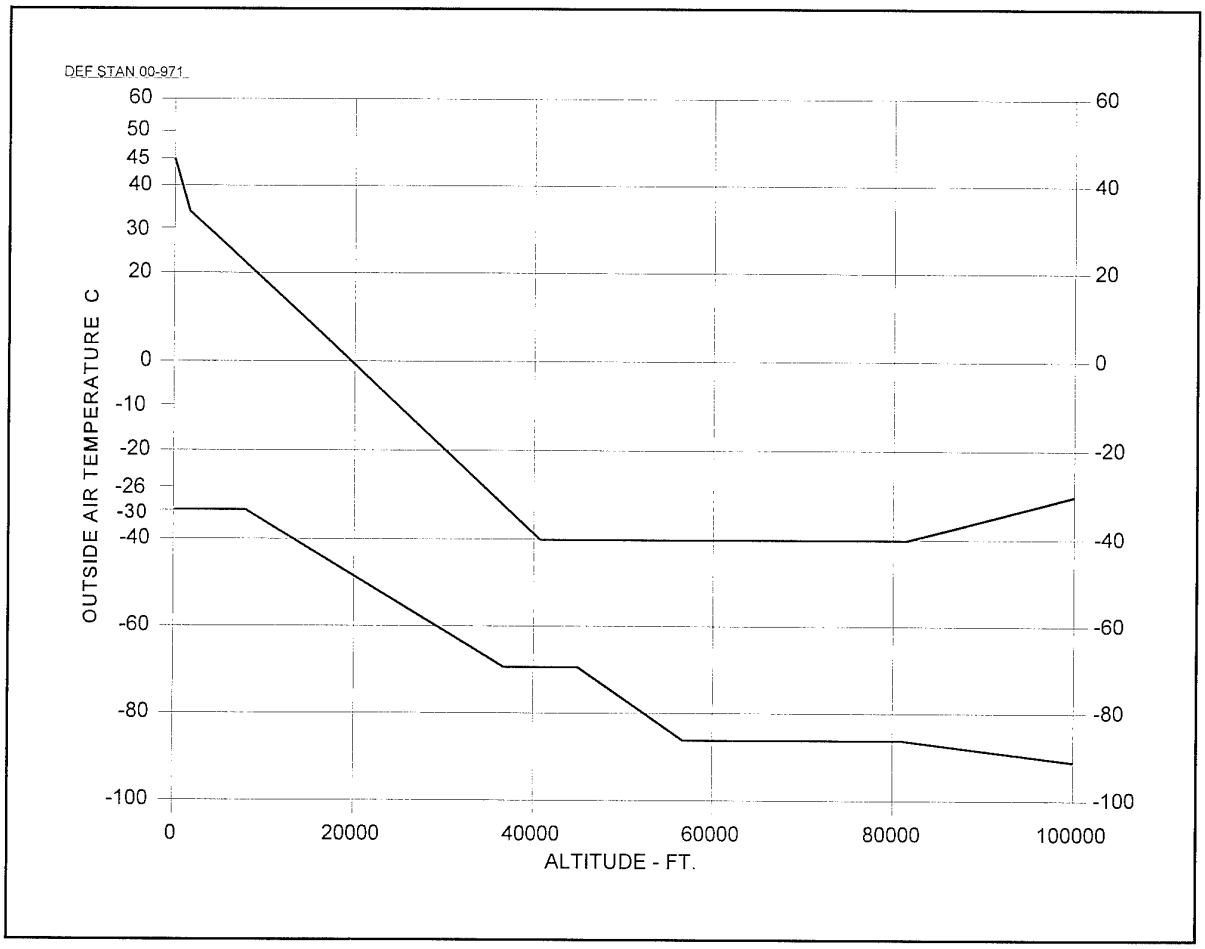

Figure 6-2

Maximum and Minimum Atmospheric Temperatures for Design Purposes
(Reference 8.2, 8.3 & 9.1)
(Reproduced from Def Stan 00-970 Vol 1 Chap 101)

7. MEASUREMENT OF INGESTED QUANTITIES AND CONDITIONS[1]

7.1 SCOPE

Previous chapters have discussed the influence of water in its various forms on the performance of gas turbine engines and their components. These influences can be significant, and if they are to be quantified some measurement of water content is required. Consequently this chapter discusses both methods and problems to be encountered in assessing and quantifying the presence of rain, hail and/or moisture content in a gas turbine engine or test plant and the influence the presence of water in any form may have on conventional instrumentation. The topic is extremely broad and includes many areas where inadequate data are available.

The chapter does not attempt to define all aspects of good instrumentation practice for 'fair weather' conditions and should be examined with other documentation on this subject, e.g. References 7.1 and 7.2. This chapter does attempt, however, to amplify these references and to extend the recommendations for inclement weather operation and define areas where caution should be exercised. In addition, it presents instrumentation methods specifically designed to assess and quantify the presence of vapour, droplets and particles (frozen droplets) in the flow and to describe the influence of 'water' on various routine measurements used for testing engines and their inflight control.

As already indicated, this chapter deals with the measurement of Humidity (gaseous water), Particles (as particles - liquid and solid) and Velocity (particles in the flow). To assist the reader, an overview of techniques (under the section headings used in the text) is given in Tables 7-1 (for Humidity), 7-2 (for Particles) and 7-3 (for Velocity Measurement).

7.2 HUMIDITY

In this section, we consider only that fraction of water existing in the form of vapour. The condensed phase (water, snow, hail, ice) is treated in Section 7.3.

Humid air is considered as a mixture of two gases obeying Dalton's Law

$$P_S = P_{Sd,a} + P_{Sv} \qquad 7\text{-}1$$

where P_S = static pressure of the mix,
$P_{Sd,a}$ = partial pressure of dry air,
P_{Sv} = partial pressure of water vapour.

T_S is the common temperature of the two gases and is called the "dry bulb temperature".

In the range of temperatures and pressures encountered in gas turbines, the gaseous mixture (air and water vapour) can usually be treated as a perfect gas, (see Equation 3-16):

$$P_{S\,d,a} = \frac{m_{d,a} R_{d,a} T_S}{V} \qquad 7\text{-}2(a)$$

$$P_{Sv} = \frac{m_v R_w T_S}{V} \qquad 7\text{-}2(b)$$

The hygrometric state of the atmosphere (amount of water vapour and other variables) can be specified in several different ways. The following are the principal quantities which may be measured or inferred:

(i) air temperature
(ii) absolute humidity (mass per unit volume)
(iii) partial pressure of vapour present
(iv) relative humidity
(v) dewpoint
(vi) wet-bulb depression (for a given type of instrument).

A knowledge of (i) and one other quantity determines the rest. Hygrometric tables define these relationships and make it possible to measure humidity in a number of ways.

---

[1] Tables and Figures for Chapter 7 begin on page 7-18

7.2.1 Terms Concerning Humidity Sensors

Many of the relevant terms used in hygrometry have been defined in previous chapters. The terms of importance to this discussion are summarized here with references to previous sections:

a) Absolute Humidity: (also called Mixing Ratio or Water Air Ratio) - **war** - The ratio of the mass m_v of water vapour to the mass $m_{d,a}$ of dry air with which the water vapour is associated in a given volume (see also Section 2.1.2 and Section 3.2.2, Equation 3-8).

$$\mathbf{war} = \frac{m_v}{m_{d,a}} = \frac{R_{d,a}}{R_w} \cdot \frac{P_{Sv}}{P_S - P_{Sv}} = 0.622 \frac{P_{Sv}}{P_S - P_{Sv}} \qquad 7\text{-}3$$

b) Saturated pressure of water vapour: P_{sat} - The static pressure, at a given temperature T_S and pressure P_S, of the water vapour in equilibrium with a plane surface of liquid water or pure ice: ($P_{sat} = f(T)$, see Section 2.1.2 and Figure 7.1(a) and (b)).

c) Relative Humidity: RH - The ratio of the partial water vapour pressure and the saturation pressure at the same temperature T:

$$RH = P_{Sv} / P_{sat} \approx \varphi \qquad 7\text{-}4(a)$$

which is often expressed as a percentage.

d) Dew point temperature and frost point temperature: Td, Tf - The temperature to which the humid air has to be brought (at constant P and **war**) in order that its water vapour pressure is equal to the saturated water vapour pressure at this temperature:

$$Td \text{ or } Tf = T_{sat\ (Psat)} \qquad 7\text{-}5$$

Note that for $T < 0$ °C, this temperature is the dew point temperature if the vapour is in equilibrium with subcooled-water and is the frost point temperature if the vapour is in equilibrium with ice (see Figure 7-1(b)).

e) Temperature of adiabatic saturation: Thermodynamic temperature of the wet bulb thermometer (in air) having pressure P_S, the temperature T_S, and the mixing ratio **war**. When water evaporates, a comparatively large amount of heat is taken up by the vapour. If the source of water in an air stream is thermally isolated from its surroundings, the temperature of the source will fall until all the heat required for evaporation is extracted through the boundary layer of gas adjacent to the water source. This limit temperature is the temperature of adiabatic saturation. As a first approach, it is the temperature indicated by the wet bulb thermometer of a psychrometer (T_{wb}), whereas the dry bulb thermometer (T_{db}) is the air temperature indicated by a thermometer whose sensitive element is perfectly clean and dry.

7.2.2 Technical Classification of Sensors

Humidity sensors can be classified into three types:

(i) Direct Determination of humid air parameters (e.g. wet and dry/ dewpoint hygrometers) (Section 7.2.3),

(ii) Indirect Determination of humidity. These sensors use an element whose characteristic (electrical or mechanical) is sensitive to humidity (Section 7.2.4),

(iii) Other Methods using special properties of the water vapour, including infrared absorption, change in the velocity of sound in air, etc. (Section 7.2.5)

Most of the typical instrument descriptions presented in the following sections are given by courtesy of SIRA (References 7.3 and 7.4)

7.2.3. Direct Methods

7.2.3.1 *Psychrometer (wet and dry hygrometer)*

Psychrometers measure the humidity by determining the ambient temperature (dry bulb temperature T_{db}), and the temperature of an evaporating water source (wet bulb temperature T_{wb}). These exist in many forms, an example of which is given in Figure 7.2.

The simplified heat balance for the wet bulb thermometer gives a simple relationship between the difference of the two temperatures T_{db} and T_{wb} and the amount of evaporated water (note that T_{wb} is a saturated temperature):

$$h_{fg}(\mathbf{war}_{wb} - \mathbf{war}_{db}) = c_{p\ mix}(T_{db} - T_{wb}) \qquad 7\text{-}6$$

assuming $P_v << P_a$, and

where h_{fg} is the latent heat of evaporation,
$c_{p\ mix}$ is the specific heat of humid air.

Using the relation for **war** of Equation 7-3, we get the following approximation for the partial pressure of the water vapour:

$$P_{S\,v,T_{db}} = P_{S\,v,T_{wb}} - \frac{R_w\, c_{p\ mix}}{R_a\ h_{fg}} P_S (T_{db}-T_{wb}) \qquad 7\text{-}7$$

and the relative humidity is obtained using Equation 7-4. Such calculations are usually achieved with the use of hygrometric tables, as previously described. The source of moisture is usually a moistened textile wick surrounding a thermometer. However, other porous materials are used occasionally. Perhaps the most important recent innovation is the use of a small pool of water that avoids the use of a wick altogether.

The psychometric method is simple, but is very sensitive to small temperature errors, which may occur for several reasons, especially:

- Thermometer uncertainties: The accuracy of the humidity measurement is much more dependent on the difference between the two thermometers than the absolute accuracy.
- Wet bulb temperature: Insufficient air flow is a major source of uncertainty. For accurate measurement, the required velocity is between 3 and 5 m/s.
- Contamination: Contamination on the wet bulb is another major source of uncertainty and water purity is essential as all the soluble contaminants in the water end up on the wick. Contaminants are also accumulated on the wick from the air and it is essential to ensure that the wick on the wet thermometer is cleaned regularly. Some psychrometers are badly designed and it is difficult to change the wick without contamination. For high accuracy, wicks may need to be replaced (new wicks may need to be boiled) or cleaned (by boiling or flushing with deionised water) every day.

The main advantages of the psychometric method are price, simplicity and its ability to withstand condensation. Contamination is tolerated insofar as replacement or cleaning of the wick restores the original calibration.

7.2.3.2 ***The Condensation Dewpoint Hygrometer***

The dewpoint (Td) of a sample of air is defined as the temperature at which the Saturated Water Vapour Pressure matches the partial pressure of the water vapour present, - alternatively, it is the temperature of onset of condensation when the sample of air is cooled under conditions of constant pressure.

The measurement of condensation dewpoint temperature is almost as old as humidity measurement. The process involves cooling a test surface until condensation is observed. Cooling is achieved by means of evaporating alcohol, or by other means, depending on the temperature required. The formation of dew is observed by the operator. The test surface is usually silvered, and observation is performed with the aid of a microscope. The accuracy of a manually operated dewpoint hygrometer depends on the skill of the operator in applying cooling at a slow rate to determine the temperature at which dew forms, and allowing the temperature to rise slowly to determine the temperature at which the dew disappears. Measurement of the dewpoint and air temperatures permits the relative humidity to be defined by use of the hygrometric tables.

The development of the modern condensation dewpoint hygrometer followed the development of efficient Peltier coolers (to cool the mirrors) and reliable opto-electronics (to observe condensation). The usual measurement configuration of a condensation dewpoint hygrometer is shown in Figure 7-3 where the rate of cooling is controlled to maintain a constant dew layer. Other means of detecting the dew, include capacitance change and sonar. A temperature sensor, normally a platinum resistance thermometer (PRT), is used to measure the condensation temperature. Electronic control of mirror temperature to maintain a constant layer of condensate, together with a PRT mirror temperature sensor, can give excellent long-term stability. An accuracy of ± 0.15 K dp (dp: dew point temperature) is possible with reproducibility better than ± 0.05 K dp. This is better than the performance of any other commercially available type of hygrometer at the present time. Also the instrument is, in principle, capable of operation over the whole of the normal operating range of hygrometers, from very low humidities to near saturation.

This apparatus can be considered as a reference method. The main source of error is the role of contamination. For example, traces of soluble contamination on the test surface are a potential source of large errors.

7.2.4. Indirect Methods

7.2.4.1 ***Mechanical hygrometer***

The dimensions of many natural organic and other materials change in response to a humidity change. Hair (usually human) and animal membrane are the most common materials used in older instruments, but various plastic materials, polymers, and textiles are becoming more common. The change in length, (which, for human hair, is 2% for a change from 0 to 100% RH) is related to the relative humidity (as opposed to other humidity parameters), and is non-linear.

Such an instrument is generally used at ambient temperatures and humidities (typical range 20 to 80% RH). Response is slow, particularly for decreasing humidity, and there is broad hysteresis, 3% RH or more. The characteristic output is subject to ageing and the instrument is sensitive to vibration. Mechanical systems can be used to linearise the output and/or operate a pen recorder. Electromechanical and pneumatic systems are sometimes used to provide suitable remote outputs. The main advantage of the instrument is its comparatively low cost, and it is the most common type of hygrometer in use, being the primary instrument for environmental monitoring and control of air conditioning systems. Accuracy is unlikely to be much better than ±10% RH even when a careful calibration schedule is employed.

7.2.4.2 ***Electronic sensors***

In many relative humidity measurement applications, hygrometers which use electrical relative humidity sensors have replaced mechanical hygrometers and psychrometers in recent years.

There are many types of sensors available but all usually consist of a hygroscopic material whose electrical impedance varies with relative humidity. Often this is lithium chloride, or another salt, which may be held in a gel or matrix of some kind. However, many modern sensors are constructed using thin film technology, or other means, and the sensor configuration may be resistive, capacitive or some combination. The important distinction for instruments in this group is that the measured electrical property changes in relation to the relative humidity, rather than the dewpoint. Calibration is essential, usually frequently.

Sensors often have a significant temperature coefficient though this is rarely specified. Many sensors have a limitation on the range, either close to 100% RH or close to 0% RH. There may be a severe non-linearity at these extremities, and in some cases sensor damage may occur. Despite this, many manufacturers claim 0 to 100% RH and it is difficult to decide which claims are justified.

These instruments have fast response and direct readout (nowadays usually digital). The operating range is typically 15 to 95% RH for humidity and -30 to +70°C for temperature, but some now operate over a wider range. Generally an accuracy of ±3% of the reading is the normal limit of accuracy, though once again many manufacturers claim better.

Used carefully, calibration drift is small but a short period at saturation conditions, or the presence of low concentrations of certain contaminants (depending on the particular sensor), can cause a calibration change. It is difficult to know when such conditions have occurred but checks using saturated salts are useful to confirm performance between calibrations. Additional information on two sensors is provided below.

a) Electrolytic (Coulometric) hygrometer: This hygrometer is based on the measurement of the quantity of electricity (or intensity of current) produced by the electrolysis of a compound, being formed through the effect of humidity on an anhydric compound. An example is the electrolysis of phosphoric acid formed by water vapour absorption on anhydric phosphorous where the electrolysis current is proportional to the amount of absorbed water vapour, and the anhydric phosphorous is reactivated by the electrolysis itself.

Until the advent of the optical dewpoint hygrometer, the electrolytic hygrometer was the only type of hygrometer suitable for measurement of low humidities (e.g. below **war**$=10^{-3}$). In this domain humidities are sometimes expressed in PPMw (parts per million by weight = 10^6 **war**) or in PPMv (parts per million by volume = $10^6(P_{Sv}/P_S)$ = 10^6 (**war**/0.622). The most important application range for the instrument is below 500 PPMv, and below about 5 PPMv it is still the best instrument in some respects. Response is fairly fast. At very low humidities the cell life is shortened as the phosphorus pentoxide can be "blown" off the cell. Accuracy is normally about ±10% of reading but, with high precision gas flowrate measurement and proper precautions when the cell electrodes are recoated, an accuracy of ±5% can be achieved.

b) Saturated (heated) lithium chloride sensor: This type of instrument operates on the principle that dry lithium chloride (LiCl) does not conduct electricity, whereas a solution is a conductor. The sensor consists of a bifilar winding on a LiCl-impregnated bobbin. The hygroscopic salt passes the supplied alternating current only when moist. This raises the temperature of the bobbin until an equilibrium relative humidity is achieved and the solution neither absorbs moisture from nor gives up moisture to the surrounding atmosphere. The instrument acts as a self-regulating heater to establish this equilibrium temperature and the output is interpreted in terms of dewpoint. The instrument range is -45 to +60°C dp with an accuracy of the order of ±1 K dp. There are further constraints because of the use of a hygroscopic salt. Operation is limited at high humidity because of the possible loss of hygroscopic salt under wet conditions, and, at low humidity,operation is limited to approximately 10% RH

because this is the minimum equilibrium relative humidity obtained with the salt. Response is slow.

7.2.5. Other Methods

7.2.5.1 *Spectroscopic hygrometers*

A number of absorption bands characterising the water molecule fall in the infrared region (1 - 10 μm). Most commercial infrared hygrometers use the 1.9, 2.7 and 6.3 μm bands, since these display the strongest absorption. The fraction of energy transmitted through a sample cell depends on water concentration, path length, and wavelength. At low moisture level, a long path length is required to maintain sensitivity. The basic instrument consists of a source, a filter for isolating wavelengths in the spectral region of interest, a sample cell, and detection system. Instruments usually compare transmission at two similar wavelengths (one being absorbed more than the other by water vapour) and use a broad-band solid-state detector, or else they use a strongly-absorbed wavelength and compare the transmission of the sample cell with that of a standard reference cell (Luft detector). None of the other constituent sample gases should have absorption bands overlapping with those of water.

The technique is relatively expensive, but is non-contact, and can therefore be used in the presence of aggressive gases. It would also be an economic method where a gas analyser is required for other components of the gas. Various research instruments of this type exist but commercial versions are also becoming available (Reference 4.14).

In the ultra-violet range, the Lyman-Alpha device is commonly used for inflight measurement (see Reference 7.6 and Section 7.3.3 b) because of its very fast response, despite the need for calibration.

7.2.5.2 *Refractometer*

A microwave refractometer measures the refractive index of air using a microwave (9 GHz) resonant cavity extended into the region of interest. It offers fast response and direct measurement of refractive index. Some drawbacks are present including a temperature dependence (Reference 7.3).

7.2.5.3 *Other*

There are several other types of instrument "more or less" commercially available. Principles employed include measurement of sound velocity, temperature rise of sulphuric acid, oscillation frequency of hygroscopically coated quartz crystal (piezoelectric), detection of oxygen concentration (using the zirconia sensor) and mist formation during adiabatic expansion.

7.3 PARTICLES

7.3.1 Particle Size Measurement

In the following sections various aspects of particle size and concentration measurement are considered. The domains of interest can be defined generally as follows:

Large particles ($>$ 10 μm) - rain drops, snow, hail, which often do not follow the flow.

Small particles ($<$ 10 μm) - droplets of condensation (fog), which generally follow the flow.

Very small particles ($<$ 1 μm) - atmospheric aerosols, which do follow the flow. Such particles include the solid and liquid particles in the earth's atmosphere which act as condensation nuclei for cloud droplets and play a role in the formation of smog and acid rain. From the point of view of particle characterization and measurement, the aerosols' subdivision introduced by Young (Reference 7.7) is convenient:

Aitken particles: $r < 0.1$ μm

Large aerosol particles: $0.1 < r < 1.0$ μm

Giant aerosol particles: $r > 1$ μm (Small particles in our more general classification.)

The following is a review of the main particle sizing techniques in multiphase flow. With most conventional methods, the sampling of small particles is achieved by extracting 'particle laden' samples from the flow and the measurement is therefore representative only of the extraction location. With large particles conventional methods are intrusive, whereas for medium sized particles some intrusive methods are used but care has to be taken to avoid corrupting the sample through the extraction process (iso-kinetic sampling should be used where local and probe sampling velocities are kept equal). Optical methods are generally non-intrusive and some can measure over a considerable range. Optical methods tend to suffer, however, from lengthy analysis and difficulties with densely laden flows. Considerable relevant work has been undertaken in the study of two phase flows in steam turbines, for example References 7.8 and 7.9.

7.3.1.1 ***Conventional (Non-Optical) Methods***

a) Large Particles: typical methods use the following techniques:

Sample Extraction - Sedimentation or sieving of particles collected in batches (liquids drops can be frozen).

Impact Method - Particles may be sized by microscopic examination after capture on solid surfaces (magnesium oxide, soot or vaseline, or in thin, viscous liquid films for liquid drops).

Evaporation Method - The method consists of impinging the drops onto a hot surface and then observing their evaporation.

Electrical Method (conductance) - This method uses the low resistivity of the drop to complete a bridge between a pair of needle electrodes. For a known electrode separation B, a current pulse is produced from drops of diameter equal to or greater than B. Drop size distribution is then deduced by making measurements at various probe separations. The advantage of this technique is the possibility to insert a probe in the flow to take on-line measurements (see Figure 7-4 and Reference 7.8).

b) Small and Very Small Particles: Conventional measurement methods are based on the dynamic or electrical mobility of submicronic aerosol particles and can be divided into the following three groups:

Inertial Method (Figure 7-5) - This method consists of two main steps:

- selection of particle size by application of an external force (gravity, centrifugal force, electrical force) or by sudden change in the velocity vector of the fluid;
- detection of size after collection on a support (solid particles) or by optical detectors.

In the most commonly used devices, these operations are rarely performed simultaneously and measurements are therefore relatively time-consuming.

Diffusion Methods - These methods are based on the theory of Brownian motion and the diffusion of small particles suspended in a gas. In this situation the gas molecules rebound when they collide with a wall, whereas the particles adhere to the wall. The deposition rate depends on their diffusion coefficient and, therefore, on their size. The selection principle generally operates by circulating the particle laden gas through a bundle of cylindrical tubes or parallel plates. The detection of small particles often requires a battery of such devices.

Electrical Methods - Three successive steps are usually employed:

- labelling of particles by applying a known number of electric charges (for example, particles are placed in contact with a cloud of bipolar ions),
- selection of particles by application of an electric field in an electrostatic precipitator,
- counting selected particles (to give concentrations) either by electrical measurements or by use of optical counters or condensation nuclei counters.

A sophisticated example of such an instrument for measuring modest concentrations of small droplets (or particles) is the Differential Mobility Particle Size Analyser (DMPSA). The DMPSA measures airborne particle distributions of samples taken from the air in the 0.02 - 0.9 μm range with high resolution. It consists of a Differential Mobility Analyser (DMA - to label and select a particular range of particles) and a Condensation Nucleus Counter (CNC - to count the concentration of selected particles). Studies using the DMPSA are detailed in Section 4.6.2 and a brief description of its operation is provided here.

Differential Mobility Analyser (DMA) (Figure 7-6) - The mobility analyser categorises the sample into selectively sized groups.

Before entering the Analyser, the gas sample enters an impactor designed to remove particles greater than one micron that would otherwise interfere with the measurement. The impactor is a calibrated orifice that directs the sample flow onto a removable impaction plate. The impaction plate is covered with a thin layer of vacuum grease and is designed such that particles greater than a predictable upper size are removed from the sample. The pressure drop across the orifice is also used to give an indication of inlet flow. The submicron aerosol then passes through to the "labelling" and "selection" procedure.

The "labelling" process involves exposing the flow to a radioactive source of two millicuries of Krypton 85 providing a high concentration of both positive and negative ions. The particles acquire a known charge level described by Boltzmann's equilibrium charge distribution and enter the "selection" process or electrostatic classifier.

The classifier employs two concentric cylindrical electrodes. A high voltage supply controlled by the computer maintains the centre electrode at a precise negative potential. The outer electrode is at ground potential. An inner core of particle-free sheath air and an outer annular ring of the sample aerosol flow laminarly down between the electrodes with no mixing of the two air streams. Particles with positive charges are attracted through the sheath air toward the negatively charged inner electrode. The trajectory of such a particle is a function of the flow rate, analyser

geometry, electric field, particle diameter and narrow slot, and only those particles with a narrow, predictable mobility range pass through an orifice to the detector (counter).

Condensation Nucleus Counter (CNC) (Figure 7-7) - The condensation nucleus counter is the instrument used to count the number of sized particles from the electrostatic classifier. The particles pass through a saturated alcohol vapour and then into a condenser. Each particle acts as a nucleation site that the alcohol condenses around forming a relatively large droplet, that is able to scatter a detectable amount of light from the optical detector.

The dry particle, being a similar size to the wavelength of light (violet 0.4, red 0.74 microns), would have been too small to be detected. The droplet size, however, is nearly independent of the size of the original particle, so the light scattered is a function of concentration (number) only.

The counter is also able to operate in two counting modes, a single pulse counting mode that allows accurate measurement of low concentrations from 0.1 to 1000 particles/cm^3. As the concentration becomes stronger and individual pulses can no longer be resolved, the counter enters a photometric mode and measures the total light scattered from all droplets in the viewing volume, allowing concentration measurements from 1000 to 10,000,000 particles/cm^3.

Although this is basically an optical scattering method it has been included here because it is most often used as a part of an 'Electrical Method'.

The above methods are versatile, but do not cover all applications, notably the detection in real time of very low concentrations of aerosols (less than 1 μm).

7.3.1.2 *Optical Methods*

There is a tendency for conventional methods to be superseded by optical methods, though these latter are more expensive. Practically all optical methods are based on the properties of the light scattered by particles when illuminated by an external light source. For practical purposes, these methods can be divided into four groups:

a) Imagery (for large particles (>10 μm)):

High Speed Photography (Figure 7-8, Reference 7.9) - The most suitable technique is the shadowgraphy (backside lighting using a pulsed laser diode or a fast timed flash) associated with a video CCD camera (equipped with an enlarging optic) which records image shadows at the frequency of 25 Hz. The measuring volume is small and numerous images (e.g. 500) are needed to obtain a realistic histogram of the fog. Real time (25 Hz) automatic image analysis systems should be available in the near future which will greatly assist the analysis of data. The use of a double-pulsed laser diode or flash offers the potential of defining particle velocity in addition to size. Inherently, the method is used for measurement over a field but is limited in densely laden flows.

Holography - Holography (three dimensional object reconstruction) has long been considered as the most suitable technique for particle sizing. It provides images of large particles of any shape, as 'frozen' in space, which then can be analysed in their entirety at leisure (for example, with a video camera system). The main limitation of this technique is the amount of time necessary for analysing holograms and the cost of the apparatus (ruby or YAG laser). Automatic analysis systems (using digital image processing) should be available in the near future. Figure 7-9 shows a holographic probe designed for measurements in industrial environments. Again, the method is a field system but has difficulties in heavily laden flows (Reference 7.9).

b) Scattering: The intensity (I) of light scattered by a particle depends on the intensity of the illuminating radiation, the diameter and refractive index of the particle, the wavelength and polarisation of the light and the direction of the observation relative to that of the illumination. Complete calculation codes for spherical particles are now available on the basis of Lorentz-Mie theory in the case of a plane monochromatic incident wave. The structure of the angular distribution is very complex and three regions are to be considered according to the size parameter $\alpha = \pi D/\lambda$, (λ = wavelength of light):

$\alpha < 0.1$	- Rayleigh zone
$0.1 < \alpha < 30$	- Mie zone
$\alpha > 30$	- geometrical optical laws are applicable

The most complicated zone to compute is the 'Mie' zone where the intensity oscillations I(θ) are very important. (See Figures 7-10 and 7-11).

The basic technique consists of collecting at a given angle (θ) the light scattered by a particle, and of correlating the signal intensity with the particle diameter as shown in Figure 7-10 for $\theta = 90$ degrees. This technique gives a quasi monotonical response curve in two regions:

- large particles (with white light source)

$$I = kD^2$$ 7-8

- small particles (Rayleigh region):

$$I = kD^6 \qquad 7\text{-}9$$

In the latter case, the use of a laser is necessary to increase the intensity of illumination. Hence, the scattered intensity depends on the location of the particle in the Gaussian laser beam. Correlation techniques are needed to extract size and velocity information. Many methods have been developed to minimize the trajectory ambiguity (correlation techniques, two color beams, etc.). Some instruments use the rates of intensities scattered from different positions in space.

c) Laser Doppler: Doppler techniques can be used for single particle sizing (see Section 7.3.2.1).

d) Extinction: (References 7.8 and 7.9). The attenuation of a parallel beam of light (Figure 7-11) due to scattering from droplets is a function of each particle size parameter and the number N of particles. Using numerical inversion techniques, the size distribution can be determined from the attenuation measured at various wavelengths. This technique has been widely used in wet steam fog studies. Both point and field applications are available although the most common are point instruments. The use of moderate power lasers permits application in reasonably dense fields. A simple implementation of an extinction method is also discussed in Section 4.3.1.3 for engine testing.

e) Diffraction: The technique (Figure 7-12 and References 7.14, 7.31, and 7.32) uses the intensity variation within the diffraction pattern produced by particles at small angles. This diffraction pattern depends only on the size of the particle and is independent of the refractive index and the position of the particle in the measuring volume. Therefore, a collection of particles of the same size will give identical diffraction patterns which will be superimposed at the recording plane.

For a polydispersed fog, the size distribution can be obtained using special algorithms. In the most common applications, a relative distribution is achieved by adjusting coefficients of a given distribution function (log-normal, upper limit function, etc.).

f) Other Methods: Other methods include multi-wavelength solar radiometry using the sun as a known source and measuring extinction, and back-scatter systems. A global term for such methods is the acronym LIDAR (Light Detection and Ranging) which includes many of the processes amenable to laser remote sensing (Reference 7.11).

Note: Methods (a), (b) and (c) are single particle size measurements; methods (d), (e) and (f) are ensemble particle sizing measurements.

7.3.1.3 *Summary*

Table 7-2 reviews the advantages and problems for each method. For gas turbine applications the following appear to be the most suitable:

for large particles (rain, snow, hail): high speed video, shadowgraph, and holography;

for small droplets (condensation fog): extinction and scattering (with calibration);

for air pollution: one of the conventional sampling methods.

For inflight measurement, Knollenberg manufactures equipment suitably packaged in various configurations. Such equipment is widely used in atmospheric research studies (Reference 7.12). Figure 7-13 illustrates (a) a spectrometric probe based on forward scattering (a mask is needed to eliminate the direct beam), and (b) an optical array probe based on one-dimensional shadowgraphy. Figure 7.14 shows a typical flight probe.

Care should be taken using optical techniques, as with the exception of imagery and diffraction techniques, optical methods depend on the refractive index and the shape of particles. Figure 7-15 indicates ice crystal shapes which can occur and which can confuse measurements, Reference 7.13.

7.3.2 Velocity Measurement

7.3.2.1 *Velocity Measurement Techniques*

a) Point Measurement:

Laser Doppler Method - (Figure 7-16 and References 7.31 and 7.32) - Laser Doppler anemometers use the frequency information contained in the light scattered by individual particles passing through a fringe pattern to determine the particle velocity. The fringe pattern is obtained either by two interfering laser beams (LDA) or by using gratings imaged into the measuring volume (Reference 7.14). Additionally, information on size can be obtained through two methods:

- Visibility technique,
- Phase difference between the signals produced by two detectors located at two different points in space and looking at the same particle.

The latter method seems to be the more powerful technique, and significant advances have been achieved recently (Reference 7.15).

Laser Two Focus - An alternative optical method of defining the velocity of particles is the Laser Two Focus (L2F) or Transit Anemometer (Reference

7.16). In this method the interference fringes of the Doppler system are replaced by two highly focussed laser beams which become the optical gates of the system. The spots from the laser beams are rotated until they are aligned with the flow when the individual transit times are most consistent. (When the spots are not aligned the 'apparent' transit times are the result of different particles passing through the same spots and these 'apparent' transit times are inconsistent). The tech-nique has the benefit of good signal strength and good spatial resolution but the disadvantage of having to rotate the spots (by comparison, Doppler systems measure components). The technique has not been used for the assessment of particle sizes but has been used to track particles where their sizes are known (Reference 7.17).

b) Field Measurement Method: Such techniques are now becoming available in the forms of Particle Image Velocimetry (PIV) and Doppler Global Velocimetry (DGV).

Particle Image Velocimetry - PIV is the more established method and has various formats (Reference 7.18). The principle involves a double exposure of particles and the subsequent analysis of the particle movement between exposures. Knowing the movement and the time between exposures provides the velocity informa- tion required. In many ways, PIV is the field interpretation of the Transit Anemometer.

Doppler Global Velocimetry - In much the same way, DGV is the field analogue of the Doppler Anemometer in that it measures the frequency shift of light scattered from particles moving through a laser light sheet (Reference 7.19). The detection method uses the absorption characteristics of an iodine cell to measure the frequency shift.

DGV is the more recently researched method and appears to hold advantages over PIV systems where the velocity is high, but much research has yet to be undertaken. In both cases, however, current development has been for the measurement of flow (using small particles) but there are obvious applica-cations for the measurement of the velocity of larger particles, although (to date) neither method has been used to measure particle size.

7.3.3 Quantity of particulate

a) Ground Measurement: Two "lump parameter" quantities generally used to describe rain are rainfall rate (Rr) and liquid water content (LWC). Rainfall rate is the linear accumulation depth at ground level per unit time and is typically used to characterize rainfall at ground level. For airborne measurements, the liquid water content (LWC), the mass of liquid water per unit volume usually expressed as g/m^3, is the more meaningful parameter. The relationship between LWC and Rr is uniquely dependent on the type of storm and the intensity level of the storm. In the absence of a vertical wind velocity, the LWC is directly related to the rainfall rate and the drop size distribution.

Rainfall rate Rr is usually measured using either collection pans or storage flasks which provide the average rainfall over some considerable time or using a 'rocking meter' with two small containers, one of which is empty and the other filling. When the 'filling' container is full the system 'rocks' and initiates filling of the second container and empties the first. The rainfall is measured by the rate of 'rocking'.

The lack of rainfall measurements over very short time constants, in the order of seconds, has led to the development of a ground-based natural rainfall measurement technique by Melson (Reference 7.20). His technique acquires data over very short time constants, as short as one sample per second. The maximum rainfall rate measured of 720 mm/hr (28 in/hr) occurred for just under ten seconds at NASA Wallops Flight Facility in 1990.

An emerging method for the remote measurement of precipitation (rain, hail, snow) uses radar and the relationship between the rainfall rate (Rr), and the radar reflectivity factor (Z) for the particles (rain, snow, hail) (see also Section 2.4.4). The factor (Z) determines the amount of power scattered by the raindrops in a unit volume at a given distance back to a receiving antenna. (This relationship is often described as the Z-R relationship.) Raindrops, some of which have diameters less than 1 mm, are small compared with the wavelengths of weather radars (usually 3, 5, or 10 cm). Thus the radar reflectivity is very small and, to accommodate this, the relationship is modified and it has become the custom to express it in the form:

$$Z = z_1 Rr^{z_2}$$

where z_1 and z_2 are constants depending on the type of particles: droplet, snow, hail (References 7.21, 7.22 and 7.23). By careful calibration and some further knowledge (or possibly several measurements from different 'viewpoints') the position, type and rate of fall can be established.

b) Inflight Measurements: The following methods are used:

Imagery Technique - The quantity of droplets can be deduced from optical measurement

techniques, if the velocity and the measuring volume are known. Scattering techniques or high speed photography could be used for this purpose but the accuracy is limited to 5 - 10 % (see also Section 7.3.1.2).

Hot Wire Technique (Figure 7-17) - In this method a calibrated resistance wire which has been mounted in the airstream is connected as one branch of a balanced bridge circuit and is heated by an electric current. As the water droplets in the cloud strike the wire, they are evaporated, thus cooling the wire and thereby decreasing its resistance. The change in resistance causes the bridge to become unbalanced, and the degree of unbalance is a function of the liquid-water content of the cloud.

A second resistance wire, mounted with its axis parallel to the airstream direction and hence not subject to water-drop impingement, is connected as an adjacent branch of the bridge. This wire serves to compensate for variations in airspeed, altitude, and air temperature, so that the bridge becomes unbalanced only in the presence of water droplets. The output of the bridge is proportional to the rate of impingement of water on the sensing wire. This signal is converted to concentration of water per unit volume of air by means of an adjustment for true airspeed.

Absorption Method - An example of such an instrument for inflight applications is described by the Meteorological Research Flight publication (Reference 7.24). This is a Lyman-Alpha absorption device which measures absorption due to water vapour of a sample which has passed through a heater which evaporates solid and liquid water. From this absorption, the total water content by mass is calculated (e.g. see Figure 7.18a). The instrument can also be considered as a humidity instrument when used in cloud (particle) free conditions. Humidity can also be measured after droplet separation (e.g. see Figure 7.18b).

Total Water Content is a quantity which is conserved in the absence of precipitation of mixing processes, and it is therefore useful to be able to measure it directly rather than by the separate measurement of different phases, i.e. liquid plus vapour (e.g. see Figure 7-18a).

Typical devices have an isokinetic sampling inlet to ensure that all sizes of liquid or ice particles are correctly sampled. Condensed water is evaporated as it passes through high-efficiency heaters consisting of a barium titanate matrix with steel mesh screens to further break up any drops. The humidity of the resulting air/water vapour mixture is then measured using a Lyman-Alpha absorption hygrometer. UV radiation at 121.56 nm is emitted by a hydrogen source tube. The absorption of this wavelength can be related to the water vapour concentration, after allowances for some absorption by oxygen and ozone. The detector tube is a nitric oxide ion detector. The ionisation current is greatly amplified and linearised by means of a logarithmic amplifier. The voltage output is then digitised and recorded. Instruments are calibrated from other humidity sensors, such as dew-point hygrometer. Calibration constants in the form of an offset voltage and sensitivity factor may then be obtained.

Instruments typically have a resolution of ± 0.005 g/kg, a range of 0 to 20 g/kg and an accuracy of ± 0.15 g/kg. Sample rates are about 10 l/s and the response time is about 2 ms for vapour only, rising to 0.2 s when drops of 1 mm radius are being evaporated.

The instrument has a very fast response and provides high quality and useful data. The absolute accuracy does, however, depend entirely on the calibration and requires a certain degree of expertise to achieve the optimum results.

c) Other Ground/Inflight Methods: Reference should also be made to Section 7.3.1, which considers the sizing of individual particles and, in some cases, the estimation of the number of particles present in a sample. Such sampling methods are generally suitable for both 'ground' and 'inflight' measurement.

7.4 EFFECT OF WATER ON TEMPERATURE MEASUREMENT

It appears to the authors that, where water is in vapour form and mixed with the incoming air, contact sensor techniques such as thermocouples and PRT's arranged as described in Reference 7.1 will provide meaningful readings of the mixed gas temperature. Care should be taken, however, where attempts are made to use temperature to infer an enthalpy level, or where static to total transformations are involved, as this requires a knowledge of the gas composition (see Chapter 3).

Where small particles of water (from condensation or rain) are present, the situation becomes much more complicated as the droplets will impact on the sensor tending to mask the gas temperature. Subsequent evaporation from the sensor, the meaning

of any Recovery Factor (r_f) and the possibility of non-equilibrium temperature between the particles and gas flow add to the problem to the extent that in most instances the reading becomes unreliable. No reliable correction exists for these circumstances and, indeed, the greater present problem is the detection of these conditions.

A partial solution to the problem is to use a centrifuge sensor, such as the Rosemount sensor (Reference 7.26), which, before bringing the flow to rest in the stagnation chamber, centrifuges particles out of the sensed gas flowpath. These sensors have been further developed for use in icing conditions by installation of a heating element in the centrifuge system but, while enabling some form of measurement to be made, care must be taken because the heating element can introduce errors in the recorded gas temperature. Some further user experiences are reported below. These attempts to overcome the problem, however, leave much to be desired as, even if successful, they only define the gas flow temperature and not the particulate or average temperature.

7.4.1 The Rosemount (Centrifuge) Sensors

Details of sensors which have a centrifuge to separate the flow and particles are discussed in Reference 7.26 and have two forms, one of which contains a heater to prevent icing in icing conditions while the other does not. Each sensor assembly is made up of two parts - a sensing element and a housing which supports and protects the element. The element is a pure platinum wire of diameter .025 mm and length 250 mm, wound in a spiral on a rigid mica former to finish as a structure some 6 mm long with a square cross section of side 4 mm. The ice-point resistance is 50 ohms. The housing holds the element at right angles to the main air flow and the design means that the bleed air reaching the element has undergone a right angle turn which achieves inertial separation of solid particles or water droplets and thereby attempts to avoid damage to and wetting of the fragile platinum wire. Data from the de-iced sensor is typically recorded at 32 Hz with a resolution of about 0.0025 K. A comparison of the sensitivity to moisture between a standard probe and a special probe is given in Figure 7-19 (Reference 7.26).

Several potential sources of error need to be considered in deriving temperature from the sensor measurements:

Resistance/temperature calibration - This is based on fixed point calibrations and gives rise to a calibration tolerance of $\pm 0.25\ ^{\circ}C + 0.5\%$ T over the range -70 to +50°C where T is the temperature in °C.

Recovery error - This results from the inability to achieve 100% adiabatic compression within the housing which means that the recovery temperature (T_r) is less than T_T. The recovery factor relates T_T and T_S to T_r:

$$r_f = \frac{T_r - T_S}{T_T - T_S} \qquad 7\text{-}10$$

and for sensors with a constant adiabatic recovery factor, the recovery temperature is:

$$\frac{T_r}{T_S} = 1 + r_f \left(\frac{\gamma - 1}{2} \right) Ma^2 \qquad 7\text{-}11$$

Clearly, the presence of evaporating moisture will influence the process.

De-icing heater error - This arises from heating of the air flow by the heated housing of the deiced sensor. The correction applied is based on figures supplied by Rosemount for various temperatures and Mach numbers. The size of the correction is typically 0.2 K which is only applied when the heater is switched on.

Time constant - The time constant of a temperature sensor is not a simple parameter to quantify. As well as having a dependence on the construction of the sensing element itself, it is also related to the way the element is supported (there are conduction losses to the structure) and to the nature of the fluid flow around it. For the Rosemount 102 sensor there is a well documented double time constant response (References 7.28 and 7.29) with a rapid response to a step change from the element itself followed by a much slower one due to the effects of thermal conduction to the housing. Numerical techniques are available to retrieve some 'lost' high frequency data and take the level response up to about 3 Hz.

Sensor wetting - The construction of the Rosemount sensor housing is designed to inertially remove particulate matter and water drops from the sample flow. The fact that this is not 100% successful is evidenced by the fact that salt crystals have been observed on the element after removal from the housing. In this case the platinum wire is acting partially as a wet bulb thermometer and will therefore be under-reading (Reference 7.30). When flying in

cloud with a high concentration of water droplets, the probability of the occurrence of some sensor wetting is increased to a near certainty. The magnitude of the error is typically a few tenths of a degree K (Reference 7.30) and is dependent on the liquid water content of the cloud (Reference 7.31).

Overall performance - The overall accuracy of measurements made by the deiced sensor is estimated to be ± 0.3 K. Response starts to fall off at about 0.1 Hz unless a numerical correction scheme is employed, which can maintain a level response up to about 3 Hz.

7.4.2 Temperature Measurement by a Non-Contact Instrument (Reference 7.27)

Many of the problems associated with the immersion type of thermometer are avoided by using a radiation or 'non-contact' instrument. Such instruments measure the incoming radiation in a clearly defined passband and, by inversion of the Planck function, the temperature is obtained.

Such an instrument is fully described in Rudman (Reference 7.32). Essentially it comprises a radiometer looking at the 4.3 μm carbon dioxide absorption band, which is used because of the relative uniformity of CO_2 in the atmosphere. The in-coming radiation is chopped against an internal black body at 3.2 kHz. Combining this rate with a fast detector means that meaningful data at 32 Hz are obtained - a sampling interval of around 3 m at typical airspeeds. Two optical filters are used, the first being a solar blocker to reduce the sensitivity of the instrument to short wave radiation and the second a narrow band filter to define the passband. The chopper is an aluminium alloy disk with 8 holes and with a reflecting film deposited on the in-board surface to reflect radiation from the reference black body into the optical path. The strength of the 4.3 μm absorption line (in reality a series of lines) defines the effective sampling volume.

Recovery, de-icing heater and sensor wetting errors are avoided, although the instrument requires careful and relatively frequent calibration to compensate for drifts and degradation of the optical surfaces. Procedures usually involve regular calculation by comparison with thermocouple measurements in clear air. When properly calibrated, the instrument can provide temperature accuracies of about 0.3 K at low temperatures and about 1 K at high temperatures. Operation below about 200 K is not possible because of the poor signal to noise ratio. The instrument is expensive, however, and it is difficult to foresee how it can replace the banks of thermocouples normally used on engines.

7.4.3 Summary for Temperature Measurement (Reference 7.27)

(i) Where a fast response (say >1 Hz) is not required, and in a cloud-free atmosphere, Rosemount thermometers supply adequate data.

(ii) For data when condensing conditions prevail, difficulties can be anticipated and care should be taken. Some form of non-contact probe would be preferred but these look unlikely in the near future.

7.5 EFFECT OF WATER ON PRESSURE MEASUREMENT

The pressure which would be attained in a pitot tube facing a stream of moist air in which drops have condensed owing to the fall in temperature which occurs in the low pressure intake flow can be studied by means of a (pressure/specific volume) diagram, Figure 7-20 (Reference 7.33).

Now suppose that the moisture-laden air meets a pitot tube. If the drops evaporate so rapidly as to maintain saturation conditions, the representative point will travel back along *EDB* to *B* and will then run up the dry adiabatic towards *A*. If the drops do not evaporate at all, the point will travel up a curve *EF* which is practically identical with the dry adiabatic through *E*. Partial evaporation will be represented by an intermediate line.

The diagram may be used to determine the velocity of air at any point since Bernoulli's equation may be written:

$$\frac{1}{2}V^2 = \int_P^{P_0} \frac{dP}{\rho} \qquad 7\text{-}12$$

where P_0 is the pressure in the reservoir and V the stream velocity. A pitot tube brings the air to rest so that if P_1 is the pitot pressure

$$\int_{P_1}^{P_0} \frac{dP}{\rho} = 0 \qquad 7\text{-}13$$

the integral being taken round the path followed by the representative point. Therefore, to find the pitot pressure, all that is necessary is to follow the

representative point until the total area swept out by the *abscissa* is zero. It will be seen that if no condensation occurs or if the air remains exactly saturated after first reaching saturation (i.e. if the representative point travels down and returns up the saturation line *BDE*) the condition can only be satisfied when $P_1 = P_o$ so that the pitot pressure is the same as that of the reservoir.

If the representative point travels down the dry adiabatic until, say, 4-fold supersaturation is attained at *C* the representative point then follows the path *CDEGH* till all drops are evaporated before reaching the pitot at the point *H* (which lies on the dry adiabatic). It will then run up the line *BHA* to the point *K* where the area *HBCDEGH* is equal to the area *LAKN*. At this point the condition is satisfied so that the ordinate *KS* of *K* represents P_1, the pressure attained in the pitot tube.

It may happen that the drops do not evaporate before reaching the pitot tube. In this case the abscissa of the representative point will have swept out zero area before reaching the dry adiabatic. Such a case is represented by the path *ABCDEO*. If *OR* is the abscissa of *O* and *OR* cuts the dry adiabatic line at *Q*, *O* is determined by the condition at the area *ABQRLA*. In that case, the pitot pressure P_1 is represented by the ordinate of *O* which is shown as *OT*.

It is of interest, (Reference 7.34), to note that if a nuclei-free saturated gas contained in a Wilson chamber is supersaturated by rapid expansion, no condensation will occur until the gas pressure reaches about four times the saturation pressure, when the supersaturated system will in every case collapse. Pearcey also reports that Oswatitch suggests that the numbers of condensation nuclei in atmospheric air are probably far too small to have any appreciable effect on condensation phenomena at high speeds, and Oswatitch found experimentally for his supersonic nozzles that rapid condensation began when P_v/P_{sat} was about 4.0, *i.e.* the same value as for the cloud-chamber tests. This process takes place within an atmosphere with few particles and is largely homogeneous (see Chapter 4). In gas turbines operating at sea level the process is likely to be precipitated by atmospheric particles (heterogeneous condensation) and lower levels of supersaturation are probable.

The error introduced by the process is difficult to generalize because of the uncertainties associated with the condensation process. Awareness of the problem, however, is recommended as the best precaution.

A further serious consideration is the accumulation of water (or ice) in the lines connecting probes and sensors. Such accumulation will lead to failure of the measurement system when the tube is completely blocked, although even a liquid slug can cause severe problems, especially in low pressure systems. Where accumulation is possible, lines should be appropriately sized and fitted with water traps. Sensors should either be sufficiently robust not to be influenced by droplet formation or be situated where this will not occur or (possibly) heated.

7.6 SENSORS AND ELECTRONICS FOR FLIGHT

7.6.1 Function and Location of the Sensors

The function and location of pressure and temperature sensors on an aircraft (Figure 7-21) are generally as follows:

a) Pressure Sensors: In flight, we can measure the static pressure P_S and the total pressure (or stagnation pressure) P_T, either with the help of a combination (or Pitot-Static) probe or a total pressure probe and separate static pressure tappings.

The measurement of these two pressures permits the presentation of the following information to the pilot:

- altitude (on the altimeter),
- the conventional air speed (on the anemometer),
- the Mach number (Ma),
- the vertical speed read on the variometer obtained by the pneumatic derivation of the static pressure.

Note: The pressure recording device is generally remote from the measuring point, the pressure being transmitted via small-diameter tubing; care should always be exercised to avoid particulates blocking these lines.

b) Temperature Sensors: Here, only the total temperature (or stagnation temperature) T_T is accessible through direct measurement. Nevertheless, from Equations 7-14 and 7-15:

$$T_T = T_S\left(1 + \frac{\gamma - 1}{2} Ma^2\right) \qquad 7\text{-}14$$

$$V_{ar} = \sqrt{\gamma R T_S}.Ma \qquad 7\text{-}15$$

the static temperature T_S and the speed of the aircraft V_{ar} can be calculated.

c) Others: It is equally possible to measure the angle of incidence of the aircraft (with the help of a weather-cock), its positions and angular speeds (gyroscopic), its altitude with the help of a radioelectric sensor, and its ground speed by the Doppler effect.

Humidity has nearly no influence on these particular measurements, except the radioelectric sensor whose antenna is defrosted by the help of an electrical resistance.

7.6.2 Protection Used Against Humidity

Humidity can be the source of errors in many of the different measurements described above. Humidity influences air density and its isentropic exponent γ which can lead to errors in the anemometer, altimeter and temperature.

The water vapour contained in air can be sucked into the pressure line and possibly condense giving rise to droplets thereby risking the blockage of the duct. Still worse, if droplets freeze, it could cause a breakdown of the installation in a non-recoverable manner. Finally, the drops of water or the melted balls of snow can obstruct the transmitting pressure lines.

The following technical solutions have been formulated:

a) For temperature measurement

The influence of humidity on γ is very large in the case where we simultaneously have:

- a high static temperature,
- a very high degree of humidity,
- a high Mach number flight.

This kind of flight is relatively rare in our latitudes and only military aircraft are likely to incur such conditions. Under normal conditions, the high speeds required are only achieved at very high altitudes where the static temperature and degree of humidity are relatively low. In such cases the influence of humidity can usually be neglected.

Potential damage to probes caused by droplets, snow balls and ice is usually avoided by well-designed (and positioned) probes. However, they can be progressively covered by a fine layer of water or ice which interferes with the measurement as the air stream evaporates (totally or partially) the water and cools the sensor. To solve this problem the probes used have an internal deflector and/or an electrical heater which eliminates the risk of deposit of ice or water on the probe. These have been discussed in Section 7.4.

b) For pressure measurement

Humidity can modify the pressure measurement (as previously described) and thus, for example, the altimetric measurements.

The influence, however, is less than 3% in tropical countries and close to the ground level (saturated air at 40°C). Even if the relative humidity is 100% at altitude, the corresponding absolute humidity (**war**) decreases rapidly with the temperature, so that the error in pressure measurement will be less than about 1%. As humid air is lighter than dry air, the error introduced is conservative.

It is very important to prevent water blocking the lines, so tubing should have an adequate diameter. Pitot tubes often have lines consisting of chicanes and decantation chambers with evacuation holes to avoid the problem.

7.7 CONCLUSIONS AND RECOMMENDATIONS

As explained in the scope, this chapter is very broad and, in several areas, incomplete. Although various techniques exist to determine humidity, particle size and particle velocity, they are often ill-suited to measurement in the gas turbine environment, or laborious, or expensive. It is also clear that the presence of water as liquid or ice can significantly influence temperature measurements, and, to a lesser extent, pressure measurements, without a satisfactory method of compensation. In such cases, extreme care must be exercised. On a more positive note it is hoped that this chapter serves to define suitable measurement systems where available, prompts due care where techniques are inadequate, and will lead to improved measurements systems in the future. The following specific recommendations are made:

(i) Generally improve the packaging and reliability of complex measuring systems for gas turbine test environments.

(ii) Develop robust particle sizing methods for liquid and solid particulates for routine use in the engine and component test environment. These might be of at least two categories - the first to detect some critical level of particulate, and the second to quantify the particulates more precisely. The range of particle sizes that may be encountered is considerable and depends on the test program. The question of sampling with multi-point probes or using field measurement techniques must be addressed. Where the particulates are dense and maldistributed, current methods are particularly inadequate.

(iii) Methods for defining total temperature in the presence of particulates (condensate, rain, hail, etc.) need to be improved. Again this must address the matter of spatial sampling. Techniques are required which provide both a meaningful measurement of gaseous temperature and particulate temperature so that a combination of this information and the particle measuring method can be used to define the enthalpy of the two (or even three) states separately.

7.8 REFERENCES

7.1 *Recommended Practices for Measurement of Gas Path Pressures and Temperatures for Performance Assessment of Aircraft Turbine Engines and Components*, AGARD Advisory Report No. 245, 1990.

7.2 Ower, E., and Pankhurst, R.C., *The Measurement of Air Flow*, Pergamon Press, 5th Edition, 1977.

7.3 *Humidity and Moisture Measurement*, SIRA Ltd, Chislehurst, South Hill, Kent BR7 5EH, England, communication, 1993.

7.4 Pragnell, R.F., *Recording humidity: no need to lose your hair*, Environmental Engineering, September, 1990.

7.5 *L'Air Humide - Mesures d'humidité*, Revue Technique de l'Ingénieur, 21 rue Cassette, Paris, 1986 - 1993.

7.6 *Humidity Measurement*, Meteorological Research Flight Instrument Note 6, Meterorological Research Flight, Farnborough, U.K., 1991.

7.7 Young, J.B., *Condensation in Jet Engine Intake Ducts during Stationary Operation*, ASME Paper 93-GT-5, International Gas Turbine and Aeroengine Congress and Exposition, Cincinnati, USA, May 24-27, 1993.

7.8 Moore, M.J. and Sieverding, C.H., *Ed., Phase Steam Flow in Turbines and Separators*, Von Karman Institute Book, McGraw-Hill Book Company, London, 1979.

7.9 Kleitz, A. and Courant, J.J., *Three Probes for Water Droplet Sizing in Wet Steam Turbines*, European Conference on Turbomachines, London, 1991.

7.10 Gebhart, J., and Anseln, A., *Effect of Particle Shape on the Response of Single Particle Optical Counters*, in *Optical Particle Sizing*, edited by Gouesbet, G. and Grehan, G., Plenum Press, 1988.

7.11 Measures, R.M., *Laser Remote Sensing: Fundamentals and Applications*, Wiley & Sons, 1989.

7.12 *Setting up of the EDF-INAG Test Station for Low Atmospheric Exploration on board the HD-34 (Hurel-Dubois) Airplane of the Institute Géogrphique National*, Technical Report, July, 1980.

7.13 Angot, A., *Traité de Météorologie*, Ed. Gauthier-Villars, Paris, 1944.

7.14 Tayali, N.E., and Bates, C.D., *Particle Sizing Techniques in Multiphase Flows: A Review*, Flow Measurement Instrumentation, Butterworth and Co. Ltd., U.K., 1990.

7.15 *Applications of Laser Techniques to Fluid Mechanics*, Fourth and Fifth International Symposiums, Lisbon, Ed. Springer-Verlag, Berlin (ISBN 3-540 54318X), 1989 - 1990.

7.16 Schodl, R., *Laser Dual Beam Method for Flow Measurements in Turbomachines*, ASME Paper 74-GT-157, 1974.

7.17 Elder, R.L., Harris, P.K., and Tan, S.C., *Particle Trajectories in Gas Turbine Engines*, AGARD Conference Proceedings 558, 1994.

7.18 Willert, C.E., and Gharib, M., *Digital Particle Image Velocimetry*, Exp. Fluids, 1991, Vol. 10, 181-193.

7.19 Meyers, J.F., and Komine, H., *Doppler Global Velocimetry: A New Way to Look at Velocity* - ASME 4th International Conference on Laser Anemometry Advances and Applications, Cleveland, Ohio, Aug 5-9, 1991.

7.20 Melson, W.E., Jr., Referenced in *A Summary of NASA Research on Effects of Heavy Rain on Airfoils*, by Dunham D.J., Dunham, E., Jr., and Bezos, G.M. in *Effects of Adverse Weather on Aerodynamics*, AGARD Conf. Proc. CP 496, 1991.

7.21 Kessler, E. and Wilk K.E., *Radar Measurement of Precipitation for Hydrological Purposes*, WMO/IHD Proj. Rep. 5, 46pp., World Meteorological Organ., Geneva, 1968.

7.22 Barge, B.L. and Humphries, R.G., *Rainfall Measurements by Weather Radar: Application to Hydrology*, Water Resources Research, 1979.

7.23 Atkinson, N.C. and McMahon, B.B., *Rain, Hail Measurement by Weather Radar - Applications to Hydrology*, Water Resources Research, 1979.

7.24 *Cloud Physics Instrumentation*, Meteorological Research Flight MRF Note 3, Meteorological Research Flight, Farnborough, U.K., 1991.

7.25 Gribhoff, A., *Qualification d'un nouveau capteur pour la mesure des teneurs en eau á l'intérieur des nuages*. Thèse á l'université de Clermont II, France, 1983.

7.26 Rosemount Technical Report 5755, Rosemount Co., Minneapolis, USA, 1981 (see also Probe Type 154 Brochure).

7.27 *Temperature Measurement*, Meteorological Research Flight MRF Note 9, Meteorological Research Flight, Farnborough, U.K., 1991.

7.28 Spyers-Duran, P. and Baumgardner, D., *In-Flight Estimation of the Time Response of Airborne Temperature Sensors*, Fifth Symposium Met. Obs. and Instrum., Toronto, 1983.

7.29 McCarthy, J., *A Method for Correcting Airborne Temperature Data for Sensor Response Time*, J. Appl. Meteorology, pp.211-214, 1973

7.30 Lawson, R.P. and Cooper, W.A., *Performance of Some Airborne Thermometers in Cloud*, J. Atmos. Oceanic Technol. **7**, pp.480-494, 1990.

7.31 Lenschow, D.H., *Probing the Atmospheric Boundary Layer*, American Meteorological Society, 1986.

7.32 Rudman , S.D., In preparation by the Meteorological Research Flight, Farnborough, U.K.

7.33 Taylor, G.I., *Pitot Pressures in Moist Air*, Aeronautical Research Council (UK) Report, 1948.

7.34 Pearcey, H.H., *The Effect of the Condensation of Atmospheric Water Vapour on Total Head and other Measurements in the N P L High Speed Tunnels*, Aeronautical Research Council (UK) Report, 1951.

7.35 Mayinger, F. (Editor), *Optical Measurement Techniques and Applications*, Springer-Verlag, 1994.

7.36 Chigier, N. (Editor), *Combustion Measurements*, Dept. of Mechanical Engineering, Carnegie-Mellon University, Pittsburg, U.S.A., 1991.

Table 7-1

HUMIDITY MEASUREMENT

Method	Accuracy	User Complexity	Cost	Suitability for Inflow Use	Comments
Direct Methods					
Psychrometer (wet and dry bulb)	Medium (with care)	Low	Low	Yes (by sampling)	Widely used
Condensation Hygrometer	Good (0.15 K) (with care)	Medium	Various	Yes (by sampling)	
Indirect Methods					
Mechanical Hygrometer (material response)	Poor (10 % RH)	Low	Low	Yes (by sampling)	Very widely used
Electronic Sensors	Fair (3 % of reading)	Low	Moderate	Yes (by sampling)	
Electrolytic Hygrometer	Poor (10 % RH)	Low	Moderate	Yes (by sampling)	Good at low RH
Saturated LiCl Sensors	Fair (1 K dp)	Low	Moderate	Yes (by sampling)	Above 10 % RH
Spectroscopic Hygrometer	Regular calibration required	High	High	Yes	Fast response
Refractometer	Reasonable, but temperature dependent	High	High	Yes (by sampling)	Fast response

Table 7-2

PARTICLE SIZE MEASUREMENT

Method	Accuracy	Complexity	Cost	Suitability for Inflow Use	Comments
Conventional (Large Particles > 10 μm)					
Extraction	Reasonable with care	Medium	Low	Yes (by sampling)	Laborious
Impact	"	"	"	"	"
Evaporation	"	"	Medium	"	"
Electrical (conductance)	"	"	Low	"	Fast Response
Conventional (Small Particles < 10 μm)					
Inertial	Reasonable with care	Medium	Medium	Yes (by sampling)	
Diffusion	"	"	"	"	
Electrical (DMPSA)	Good	High	High	"	for small particles
Optical (all are limited when the particle density is high)					
High Speed Photography	Good	Medium	Medium	Yes	Fast response (off-line analysis). Large particles.
Holography	"	High	Very High	"	Time consuming. Large particles.
Scattering	"	"	Medium	"	Fast response
Extinction	"	"	High	"	"
Diffraction	"	"	"	"	"

Table 7-3

PARTICLE VELOCITY MEASUREMENTS

Method	Accuracy	Complexity	Cost	Suitability for Inflow Use	Comments
Point Measurement					
Laser Doppler	Good	High	High	Yes	(Phase Doppler also gives particle size)
Laser Transit	Good	High	High	Yes	
Field Measurement					
Particle Image	Reasonable	High	High	Yes	Better at Low Velocities
Doppler Global	Not yet Known	High	High	Yes	Better at High Velocities

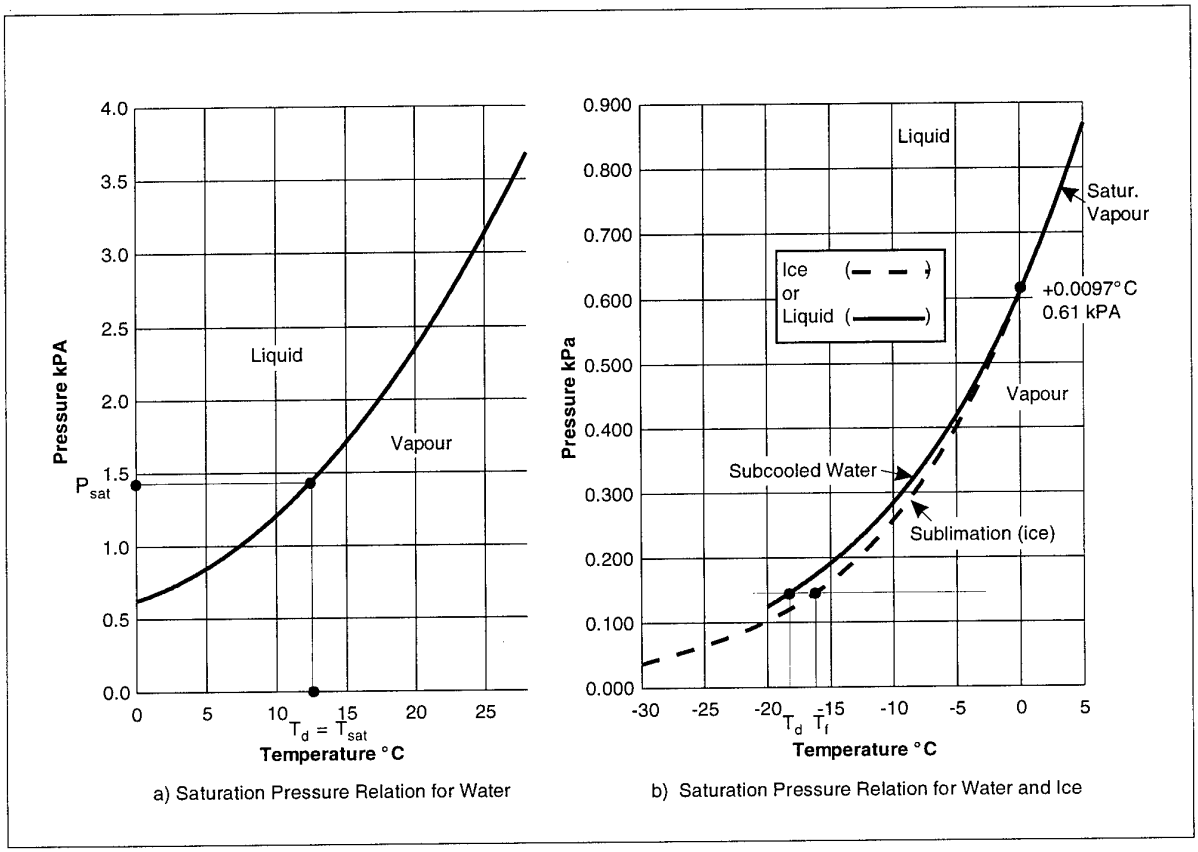

Figure 7-1

Vaporization, Freezing and Sublimation Relationships

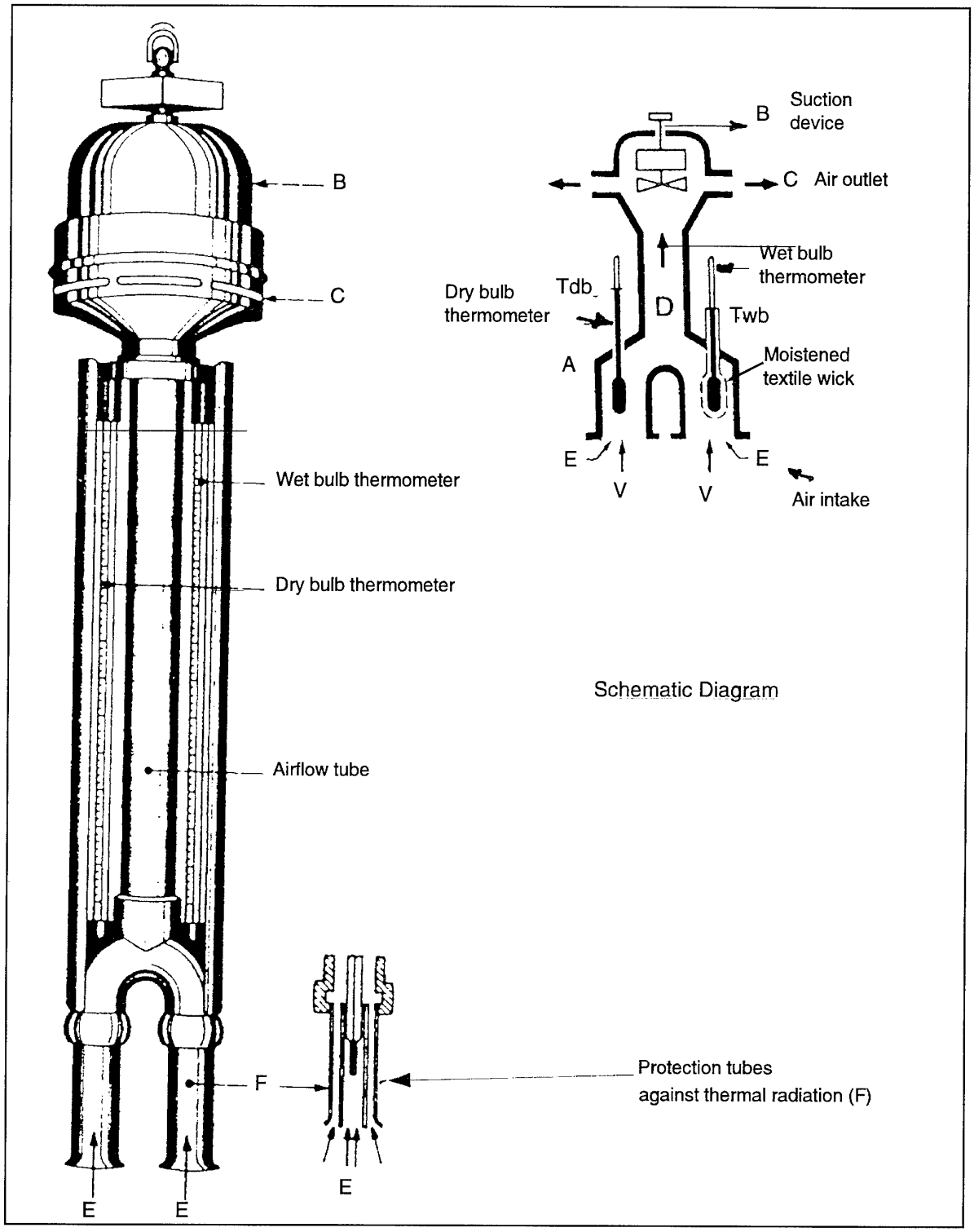

Figure 7-2

"Assman" Psychrometer
(Reference 7.5)

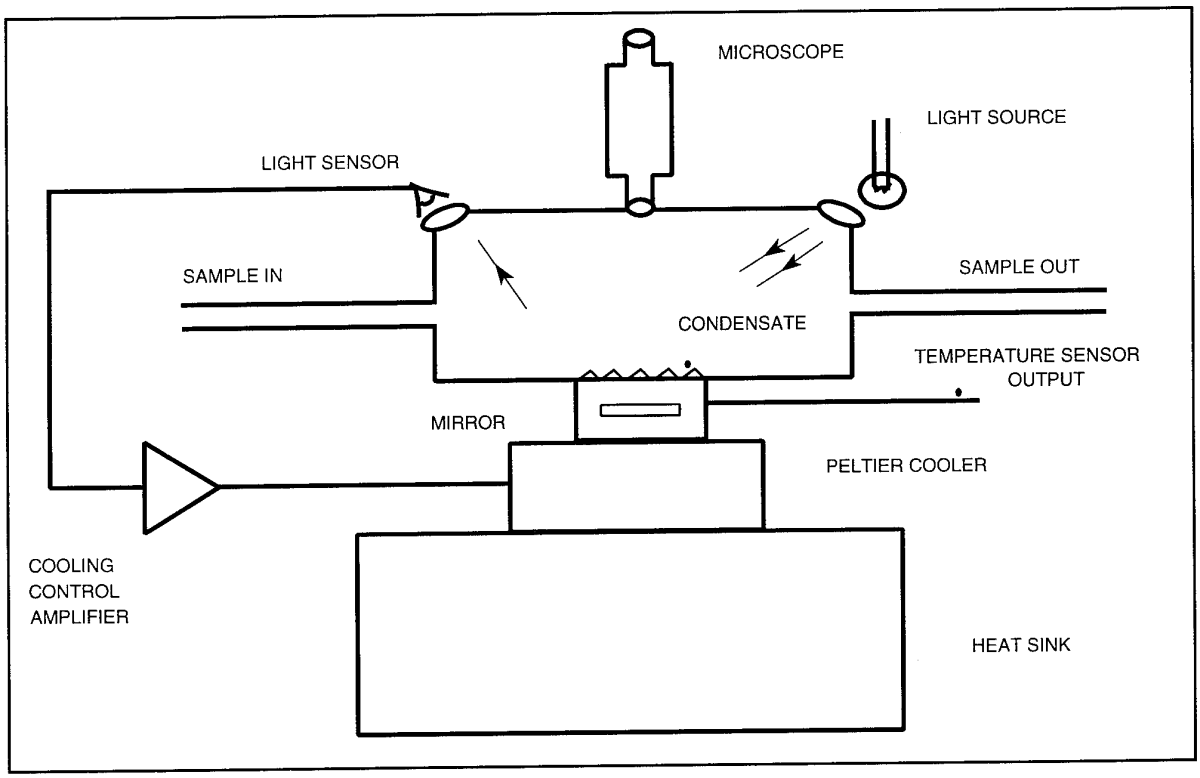

Figure 7-3

Optical Dewpoint Hygrometer
(Reference 7.3)

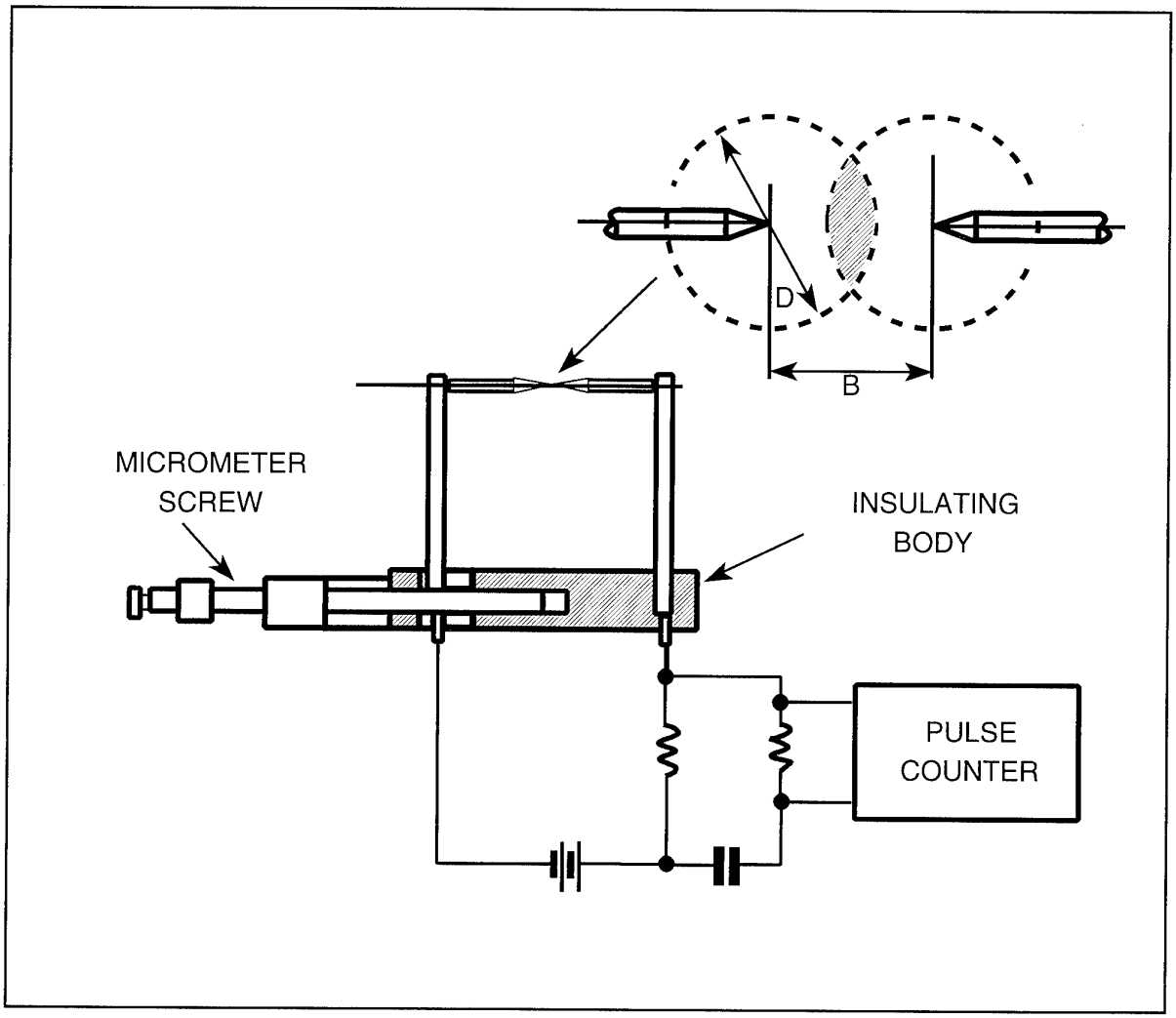

Figure 7-4

Needle Probe for Large Droplet Sizing (Electrical Method)
(Reference 7.8)

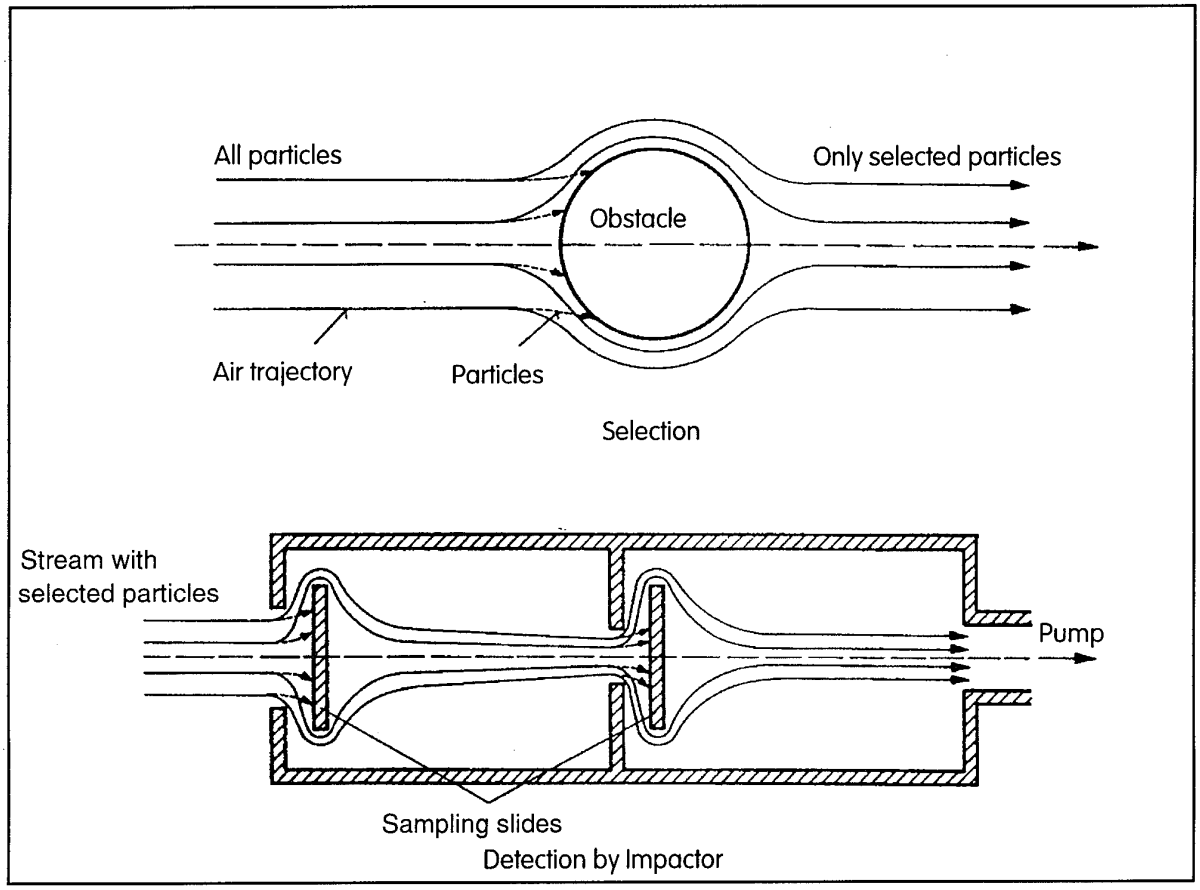

Figure 7-5

Selection and Detection of Particles by Inertial Methods

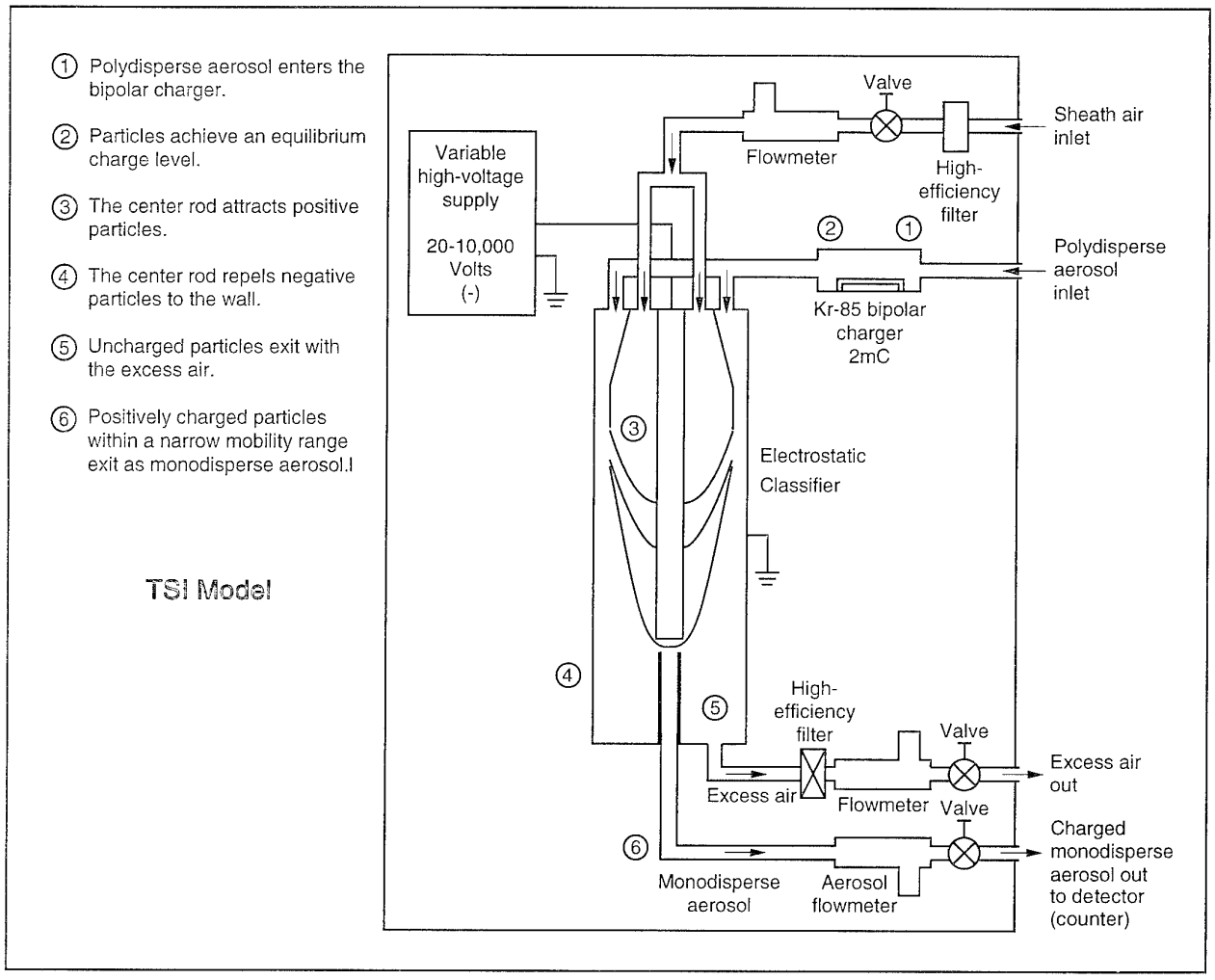

Figure 7-6

Differential Mobility Analyser

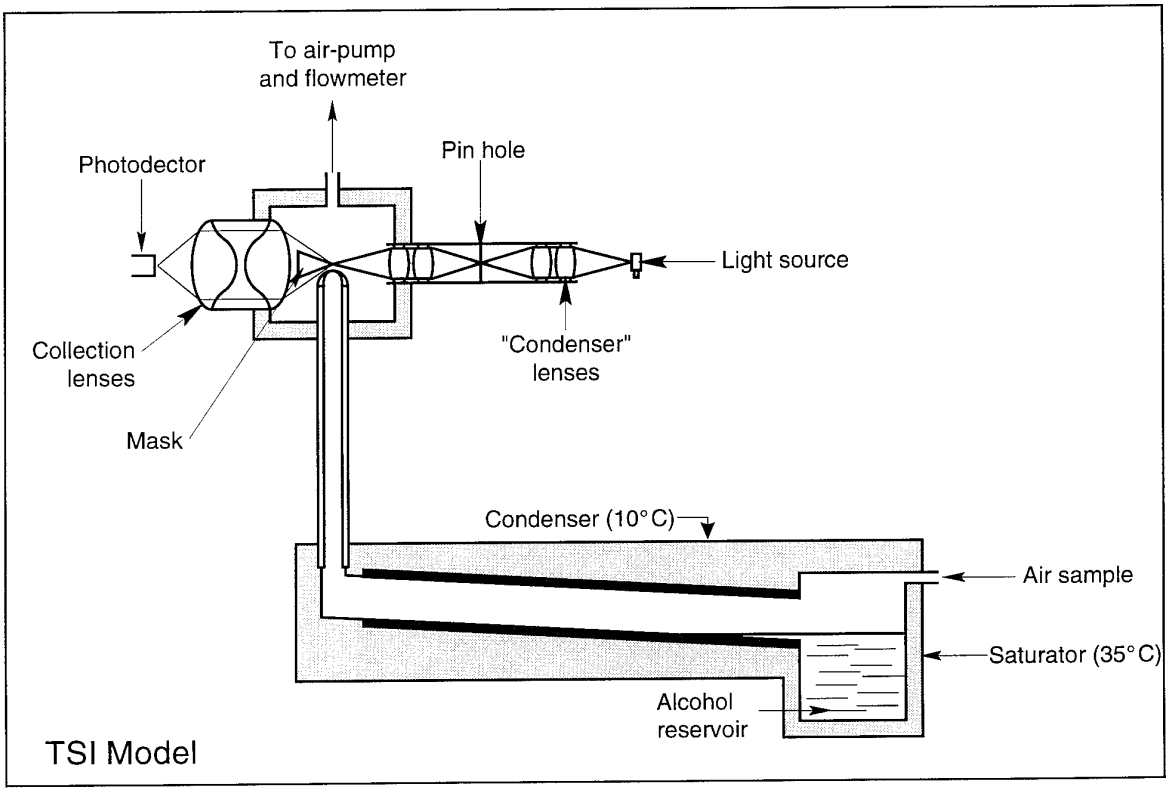

Figure 7-7

Condensation Nucleus Counter (CNC)

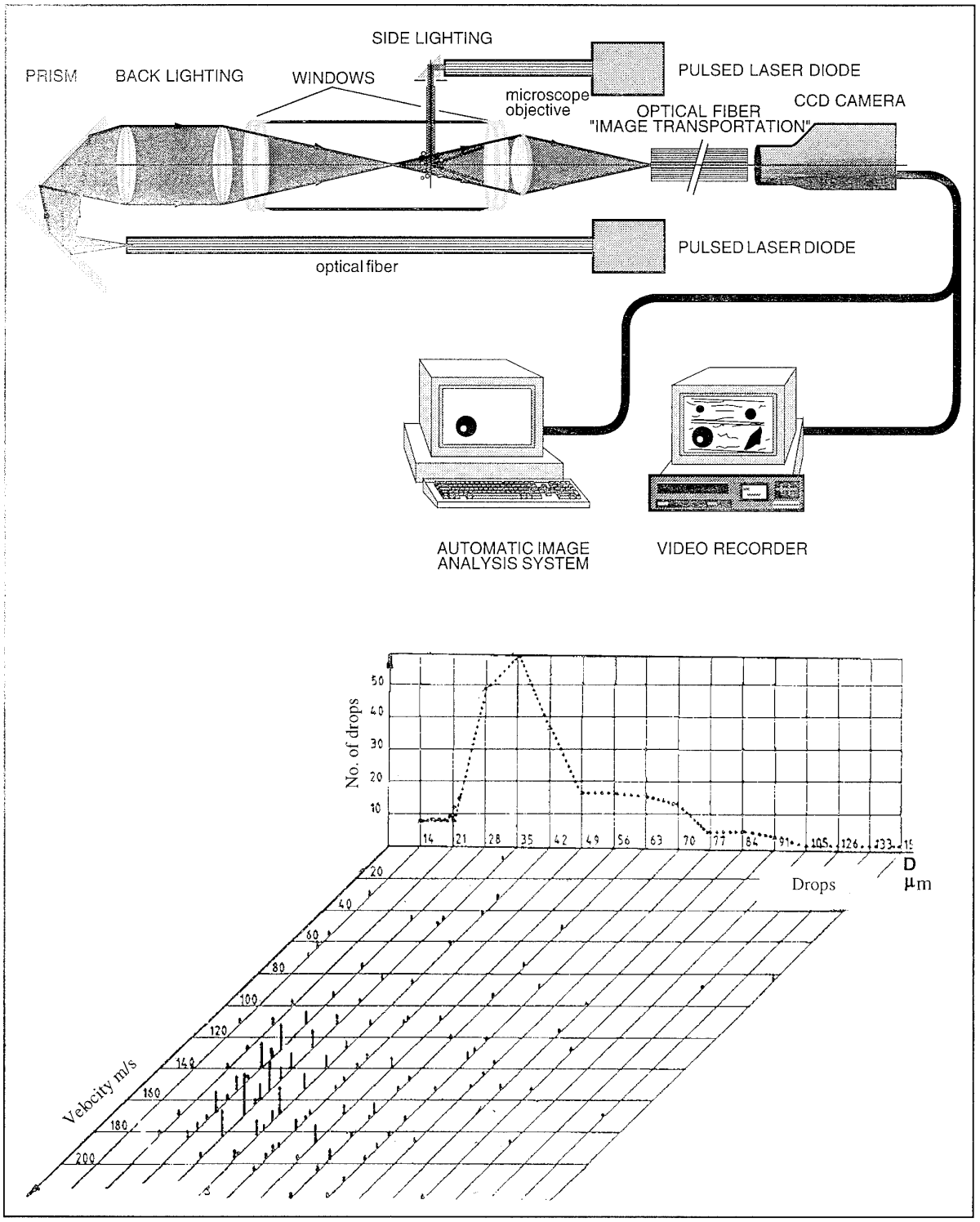

Figure 7-8

Microvideo Probe (Shadowgraphy)
(Reference 7.9)

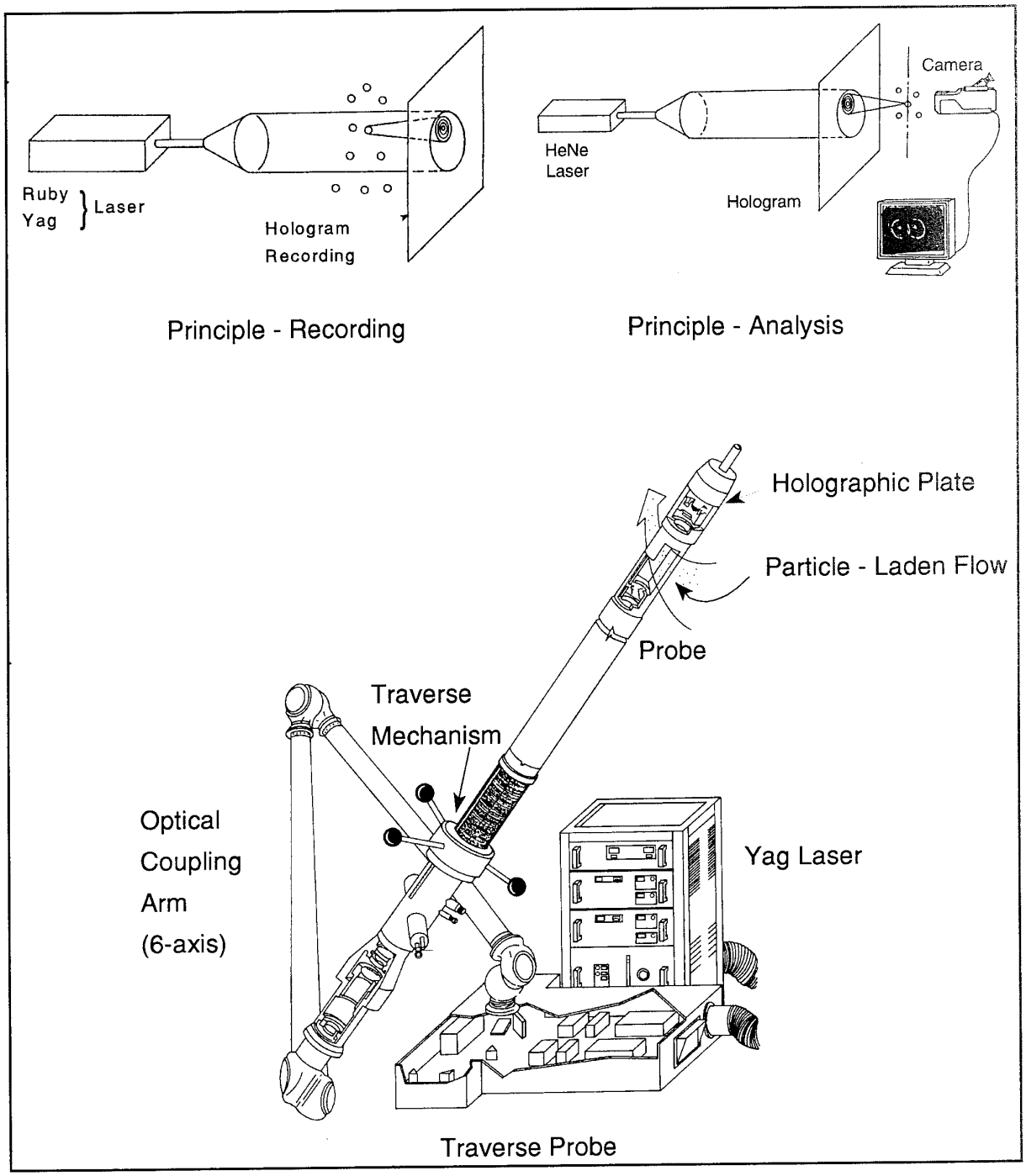

Figure 7-9

Holographic Probe
(Reference 7.9)

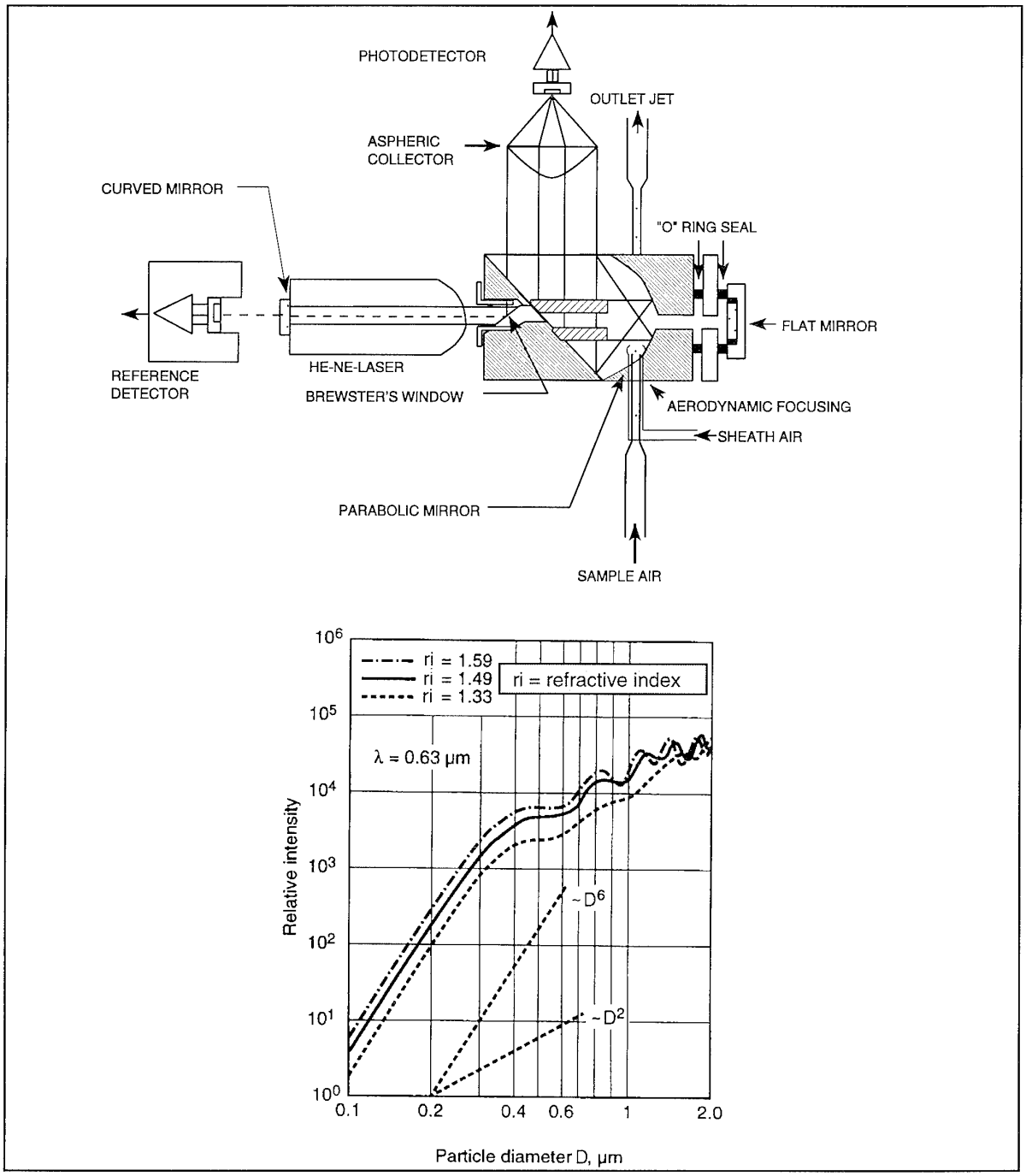

Figure 7-10

Intensity Based Scattering Method for Particle Detection
PMS - Sensor and Theoretical Calibration Curves for the Laser, Particle Counter Royco 236
(Reference 7.10)

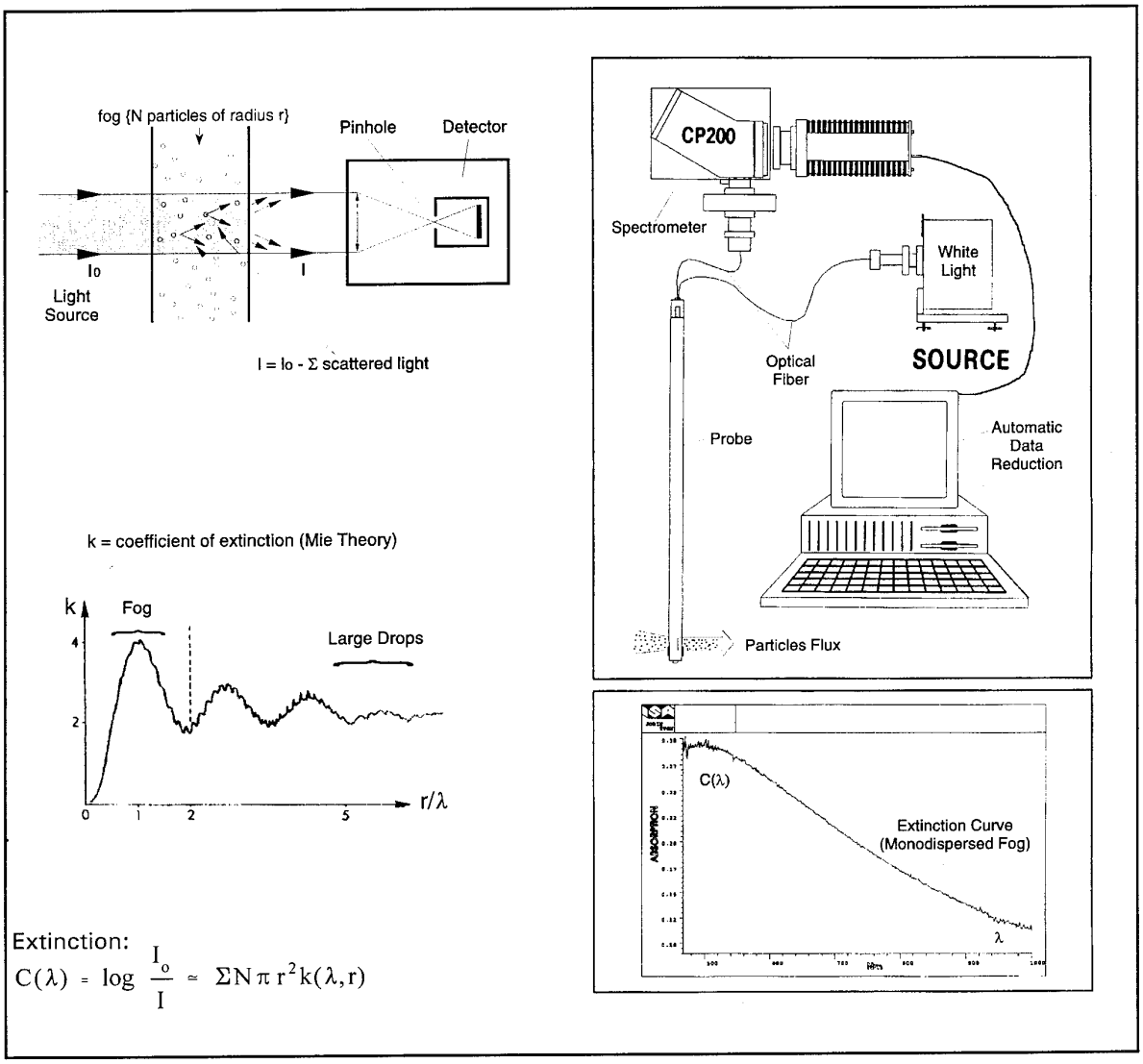

Figure 7-11

Extinction (Attenuation) Method
(Reference 7.9)

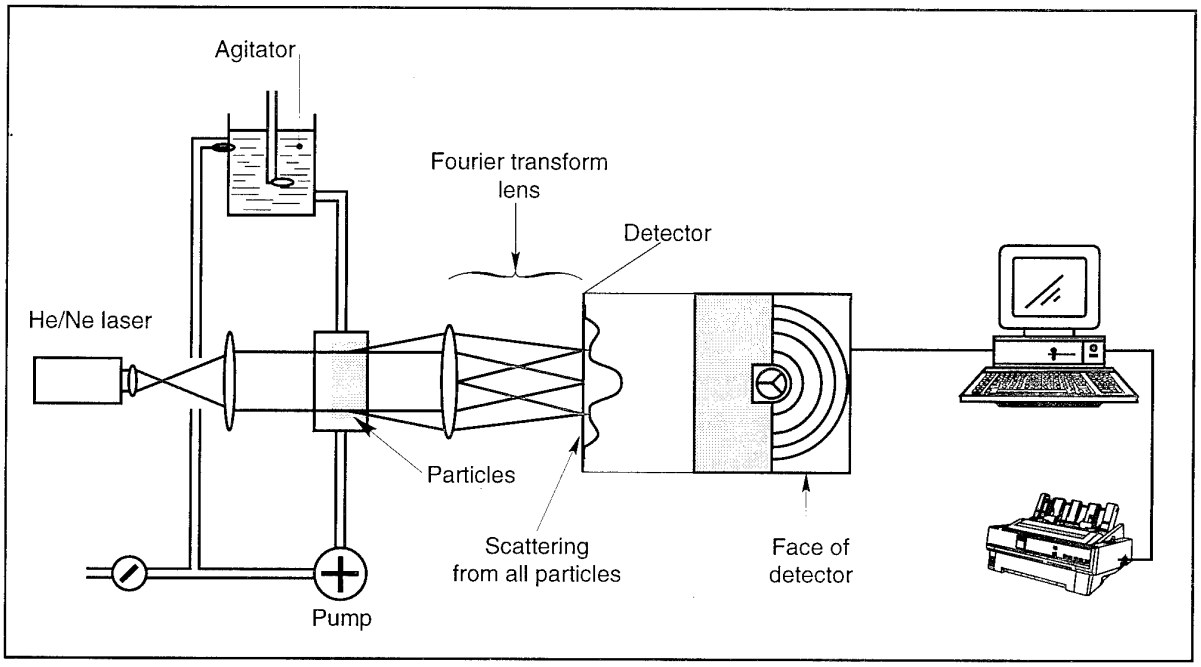

Figure 7-12

Diffraction Technique

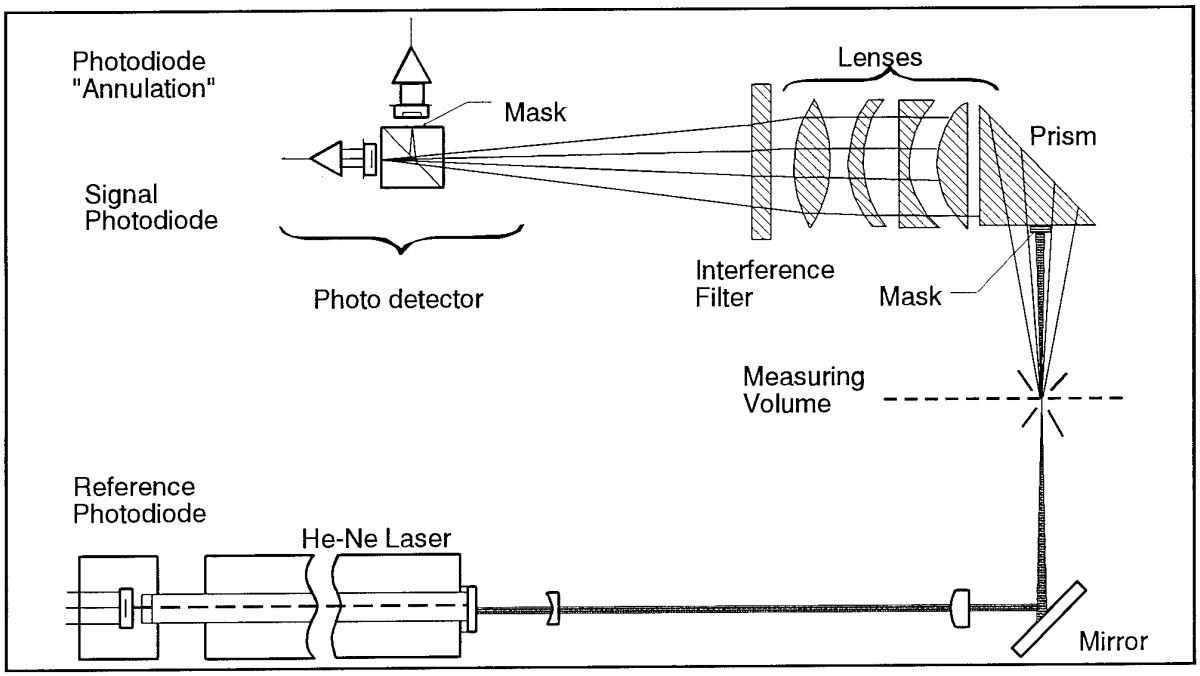

a) Forward Scattering (θ=0°) Spectrometer Probe (FSSP100)

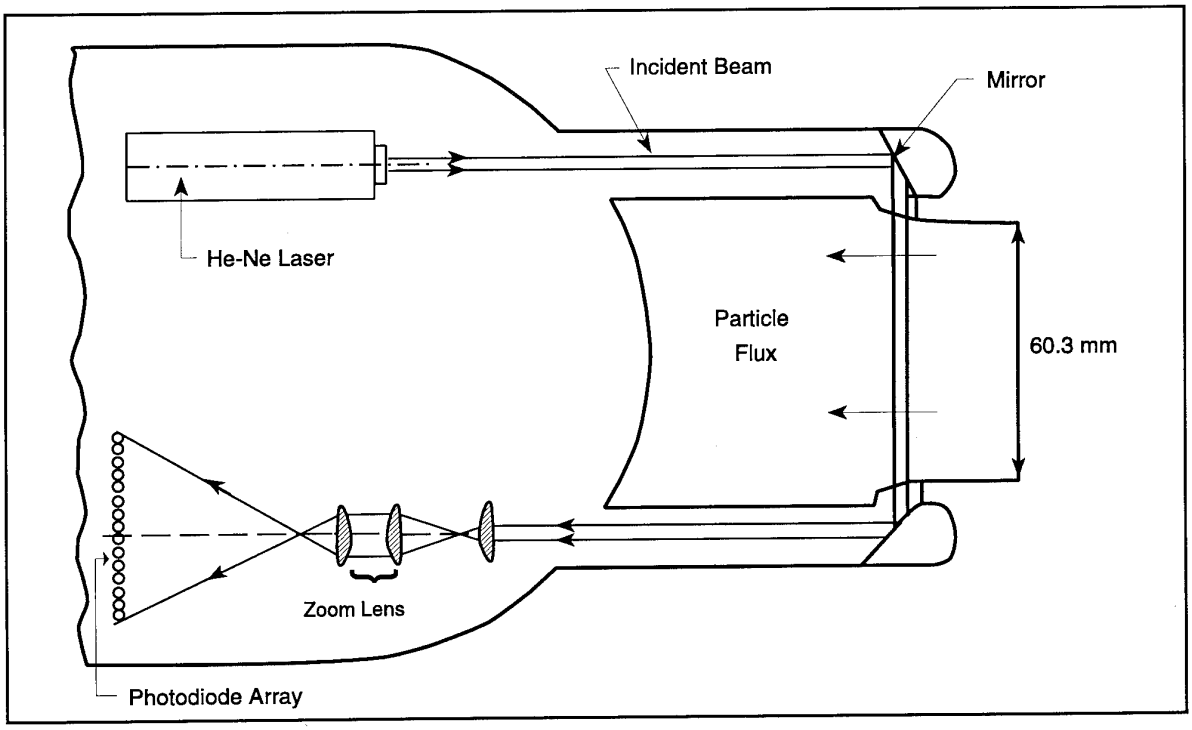

b) Optical Array Cloud Droplet Probe (OAP 200X)

Figure 7-13

Inflight Optical Devices (Knollenberg)

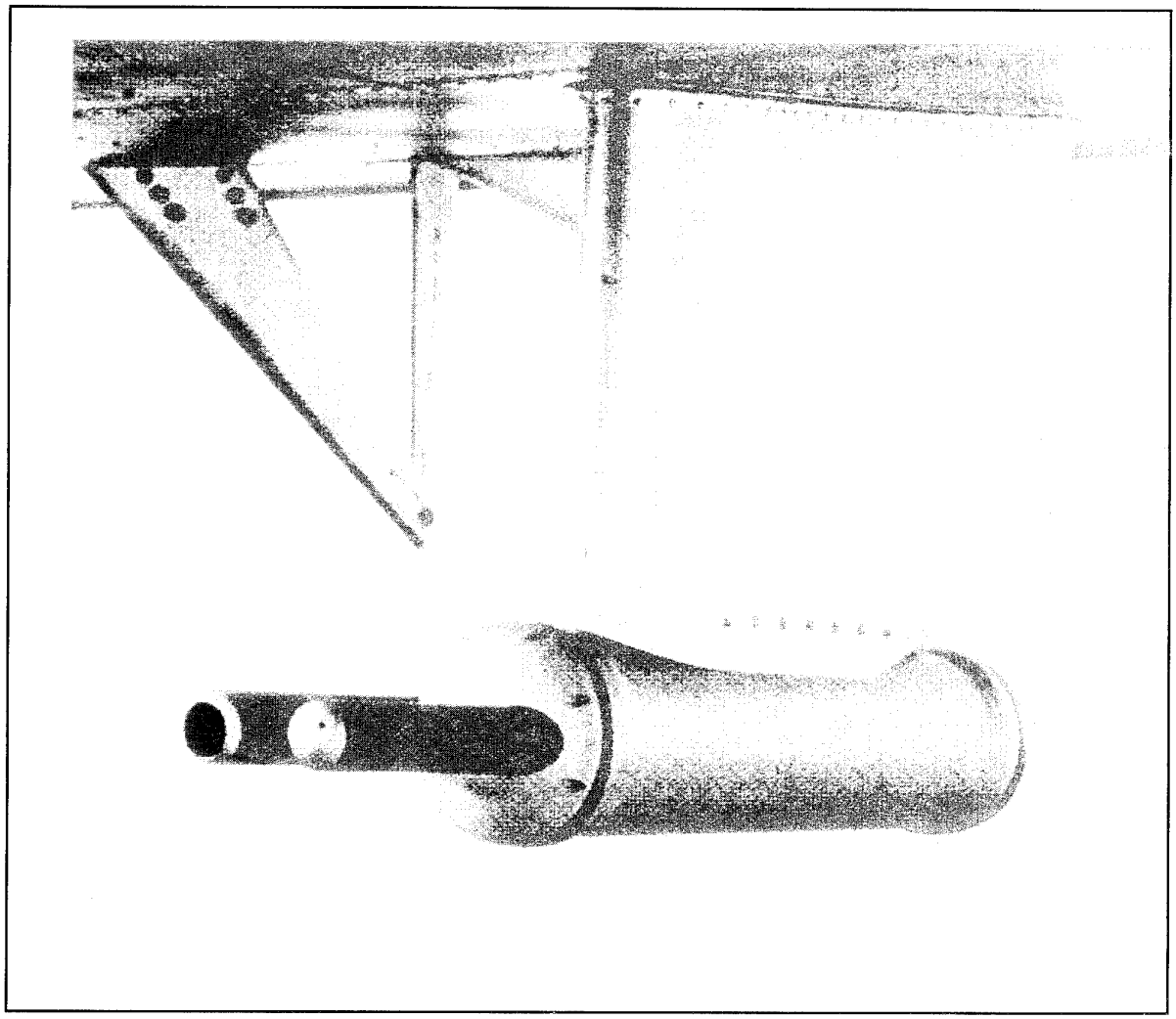

Figure 7-14

Knollenberg Probe Arranged for In-Flight Use
(Reference 7.12)

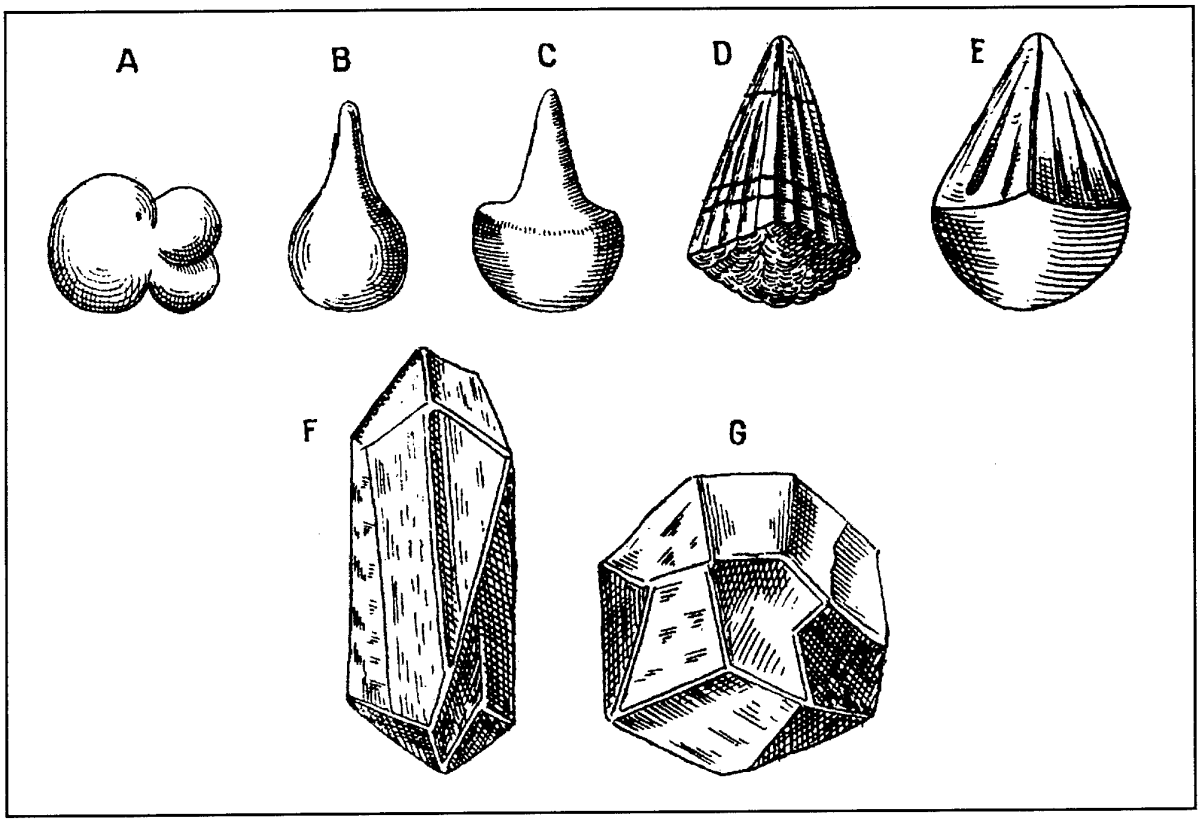

Figure 7-15

Ice Crystal Shapes
(Reference 7.13)

a) Principle of L.D.A

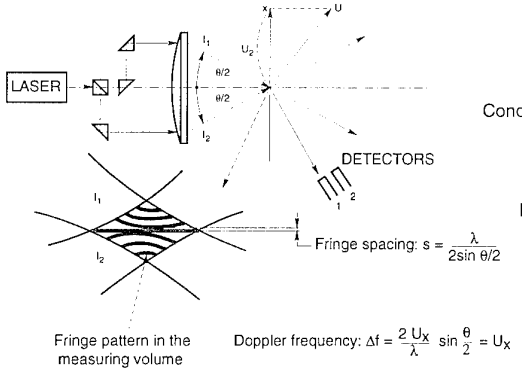

b) Grid technique

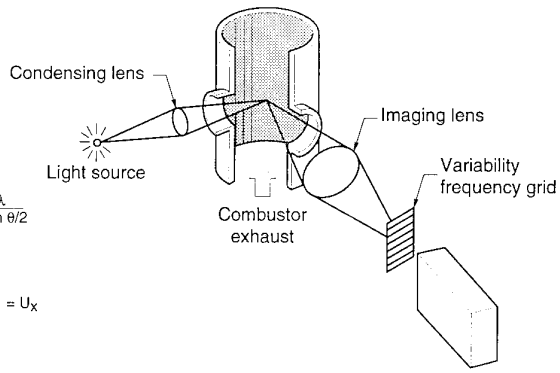

c) Particle sizing adaptations

c1) Variation of visibility with particle diameter ior spheres crossing fully-modulated fringes.

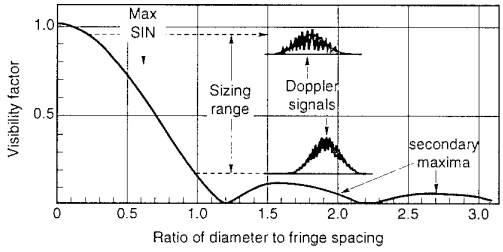

c2) Phase shift

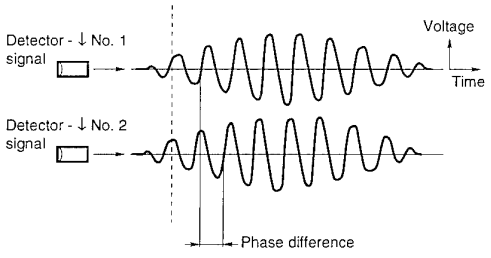

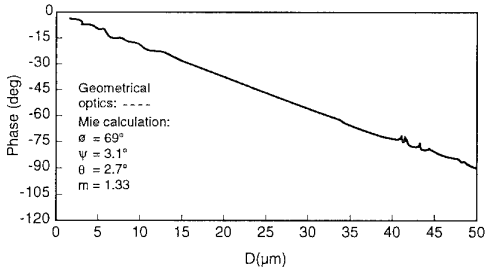

Figure 7-16

Doppler Measurement Techniques
(Reference 7-14)

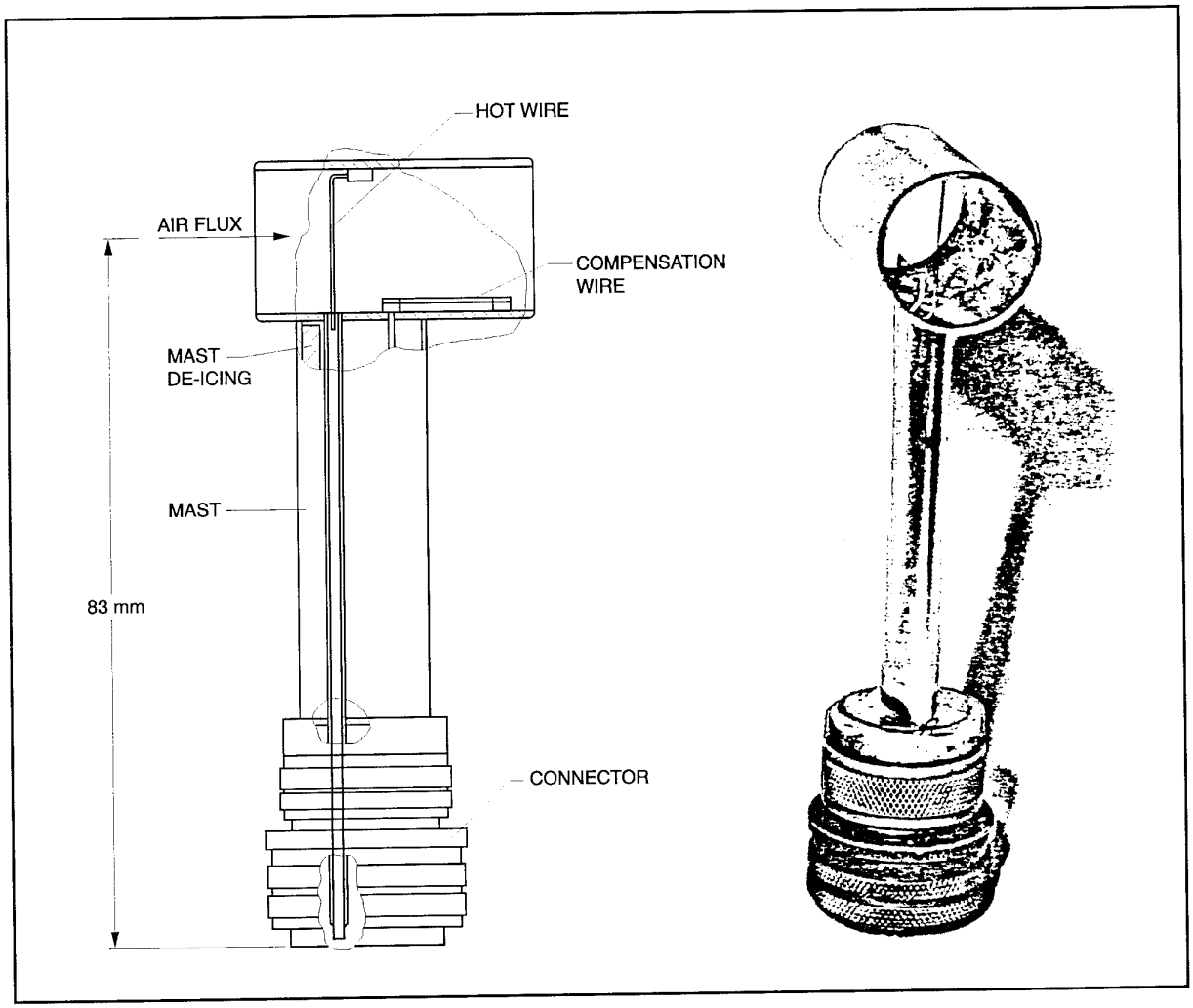

Figure 7-17

Hot Wire Technique
(Reference 7.24)

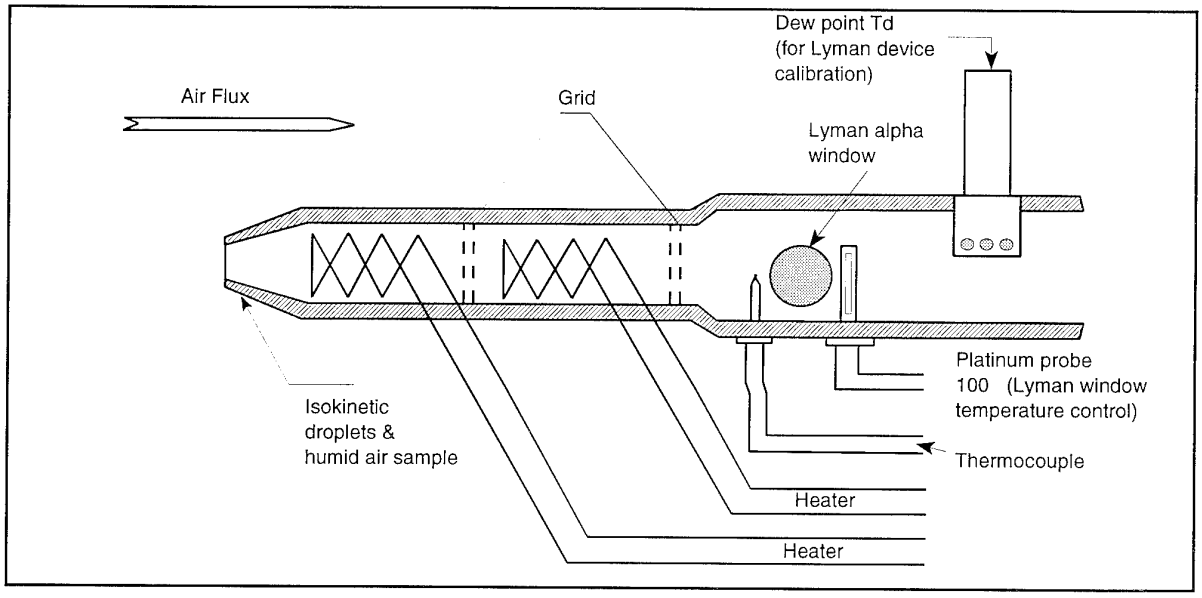

a) Total Water Content: Absorption Calorimeter

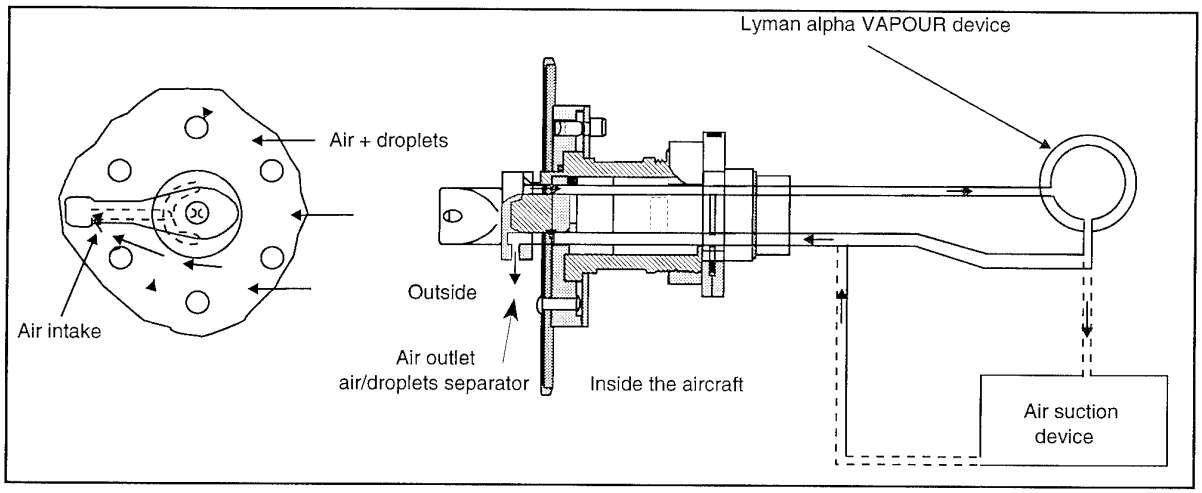

b) Humidity Measurement After Liquid Separator

Figure 7-18

Water Content Absorption Instruments
(Reference 7.25)

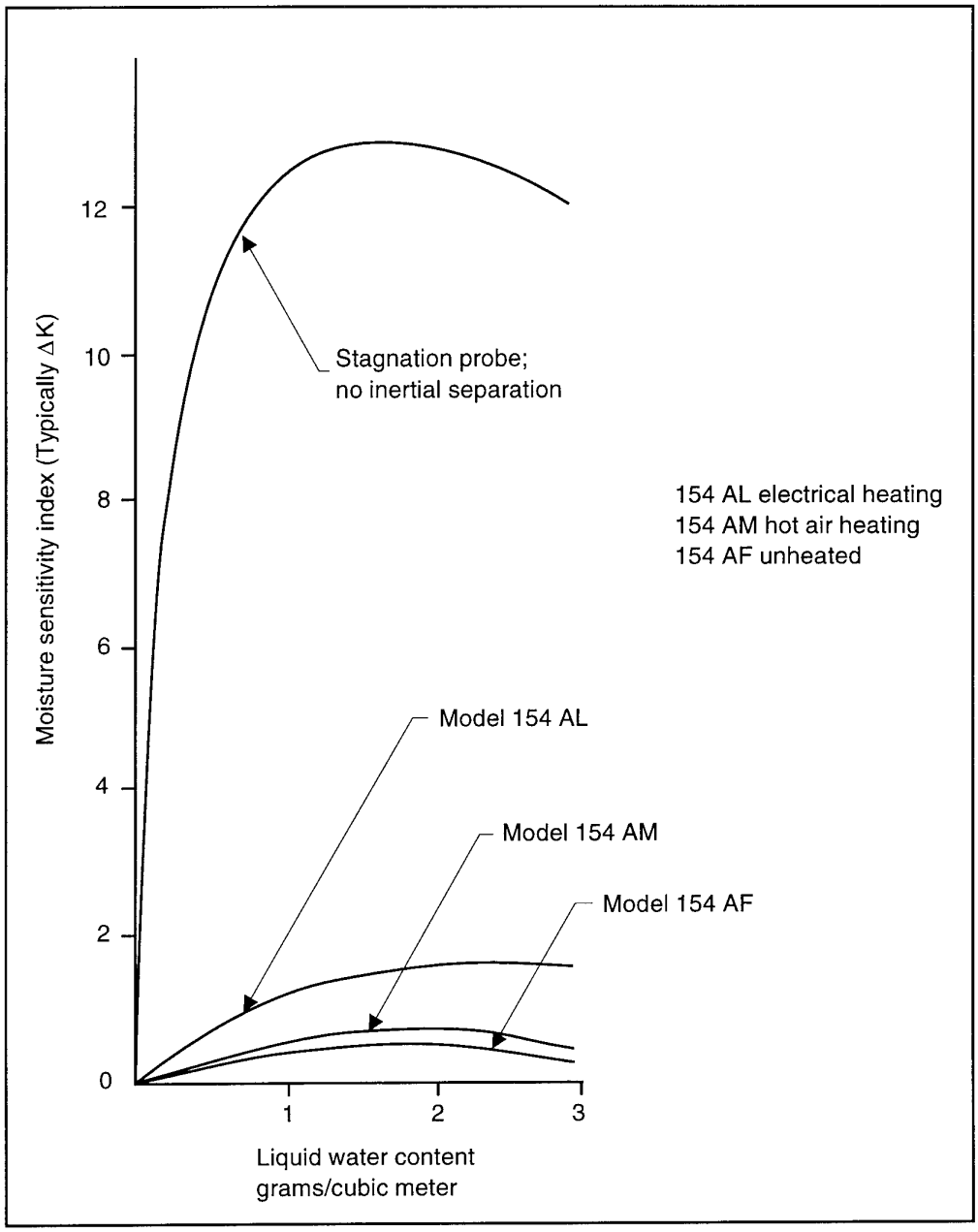

Figure 7-19

Sensitivity of Rosemount Sensors to Moisture
(Reference 7.26)

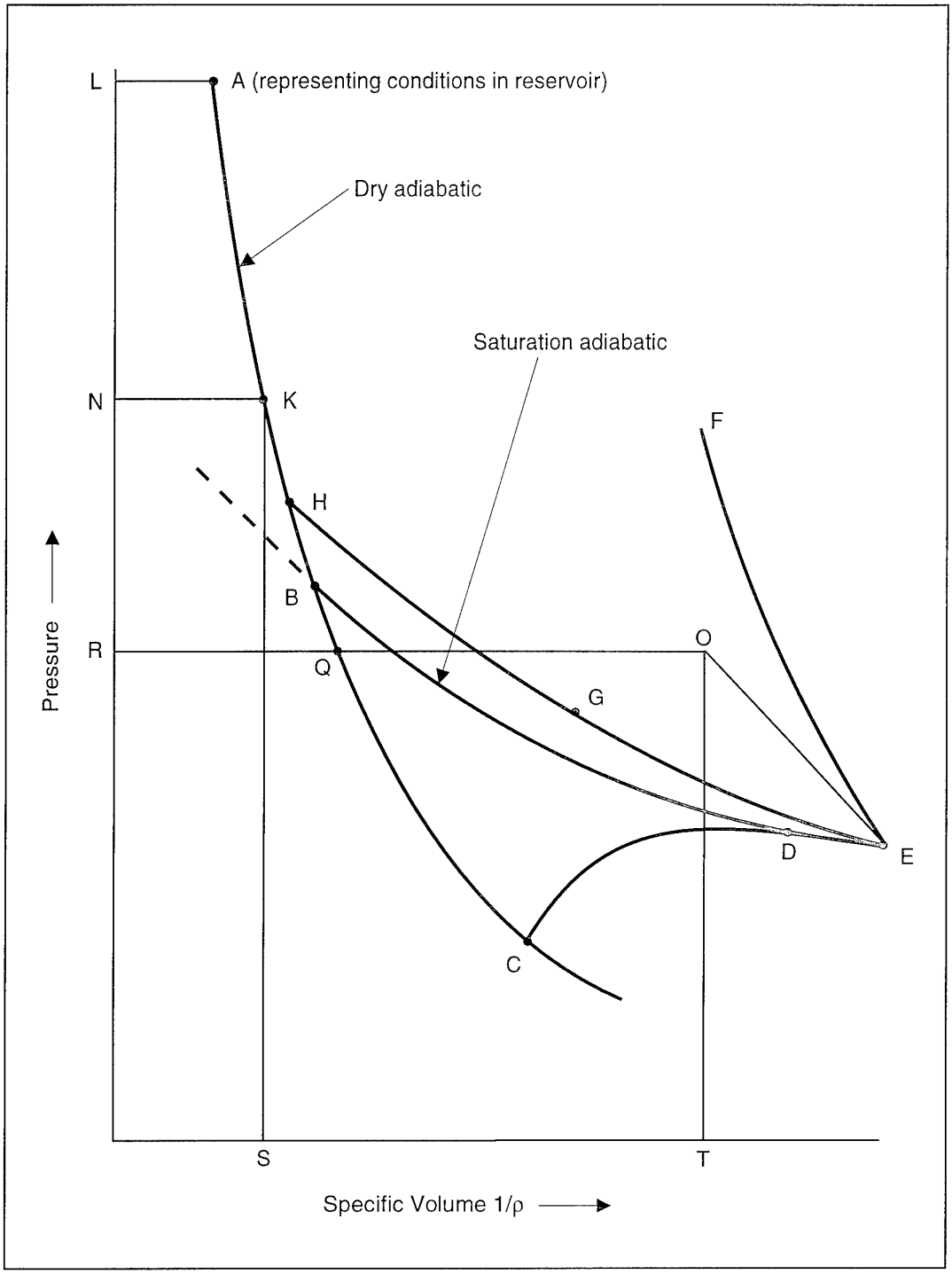

Figure 7-20

Condensation and Re-Vaporisation Process
(Reference 7.30)

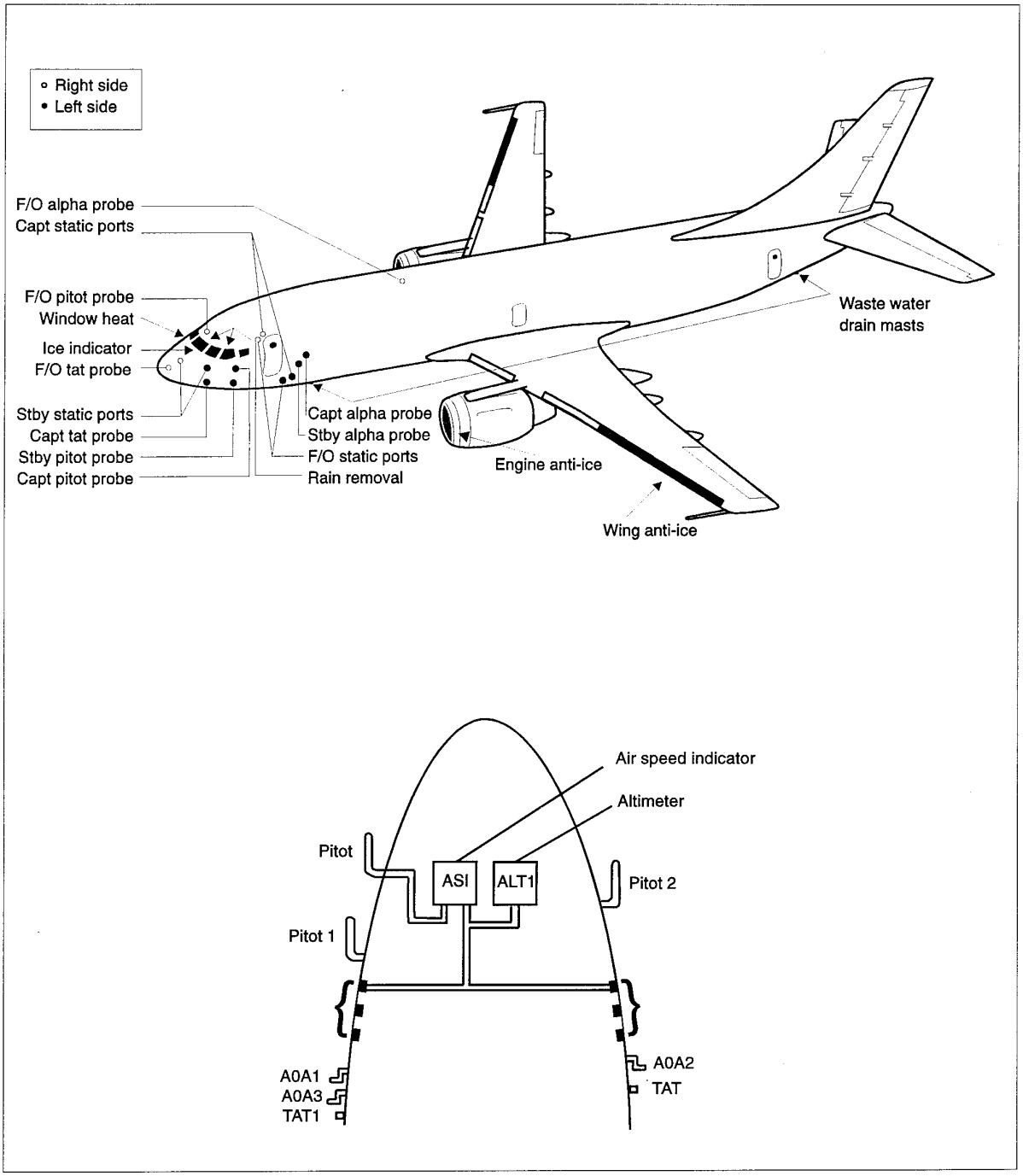

Figure 7-21

Sensors Location and Anti-Icing Devices on A320

8. DUPLICATION/SIMULATION OF WATER INGESTION FOR TESTING OF COMPONENTS AND ENGINES[1]

Test capabilities are currently available in either ground level test facilities, altitude test facilities, or flight test aircraft to duplicate or simulate most of the water ingestion conditions encountered during operations of military and civil aircraft propulsion systems. There are, however, some conditions for which test capabilities are lacking and new testing technologies are needed in test equipment, test techniques, and/or instrumentation.

By far the greatest amount of testing of engines is conducted in ground test facilities using ambient air with naturally occurring gaseous humidity. At many test sites the ambient relative humidity is sometimes high enough to produce potentially condensing flows. Ground level facilities are also widely used for both simulated rain and hail ingestion testing. Significant amounts of testing are conducted in altitude test facilities and in enclosed test facilities which can provide inlet air humidity, pressure and temperature conditioning. The range of water ingestion testing is summarized in Table 8-1.

In this chapter, each of the five forms of water ingestion is addressed separately. For each form, the goals of testing are identified first, and then the current practices and the required instrumentation are described. Finally, the shortfalls and recommended new research/development capabilities are listed.

8.1 TESTING WITH GASEOUS WATER INGESTION (NO CONDENSATION)

8.1.1 Goals of Testing

Most testing in ground test facilities is done to provide performance data for engines following initial build, rebuild, or significant rework. Similar testing is done to provide diagnostic data for engine fault analysis. This testing is, in general, accomplished with naturally occurring humidity present. Correction of the observed data to a reference level of humidity (usually zero) is required. The major goal for testing with gaseous humidity present is, therefore, to determine the engine performance at a reference humidity level.

Other goals for testing conducted with gaseous humidity present are to verify component and engine performance models and to assure compliance with engine design and development goals. Approaches discussed in Chapter 3 are used to develop appropriate component and engine models. Design goal compliance is required to assure delivery of a system which will adequately perform its mission over the full range of expected environmental conditions. It is in meeting the performance specifications that the accurate knowledge of the quantitative effects of gaseous humidity is most often required. In all cases, performance data should be adjusted to the specified reference humidity level (zero is preferred) to allow direct comparison of results.

Gaseous humidity levels have no significant effects on engine operability so no special humidity level testing is required for operability certification.

8.1.2 Current Practices

The level of humidity at ground level test facilities varies with geographical location and with annual and diurnal patterns. In general, so long as no condensation occurs, no limitations exist on measured levels of gaseous humidity. Testing is generally limited to those conditions of ambient humidity for which the relative humidity of the air at the engine face is less than a specified value, ranging from 100 percent upwards to perhaps 200 percent (see 4.5.2). Some facilities limit testing at higher engine speeds to ambient air relative humidities less than a specified amount (e.g. 75 percent) to assure that no local condensation occurs. The actual allowable ambient relative humidity level is a function of inlet duct Mach number, inlet airflow particulate characteristics, inlet duct length and configuration, and the type of testing being done. For example, the presence of flow distortion devices, such as screens, which produce adiabatic pressure losses reduces the level of ambient humidity at which condensation occurs. This is a result of the higher

[1] Tables and Figures for Chapter 8 begin on page 8-10.

Mach numbers produced in the screen passages. Some engines have inlet temperature sensors which can be read from the engine data system. For these engines, a comparison of ambient air temperature and the engine sensed inlet temperature can be made to assure that no significant condensation is present (i.e. engine inlet temperature equals ambient temperature). For all cases, it is imperative to know that condensation is not present because condensation can produce significant shifts in the controlled point of engine operation and cause engine cycle rematch.

The models mentioned in Section 8.1.1 provide adequate bases for adjusting data to specified humidity levels. One such model (Reference 8.1) has been constructed for bypass ratios from 0 to 4.0 and the results reduced to a set of polynomial equations with absolute humidity as the independent variable. Experience documented in References 8.2 through 8.4 suggests that such a presentation format may be sufficient for providing an easy-to-apply adjustment methodology. However, a complete understanding of cycle assumptions, control method, and operating conditions is needed to ensure applicability.

Careful measurement of inlet humidity is also required to define the emission characteristics of an engine. In particular, the quantities of oxides of nitrogen are dependent on humidity at the combustor. Current practice (see, for example, Reference 3.3) is to measure the humidity and adjust emission data to standard operating conditions (again, usually zero humidity).

Flight testing near ground level generally has humidity constraints similar to ground level facility testing insofar as performance is concerned. At lower altitudes local humidities may vary significantly over the flight path, thus requiring in-flight measurement of humidity and subsequent coordination of the observed humidity with engine performance variations.

Providing accurate assessments of gaseous humidity effects is difficult because the induced effects over the full range of humidities possible are of the same order as the measurement uncertainties of the performance parameters. Therefore, testing over a period of time (e.g. day-to-day) with various humidity levels results in the humidity effects being obscured by the fundamental performance measurement uncertainties.

Altitude test facilities generally use some mechanism to dry the air being processed for delivery to test systems. Two common drying mechanisms are desiccants and refrigeration with subsequent reheat, if required. In both cases, the relative humidity levels are typically reduced to levels of 0.05 percent or less, thus effectively reducing the magnitude of gaseous humidity effects to negligible levels.

Because humidity can be precisely controlled during testing in altitude facilities with a defined measurement process, the bias term contribution to overall uncertainty is identical for adjacent data points and only the precision term impacts the performance derivative measured. Thus, the effects of humidity can be accurately assessed. One method used to provide such humidity control is described in References 8.2 through 8.4. In this method, air at a known low humidity (of the order of 0.02 percent) is purposely rehumidified using carefully measured superheated steam injected into a plenum upstream of the engine face. Adequate mixing is provided to ensure a uniform distribution of the humid air at the engine face so that natural atmospheric humidity conditions are duplicated.

8.1.3 Required Instrumentation

Engine or component instrumentation required is identical to that used for normal performance and operability testing. Air supply instrumentation is required to identify inlet pressure, temperature, and relative humidity (See Chapter 7) at the engine face. For the case of an altitude facility testing to a specified humidity level, it will be necessary to provide a means of measuring the steam quality (to assure the necessary superheating) and the amounts of injected steam. In that case, conventional calorimeters can be used quite successfully for quality determination.

8.1.4 Shortfalls and Recommended New Research/Development Capabilities

Ground level facility testing methodologies for gaseous humidity effects are well in hand and follow normal performance testing practices. Testing to determine the effects of gaseous humidity on operability is not normally done. Use of an engine cycle model is recommended to adjust for the effects of humidity.

At present, rapid determination of inlet air humidity over a wide range of pressures (0.5 to 2.0 std atmospheres), temperature (260 K to 320 K), and water vapour concentration (0 to 100 percent relative humidity) is difficult. Existing measurement devices, e.g. chilled mirror or various salts, all suffer various shortfalls. A simple, reliable, accurate ($\pm$5 percent relative humidity), and fast (characteristic response time $\leq$ 0.5 sec) humidity measurement system is needed.

8.2 TESTING WITH CONDENSATE WATER INGESTION

8.2.1 Goals of Testing

The operation of engines in environments in which condensation occurs due to acceleration of the flow in the inlet duct is not uncommon (References 8.5 and 8.6). Such condensing flows lead to an increase in engine inlet total temperature and an increase in inlet specific volume, which produce a significant shift in the measured performance and in engine control schedules. Such shifts introduce problems in interpretation of test data in three distinct areas:

1. Ground test performance acceptance or pass-off testing.
2. Installed performance in the aircraft.
3. Operability and durability impacts such as the effect of mis-set trim.

In all cases, the desired goal, which is to adjust the observed performance to a reference condition (usually zero humidity), cannot be achieved by analytical methods when condensate is present.

The effects of condensing flow on engine sensors must be defined. Although it is suspected (see Chapter 4) that condensing flows produce small ($< 5\mu$) drops or ice particles which follow streamlines, the effects of liquid droplets impacting temperature sensors can be significant and may require demonstration for design/development compliance and certification testing. In any case, the effect of condensing flow on inlet air stagnation temperature and the subsequent effects on engine and component performance must be evaluated. The reader is referred to Chapter 4 of this report and References 8.5 and 8.6 for a detailed consideration of condensation effects.

Passage of the condensate through the engine, and the subsequent re-vaporization of the condensate, must also be evaluated. Because the degree of supercooling tolerated by a flow is a function of particulate levels and particle size distribution, an empirical approach to define condensation effects on temperature levels is usually required. The effects of liquid condensate flow and re-evaporation may be analyzed by coupling a thermodynamic, stage-by-stage compressor model with a droplet evaporation model.

8.2.2 Current Practices

Condensing flow is usually produced in ground facility testing only as an undesired consequence of high inlet relative humidity and high engine speeds. Because of the complex dependence of condensation on the amount of cooling below saturation temperature, number of nucleation centers present, and time, no comprehensive prediction method exists for determining when and to what degree condensation will occur (see Chapter 4). Current best practice recommends stopping testing when conditions which will produce significant condensation are encountered.

However, in some cases, testing must be done with high speeds and high humidity and, for these cases, empirically determined relations are used to define the effects of condensation on inlet temperature for specific geographic locales and specific inlet geometries (Section 4.5.3). Such empirical relations are usually expressed by showing temperature rise as a function of inlet air relative humidity and engine speed or corrected air flow. Even for facilities which routinely dry the inlet air, cooling below the saturation temperature may occur for operation at very low temperatures, i.e. < 250 K. For facilities which dry the air, the thermodynamic effects of condensation are small because the absolute humidity is low. The major impact is potential snow accumulation on fine mesh (finer than 8-wires/cm) screens used to prevent foreign object damage and accumulation in forward facing probes. This presents a potential safety-of-operation issue. Similar test practices are followed in component rig tests.

While the actual total temperature rise caused by the condensation of water is a function of many variables (number of condensation nuclei, time at condition, etc.), the potential range may be estimated by employing the thermodynamic relations described in Section 4.2. As an example, consider the following typical case:

Ambient pressure, P_T = 1 std. atmosphere
= 101.325 kPa (14.696 lb/in^2)
Ambient Temperature, T_T = 310.8 K (100°F)
Relative Humidity, RH = 70%
Using Equation 4-3(b):

$$\mathbf{war}_{sat} = 0.622\left[\frac{P_{sat}}{P_{Smix} - P_{sat}}\right] = 0.04295$$

From Table 3-2, since RH = 70%,
$\mathbf{war}_{amb}$ = (0.7) (0.04295) =0.03006

For simplicity, assume
$\gamma = 1.4$ = constant, and
$c_p = [c_p(\text{ambient}) + c_p(\text{inlet face})]/2$, from, for example, Figure 3-3.

Further, assume the engine inlet face Mach number, Ma = 0.6.

From Equations 4-1 and 4-2:

$$T_S = \frac{T_T}{1 + \frac{\gamma-1}{2} Ma^2} = 290°K \ (62.4°F)$$

$$P_S = \frac{P_T}{\left(1 + \frac{\gamma-1}{2} Ma^2\right)^{\frac{\gamma}{\gamma-1}}} = 79.44\,kPa\,(11.52\,lb/in^2)$$

The lower bounding limit of total temperature rise is obviously zero, i.e. no condensation. However, the condensation process can proceed along either equilibrium or non-equilibrium paths. The maximum total temperature rise is experienced in an extremely non-equilibrium process when all possible condensation occurs instantaneously at the engine inlet static pressure as calculated in the previous paragraph.

Specifically, the minimum **war** occurs with $\mathbf{war}_{local}$ evaluated at the engine inlet for saturated conditions:

$$\mathbf{war}_{local} = 0.622\left(\frac{P_{Sv}}{P_{Smix} - P_{Sv}}\right) = 0.0154$$

Using Equations 4-7 and 4-8(a) yields the maximum possible temperature rise:

$$Wr_f = \mathbf{war}_{amb} - \mathbf{war}_{local} = 0.0146$$

$$T_T - T_{amb} = \frac{Wr_f\, h_{fg}}{c_{p\,mix}} = 35 \ K \ (63°F)$$

However, if the process proceeds in complete equilibrium, the total temperature rise will be much less. Equations 4-1, 4-2, 4-7 and 4-8 must be simultaneously solved to identify the equilibrium temperature rise. For simplicity, the loss in total pressure may be neglected without seriously affecting the final answer. For the example identified in this section, a total temperature rise of 9.0 K (16.3°F) may be calculated for equilibrium conditions, assuming no total pressure loss.

Thus it may be seen that the potential total temperature rise may range over a very wide set of values.

Current practice to define the effects of inlet-specific-induced condensation on performance is to operate the engine behind the actual inlet under field conditions. All the problems discussed for ground test facilities in determining the amount of condensate are avoided. However, the measurement of small performance changes in an aircraft installation must be addressed.

Flight testing for performance determination at relatively high altitudes is generally conducted under conditions where no significant condensation occurs. However, performance and operability testing is conducted for takeoff, landing and certain parts of the envelope to define overall effects of inlet duct condensation for operation over a full range of inlet humidities. Direct correlation of the degree of condensation versus performance or operability change is not required.

8.2.3 Required Instrumentation

The instrumentation requirements are identical to those of gaseous humidity testing because, in general, no capability exists to define the detailed characteristics of the condensate (size, number density, and particle shape) under realistic test conditions.

8.2.4 Shortfalls and Recommended New Research/Development Capabilities

A need exists for a simple, reliable indicator of the presence of condensation as indicated in Section 4.1. To a lesser degree, there is a need to quantify the level of condensation.

An "at-least-academic" need exists for a method to characterize the condensation phenomena as functions of degree of supersaturation, number of condensation nuclei, and time. The method should be capable of addressing local flow characteristics, such as accelerations produced by a bellmouth or actual inlet hardware. If such a method existed, the effects of both stagnation temperature change and subsequent re-evaporation could be addressed. At present, however, no over-riding driver for such an understanding has emerged.

8.3 TESTING WITH RAIN INGESTION

8.3.1 Goals of Testing

There are two major goals of testing for rain ingestion effects: assessments of mechanical damage and determination of operability effects. Mechanical damage effects, such as erosion due to water drop impacts and mechanical interference damage due to case shrinkage, have been experienced. Operability effects such as significant power loss, compressor stall, and combustor flameout result from the combination of effects discussed in Chapter 5. The scope of this report is limited to thermodynamic effects and does not address mechanical damage. Therefore, for the purpose of this report, the goal of rain ingestion testing is to determine the effects on engine operability. Key parameters to be simulated include water drop size, water-to-air ratios, and distribution at an appropriate reference plane as well as any sheets, streams, or other continuum flows which may be generated by the inlet.

8.3.2 Current Practices

Rain ingestion is currently simulated by means of atomizing water nozzle arrays positioned in front of engines on open air test stands (Figure 8-1) or by in-flight spray generation (Figure 8-2), or by locating a suitable nozzle array interior to the engine in front of a selected engine component (Figure 8-3). Each method has some advantages and difficulties.

Ground testing with inlet water sprays is generally done with a nozzle producing known, desired water spray drop and spatial position characteristics. The ratio of water to air can be carefully controlled. However, because of the different shearing characteristics of large ($\sim$2500 μ) and small ($<$300 μ) drops when injected into a moving airstream at velocities different than those of the airstream, the actual drop size at the engine face may be different and unknown (See Reference 8.7 for a brief discussion). Of even more importance is the fact that the engine airflow pattern is radically different in the ground facility compared to flight because of the external diffusion or external acceleration forward of the inlet. The resulting variations in the amount of free-stream air captured by the inlet (referred to as "scoop factor" in Chapter 5) significantly alter the **war** entering the inlet. The maximum amount of rain enters the inlet when the inlet capture area ratio is much less than one, e.g. at aircraft descent conditions when the flight speeds are relatively high and the engine power settings are very low. The distribution of raindrops at the core of a large, high bypass turbofan will, in general, be radically different for ground test conditions compared to the in-flight distributions. A careful analysis of the trajectories of the various water drops is required to determine the in-flight distribution value to be simulated in the ground test facility. Similar effects, compounded by more interaction with the flow turning and diffusion in the inlet duct are encountered in tactical military aircraft.

One technique used to address the above problems for large, high bypass turbofans, is to position the water injection sprays behind the fan and in front of the core compressor (Figure 8-3). Assuming a correct calculation of external diffusion effects, spinner and fan deflection effects on particle size and trajectories, and for centrifuging effects on trajectories, this technique can be used to set a more precise water-to-air ratio in the core engine. However, the effects of velocity and drop size mismatches are not known.

In both the ground test methods, the effects of altitude are addressed by maintaining the water-to-air mass ratio expected to be encountered in flight. The results of ground testing are then correlated using engine mathematical models and various heat transfer models to adjust to the desired conditions.

In-flight testing is generally accomplished using an aircraft tanker with a trailing boom to which an atomizing nozzle is attached. Airflow patterns into the inlet are duplicated by this technique; however, provision of a known drop size and distribution characteristic is difficult. Because the spray pattern produced by the tanker aircraft is limited to a diameter on the order to 1.8 to 3 metres (6 to 10 feet), maintaining the aircraft inlet in the correct, required position is not easy. Also, as commercial aircraft engines grow larger, the adequacy of existing equipment to continuously cover the full inlet becomes even more difficult if not impossible.

8.3.3 Required Instrumentation

A full complement of engine performance and operability instrumentation is required. The set should be as extensive as resources and engine operating characteristics will permit. In addition, two additional instrumentation requirements must be addressed.

First, the capability of conventional probes to measure either total pressure or total temperature in the presence of liquid water is not very good. Several attempts (see, for example, References 8.8 and 8.9) have been made to provide for the measurement of total pressure with a fair degree of success. Likewise,

use of properly designed thermocouples has been shown to provide some success (Reference 8.10). In both cases, however, very careful attention must be paid to probe design and data interpretation.

Second, the water drop size and spatial distribution characteristics at a relevant reference plane must be determined. Existing methodologies, such as laser interferometric systems, tend to suffer if the water-to-air ratio is large and if the area required to be surveyed is extensive.

One method, used occasionally, is to measure the quantity of water at the discharge of the core engine turbine to ascertain the amount of water ingested by the core. Such measurements can be made in a number of ways by various available sensors and measurement systems. One typical system uses one or more of the 1 to 6 μ wavelength water absorption bands in the near infrared region. Other systems have used non-dispersive infrared measurements which are then compared to a calibration cell with known absorption characteristics. Use of the latter method generally is less accurate and requires more assumptions concerning the combustion efficiency.

Measurement of combustion efficiency can be directly accomplished by determining the relative ratios of the various common carbon bearing compounds of CO_2, CO, and unburned hydrocarbons. A wide range of commercial instrumentation is available for these measurements.

8.3.4 Shortfalls and Recommended New Research/Development Capabilities

Testing techniques for addressing current certification requirements for commercial engines are generally thought to be adequate, although the certification requirements themselves are not. As new requirements are developed, it will be necessary to examine them for test techniques.

Certification requirements for tactical military engines are somewhat more difficult to ascertain. However, a facility to test the complete aircraft propulsion system at a high angle of attack in heavy rain would have a strong potential for extending adverse weather operational capability. Such a facility would most likely be a freejet installation such as that at the AEDC (Reference 8.11).

Two specific instrumentation needs currently exist. First, a method is needed to quickly and economically determine water drop size and spatial distribution over a relevant reference plane. Such a method would apply to both subsonic transport and tactical military aircraft external diffusion effects. Second, continued improvement is required in the ability to measure total pressure and temperature in the presence of water drops.

8.4 TESTING WITH SNOW/SLUSH WATER INGESTION

8.4.1. Goals of Testing

Goals for snow and slush ingestion are virtually identical to those for rain ingestion: assessment of mechanical damage and engine operability effects. Meeting these goals requires simulation of appropriate characteristics for the ingested materials.

8.4.2 Current Practices

Some limited capabilities exist to provide snow blown at an intake. However, no capability currently exists to provide standardized ground testing of snow/slush effects with uninstalled engines because of an inability to adequately produce and distribute representative snow and an inability to adequately define the expected distributions of slush across the engine face produced by wheel splash.

Ingestion of snow in flight is not currently assessed by formal ground facility tests or flight testing. Some testing may result from encounters with snowstorms (Section 2.1.4). In all cases, the total moisture content of the snow laden air is substantially less than that produced by rain ingestion. Therefore, the effects may be adequately addressed by low level raindrop ingestion testing.

Substantial quantities of snow (up to 390 g/m^3, Section 2.1.4) and slush may be ingested during ground operation. The maximum quantities may be encountered as a result of tire-driven splash with subsequent ingestion into the engine or as a result of hovering operation of rotary-wing aircraft.

In general, careful attention to these conditions is paid during aircraft design to ensure that such ingestion is minimized. Testing, for the most part, consists of high speed runway operations into controlled depths of slush and snow or actual hovering. The effects of inlet screens on rotary wing or reduced radar signature fixed wing aircraft are not measured currently by any standardized test methodology.

A second possible mode of operation which can cause ingestion of snow (primarily) and slush

(secondarily) is thrust reverser operation. Again, testing consists of high speed runway operations.

A third possible mode of operation is with a strong ground vortex entraining snow and slush. Since this mode is avoided to the maximum extent possible because of other, more serious effects (e.g. foreign object damage and surge margin loss), little, if any, testing is done. A rain ingestion test setup can be used to simulate water ingestion caused by vortex entrainment by focusing a water stream into discrete areas of the engine inlet.

Characterization of snow is generally based on water-to-air mass ratios and equivalent density of the snow material. Large snowflakes generally disintegrate and follow the streamlines of the airflow. Smaller, denser snow may be treated as very small hail particles (diameters on the order of 500-1000 μ).

Slush may be characterized by density, and, to a lesser extent, by temperature. Slush, formed in locations where substantial contamination by deicing fluids may occur, may be colder than pure water-based slush.

8.4.3 Required Instrumentation

A set of engine operability and performance assessment instrumentation similar to that required for rain ingestion testing is required. A visual record of the time dependent ingestion flows is also required to allow correlation to observed results.

Characterization of slush requires only a means of measuring the density and temperature of the slush before ingestion. Interpretation of the visual record is marginally adequate to assess the effects of the ingested slush. Snow characterization requires a means of determining snowflake sizes and number density.

8.4.4 Shortfalls and Recommended New Research/Development Capabilities

No known shortfalls exist as determined by ability to meet development and certification requirements. In general, testing with liquid water ingestion at identical water-to-air mass ratios is adequate. A need may exist for a testing methodology to evaluate snow accumulation on inlet screens.

8.5 TESTING WITH HAIL INGESTION

8.5.1 Goals of Testing

The goals of testing with hail ingestion are identical to those for rain ingestion, however, as previously stated, mechanical damage assessment testing is not within the scope of this report. Therefore, only the effects associated with operability will be treated.

8.5.2 Current Practices

Naturally occurring hail distributions identified in Section 2.4.4 have a lower limit of 0.5 cm diameter and a mean diameter of 0.95 cm with approximately 90% of the stones below 1.5 cm diameter. Ground facility testing for hail ingestion typically uses stones ranging from 1 cm to 5 cm in diameter with ice temperatures from -6.7°C to -17.8°C. Geometrical shapes range from spherical to irregular shapes of layered ice. No industry-wide standard has been defined.

Two significantly different approaches are currently in use for ground testing with hail ingestion. One technique uses direct impingement of hailstones on the face of an operating engine at desired locations, velocities, and impact number rates (Reference 8.12). The other uses an analytical calculation of ice trajectories based on data acquired from hailstone impact tests on surfaces at various angles and hailstone velocity and temperature (see Section 5.2.3). Both methods were derived to meet mechanical damage assessment criteria.

Deliberate, flight test bed encounters with hailstorms is not in practice at this time.

The reader is referred to Section 5.2.3 for details on the calculated trajectory method. The direct impingement method uses an air-powered "hail cannon" with multiple launch tubes and variable projectile velocities and number rate (Figure 8-4). Impact points may be selected for any of the individual tubes to meet various regulatory requirements.

A significant finding of current testing is that hailstones on the order of 1 cm (0.5-in) diameter cause the most significant performance losses for current engines.

8.5.3 Required Instrumentation

Instrumentation is required to assess engine performance and operability as for rain ingestion testing. Additional instrumentation to determine hailstone velocities and trajectories is required. This may be in the form of relatable parameters (driving pressure for a hail gun, etc.) which can be used to enter calibration curves. Other internal instrumentation is required as for rain ingestion testing.

8.5.4 Shortfalls and Recommended New Research/Development Capabilities

No methodology currently exists to assess the tri-phase character of the ingested water (solid, liquid, and gas) as it proceeds through the engine. A set of sensors/ methodology to make this assessment is needed. Sensors should be capable of measuring total pressure and total temperature in the presence of all phases of water. This capability is needed to permit assessment of the effectiveness of such techniques as using compressor bleeds for removal of significant quantities of solid and liquid water.

8.6 CONCLUSIONS AND RECOMMENDATIONS

Adequate testing methodologies are available for determining gaseous humidity effects. Testing methodologies for flows with condensation are only marginally made satisfactory by using statistical manipulations of a large number of test points. Rain and hail ingestion testing methodologies are adequate for defining regulatory compliance of simple, short pitot intakes; however, no satisfactory testing method has been developed for more complex intakes such as are found on many tactical military aircraft. No standardized testing methodology exists for determination of snow ingestion effects.

8.6.1 Gaseous Water Ingestion

Adequate testing methodologies exist to determine the effects of gaseous humidity on performance characteristics. However, because testing of this type is usually expensive and because the effects are small for the full range of expected atmospheric encounters, the use of such testing is generally restricted to validating a suitable analytical model.

No operability effects are known to occur as a result of operation with gaseous humidity ingestion. Therefore, no testing methodology is needed and none has been developed.

8.6.2 Condensate Water Ingestion

No fully satisfactory testing methodology has been developed. Because condensation is a path-dependent thermodynamic process, and a process which is influenced by a large number of variables (such as particle concentration, size and electrical charge; time at condition; inlet geometry and resulting local flow fields), development of an appropriate methodology is expected to be prohibitively expensive. Therefore, testing with a given, minimum number of variables, in an environment such as occurs in developmental ground test stands, has resorted to the use of statistical treatment of data to obtain empirical coefficients. This treatment is marginally satisfactory for determining "pass/fail" for acceptance testing.

8.6.3 Rain Ingestion

Direct water sprays are used to simulate rain ingestion. This technique is highly dependent on accurate calculations of particle trajectories for a particular intake and flight condition. The technique meets the regulatory standards for civil aircraft using simple, short pitot intakes but has not been shown to be adequate for more complex inlets. In particular, adequacy of testing has not been shown for intakes for (1) transonic and supersonic tactical and strategic military aircraft, (2) supersonic civil transport aircraft, and (3) subsonic/transonic/supersonic aircraft with reduced infrared, acoustic, and/or radar signatures.

8.6.4 Snow/Slush Ingestion

No standardized testing methodologies exist for snow ingestion. Altitude encounters with snow are adequately addressed by methodologies identified in Reference 9.1.

8.6.5 Hail Ingestion

Comments made for rain ingestion apply to hail ingestion.

8.7 REFERENCES

8.1 Fishbeyn, B.D. and Pervyshin, N.V. *Determination of the Effect of Atmospheric Humidity on the Characteristics of a Turbofan Engine,* 1970, Translation by Foreign Technology Division, Wright-Patterson AFB, FTD-HT-23-290-68 (AD) 715232.

8.2 Lazalier, G. R., Palmer, J. D., and Harper, R. E., *Altitude Development of the F100-PW-100 Turbofan Engine Phase IX*, June, 1975, AEDC/PA 90-104.

8.3 Counts, H. J., and Lazalier, G. R., *Baseline Performance of Newly Overhauled J75-P-17 Turbojet Engines*, February, 1978, AEDC/PA 90-104.

8.4 *Altitude Evaluation of an Overhauled TF41-A-1 Turbofan Engine (S/N 141683),* August 1977, AEDC/PA 90-104.

8.5 Spencer, James H., and Archer, David D., *The Effects of Condensation within an Aircraft Inlet Duct on Installed Turbofan Engine Performance*, Proceedings of the Tenth National Conference on Environmental Effects on Aircraft and Propulsion Systems, Philadelphia, May 1971.

8.6 Blake, J. C., *Effects of Condensation in the JT9D Turbofan Engine Bellmouth Inlet*, AIAA Paper No. 75-1325, AIAA/SAE 11th Propulsion Conference, Anaheim, California, September 29-October 1, 1975.

8.7 Russell, R. E., and Victor, I.W., *Evaluation and Correction of the Adverse Effects of (i) Inlet Turbulence and (ii) Rain Ingestion on High Bypass Engines*, AIAA Paper No. 84-2486, October 31-November 2, 1984.

8.8 Murthy, S. N. B., Leonardo, M., and Ehresman, C. M., *A Stagnation Pressure Probe for Droplet-Laden Air Flow*, AIAA Paper No. 85-0330, presented at AIAA 23rd Aerospace Sciences Meeting, January 14-17, 1985.

8.9 Dussourd, Jules L., and Shapiro, Ascher H., *A Deceleration Probe for Measuring Stagnation Pressure and Velocity of a Particle-Laden Gas Stream*, Jet Propulsion, January, 1958.

8.10 Pelton, J. M., Clark, H. K., and Paulk, R. A., *The Development of a Temperature Measuring Probe for Use in a Two-Phase (Gas-Liquid) Environment*, AEDC TR-72-19, June 1972..

8.11 Duesterhaus, D.A. and Maywald, P.V., *Freejet Test Capability for the Aeropropulsion Systems Test Facility*, AIAA Paper No. 89-2537, July 10-12, 1989.

8.12 Volk, Larry, *Power Loss in Inclement Weather*, FSF 45th IASS & 22nd IFA Conference, Long Beach, California, November 2-5, 1992

Table 8-1

Range of Water Ingestion Occurrence for Component/Engine Testing

Test Mode	Form of Water Ingestion				
	Gaseous	Condensate	Rain	Snow/Slush	Hail
Component Rig (Fan/Compressor)	Natural[1]	Not generally available[1]	Induced	Not generally available	Induced
Ground Facility Engine	Natural[2]	Not generally available[2]	Induced	Not generally available	Induced
Altitude Facility Engine	Natural[3]	Not generally available[3]	Induced	Not generally available	Induced
Flight Test Aircraft	Natural	Natural	Natural	Natural	Natural

[1] Generally at or below ambient absolute humidity
[2] Generally at ambient levels
[3] Generally well below facility ambient levels

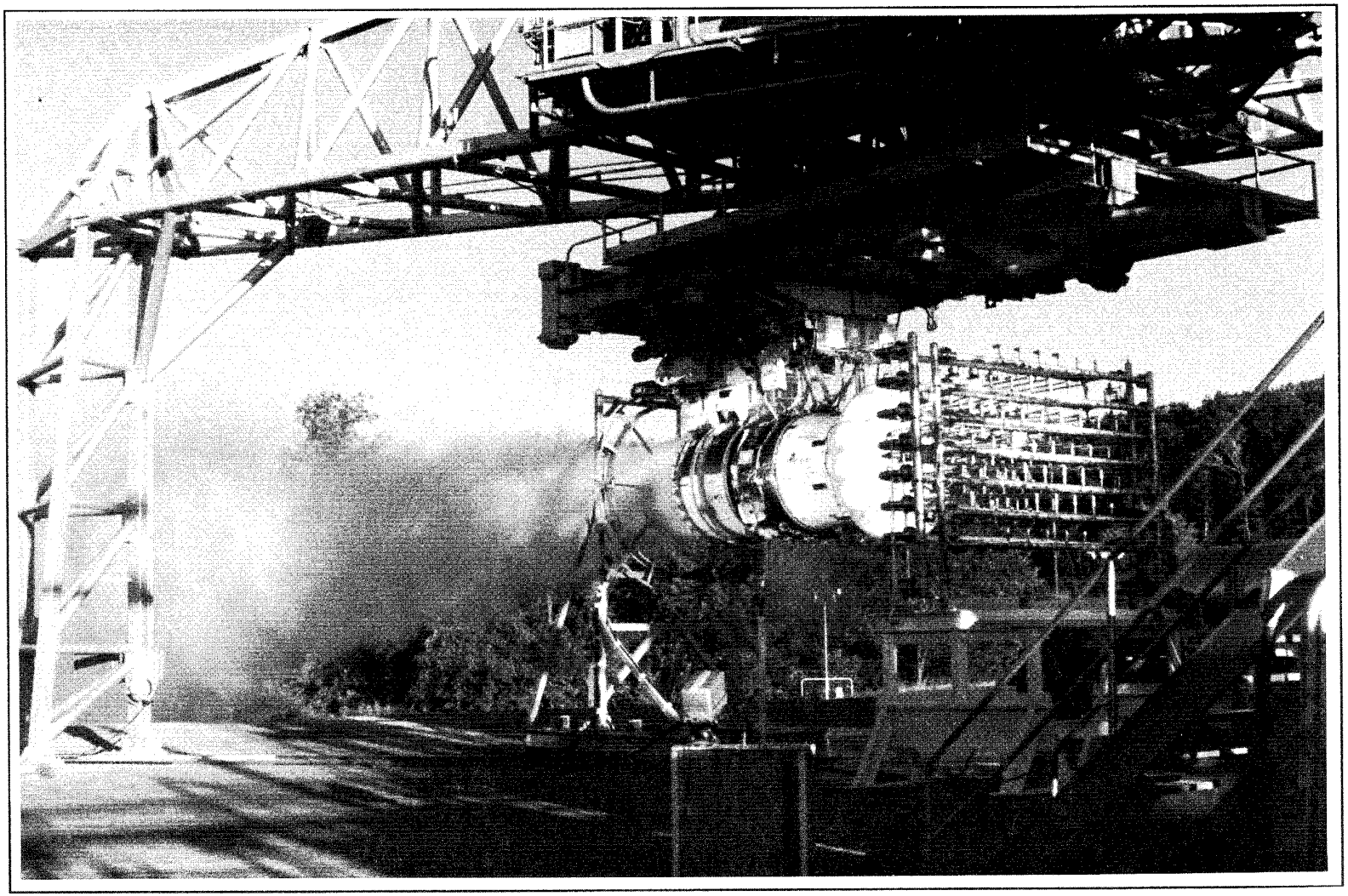

Figure 8-1

Engine Water Ingestion Ground Tests
(Reference 8.12)

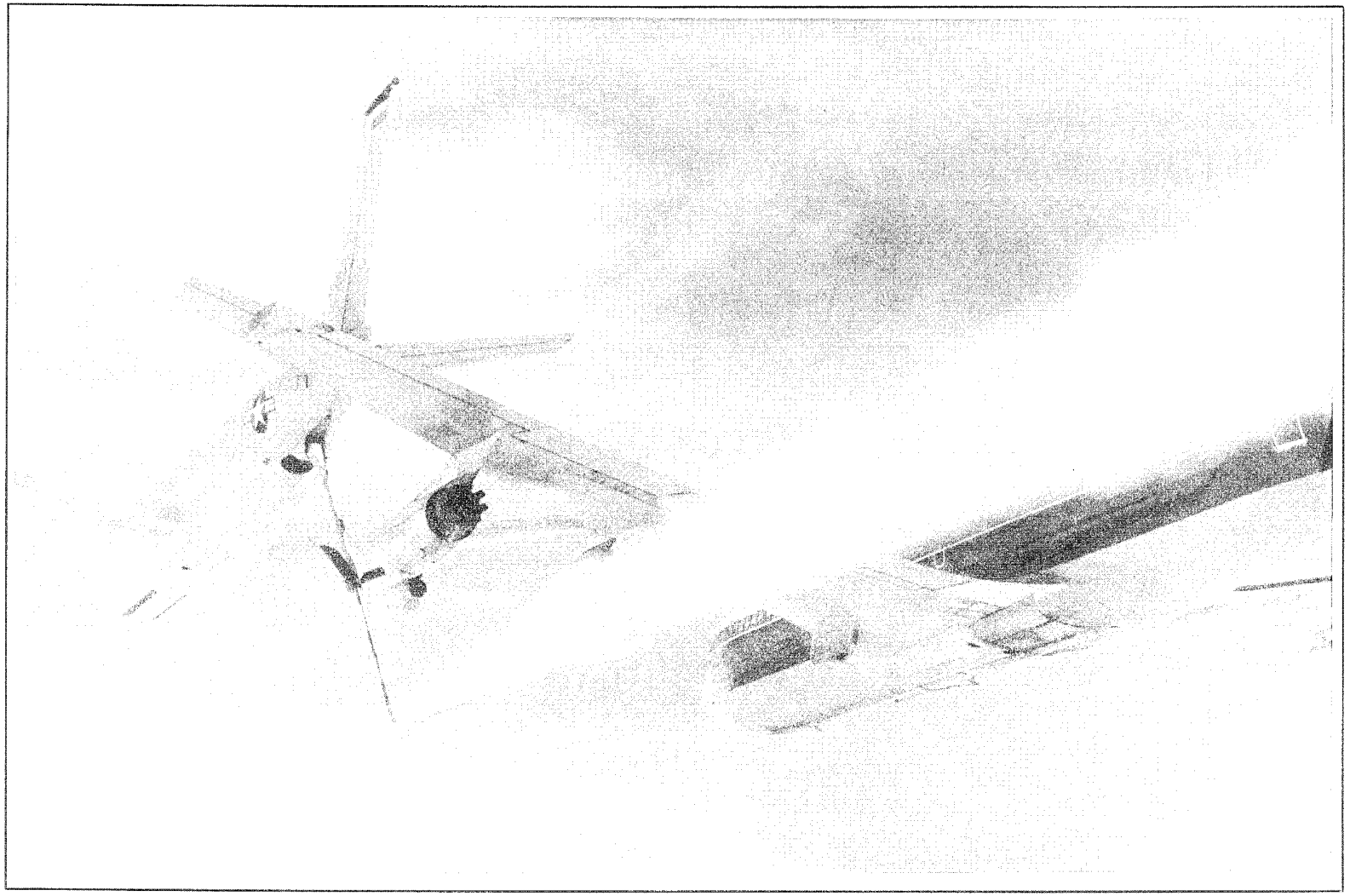

Figure 8-2

CFM56-3 Engine Water Ingestion Flight Tests
(Reference 8.12)

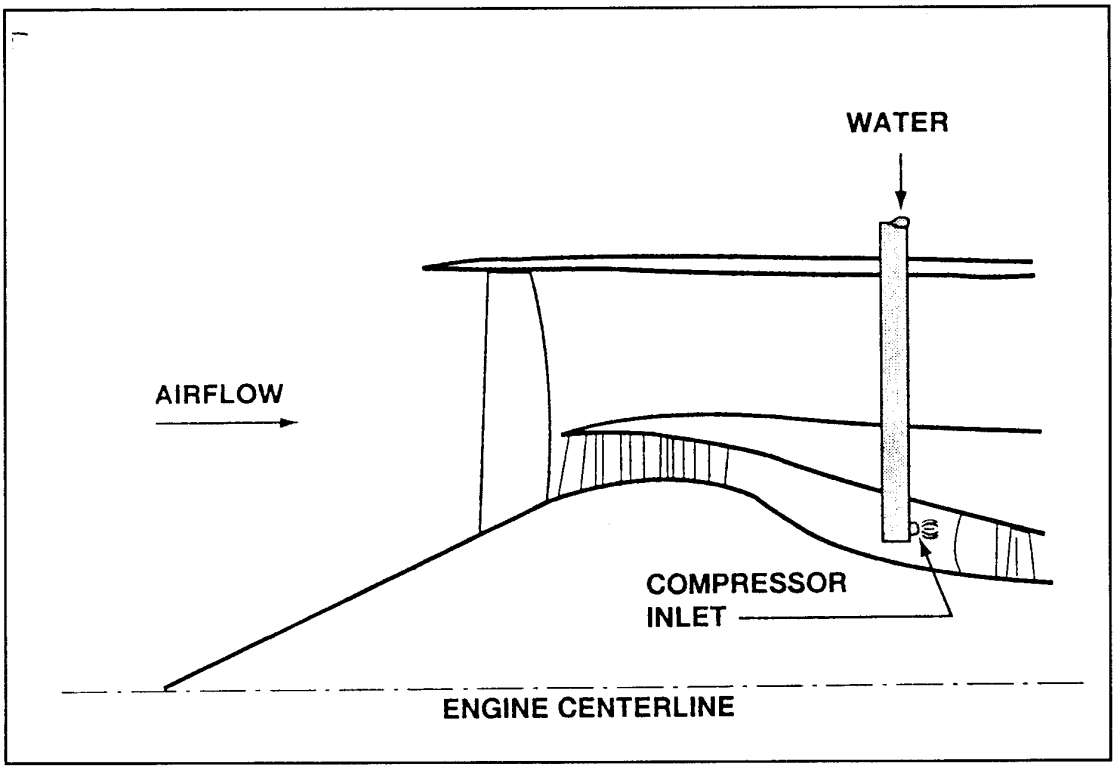

Figure 8-3

Schematic Configuration for Direct Compressor Water Ingestion Testing

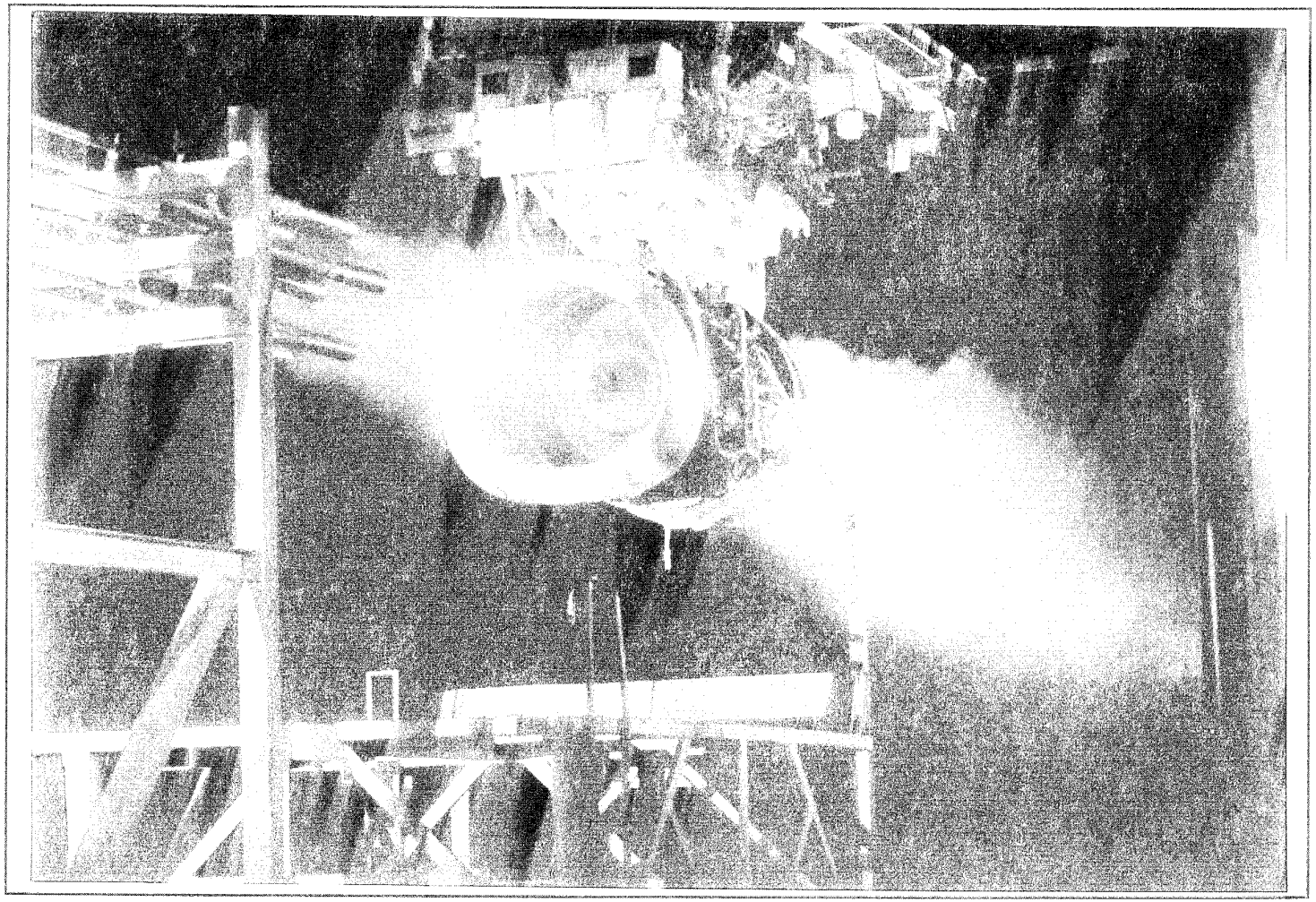

Figure 8-4

Engine Hail Ingestion Tests
(Reference 8.12)

9. CONCLUSIONS AND RECOMMENDATIONS[1]

9.1 OVERVIEW

Ingestion of water — in the forms of vapour, condensed droplets, rain, snow, and hail -- from the atmosphere into the inlet of gas turbine engines can significantly affect their performance and operability during take-off, flight, and landing. In turn, these characteristics directly affect key aircraft parameters such as range, mission cost, payload, mission suitability, and safety of flight. Therefore, precise understanding of engine responses to ingested water - in all natural forms and in quantities likely to be encountered during flight operations - must be established during the engine design and development processes and then verified as part of the engine certification process.

The primary objective of this study was to select and recommend the preferred practices from all those currently in use by government and industry to measure the effects of all forms of water ingestion on the performance and operability of gas turbine engines. Water from the natural environment is ingested by turbine engines in five different physical/thermodynamic states, i.e., gaseous humidity, condensation droplets, rain, snow, and hail. Each of these five states was addressed independently during this study. Both analytical and experimental methods as well as combinations of analyses and experiments which are currently in use to measure ingestion effects were evaluated. A unique and essential part of this study was the definition of the probable levels of water ingestion (the threat) for all types of aircraft engaged in both civil and military operations on a worldwide basis.

As expected, a number of different analytical and experimental practices are in use within the NATO community to measure the effects of the different forms of water ingestion on engine performance and operability. Each of the several practices was evaluated, and the practices recommended in this report are based on minimizing the uncertainty of and maximizing the confidence in the measured response of engines to water ingestion.

This study also confirmed the highly specialized nature and in some cases the relative immaturity of the certification requirements for turbine engine tolerance of ingested water. Further, the study also confirmed the unique characteristics of the required test instrumentation and the testing techniques required to duplicate or simulate water ingestion during development and certification tests of an engine. Therefore, separate chapters were devoted to each of these two areas.

A very useful byproduct of this study was the assessment of the current state-of-the-art of the enabling technologies required to measure the effects of water ingestion. This assessment permitted identification of shortfalls in supporting technologies. The identified areas in which improvements in the underlying technology base will provide better understanding of the effects of water ingestion on the performance and/or operability of engines are summarized separately in this chapter. This summary provides a road map which can be used to guide selection of future technology development initiatives.

Two notable areas were excluded from the scope of this work. First, recommended practices to measure the effects of water ingestion on the durability, e.g. erosion of fan/compressor blades and vanes, wear of blade tips and case rub strips and wear of air seals, and structural integrity, e.g. bending, cracking, and fracture of static and rotating blades, vanes, and struts, of engines were excluded from this study. Certainly, the effects of ingestion of rain and hail on the engine structures can be very significant, and the development of recommended practices to assess the structural effects during the design, development, and certification processes could be the subject of a further study. Such a study could be closely aligned with an overall study of hard and soft foreign object ingestion. Second, recommended practices to measure the effect of ingestion of ice crystals and supercooled water droplets were excluded from this work because this topic was specifically addressed during a 1990 symposium sponsored by the Propulsion and Energetics Panel (PEP) of AGARD (Reference 9.1).

---

[1] Tables for Chapter 9 begin on Page 9-9

This chapter should be read carefully by anyone that uses this report. Although each individual chapter attempts to highlight the state of knowledge and its influence on the engine, these are collated in this final chapter and a balanced view can then be formed. Areas of lack of information and knowledge are identified which gives rise to indications of where further research or application should be made. Above all it is hoped that any reader of this report will have had their awareness raised and that throughout their dealings with the gas turbine will note the efforts made to make flying a safe situation whatever the weather!

9.2 CONCLUSIONS

Overall conclusions and interrelated conclusions from each of the eight chapters are presented in this section. Additional detailed conclusions related to each individual subject area are presented at the end of Chapters 2 through 8.

9.2.1 Assessment of Environmental Water

The probable ranges of relative humidity and specific humidity in the earth's atmosphere are well defined and documented for day/night, annual seasons, and geographic locations throughout most of the world. Verified data have been available over a long period of time. Atmospheric standards including probable ranges of humidity are maintained for certification of civil and military aircraft turbine engines in most NATO countries.

The onset of condensation of water droplets in the engine inlet flow field is not only a function of atmospheric conditions but is also a strong function of the air intake geometry, aircraft speed, and engine airflow hence engine power setting. Therefore, there are no generalized ranges of condensed particle size distribution, particle number density, or particle spatial distribution. Each intake/engine configuration, aircraft/engine operating condition, and local value of humidity must be analyzed on a case-by-case basis to define the condensed droplet flow field. Current computational models of the nucleation and condensation processes are highly empirical and are subject to large uncertainties. Direct experimental measurements of the condensed droplet flow field at the engine inlet are very difficult and time consuming even at a local point in the flow field. Today, it is virtually impossible to obtain spatially integrated values and local spatial distributions of a condensed droplet flow field at the engine inlet.

In recent years substantial improvements have been made in the global definition of the particle size distribution, concentration, geographic extent, and probability of occurrence of rain, snow/ice crystals, and hail including graupel. These improvements have been achieved largely because of the requirements to improve turbine engine certification requirements in the civil aviation sector. Organizations such as the Aerospace Industries Association (AIA) in the United States and civil aviation organizations in other NATO countries have been responsible for these improvements. Cooperation between many meteorological organizations in Europe, Turkey, and the U.S. generated a vast pool of meteorological data. Reliable estimates of the probability of encountering upper limit values of rain, snow, and hail are now available. However, substantial extrapolation of the existing data base with an attendant increase in uncertainty is required for the lower probability/higher concentration conditions, e.g. probability less than one in 10^7.

9.2.2 Effects of Gaseous Humidity

Reliable analytical and experimental methods are available to assess the effect of gaseous humidity on the performance of both complete engines and engine components. It is generally assumed that the effects of gaseous humidity on engine operability are negligible.

Engine component performance is affected by gaseous humidity in two ways.The larger effect results from changes in the gas constant of the working fluids and can be accounted for by thermodynamically exact methods. The smaller effect results from changes in the local isentropic exponent of the working fluid and the effect on component performance can only be approximated. The effect of gaseous humidity on overall engine performance is clearly the summation of the effects on each individual component as modified by changes in the component matching and by changes in engine control system response. Changes in the control system operating point induced by gaseous humidity can be as large as the effect of the change in gas constant and may be of the same sign or opposite sign.

The recommended analytical method is based on the use of standard algorithms for both thermodynamic properties of the working fluid and engine

cycle calculations and a validated model of the engine control system behavior. The experimental method is relatively expensive and is used only infrequently to validate the analytical methods (see Chapter 8).

The capabilities of the recommended practices to measure the effects of gaseous humidity on engine performance and operability are summarized in Table 9-1. As shown in Table 9-1, the assessment method for gaseous humidity is dominated by the analytical method. Experimental testing is required to measure the effect of gaseous humidity on engine starting. It is encouraging to note that the recommended practices provide high confidence in measuring the effects of gaseous humidity in essentially all of the areas of interest.

9.2.3 Effects of Condensing Flow

Only approximate methods are available to assess the effects of condensing flow on the performance and operability of engines. In almost all cases, a combination of analytical and experimental test methods is required because neither alone can provide results having adequate confidence. These methods are generally restricted to operation of engines on development test stands because the very large populations of data required are generated only during engine development. Large data populations are required to derive pooled empirical coefficients with usable levels of accuracy. Each individual coefficient is relatively imprecise because it is inferred from correlations of a small difference in observed overall engine performance. The quality of the pooled coefficients is substantially improved when instrumentation is used to verify the presence or absence of condensation droplets at the fan or compressor inlet during each test data record.

Currently there are no recommended practices for measuring the effects of condensation droplets on test results from engine component rigs. Similarly, there are no recommended practices for measuring the effect of condensation on the performance and operability of complete intake-engine systems when installed in the aircraft.

The capabilities of the recommended practices to measure the effects of condensing flow at the engine inlet on engine performance and operability are summarized in Table 9-2. Although the capabilities shown in this Table are tabulated on a component basis, the information is only applicable to components operating within a complete engine. There are no recommended practices for engine components operating in a component test rig with condensation present. In fact, it is recommended that operation with condensation should be avoided (Section 4.5.1). Note that in essentially all cases, a combination of analysis and test is required to assess the effects of condensing flow. Also note that for the inlet, fan/splitter, compressor, and control the influence of condensation is high and the recommended practices provide only low or medium confidence in the corrections. The lower confidence reflects the relatively immature state-of-the-art for assessment of both the amount of condensation and the effects of any subsequent re-evaporation.

It is important to note that the condensation droplets are revaporized by the work added to the flow as it passes through the fan and/or compressor. Thus, for all components downstream of the compression system when operating as a part of a complete engine, the assessment methods for the condensing flow case are the same as for the gaseous humidity case. Therefore, the entries in Tables 9-1 and 9-2 for the combustor, turbine, and nozzles are identical. The reduced confidence for engine controls which have sensing elements in the air intake and/or in the early stages of the compression system is highlighted in this table.

9.2.4 Effects of Liquid Water, Snow and Hail

Newly developed methods are available to assess the effects of liquid water and hail on the performance and operability of engines. In all cases a combination of analytical and experimental methods is required. As is well known, the rain or hail properties which exist in the natural environment are substantially modified by the flow turning and the diffusion or expansion which occurs in the flow field forward of the aircraft air intake cowl. The rain, snow, or hail properties are further modified by the flow turning and the diffusion which occur within the aircraft air intake (including effects of the engine inlet spinner or bulletnose). In this report these effects have been grouped together and evaluated as a part of the "scoop factor". Analytical techniques are recommended to establish the quantitative transfer functions which describe the changes in the size, concentration, and spatial distribution of the rain or hail particles as they are captured by the aircraft inlet system and delivered to the engine inlet. The results of this particle analysis program is then used to define the rain/hail characteristics that must be simulated at the engine inlet for testing of engines or components on a test stand.

For the larger size particles that occur naturally in rain storms or hail storms, the scoop factor

can increase the concentration of rain or hail at the engine face to several times the free-stream concentration. The scoop factor is a strong function of the aircraft inlet configuration and of the operating condition of the aircraft, e.g. take-off, climb, cruise, descent, and of the engine power setting, e.g., take-off, cruise, or idle. Therefore, the effects of rain and hail on engine performance and operability are very configuration dependent and must be assessed on a case-by-case basis.

Some empirical terms in the analytical programs for the scoop factor are related to the shape of the particles (which is not well defined) and to the effects of multiple collisions between adjacent particles and between particles and adjacent aircraft or engine structures, e.g. cowl, duct, spinner, blades, vanes. In some cases these empirical coefficients are relatively imprecise. The currently recommended practices include allowances in the analysis which ensure that the derived engine inlet conditions for ingestion of liquid water or hail represent a safe, conservative, worst-case scenario.

Currently, there are no recommended practices for measuring the effect of snow on engine performance and operability. There are recommended practices for assessing the effects of atmospheric ice ingestion which are closely related to snow ingestion under some conditions. The recommended practices for assessing the effects of ice ingestion were the subject of an earlier symposium sponsored by AGARD-PEP (Reference 9.1). The potential for a severe influence of snow on engine performance and operability exists for propulsion system configurations which include particle collection/protection devices, e.g. screens and grids, in the engine inlet duct. Such devices are frequently used on helicopters and in turbine engine ground test facilities.

The capabilities of the recommended practices to measure the effects of rain and hail on engine performance and operability are summarized in Table 9-3. In all cases, a combination of analysis and test is required to assess the effects of rain or hail. Analytical methods are required to transform the rain/hail environment from the atmosphere to the fan or compressor inlet plane. Testing is then required to measure the effects of the rain/hail ingestion on engine performance and operability. Even though measurement of these effects is a relatively new requirement, the state-of-the-art has advanced rapidly because of the major importance of certifying engines which will withstand the rain/hail threat on a global basis. However, as shown in Table 9-3, there are still several areas in which the confidence in the assessment of performance effects is low, but fortunately in most of these cases, the influence of rain or hail on performance is also low.

9.2.5 Specifications and Test Requirements

Within the NATO countries, the existing engine specification requirements and test requirements for gaseous humidity are generally consistent with maximum probable levels that would be encountered during flights of military and civil aircraft.

The existing specification requirements for liquid water (rain) tolerance warrant re-evaluation to ensure that the recent meteorological data and the aircraft installation effects (scoop factor) have been properly addressed. The Notice of Proposed Rulemaking as prepared by the U.S. FAA does include revisions to the liquid water requirements based on more complete meteorological data and improved understanding of the scoop factor. This notice is currently under review in the U.S. and is being considered by other air-worthiness agencies. These changes as proposed affect only the specifications for civil aircraft. So far as can be determined, there are no similar changes to military specifications undergoing review at this time.

In a manner similar to the specification for liquid water (rain), the existing specifications for hail tolerance warrant revision to upgrade the requirements to include the hail threat as defined in the recent AIA studies. Again, the proposed changes for hail are addressed in the FAA Notice of Proposed Rulemaking as applicable to civil aircraft. So far as can be determined, there are no similar changes to military specifications undergoing review at this time.

9.2.6 Measurement of Ingested Quantities and Conditions

The results of the assessment of the instrumentation required to sense the quantities and to define the condition of water in all its phases during ingestion into gas turbines engines are very positive. However, the more capable devices are generally bulky, expensive, and require expert attention. Much of the required instrumentation is state-of-the-art and can provide the required accuracy of measurement, durability, productivity, and accessibility when sufficient investigation and care are taken although such instrumentation is rarely used to its full potential. There are two notable exceptions to the instrumentation availability. First, instrumentation to measure gas phase total temperature and gas phase total pressure in the

presence of water droplets entrained in the flow is not available. Second, instrumentation to measure the gaseous humidity of the engine inlet flow and to measure the size, shape, number density, and velocity of ingested water particles is not packaged in configurations which are compatible with installation requirements at the inlet of gas turbine engines or which are highly productive in gas turbine test applications. Even though the basic principles of advanced instrumentation which will meet this second class of needs have been demonstrated, the application engineering work remains to package the instrumentation in suitable configurations.

9.2.7 Duplication/Simulation of Water Ingestion for Testing

The state-of-the-art assessment of the test capabilities required to support development testing and certification testing for water ingestion tolerance of gas turbine engines was very positive for current day subsonic transport aircraft. Specialized test capabilities are available which meet required levels of productivity and cost effectiveness for subsonic aircraft equipped with simple pitot air-intakes. On the other hand, the specialized test capabilities are not available for many higher performance intake/engine configurations currently in use on military and some civil aircraft. These configurations include all the non-pitot intake systems for subsonic, transonic, and supersonic aircraft. Examples of such systems are (1) transonic and supersonic tactical and strategic military aircraft, (2) supersonic civil transport aircraft, and (3) subsonic,transonic, and supersonic aircraft with reduced infrared, acoustic, and radar signatures.

9.3 RECOMMENDATIONS

During this study several technical and management shortfalls were identified which warrant additional research and development. Advances in each of these areas could contribute to improvements in the accuracy and reliability of the measurements of the effects of water ingestion on the performance and operability of gas turbine engines. Recommendations for specific improvements are summarized below. Additional detailed recommendations related to each subject area are presented at the end of each chapter 2 through 8.

This list of recommendations is intended to serve as a road map to assist in planning and prioritizing future efforts.

A. Assessment of Environmental Water - (Chapter 2)

1. Incorporate additional meteorological data for rain and hail into the respective data bases to increase the level of confidence and to reduce the extrapolation for probability of occurrence less than one in 10^7.

2. Determine average and extreme temperatures of natural hailstones and ambient liquid water to assess the impact on engine operability.

3. Determine the breakup characterisitics of natural and simulated hailstones over a wide range of physical properties, e.g. density, shape, temperature and quantity of surface water.

4. Define the environmental water threat from combinations of rain and hail.

B. Effects of Gaseous Humidity - (Chapter 3)

1. Develop improved methods for describing the effects of isentropic exponent on turbomachinery performance. Enlarge the published data base of detailed compressor and turbine performance calculations to increase the range of turbomachinery design approaches, e.g., stage pressure coefficients and flow coefficients and configuration variables.

C. Effects of Condensing Flow - (Chapter 4)

1. Improve computational modeling of condensation flow fields forward of the air intake cowl plane and between the air intake cowl plane and the engine inlet plane for

two dimensional (axisymmetric) and three dimensional (non-axisymmetric) configurations.

2. Develop easily applied methods for modelling the influence of condensation (and re-evaporation) on engine components and, in particular, the stage matching and stage performance within multistage axial flow compressors.

3. Develop instrumentation to measure local and average total temperatures of the engine inlet air in the presence of condensed liquid water droplets (same as Recommendation F.1).

4. Improve instrumentation to measure particle size, number density, and spatial distribution at the engine inlet plane (included in Recommendation F.3). Atmospheric particles, droplets, rain, etc., are included in this capability.

5. Develop new or improved inlet condensation monitoring systems (e.g. video or absorption/extinction), tailored to provide continuous, real-time detection of condensate at the inlet of engines during test operation.

6. Identify controlling parameters and ranges of water vapour subcooling before onset of droplet formation and ranges of droplet superheating before droplet revaporization.

D. Effects of Liquid Water, Snow, and Hail - (Chapter 5)

1. Improve computational models of the "scoop factor" for the air intake to account for the effects of various design approaches, aircraft speeds, engine power settings and sizes and shapes of raindrops and hailstones.

2. Improve computational models of the radial and streamwise trajectories of raindrops and hailstones external to the air intake cowl plane and between the air intake cowl plane and the engine inlet plane.

3. Improve computational models of the flow of liquid raindrops and solid hailstones through engine fans and compressors as a function of engine spinner/bulletnose configuration and fan/compressor design parameters, e.g., inlet guide vane arrangements (if any), relative Mach number of blading, and stagger, solidity, and aspect ratio of blades and vanes.

4. Improve data base for shattering and agglomeration of raindrops and breakup of hailstones upon impact with static structure and rotating blades.

5. Develop generation systems and measurement equipment for artificial snow which have capacities appropriate for engine testing.

6. Improve modelling of phase changes within the components of engines.

E. Specifications and Test Requirements - (Chapter 6)

1. Reconcile the differences in adverse weather, i.e. rain and hail, requirements for certification of aircraft turbine engines for military and civil applications.

F. Measurement of Ingested Quantities and Conditions - (Chapter 7)

1. Develop instrumentation to measure local and average total temperature of the engine inlet air in the presence of condensed liquid water droplets (same as Recommendation C.3).

2. Improve packaging and application engineering of humidity measuring systems for gas turbine testing.

3. Improve instrumentation to measure size, shape, number density, velocity, and spatial distribution of liquid water droplets and hailstones at the engine inlet plane (see also Recommendation C.4). Improve the durability of this instrumentation to operate in the engine environment.

G. Duplication/Simulation of Water Ingestion for Testing - (Chapter 8)

1. Develop and validate test techniques and test equipment for certification of non-pitot inlet/engine configurations for aircraft operation at subsonic, transonic, and supersonic flight speeds with simulated rain and hail storm environments.

9.4 REFERENCES

9.1 *Low Temperature Environment Operations of Turboengines (Design and User's Problems*, AGARD Conference Proceedings, CP 480, May, 1991.

DEFINITION OF TERMS - TABLES 9-1, 9-2 AND 9-3

CONFIDENCE: The degree to which the recommended analytical practices and/or test practices measure the true shift in the performance or operability characteristics of the component or the process as a function of water ingestion.

INFLUENCE: The degree to which a component or a process embedded within the engine system affects the overall system characteristics.

A	Analytical, computational
T	Experimental, test
H	High
M	Medium
L	Low
N/A	Not applicable
N/K	Not known

Table 9-1

CAPABILITIES OF RECOMMENDED PRACTICES TO ASSESS THE EFFECTS OF INGESTED GASEOUS HUMIDITY

	ASSESSMENT METHOD	PERFORMANCE		OPERABILITY		COMMENTS
		Influence	Confidence	Influence	Confidence	
Components:						Measurement of gaseous humidity effects is important whenever 1-2% changes in engine performance are to be evaluated.
Inlet	A	M	H	L	H	
Fan/Splitter	A	M	H	L	H	
Compressor	A	M	H	L	H	
Combustor	A	M	H	L	H	
Turbine	A	M	H	L	H	
Nozzle: Core	A	L	H	L	H	
Nozzle: ByPass	A	L	H	L	H	
Engine:						
Controls (Sensors and Logic)	A	M	M	L	H	
Starting	A + T	N/A	N/A	L	M	
Power Transients	A	M	M	L	L	
Determining Core Water	N/A	N/A	N/A	N/A	N/A	

Table 9-2

CAPABILITY OF RECOMMENDED PRACTICES TO ASSESS THE EFFECTS OF INGESTED CONDENSING FLOW

	ASSESSMENT METHOD	PERFORMANCE		OPERABILITY		COMMENTS
		Influence	Confidence	Influence	Confidence	
Components:						Assessment is restricted to ground testing of complete engines only. Not applicable to rig tests or to airframe/engine installations.
Inlet	A + T	H	L	L	H	
Fan/Splitter	A + T	H	L	H	L	
Compressor	A + T	H	L	H	L	
Combustor	T	M	H	L	H	
Turbine	A + T	M	H	L	H	
Nozzle: Core	A + T	L	H	L	H	
Nozzle: ByPass	A + T	L	H	L	H	
Engine:						
Controls (Sensors and Logic)	A + T	M	M	L	H	
Starting	T	N/A	N/A	L	M	
Power Transients	T	M	M	L	L	
Determining Core Water	N/A	N/A	N/A	N/A	N/A	

Table 9-3

CAPABILITIES OF RECOMMENDED PRACTICES TO ASSESS THE EFFECTS OF LIQUID WATER (RAIN) AND HAIL

	ASSESSMENT METHOD	PERFORMANCE		OPERABILITY		COMMENTS
		Influence	Confidence	Influence	Confidence[2]	
Components:						
Inlet	A + T[1]	L	L	M	M	
Fan/Splitter	A + T[1]	L	L	M	M	
Compressor	A + T[1]	M	L	H	M	
Combustor	A + T[1]	H	M	H	L-M	
Turbine	A	M	L	L	H	
Nozzle: Core	A	L	H	L	H	
Nozzle: ByPass	A	L	H	L	H	
Engine:						
Controls (Sensors and Logic)	A + T[1]	H	N/K	H	M	
Starting	A + T[1]	N/A	N/A	H	L	
Power Transients	A + T[1]	N/K	N/K	H	M	
Determining Core Water	A + T[1]	L	M	L	M	

1 Analysis: Required to establish engine inlet environment transformed from atmospheric environment.
Test: Required to measure effect of water/hail ingestion.

2 Required Analytical and Test Procedures are defined so that confidence in Engine Capability is very high.

REPORT DOCUMENTATION PAGE

1. Recipient's Reference	2. Originator's Reference	3. Further Reference	4. Security Classification of Document
	AGARD-AR-332	ISBN 92-836-1022-9	UNCLASSIFIED/ UNLIMITED

5. Originator Advisory Group for Aerospace Research and Development
North Atlantic Treaty Organization
7 rue Ancelle, 92200 Neuilly-sur-Seine, France

6. Title

Recommended Practices for the Assessment of the Effects of Atmospheric Water Ingestion on the Performance and Operability of Gas Turbine Engines

7. Presented at/sponsored by

The Propulsion and Energetics Panel of AGARD.

8. Author(s)/Editor(s)	9. Date
	September 1995
10. Author's/Editor's Address	**11. Pages**
	368

12. Distribution Statement There are no restrictions on the distribution of this document. Information about the availability of this and other AGARD unclassified publications is given on the back cover.

13. Keywords/Descriptors

Gas turbine engines	Hail
Aircraft engines	Humidity
Engine inlets	Performance
Ingestion (engines)	Specifications
Atmospheric condensation	Standards
Water vapour	Measurement
Snow	Aviation safety
Rain	Hazardous conditions

14. Abstract

The ingestion of water from the atmosphere into the inlet of a gas turbine engine can significantly influence the performance and operability of the engine. The objective of this report is to identify preferred practices to measure the effect of water ingestion on engine performance and operability. Atmospheric water is considered in all its forms: gaseous humidity, condensation droplets, rain, snow and hail.

The Introduction in Chapter 1 summarizes the purpose and background to the report and identifies the intended audience. Chapter 2 provides a quantitative assessment of the hazardous weather threat due to water for all types of aircraft using data collected from international sources. Chapters 3, 4 and 5 examine analytical and experimental techniques currently in use to measure and to predict the effects of the different forms of ingested water on engine performance and operability. Chapter 6 summarizes current acceptance and certification specifications used by different national agencies in assessing the effects of ingested water. In Chapter 7 a review is made of current instrumentation used to assess and quantify the presence of vapour, liquid droplets and particles (frozen droplets) in the flow. Chapter 8 describes briefly current methods for testing gas turbine engines under typical weather threat conditions. The final chapter of the report summarizes the collected information on the effects of water ingestion from the preceding chapters and presents a set of conclusions and recommendations for future research.

It is hoped that this comprehensive review of the potential impact of atmospheric water ingestion will stimulate the development and application of new and improved methods for the measurement and assessment of ingested water effects on aircraft gas turbines and, hence, will lead to increased safety of aircraft operating in extreme weather conditions.

AGARD

NATO OTAN

7 RUE ANCELLE • 92200 NEUILLY-SUR-SEINE

FRANCE

Télécopie (1)47.38.57.99 • Télex 610 176

DIFFUSION DES PUBLICATIONS

AGARD NON CLASSIFIEES

Aucun stock de publications n'a existé à AGARD. A partir de 1993, AGARD détiendra un stock limité des publications associées aux cycles de conférences et cours spéciaux ainsi que les AGARDographies et les rapports des groupes de travail, organisés et publiés à partir de 1993 inclus. Les demandes de renseignements doivent être adressées à AGARD par lettre ou par fax à l'adresse indiquée ci-dessus. *Veuillez ne pas téléphoner.* La diffusion initiale de toutes les publications de l'AGARD est effectuée auprès des pays membres de l'OTAN par l'intermédiaire des centres de distribution nationaux indiqués ci-dessous. Des exemplaires supplémentaires peuvent parfois être obtenus auprès de ces centres (à l'exception des Etats-Unis). Si vous souhaitez recevoir toutes les publications de l'AGARD, ou simplement celles qui concernent certains Panels, vous pouvez demander à être inclu sur la liste d'envoi de l'un de ces centres. Les publications de l'AGARD sont en vente auprès des agences indiquées ci-dessous, sous forme de photocopie ou de microfiche.

CENTRES DE DIFFUSION NATIONAUX

ALLEMAGNE
Fachinformationszentrum,
Karlsruhe
D-76344 Eggenstein-Leopoldshafen 2

BELGIQUE
Coordonnateur AGARD-VSL
Etat-major de la Force aérienne
Quartier Reine Elisabeth
Rue d'Evere, 1140 Bruxelles

CANADA
Directeur, Services d'information scientifique
Ministère de la Défense nationale
Ottawa, Ontario K1A 0K2

DANEMARK
Danish Defence Research Establishment
Ryvangs Allé 1
P.O. Box 2715
DK-2100 Copenhagen Ø

ESPAGNE
INTA (AGARD Publications)
Pintor Rosales 34
28008 Madrid

ETATS-UNIS
NASA Headquarters
Code JOB-1
Washington, D.C. 20546

FRANCE
O.N.E.R.A. (Direction)
29, Avenue de la Division Leclerc
92322 Châtillon Cedex

GRECE
Hellenic Air Force
Air War College
Scientific and Technical Library
Dekelia Air Force Base
Dekelia, Athens TGA 1010

ISLANDE
Director of Aviation
c/o Flugrad
Reykjavik

ITALIE
Aeronautica Militare
Ufficio del Delegato Nazionale all'AGARD
Aeroporto Pratica di Mare
00040 Pomezia (Roma)

LUXEMBOURG
Voir Belgique

NORVEGE
Norwegian Defence Research Establishment
Attn: Biblioteket
P.O. Box 25
N-2007 Kjeller

PAYS-BAS
Netherlands Delegation to AGARD
National Aerospace Laboratory NLR
P.O. Box 90502
1006 BM Amsterdam

PORTUGAL
Força Aérea Portuguesa
Centro de Documentação e Informação
Alfragide
2700 Amadora

ROYAUME-UNI
Defence Research Information Centre
Kentigern House
65 Brown Street
Glasgow G2 8EX

TURQUIE
Millî Savunma Başkanliği (MSB)
ARGE Dairesi Başkanliği (MSB)
06650 Bakanliklar-Ankara

Le centre de distribution national des Etats-Unis ne détient PAS de stocks des publications de l'AGARD.

D'éventuelles demandes de photocopies doivent être formulées directement auprès du NASA Center for AeroSpace Information (CASI) à l'adresse ci-dessous. Toute notification de changement d'adresse doit être fait également auprès de CASI.

AGENCES DE VENTE

NASA Center for
AeroSpace Information (CASI)
800 Elkridge Landing Road
Linthicum Heights, MD 21090-2934
Etats-Unis

ESA/Information Retrieval Service
European Space Agency
10, rue Mario Nikis
75015 Paris
France

The British Library
Document Supply Division
Boston Spa, Wetherby
West Yorkshire LS23 7BQ
Royaume-Uni

Les demandes de microfiches ou de photocopies de documents AGARD (y compris les demandes faites auprès du CASI) doivent comporter la dénomination AGARD, ainsi que le numéro de série d'AGARD (par exemple AGARD-AG-315). Des informations analogues, telles que le titre et la date de publication sont souhaitables. Veuiller noter qu'il y a lieu de spécifier AGARD-R-nnn et AGARD-AR-nnn lors de la commande des rapports AGARD et des rapports consultatifs AGARD respectivement. Des références bibliographiques complètes ainsi que des résumés des publications AGARD figurent dans les journaux suivants:

Scientific and Technical Aerospace Reports (STAR)
publié par la NASA Scientific and Technical
Information Division
NASA Headquarters (JTT)
Washington D.C. 20546
Etats-Unis

Government Reports Announcements and Index (GRA&I)
publié par le National Technical Information Service
Springfield
Virginia 22161
Etats-Unis
(accessible également en mode interactif dans la base de
données bibliographiques en ligne du NTIS, et sur CD-ROM)

Imprimé par le Groupe Communication Canada
45, boul. Sacré-Cœur, Hull (Québec), Canada K1A 0S7

AGARD

NATO OTAN

7 RUE ANCELLE • 92200 NEUILLY-SUR-SEINE

FRANCE

Telefax (1)47.38.57.99 • Telex 610 176

DISTRIBUTION OF UNCLASSIFIED

AGARD PUBLICATIONS

AGARD holds limited quantities of the publications that accompanied Lecture Series and Special Courses held in 1993 or later, and of AGARDographs and Working Group reports published from 1993 onward. For details, write or send a telefax to the address given above. *Please do not telephone.*

AGARD does not hold stocks of publications that accompanied earlier Lecture Series or Courses or of any other publications. Initial distribution of all AGARD publications is made to NATO nations through the National Distribution Centres listed below. Further copies are sometimes available from these centres (except in the United States). If you have a need to receive all AGARD publications, or just those relating to one or more specific AGARD Panels, they may be willing to include you (or your organisation) on their distribution list. AGARD publications may be purchased from the Sales Agencies listed below, in photocopy or microfiche form.

NATIONAL DISTRIBUTION CENTRES

BELGIUM
Coordonnateur AGARD — VSL
Etat-major de la Force aérienne
Quartier Reine Elisabeth
Rue d'Evere, 1140 Bruxelles

CANADA
Director Scientific Information Services
Dept of National Defence
Ottawa, Ontario K1A 0K2

DENMARK
Danish Defence Research Establishment
Ryvangs Allé 1
P.O. Box 2715
DK-2100 Copenhagen Ø

FRANCE
O.N.E.R.A. (Direction)
29 Avenue de la Division Leclerc
92322 Châtillon Cedex

GERMANY
Fachinformationszentrum
Karlsruhe
D-76344 Eggenstein-Leopoldshafen 2

GREECE
Hellenic Air Force
Air War College
Scientific and Technical Library
Dekelia Air Force Base
Dekelia, Athens TGA 1010

ICELAND
Director of Aviation
c/o Flugrad
Reykjavik

ITALY
Aeronautica Militare
Ufficio del Delegato Nazionale all'AGARD
Aeroporto Pratica di Mare
00040 Pomezia (Roma)

LUXEMBOURG
See Belgium

NETHERLANDS
Netherlands Delegation to AGARD
National Aerospace Laboratory, NLR
P.O. Box 90502
1006 BM Amsterdam

NORWAY
Norwegian Defence Research Establishment
Attn: Biblioteket
P.O. Box 25
N-2007 Kjeller

PORTUGAL
Força Aérea Portuguesa
Centro de Documentação e Informação
Alfragide
2700 Amadora

SPAIN
INTA (AGARD Publications)
Pintor Rosales 34
28008 Madrid

TURKEY
Millî Savunma Başkanliği (MSB)
ARGE Dairesi Başkanliği (MSB)
06650 Bakanliklar-Ankara

UNITED KINGDOM
Defence Research Information Centre
Kentigern House
65 Brown Street
Glasgow G2 8EX

UNITED STATES
NASA Headquarters
Code JOB-1
Washington, D.C. 20546

The United States National Distribution Centre does NOT hold stocks of AGARD publications.
Applications for copies should be made direct to the NASA Center for AeroSpace Information (CASI) at the address below. Change of address requests should also go to CASI.

SALES AGENCIES

NASA Center for
AeroSpace Information (CASI)
800 Elkridge Landing Road
Linthicum Heights, MD 21090-2934
United States

ESA/Information Retrieval Service
European Space Agency
10, rue Mario Nikis
75015 Paris
France

The British Library
Document Supply Centre
Boston Spa, Wetherby
West Yorkshire LS23 7BQ
United Kingdom

Requests for microfiches or photocopies of AGARD documents (including requests to CASI) should include the word 'AGARD' and the AGARD serial number (for example AGARD-AG-315). Collateral information such as title and publication date is desirable. Note that AGARD Reports and Advisory Reports should be specified as AGARD-R-nnn and AGARD-AR-nnn, respectively. Full bibliographical references and abstracts of AGARD publications are given in the following journals:

Scientific and Technical Aerospace Reports (STAR)
published by NASA Scientific and Technical
Information Division
NASA Headquarters (JTT)
Washington D.C. 20546
United States

Government Reports Announcements and Index (GRA&I)
published by the National Technical Information Service
Springfield
Virginia 22161
United States
(also available online in the NTIS Bibliographic
Database or on CD-ROM)

Printed by Canada Communication Group
45 Sacré-Cœur Blvd., Hull (Québec), Canada K1A 0S7

ISBN 92-836-1022-9